TECHNISCHE UNIVERSITÄT MÜNCHEN
Institut für Theoretische Physik T30f

Heavy Quark-Antiquark Pairs at Zero and Finite Temperature with Effective Field Theories of QCD

Matthias Wilhelm Georg Berwein

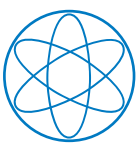

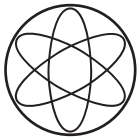

TECHNISCHE UNIVERSITÄT MÜNCHEN
Institut für Theoretische Physik T30f

Heavy Quark-Antiquark Pairs at Zero and Finite Temperature with Effective Field Theories of QCD

Matthias Wilhelm Georg Berwein

Vollständiger Abdruck der von der Fakultät für Physik der Technischen Universität München zur Erlangung des akademischen Grades eines

Doktors der Naturwissenschaften (Dr. rer. nat.)

genehmigten Dissertation.

Vorsitzende:	Prof. Dr. Laura Fabbietti
Prüfer der Dissertation:	1. Prof. Dr. Nora Brambilla
	2. Prof. Dr. Norbert Kaiser
	3. Prof. Dr. Eric Braaten (Ohio State University, schriftliche Beurteilung)

Die Dissertation wurde am 19.09.2016 bei der Technischen Universität München eingereicht und durch die Fakultät für Physik am 17.10.2016 angenommen.

Abstract

We use effective field theories to study the interactions of heavy quarks in the vacuum and in medium. First, we show how the concept of a non-relativistic effective theory (in particular NRQCD and pNRQCD) is compatible with the inherent Poincaré invariance of the underlying fundamental theory of QCD. Boost transformations, though not explicitly realized in the effective theory, may nevertheless be introduced as non-linear transformations on the non-relativistic fields. By requiring the effective Lagrangian to be invariant under these transformations, exact relations can be derived for the Wilson coefficients.

We also study the exotic bound states of heavy quarks, called hybrids, where the binding gluons are in an excited configuration. Using arguments from both NRQCD and pNRQCD, we derive a coupled Schrödinger equation, the eigenvalues of which give the leading order masses of the hybrids. The results are compared to previous theoretical approaches like the Born-Oppenheimer approximation, as well as results from experiments, lattice QCD and sum rules.

Finally, we study the behavior of heavy quarks in a hot medium by calculating the Polyakov loop and the Polyakov loop correlator at finite temperature in the weak coupling expansion. For the Polyakov loop, we present a next-to-next-to-leading-order result, using the effective theories EQCD and MQCD as well as a direct calculation. A comparison to lattice data is also given. For the correlator, we present a next-to-next-to-next-to-leading-order result in the short distance limit, which follows directly from the result for the Polyakov loop and a novel exponentiated expression for the Polyakov loop correlator in terms of singlet and adjoint free energies. We also compare these in a matching to pNRQCD.

Zusammenfassung

Wir untersuchen das Verhalten von schweren Quarks im Vakuum und bei endlicher Temperatur mit Hilfe von effektiven Feldtheorien. Zunächst zeigen wir, wie das Konzept einer nicht-relativistischen effektiven Theorie mit der zu Grunde liegenden Poincaré-Invarianz der fundamentalen Theorie QCD in Einklang gebracht werden kann. Obwohl Boost-Transformationen in der effektiven Theorie nicht explizit realisiert sind, lassen sie sich dennoch in Form von nicht-linearen Transformationen für die nicht-relativistischen Felder einführen. Indem wir die Invarianz der effektiven Lagrange-Dichte unter diesen Transformationen fordern, erhalten wir exakte Beziehungen zwischen den Wilson-Koeffizienten.

Weiterhin untersuchen wir exotische Bindungszustände von schweren Quarks, bei denen sich die bindenden Gluonen in einem angeregten Zustand befinden und die deshalb Hybrids genannt werden. Durch Verwendung von Argumenten aus NRQCD und pNRQCD erhalten wir eine gekoppelte Schrödingergleichung, deren Eigenwerte die Hybrid-Massen in führender Ordnung darstellen. Wir vergleichen unsere Ergebnisse mit vorherigen theoretischen Herangehensweisen, und darüber hinaus auch mit experimentellen Resultaten, Gitter-QCD oder Summenregeln.

Schließlich untersuchen wir das Verhalten von schweren Quarks in heißer Materie, indem wir den Polyakov Loop und den Polyakov Loop Korrelator bei endlicher Temperatur und in der Entwicklung für schwache Kopplung berechnen. Wir erhalten den Polyakov Loop in zweiter Korrektur zur führenden Ordnung unter Verwendung der effektiven Theorien EQCD und MQCD sowie durch direkte Berechnung. Das Ergebnis wird auch mit Gitter-QCD-Daten ver-

glichen. Für den Polyakov Loop Korrelator erhalten wir die dritte Korrektur zur führenden Ordnung, welche direkt aus dem Ergebnis zum Polyakov Loop folgt sowie durch eine neue exponentielle Formulierung des Korrelators durch die freien Energien in Singlet- und adjungierter Darstellung. Wir vergleichen diese ebenfalls mit pNRQCD durch ein Matching.

Contents

Contents

Chapter 1

Introduction

1.1 Phenomenology of the Strong Interaction

The strong interaction is a particularly interesting field in particle physics in that great advances have been made over the last century, with the discovery of a multitude of strongly interacting particles in collider experiments (half jokingly referred to as the particle zoo), which ultimately turned out to be perfectly described by a comparatively simple theory as bound states of only a few elementary particles called quarks; and yet they continue to this day to challenge both theorists and experimentalists alike, with new particles still being discovered (that require interpretation) or predicted (that require detection). The (by now) well established theory for the strong force is called quantum chromodynamics (QCD), for recent reviews on the state of the art and current open problems see [1–3]. Even though its Lagrangian takes only one line to write down, it is an extremely rich theory allowing for vastly different phases of matter that we are just beginning to understand.

One of the most fascinating aspects of the strong force is confinement, the property that quarks or gluons at low energies can never be observed in isolation, but only in color neutral bound states. Since confinement is a low-energy phenomenon, it is expected theoretically that if nuclear matter is heated up to sufficiently high temperatures, where the average energy per particle is larger than the confinement scale Λ_{QCD}, it should undergo a phase transition from confining to deconfined, the so-called quark gluon plasma (QGP). Such a phase transition has indeed been seen at temperatures of around 160 MeV in lattice studies [4, 5]. A concurrent phenomenon is the restoration of chiral symmetry, and the close proximity of the two transition temperatures has sparked intense discussions whether the two effects are related, an issue that is still not resolved. With heavy ion collisions, currently conducted in the experimental facilities RHIC (Relativistic Heavy Ion Collider) at the Brookhaven National Laboratory and LHC (Large Hadron Collider) at CERN (the European Organization for Nuclear Research), there is also a great experimental effort to study this new phase of matter, which is believed to have been the state of the universe in the early stages after the big bang [6].

A particularly useful probe for the QGP are heavy quarks, which may not be thermalized at temperatures of a few hundred MeV because of their large mass and therefore can be used to observe the hot medium. This idea was originally proposed by Matsui and Satz [7], who argued that the screening of the strong force through the medium would lead to a breaking of heavy quarkonium bound states. Since different excitations of quarkonium states correspond to different sizes, they would melt at different temperatures, when the screening length would become smaller than the mean distance. So the suppression of quarkonium states would

be an indicator of the temperature of the QGP. While the main idea of using quarkonia as an effective thermometer for the medium has remained, recent studies have shown that the process of quarkonium melting is in fact dominated through a thermal decay width due to an imaginary part in the interquark potential rather than through color screening, at least in the weak coupling regime [8]. An exact prediction of the quarkonium yield in such experiments is further complicated by other effects, such as cold nuclear matter or recombination effects, so this problem is currently subject to very active study.

The advances in the understanding of quarkonium dissociation demonstrated in [8] have been achieved through effective field theories (EFTs), which are among the most modern tools used at the frontier of research, complemented by lattice calculations in QCD. While the concept of describing heavy quark bound states through a potential has been used in numerous models to varying success, it is EFTs that provide the appropriate framework for the definition of a potential and establish a rigorous connection to the underlying theory of QCD [9]. In the EFT approach, potentials arise naturally as non-local interaction terms for quarkonium fields, but the theory is completely general and also describes all non-potential effects. Through this approach it has been possible to achieve an accurate description of the quarkonium spectrum in the vacuum for states below the open flavor threshold in a way that is firmly based on QCD, which shows the great importance of EFTs for the study of multiscale systems [9, 10].

In an EFT a given hierarchy of scales is exploited through a systematic expansion of the Lagrangian in ratios of these scales. The heavy scales are sequentially integrated out, generating a tower of effective theories. At each step, equivalence with the fundamental theory is ensured through a matching calculation, which determines the parameters of the EFT. Then all higher energy effects are fully contained in the parameters and only the lower scales remain dynamical. In this way high energy effects are factorized from low energy effects, and while the former can usually be calculated through perturbation theory, the latter can be defined through correlators of the effective degrees of freedom, which are then suitable for lattice evaluations. Thus perturbative and non-perturbative methods are well connected through the EFT.

A great example for this are the exotic XYZ states, which were discovered recently and continue to be subject of intense experimental study at facilities like BESIII, LHC, or also in future experiments at Belle2 and Panda at FAIR, aiming at higher precision and statistics as well as more information on production mechanisms or decays. They are typically found at or above the open flavor threshold; a list of known exotics can be found e.g. in [1], although other states have been found in the meantime like the famous "charmonium-pentaquark" state at LHCb [11]. Also in lattice QCD there has been great effort and progress regarding the study of excited quarkonia, even though a direct study is still far from being without problems [12–16].

A particularly clear indication for exotic properties is the appearance of electric charge in states which are expected to belong to the charmonium or bottomonium spectrum based on their mass and decay channels (these states are typically given the label Z). Since the combination of a quark and its antiquark is electrically neutral, the charge can only be generated by some non-trivial light quark content, thus favoring a tetraquark interpretation. But also non-trivial gluonic content may result in exotic properties, like quantum numbers that are excluded in standard interpretations of quarkonia. In this case, the states are called hybrids (i.e. a hybrid between a pure quark-antiquark bound state and a purely gluonic state like glueballs) [17].

Even if there are no inherently exotic properties, just the number of states found in the charmonium and bottomonium sectors suggests that there is more than one way to form a bound state. Accordingly, there are numerous proposed models for exotic bound states. Among

these are bound states between heavy-light mesons, or any other color combination between a heavy and a light quark like diquarkonium, three-body treatments with a constituent gluon or molecular approaches. Usually, these models are based on an assumption about the relevant degrees of freedom and a phenomenological Hamiltonian. However, even if for some special states a well defined theoretical description has been established, like for the $X(3872)$ [18, 19], a consistent framework for all these states with a well founded connection to QCD is still lacking. In this work we will explore to what extent EFTs may be used to organize the different descriptions for exotic quarkonia, focusing on hybrids.

The rest of this work is organized as follows. In the remaining sections of this introductory chapter some basic theoretical concepts and tools are summarized, including QCD and EFTs for heavy quarks at zero and finite temperature. The next chapter 2 deals with the question, how the concept of boost transformations can be implemented in the non-relativistic framework of certain EFTs. Since the underlying fundamental theory of QCD is relativistic and therefore invariant under boosts, this symmetry needs to be somehow hidden in the effective theories. We will demonstrate how non-linear field transformations can be used to implement boost transformations. The EFTs studied in chapter 2 are then applied to study hybrid quarkonium in chapter 3. Combining information from the perturbative short-range regime and lattice results for intermediate ranges, a coupled Schrödinger equation is obtained whose eigenvalues give the leading order hybrid masses. The quantum numbers of these states are explained, and the results are compared to various other data, including experiments, direct lattice calculations or results from sum rules.

In the second part of this work, the behavior of heavy quarks in a hot plasma is studied in chapter 4. We calculate the Polyakov loop at $\mathcal{O}(g^5)$ in perturbation theory (i.e. up to three loops), which is the penultimate order at which perturbation theory can be used before the expansion breaks down due to thermal low-energy effects. We use both resummed perturbation theory and EFT methods and obtain results that are in agreement. A comparison to lattice data is also presented. These results can be applied directly to the calculation of the Polyakov loop correlator, for which we present a novel expression in terms of singlet and octet free energies derived in the framework of Wilson-line exponentiation. This new result greatly simplifies the calculation and allows us to give the perturbative expansion of the Polyakov loop correlator for short distances up to $\mathcal{O}(g^7)$. We also discuss the EFT description of this operator. Finally, chapter 5 contains our conclusions and an outlook, while the appendices give further detail on the calculations or related discussions.

Parts of the contents of this thesis have previously been published in [20], [21], and [22], or are being prepared for publication [23, 24].

1.2 Quantum Chromodynamics

Quantum Chromodynamics (QCD) is widely accepted as the theory for the strong interaction. Strictly speaking, it is an SU(3) gauge theory (i.e. non-Abelian) with 6 massive Dirac fields describing the quarks, which transform in the fundamental representation of SU(3), while the gluons take on the role of the gauge field. The different components of the gauge group representation are called *colors* and the different types of quark fields are called *flavors*. The Lagrangian density is given by:

$$\mathcal{L}_{\text{QCD}} = \sum_q \bar{q} \left(i \not{D} - m_q \right) q - \frac{1}{4} F^a_{\mu\nu} F^{a\,\mu\nu} \,. \tag{1.1}$$

In this notation, several indices have been suppressed. The quark fields have a Dirac index, which is contracted with the Dirac matrices implied by the shorthand $\not{D} \equiv D_\mu \gamma^\mu$, as well as a color index, which is contracted with the color indices of the covariant derivative D_μ. The mass terms m_q act as unity with respect to both of these indices.

The 6 quark masses are vastly different, ranging from a few MeV to a few hundred GeV. A common approximation to QCD is therefore to neglect the heavy quarks and treat the light quarks as massless (this can be done rigorously in the context of effective field theories, which also allow for the treatment of the heavy quarks, compare the following sections). The theory is also chirally symmetric in this limit. The term "heavy quarks" usually refers to charm, bottom, and top flavors (c, b, and t), while up and down (u and d) belong to the light quark flavors. The strange quark flavor (s) is somewhat in-between, sometimes it is counted towards the light quarks and in other cases its mass is not neglected.

Another observation is that the degree of the gauge group of this theory has only very little effect on its properties; usually it only appears in the form of coefficients. It is therefore straightforward to consider QCD as a special case of a more general class of theories, i.e. SU(N) gauge theories with N colors and n_f light quarks. For the majority of this work we will use the term QCD to refer to this general class of theories.

The gauge fields enter the Lagrangian through the covariant derivatives: $D_\mu \equiv \partial_\mu + igA_\mu$, or through the related field strength tensor:

$$F_{\mu\nu} \equiv \frac{1}{ig} \big[D_\mu, D_\nu \big] \,, \tag{1.2}$$

where the square brackets denote the commutator: $\big[X, Y\big] \equiv XY - YX$. Here and in the following, if a color index is suppressed on a field, it means it is contracted with a generator of the gauge group T^a: $A_\mu \equiv A^a_\mu T^a$ or $F_{\mu\nu} \equiv F^a_{\mu\nu} T^a$.

Sometimes also the opposite sign is used for the gauge field in the covariant derivative. This sign is arbitrary; it can be interpreted as a redefinition of the coupling constant g, and since g always appears to even powers in perturbative results, i.e. in the combination $\alpha_\text{s} \equiv g^2/4\pi$, a sign change has no effects. Alternatively, it can be removed through a field redefinition of the gauge fields in the path integral, which also does not affect results. This is a big difference to U(1) gauge theories, where different elementary charges for different fields are possible; in non-Abelian theories all fields carry the same charge, so a redefinition affects each field in the same way. In this work we will use both signs, whichever will seem more convenient; the exact sign will be specified where relevant.

The generators of the gauge group are denoted by T^a, where a is the color index. When necessary, the representation will also be given by an index T^a_R; if the representation index is

missing, then the fundamental representation will be understood. We will also call these *color matrices*. They share several features which are independent of the degree N of the gauge group. First, the defining property for generators of a Lie group is, that any element U of the group can be written as

$$U(\alpha^a) = \exp\left[iT^a\alpha^a\right] , \tag{1.3}$$

for some real parameters α^a. This relation applies to any representation of the group, but in the fundamental representation, the resulting matrices U have to be unitary $N \times N$ matrices with determinant 1, which implies that the T^a have to be hermitian and traceless. Any set of independent $N \times N$ matrices that satisfy these properties can be used as color matrices for that group; it will always contain $N^2 - 1$ elements.

However, it is convenient to use a set of matrices that are orthogonal with respect to the scalar product of the vector space of complex $N \times N$ matrices, which is $\langle X, Y\rangle = X^*_{ij}Y_{ij}$. Because of the hermiticity of the color matrices, the condition for orthogonality can also be written as

$$T^{a\,*}_{ij}T^b_{ij} = \mathrm{Tr}\left[T^aT^b\right] \propto \delta^{ab} . \tag{1.4}$$

Instead of normalizing the color matrices to 1 under this scalar product, it is conventional to use instead

$$\mathrm{Tr}\left[T^aT^b\right] = \frac{\delta^{ab}}{2} . \tag{1.5}$$

Sometimes also a general normalization factor denoted as T_F is used. However, this factor is completely irrelevant for any results, since each generator in the Lagrangian is accompanied by a power of the coupling g and vice versa. A different normalization for the color matrices can therefore be fully absorbed by a redefinition of the coupling parameter. This also means that in any result the power of T_F will always be the same as the power of α_s[1]. We prefer therefore to use the conventional choice of $T_F = 1/2$.

The unit matrix does not belong to the color matrices, because it is not traceless, and it is straightforward to see that it is orthogonal to any generator. The set of color matrices complemented by the unit matrix (which contains exactly N^2 elements) therefore forms an orthogonal (but not normalized) basis for the space of complex $N \times N$ matrices. This means that for any matrix X we can write:

$$X = \frac{1}{N}\mathrm{Tr}[\mathbb{1}X]\mathbb{1} + 2\mathrm{Tr}[T^aX]T^a . \tag{1.6}$$

Through a slight rearrangement of this expression, we can obtain the Fierz identity:

$$T^a_{ij}T^a_{kl} = \frac{1}{2}\delta_{il}\delta_{kj} - \frac{1}{2N}\delta_{ij}\delta_{kl} . \tag{1.7}$$

This relation is only valid in the fundamental representation, since it is only in this case that the number of generators plus the unit matrix equals the dimension of the matrix space.

The commutator of two color matrices is necessarily orthogonal to the unit matrix, since the trace of it vanishes trivially because of the cyclic property of the trace, so we can write:

$$\left[T^a, T^b\right] = if^{abc}T^c , \tag{1.8}$$

[1] Or at least they will differ by a constant number, in case color matrices are already present in the initial expression.

where the coefficients f^{abc} are called *structure constants*. It is straightforward to see that they are real by taking the hermitian conjugation of Eq. (1.8) and keeping in mind that all color matrices are hermitian. Because of Eq. (1.5) we can express them directly as:

$$f^{abc} = -2i \operatorname{Tr}\Big(\big[T^a, T^b\big]\, T^c \Big) \,. \tag{1.9}$$

So we see that, while the first two indices of the structure constants are antisymmetric by definition, for an orthogonal set of color matrices the structure constants are fully antisymmetric in all indices. Other representations are then defined through Eq. (1.8): any set of matrices that satisfy this relation may be used as generators of the gauge group in their respective representation. If there is no similarity transformation that makes the generators block diagonal, then the representation is called irreducible.

One can also define symmetric structure constants. In analogy to the antisymmetric structure constants, we write:

$$d^{abc} = 2 \operatorname{Tr}\Big(\big\{T^a, T^b\big\}\, T^c \Big) \,, \tag{1.10}$$

where the curly brackets denote the anticommutator $\{X, Y\} \equiv XY + YX$. The symmetric structure constants play a role in the decomposition of products of color matrices. Since the product of two color matrices necessarily needs to be a linear combination of the unit matrix and the color matrices (as those form a basis of matrix space), we can determine this expression by calculating the projections:

$$T^a T^b = \frac{1}{N} \operatorname{Tr}\big[T^a T^b\big]\, \mathbb{1} + 2 \operatorname{Tr}\big[T^a T^b T^c\big] T^c = \frac{\delta^{ab}}{2N} \mathbb{1} + \left(\frac{1}{2} d^{abc} + \frac{i}{2} f^{abc} \right) T^c \,, \tag{1.11}$$

where in the second term we have written the product through commutator and anticommutator: $T^a T^b = \{T^a, T^b\}/2 + [T^a, T^b]/2$. In this way, any product of color matrices can be decomposed in terms of structure constants, color matrices and the unit matrix by iterated application of this relation. Unlike the antisymmetric structure constants, however, the symmetric structure constants have no direct relation to higher representations; for other representations there is no way to simplify the anticommutator of two generators.

Through repeated use of the commutation relations (1.8) for the color matrices, or alternatively through the explicit expressions for the structure constants and the Fierz identity, one can show the Jacobi identity:

$$f^{abe} f^{ecd} + f^{bce} f^{ead} + f^{cae} f^{ebd} = 0 \,. \tag{1.12}$$

From this one can see, that the structure constants themselves form a representation of $\mathrm{SU}(N)$, the so-called *adjoint representation*. Its generators are defined as:

$$(T^a_A)_{bc} = -i f^{abc} \,. \tag{1.13}$$

Inserting this in Eq. (1.8) and using the antisymmetry of the structure constants, one can show that for the adjoint representation the commutation relation corresponds to the Jacobi identity.

There is a useful relation between fields $\mathcal{F}$ that transform under the adjoint representation and transformation matrices U in the fundamental representation by contracting the color index with a color matrix:

$$\mathcal{F} = \mathcal{F}^a T^a \xrightarrow{\mathrm{SU}(N)} U \mathcal{F} U^\dagger \,. \tag{1.14}$$

The easiest way to show this is by considering only an infinitesimal transformation $\alpha^a \to 0$. The left-hand side transforms as:

$$\mathcal{F}^a \xrightarrow{\mathrm{SU}(N)} \mathcal{F}^a + i\alpha^c \left(T_A^c\right)_{ab} \mathcal{F}^b + \mathcal{O}\left(\alpha^2\right) = \mathcal{F}^a + f^{abc}\alpha^c \mathcal{F}^b + \mathcal{O}\left(\alpha^2\right) , \tag{1.15}$$

while the right-hand side gives:

$$U\mathcal{F}U^\dagger = \mathcal{F} - i\big[\mathcal{F}, \alpha\big] + \mathcal{O}\left(\alpha^2\right) = \mathcal{F}^a T^a + f^{abc}\alpha^c \mathcal{F}^b T^a + \mathcal{O}\left(\alpha^2\right) . \tag{1.16}$$

Since a finite transformation can be written as a succession of infinitesimal transformations, and at each step left-hand and right-hand sides agree, we see that Eq. (1.14) is indeed valid also for finite transformations. An alternative way to prove this directly for finite transformations is through the Baker-Campbell-Hausdorff formula (see below).

Since QCD is a gauge theory, the gauge transformations are local, which means that the parameters α^a in Eq. (1.3) depend on the space-time coordinates. The quark fields transform as:

$$q(x) \xrightarrow{\mathrm{SU}(N)} U(x)q(x) . \tag{1.17}$$

In order for the Lagrangian to remain invariant, the gauge fields have to transform in a way that the covariant derivatives transform as:

$$D_\mu \xrightarrow{\mathrm{SU}(N)} U(x)D_\mu U^\dagger(x) , \qquad \text{so} \qquad A_\mu(x) \xrightarrow{\mathrm{SU}(N)} U(x)A_\mu(x)U^\dagger(x) + \frac{1}{ig}U(x)\partial_\mu U^\dagger(x) . \tag{1.18}$$

Such a transformation is only possible, if there are sufficient degrees of freedom. The gauge field A_μ is a matrix that is constructed only from the color matrices; it therefore contains no component proportional to the unit matrix and its trace vanishes. The transformed field cannot have a component proportional to the unit matrix either, so also its trace has to vanish.

For the first term (which transforms like an adjoint field) it is straightforward to show that the trace vanishes, since the trace is cyclic and the order of the matrices can be shifted such that $U(x)$ and $U^\dagger(x)$ cancel each other. For the second term we may use the Baker-Campbell-Hausdorff formula:

$$U(x)\partial_\mu U^\dagger(x) = \sum_{k=1}^{\infty} \frac{(-i)^k}{k!} \big[\partial_\mu, \alpha(x)\big]_k , \tag{1.19}$$

where the nested commutators are defined recursively as:

$$[X, Y]_k \equiv \big[[X, Y]_{k-1}, Y\big] , \qquad \text{with} \qquad [X, Y]_1 \equiv [X, Y] . \tag{1.20}$$

The trace vanishes for all terms with $k \geq 2$ because of the commutator; for $k = 1$ we have $[\partial_\mu, \alpha(x)] = [\partial_\mu \alpha^a(x)]T^a$, so also this term contains no component proportional to the unit matrix and its trace vanishes.

It is also straightforward to show that also the field strength tensor indeed has no component proportional to the unit matrix and can be written as a linear combination of color matrices, as claimed above. We write it explicitly:

$$F_{\mu\nu} = \partial_\mu A_\nu - \partial_\nu A_\mu + ig\big[A_\mu, A_\nu\big] , \tag{1.21}$$

and we see that the trace over all these three terms vanishes. In addition, it follows from the transformation of the covariant derivatives that the field strength tensor is an adjoint field:

$$F_{\mu\nu}(x) = \frac{1}{ig}[D_\mu, D_\nu] \xrightarrow{\mathrm{SU}(N)} \frac{1}{ig}\big[U(x)D_\mu U^\dagger(x), U(x)D_\nu U^\dagger(x)\big] = U(x)F_{\mu\nu}(x)U^\dagger(x) . \tag{1.22}$$

So the gauge field part of the Lagrangian, which can also be written as:

$$-\frac{1}{4}F^a_{\mu\nu}F^{a\,\mu\nu} = -\frac{1}{2}\mathrm{Tr}\left[F_{\mu\nu}F^{\mu\nu}\right] , \tag{1.23}$$

is indeed gauge invariant, since the transformation matrices cancel in the trace. For the different components of the field strength tensor, the expressions (chromo) electric and (chromo) magnetic fields are common:

$$E^i \equiv F^{i0} \qquad \text{and} \qquad \epsilon_{ijk}B^k \equiv -F^{ij} , \tag{1.24}$$

where ϵ_{ijk} is the Levi-Civita tensor of rank 3.

In addition to the gauge symmetry, the fields in QCD show the typical behavior of Dirac or vector fields under Poincaré transformations as well as the discrete P, C, and T transformations. The QCD Lagrangian is invariant under each of these transformations. In principle, it is possible to add terms to the QCD Lagrangian which would break the CP symmetry. However, the experimental bounds on the parameters of these extra terms are such that their effects are extremely suppressed [25]. We will therefore not include any of these terms, so the discrete symmetries are assumed to be exact. The as yet unsolved question why no such effects appear in the strong force, even though they would be allowed theoretically, is known as the *strong CP problem*.

1.2.1 Running Coupling

Like most quantum field theories, QCD suffers from ultraviolet (UV) divergences that need to be renormalized in order to obtain meaningful predictions. A convenient regularization technique for perturbative calculations is *dimensional regularization*, whereby the momentum integrals appearing in loop diagrams are analytically continued to $D = 4-2\varepsilon$ dimensions. The divergences of the unregulated integrals are reobtained in the $\varepsilon \to 0$ limit (or in some cases this limit may even be finite).

The $1/\varepsilon$ poles of the dimensionally regulated diagrams need to be absorbed in redefinitions of the parameters of the theory. Since QCD has only one free parameter (in the absence of quark masses or CP breaking terms), the renormalization of these UV divergences can be achieved by replacing the bare coupling constant g_B through its renormalized value g_R. Since the coupling constant is the only parameter that needs to be redefined in order to renormalize the QCD Lagrangian, this process is also known as *charge renormalization*. However, certain operators may require further renormalization constants.

The explicit relation between g_B and g_R is given by:

$$g_B^2\mu^{-2\varepsilon} = g_R^2(\mu) - \frac{g_R^4(\mu)}{(4\pi)^2}\left(\frac{11}{3}N - \frac{2}{3}n_f\right)\left(\frac{1}{\varepsilon} - \gamma_E + \ln 4\pi\right) + \mathcal{O}\left(g^6\right) , \tag{1.25}$$

where γ_E is the Euler-Mascheroni constant. The inclusion of the constant terms beside the $1/\varepsilon$ poles is arbitrary; different choices define different renormalization schemes. Here we have chosen the so-called $\overline{\mathrm{MS}}$-scheme, which we will use throughout this work. Physical results ultimately do not depend on the choice of scheme, as long as one consistently uses the same scheme for any result.

The bare coupling in the dimensionally regularized theory needs to have mass dimension 2ε in order for the action to be dimensionless. For the renormalized coupling, this has been

separated into the mass scale μ, which is in principle arbitrary, such that g_R is dimensionless. However, this step introduces an explicit μ dependence into the renormalized results in the form of logarithms of μ^2. Since the unrenormalized expression does not depend on μ, the renormalized coupling g_R needs to depend on μ implicitly in order to cancel the explicit dependence. This scale dependence of the renormalized coupling constant is known as *running coupling*.

The running is described by the so-called *beta function*, which is defined as the logarithmic derivative of the coupling with respect to μ. It is usually expressed through α_s instead of g, and it can be expanded in powers of α_s in perturbation theory:

$$\beta(\alpha_\mathrm{s}) = \mu^2 \frac{d\alpha_\mathrm{s}(\mu)}{d\mu^2} = -\sum_{k=0}^{\infty} \beta_k \alpha_\mathrm{s}(\mu) \left(\frac{\alpha_\mathrm{s}(\mu)}{4\pi}\right)^{1+k} . \tag{1.26}$$

We can obtain the first coefficient of the beta function directly from Eq. (1.25) (after multiplying with $\mu^{2\varepsilon}/4\pi$) by taking the derivative on both sides. Since the bare coupling does not depend on μ, the left-hand side gives zero, and through some rearrangement of the terms on the right hand side and we get $\beta_0 = (11N - 2n_f)/3$. So we see that the sign of the beta function depends on the number of colors and light quarks; for standard QCD it is negative.

This has great consequences on the scale dependence of the coupling constant. If we include only the first term in the beta function, we can solve the differential equation for $\alpha_\mathrm{s}(\mu)$ as:

$$\alpha_\mathrm{s}(\mu) = \frac{\alpha_\mathrm{s}(\mu')}{1 + \dfrac{\beta_0 \alpha_\mathrm{s}(\mu')}{4\pi} \ln \dfrac{\mu^2}{\mu'^2}} , \tag{1.27}$$

where μ' is some reference scale. This function has a pole at a certain scale, which is called Λ_QCD, and if we now choose $\mu' = \Lambda_\mathrm{QCD}$, then the running coupling takes on the form:

$$\alpha_\mathrm{s}(\mu) = \left(\frac{\beta_0}{4\pi} \ln \frac{\mu^2}{\Lambda_\mathrm{QCD}^2}\right)^{-1} . \tag{1.28}$$

Since β_0 is positive, we see that the coupling constant becomes small at large energy scales $\mu \gg \Lambda_\mathrm{QCD}$, which is the opposite behavior compared to U(1) gauge theories, for instance. This feature of QCD is known as *asymptotic freedom*. Conversely, the coupling constant becomes large at small energy scales, which means that in this case perturbation theory cannot be used. Note that Eq. (1.28) may only be used in the asymptotically free regime, since it was derived from the assumption that terminating the expansion of the beta function after the first term is a good approximation.

1.3 The Imaginary-Time Formalism

The main idea behind the imaginary time formalism is the observation that the exponential of the Hamiltonian operator divided by the temperature T, which appears in the calculation of thermal averages, has the same form as the time evolution operator, except that the exponent

[2] In calculations we may just equip each integral from the start with the appropriate power of μ to give it integer dimension, i.e. $\int d^4x \to \mu^{-2\varepsilon} \int d^D x$ and $\int d^4p \to \mu^{2\varepsilon} \int d^D p$, since the number of loop momenta is always the same as the power of g, so charge renormalization will always provide the required μ terms.

is real instead of imaginary. The two operators are formally equivalent by inserting $t = -i/T$, which relies on the assumption that the time coordinate t can be analytically continued to the complex plane: $t \to -i\tau$. The new coordinate τ is called the *imaginary time* because of this relation, although τ itself is a real parameter.

By exploiting this analogy, it can be shown that the calculation of thermal averages is equivalent to calculating vacuum expectation values in a theory, where the time coordinate t has been replaced by the imaginary time coordinate τ. This theory now has a Euclidean instead of a Minkowski metric, because the square of the imaginary unit that comes from the change $t \to -i\tau$ yields another minus. Accordingly, all vector indices are written as lower indices in this theory, and the usual Minkowski interpretation in terms of covariant and contravariant vectors is dropped.

Also several other modification have to be done for this Euclidean theory: since $\partial_t \to i\partial_\tau$, we also need to change $A_0 \to iA_0$ in order for the covariant derivative to change uniformly as $D_0 \to iD_0$ (sometimes the index is also changed from 0 to 4 in the Euclidean theory, but we will keep 0 in this work). In addition, while in the Minkowski theory one usually identifies the gauge field with the upper index with the 3-vector field $\boldsymbol{A}$, in the Euclidean theory it is the gauge field with the lower index, so there is a sign difference of $\boldsymbol{A}$ between Minkowski and Euclidean theory. Accordingly, the components of the field strength tensor change as $\boldsymbol{E} \to i\boldsymbol{E}$ and $\boldsymbol{B} \to -\boldsymbol{B}$. In order to also write the $\not{D}$ in the quark sector as a Euclidean product, we redefine the Dirac matrices as $(\gamma_E)_0 = (\gamma_M)_0$ and $(\gamma_E)_i = -i(\gamma_M)^i$, such that $\not{D} \to iD_\mu(\gamma_E)_\mu$. After these modifications, there is an overall minus sign in the Euclidean Lagrangian, which is usually combined with the factor $-i$ from the time integral in the action, such that the phase factor in the path integral changes as $\exp[iS_M] \to \exp[-S_M]$. In summary, the Euclidean Lagrangian is obtained from the Minkowski through:

$$\mathcal{L}_E = -\mathcal{L}_M \left(D_0 \to iD_0, \boldsymbol{\gamma} \to -i\boldsymbol{\gamma}\right) . \tag{1.29}$$

The imaginary time coordinate is restricted to take values between 0 and $1/T$. The bosonic fields obey periodic boundary conditions $A_\mu(1/T) = A_\mu(0)$, while the fermionic fields obey antiperiodic boundary conditions $q(1/T) = -q(0)$. As a consequence, the connection to momentum space is obtained through a discrete Fourier transformation for the imaginary time coordinate, which we denote by a sum-integral symbol:

$$\begin{aligned} A_\mu(x) = &\sum\!\!\!\!\!\!\int_K e^{iK_\nu x_\nu} \widetilde{A}_\mu(K) \equiv \sum_{k_0} \int_k e^{i(k_0\tau + \boldsymbol{k}\cdot\boldsymbol{x})} \widetilde{A}_\mu(k_0, \boldsymbol{k}) \\ &\equiv T \sum_{n\in\mathbb{Z}} \int \frac{d^dk}{(2\pi)^d} e^{i(2\pi T\tau n + \boldsymbol{k}\cdot\boldsymbol{x})} \widetilde{A}_\mu(2\pi Tn, \boldsymbol{k}) , \end{aligned} \tag{1.30}$$

$$\begin{aligned} q(x) = &\sum\!\!\!\!\!\!\int_{\{K\}} e^{iK_\mu x_\mu} \widetilde{q}(K) \equiv \sum_{\{k_0\}} \int_k e^{i(k_0\tau + \boldsymbol{k}\cdot\boldsymbol{x})} \widetilde{q}(k_0, \boldsymbol{k}) \\ &\equiv T \sum_{n\in\mathbb{Z}} \int \frac{d^dk}{(2\pi)^d} e^{i(\pi T\tau(2n+1) + \boldsymbol{k}\cdot\boldsymbol{x})} \widetilde{q}(\pi T(2n+1), \boldsymbol{k}) , \end{aligned} \tag{1.31}$$

where the dimensionally regularized integral is now performed in $d = 3 - 2\varepsilon$ dimensions. The zero components of the momentum $K = (k_0, \boldsymbol{k})$ are called bosonic (for $k_0 = 2\pi Tn$) or fermionic (for $k_0 = \pi T(2n+1)$) *Matsubara frequencies*.

The discrete nature of the Matsubara frequencies has far reaching consequences. The sum over all frequencies (called Matsubara sum) usually introduces the bosonic or fermionic

distribution functions $n_{B/F}(k) = 1/(\exp[k/T] \mp 1)$ into the propagators. In addition, the fact that for $n = 0$ the bosonic frequency vanishes (the so-called zero mode) introduces infrared (IR) divergences to many diagrams, which are not removed with charge renormalization. The treatment of these divergences requires a more careful approach than naive perturbation theory, because soft gluonic modes need to be resummed [26, 27] (see also chapter 4).

Since in the imaginary-time formalism the time coordinate is traded in for the imaginary time coordinate, it is only suitable for the study of time-independent operators in an equilibrium system. In case one is interested in explicitly time-dependent quantities or non-equilibrium dynamics, other forms of thermal field theory have to be used, i.e. the *real time formalism*. Since we will only need the imaginary time formalism in this work, we will not discuss these further here.

1.4 Effective Field Theories

In many physical systems there are several scales present which satisfy a certain hierarchy, meaning that ratios of these scales are different from one by orders of magnitude (examples will follow shortly). Multiscale systems are typically very difficult to solve, so one of the most promising approaches to obtaining an approximate result is to expand in these ratios. This is what effective field theories (EFTs) achieve in a systematic fashion by implementing the expansion at the Lagrangian level.

The way an EFT is constructed from a fundamental theory is the following: one assumes a scale hierarchy, i.e. that the scale which we will generically call M here is much larger than any other scale in the system, and figures out the effective degrees of freedom as well as the symmetries. Usually, this is done by considering how the system would be described if M were infinitely large. Then the effective Lagrangian is given by the most general collection of operators that can be constructed from these effective degrees of freedom and which are allowed by the symmetries. Each of these operators is equipped with a coefficient, called *Wilson coefficient*, and divided by the appropriate power of M to get the right mass dimension:

$$\mathcal{L}_{\text{EFT}} = \sum_i \frac{c_i(\mu_M/M)}{M^{d_i-4}} O_i(\mu_M)\,, \tag{1.32}$$

where d_i is the mass dimension of the operator O_i.

The effective degrees of freedom are restricted to carry only energies or momenta which are much smaller than M. This is denoted by writing $O_i(\mu_M)$, where μ_M acts as a cutoff between the lower energy scales and M. In this way, M has been completely removed from the dynamics of the effective theory, which is why this process is also known as *integrating out* the scale M. All information from processes that happen at the scale M are contained in the Wilson coefficients, which are also the only elements that may contain non-analyticities in M.

Unlike for theories that can be considered to be truly fundamental, like e.g. QCD or the full Standard Model, there is no requirement on effective theories to include only operators that are renormalizable. This means that usually there is an infinite number of operators to be included in the EFT. However, each of these operators scales at most like $\mu_M^{d_i}$, and if we only include operators up to a maximal order in μ_M/M, then there is only a finite number of them; this order is then the accuracy to which the calculation is performed. Renormalizability is then not an issue: it can be performed order by order in the expansion parameter [28, 29].

In practice, however, there may be more than one energy scale left in the EFT, so operators with the same mass dimension may scale very differently, depending on which scale they are associated with. In order to obtain a systematic expansion, it is essential that a *power counting* is established, which determines the scaling behavior of each operator. Without such a power counting, it is not possible to give a reliable estimate of the size of the contributions that are neglected after the expansion terminates. Often the best way to establish such a power counting is to construct lower order EFTs by integrating out further scales in order to uniquely define the power counting for certain operators.

The Wilson coefficients of the effective Lagrangian need to be fixed in what is called a *matching calculation* in order to ensure equivalence with the fundamental theory in the low energy regime. This is usually done by calculating equivalent correlators in the effective and in the fundamental theory up to the same order in the expansion parameter and equating the results. In doing this, one needs to keep in mind that also operators in the fundamental and the effective theory need to be matched.

In this way EFTs disentangle contributions from different energy scales: the high energy processes at the scale M are factorized in the Wilson coefficients and the low energy processes are dynamically generated by the effective degrees of freedom. This separation is also particularly useful regarding the applicability of perturbation theory; since the matching calculation is performed at the scale that is being integrated out, it can always be done perturbatively as long as $M \gg \Lambda_{\mathrm{QCD}}$. Then calculations in the EFT may or may not be perturbative, depending on the relation of the remaining energy scales to Λ_{QCD}. In this way EFTs can also separate perturbative from non-perturbative contributions.

1.4.1 NRQCD and pNRQCD

In the study of the interactions of heavy quarks, the heavy quark mass is a very convenient parameter to integrate out, since it is typically much larger than e.g. the energy scales of processes that lead to the formation of bound states. The effective degrees of freedom can be figured out by considering the infinite mass limit. In that case, the heavy quark or antiquark is a static particle, which may still act as a color source or sink and has a spin, but can no longer be created or annihilated. Accordingly, in the effective theory they are described by two independent, non-relativistic Pauli spinor fields: ψ annihilates a heavy quark and χ creates a heavy antiquark. Since there is no pair creation or annihilation, the two fields anticommute and quark and antiquark number are separately conserved.

The other effective degrees of freedom look the same as in QCD: gluons and n_f flavors of massless quarks described by Dirac spinors. Only in the effective theory they must not have energies or momenta of the order of M or larger. All fields still carry color charge, so the effective Lagrangian must obey the gauge symmetry. The discrete symmetries P, C, and T are also present in the effective theory as well as rotational invariance, only boost transformations are no longer explicit symmetries of the effective Lagrangian. More details on this can be found in chapter 2.

Since the heavy quarks and antiquarks are described by non-relativistic fields, this theory is called *Non-Relativistic QCD* (NRQCD) [30–32]. Its Lagrangian at next-to-leading order

(NLO) is given by:

$$\mathcal{L}_{\text{NRQCD}} = \psi^\dagger \left(iD_0 + \frac{1}{2M}\boldsymbol{D}^2 + \frac{c_F}{2M} g\boldsymbol{B}\cdot\boldsymbol{\sigma} \right) \psi + \chi^\dagger \left(iD_0 - \frac{1}{2M}\boldsymbol{D}^2 - \frac{c_F}{2M} g\boldsymbol{B}\cdot\boldsymbol{\sigma} \right) \chi + \sum_{l=1}^{n_f} \bar{q}_l i\not{D} q_l - \frac{1}{4} F^a_{\mu\nu} F^{a\,\mu\nu} + \mathcal{O}\left(M^{-2}\right) . \tag{1.33}$$

Note that the spatial covariant derivative is identified with D_i, so in vector notation the sign in front of the gauge field differs from that of the temporal derivative: $D_0 = \partial_0 + igA_0$ and $\boldsymbol{D} = \boldsymbol{\nabla} - ig\boldsymbol{A}$.

In case one is interested in situations where there is only a heavy quark but no antiquark (or vice versa), like e.g. heavy-light mesons, the effective Lagrangian contains only the heavy (anti)quark terms and the theory is called *Heavy Quark Effective Theory* (HQET) [33, 34]. Both theories have the same Lagrangian (except for the missing (anti)quark sector), but the hierarchy of scales and power counting are different. Also C symmetry is obviously not satisfied in HQET for the heavy (anti)quarks.

The construction of NRQCD is a very important step for the description of heavy quark-antiquark bound states. However, attempts to study these bound states directly in NRQCD often encounter serious problems, because there are still several physical scales present. In order to disentangle these scales, one needs to construct another EFT. Typical scales in a quarkonium system are the relative momentum p_r, the distance r between quark and antiquark, or the binding energy E_b, and the usual power counting is $p_r \sim 1/r \sim Mv$ and $E_b \sim Mv^2$, where $v \ll 1$ can be interpreted as the non-relativistic velocity. These scales are usually also referred to as the *soft scale* for Mv and the *ultrasoft scale* for Mv^2, while M corresponds to the *hard scale*.

So in order to integrate out the soft scale, we have to consider a heavy quark-antiquark system at vanishing distance r. The individual quarks can no longer be resolved, so the effective degrees of freedom have to be quarkonium fields that describe both particles together. Those can have either a singlet or an adjoint color configuration (or singlet and octet in the case of SU(3)), so they are called S and O^a. The remaining massless quarks and gluons can depend only on the center-of-mass coordinate $\boldsymbol{R}$, and any dependence on the relative coordinate $\boldsymbol{r}$ needs to be expanded, which is why this is also called *multipole expansion* in analogy to electrodynamics. The Wilson coefficients of this theory depend on the scale that is integrated out, which is r, so they constitute non-local interactions in the form of potentials. Therefore, this theory is called *potential NRQCD* (pNRQCD) [9, 10].

The Lagrangian now contains a double expansion in the parameters M and r. At leading order (LO) in $1/M$ and next-to-leading order (NLO) in r, it is given by:

$$\mathcal{L}_{\text{pNRQCD}} = \int d^3r \left[S^\dagger (i\partial_0 - V_s) S + O^{\dagger\,a} \left(iD_0^{ab} - V_o \delta^{ab} \right) O^b \right] - \frac{1}{4} F^a_{\mu\nu} F^{a\,\mu\nu} + \sum_{l=1}^{n_f} \bar{q}_l i\not{D} q_l + \int d^3r \left[\frac{V_A}{\sqrt{2N}} \left(S^\dagger (\boldsymbol{r}\cdot g\boldsymbol{E}^a) O^a + O^{\dagger\,a} (\boldsymbol{r}\cdot g\boldsymbol{E}^a) S \right) + \frac{V_B}{2} d^{abc} O^{\dagger\,a} (\boldsymbol{r}\cdot g\boldsymbol{E}^b) O^c \right] , \tag{1.34}$$

where D_0^{ab} is the covariant time derivative for the adjoint representation, V_s and V_o are the static singlet and octet potentials, and V_A and V_B are the coefficients for the singlet-octet and

octet-octet transitions under interactions with a chromoelectric field. Unlike the heavy mass M, the distance r can take different values, so the Lagrangian is an integral over all possible values of r. But only the quarkonium fields S and O^a (and the potentials) depend on $\boldsymbol{r}$, all other fields can depend only on $\boldsymbol{R}$. All symmetries of NRQCD also remain in pNRQCD, however, the local gauge symmetry is now reduced to transformations depending only on $\boldsymbol{R}$, which also do not resolve distances of the order of $\boldsymbol{r}$.

Throughout this section it has been assumed that Λ_{QCD} is much smaller than the scales that are being integrated out. While this is certainly the case for the heavy quark mass M, it does not necessarily have to be for the other energy scales. For example, Λ_{QCD} may be comparable to r for some excited quarkonia, which means that it has to be integrated out together with r. If one integrates out Λ_{QCD}, that means that the effective degrees of freedom may not contain any colored fields, so in the case of pNRQCD only the singlet field may appear, together with pions or other light mesons. These two different versions of pNRQCD are called *strongly coupled* or *weakly coupled* depending on whether Λ_{QCD} is integrated out or not, respectively (see [35] or [36] for a review). The matching calculation for the potentials as well as calculations within the EFT may only be carried out perturbatively in weakly coupled pNRQCD, so we will focus on this theory in this work.

1.4.2 EQCD and MQCD

At finite temperature, there appear more physical scales related to the properties of the medium. Among these naturally is the temperature T (or rather πT, since T always appears with a coefficient π in calculations), but also thermal screening masses (see below). Assuming that the temperature is the largest scale (i.e. we work with QCD without heavy quarks), we can construct an EFT that describes only the lower energy dynamics by integrating out the temperature. In this case it is a bit more complicated to explain what are the effective degrees of freedom.

We will use a geometric argument. The finite temperature theory of the imaginary time formalism is essentially defined on a compactified (and Euclidean) space-time of $\mathbb{R}^d \times S^1$, where S^1 denotes the circle of the imaginary time direction with periodic boundary conditions. If we now consider the situation of infinite temperature, then this circle has a radius of zero, so there is no longer any extent in the imaginary time direction. Accordingly, the effective degrees of freedom cannot depend on the imaginary time and this coordinate no longer appears in the EFT at all. Moreover, since the fermionic fields have to obey antiperiodic boundary conditions, they vanish completely, because it is only possible for them to be both positive and negative at the same point if they are zero everywhere. So the effective degrees of freedom contain only the gluon fields, which depend only on the spatial coordinates. The P and C symmetries remain in the EFT as well as rotations. Time reversal obviously has no more meaning, and boost transformations already were not a symmetry of the fundamental theory, because the existence of the medium explicitly breaks this symmetry (we are working in the rest frame of the medium).

As there is no longer a time coordinate, the A_0-field loses its interpretation as a gauge field; what remains is just an adjoint scalar field. As such, there is nothing that prevents it from having a mass term in the effective Lagrangian, so this has to be included as a matching coefficient in the EFT. This mass provides a natural IR cutoff and thus the problems with IR divergences at finite temperature are (at least partially) solved in this EFT. The chromoelectric field is now simply the covariant derivative of this scalar field $\boldsymbol{E}^a = \boldsymbol{D}^{ab} A_0^b$, which is why this

mass is called the *electric mass* m_E. It turns out that this mass is the largest remaining scale in this EFT. Because of this and the absence of a time coordinate, this theory is called *electrostatic QCD* (EQCD) [37, 38] (for earlier and related works on this subject see Refs. [39–55]).

Because of the reduced dimension of this theory, the gluons no longer have mass dimension $(d-1)/2$, but instead $(d-2)/2$, which we will express by a tilde over the fields. Then the effective Lagrangian is given by

$$\mathcal{L}_{\mathrm{EQCD}} = \frac{1}{2}\widetilde{\boldsymbol{E}}^a \cdot \widetilde{\boldsymbol{E}}^a + \frac{m_E^2}{2}\widetilde{A}_0^a \widetilde{A}_0^a + \frac{1}{4}\widetilde{F}_{ij}^a \widetilde{F}_{ij}^a + \dots \,, \tag{1.35}$$

where the dots contain interactions with four $\widetilde{A}_0$-fields, which are not suppressed by πT with respect to the given terms, but instead by higher powers in α_{s}, and of course also higher order operators. The effective coupling constant becomes another matching coefficient g_E and like the fields it also changes its mass dimension from $(3-d)/2$ to $(4-d)/2$. The leading-order results for these parameters are $g_E^2 = g^2 T + \mathcal{O}(\alpha_{\mathrm{s}}^2)$ and $m_E^2 = (N/3 + n_f/6) g^2 T^2 + \mathcal{O}(\alpha_{\mathrm{s}}^2)$. We will also call this leading order result for m_E the *Debye mass* m_D.

Since we assumed that the temperature is the largest scale in the system, the scale hierarchy $\pi T \gg m_D$ needs to be satisfied. But m_D is also proportional to the temperature, so it depends only on the size of g whether this hierarchy is satisfied or not. More specifically, one needs $\sqrt{N/3 + n_f/6}\, g/\pi \ll 1$, which is a much stronger requirement than $g^2/4\pi \ll 1$ that usually appears in perturbative vacuum calculations[3]. This means that EQCD can only be applied for very large temperatures, where the plasma becomes weakly coupled enough to satisfy this condition.

One can proceed and integrate out the scale m_D to describe even lower energy processes. The $\widetilde{A}_0$ field cannot have momenta lower than m_D because of the mass in its propagator, so it can no longer appear in this lower order EFT. What remains is a pure SU(N) gauge theory in d space dimensions without any additional fields. Since only the chromomagnetic field is left in this EFT, it is called *magnetostatic QCD* (MQCD).

The typical scale of this theory can be determined like for EQCD by looking at the gluon propagator. In the matching, one finds that m_D^2 is given by the LO gluon self-energy for the temporal gluon field A_0 at vanishing momentum. Similarly, one can show that the self-energy of the spatial gluon field $\boldsymbol{A}$ at vanishing momentum is of order $g^4 T^2$. Therefore, the typical scale of MQCD, which is called the *magnetic mass* scale m_M, is of order $g^2 T$. However, unlike in EQCD, this magnetic mass is not related to a mass term in the effective Lagrangian, since the spatial gluons are still gauge fields and a mass term would break the gauge symmetry.

The coupling constant g_M is the same as g_E at leading order. It follows that the terms in the Lagrangian which are usually considered perturbations (the three- and four-gluon interactions) are actually of the same order as the kinetic terms for the gluons, since all fields and derivatives scale as m_M. This means that MQCD is completely non-perturbative, even if g is a small parameter. One can confirm this by looking at the gluon propagator and its self-energy: it follows from straightforward power counting arguments that, if the momenta are of order $g^2 T$, then each loop order in a perturbative expansion contributes at the same order in g to the self-energy, rendering the perturbative expansion useless. It is therefore impossible to continue perturbation theory to any order at finite temperature; as soon as the magnetic scale enters a calculation one has to include inherently non-perturbative contributions. However, the EFT

[3]For comparison, the latter expression is smaller than 0.1 for g smaller than 1.12, while for the former expression one needs 0.21 with $N = 3$ and $n_f = 3$.

framework allows one to absorb all non-perturbative effects into a few parameters which are defined in MQCD and need to be calculated e.g. on the lattice, and beyond that one may still continue the perturbative expansion within EQCD as long as g is small enough [37, 38, 42]. Using this sequence of effective theories the weak coupling expansion of the QCD pressure has been calculated [37] finding a solution to the well-known infrared problem [56].

Chapter 2

Poincaré Invariance in Nonrelativistic Effective Field Theories

2.1 Introduction and Outline

We have already discussed in the previous sections how effective theories for heavy quarks are constructed. One feature of these effective theories is that the heavy quark or antiquark fields are treated essentially as non-relativistic fields, even though the underlying fundamental theory of QCD is fully relativistic. As a consequence, the theory no longer explicitly displays the symmetry under boosts. However, this symmetry is only hidden in the EFT and appears in the form of exact relations between certain Wilson coefficients. This issue will be explained in detail in this chapter, including explicit constructions of the boost transformations as well as the other elements of the Poincaré group. Apart from clarifying these conceptual issues, the results of this chapter also have some very practical applications, since for each relation that is found for the Wilson coefficients, one less matching calculation needs to be performed.

During the past few decades, there have been several different approaches to reducing the number of coefficients or finding relations thereof in EFTs. In HQET, which is parametrized by velocity and residual momentum of the heavy quark fields, requiring reparametrization invariance (i.e. invariance under a shift of velocity resulting in a redefinition of its residual momentum) yields relations between the Wilson coefficients [57]; in fact, reparametrization invariance turned out to be equivalent to Poincaré invariance of the theory [58].

In [58] a direct implementation of Poincaré invariance was achieved and applied to NRQCD and pNRQCD. Although non-relativistic EFTs no longer explicitly display the full symmetry, in particular invariance under boosts, it is still hidden in the EFT, since it is a symmetry of the underlying theory QCD. So one can show that it is possible to construct all generators of this symmetry group in these EFTs. Since the symmetries of time translations, space translations, and rotations are explicitly realized, the corresponding generators are obtained in the usual way from the associated conserved Noether currents. For the generator of boosts one has to make a general ansatz, including all operators allowed by the other symmetries up to a certain order in the expansion parameters. By demanding that these generators satisfy the commutation relations of the Poincaré algebra, one can obtain relations between the Wilson coefficients of the EFTs.

Although this method yields the desired constraints and is probably the most fundamental approach, since it works in the quantized theory, continuing in this way to higher orders of

the expansion parameters quickly becomes a formidable task. Recently, another approach was suggested for deriving constraints in EFTs through Poincaré invariance, which employs Wigner's *induced representation* [59]. It was proposed in [60] that a free non-relativistic field ϕ in the rest frame, which has well defined transformation behavior under rotations R as $\phi(x) \to D[R]\phi(R^{-1}x)$, should transform under a generic Lorentz transformation Λ as

$$\phi(x) \to D[W(\Lambda, i\partial)]\phi(\Lambda^{-1}x)\,, \tag{2.1}$$

where the *little group element* W is a particular rotation associated with Λ. This little group element is defined through the momentum after the Lorentz transformation, which leads to a dependence on derivatives of ϕ in position space. This expression is then expanded, such that one has the boost transformation at the same order as the Lagrangian.

While this seems to work well for non-interacting fields, in an interacting gauge theory some problems arise. First, this boost transformation does not have the right behavior under gauge transformations. One would like to have the boosted field to transform in the same way as the original field would at the new coordinates, but this is not possible because of the derivatives in the induced representation. Promoting the derivatives to covariant derivatives fixes this problem, but introduces a new ambiguity in how the covariant derivatives should be ordered. Even with this covariantized induced boost transformation, the Lagrangian of the EFT is still not invariant, but requires the introduction of additional gauge field terms to the boost. Nevertheless, the constraints obtained in this way agree with the previous results, and the derivation is much simpler.

So in this chapter we will address some of the open questions related to this method. First, the appearance of additional gauge field terms in the boost transformation, whose coefficients turn out to be given by Wilson coefficients from the Lagrangian, is very reminiscent of the construction of EFT Lagrangians, where one includes all terms allowed by the symmetries. However, in the usual EFT approach each term gets a coefficient that contains the contributions from the scales that were integrated out, while in the approach suggested in [60] the terms in the boost that derive from the induced representation have no such coefficients. We are not aware of an a priori justification for that assumption.

The second issue we want to study in this chapter deals with the question, which additional terms to include in the boost. At higher orders in the expansion there may be several terms one could add to the boost in order to make the Lagrangian gauge invariant, so it is not clear which effects this ambiguity might have or if there is a loss in generality if one chooses only one of several possible terms.

So we will take from [60] that the boost transformation of the non-relativistic fields is realized in a nonlinear way, and that requiring invariance of the Lagrangian under this boost leads to constraints on the Wilson coefficients, but apart from that we will not refer to the induced representation and instead follow the EFT approach, where one includes all terms in the boost transformation that are allowed by the other symmetries of the theory and gives a matching coefficient to each of them. Even though we will start from the most general expression, we will exploit the possibility to redefine the effective fields in order to remove redundant terms from this ansatz.

Lastly, since the boost transformation defined in this way has to satisfy the Poincaré algebra, we will also demonstrate how the usual commutation relations need to be modified for nonlinear boost generators. Requiring all commutators of the Poincaré algebra to be satisfied will lead to additional constraints on the boost parameters and Wilson coefficients.

We should note here that, unlike in [58], this approach is defined for the classical and not the quantized field theory. However, since in the fundamental theory of QCD there are no quantum effects on the spacetime symmetries of the Poincaré group, we also do not expect quantum effects to show up for the EFTs.

This chapter is organized as follows. In section 2.2 we study NRQCD, first discussing the different generators of the Poincaré group in the EFT approach in 2.2.1 and how they satisfy the Poincaré algebra. Then we derive the constraints of the Wilson coefficients up to order M^{-2} in the two-fermion sector in 2.2.2, and up to order M^{-3} in the four-fermion sector in 2.2.3. We also comment on the Noether charges obtained from these transformations in 2.2.2 and how they correspond to the quantum field generators constructed in [58]. Next we continue the discussion to pNRQCD in section 2.3. First we study how quarkonium fields are expected to transform under boosts in 2.3.1, then we use field redefinitions to remove redundant terms from the most general boost generator in 2.3.2, and finally we derive constraints on the Wilson coefficients of pNRQCD in 2.3.3.

2.2 Constraints in NRQCD

As explained in section 1.4.1, Non-Relativistic QCD (NRQCD) is the EFT obtained from QCD after integrating out the scale of the heavy quark mass M [30, 32]. Its Lagrangian up to $\mathcal{O}\left(M^{-2}\right)$ is given by:

$$\begin{aligned}\mathcal{L}_{\text{NRQCD}} = \psi^\dagger \left\{ iD_0 + \frac{c_2}{2M}\boldsymbol{D}^2 + \frac{c_F}{2M} g\boldsymbol{B}\cdot\boldsymbol{\sigma} + \frac{c_D}{8M^2}\left[\boldsymbol{D}\cdot, g\boldsymbol{E}\right] + \frac{ic_S}{8M^2}\left[\boldsymbol{D}\times, g\boldsymbol{E}\right]\cdot\boldsymbol{\sigma} \right\} \psi \\ + \chi^\dagger \left\{ iD_0 - \frac{c_2}{2M}\boldsymbol{D}^2 - \frac{c_F}{2M} g\boldsymbol{B}\cdot\boldsymbol{\sigma} + \frac{c_D}{8M^2}\left[\boldsymbol{D}\cdot, g\boldsymbol{E}\right] + \frac{ic_S}{8M^2}\left[\boldsymbol{D}\times, g\boldsymbol{E}\right]\cdot\boldsymbol{\sigma} \right\} \chi \\ + \frac{1}{2}\boldsymbol{E}^a\cdot\boldsymbol{E}^a - \frac{1}{2}\boldsymbol{B}^a\cdot\boldsymbol{B}^a + \sum_{l=1}^{n_f} \bar{q}_l i\not{D} q_l \,, \end{aligned} \tag{2.2}$$

where $\boldsymbol{\sigma}$ denotes the Pauli matrices, which are given by:

$$\sigma_1 \equiv \begin{pmatrix} 0 & 1 \\ 1 & 0 \end{pmatrix}, \qquad \sigma_2 \equiv \begin{pmatrix} 0 & -i \\ i & 0 \end{pmatrix}, \qquad \text{and} \quad \sigma_3 \equiv \begin{pmatrix} 1 & 0 \\ 0 & -1 \end{pmatrix}. \tag{2.3}$$

We have neglected $\mathcal{O}\left(M^{-2}\right)$ interaction terms between only gluons or light quarks, because they will be irrelevant to the following discussion (in fact, we will completely ignore the light quarks from here on), as well as interactions between four heavy particles, since they will be given separately. We also have made use of the equations of motion to remove all higher time derivatives [61], as well as removed a possible mass term $-M\psi^\dagger\psi + M\chi^\dagger\chi$ through the field redefinitions $\psi \to e^{-iMt}\psi$ and $\chi \to e^{iMt}\chi$.

2.2.1 Poincaré Algebra for Field Transformations

The Poincaré group contains space-time translations, rotations and boosts. In this chapter we will be mainly concerned with boosts, because the other transformations are fairly straightforward to implement. The translations act only on the coordinates, shifting the origin by a constant vector a^μ. The transformed field in the new coordinate system has to correspond

to the original field at the coordinates before the transformation. But because of the field redefinition we used to remove the $\mathcal{O}(M)$-term from the Lagrangian there is an additional factor of $\exp(-iMa^0)$. So for an infinitesimal transformation (where we neglect all powers of the transformation parameter beyond the linear), we have:

$$\psi(x) \xrightarrow{P_\mu} \psi'(x) = e^{-iMa^0}\psi(x+a) = (1-iMa^0)\psi(x) + \left[a^\mu\partial_\mu, \psi(x)\right] \equiv (1 - ia^\mu P_\mu)\,\psi(x)\,, \quad (2.4)$$

and analogous for the other fields, although the mass term is only there for the heavy quark, and for the heavy antiquark it has opposite sign. We have written the derivative as a commutator to stress the fact that it only acts on this field and not any other. The generators of translations are then $P_\mu = i\partial_\mu$ (i.e. $P_0 = i\partial_0$ for time translations and $\boldsymbol{P} = -i\boldsymbol{\nabla}$ for space translations). There is no dependence on the field apart from the mass term.

Rotations act both on the coordinates and on the field components. The coordinates are transformed under infinitesimal rotations such that $\boldsymbol{r}$ in the new coordinate system corresponds to $\boldsymbol{r} + \boldsymbol{\alpha} \times \boldsymbol{r}$ in the old, where the direction of $\boldsymbol{\alpha}$ gives the rotation axis and the absolute value gives the infinitesimal rotation angle. The components of the Pauli spinor fields are rotated with the Pauli matrix $\boldsymbol{\sigma}/2$, while the gauge fields transform as vectors:

$$A_0(x) \xrightarrow{J} A_0'(x) = A_0(x) + \left[\boldsymbol{\alpha}\cdot(\boldsymbol{r}\times\boldsymbol{\nabla}), A_0(x)\right] \equiv (1 + i\boldsymbol{\alpha}\cdot\boldsymbol{j}_0)\,A_0(x)\,, \quad (2.5)$$

$$\psi(x) \xrightarrow{J} \psi'(x) = \left(1 + \frac{i}{2}\boldsymbol{\alpha}\cdot\boldsymbol{\sigma}\right)\psi(x) + \left[\boldsymbol{\alpha}\cdot(\boldsymbol{r}\times\boldsymbol{\nabla}), \psi(x)\right] \equiv \left(1 + i\boldsymbol{\alpha}\cdot\boldsymbol{j}_{1/2}\right)\psi(x)\,, \quad (2.6)$$

$$\chi(x) \xrightarrow{J} \chi'(x) = \left(1 + \frac{i}{2}\boldsymbol{\alpha}\cdot\boldsymbol{\sigma}\right)\chi(x) + \left[\boldsymbol{\alpha}\cdot(\boldsymbol{r}\times\boldsymbol{\nabla}), \chi(x)\right] \equiv \left(1 + i\boldsymbol{\alpha}\cdot\boldsymbol{j}_{1/2}\right)\chi(x)\,, \quad (2.7)$$

$$\boldsymbol{A}(x) \xrightarrow{J} \boldsymbol{A}'(x) = \boldsymbol{A}(x) - \boldsymbol{\alpha}\times\boldsymbol{A}(x) + \left[\boldsymbol{\alpha}\cdot(\boldsymbol{r}\times\boldsymbol{\nabla}), \boldsymbol{A}(x)\right] \equiv (1 + i\boldsymbol{\alpha}\cdot\boldsymbol{j}_1)\,\boldsymbol{A}(x)\,. \quad (2.8)$$

The $\boldsymbol{E}$ and $\boldsymbol{B}$ fields transform in the same way as $\boldsymbol{A}$.

So, all the different rotation generators have a term $\boldsymbol{r}\times(-i\boldsymbol{\nabla})$ for the coordinate transformation and some matrix for the transformation of the components depending on the representation of the fields. We use a capital $\boldsymbol{J}$ to denote the generators of rotations in general, and a lowercase $\boldsymbol{j}$ with an index for the particular representation. Note that the sign of the transformation of the components of the vector field is opposite to that of the coordinate transformation. This is because we use the inverse transformation in order to connect the new coordinate system to the old, or in other words, the components are rotated with a passive transformation, while the coordinates rotate with an active transformation.

Derivatives acting on the transformed fields can be written such that they transform in the same way as the gauge fields and the covariant derivatives have uniform transformation behavior:

$$D_0' = \partial_0 + igA_0' = D_0 + \left[\boldsymbol{\alpha}\cdot(\boldsymbol{r}\times\boldsymbol{\nabla}), D_0\right], \quad (2.9)$$

$$\boldsymbol{D}' = \boldsymbol{\nabla} - ig\boldsymbol{A}' = \boldsymbol{D} - \boldsymbol{\alpha}\times\boldsymbol{D} + \left[\boldsymbol{\alpha}\cdot(\boldsymbol{r}\times\boldsymbol{\nabla}), \boldsymbol{D}\right]. \quad (2.10)$$

For D_0' the commutator of the time derivative and the $\boldsymbol{\alpha}$-dependent term vanishes, while for $\boldsymbol{D}'$ the commutator gives a term that cancels the new derivative term that was introduced in $-\boldsymbol{\alpha}\times\boldsymbol{D}$. In this way, we have e.g.

$$\boldsymbol{D}\psi \xrightarrow{J} \boldsymbol{D}'\psi' = \boldsymbol{D}\psi - (\boldsymbol{\alpha}\times\boldsymbol{D})\psi + \boldsymbol{D}\left(\frac{i}{2}\boldsymbol{\alpha}\cdot\boldsymbol{\sigma}\right)\psi + \left[\boldsymbol{\alpha}\cdot(\boldsymbol{r}\times\boldsymbol{\nabla}), \boldsymbol{D}\psi\right]. \quad (2.11)$$

For any product of fields, the coordinate transformations take the form of a single commutator of $\boldsymbol{\alpha}\cdot(\boldsymbol{r}\times\boldsymbol{\nabla})$ with the whole expression, while the component transformations appear for each field or derivative individually.

Finally, for boosts we expect the transformed fields at coordinates $(t,\boldsymbol{r})$ to correspond to the original fields at $(t+\boldsymbol{\eta}\cdot\boldsymbol{r},\boldsymbol{r}+\boldsymbol{\eta}t)$, where $\boldsymbol{\eta}$ is the boost parameter. So the generators $\boldsymbol{K}$ for a generic infinitesimal boost transformation $1-i\boldsymbol{\eta}\cdot\boldsymbol{K}$ will always contain the term $it\boldsymbol{\nabla}+i\boldsymbol{r}\partial_0$ for the coordinate transformations. The heavy quark and antiquark fields will also obtain a term $\pm Mr$ in the generators from the field redefinitions.

For the gluon fields the transformation of the components is clear: they are those of a vector field. We will again express them in the form of the covariant derivatives:

$$D_0' = D_0 + [\boldsymbol{\eta}\cdot t\boldsymbol{\nabla} + \boldsymbol{\eta}\cdot\boldsymbol{r}\partial_0, D_0] + \boldsymbol{\eta}\cdot\boldsymbol{D}\,, \tag{2.12}$$

$$\boldsymbol{D}' = \boldsymbol{D} + [\boldsymbol{\eta}\cdot t\boldsymbol{\nabla} + \boldsymbol{\eta}\cdot\boldsymbol{r}\partial_0, \boldsymbol{D}] + \boldsymbol{\eta}D_0\,, \tag{2.13}$$

from which follow the transformation rules for the $\boldsymbol{E}$ and $\boldsymbol{B}$ fields:

$$\boldsymbol{E}'(x) = \boldsymbol{E}(x) + [\boldsymbol{\eta}\cdot t\boldsymbol{\nabla} + \boldsymbol{\eta}\cdot\boldsymbol{r}\partial_0, \boldsymbol{E}(x)] + \boldsymbol{\eta}\times\boldsymbol{B}(x)\,, \tag{2.14}$$

$$\boldsymbol{B}'(x) = \boldsymbol{B}(x) + [\boldsymbol{\eta}\cdot t\boldsymbol{\nabla} + \boldsymbol{\eta}\cdot\boldsymbol{r}\partial_0, \boldsymbol{B}(x)] - \boldsymbol{\eta}\times\boldsymbol{E}(x)\,. \tag{2.15}$$

For the heavy quark and antiquark fields the transformation behavior is not clear, since they were constructed to have only well-defined behavior under translations and rotations. A generator like $\pm i\sigma$, for instance, would satisfy the Poincaré algebra, but violate the required behavior under parity transformations (see below). On the other hand, there needs to be some way to implement boost transformations also for these non-relativistic fields, since it is a symmetry of the underlying theory. So we will take the EFT approach and write down the most general ansatz for the boost-transformed fields, i.e. including all terms that are allowed by the other symmetries and attributing a Wilson coefficient to each of them, which has to be determined through a matching calculation or some other means. In particular, this boost transformation will be nonlinear in the fields, so we write:

$$\psi(x) \xrightarrow{K} \psi'(x) = \Big(1 - i\boldsymbol{\eta}\cdot\boldsymbol{k}_\psi(\boldsymbol{D},\boldsymbol{E},\boldsymbol{B},\psi,\chi,x)\Big)\psi(x)\,, \tag{2.16}$$

$$\chi(x) \xrightarrow{K} \chi'(x) = \Big(1 - i\boldsymbol{\eta}\cdot\boldsymbol{k}_\chi(\boldsymbol{D},\boldsymbol{E},\boldsymbol{B},\psi,\chi,x)\Big)\chi(x)\,. \tag{2.17}$$

An important requirement determining which terms can appear in $\boldsymbol{k}_\psi$ and $\boldsymbol{k}_\chi$ is that they need to have the right behavior under the discrete transformations P, C, and T, i.e. parity, charge conjugation, and time reversal, respectively. The fields transform as

$$\psi(t,\boldsymbol{r}) \xrightarrow{P} \psi(t,-\boldsymbol{r})\,, \qquad \psi(t,\boldsymbol{r}) \xrightarrow{C} -i\sigma_2\chi^*(t,\boldsymbol{r})\,, \qquad \psi(t,\boldsymbol{r}) \xrightarrow{T} i\sigma_2\psi(-t,\boldsymbol{r})\,, \tag{2.18}$$

$$\chi(t,\boldsymbol{r}) \xrightarrow{P} -\chi(t,-\boldsymbol{r})\,, \qquad \chi(t,\boldsymbol{r}) \xrightarrow{C} i\sigma_2\psi^*(t,\boldsymbol{r})\,, \qquad \chi(t,\boldsymbol{r}) \xrightarrow{T} i\sigma_2\chi(-t,\boldsymbol{r})\,, \tag{2.19}$$

$$\boldsymbol{E}(t,\boldsymbol{r}) \xrightarrow{P} -\boldsymbol{E}(t,-\boldsymbol{r})\,, \qquad \boldsymbol{E}(t,\boldsymbol{r}) \xrightarrow{C} -\boldsymbol{E}^*(t,\boldsymbol{r})\,, \qquad \boldsymbol{E}(t,\boldsymbol{r}) \xrightarrow{T} \boldsymbol{E}(-t,\boldsymbol{r})\,, \tag{2.20}$$

$$\boldsymbol{B}(t,\boldsymbol{r}) \xrightarrow{P} \boldsymbol{B}(t,-\boldsymbol{r})\,, \qquad \boldsymbol{B}(t,\boldsymbol{r}) \xrightarrow{C} -\boldsymbol{B}^*(t,\boldsymbol{r})\,, \qquad \boldsymbol{B}(t,\boldsymbol{r}) \xrightarrow{T} -\boldsymbol{B}(-t,\boldsymbol{r})\,. \tag{2.21}$$

Since the boosted fields have to satisfy the same transformation behavior, with $\boldsymbol{\eta}$ replaced by $-\boldsymbol{\eta}$ for P and T, we require

$$\boldsymbol{k}_\psi \xrightarrow{P} -\boldsymbol{k}_\psi\,, \qquad \boldsymbol{k}_\psi \xrightarrow{C} -\sigma_2\boldsymbol{k}_\chi^*\sigma_2\,, \qquad \boldsymbol{k}_\psi \xrightarrow{T} \sigma_2\boldsymbol{k}_\psi\sigma_2\,, \tag{2.22}$$

$$\boldsymbol{k}_\chi \xrightarrow{P} -\boldsymbol{k}_\chi\,, \qquad \boldsymbol{k}_\chi \xrightarrow{C} -\sigma_2\boldsymbol{k}_\psi^*\sigma_2\,, \qquad \boldsymbol{k}_\chi \xrightarrow{T} \sigma_2\boldsymbol{k}_\chi\sigma_2\,, \tag{2.23}$$

where we also keep in mind that the T operation takes the complex conjugate of all coefficients in $\boldsymbol{k}$.

The most general expression for $\boldsymbol{k}_\psi$ and $\boldsymbol{k}_\chi$ up to $\mathcal{O}(M^{-3})$ is then given by:

$$\begin{aligned}\boldsymbol{k}_\psi(\boldsymbol{D},\boldsymbol{E},\boldsymbol{B},\psi,\chi,x) = {}& it\boldsymbol{\nabla} + i\boldsymbol{r}\partial_0 + M\boldsymbol{r} - \frac{k_D}{2M}\boldsymbol{D} - \frac{ik_{DS}}{4M}\boldsymbol{D}\times\boldsymbol{\sigma} + \frac{k_E}{8M^2}g\boldsymbol{E} \\ & + \frac{ik_{ES}}{8M^2}g\boldsymbol{E}\times\boldsymbol{\sigma} - \frac{k_{D3}}{4M^3}\boldsymbol{D}(\boldsymbol{D}^2) - \frac{ik_{D3S}}{16M^3}(\boldsymbol{D}\times\boldsymbol{\sigma})(\boldsymbol{D}^2) \\ & + \frac{ik_{B1}}{16M^3}[\boldsymbol{D}\times, g\boldsymbol{B}] + \frac{ik_{B2}}{16M^3}\{\boldsymbol{D}\times, g\boldsymbol{B}\} + \frac{k_{BS1}}{16M^3}[\boldsymbol{D}, (g\boldsymbol{B}\cdot\boldsymbol{\sigma})] \\ & + \frac{k_{BS2}}{16M^3}\{\boldsymbol{D}, (g\boldsymbol{B}\cdot\boldsymbol{\sigma})\} + \frac{k_{BS3}}{16M^3}[(\boldsymbol{D}\cdot\boldsymbol{\sigma}), g\boldsymbol{B}] \\ & + \frac{k_{BS4}}{16M^3}\{(\boldsymbol{D}\cdot\boldsymbol{\sigma}), g\boldsymbol{B}\} + \frac{k_{BS5}}{16M^3}\{\boldsymbol{D}\cdot, g\boldsymbol{B}\}\,\boldsymbol{\sigma}\,, \end{aligned} \tag{2.24}$$

$$\begin{aligned}\boldsymbol{k}_\chi(\boldsymbol{D},\boldsymbol{E},\boldsymbol{B},\psi,\chi,x) = {}& it\boldsymbol{\nabla} + i\boldsymbol{r}\partial_0 - M\boldsymbol{r} + \frac{k_D}{2M}\boldsymbol{D} + \frac{ik_{DS}}{4M}\boldsymbol{D}\times\boldsymbol{\sigma} + \frac{k_E}{8M^2}g\boldsymbol{E} \\ & + \frac{ik_{ES}}{8M^2}g\boldsymbol{E}\times\boldsymbol{\sigma} + \frac{k_{D3}}{4M^3}\boldsymbol{D}(\boldsymbol{D}^2) + \frac{ik_{D3S}}{16M^3}(\boldsymbol{D}\times\boldsymbol{\sigma})(\boldsymbol{D}^2) \\ & - \frac{ik_{B1}}{16M^3}[\boldsymbol{D}\times, g\boldsymbol{B}] - \frac{ik_{B2}}{16M^3}\{\boldsymbol{D}\times, g\boldsymbol{B}\} - \frac{k_{BS1}}{16M^3}[\boldsymbol{D}, (g\boldsymbol{B}\cdot\boldsymbol{\sigma})] \\ & - \frac{k_{BS2}}{16M^3}\{\boldsymbol{D}, (g\boldsymbol{B}\cdot\boldsymbol{\sigma})\} - \frac{k_{BS3}}{16M^3}[(\boldsymbol{D}\cdot\boldsymbol{\sigma}), g\boldsymbol{B}] \\ & - \frac{k_{BS4}}{16M^3}\{(\boldsymbol{D}\cdot\boldsymbol{\sigma}), g\boldsymbol{B}\} - \frac{k_{BS5}}{16M^3}\{\boldsymbol{D}\cdot, g\boldsymbol{B}\}\,\boldsymbol{\sigma}\,. \end{aligned} \tag{2.25}$$

Again we did not include any temporal derivatives, because we assume they have been removed through the equations of motion. Every term in these expressions transforms as a vector under rotations, which is important in order to satisfy one of the relations from the Poincaré algebra (see below). Further symmetries constraining the form of the boosts are the gauge symmetry, under which they have to transform like

$$\boldsymbol{K} \xrightarrow{U} U\boldsymbol{K}U^\dagger + \big[it\boldsymbol{\nabla} + i\boldsymbol{r}\partial_0, U\big]U^\dagger\,, \tag{2.26}$$

and heavy quark or antiquark number conservation, which excludes terms like $i\psi\chi^\dagger\boldsymbol{\sigma}$ with a heavy quark and antiquark field. In the following it will be sufficient to study only the heavy quark sector, since the antiquark sector will follow just from charge conjugation.

The nonlinear boost transformations defined in this way have to satisfy the Poincaré algebra:

$$\begin{aligned} &\big[P_0, P_i\big] = 0\,, && \big[P_0, J_i\big] = 0\,, && \big[P_0, K_i\big] = -iP_i\,, \\ &\big[P_i, P_j\big] = 0\,, && \big[P_i, J_j\big] = i\epsilon_{ijk}P_k\,, && \big[P_i, K_j\big] = -i\delta_{ij}P_0\,, \\ &\big[J_i, J_j\big] = i\epsilon_{ijk}J_k\,, && \big[K_i, J_j\big] = i\epsilon_{ijk}K_k\,, && \big[K_i, K_j\big] = -i\epsilon_{ijk}J_k\,. \end{aligned} \tag{2.27}$$

Note that we are not using covariant notation here and in the rest of this chapter; unless otherwise specified we write all vector indices as lower indices.

The commutation relations of the Poincaré algebra not involving boosts are trivially satisfied, but for the boosts they provide nontrivial information. It is straightforward to check that

the commutators of a boost with the generators of translations are satisfied. Also the commutator of a boost with a rotation gives the right result, because we have implicitly constructed all terms in the generators as vectors. We have confirmed this in an explicit calculation along the lines of the following discussion, but since the result is not very interesting, we will not show that calculation here. Finally, the commutator of two boosts really gives new constraints on the boost parameters.

Since the boost for the heavy quark field is realized in a nonlinear way, calculating the commutator is a bit more involved. Conceptually, it is nothing but the difference in performing two successive operations in opposite orders. So we write the commutation relation as

$$[1 - i\boldsymbol{\xi}\cdot\boldsymbol{K}, 1 - i\boldsymbol{\eta}\cdot\boldsymbol{K}] = i(\boldsymbol{\xi}\times\boldsymbol{\eta})\cdot\boldsymbol{J}\,. \tag{2.28}$$

Applying this to the heavy quark field, we write the two successive boosts as:

$$\begin{aligned}
\psi(x) &\xrightarrow{K_\eta} \psi'_\eta(x) = \Big(1 - i\boldsymbol{\eta}\cdot\boldsymbol{k}_\psi(\boldsymbol{D},\boldsymbol{E},\boldsymbol{B},\psi,\chi,x)\Big)\psi(x)\,,\\
\psi'_\eta(x) &\xrightarrow{K_\xi} \psi''_{\xi\eta}(x) = \Big(1 - i\boldsymbol{\xi}\cdot\boldsymbol{k}_\psi(\boldsymbol{D}'_\eta,\boldsymbol{E}'_\eta,\boldsymbol{B}'_\eta,\psi'_\eta,\chi'_\eta,x)\Big)\psi'_\eta(x)\,.
\end{aligned} \tag{2.29}$$

Expanding to linear order in $\boldsymbol{\xi}$ and $\boldsymbol{\eta}$ gives

$$\begin{aligned}
&[1 - i\boldsymbol{\xi}\cdot\boldsymbol{K}, 1 - i\boldsymbol{\eta}\cdot\boldsymbol{K}]\psi(x) = \psi''_{\xi\eta}(x) - \psi''_{\eta\xi}(x)\\
&= \Big(1 - i\boldsymbol{\xi}\cdot\boldsymbol{k}_\psi(\boldsymbol{D}'_\eta,\boldsymbol{E}'_\eta,\boldsymbol{B}'_\eta,\psi'_\eta,\chi'_\eta,x)\Big)\psi'_\eta(x) - \Big(1 - i\boldsymbol{\eta}\cdot\boldsymbol{k}_\psi(\boldsymbol{D}'_\xi,\boldsymbol{E}'_\xi,\boldsymbol{B}'_\xi,\psi'_\xi,\chi'_\xi,x)\Big)\psi'_\xi(x)\\
&= \Big(1 - i\boldsymbol{\xi}\cdot\boldsymbol{k}_\psi(\boldsymbol{D},\boldsymbol{E},\boldsymbol{B},\psi,\chi,x)\Big)\Big(1 - i\boldsymbol{\eta}\cdot\boldsymbol{k}_\psi(\boldsymbol{D},\boldsymbol{E},\boldsymbol{B},\psi,\chi,x)\Big)\psi(x)\\
&\quad - i\Big(\boldsymbol{\eta}D_0\cdot\boldsymbol{\delta}_D + (\boldsymbol{\eta}\times\boldsymbol{B})\cdot\boldsymbol{\delta}_E - (\boldsymbol{\eta}\times\boldsymbol{E})\cdot\boldsymbol{\delta}_B - i(\boldsymbol{\eta}\cdot\hat{\boldsymbol{k}}_\psi)\delta_\psi - i(\boldsymbol{\eta}\cdot\hat{\boldsymbol{k}}_\chi)\delta_\chi\Big)\,\boldsymbol{\xi}\cdot\hat{\boldsymbol{k}}_\psi\,\psi(x)\\
&\quad - i\Big[\boldsymbol{\eta}\cdot t\boldsymbol{\nabla} + \boldsymbol{\eta}\cdot\boldsymbol{r}\partial_0, \boldsymbol{\xi}\cdot\hat{\boldsymbol{k}}_\psi(\boldsymbol{D},\boldsymbol{E},\boldsymbol{B},\psi,\chi,x)\Big]\,\psi(x) - (\boldsymbol{\xi}\leftrightarrow\boldsymbol{\eta})\\
&= (\boldsymbol{\xi}\times\boldsymbol{\eta})\cdot(\boldsymbol{r}\times\boldsymbol{\nabla})\psi(x) - \Big[\boldsymbol{\xi}\cdot\hat{\boldsymbol{k}}_\psi(\boldsymbol{D},\boldsymbol{E},\boldsymbol{B},\psi,\chi,x), \boldsymbol{\eta}\cdot\hat{\boldsymbol{k}}_\psi(\boldsymbol{D},\boldsymbol{E},\boldsymbol{B},\psi,\chi,x)\Big]\,\psi(x)\\
&\quad - i\Big(\boldsymbol{\eta}D_0\cdot\boldsymbol{\delta}_D + (\boldsymbol{\eta}\times\boldsymbol{B})\cdot\boldsymbol{\delta}_E - (\boldsymbol{\eta}\times\boldsymbol{E})\cdot\boldsymbol{\delta}_B - i(\boldsymbol{\eta}\cdot\hat{\boldsymbol{k}}_\psi)\delta_\psi - i(\boldsymbol{\eta}\cdot\hat{\boldsymbol{k}}_\chi)\delta_\chi\Big)\,\boldsymbol{\xi}\cdot\hat{\boldsymbol{k}}_\psi\,\psi(x)\\
&\quad + i\Big(\boldsymbol{\xi}D_0\cdot\boldsymbol{\delta}_D + (\boldsymbol{\xi}\times\boldsymbol{B})\cdot\boldsymbol{\delta}_E - (\boldsymbol{\xi}\times\boldsymbol{E})\cdot\boldsymbol{\delta}_B - i(\boldsymbol{\xi}\cdot\hat{\boldsymbol{k}}_\psi)\delta_\psi - i(\boldsymbol{\xi}\cdot\hat{\boldsymbol{k}}_\chi)\delta_\chi\Big)\,\boldsymbol{\eta}\cdot\hat{\boldsymbol{k}}_\psi\,\psi(x)\,,
\end{aligned} \tag{2.30}$$

where we have introduced $\hat{\boldsymbol{k}}_\psi$ to mean $\boldsymbol{k}_\psi$ without the coordinate transformations $it\boldsymbol{\nabla} + i\boldsymbol{r}\partial_0$.

The first line contains the terms one would have obtained from a naive application of the commutator to the generators, while the second and third lines contain additional terms arising from the fact that one has to use boosted fields in the generators of the second transformation. In order to make the expression more concise, we have introduced a notation with "derivatives" δ, which are defined such that they give the right ordering for noncommuting operators:

$$A\delta_B f(B) \equiv \partial_x f(B + xA)\Big|_{x=0}\,. \tag{2.31}$$

In short, what this operation does is replace each field in $\hat{\boldsymbol{k}}_\psi$ (one at a time) with its boosted expression, such that e.g.:

$$(\boldsymbol{\eta}D_0\cdot\boldsymbol{\delta}_D)\,\boldsymbol{D}^2 = \{\boldsymbol{\eta}\cdot\boldsymbol{D}, D_0\}\,. \tag{2.32}$$

For the boost transformation defined in Eq. (2.24) this gives at $\mathcal{O}(M^{-2})$

$$
\begin{aligned}
&[1 - i\boldsymbol{\xi}\cdot\boldsymbol{K}, 1 - i\boldsymbol{\eta}\cdot\boldsymbol{K}]\psi(x) \\
&= \Bigg\{ (\boldsymbol{\xi}\times\boldsymbol{\eta})\cdot(\boldsymbol{r}\times\boldsymbol{\nabla}) + \frac{ik_{DS}}{2}(\boldsymbol{\xi}\times\boldsymbol{\eta})\cdot\boldsymbol{\sigma} - \frac{k_{DS}}{2M}(\boldsymbol{\xi}\times\boldsymbol{\eta})\cdot\boldsymbol{\sigma}D_0 - \frac{ik_E}{4M^2}(\boldsymbol{\xi}\times\boldsymbol{\eta})\cdot g\boldsymbol{B} \\
&\quad + \frac{k_{ES}}{8M^2}(\boldsymbol{\xi}\times\boldsymbol{\eta})\cdot(g\boldsymbol{B}\times\boldsymbol{\sigma}) + \frac{ik_D^2}{4M^2}(\boldsymbol{\xi}\times\boldsymbol{\eta})\cdot g\boldsymbol{B} - \frac{k_Dk_{DS}}{8M^2}(\boldsymbol{\xi}\times\boldsymbol{\eta})\cdot(g\boldsymbol{B}\times\boldsymbol{\sigma}) \\
&\quad - \frac{ik_{DS}^2}{16M^2}(\boldsymbol{\xi}\times\boldsymbol{\eta})\cdot g\boldsymbol{B} + \frac{ik_{DS}^2}{16M^2}(\boldsymbol{\xi}\times\boldsymbol{\eta})\cdot\big\{\boldsymbol{D},(\boldsymbol{D}\cdot\boldsymbol{\sigma})\big\} - \frac{ik_{D3}}{2M^2}(\boldsymbol{\xi}\times\boldsymbol{\eta})\cdot g\boldsymbol{B} \\
&\quad + \frac{ik_{D3S}}{4M^2}(\boldsymbol{\xi}\times\boldsymbol{\eta})\cdot\boldsymbol{\sigma}(\boldsymbol{D})^2 - \frac{ik_{D3S}}{16M^2}(\boldsymbol{\xi}\times\boldsymbol{\eta})\cdot\big\{\boldsymbol{D},(\boldsymbol{D}\cdot\boldsymbol{\sigma})\big\} + \frac{k_{D3S}}{16M^2}(\boldsymbol{\xi}\times\boldsymbol{\eta})\cdot(g\boldsymbol{B}\times\boldsymbol{\sigma}) \\
&\quad - \frac{ik_{B1}}{4M^2}(\boldsymbol{\xi}\times\boldsymbol{\eta})\cdot g\boldsymbol{B} - \frac{k_{BS4}}{8M^2}(\boldsymbol{\xi}\times\boldsymbol{\eta})\cdot(g\boldsymbol{B}\times\boldsymbol{\sigma}) + \frac{k_{BS5}}{8M^2}(\boldsymbol{\xi}\times\boldsymbol{\eta})\cdot(g\boldsymbol{B}\times\boldsymbol{\sigma})\Bigg\}\psi(x) \\
&= (\boldsymbol{\xi}\times\boldsymbol{\eta})\cdot\Bigg\{\boldsymbol{r}\times\boldsymbol{\nabla} + \frac{ik_{DS}}{2}\boldsymbol{\sigma} \\
&\quad + \frac{i}{4M^2}(k_{D3S} - k_{DS}c_2)\boldsymbol{\sigma}(\boldsymbol{D}^2) + \frac{i}{16M^2}(k_{DS}^2 - k_{D3S})\big\{\boldsymbol{D},(\boldsymbol{D}\cdot\boldsymbol{\sigma})\big\} \\
&\quad - \frac{i}{16M^2}(4k_{DS}c_F + 4k_E - 4k_D^2 + k_{DS}^2 + 8k_{D3} + 4k_{B1})\,g\boldsymbol{B} \\
&\quad + \frac{1}{16M^2}(4k_{DS}c_F + 2k_{ES} - 2k_Dk_{DS} + k_{D3S} - 2k_{BS4} + 2k_{BS5})(g\boldsymbol{B}\times\boldsymbol{\sigma})\Bigg\}\psi(x) \qquad (2.33) \\
&\stackrel{!}{=} i(\boldsymbol{\xi}\times\boldsymbol{\eta})\cdot\Bigg\{\boldsymbol{r}\times(-i\boldsymbol{\nabla}) + \frac{1}{2}\boldsymbol{\sigma}\Bigg\}\psi(x)\,. \qquad (2.34)
\end{aligned}
$$

For the commutator of two boosts to be equivalent to a rotation, the coefficients thus need to satisfy the following relations:

$$k_{DS} = 1\,, \quad k_{D3S} = 1\,, \quad c_2 = 1\,, \qquad (2.35)$$

$$c_F + k_E - k_D^2 + 2k_{D3} + k_{B1} = -\frac{1}{4}\,, \qquad (2.36)$$

$$2c_F + k_{ES} - k_D - k_{BS4} + k_{BS5} = -\frac{1}{2}\,. \qquad (2.37)$$

In this derivation we have used the equation of motion for the heavy quark field at $\mathcal{O}(M^{-1})$

$$iD_0\psi(x) = \Bigg\{-\frac{c_2}{2M}\boldsymbol{D}^2 - \frac{c_F}{2M}g\boldsymbol{B}\cdot\boldsymbol{\sigma}\Bigg\}\psi(x)\,. \qquad (2.38)$$

2.2.2 Invariance of the Lagrangian

Now that we have constructed a nonlinear boost transformation for the heavy quark fields that satisfies the Poincaré algebra, we can proceed to check which conditions need to be satisfied such that the Lagrangian is invariant under this transformation. We will start with the heavy quark sector. The Lagrangian at $\mathcal{O}(M^{-2})$ was already given in Eq. (2.2), but in order to study the transformed Lagrangian at this order, we also need the $\mathcal{O}(M^{-3})$ terms that contain

a derivative:

$$\mathcal{L}^{(3)}\Big|_{\boldsymbol{D}} = \psi^\dagger\Big\{\frac{c_4}{8M^3}(\boldsymbol{D}^2)^2 + \frac{c_{W1}}{8M^3}\big\{\boldsymbol{D}^2, g\boldsymbol{B}\cdot\boldsymbol{\sigma}\big\} - \frac{c_{W2}}{4M^3}D_i(g\boldsymbol{B}\cdot\boldsymbol{\sigma})D_i \\ + \frac{c_{p'p}}{16M^3}\Big\{(\boldsymbol{D}\cdot\boldsymbol{\sigma}), \big\{\boldsymbol{D}\cdot, g\boldsymbol{B}\big\}\Big\} + \frac{ic_M}{8M^3}\Big\{\boldsymbol{D}\cdot, \big\{\boldsymbol{D}\times, g\boldsymbol{B}\big\}\Big\}\Big\}\psi\,. \tag{2.39}$$

The reason for this is that the term $-iM\boldsymbol{r}$ from the boost transformation adds a power of M to the $\mathcal{O}(M^{-3})$ Lagrangian, but the commutator with this term vanishes unless there appears a derivative.

By invariance of the Lagrangian we mean invariance up to total derivatives. With the Lagrangian defined in Eqs. (2.2) and (2.39) we obtain the following transformation behavior at $\mathcal{O}(M^{-2})$:

$$\partial_\mu\Delta^\mu\mathcal{L} = \mathcal{L}\big(\boldsymbol{D}', \boldsymbol{E}', \boldsymbol{B}', \psi', \chi', x\big) - \mathcal{L}\big(\boldsymbol{D}, \boldsymbol{E}, \boldsymbol{B}, \psi, \chi, x\big) \tag{2.40}$$

$$= \boldsymbol{\eta}\cdot(\boldsymbol{r}\partial_0 + t\boldsymbol{\nabla})\mathcal{L} + \boldsymbol{\eta}\cdot\psi^\dagger\Big\{i(1-c_2)\boldsymbol{D} + \frac{1}{2M}(c_2 - k_D)\big\{D_0, \boldsymbol{D}\big\} \\ + \frac{1}{4M}(k_{DS} - 2c_F + c_S)g\boldsymbol{E}\times\boldsymbol{\sigma} + \frac{i}{4M^2}(c_2k_D - c_4)\big\{\boldsymbol{D}, \boldsymbol{D}^2\big\} + \frac{1}{8M^2}(c_D + k_E)\big[D_0, \boldsymbol{E}\big] \\ + \frac{i}{8M^2}(c_S + k_{ES})\big\{D_0, g\boldsymbol{E}\big\}\times\boldsymbol{\sigma} + \frac{1}{8M^2}(2c_M - c_D + c_Fk_{DS})\big\{\boldsymbol{D}\times, g\boldsymbol{B}\big\} \\ + \frac{i}{8M^2}(c_S - c_Fk_{DS} - c_{p'p})\big\{\boldsymbol{D}\cdot, g\boldsymbol{B}\big\}\boldsymbol{\sigma} + \frac{i}{8M^2}(c_Fk_{DS} - c_2k_{DS} - c_{p'p})\big\{(\boldsymbol{D}\cdot\boldsymbol{\sigma}), g\boldsymbol{B}\big\} \\ + \frac{i}{8M^2}(c_2k_{DS} + 2c_Fk_D - c_S - 2c_{W1} + 2c_{W2})\big\{\boldsymbol{D}, (g\boldsymbol{B}\cdot\boldsymbol{\sigma})\big\}\Big\}\psi \\ + \boldsymbol{\nabla}\cdot\boldsymbol{\eta}\,\psi^\dagger\left\{\frac{k_D}{2M}D_0 - \frac{ic_2k_D}{4M^2}\boldsymbol{D}^2 - \frac{ic_Fk_D}{4M^2}g\boldsymbol{B}\cdot\boldsymbol{\sigma}\right\}\psi \\ + \boldsymbol{\nabla}\cdot\boldsymbol{\eta}\times\psi^\dagger\left\{\frac{ik_{DS}}{4M}D_0\boldsymbol{\sigma} + \frac{c_2k_{DS}}{8M^2}(\boldsymbol{D}^2)\boldsymbol{\sigma} + \frac{c_Fk_{DS}}{8M^2}g\boldsymbol{B} + \frac{ic_Fk_{DS}}{8M^2}g\boldsymbol{B}\times\boldsymbol{\sigma}\right\}\psi\,. \tag{2.41}$$

Here we included the total spatial derivatives in the last two lines for completeness, although they will play no role in the following discussion. They arise from covariant derivatives in the boost transformation of $\psi^\dagger$ through

$$(\boldsymbol{D}\psi)^\dagger = \boldsymbol{\nabla}\psi^\dagger - \psi^\dagger\boldsymbol{D}\,. \tag{2.42}$$

Only the time derivative will be important when we want to calculate the conserved Noether charge associated with a boost transformation.

All terms which are not total derivatives have to vanish, from which we get the constraints

$$c_2 = 1\,,\quad k_D = 1\,,\quad c_4 = 1\,,\quad k_E = -c_D\,,\quad k_{ES} = -c_S\,,\quad k_{DS} = 1\,, \tag{2.43}$$

$$c_S = 2c_F - 1\,,\quad 2c_M = c_D - c_F\,,\quad c_{p'p} = c_F - 1\,,\quad c_{W2} = c_{W1} - 1\,. \tag{2.44}$$

We see that they are consistent with the constraints obtained from the commutator of two boosts. By combining both results we can simplify the additional constraints from the commutator of two boosts:

$$k_{B1} = c_D - c_F + \frac{3}{4} - 2k_{D3}\,,\quad k_{BS5} = k_{BS4} - \frac{1}{2}\,. \tag{2.45}$$

Also note that the relation $k_{DS} = 1$ is obtained from the commutator of two boosts at $\mathcal{O}(M^{-1})$ and $c_2 = 1$ at $\mathcal{O}(M^{-2})$, while from the invariance of the Lagrangian the situation is reversed. Ultimately, if one were able to do an all orders calculation, it is believed that each calculation by itself would give all constraints, since the Wilson coefficients of the Lagrangian enter the calculation of the commutator of two boosts through the equations of motion, but at any finite order both calculations provide complementary information.

So far k_{D3} has not been fixed, but it can be easily seen that there is a term

$$\psi^\dagger \frac{1}{8M^3}(c_4 - k_{D3})\Big\{\big\{D_0, \boldsymbol{\eta}\cdot\boldsymbol{D}\big\}, \boldsymbol{D}^2\Big\}\psi \tag{2.46}$$

in $\partial_\mu \Delta^\mu \mathcal{L}$ that can not be canceled by any other term, because those all contain at least one gluon field $\boldsymbol{E}$ or $\boldsymbol{B}$. So we get the constraint $k_{D3} = 1$ at $\mathcal{O}(M^{-3})$.

If we compare this to the boost transformation used in [60] (which deals with NRQED instead of NRQCD, but at low orders in $1/M$ the two calculations are analogous), we see that the two are the same. The boost coefficients k_D, k_{DS}, k_{D3}, and k_{D3S}, which we have included in our general EFT approach but are absent in [60], turned out to be constrained to be exactly 1. While this is not a general proof that all terms that appear in the induced representation for non-interacting fields do not get loop corrections from the matching, i.e. that there can be no coefficients different from 1, it shows at least that the assumption was justified for the low order terms.

Noether Charges

Now that we have determined the boost transformation of the heavy quark fields we can obtain the corresponding Noether charge $\boldsymbol{\mathcal{K}}$:

$$\begin{aligned}
\boldsymbol{\mathcal{K}} &= \int d^3r \left(\frac{\partial\mathcal{L}}{\partial(\partial_0\phi_i)}(-i\boldsymbol{k}_\phi\phi_i) - \Delta^0\mathcal{L}\right) \\
&= \int d^3r \left(\frac{\partial\mathcal{L}}{\partial(\partial_0\phi_i)}(t\boldsymbol{\nabla} + \boldsymbol{r}\partial_0)\phi_i + \psi^\dagger\hat{\boldsymbol{k}}_\psi\psi + \chi^\dagger\hat{\boldsymbol{k}}_\chi\chi - \boldsymbol{\Pi}^a A_0^a - \boldsymbol{r}\mathcal{L}\right) \\
&= -t\boldsymbol{\mathcal{P}} + \int d^3r \left(\boldsymbol{r}h + \psi^\dagger\hat{\boldsymbol{k}}_\psi\psi + \chi^\dagger\hat{\boldsymbol{k}}_\chi\chi\right), \qquad (2.47) \\
&= -t\boldsymbol{\mathcal{P}} + \frac{1}{2}\int d^3r \left\{\boldsymbol{r}, h + M\psi^\dagger\psi - M\chi^\dagger\chi\right\} - \int d^3r\, \psi^\dagger\left(\frac{i}{4M}\boldsymbol{D}\times\boldsymbol{\sigma} + \frac{c_D}{8M^2}g\boldsymbol{E}\right)\psi \\
&\quad + \int d^3r\, \chi^\dagger\left(\frac{i}{4M}\boldsymbol{D}\times\boldsymbol{\sigma} - \frac{c_D}{8M^2}g\boldsymbol{E}\right)\chi + \mathcal{O}(M^{-3}), \qquad (2.48)
\end{aligned}$$

where ϕ_i stands for all three fields ψ, χ, and $\boldsymbol{A}$, while $\boldsymbol{\Pi}$ is the canonical momentum field associated to $\boldsymbol{A}$:

$$\Pi_i^a = \frac{\partial\mathcal{L}}{\partial(\partial_0 A_i^a)} = -E_i^a + \mathcal{O}(M^{-2}). \tag{2.49}$$

$\boldsymbol{\mathcal{P}}$ is the Noether charge associated with spatial translations

$$\boldsymbol{\mathcal{P}} = \int d^3r \left(\frac{\partial\mathcal{L}}{\partial(\partial_0\phi_i)}(-\boldsymbol{\nabla})\phi_i\right) = \int d^3r \left(\psi^\dagger(-i\boldsymbol{D})\psi + \chi^\dagger(-i\boldsymbol{D})\chi - \mathrm{Tr}\big[\boldsymbol{\Pi}\times, \boldsymbol{B}\big]\right), \tag{2.50}$$

where we have used the equations of motion (i.e. the Gauss law)

$$\big[\boldsymbol{D}\cdot, \boldsymbol{\Pi}\big] = -\left(\psi^\dagger g T^a\psi + \chi^\dagger g T^a\chi\right)T^a, \tag{2.51}$$

in order to make the expression explicitly gauge invariant. The Hamiltonian density h is given through the Hamiltonian

$$\mathcal{H} = \int d^3r \left(\frac{\partial \mathcal{L}}{\partial(\partial_0 \phi_i)} \partial_0 \phi_i - \mathcal{L} \right) = \int d^3r \left(\psi^\dagger h_\psi \psi + \chi^\dagger h_\chi \chi + \mathrm{Tr}\big[\boldsymbol{\Pi}^2 + \boldsymbol{B}^2\big] \right) \equiv \int d^3r \, h \,, \tag{2.52}$$

where h_ψ and h_χ are defined through the Lagrangian as

$$\mathcal{L} = \psi^\dagger (iD_0 - h_\psi)\psi + \chi^\dagger (iD_0 - h_\chi)\chi + \mathrm{Tr}\big[\boldsymbol{E}^2 + \boldsymbol{B}^2\big] \,, \tag{2.53}$$

and we have made use of the Gauss law again. The initial expression $\dfrac{\partial \mathcal{L}}{\partial(\partial_0 \phi_i)} \partial_0 \phi_i - \mathcal{L}$ and h, as defined in the final expression, differ by a derivative term $-\boldsymbol{\nabla} \cdot (\boldsymbol{\Pi}^a A_0^a)$, which vanishes in $\mathcal{H}$, but gives a contribution to $\boldsymbol{\mathcal{K}}$ that exactly cancels the extra terms from the boost of the $\boldsymbol{A}$ field. In the last expression for $\boldsymbol{\mathcal{K}}$, we have replaced $\boldsymbol{r}h$ by $\frac{1}{2}\{\boldsymbol{r}, h\} - \frac{1}{2}[h, \boldsymbol{r}]$ in order to obtain an explicitly hermitian expression; the antihermitian terms from $\psi^\dagger \hat{\boldsymbol{k}}_\psi \psi$ and $\chi^\dagger \hat{\boldsymbol{k}}_\chi \chi$ cancel against $\frac{1}{2}[h, \boldsymbol{r}]$.

This $\boldsymbol{\mathcal{K}}$ corresponds exactly to the boost operator of the quantized theory obtained in [58] and extends it to $\mathcal{O}(M^{-2})$. Note that in [58] the field redefinitions that remove the $\mathcal{O}(M)$ terms from the Lagrangian have not been performed, therefore their definition of h differs from ours by $M\psi^\dagger\psi - M\chi^\dagger\chi$, which thus appears explicitly in our expression for $\boldsymbol{\mathcal{K}}$. Also note that time translations after the redefinition of ψ and χ are given by $i\partial_0 \pm M$, so the proper Noether charge of time translations is the Hamiltonian $\mathcal{H}$ given above plus $M \int d^3r (\psi^\dagger\psi - \chi^\dagger\chi)$, which is exactly the same as in [58].

2.2.3 The Four-Fermion Lagrangian

We will now turn to the four-fermion sector of NRQCD, or more specifically the part consisting of two heavy quark and two heavy antiquark fields. The lowest order terms of the Lagrangian are given by:

$$\begin{aligned} \mathcal{L}^{(2)}\Big|_{4f} = \frac{1}{M^2} \Big\{ & f_1(^1S_0)\, \psi^\dagger \chi \chi^\dagger \psi + f_1(^3S_1)\, \psi^\dagger \boldsymbol{\sigma} \chi \cdot \chi^\dagger \boldsymbol{\sigma} \psi \\ & + f_8(^1S_0)\, \psi^\dagger T^a \chi \chi^\dagger T^a \psi + f_1(^3S_1)\, \psi^\dagger \boldsymbol{\sigma} T^a \chi \cdot \chi^\dagger \boldsymbol{\sigma} T^a \psi \Big\} \,. \end{aligned} \tag{2.54}$$

These coefficients are related by Poincaré invariance to the coefficients of the next order four-fermion Lagrangian, which in this case is $\mathcal{O}(M^{-4})$ [62]. It is easy to see that the $\mathcal{O}(M)$ terms of $\boldsymbol{k}_\psi$ and $\boldsymbol{k}_\chi$ cancel in the boost transformation of the leading order Lagrangian. Therefore, the first constraints will be obtained at $\mathcal{O}(M^{-3})$.

The $\mathcal{O}(M^{-4})$ Lagrangian will contribute with only the $\mathcal{O}(M)$ terms of $\boldsymbol{k}_\psi$ and $\boldsymbol{k}_\chi$, which are given by $\pm M\boldsymbol{r}$. Since in terms with two left-right derivatives (see below), like e.g. in $\psi^\dagger \overleftrightarrow{\boldsymbol{D}} \chi \cdot \chi^\dagger \overleftrightarrow{\boldsymbol{D}} \psi$, or in the terms with a chromomagnetic field $\boldsymbol{B}$ the $\mathcal{O}(M)$ terms cancel, only the terms with at least one "center-of-mass" derivative (i.e. a derivative acting on two heavy fields like $\boldsymbol{\nabla}\chi^\dagger\psi$) give nonvanishing contributions after a boost transformation. Including only such terms, the Lagrangian is given by:

$$\begin{aligned} \mathcal{L}^{(4)}\Big|_{4f,\,cm} = & -\frac{i f_{1cm}}{2M^4} \big(\psi^\dagger (\overleftrightarrow{\boldsymbol{D}} \times \boldsymbol{\sigma}) \chi \cdot \boldsymbol{\nabla} \chi^\dagger \psi + (\boldsymbol{\nabla} \psi^\dagger \chi) \cdot \chi^\dagger (\overleftrightarrow{\boldsymbol{D}} \times \boldsymbol{\sigma}) \psi \big) \\ & - \frac{i f_{8cm}}{2M^4} \big(\psi^\dagger (\overleftrightarrow{\boldsymbol{D}} \times \boldsymbol{\sigma}) T^a \chi \cdot \boldsymbol{D}^{ab} \chi^\dagger T^b \psi + (\boldsymbol{D}^{ab} \psi^\dagger T^b \chi) \cdot \chi^\dagger (\overleftrightarrow{\boldsymbol{D}} \times \boldsymbol{\sigma}) T^a \psi \big) \end{aligned}$$

$$
\begin{aligned}
&+\frac{if'_{1cm}}{2M^4}\big(\psi^\dagger\overleftrightarrow{\boldsymbol{D}}\chi\cdot(\boldsymbol{\nabla}\times\chi^\dagger\boldsymbol{\sigma}\psi)+(\boldsymbol{\nabla}\times\psi^\dagger\boldsymbol{\sigma}\chi)\cdot\chi^\dagger\overleftrightarrow{\boldsymbol{D}}\psi\big)\\
&+\frac{if'_{8cm}}{2M^4}\big(\psi^\dagger\overleftrightarrow{\boldsymbol{D}}T^a\chi\cdot(\boldsymbol{D}^{ab}\times\chi^\dagger\boldsymbol{\sigma}T^b\psi)+(\boldsymbol{D}^{ab}\times\psi^\dagger\boldsymbol{\sigma}T^b\chi)\cdot\chi^\dagger\overleftrightarrow{\boldsymbol{D}}T^a\psi\big)\\
&+\frac{g_{1acm}}{M^4}\left(\nabla_i\psi^\dagger\sigma_j\chi\right)\left(\nabla_i\chi^\dagger\sigma_j\psi\right)+\frac{g_{8acm}}{M^4}\left(D_i^{ab}\psi^\dagger\sigma_jT^b\chi\right)\left(D_i^{ac}\chi^\dagger\sigma_jT^c\psi\right)\\
&+\frac{g_{1bcm}}{M^4}\left(\boldsymbol{\nabla}\cdot\psi^\dagger\boldsymbol{\sigma}\chi\right)\left(\boldsymbol{\nabla}\cdot\chi^\dagger\boldsymbol{\sigma}\psi\right)+\frac{g_{8bcm}}{M^4}\left(\boldsymbol{D}^{ab}\cdot\psi^\dagger\boldsymbol{\sigma}T^b\chi\right)\left(\boldsymbol{D}^{ac}\cdot\chi^\dagger\boldsymbol{\sigma}T^c\psi\right)\\
&+\frac{g_{1ccm}}{M^4}\left(\boldsymbol{\nabla}\psi^\dagger\chi\right)\cdot\left(\boldsymbol{\nabla}\chi^\dagger\psi\right)+\frac{g_{8ccm}}{M^4}\left(\boldsymbol{D}^{ab}\psi^\dagger T^b\chi\right)\cdot\left(\boldsymbol{D}^{ac}\chi^\dagger T^c\psi\right)\,. \qquad (2.55)
\end{aligned}
$$

Covariant derivatives with color indices are understood in the adjoint representation. The left-right derivatives are defined as follows:

$$
\psi^\dagger(\overleftrightarrow{\boldsymbol{D}})^nT\chi=\sum_{k=0}^{n}(-1)^k\binom{n}{k}\left(\boldsymbol{D}^k\psi\right)^\dagger T\left(\boldsymbol{D}^{n-k}\chi\right)\,, \qquad (2.56)
$$

where the order of the $\boldsymbol{D}$'s is the same in each term and T stands for either the unit or a color matrix. In particular it follows from this expression that $\overleftrightarrow{\boldsymbol{D}}$ does not act on any field outside of $\psi^\dagger$ and χ.

From this we get at $\mathcal{O}(M^{-3})$

$$
\begin{aligned}
\partial_\mu\widehat{\Delta}^\mu\mathcal{L}^{(4f)}=&-\frac{1}{2M^3}\left(f_1(^1S_0)+4g_{1ccm}\right)\left[(\boldsymbol{\eta}\cdot i\boldsymbol{\nabla}\psi^\dagger\chi)\chi^\dagger\psi+h.c.\right]\\
&-\frac{1}{2M^3}\left(f_8(^1S_0)+4g_{8ccm}\right)\left[(\boldsymbol{\eta}\cdot i\boldsymbol{D}^{ab}\psi^\dagger T^b\chi)\chi^\dagger T^b\psi+h.c.\right]\\
&+\frac{1}{4M^3}\left(f_1(^1S_0)-f_{1cm}\right)\left[\psi^\dagger\boldsymbol{\eta}\cdot(\overleftrightarrow{\boldsymbol{D}}\times\boldsymbol{\sigma})\chi\chi^\dagger\psi+h.c.\right]\\
&+\frac{1}{4M^3}\left(f_8(^1S_0)-f_{8cm}\right)\left[\psi^\dagger\boldsymbol{\eta}\cdot(\overleftrightarrow{\boldsymbol{D}}\times\boldsymbol{\sigma})T^a\chi\chi^\dagger T^a\psi+h.c.\right]\\
&-\frac{1}{2M^3}\left(f_1(^3S_1)+4g_{1acm}\right)\left[(\boldsymbol{\eta}\cdot i\boldsymbol{\nabla}\psi^\dagger\sigma_i\chi)\chi^\dagger\sigma_i\psi+h.c.\right]\\
&-\frac{1}{2M^3}\left(f_8(^3S_1)+4g_{8acm}\right)\left[(\boldsymbol{\eta}\cdot i\boldsymbol{D}^{ab}\psi^\dagger\sigma_iT^b\chi)\chi^\dagger\sigma_iT^b\psi+h.c.\right]\\
&+\frac{1}{4M^3}\left(f_1(^3S_1)-f'_{1cm}\right)\left[\psi^\dagger(\boldsymbol{\eta}\times\overleftrightarrow{\boldsymbol{D}})\chi\cdot\chi^\dagger\boldsymbol{\sigma}\psi+h.c.\right]\\
&+\frac{1}{4M^3}\left(f_8(^3S_1)-f'_{8cm}\right)\left[\psi^\dagger(\boldsymbol{\eta}\times\overleftrightarrow{\boldsymbol{D}})T^a\chi\cdot\chi^\dagger\boldsymbol{\sigma}T^a\psi+h.c.\right]\\
&+\frac{2}{M^3}g_{1bcm}\left[\psi^\dagger(\boldsymbol{\eta}\cdot\boldsymbol{\sigma})\chi(i\boldsymbol{\nabla}\cdot\chi^\dagger\boldsymbol{\sigma}\psi)+h.c.\right]\\
&+\frac{2}{M^3}g_{8bcm}\left[\psi^\dagger(\boldsymbol{\eta}\cdot\boldsymbol{\sigma})T^a\chi(i\boldsymbol{D}^{ab}\cdot\chi^\dagger\boldsymbol{\sigma}T^b\psi)+h.c.\right]\,, \qquad (2.57)
\end{aligned}
$$

where we use $\widehat{\Delta}$ to denote the boost transformation except for the coordinate transformations, and $h.c.$ means the hermitian conjugate of the preceding term in the brackets. None of these terms has the form of a total derivative, so all coefficients have to be equal to zero, which means:

$$
g_{1acm}=-\frac{1}{4}f_1(^3S_1)\,,\quad g_{1ccm}=-\frac{1}{4}f_1(^1S_0)\,,\quad g_{8acm}=-\frac{1}{4}f_8(^3S_1)\,,\quad g_{8ccm}=-\frac{1}{4}f_8(^1S_0)\,, \qquad (2.58)
$$

$$f_{1cm} = \frac{1}{4} f_1(^1S_0)\,, \quad f'_{1cm} = \frac{1}{4} f_1(^3S_1)\,, \quad f_{8cm} = \frac{1}{4} f_8(^1S_0)\,, \quad f'_{8cm} = \frac{1}{4} f_8(^3S_1)\,, \tag{2.59}$$

$$g_{1bcm} = g_{8bcm} = 0\,. \tag{2.60}$$

These relations were first derived in [62] and later confirmed in [63] for the singlet sector, which is at this order equivalent to NRQED.

2.2.4 NLO Calculation in the Four-Fermion Sector

Going to next order in $1/M$ we have to include two-fermion terms in $\boldsymbol{k}_\psi$ and $\boldsymbol{k}_\chi$, which we can parametrize as follows:

$$\begin{aligned}
\hat{\boldsymbol{k}}_\psi^{(2f)} = {} & \frac{a_{11}}{M^4}\overleftrightarrow{\boldsymbol{D}}\chi\chi^\dagger + \frac{a_{12}}{M^4}\chi\boldsymbol{\nabla}\chi^\dagger + \frac{a_{13}}{M^4}\chi\chi^\dagger\overleftrightarrow{\boldsymbol{D}} \\
& + \frac{a_{81}}{M^4}\overleftrightarrow{\boldsymbol{D}}T^a\chi\chi^\dagger T^a + \frac{a_{82}}{M^4}T^a\chi\boldsymbol{D}^{ab}\chi^\dagger T^b + \frac{a_{83}}{M^4}T^a\chi\chi^\dagger\overleftrightarrow{\boldsymbol{D}}T^a \\
& + \frac{ib_{11}}{M^4}\overleftrightarrow{\boldsymbol{D}}\times\boldsymbol{\sigma}\chi\chi^\dagger - \frac{ib_{12}}{M^4}\boldsymbol{\sigma}\chi\times\boldsymbol{\nabla}\chi^\dagger - \frac{ib_{13}}{M^4}\boldsymbol{\sigma}\chi\times\chi^\dagger\overleftrightarrow{\boldsymbol{D}} \\
& + \frac{ib_{14}}{M^4}\overleftrightarrow{\boldsymbol{D}}\chi\times\chi^\dagger\boldsymbol{\sigma} + \frac{ib_{15}}{M^4}\chi\boldsymbol{\nabla}\times\chi^\dagger\boldsymbol{\sigma} + \frac{ib_{16}}{M^4}\chi\chi^\dagger\overleftrightarrow{\boldsymbol{D}}\times\boldsymbol{\sigma} \\
& + \frac{ib_{81}}{M^4}\overleftrightarrow{\boldsymbol{D}}\times\boldsymbol{\sigma}T^a\chi\chi^\dagger T^a - \frac{ib_{82}}{M^4}\boldsymbol{\sigma}T^a\chi\times\boldsymbol{D}^{ab}\chi^\dagger T^b - \frac{ib_{83}}{M^4}\boldsymbol{\sigma}T^a\chi\times\chi^\dagger\overleftrightarrow{\boldsymbol{D}}T^a \\
& + \frac{ib_{84}}{M^4}\overleftrightarrow{\boldsymbol{D}}T^a\chi\times\chi^\dagger\boldsymbol{\sigma}T^a + \frac{ib_{85}}{M^4}T^a\chi\boldsymbol{D}^{ab}\times\chi^\dagger\boldsymbol{\sigma}T^b + \frac{ib_{86}}{M^4}T^a\chi\chi^\dagger\overleftrightarrow{\boldsymbol{D}}\times\boldsymbol{\sigma}T^a \\
& + \frac{c_{11}}{M^4}(\overleftrightarrow{\boldsymbol{D}}\cdot\boldsymbol{\sigma})\chi\chi^\dagger\boldsymbol{\sigma} + \frac{c_{12}}{M^4}\sigma_i\chi\nabla_i\chi^\dagger\boldsymbol{\sigma} + \frac{c_{13}}{M^4}\sigma_i\chi\chi^\dagger\overleftrightarrow{D_i}\boldsymbol{\sigma} \\
& + \frac{c_{14}}{M^4}\overleftrightarrow{D_i}\boldsymbol{\sigma}\chi\chi^\dagger\sigma_i + \frac{c_{15}}{M^4}\boldsymbol{\sigma}\chi\nabla_i\chi^\dagger\sigma_i + \frac{c_{16}}{M^4}\boldsymbol{\sigma}\chi\chi^\dagger(\overleftrightarrow{\boldsymbol{D}}\cdot\boldsymbol{\sigma}) \\
& + \frac{c_{17}}{M^4}\overleftrightarrow{\boldsymbol{D}}\sigma_i\chi\chi^\dagger\sigma_i + \frac{c_{18}}{M^4}\sigma_i\chi\boldsymbol{\nabla}\chi^\dagger\sigma_i + \frac{c_{19}}{M^4}\sigma_i\chi\chi^\dagger\overleftrightarrow{\boldsymbol{D}}\sigma_i \\
& + \frac{c_{81}}{M^4}(\overleftrightarrow{\boldsymbol{D}}\cdot\boldsymbol{\sigma})T^a\chi\chi^\dagger\boldsymbol{\sigma}T^a + \frac{c_{82}}{M^4}\sigma_i T^a\chi D_i^{ab}\chi^\dagger\boldsymbol{\sigma}T^b + \frac{c_{83}}{M^4}\sigma_i T^a\chi\chi^\dagger\overleftrightarrow{D_i}\boldsymbol{\sigma}T^a \\
& + \frac{c_{84}}{M^4}\overleftrightarrow{D_i}\boldsymbol{\sigma}T^a\chi\chi^\dagger\sigma_i T^a + \frac{c_{85}}{M^4}\boldsymbol{\sigma}T^a\chi D_i^{ab}\chi^\dagger\sigma_i T^b + \frac{c_{86}}{M^4}\boldsymbol{\sigma}T^a\chi\chi^\dagger(\overleftrightarrow{\boldsymbol{D}}\cdot\boldsymbol{\sigma})T^a \\
& + \frac{c_{87}}{M^4}\overleftrightarrow{\boldsymbol{D}}\sigma_i T^a\chi\chi^\dagger\sigma_i T^a + \frac{c_{88}}{M^4}\sigma_i T^a\chi\boldsymbol{D}^{ab}\chi^\dagger\sigma_i T^b + \frac{c_{89}}{M^4}\sigma_i T^a\chi\chi^\dagger\overleftrightarrow{\boldsymbol{D}}\sigma_i T^a\,,
\end{aligned} \tag{2.61}$$

$$\hat{\boldsymbol{k}}_\chi^{(2f)} = \hat{\boldsymbol{k}}_\psi^{(2f)}(\psi\leftrightarrow\chi)\,. \tag{2.62}$$

Here the definition of the left-right derivatives on the left-hand side of $\chi\chi^\dagger$ is a bit trickier. We will understand them as follows

$$\overleftrightarrow{\boldsymbol{D}}T\chi\chi^\dagger T\psi = T(\boldsymbol{D}\chi)\chi^\dagger T\psi + \boldsymbol{D}(T\chi\chi^\dagger T\psi)\,, \tag{2.63}$$

and implicitly perform integration by parts on the second term. The overall spatial derivatives introduced by this integration are irrelevant for everything that will be discussed in this chapter, so we will ignore them. But this definition then implies that the left-derivative part of $\overleftrightarrow{\boldsymbol{D}}$ acts also on the terms outside the bilinear in which it appears. The left-right derivatives on the right-hand side of $\chi\chi^\dagger$ are defined as above and act only within their bilinear.

As an example we give the boost transformation proportional to a_{11} and a_{13} due to the χ field in $\psi^\dagger\chi\chi^\dagger\psi$:

$$\psi^\dagger(\hat{\boldsymbol{k}}\chi)\chi^\dagger\psi = \frac{a_{11}}{M^4}(\psi^\dagger\overleftrightarrow{\boldsymbol{D}}\psi)\psi^\dagger\chi\chi^\dagger\psi - \frac{a_{11}}{M^4}\psi^\dagger\psi\psi^\dagger\chi(\boldsymbol{\nabla}\chi^\dagger\psi) + \frac{a_{13}}{M^4}\psi^\dagger\psi(\psi^\dagger\overleftrightarrow{\boldsymbol{D}}\chi)\chi^\dagger\psi + \dots\,. \tag{2.64}$$

When we now calculate the commutator of two boosts at $\mathcal{O}(M^{-3})$ and consider only the two-fermion part, we get some constraints on these boost coefficients a, b and c. As above, we see that at this order only the terms with a center-of-mass derivative do not cancel automatically, and none of the a coefficients can appear, because they do not give terms antisymmetric in $\boldsymbol{\xi}$ and $\boldsymbol{\eta}$.

There are three contributions to this commutator, the first is

$$\begin{aligned}
&-\left[\boldsymbol{\xi}\cdot\hat{\boldsymbol{k}}_\psi^{(2f)}, M\boldsymbol{\eta}\cdot\boldsymbol{r}\right]+\left[\boldsymbol{\eta}\cdot\hat{\boldsymbol{k}}_\psi^{(2f)}, M\boldsymbol{\xi}\cdot\boldsymbol{r}\right]\\
&= -\frac{2i}{M^3}(b_{11}+b_{12}+b_{13})(\boldsymbol{\xi}\times\boldsymbol{\eta})\cdot\boldsymbol{\sigma}\chi\chi^\dagger-\frac{2i}{M^3}(b_{14}+b_{15}+b_{16})\chi\chi^\dagger(\boldsymbol{\xi}\times\boldsymbol{\eta})\cdot\boldsymbol{\sigma}\\
&\quad-\frac{2i}{M^3}(b_{81}+b_{82}+b_{83})(\boldsymbol{\xi}\times\boldsymbol{\eta})\cdot\boldsymbol{\sigma}T^a\chi\chi^\dagger T^a-\frac{2i}{M^3}(b_{84}+b_{85}+b_{86})T^a\chi\chi^\dagger(\boldsymbol{\xi}\times\boldsymbol{\eta})\cdot\boldsymbol{\sigma}T^a\\
&\quad+\frac{1}{M^3}(c_{11}+c_{12}+c_{13}-c_{14}-c_{15}-c_{16})(\boldsymbol{\xi}\times\boldsymbol{\eta})\cdot(\boldsymbol{\sigma}\chi\times\chi^\dagger\boldsymbol{\sigma})\\
&\quad+\frac{1}{M^3}(c_{81}+c_{82}+c_{83}-c_{84}-c_{85}-c_{86})(\boldsymbol{\xi}\times\boldsymbol{\eta})\cdot(\boldsymbol{\sigma}T^a\chi\times\chi^\dagger\boldsymbol{\sigma}T^a)\,.
\end{aligned}\tag{2.65}$$

The second contribution comes from the transformation of the χ fields inside $\hat{\boldsymbol{k}}_\psi^{(2f)}$

$$\begin{aligned}
&-(M\boldsymbol{\xi}\cdot\boldsymbol{r}\delta_\chi-M\boldsymbol{\xi}\cdot\boldsymbol{r}\delta_{\chi^\dagger})(\boldsymbol{\eta}\cdot\hat{\boldsymbol{k}}_\psi^{(2f)})+(M\boldsymbol{\eta}\cdot\boldsymbol{r}\delta_\chi-M\boldsymbol{\eta}\cdot\boldsymbol{r}\delta_{\chi^\dagger})(\boldsymbol{\xi}\cdot\hat{\boldsymbol{k}}_\psi^{(2f)})\\
&=\frac{2i}{M^3}(b_{11}-b_{12}+b_{13})(\boldsymbol{\xi}\times\boldsymbol{\eta})\cdot\boldsymbol{\sigma}\chi\chi^\dagger+\frac{2i}{M^3}(b_{14}-b_{15}+b_{16})\chi\chi^\dagger(\boldsymbol{\xi}\times\boldsymbol{\eta})\cdot\boldsymbol{\sigma}\\
&\quad+\frac{2i}{M^3}(b_{81}-b_{82}+b_{83})(\boldsymbol{\xi}\times\boldsymbol{\eta})\cdot\boldsymbol{\sigma}T^a\chi\chi^\dagger T^a+\frac{2i}{M^3}(b_{84}-b_{85}+b_{86})T^a\chi\chi^\dagger(\boldsymbol{\xi}\times\boldsymbol{\eta})\cdot\boldsymbol{\sigma}T^a\\
&\quad-\frac{1}{M^3}(c_{11}-c_{12}+c_{13}-c_{14}+c_{15}-c_{16})(\boldsymbol{\xi}\times\boldsymbol{\eta})\cdot(\boldsymbol{\sigma}\chi\times\chi^\dagger\boldsymbol{\sigma})\\
&\quad-\frac{1}{M^3}(c_{81}-c_{82}+c_{83}-c_{84}+c_{85}-c_{86})(\boldsymbol{\xi}\times\boldsymbol{\eta})\cdot(\boldsymbol{\sigma}T^a\chi\times\chi^\dagger\boldsymbol{\sigma}T^a)\,.
\end{aligned}\tag{2.66}$$

The last contribution comes from the term $-\frac{1}{2M}(\boldsymbol{\xi}\times\boldsymbol{\eta})\cdot\boldsymbol{\sigma}D_0$ that has already been derived above. When we use the equation of motion for $iD_0\psi$ this becomes in the two-fermion sector

$$\begin{aligned}
&-\frac{i(\boldsymbol{\xi}\times\boldsymbol{\eta})\cdot\boldsymbol{\sigma}}{2M^3}\Big\{f_1(^1S_0)\,\chi\chi^\dagger+f_1(^3S_1)\,\boldsymbol{\sigma}\chi\cdot\chi^\dagger\boldsymbol{\sigma}+f_8(^1S_0)\,T^a\chi\chi^\dagger T^a+f_1(^3S_1)\,\boldsymbol{\sigma}T^a\chi\cdot\chi^\dagger\boldsymbol{\sigma}T^a\Big\}\\
&=-\frac{if_1(^1S_0)}{2M^3}(\boldsymbol{\xi}\times\boldsymbol{\eta})\cdot\boldsymbol{\sigma}\chi\chi^\dagger-\frac{if_8(^1S_0)}{2M^3}(\boldsymbol{\xi}\times\boldsymbol{\eta})\cdot\boldsymbol{\sigma}T^a\chi\chi^\dagger T^a\\
&\quad-\frac{if_1(^3S_1)}{2M^3}\chi\chi^\dagger(\boldsymbol{\xi}\times\boldsymbol{\eta})\cdot\boldsymbol{\sigma}-\frac{if_8(^3S_1)}{2M^3}T^a\chi\chi^\dagger(\boldsymbol{\xi}\times\boldsymbol{\eta})\cdot\boldsymbol{\sigma}T^a\\
&\quad-\frac{f_1(^3S_1)}{2M^3}(\boldsymbol{\xi}\times\boldsymbol{\eta})\cdot(\boldsymbol{\sigma}\chi\times\chi^\dagger\boldsymbol{\sigma})-\frac{f_8(^3S_1)}{2M^3}(\boldsymbol{\xi}\times\boldsymbol{\eta})\cdot(\boldsymbol{\sigma}T^a\chi\times\chi^\dagger\boldsymbol{\sigma}T^a)\,.
\end{aligned}\tag{2.67}$$

The sum of these three contributions has to vanish, so we have

$$\begin{aligned}
0=&-\frac{i}{2M^3}\left(8b_{12}+f_1(^1S_0)\right)(\boldsymbol{\xi}\times\boldsymbol{\eta})\cdot\boldsymbol{\sigma}\chi\chi^\dagger-\frac{i}{2M^3}\left(8b_{82}+f_8(^1S_0)\right)(\boldsymbol{\xi}\times\boldsymbol{\eta})\cdot\boldsymbol{\sigma}T^a\chi\chi^\dagger T^a\\
&-\frac{i}{2M^3}\left(8b_{15}+f_1(^3S_1)\right)\chi\chi^\dagger(\boldsymbol{\xi}\times\boldsymbol{\eta})\cdot\boldsymbol{\sigma}-\frac{i}{2M^3}\left(8b_{85}+f_8(^3S_1)\right)T^a\chi\chi^\dagger(\boldsymbol{\xi}\times\boldsymbol{\eta})\cdot\boldsymbol{\sigma}T^a\\
&+\frac{1}{2M^3}\left(4c_{12}-4c_{15}-f_1(^3S_1)\right)(\boldsymbol{\xi}\times\boldsymbol{\eta})\cdot(\boldsymbol{\sigma}\chi\times\chi^\dagger\boldsymbol{\sigma})\\
&+\frac{1}{2M^3}\left(4c_{82}-4c_{85}-f_8(^3S_1)\right)(\boldsymbol{\xi}\times\boldsymbol{\eta})\cdot(\boldsymbol{\sigma}T^a\chi\times\chi^\dagger\boldsymbol{\sigma}T^a)\,,
\end{aligned}\tag{2.68}$$

which fixes the two-fermion boost parameters to be

$$b_{12} = -\frac{1}{8} f_1({}^1S_0)\,, \quad b_{15} = -\frac{1}{8} f_1({}^3S_1)\,, \quad b_{82} = -\frac{1}{8} f_8({}^1S_0)\,, \quad b_{85} = -\frac{1}{8} f_8({}^3S_1)\,, \tag{2.69}$$

$$c_{12} - c_{15} = \frac{1}{4} f_1({}^3S_1)\,, \quad c_{82} - c_{85} = \frac{1}{4} f_8({}^3S_1)\,. \tag{2.70}$$

At $\mathcal{O}(M^{-4})$ there is no new information from the two-boost commutator. The $\mathcal{O}(M^{-5})$ terms of $\hat{\boldsymbol{k}}_\psi^{(2f)}$ can either contain two derivatives or one gluon field for dimensional reasons, but only the chromoelectric field has the right parity transformation behavior. So there can be no $\mathcal{O}(M^{-5})$ terms with derivatives, and therefore the commutator of the $\mathcal{O}(M^{-5})$ $\hat{\boldsymbol{k}}_\psi^{(2f)}$ with $M\boldsymbol{r}$ vanishes. The boost transformation of the fields inside $\hat{\boldsymbol{k}}_\psi^{(2f)}$ at $\mathcal{O}(M^{-4})$ gives only temporal derivatives, which have to be replaced through the equations of motion for ψ and χ and thus contribute only at $\mathcal{O}(M^{-5})$. And there are no four-fermion $\mathcal{O}(M^{-3})$ terms that could give a contribution at $\mathcal{O}(M^{-4})$ from $-\frac{1}{2M}(\boldsymbol{\xi}\times\boldsymbol{\eta})\cdot\boldsymbol{\sigma} D_0$.

In order to get the constraints from the boost transformation of $\mathcal{L}$ at $\mathcal{O}(M^{-4})$ we need all four-fermion terms at $\mathcal{O}(M^{-4})$, most of which can be found in [62], and all center-of-mass derivative terms at $\mathcal{O}(M^{-5})$, which were not included in [62].

$$\begin{aligned}
\mathcal{L}^{(4f)}_{M^{-4}} = &-\frac{g_1({}^1S_0)}{8M^4}\left(\psi^\dagger \overleftrightarrow{\boldsymbol{D}}^2 \chi\chi^\dagger\psi + \psi^\dagger\chi\chi^\dagger \overleftrightarrow{\boldsymbol{D}}^2\psi\right)\\
&-\frac{g_1({}^3S_1)}{8M^4}\left(\psi^\dagger(\overleftrightarrow{\boldsymbol{D}}^2)\boldsymbol{\sigma}\chi\cdot\chi^\dagger\boldsymbol{\sigma}\psi + \psi^\dagger\boldsymbol{\sigma}\chi\chi^\dagger(\overleftrightarrow{\boldsymbol{D}}^2)\boldsymbol{\sigma}\psi\right)\\
&-\frac{g_1({}^3S_1,{}^1S_0)}{8M^4}\left(\frac{1}{2}\psi^\dagger\left\{(\overleftrightarrow{\boldsymbol{D}}\cdot\boldsymbol{\sigma}),\overleftrightarrow{\boldsymbol{D}}\right\}\chi\cdot\chi^\dagger\boldsymbol{\sigma}\psi - \frac{1}{3}\psi^\dagger\overleftrightarrow{\boldsymbol{D}}^2\chi\chi^\dagger\psi + h.c.\right)\\
&-\frac{g_8({}^1S_0)}{8M^4}\left(\psi^\dagger \overleftrightarrow{\boldsymbol{D}}^2 T^a\chi\chi^\dagger T^a\psi + \psi^\dagger\chi\chi^\dagger \overleftrightarrow{\boldsymbol{D}}^2 T^a\psi\right)\\
&-\frac{g_8({}^3S_1)}{8M^4}\left(\psi^\dagger(\overleftrightarrow{\boldsymbol{D}}^2)\boldsymbol{\sigma}T^a\chi\cdot\chi^\dagger\boldsymbol{\sigma}T^a\psi + \psi^\dagger\boldsymbol{\sigma}T^a\chi\chi^\dagger(\overleftrightarrow{\boldsymbol{D}}^2)T^a\boldsymbol{\sigma}\psi\right)\\
&-\frac{g_8({}^3S_1,{}^1S_0)}{8M^4}\left(\frac{1}{2}\psi^\dagger\left\{(\overleftrightarrow{\boldsymbol{D}}\cdot\boldsymbol{\sigma}),\overleftrightarrow{\boldsymbol{D}}\right\}T^a\chi\cdot\chi^\dagger\boldsymbol{\sigma}T^a\psi - \frac{1}{3}\psi^\dagger\overleftrightarrow{\boldsymbol{D}}^2T^a\chi\chi^\dagger T^a\psi + h.c.\right)\\
&-\frac{f_1({}^1P_1)}{4M^4}\psi^\dagger\overleftrightarrow{\boldsymbol{D}}\chi\cdot\chi^\dagger\overleftrightarrow{\boldsymbol{D}}\psi\\
&-\frac{f_1({}^3P_0)}{12M^4}\psi^\dagger(\overleftrightarrow{\boldsymbol{D}}\cdot\boldsymbol{\sigma})\chi\chi^\dagger(\overleftrightarrow{\boldsymbol{D}}\cdot\boldsymbol{\sigma})\psi\\
&-\frac{f_1({}^3P_1)}{8M^4}\left(\psi^\dagger\overleftrightarrow{D_i}\sigma_j\chi\chi^\dagger\overleftrightarrow{D_i}\sigma_j\psi - \psi^\dagger\overleftrightarrow{D_i}\sigma_j\chi\chi^\dagger\overleftrightarrow{D_j}\sigma_i\psi\right)\\
&-\frac{f_1({}^3P_2)}{4M^4}\left(\frac{1}{2}\psi^\dagger\overleftrightarrow{D_i}\sigma_j\chi\chi^\dagger\overleftrightarrow{D_i}\sigma_j\psi + \frac{1}{2}\psi^\dagger\overleftrightarrow{D_i}\sigma_j\chi\chi^\dagger\overleftrightarrow{D_j}\sigma_i\psi - \frac{1}{3}\psi^\dagger(\overleftrightarrow{\boldsymbol{D}}\cdot\boldsymbol{\sigma})\chi\chi^\dagger(\overleftrightarrow{\boldsymbol{D}}\cdot\boldsymbol{\sigma})\psi\right)\\
&-\frac{f_8({}^1P_1)}{4M^4}\psi^\dagger\overleftrightarrow{\boldsymbol{D}}T^a\chi\cdot\chi^\dagger\overleftrightarrow{\boldsymbol{D}}T^a\psi\\
&-\frac{f_8({}^3P_0)}{12M^4}\psi^\dagger(\overleftrightarrow{\boldsymbol{D}}\cdot\boldsymbol{\sigma})T^a\chi\chi^\dagger(\overleftrightarrow{\boldsymbol{D}}\cdot\boldsymbol{\sigma})T^a\psi\\
&-\frac{f_8({}^3P_1)}{8M^4}\left(\psi^\dagger\overleftrightarrow{D_i}\sigma_j T^a\chi\chi^\dagger\overleftrightarrow{D_i}\sigma_j T^a\psi - \psi^\dagger\overleftrightarrow{D_i}\sigma_j T^a\chi\chi^\dagger\overleftrightarrow{D_j}\sigma_i T^a\psi\right)
\end{aligned}$$

$$
\begin{aligned}
&- \frac{f_8(^3P_2)}{4M^4}\left(\frac{1}{2}\psi^\dagger\overleftrightarrow{D_i}\sigma_j T^a\chi\chi^\dagger\overleftrightarrow{D_i}\sigma_j T^a\psi + \frac{1}{2}\psi^\dagger\overleftrightarrow{D_i}\sigma_j T^a\chi\chi^\dagger\overleftrightarrow{D_j}\sigma_i T^a\psi\right.\\
&\qquad\left.-\frac{1}{3}\psi^\dagger(\overleftrightarrow{\boldsymbol{D}}\cdot\boldsymbol{\sigma})T^a\chi\chi^\dagger(\overleftrightarrow{\boldsymbol{D}}\cdot\boldsymbol{\sigma})T^a\psi\right)\\
&- \frac{if_{1cm}}{2M^4}\left(\psi^\dagger(\overleftrightarrow{\boldsymbol{D}}\times\boldsymbol{\sigma})\chi\cdot\boldsymbol{\nabla}\chi^\dagger\psi + (\boldsymbol{\nabla}\psi^\dagger\chi)\cdot\chi^\dagger(\overleftrightarrow{\boldsymbol{D}}\times\boldsymbol{\sigma})\psi\right)\\
&+ \frac{if'_{1cm}}{2M^4}\left(\psi^\dagger\overleftrightarrow{\boldsymbol{D}}\chi\cdot(\boldsymbol{\nabla}\times\chi^\dagger\boldsymbol{\sigma}\psi) + (\boldsymbol{\nabla}\times\psi^\dagger\boldsymbol{\sigma}\chi)\cdot\chi^\dagger\overleftrightarrow{\boldsymbol{D}}\psi\right)\\
&- \frac{if_{8cm}}{2M^4}\left(\psi^\dagger(\overleftrightarrow{\boldsymbol{D}}\times\boldsymbol{\sigma})T^a\chi\cdot\boldsymbol{D}^{ab}\chi^\dagger T^b\psi + (\boldsymbol{D}^{ab}\psi^\dagger T^b\chi)\cdot\chi^\dagger(\overleftrightarrow{\boldsymbol{D}}\times\boldsymbol{\sigma})T^a\psi\right)\\
&+ \frac{if'_{8cm}}{2M^4}\left(\psi^\dagger\overleftrightarrow{\boldsymbol{D}}T^a\chi\cdot(\boldsymbol{D}^{ab}\times\chi^\dagger\boldsymbol{\sigma}T^b\psi) + (\boldsymbol{D}^{ab}\times\psi^\dagger\boldsymbol{\sigma}T^b\chi)\cdot\chi^\dagger\overleftrightarrow{\boldsymbol{D}}T^a\psi\right)\\
&+ \frac{g_{1acm}}{M^4}\left(\nabla_i\psi^\dagger\sigma_j\chi\right)\left(\nabla_i\chi^\dagger\sigma_j\psi\right) + \frac{g_{8acm}}{M^4}\left(D_i^{ab}\psi^\dagger\sigma_j T^b\chi\right)\left(D_i^{ac}\chi^\dagger\sigma_j T^c\psi\right)\\
&+ \frac{g_{1bcm}}{M^4}\left(\boldsymbol{\nabla}\cdot\psi^\dagger\boldsymbol{\sigma}\chi\right)\left(\boldsymbol{\nabla}\cdot\chi^\dagger\boldsymbol{\sigma}\psi\right) + \frac{g_{8bcm}}{M^4}\left(\boldsymbol{D}^{ab}\cdot\psi^\dagger\boldsymbol{\sigma}T^b\chi\right)\left(\boldsymbol{D}^{ac}\cdot\chi^\dagger\boldsymbol{\sigma}T^c\psi\right)\\
&+ \frac{g_{1ccm}}{M^4}\left(\boldsymbol{\nabla}\psi^\dagger\chi\right)\cdot\left(\boldsymbol{\nabla}\chi^\dagger\psi\right) + \frac{g_{8ccm}}{M^4}\left(\boldsymbol{D}^{ab}\psi^\dagger T^b\chi\right)\cdot\left(\boldsymbol{D}^{ac}\chi^\dagger T^c\psi\right)\\
&+ \frac{s_{1-8}(^1S_0,{}^3S_1)}{2M^4}\left(\psi^\dagger g\boldsymbol{B}\cdot\boldsymbol{\sigma}\chi\chi^\dagger\psi + \psi^\dagger\chi\chi^\dagger g\boldsymbol{B}\cdot\boldsymbol{\sigma}\psi\right)\\
&+ \frac{s_{1-8}(^3S_1,{}^1S_0)}{2M^4}\left(\psi^\dagger g\boldsymbol{B}\chi\cdot\chi^\dagger\boldsymbol{\sigma}\psi + \psi^\dagger\boldsymbol{\sigma}\chi\cdot\chi^\dagger g\boldsymbol{B}\psi\right)\\
&+ \frac{s_{8-8}(^1S_0,{}^3S_1)}{2M^4}d^{abc}g\boldsymbol{B}^a\cdot\left(\psi^\dagger\boldsymbol{\sigma}T^b\chi\chi^\dagger T^c\psi + \psi^\dagger T^b\chi\chi^\dagger\boldsymbol{\sigma}T^c\psi\right)\\
&+ \frac{s_{8-8}(^3S_1,{}^3S_1)}{2M^4}f^{abc}g\boldsymbol{B}^a\cdot\left(\psi^\dagger\boldsymbol{\sigma}T^b\chi\times\chi^\dagger\boldsymbol{\sigma}T^c\psi\right)\,. \qquad (2.71)
\end{aligned}
$$

For dimensional reasons the $\mathcal{O}(M^{-5})$ four-fermion Lagrangian can either contain three derivatives or one derivative and one gluon field. Parity allows only the combination of a chromoelectric field and a derivative. As stated above, only center-of-mass derivatives are relevant for this order of the boost transformation.

$$
\begin{aligned}
\mathcal{L}^{(4f)}_{M^{-5}cm} = &\frac{is_{1-8\,cm}}{2M^5}\left(\psi^\dagger g\boldsymbol{E}\times\boldsymbol{\sigma}\chi\cdot\boldsymbol{\nabla}\chi^\dagger\psi - (\boldsymbol{\nabla}\psi^\dagger\chi)\cdot\chi^\dagger g\boldsymbol{E}\times\boldsymbol{\sigma}\psi\right)\\
&- \frac{is'_{1-8\,cm}}{2M^5}\left(\psi^\dagger g\boldsymbol{E}\chi\cdot(\boldsymbol{\nabla}\times\chi^\dagger\boldsymbol{\sigma}\psi) - (\boldsymbol{\nabla}\times\psi^\dagger\boldsymbol{\sigma}\chi)\cdot\chi^\dagger g\boldsymbol{E}\psi\right)\\
&+ \frac{is_{8-8\,cm}}{2M^5}d^{abc}g\boldsymbol{E}^a\cdot\left(\psi^\dagger\boldsymbol{\sigma}T^b\chi\times\boldsymbol{D}^{cd}\chi^\dagger T^d\psi + (\boldsymbol{D}^{bd}\psi^\dagger T^d\chi)\times\chi^\dagger\boldsymbol{\sigma}T^c\psi\right)\\
&+ \frac{is'_{8-8\,cm}}{2M^5}f^{abc}gE_i^a\left(\psi^\dagger\sigma_i T^b\chi(\boldsymbol{D}^{cd}\cdot\chi^\dagger\boldsymbol{\sigma}T^d\psi) + (\boldsymbol{D}^{bd}\cdot\psi^\dagger\boldsymbol{\sigma}T^d\chi)\chi^\dagger\sigma_i T^c\psi\right)\,. \qquad (2.72)
\end{aligned}
$$

In principle one can write more terms with a center-of-mass derivative, but those can be integrated by parts, neglecting overall derivatives, and they give a derivative that acts only on the chromoelectric field, e.g.

$$
if^{abc}g\boldsymbol{E}^a\cdot\left(\psi^\dagger T^b\chi\boldsymbol{D}^{cd}\chi^\dagger T^d\psi + (\boldsymbol{D}^{bd}\psi^\dagger T^d\chi)\chi^\dagger T^c\psi\right) = -(\boldsymbol{D}^{ad}\cdot g\boldsymbol{E}^d)\,if^{abc}\psi^\dagger T^b\chi\chi^\dagger T^c\psi\,. \qquad (2.73)
$$

These terms obviously do not contribute to the boost transformation of the Lagrangian at $\mathcal{O}(M^{-4})$, we therefore chose a minimal basis of operators where only the terms given above have explicit center-of-mass derivatives.

After a lengthy calculation of the boost transformation of the Lagrangian at $\mathcal{O}(M^{-4})$, we obtain the following constraints:

$$a_{11} = \frac{1}{4} g_1({}^1S_0)\,, \quad a_{12} = g_{1ccm}\,, \quad a_{13} = \frac{1}{4} f_1({}^1P_1)\,,$$

$$a_{81} = \frac{1}{4} g_8({}^1S_0)\,, \quad a_{82} = g_{8ccm}\,, \quad a_{83} = \frac{1}{4} f_8({}^1P_1)\,,$$

$$b_{12} = -\frac{1}{2} f_{1cm}\,, \quad b_{15} = -\frac{1}{2} f'_{1cm}\,, \quad b_{82} = -\frac{1}{2} f_{8cm}\,, \quad b_{85} = -\frac{1}{2} f'_{8cm}\,,$$

$$b_{13} = -\frac{1}{2} f'_{1cm} + b_{14}\,, \quad b_{16} = -\frac{1}{2} f_{1cm} + b_{11}\,, \quad b_{83} = -\frac{1}{2} f'_{8cm} + b_{84}\,, \quad b_{86} = -\frac{1}{2} f_{8cm} + b_{81}\,,$$

$$c_{11} = \frac{1}{8} g_1({}^3S_1, {}^3D_1)\,, \qquad c_{13} = \frac{1}{8} \left(f_1({}^3P_2) - f_1({}^3P_1) \right)\,,$$

$$c_{14} = \frac{1}{8} g_1({}^3S_1, {}^3D_1)\,, \qquad c_{16} = \frac{1}{12} \left(f_1({}^3P_0) - f_1({}^3P_2) \right)\,,$$

$$c_{17} = \frac{1}{12} \left(4 g_1({}^3S_1) - g_1({}^3S_1, {}^3D_1) \right)\,, \qquad c_{19} = \frac{1}{8} \left(f_1({}^3P_1) + f_1({}^3P_2) \right)\,,$$

$$c_{81} = \frac{1}{8} g_8({}^3S_1, {}^3D_1)\,, \qquad c_{83} = \frac{1}{8} \left(f_8({}^3P_2) - f_8({}^3P_1) \right)\,,$$

$$c_{84} = \frac{1}{8} g_8({}^3S_1, {}^3D_1)\,, \qquad c_{86} = \frac{1}{12} \left(f_8({}^3P_0) - f_8({}^3P_2) \right)\,,$$

$$c_{87} = \frac{1}{12} \left(4 g_8({}^3S_1) - g_8({}^3S_1, {}^3D_1) \right)\,, \qquad c_{89} = \frac{1}{8} \left(f_8({}^3P_1) + f_8({}^3P_2) \right)\,,$$

$$c_{15} = -c_{12}\,, \quad c_{18} = g_{1acm}\,, \quad c_{85} = -c_{82}\,, \quad c_{88} = g_{8acm}\,,$$

$$s_{1-8\,cm} - \frac{1}{2} s_{1-8}({}^1S_0, {}^3S_1) - \frac{c_S}{4} f_1({}^1S_0) - \frac{c_S}{4} f_8({}^1S_0) - 2b_{11} - 2b_{84} = 0\,,$$

$$s'_{1-8\,cm} - \frac{1}{2} s_{1-8}({}^3S_1, {}^1S_0) - \frac{c_S}{4} f_1({}^1S_0) - \frac{c_S}{4} f_8({}^1S_0) - 2b_{14} - 2b_{81} = 0\,,$$

$$s_{8-8\,cm} - \frac{1}{2} s_{8-8}({}^1S_0, {}^3S_1) - \frac{c_S}{4} f_8({}^1S_0) - b_{81} - b_{84} = 0\,,$$

$$s'_{8-8\,cm} + \frac{1}{2} s_{8-8}({}^3S_1, {}^3S_1) - \frac{c_S}{4} f_8({}^3S_1) - \frac{1}{16} g_8({}^3S_1, {}^3D_1) + c_{82} = 0\,. \tag{2.74}$$

So far none of these constraints involves only Wilson coefficients of the Lagrangian, they rather define the boost parameters of $\hat{\boldsymbol{k}}_\psi^{(2f)}$ and $\hat{\boldsymbol{k}}_\chi^{(2f)}$. There remain two free parameters, c_{12} and one of either b_{11}, b_{14}, b_{81} or b_{84}. But if we combine them with the relations obtained from the commutator of two boosts, we get

$$c_{12} = \frac{1}{8} f_1({}^3S_1)\,, \quad c_{15} = -\frac{1}{8} f_1({}^3S_1)\,, \quad c_{82} = \frac{1}{8} f_8({}^3S_1)\,, \quad c_{85} = -\frac{1}{8} f_8({}^3S_1)\,,$$

$$s'_{8-8\,cm} + \frac{1}{2} s_{8-8}({}^3S_1, {}^3S_1) - \frac{2c_S - 1}{8} f_8({}^3S_1) - \frac{1}{16} g_8({}^3S_1, {}^3D_1) = 0\,. \tag{2.75}$$

The last equation now gives a constraint on the Wilson coefficients without any boost parameters. The other relations we got for b_{12}, b_{52}, b_{82} and b_{85} from the commutator of two boosts are consistent with the ones obtained from the transformation of the Lagrangian at $\mathcal{O}(M^{-4})$ and $\mathcal{O}(M^{-2})$.

2.3 Constraints in pNRQCD

Potential Non-Relativistic QCD (pNRQCD) is the EFT obtained from NRQCD after integrating out the scale of the relative quark-antiquark momentum. This scale is of the same order as the quark-antiquark distance r, so the expansion in this scale corresponds to a multipole expansion. In weakly coupled pNRQCD we also assume the hierarchy $1/r \gg \Lambda_{\rm QCD}$, which means that the matching can be carried out in perturbation theory. The effective degrees of freedom are color singlet S and octet O^a quarkonium fields instead of individual quark and antiquark fields. They are the only fields that can depend on the distance $\boldsymbol{r}$ and the center-of-mass coordinate $\boldsymbol{R}$, all other fields depend only on $\boldsymbol{R}$. Throughout this section, we prefer to set $N = 3$ (hence the name octet instead of adjoint field); the extension to general N is straightforward.

The Lagrangian of pNRQCD (without the gluonic part) can be written schematically as

$$\mathcal{L}_{\rm pNRQCD} = \int d^3r \,{\rm Tr}\left[S^\dagger(i\partial_0 - h_S)S + O^{a\,\dagger}(iD_0^{ab} - h_O^{ab})O^b - (S^\dagger h_{SO}^a O^a + h.c.)\right] , \qquad (2.76)$$

where the trace refers to the spin indices of the quarkonium fields. Sometimes it is more convenient to write the quarkonium fields as matrices in color space:

$$S = \frac{1}{\sqrt{3}} S\,\mathbb{1}\,, \qquad O = \sqrt{2} O^a T^a\,, \qquad (2.77)$$

and the Lagrangian:

$$\mathcal{L}_{\rm pNRQCD} = \int d^3r \,{\rm Tr}\left[S^\dagger(iD_0 - h_S)S + O^\dagger iD_0 O - \big(O^\dagger h_O O + c.c\big) - \big(S^\dagger h_{SO} O + h.c.\big)\right] , \qquad (2.78)$$

where the trace now is understood both in spin and in color space, and $c.c$ means charge conjugate. We will not use different symbols for the matrix or scalar singlet field, it should be clear from context which one is meant, or sometimes it may be irrelevant. In the octet case the matrix field is obvious from the absence of a color index. The coefficients for the matrices are such that the trace over two fields is properly normalized. The covariant derivatives are understood as commutators with everything to their right.

The matching to NRQCD is performed through interpolating fields

$$\begin{aligned} &\chi^\dagger(\boldsymbol{R} - \boldsymbol{r}/2)\phi(\boldsymbol{R} - \boldsymbol{r}/2, \boldsymbol{R} + \boldsymbol{r}/2)\psi(\boldsymbol{R} + \boldsymbol{r}/2) \\ &\to Z_S^{(0)}(r) S(\boldsymbol{r}, \boldsymbol{R}) + Z_O^{(2)}(r) r\boldsymbol{r}\cdot g\boldsymbol{E}^a(\boldsymbol{R}) O^a(\boldsymbol{r}, \boldsymbol{R}) + \mathcal{O}(r^3)\,, \qquad (2.79) \\ &\chi^\dagger(\boldsymbol{R} - \boldsymbol{r}/2)\phi(\boldsymbol{R} - \boldsymbol{r}/2, \boldsymbol{R}) T^a \phi(\boldsymbol{R}, \boldsymbol{R} + \boldsymbol{r}/2)\psi(\boldsymbol{R} + \boldsymbol{r}/2) \\ &\to Z_O^{(0)}(r) O^a(\boldsymbol{r}, \boldsymbol{R}) + Z_S^{(2)}(r) r\boldsymbol{r}\cdot g\boldsymbol{E}^a(\boldsymbol{R}) S(\boldsymbol{r}, \boldsymbol{R}) + \mathcal{O}(r^3)\,. \qquad (2.80) \end{aligned}$$

The Wilson lines ϕ act as gauge links from the quark position to that of the antiquark. Correlators of those interpolating fields in both theories have to give the same result, which determines the matching coefficients Z.

2.3.1 Coordinate Transformations for Quarkonium Fields

The interpolating fields also determine how the quarkonium fields have to transform under the spacetime symmetries. In fact, in the limit $g \to 0$ one can neglect the Wilson lines and just

determine the transformation of S and O^a from different color projections of $Q = \psi\chi^\dagger$ (this limit is not physical, since there is no non-interacting bound state, but this is irrelevant here). The coordinate transformations do not depend on the color representation, so we can just use Q for both singlet and octet.

First, we give here the transformations under the discrete symmetries:

$$Q(t,\boldsymbol{r},\boldsymbol{R}) \xrightarrow{P} -Q(t,-\boldsymbol{r},-\boldsymbol{R})\,, \tag{2.81}$$

$$Q(t,\boldsymbol{r},\boldsymbol{R}) \xrightarrow{C} \sigma_2 Q^T(t,-\boldsymbol{r},\boldsymbol{R})\sigma_2\,, \tag{2.82}$$

$$Q(t,\boldsymbol{r},\boldsymbol{R}) \xrightarrow{T} \sigma_2 Q(-t,\boldsymbol{r},\boldsymbol{R})\sigma_2\,. \tag{2.83}$$

The transposed sign on the charge conjugated fields refers both to color and spin space. Also note that charge conjugation exchanges the positions of the quark and the antiquark fields, so $\boldsymbol{r}$ goes to $-\boldsymbol{r}$.

Time translations are straightforward in pNRQCD; in the interpolating fields ψ and $\chi^\dagger$ are evaluated at the same time, so also the time argument of the quarkonium fields is shifted in the same way. The additional mass terms introduced through the field redefinitions of ψ and χ add up, so we have

$$Q(t,\boldsymbol{r},\boldsymbol{R}) \xrightarrow{P_0} Q'(t,\boldsymbol{r},\boldsymbol{R}) = (1-2iMa_0)Q(t,\boldsymbol{r},\boldsymbol{R}) + \big[a_0\partial_0, Q(t,\boldsymbol{r},\boldsymbol{R})\big]\,. \tag{2.84}$$

We assume in this chapter that the quark and the antiquark field have the same mass, so the generator of time translations is $P_0 = i\partial_0 + 2M$.

Space translations act only on the center-of-mass coordinate $\boldsymbol{R}$; both quark and antiquark are shifted by the same amount, so the relative coordinate remains unaffected. This means

$$Q(t,\boldsymbol{r},\boldsymbol{R}) \xrightarrow{P_i} Q'(t,\boldsymbol{r},\boldsymbol{R}) = Q(t,\boldsymbol{r},\boldsymbol{R}) - \big[\boldsymbol{a}\cdot\boldsymbol{\nabla}_R, Q(t,\boldsymbol{r},\boldsymbol{R})\big]\,, \tag{2.85}$$

with the generator for space translations $\boldsymbol{P} = -i\boldsymbol{\nabla}_R$.

Under rotations both $\boldsymbol{R}$ and $\boldsymbol{r}$ transform in the same way. The component transformations of ψ and χ with $i\boldsymbol{\sigma}$ each lead to a commutator with the quarkonium fields and the sigma matrix:

$$Q(t,\boldsymbol{r},\boldsymbol{R}) \xrightarrow{J} Q'(t,\boldsymbol{r},\boldsymbol{R}) = Q(t,\boldsymbol{r},\boldsymbol{R}) + \big[\boldsymbol{\alpha}\cdot(\boldsymbol{R}\times\boldsymbol{\nabla}_R + \boldsymbol{r}\times\boldsymbol{\nabla}_r + i\boldsymbol{\sigma}), Q(t,\boldsymbol{r},\boldsymbol{R})\big]\,. \tag{2.86}$$

It is conventional to use an upper index on the sigma matrices to denote whether it is supposed to be multiplied to the quarkonium field from the left or the right:

$$\boldsymbol{\sigma}^{(1)}Q = \boldsymbol{\sigma}Q \qquad \text{and} \qquad \boldsymbol{\sigma}^{(2)}Q = -Q\boldsymbol{\sigma}\,. \tag{2.87}$$

This gives the generator of rotations as $\boldsymbol{J} = \boldsymbol{R}\times(-i\boldsymbol{\nabla}_R) + \boldsymbol{r}\times(-i\boldsymbol{\nabla}_r) + \boldsymbol{\sigma}^{(1)} + \boldsymbol{\sigma}^{(2)}$. Since $\sigma_2\boldsymbol{\sigma}\sigma_2 = -\boldsymbol{\sigma}^T$ and $\boldsymbol{\sigma}^T Q^T = (Q\boldsymbol{\sigma})^T$, charge conjugation effectively exchanges $\boldsymbol{\sigma}^{(1)} \leftrightarrow \boldsymbol{\sigma}^{(2)}$.

For boosts we will first determine how the coordinates of the quarkonium fields have to transform. We still use the analogy with the interpolating fields in the $g \to 0$ limit, but now we need to write the quark and antiquark field explicitly instead of Q. So we have with $\boldsymbol{x}_1 = \boldsymbol{R} + \boldsymbol{r}/2$ and $\boldsymbol{x}_2 = \boldsymbol{R} - \boldsymbol{r}/2$

$$\begin{aligned}\psi(t,\boldsymbol{x}_1)\chi^\dagger(t,\boldsymbol{x}_2) &\xrightarrow{K} \psi(t,\boldsymbol{x}_1)\chi^\dagger(t,\boldsymbol{x}_2) - iM\boldsymbol{\eta}\cdot(\boldsymbol{x}_1+\boldsymbol{x}_2)\psi(t,\boldsymbol{x}_1)\chi^\dagger(t,\boldsymbol{x}_2)\\ &+ \big[\boldsymbol{\eta}\cdot(t\boldsymbol{\nabla}_1 + \boldsymbol{x}_1\partial_0), \psi(t,\boldsymbol{x}_1)\big]\chi^\dagger(t,\boldsymbol{x}_2) + \psi(t,\boldsymbol{x}_1)\big[\boldsymbol{\eta}\cdot(t\boldsymbol{\nabla}_2 + \boldsymbol{x}_2\partial_0), \chi^\dagger(t,\boldsymbol{x}_2)\big] + \ldots\end{aligned}$$

$$= (1 - 2iM\boldsymbol{\eta}\cdot\boldsymbol{R})\psi(t,\boldsymbol{x}_1)\chi^\dagger(t,\boldsymbol{x}_2) + \big[\boldsymbol{\eta}\cdot(t\boldsymbol{\nabla}_R + \boldsymbol{R}\partial_0), \psi(t,\boldsymbol{x}_1)\chi^\dagger(t,\boldsymbol{x}_2)\big]$$
$$+ \frac{1}{2}(\boldsymbol{\eta}\cdot\boldsymbol{r})\left(\big[\partial_0,\psi(t,\boldsymbol{x}_1)\big]\chi^\dagger(t,\boldsymbol{x}_2) - \psi(t,\boldsymbol{x}_1)\big[\partial_0,\chi^\dagger(t,\boldsymbol{x}_2)\big]\right) + \dots\,, \tag{2.88}$$

where the dots stand for all terms of the boost transformation that are not related to the coordinate transformations. The first line corresponds to the usual coordinate transformations under boosts for a scalar field with mass $2M$, where only the center-of-mass coordinate participates in the boost and the relative distance remains unaffected. In the second line, the time derivatives acting on the quark and antiquark fields cannot be written as one derivative acting on the whole quarkonium field, because they have opposite sign. But these time derivatives can be replaced by space derivatives through the equations of motion:

$$\begin{aligned}
&\frac{1}{2}(\boldsymbol{\eta}\cdot\boldsymbol{r})\left(\big[\partial_0,\psi(t,\boldsymbol{x}_1)\big]\chi^\dagger(t,\boldsymbol{x}_2) - \psi(t,\boldsymbol{x}_1)\big[\partial_0,\chi^\dagger(t,\boldsymbol{x}_2)\big]\right)\\
&= (\boldsymbol{\eta}\cdot\boldsymbol{r})\left[\frac{i}{4M}(\boldsymbol{\nabla}_1^2 - \boldsymbol{\nabla}_2^2), \psi(t,\boldsymbol{x}_1)\chi^\dagger(t,\boldsymbol{x}_2)\right] + \mathcal{O}(M^{-3})\\
&= (\boldsymbol{\eta}\cdot\boldsymbol{r})\left[\frac{i}{2M}\boldsymbol{\nabla}_R\cdot\boldsymbol{\nabla}_r, \psi(t,\boldsymbol{x}_1)\chi^\dagger(t,\boldsymbol{x}_2)\right] + \mathcal{O}(M^{-3})\,.
\end{aligned} \tag{2.89}$$

Thus these terms give corrections of order $1/M$ and higher.

The other terms in the boost transformation of the quark and antiquark fields in the $g \to 0$ limit can also be rewritten in terms of polar coordinates:

$$\begin{aligned}
&\psi(t,\boldsymbol{x}_1)\chi^\dagger(t,\boldsymbol{x}_2) \xrightarrow{K} \dots + \frac{i}{2M}\big[\boldsymbol{\eta}\cdot(\boldsymbol{\nabla}_1 + \boldsymbol{\nabla}_2), \psi(t,\boldsymbol{x}_1)\chi^\dagger(t,\boldsymbol{x}_2)\big]\\
&\quad - \frac{1}{4M}\big[(\boldsymbol{\eta}\times\boldsymbol{\nabla}_1)\cdot,\boldsymbol{\sigma}\psi(t,\boldsymbol{x}_1)\chi^\dagger(t,\boldsymbol{x}_2)\big] + \frac{1}{4M}\big[(\boldsymbol{\eta}\times\boldsymbol{\nabla}_2)\cdot,\psi(t,\boldsymbol{x}_1)\chi^\dagger(t,\boldsymbol{x}_2)\boldsymbol{\sigma}\big] + \mathcal{O}(M^{-2})\\
&= \dots + \frac{i}{2M}\big[\boldsymbol{\eta}\cdot\boldsymbol{\nabla}_R, \psi(t,\boldsymbol{x}_1)\chi^\dagger(t,\boldsymbol{x}_2)\big] - \frac{1}{8M}\left(\boldsymbol{\sigma}^{(1)} + \boldsymbol{\sigma}^{(2)}\right)\cdot\big[(\boldsymbol{\eta}\times\boldsymbol{\nabla}_R), \psi(t,\boldsymbol{x}_1)\chi^\dagger(t,\boldsymbol{x}_2)\big]\\
&\quad - \frac{1}{4M}\left(\boldsymbol{\sigma}^{(1)} - \boldsymbol{\sigma}^{(2)}\right)\cdot\big[(\boldsymbol{\eta}\times\boldsymbol{\nabla}_r), \psi(t,\boldsymbol{x}_1)\chi^\dagger(t,\boldsymbol{x}_2)\big] + \mathcal{O}(M^{-3})\,.
\end{aligned} \tag{2.90}$$

Here the dots denote the coordinate transformation terms. So we expect the boost generators in the $g \to 0$ limit to behave like

$$\begin{aligned}
\boldsymbol{k}_Q \overset{g\to 0}{=}\; & it\boldsymbol{\nabla}_R + i\boldsymbol{R}\partial_0 + 2M\boldsymbol{R} - \frac{1}{4M}\boldsymbol{\nabla}_R - \frac{1}{4M}\big\{\boldsymbol{r},(\boldsymbol{\nabla}_R\cdot\boldsymbol{\nabla}_r)\big\}\\
&- \frac{i}{8M}\boldsymbol{\nabla}_R\times\left(\boldsymbol{\sigma}^{(1)} + \boldsymbol{\sigma}^{(2)}\right) - \frac{i}{4M}\boldsymbol{\nabla}_r\times\left(\boldsymbol{\sigma}^{(1)} - \boldsymbol{\sigma}^{(2)}\right) + \mathcal{O}(M^{-3})\,.
\end{aligned} \tag{2.91}$$

This limit is interesting for the ansatz we are going to make for the singlet and octet boost generators, since it determines which coefficients we expect to be of order $1 + \mathcal{O}(\alpha_s)$. In the last two terms of the first line we have used

$$\boldsymbol{r}(\boldsymbol{\nabla}_R\cdot\boldsymbol{\nabla}_r) = \frac{1}{2}\big\{\boldsymbol{r},(\boldsymbol{\nabla}_R\cdot\boldsymbol{\nabla}_r)\big\} - \frac{1}{2}\boldsymbol{\nabla}_R\,, \tag{2.92}$$

in order to obtain terms that are explicitly hermitian or antihermitian.

Finally, we list here the behavior of the boost generators under the discrete symmetries:

$$\boldsymbol{k}_Q \xrightarrow{P} -\boldsymbol{k}_Q\,, \qquad \boldsymbol{k}_Q \xrightarrow{C} \sigma_2\boldsymbol{k}_Q^T\sigma_2\,, \qquad \boldsymbol{k}_Q \xrightarrow{T} \sigma_2\boldsymbol{k}_Q\sigma_2\,. \tag{2.93}$$

Keep in mind that P changes the sign of both $\boldsymbol{r}$ and $\boldsymbol{R}$, C changes the sign of only $\boldsymbol{r}$, T changes the sign of t and takes the complex conjugate. The transpose operation inherent to C requires some further explanation. First, the sigma matrices change like:

$$\sigma_2 \left(\boldsymbol{\sigma}^{(1/2)}\right)^T \sigma_2 = \boldsymbol{\sigma}^{(2/1)}\,, \qquad \sigma_2 \left(\boldsymbol{\sigma}^{(1/2)}\right)^* \sigma_2 = -\boldsymbol{\sigma}^{(1/2)}\,. \tag{2.94}$$

For the singlet field, transposing in color space is trivial, so we can just write $\boldsymbol{k}_S \xrightarrow{C} \sigma_2 \boldsymbol{k}_S \sigma_2$. For the octet field in matrix notation, we have to write the boost generator in two parts:

$$O \xrightarrow{K} O' = O - i\boldsymbol{\eta} \cdot \left(\boldsymbol{k}_O^{(A)} O + O \boldsymbol{k}_O^{(B)}\right)\,. \tag{2.95}$$

The two parts then are exchanged under C as $\boldsymbol{k}_O^{(A/B)} \xrightarrow{C} \sigma_2 \left(\boldsymbol{k}_O^{(B/A)}\right)^T \sigma_2$.

2.3.2 Redundancies and Field Redefinitions

In order to find the boost generators in pNRQCD, we will again use the EFT approach and write down the most general form allowed by the symmetries. However, it will turn out that several terms in this ansatz are redundant, i.e. one can make a field redefinition that removes these terms from the boost generator without changing the form of the Lagrangian. So there is no loss in generality if one chooses to work with a boost generator where these redundant terms are absent. We will work out appropriate field redefinitions in this section. Since we will calculate the transformation of the Lagrangian up to orders $M^0 r^1$ and $M^{-1} r^0$ in the next section, here we need to include all terms of order $M^0 r^2$, $M^{-1} r^0$. We will use the notation $c^{(m,n)}$ for the coefficients of terms of order $M^{-m} r^n$.

Singlet Field

For the singlet field we start with the most general ansatz for the boost generator allowed by the other symmetries. However, note that we can eliminate some terms from the outset. Also in the construction of the pNRQCD Lagrangian certain terms are neglected without an explicit matching. For example, the term $\boldsymbol{r} \cdot \boldsymbol{\nabla}_r$ is completely neutral with respect to any symmetry and also the power counting. So in principle one could add an infinite number of these terms to any operator in the Lagrangian, which would mean that at each order in the power counting one would have to match an infinite number of terms, making the construction of the EFT impossible. But by comparison with NRQCD one sees that each derivative appears with at least one power of $1/M$, so also in pNRQCD one can neglect any term where there are more derivatives than powers of $1/M$ because there would be no corresponding term in the matching to NRQCD. The same argument applies to spin-dependent terms, where also each sigma matrix has to be suppressed by a power of $1/M$. The only exception to this are the kinetic terms, where there may be one derivative more than powers of $1/M$.

By extension, these rules also apply to the construction of the boost generator, not directly (i.e. there can be terms in the boost generator where there are more derivatives and sigma matrices than powers of $1/M$), but in the following way. Operators that would lead to terms in the transformation of the Lagrangian that cannot be canceled by any other terms can immediately be ruled out. For example, operators that are antihermitian in the boost generator lead to anticommutators with the time derivative from the leading term of the Lagrangian, which can only be canceled by a term with a corresponding spatial derivative. Such a term

would be e.g. $i\boldsymbol{r}\times\left(\boldsymbol{\sigma}^{(1)}-\boldsymbol{\sigma}^{(2)}\right)/(8Mr^2)$, which is not ruled out by any symmetry argument, but the resulting term in the transformed Lagrangian would have to be canceled through a term $i\boldsymbol{D}\cdot\boldsymbol{r}\times\left(\boldsymbol{\sigma}^{(1)}-\boldsymbol{\sigma}^{(2)}\right)/(8Mr^2)$ in h_S, which is ruled out according to the arguments given above. Hermitian operators in the boost generator are less problematic, because they lead to commutators in the transformed Lagrangian, which usually reduces the number of derivatives by one.

Keeping this in mind, and writing everything in terms of explicitly hermitian or antihermitian operators (where we stay close to the nomenclature of [58]), the most general ansatz is:

$$\begin{aligned}
\boldsymbol{k}_S = {} & it\boldsymbol{\nabla}_R + i\boldsymbol{R}\partial_0 + 2M\boldsymbol{R} - \frac{k_{SD}^{(1,0)}}{4M}\boldsymbol{\nabla}_R - \frac{1}{4M}\left\{k_{Sa'}^{(1,0)}\boldsymbol{r},(\boldsymbol{\nabla}_R\cdot\boldsymbol{\nabla}_r)\right\} \\
& - \frac{1}{4M}\left\{k_{Sa''}^{(1,0)}(\boldsymbol{r}\cdot\boldsymbol{\nabla}_R),\boldsymbol{\nabla}_r\right\} - \frac{1}{4M}\left\{k_{Sa'''}^{(1,0)}\boldsymbol{r}\cdot,\boldsymbol{\nabla}_r\right\}\boldsymbol{\nabla}_R \\
& - \frac{1}{4M}\left\{\frac{k_{Sb}^{(1,0)}}{r^2}\boldsymbol{r}(\boldsymbol{r}\cdot\boldsymbol{\nabla}_R)r_i,(\nabla_r)_i\right\} - \frac{ik_{Sc}^{(1,0)}}{8M}\boldsymbol{\nabla}_R\times\left(\boldsymbol{\sigma}^{(1)}+\boldsymbol{\sigma}^{(2)}\right) \\
& - \frac{ik_{Sd''}^{(1,0)}}{8Mr^2}\left(\boldsymbol{r}\cdot\boldsymbol{\nabla}_R\right)\left(\boldsymbol{r}\times\left(\boldsymbol{\sigma}^{(1)}+\boldsymbol{\sigma}^{(2)}\right)\right) - \frac{ik_{Sd'''}^{(1,0)}}{8Mr^2}\left((\boldsymbol{r}\times\boldsymbol{\nabla}_R)\cdot\left(\boldsymbol{\sigma}^{(1)}+\boldsymbol{\sigma}^{(2)}\right)\right)\boldsymbol{r} \\
& - \frac{i}{8M}\left\{k_{Sa}^{(1,-1)},\boldsymbol{\nabla}_r\times\left(\boldsymbol{\sigma}^{(1)}-\boldsymbol{\sigma}^{(2)}\right)\right\} + \frac{i}{8M}\left[\frac{k_{Sb'}^{(1,-1)}}{r^2}\left(\boldsymbol{r}\cdot\left(\boldsymbol{\sigma}^{(1)}-\boldsymbol{\sigma}^{(2)}\right)\right)\boldsymbol{r}\times,\boldsymbol{\nabla}_r\right] \\
& - \frac{i}{8M}\left\{\frac{k_{Sb''}^{(1,-1)}}{r^2}\left(\boldsymbol{r}\times\left(\boldsymbol{\sigma}^{(1)}-\boldsymbol{\sigma}^{(2)}\right)\right)r_i,(\nabla_r)_i\right\} + \mathcal{O}\left(M^{-2}r^0,M^{-1}r^1,M^0r^3\right)\,. \qquad (2.96)
\end{aligned}$$

The coefficients depend on r, so they have to be included inside the anticommutators with the derivative $\boldsymbol{\nabla}_r$. We also have used the identity

$$\delta_{ij}\epsilon_{klm} = \delta_{ik}\epsilon_{jlm} + \delta_{il}\epsilon_{kjm} + \delta_{im}\epsilon_{klj} \qquad (2.97)$$

to eliminate some terms. For example, a term like $ik_{Sd'}^{(1,0)}(\boldsymbol{r}\times\boldsymbol{\nabla}_R)(\boldsymbol{r}\cdot(\boldsymbol{\sigma}^{(1)}+\boldsymbol{\sigma}^{(2)}))/(8Mr^2)$ is not linearly independent, because it is related to the operators of $k_{Sc}^{(1,0)}$, $k_{Sd''}^{(1,0)}$, and $k_{Sd'''}^{(1,0)}$ through this identity, which can be shown by multiplying Eq. (2.97) with $r_ir_j(\nabla_R)_k(\sigma^{(1)}+\sigma^{(2)})_l$. A similar situation is found for the operators of $k_{Sa}^{(1,-1)}$, $k_{Sb'}^{(1,-1)}$, and $k_{Sb''}^{(1,-1)}$. Note that this identity has not been used in [58].

As mentioned above, not all these terms in the boost generator are necessary, when one exploits the freedom to perform field redefinitions; i.e. one can always redefine the fields as long as the symmetry properties of the fields are not altered. In order to also keep the form of the Lagrangian intact, we will only consider unitary transformations $\mathcal{U}_S = \exp[u_S]$ with u_S antihermitian, relating the new singlet field $\widetilde{S}$ to the old one S as $S = \mathcal{U}_S\widetilde{S}$. The reason for choosing only unitary transformations is that the time derivative from the leading term of the Lagrangian appears only in commutators, since

$$\mathcal{U}_S^\dagger i\partial_0\mathcal{U}_S = i\partial_0 + [i\partial_0,u_S] + \frac{1}{2}[[i\partial_0,u_S],u_S] + \frac{1}{6}[[[i\partial_0,u_S],u_S],u_S] + \dots\,. \qquad (2.98)$$

In this and the analogous expression for the redefinition of the octet field, the commutators with the time derivative either vanish, give an electric field, or time derivatives of gluon fields,

which can be removed through the equations of motion (i.e. redefinitions of the gluon fields). So a unitary transformation does not introduce new time derivatives in the Lagrangian. It will introduce other terms, but those will be of a form already present in the Lagrangian, so their contributions can be absorbed in a redefinition of the Wilson coefficients.

In order to find a suitable unitary transformation, we need to look for terms which are antihermitian and P, C, and T invariant. Such terms can easily be found by multiplying the hermitian terms in $\boldsymbol{k}_S$ with $\boldsymbol{\nabla}_R/M$, which explains the nomenclature we use for $\mathcal{U}_S$:

$$\begin{aligned}\mathcal{U}_S = \exp\Bigg[&-\frac{1}{4M^2}\left\{q^{(1,0)}_{Sa''}\boldsymbol{r}\cdot\boldsymbol{\nabla}_R, \boldsymbol{\nabla}_r\cdot\boldsymbol{\nabla}_R\right\} - \frac{1}{4M^2}\left\{q^{(1,0)}_{Sa'''}\boldsymbol{r}\cdot, \boldsymbol{\nabla}_r\right\}\boldsymbol{\nabla}_R^2 \\ &- \frac{1}{4M^2}\left\{\frac{q^{(1,0)}_{Sb}}{r^2}(\boldsymbol{r}\cdot\boldsymbol{\nabla}_R)^2\boldsymbol{r}\cdot, \boldsymbol{\nabla}_r\right\} - \frac{iq^{(1,0)}_{Sd'''}}{8M^2r^2}(\boldsymbol{r}\cdot\boldsymbol{\nabla}_R)\left((\boldsymbol{r}\times\boldsymbol{\nabla}_R)\cdot\left(\boldsymbol{\sigma}^{(1)}+\boldsymbol{\sigma}^{(2)}\right)\right) \\ &+ \frac{i}{8M^2}\left\{q^{(1,-1)}_{Sa}, (\boldsymbol{\nabla}_r\times\boldsymbol{\nabla}_R)\cdot\left(\boldsymbol{\sigma}^{(1)}-\boldsymbol{\sigma}^{(2)}\right)\right\} \\ &- \frac{i}{8M^2}\left\{\frac{q^{(1,-1)}_{Sb'}}{r^2}\left(\boldsymbol{r}\cdot\left(\boldsymbol{\sigma}^{(1)}-\boldsymbol{\sigma}^{(2)}\right)\right)(\boldsymbol{r}\times\boldsymbol{\nabla}_R)\cdot, \boldsymbol{\nabla}_r\right\} \\ &+ \frac{i}{8M^2}\left\{\frac{q^{(1,-1)}_{Sb''}}{r^2}\left((\boldsymbol{r}\times\boldsymbol{\nabla}_R)\cdot\left(\boldsymbol{\sigma}^{(1)}-\boldsymbol{\sigma}^{(2)}\right)\right)\boldsymbol{r}\cdot, \boldsymbol{\nabla}_r\right\} + \dots\Bigg]\,, \end{aligned} \tag{2.99}$$

where the dots stand for higher order terms, which do not affect the calculations of this chapter. The coefficients q are free parameters.

We can work out the transformation of the new field $\widetilde{S}$ under boosts in the following way:

$$\begin{aligned}\widetilde{S}' = \mathcal{U}'^{\dagger}_S S' = \mathcal{U}'^{\dagger}_S(1-i\boldsymbol{\eta}\cdot\boldsymbol{k}_S)\mathcal{U}_S\widetilde{S} = \left[1-\mathcal{U}_S^{\dagger}(i\boldsymbol{\eta}\cdot\boldsymbol{k}_S)\mathcal{U}_S + \left(\delta\mathcal{U}_S^{\dagger}\right)\mathcal{U}_S\right]\widetilde{S} \\ \equiv \left(1-i\boldsymbol{\eta}\cdot\widetilde{\boldsymbol{k}}_S\right)\widetilde{S}\,,\end{aligned} \tag{2.100}$$

where

$$\begin{aligned}\delta\mathcal{U}_S^{\dagger}(\boldsymbol{\nabla}_R, \boldsymbol{E}, \boldsymbol{B}) = &\left[\boldsymbol{\eta}\cdot(t\boldsymbol{\nabla}_R + \boldsymbol{R}\partial_0), \mathcal{U}_S^{\dagger}(\boldsymbol{\nabla}_R, \boldsymbol{E}, \boldsymbol{B})\right] \\ &+ \left(\boldsymbol{\eta}\partial_0\cdot\boldsymbol{\delta}_{\nabla} + (\boldsymbol{\eta}\times\boldsymbol{B}^a)\cdot\boldsymbol{\delta}^a_E - (\boldsymbol{\eta}\times\boldsymbol{E}^a)\cdot\boldsymbol{\delta}^a_B\right)\mathcal{U}_S^{\dagger}(\boldsymbol{\nabla}_R, \boldsymbol{E}, \boldsymbol{B})\,,\end{aligned} \tag{2.101}$$

with the $\boldsymbol{\delta}$ operations defined as in Eq. (2.31).

The transformed boost generator $\widetilde{\boldsymbol{k}}_S$ has to be expanded to the same order as the original $\boldsymbol{k}_S$, so only one extra term remains:

$$\begin{aligned}\widetilde{\boldsymbol{k}}_S &= \boldsymbol{k}_S + \left[\hat{\boldsymbol{k}}_S - i\big(\partial_0\boldsymbol{\delta}_{\nabla} + \boldsymbol{B}^a\times\boldsymbol{\delta}^a_E - \boldsymbol{E}^a\times\boldsymbol{\delta}^a_B\big), u_S\right] \\ &\quad + \frac{1}{2}\left[\left[\hat{\boldsymbol{k}}_S - i\big(\partial_0\boldsymbol{\delta}_{\nabla} + \boldsymbol{B}^a\times\boldsymbol{\delta}^a_E - \boldsymbol{E}^a\times\boldsymbol{\delta}^a_B\big), u_S\right], u_S\right] \\ &\quad + \frac{1}{6}\left[\left[\left[\hat{\boldsymbol{k}}_S - i\big(\partial_0\boldsymbol{\delta}_{\nabla} + \boldsymbol{B}^a\times\boldsymbol{\delta}^a_E - \boldsymbol{E}^a\times\boldsymbol{\delta}^a_B\big), u_S\right], u_S\right], u_S\right] + \dots \\ &= \boldsymbol{k}_S + [2M\boldsymbol{R}, u_S] + \mathcal{O}(M^{-2})\,.\end{aligned} \tag{2.102}$$

Inserting the explicit field redefinition from Eq. (2.99), we obtain

$$\begin{aligned}\widetilde{\boldsymbol{k}}_S = \boldsymbol{k}_S &+ \frac{1}{2M}\left\{q^{(1,0)}_{Sa''}\boldsymbol{r}, (\boldsymbol{\nabla}_R\cdot\boldsymbol{\nabla}_r)\right\} + \frac{1}{2M}\left\{q^{(1,0)}_{Sa''}(\boldsymbol{r}\cdot\boldsymbol{\nabla}_R), \boldsymbol{\nabla}_r\right\} \\ &+ \frac{1}{M}\left\{q^{(1,0)}_{Sa'''}\boldsymbol{r}\cdot, \boldsymbol{\nabla}_r\right\}\boldsymbol{\nabla}_R + \frac{1}{M}\left\{\frac{q^{(1,0)}_{Sb}}{r^2}\boldsymbol{r}(\boldsymbol{r}\cdot\boldsymbol{\nabla}_R)r_i, (\nabla_r)_i\right\}\end{aligned}$$

$$
\begin{aligned}
&- \frac{iq_{Sd'''}^{(1,0)}}{4Mr^2}\left(\boldsymbol{r}\cdot\boldsymbol{\nabla}_R\right)\left(\boldsymbol{r}\times\left(\boldsymbol{\sigma}^{(1)}+\boldsymbol{\sigma}^{(2)}\right)\right)+\frac{iq_{Sd'''}^{(1,0)}}{4Mr^2}\left(\boldsymbol{r}\cdot\left(\boldsymbol{\nabla}_R\times\left(\boldsymbol{\sigma}^{(1)}+\boldsymbol{\sigma}^{(2)}\right)\right)\right)\boldsymbol{r}\\
&+\frac{i}{4M}\left\{q_{Sa}^{(1,-1)},\boldsymbol{\nabla}_r\times\left(\boldsymbol{\sigma}^{(1)}-\boldsymbol{\sigma}^{(2)}\right)\right\}-\frac{i}{4M}\left[\frac{q_{Sb'}^{(1,-1)}}{r^2}\left(\boldsymbol{r}\cdot\left(\boldsymbol{\sigma}^{(1)}-\boldsymbol{\sigma}^{(2)}\right)\right)\boldsymbol{r}\times,\boldsymbol{\nabla}_r\right]\\
&+\frac{i}{4M}\left\{\frac{q_{Sb''}^{(1,-1)}}{r^2}\left(\boldsymbol{r}\times\left(\boldsymbol{\sigma}^{(1)}-\boldsymbol{\sigma}^{(2)}\right)\right)r_i,(\nabla_r)_i\right\}+\mathcal{O}\left(M^{-2}\right)\,. \qquad (2.103)
\end{aligned}
$$

These extra terms can be absorbed in the operators already present in Eq. (2.96), which changes the coefficients in the following way:

$$
\begin{aligned}
&\widetilde{k}_{Sa'}^{(1,0)}=k_{Sa'}^{(1,0)}-2q_{Sa''}^{(1,0)}\,, && \widetilde{k}_{Sa''}^{(1,0)}=k_{Sa''}^{(1,0)}-2q_{Sa''}^{(1,0)}\,, && \widetilde{k}_{Sa'''}^{(1,0)}=k_{Sa'''}^{(1,0)}-4q_{Sa'''}^{(1,0)}\,,\\
&\widetilde{k}_{Sb}^{(1,0)}=k_{Sb}^{(1,0)}-4q_{Sb}^{(1,0)}\,, && \widetilde{k}_{Sd''}^{(1,0)}=k_{Sd''}^{(1,0)}+2q_{Sd'''}^{(1,0)}\,, && \widetilde{k}_{Sd'''}^{(1,0)}=k_{Sd'''}^{(1,0)}-2q_{Sd'''}^{(1,0)}\,,\\
&\widetilde{k}_{Sa}^{(1,-1)}=k_{Sa}^{(1,-1)}-2q_{Sa}^{(1,-1)}\,, && \widetilde{k}_{Sb'}^{(1,-1)}=k_{Sb'}^{(1,-1)}-2q_{Sb'}^{(1,-1)}\,, && \widetilde{k}_{Sb''}^{(1,-1)}=k_{Sb''}^{(1,-1)}-2q_{Sb''}^{(1,-1)}\,. \qquad (2.104)
\end{aligned}
$$

The seven free parameters q in the unitary operator can be chosen in any convenient way. Following the expected result in the $g\to 0$ limit from Eq. (2.91), we choose to eliminate $\widetilde{k}_{Sa''}^{(1,0)}$, $\widetilde{k}_{Sa'''}^{(1,0)}$, $\widetilde{k}_{Sb}^{(1,0)}$, $\widetilde{k}_{Sd'''}^{(1,0)}$, $\widetilde{k}_{Sb'}^{(1,-1)}$, and $\widetilde{k}_{Sb''}^{(1,-1)}$, as well as fix $\widetilde{k}_{Sa}^{(1,-1)}=1$. Then after dropping the tilde notation, the general boost transformation is simplified as follows

$$
\begin{aligned}
\boldsymbol{k}_S=&\,it\boldsymbol{\nabla}_R+i\boldsymbol{R}\partial_0+2M\boldsymbol{R}-\frac{k_{SD}^{(1,0)}}{4M}\boldsymbol{\nabla}_R-\frac{1}{4M}\left\{k_{Sa'}^{(1,0)}\boldsymbol{r},\left(\boldsymbol{\nabla}_r\cdot\boldsymbol{\nabla}_R\right)\right\}\\
&-\frac{ik_{Sc}^{(1,0)}}{8M}\boldsymbol{\nabla}_R\times\left(\boldsymbol{\sigma}^{(1)}+\boldsymbol{\sigma}^{(2)}\right)-\frac{ik_{Sd''}^{(1,0)}}{8Mr^2}\left(\boldsymbol{r}\cdot\boldsymbol{\nabla}_R\right)\left(\boldsymbol{r}\times\left(\boldsymbol{\sigma}^{(1)}+\boldsymbol{\sigma}^{(2)}\right)\right)\\
&-\frac{i}{4M}\boldsymbol{\nabla}_r\times\left(\boldsymbol{\sigma}^{(1)}-\boldsymbol{\sigma}^{(2)}\right)+\mathcal{O}\left(M^{-2}r^0,M^{-1}r^1,M^0r^3\right)\,, \qquad (2.105)
\end{aligned}
$$

in which only four undetermined coefficients remain.

Octet Field

In a similar fashion, one can proceed to determine the most general boost transformation for the octet field. The main difference is that all center-of-mass derivatives (except for the coordinate transformations) have to be replaced by covariant derivatives in the adjoint representation $\boldsymbol{D}^{ab}=\delta^{ab}\boldsymbol{\nabla}_R-f^{abc}g\boldsymbol{A}^c$ due to the color charge of the octet field. For the singlet field there were no available operators at order M^0r^2, but for the octet there are two involving the chromoelectric field. At order $M^{-1}r^0$ there are no new terms.

At this point it is more convenient to write the boost generator in components, i.e.

$$
O^a\xrightarrow{K}O^{a\prime}=\left(\delta^{ab}-i\boldsymbol{\eta}\cdot\boldsymbol{k}_O^{ab}\right)O^b\,. \qquad (2.106)
$$

The P transformation of the boost generator in component notation is the same as in matrix notation, but the C and T transformations are slightly different. Introducing a sign factor through $(T^a)^T=(T^a)^*=(-)^aT^a$ (where the double appearance of the color index on $(-)^a$ does not imply summation), the fields in the adjoint representation transform as

$$
\begin{aligned}
&O^a\xrightarrow{C}\sigma_2(-)^aO^a\sigma_2\,, && E^a\xrightarrow{C}-(-)^aE^a\,, && B^a\xrightarrow{C}-(-)^aB^a\,, && (2.107)\\
&O^a\xrightarrow{T}\sigma_2(-)^aO^a\sigma_2\,, && E^a\xrightarrow{T}(-)^aE^a\,, && B^a\xrightarrow{T}-(-)^aB^a\,. && (2.108)
\end{aligned}
$$

So the boost generator in component notation has to transform like

$$\boldsymbol{k}_O^{ab} \xrightarrow{C} (-)^a(-)^b\sigma_2\boldsymbol{k}_O^{ab}\sigma_2\,, \qquad \boldsymbol{k}_O^{ab} \xrightarrow{T} (-)^a(-)^b\sigma_2\boldsymbol{k}_O^{ab}\sigma_2\,. \tag{2.109}$$

The transformation behavior under C can be checked by using the following identities:

$$(-)^a(-)^b\delta^{ab} = \delta^{ab}\,, \qquad (-)^a(-)^b(-)^c f^{abc} = -f^{abc}\,, \qquad (-)^a(-)^b(-)^c d^{abc} = d^{abc}\,, \tag{2.110}$$

which follow from the commutation relations of the color matrices.

Then the most general ansatz for the boost generator for octets is:

$$\begin{aligned}
\boldsymbol{k}_O^{ab} = {}& \delta^{ab}(it\boldsymbol{\nabla}_R + i\boldsymbol{R}\partial_0 + 2M\boldsymbol{R}) - \frac{k_{OD}^{(1,0)}}{4M}\boldsymbol{D}_R^{ab} + \frac{i}{8}f^{abc}k_{Oa}^{(0,2)}(\boldsymbol{r}\cdot g\boldsymbol{E}^c)\boldsymbol{r} + \frac{i}{8}f^{abc}k_{Ob}^{(0,2)}r^2 g\boldsymbol{E}^c \\
& - \frac{1}{4M}\left\{k_{Oa'}^{(1,0)}\boldsymbol{r}, (\boldsymbol{\nabla}_r\cdot\boldsymbol{D}_r^{ab})\right\} - \frac{1}{4M}\left\{k_{Oa''}^{(1,0)}(\boldsymbol{r}\cdot\boldsymbol{D}_R^{ab}), \boldsymbol{\nabla}_r\right\} - \frac{1}{4M}\left\{k_{Oa'''}^{(1,0)}\boldsymbol{r}\cdot, \boldsymbol{\nabla}_r\right\}\boldsymbol{D}_R^{ab} \\
& - \frac{1}{4M}\left\{\frac{k_{Ob}^{(1,0)}}{r^2}\boldsymbol{r}(\boldsymbol{r}\cdot\boldsymbol{D}_R^{ab})r_i, (\nabla_r)_i\right\} - \frac{ik_{Oc}^{(1,0)}}{8M}\boldsymbol{D}_R^{ab}\times\left(\boldsymbol{\sigma}^{(1)}+\boldsymbol{\sigma}^{(2)}\right) \\
& - \frac{ik_{Od''}^{(1,0)}}{8Mr^2}\left(\boldsymbol{r}\cdot\boldsymbol{D}_R^{ab}\right)\left(\boldsymbol{r}\times\left(\boldsymbol{\sigma}^{(1)}+\boldsymbol{\sigma}^{(2)}\right)\right) - \frac{ik_{Od'''}^{(1,0)}}{8Mr^2}\left((\boldsymbol{r}\times\boldsymbol{D}_R^{ab})\cdot\left(\boldsymbol{\sigma}^{(1)}+\boldsymbol{\sigma}^{(2)}\right)\right)\boldsymbol{r} \\
& - \frac{i\delta^{ab}}{8M}\left\{k_{Oa}^{(1,-1)}, \boldsymbol{\nabla}_r\times\left(\boldsymbol{\sigma}^{(1)}-\boldsymbol{\sigma}^{(2)}\right)\right\} + \frac{i\delta^{ab}}{8M}\left[\frac{k_{Ob'}^{(1,-1)}}{r^2}\left(\boldsymbol{r}\cdot\left(\boldsymbol{\sigma}^{(1)}-\boldsymbol{\sigma}^{(2)}\right)\right)\boldsymbol{r}\times, \boldsymbol{\nabla}_r\right] \\
& - \frac{i\delta^{ab}}{8M}\left\{\frac{k_{Ob''}^{(1,-1)}}{r^2}\boldsymbol{r}\times\left(\boldsymbol{\sigma}^{(1)}-\boldsymbol{\sigma}^{(2)}\right)r_i, (\nabla_r)_i\right\} + \mathcal{O}\left(M^{-2}r^0, M^{-1}r^1, M^0r^3\right)\,.
\end{aligned} \tag{2.111}$$

Again, we may perform a redefinition of the octet field through a unitary transformation $\widetilde{O}^a = \mathcal{U}_O^{ab}O^b$ with $\mathcal{U}_O = \exp[u_O]$, in order to reduce the number of undetermined coefficients in $\boldsymbol{k}_O$. For this transformation matrix u_O the same arguments apply as in the singlet case, so we write:

$$\begin{aligned}
u_O^{ab} = {}& -\frac{q_{Oa}^{(0,2)}}{32M}\left\{(\boldsymbol{r}\cdot\boldsymbol{D}_R), (\boldsymbol{r}\cdot g\boldsymbol{E})\right\}^{ab} + \frac{q_{Ob}^{(0,2)}}{32M}r^2\left\{\boldsymbol{D}_R\cdot, g\boldsymbol{E}\right\}^{ab} \\
& - \frac{1}{4M^2}\left\{q_{Oa''}^{(1,0)}(\boldsymbol{r}\cdot\boldsymbol{D}_R), (\boldsymbol{\nabla}_r\cdot\boldsymbol{D}_R)\right\}^{ab} - \frac{1}{4M^2}\left\{q_{Oa'''}^{(1,0)}\boldsymbol{r}\cdot, \boldsymbol{\nabla}_r\right\}(\boldsymbol{D}_R^2)^{ab} \\
& - \frac{1}{4M^2}\left\{\frac{q_{Ob}^{(1,0)}}{r^2}\left((\boldsymbol{r}\cdot\boldsymbol{D}_R)^2\right)^{ab}\boldsymbol{r}\cdot, \boldsymbol{\nabla}_r\right\} \\
& - \frac{iq_{Od'''}^{(1,0)}}{16M^2r^2}\left\{(\boldsymbol{r}\cdot\boldsymbol{D}_R), \left((\boldsymbol{r}\times\boldsymbol{D}_R)\cdot\left(\boldsymbol{\sigma}^{(1)}+\boldsymbol{\sigma}^{(2)}\right)\right)\right\}^{ab} \\
& + \frac{i}{8M^2}\left\{q_{Oa}^{(1,-1)}, (\boldsymbol{\nabla}_r\times\boldsymbol{D}_R^{ab})\cdot\left(\boldsymbol{\sigma}^{(1)}-\boldsymbol{\sigma}^{(2)}\right)\right\} \\
& - \frac{i}{8M^2}\left\{\frac{q_{Ob'}^{(1,-1)}}{r^2}\left(\boldsymbol{r}\cdot\left(\boldsymbol{\sigma}^{(1)}-\boldsymbol{\sigma}^{(2)}\right)\right)(\boldsymbol{r}\times\boldsymbol{D}_R^{ab})\cdot, \boldsymbol{\nabla}_r\right\} \\
& + \frac{i}{8M^2}\left\{\frac{q_{Ob''}^{(1,-1)}}{r^2}\left((\boldsymbol{r}\times\boldsymbol{D}_R^{ab})\cdot\left(\boldsymbol{\sigma}^{(1)}-\boldsymbol{\sigma}^{(2)}\right)\right)\boldsymbol{r}\cdot, \boldsymbol{\nabla}_r\right\} + \dots\,,
\end{aligned} \tag{2.112}$$

where $\{A,B\}^{ab} = A^{ab'}B^{b'b} + B^{ab'}A^{b'b}$, in which we understand $\boldsymbol{E}^{ab} = -if^{abc}\boldsymbol{E}^c$.

As in the singlet case, the new boost generator after this transformation is given by:

$$\begin{aligned}
\widetilde{\boldsymbol{k}}_O^{ab} &= \boldsymbol{k}_O^{ab} + \left[2M\boldsymbol{R}, u_O^{ab}\right] + \mathcal{O}\left(M^{-2}\right) \\
&= \boldsymbol{k}_O^{ab} - \frac{i}{8}f^{abc}q_{Oa}^{(0,2)}(\boldsymbol{r}\cdot g\boldsymbol{E}^c)\boldsymbol{r} - \frac{i}{8}f^{abc}q_{Ob}^{(0,2)}r^2 g\boldsymbol{E}^c \\
&\quad + \frac{1}{2M}\left\{q_{Oa''}^{(1,0)}\boldsymbol{r}, (\boldsymbol{\nabla}_r\cdot\boldsymbol{D}_R^{ab})\right\} + \frac{1}{2M}\left\{q_{Oa''}^{(1,0)}(\boldsymbol{r}\cdot\boldsymbol{D}_R^{ab}), \boldsymbol{\nabla}_r\right\} \\
&\quad + \frac{1}{M}\left\{q_{Oa'''}^{(1,0)}\boldsymbol{r}\cdot, \boldsymbol{\nabla}_r\right\}\boldsymbol{D}_R^{ab} + \frac{1}{M}\left\{\frac{q_{Ob}^{(1,0)}}{r^2}\boldsymbol{r}(\boldsymbol{r}\cdot\boldsymbol{D}_R^{ab})r_i, (\nabla_r)_i\right\} \\
&\quad - \frac{iq_{Od'''}^{(1,0)}}{4Mr^2}\left(\boldsymbol{r}\times\left(\boldsymbol{\sigma}^{(1)}+\boldsymbol{\sigma}^{(2)}\right)\right)(\boldsymbol{r}\cdot\boldsymbol{D}_R^{ab}) + \frac{iq_{Od'''}^{(1,0)}}{4Mr^2}\left((\boldsymbol{r}\times\boldsymbol{D}_R^{ab})\cdot\left(\boldsymbol{\sigma}^{(1)}+\boldsymbol{\sigma}^{(2)}\right)\right)\boldsymbol{r} \\
&\quad + \frac{i\delta^{ab}}{4M}\left\{q_{Oa}^{(1,-1)}, \boldsymbol{\nabla}_r\times\left(\boldsymbol{\sigma}^{(1)}-\boldsymbol{\sigma}^{(2)}\right)\right\} - \frac{i\delta^{ab}}{4M}\left[\frac{q_{Ob'}^{(1,-1)}}{r^2}\left(\boldsymbol{r}\cdot\left(\boldsymbol{\sigma}^{(1)}-\boldsymbol{\sigma}^{(2)}\right)\right)\boldsymbol{r}\times, \boldsymbol{\nabla}_r\right] \\
&\quad + \frac{i\delta^{ab}}{4M}\left\{\frac{q_{Ob''}^{(1,-1)}}{r^2}\left(\boldsymbol{r}\times\left(\boldsymbol{\sigma}^{(1)}-\boldsymbol{\sigma}^{(2)}\right)\right)r_i, (\nabla_r)_j\right\} + \mathcal{O}(M^{-2})\,. \qquad (2.113)
\end{aligned}$$

This formally gives the same relations for the transformed boost coefficients as for the singlet, with the addition of the two coefficients for the chromoelectric field terms:

$$\begin{aligned}
&\widetilde{k}_{Oa}^{(0,2)} = k_{Oa}^{(0,2)} - q_{Oa}^{(0,2)}\,, && \widetilde{k}_{Ob}^{(0,2)} = k_{Ob}^{(0,2)} - q_{Ob}^{(0,2)}\,, && \\
&\widetilde{k}_{Oa'}^{(1,0)} = k_{Oa'}^{(1,0)} - 2q_{Oa''}^{(1,0)}\,, && \widetilde{k}_{Oa''}^{(1,0)} = k_{Oa''}^{(1,0)} - 2q_{Oa''}^{(1,0)}\,, && \widetilde{k}_{Oa'''}^{(1,0)} = k_{Oa'''}^{(1,0)} - 4q_{Oa'''}^{(1,0)}\,, \\
&\widetilde{k}_{Ob}^{(1,0)} = k_{Ob}^{(1,0)} - 4q_{Ob}^{(1,0)}\,, && \widetilde{k}_{Od''}^{(1,0)} = k_{Od''}^{(1,0)} + 2q_{Od'''}^{(1,0)}\,, && \widetilde{k}_{Od'''}^{(1,0)} = k_{Od'''}^{(1,0)} - 2q_{Od'''}^{(1,0)}\,, \\
&\widetilde{k}_{Oa}^{(1,-1)} = k_{Oa}^{(1,-1)} - 2q_{Oa}^{(1,-1)}\,, && \widetilde{k}_{Ob'}^{(1,-1)} = k_{Ob'}^{(1,-1)} - 2q_{Ob'}^{(1,-1)}\,, && \widetilde{k}_{Ob''}^{(1,-1)} = k_{Ob''}^{(1,-1)} - 2q_{Ob''}^{(1,-1)}\,. \qquad (2.114)
\end{aligned}$$

Again, we choose to eliminate $\widetilde{k}_{Oa''}^{(1,0)}$, $\widetilde{k}_{Oa'''}^{(1,0)}$, $\widetilde{k}_{Ob}^{(1,0)}$, $\widetilde{k}_{Od'''}^{(1,0)}$, $\widetilde{k}_{Ob'}^{(1,-1)}$, $\widetilde{k}_{Ob''}^{(1,-1)}$, and the new terms $\widetilde{k}_{Oa}^{(0,2)}$ and $\widetilde{k}_{Ob}^{(0,2)}$, as well as fix $\widetilde{k}_{Oa}^{(1,-1)} = 1$.

Then after dropping the tilde notation, the general boost transformation is simplified as follows

$$\begin{aligned}
\boldsymbol{k}_O^{ab} &= \delta^{ab}(it\boldsymbol{\nabla}_R + i\boldsymbol{R}\partial_0 + 2M\boldsymbol{R}) - \frac{k_{OD}^{(1,0)}}{4M}\boldsymbol{D}_R^{ab} - \frac{1}{4M}\left\{k_{Oa'}^{(1,0)}\boldsymbol{r}, (\boldsymbol{\nabla}_r\cdot\boldsymbol{D}_R^{ab})\right\} \\
&\quad - \frac{ik_{Oc}^{(1,0)}}{8M}\boldsymbol{D}_R^{ab}\times\left(\boldsymbol{\sigma}^{(1)}+\boldsymbol{\sigma}^{(2)}\right) - \frac{ik_{Od''}^{(1,0)}}{8Mr^2}\left(\boldsymbol{r}\cdot\boldsymbol{D}_R^{ab}\right)\left(\boldsymbol{r}\times\left(\boldsymbol{\sigma}^{(1)}+\boldsymbol{\sigma}^{(2)}\right)\right) \\
&\quad - \frac{i\delta^{ab}}{4M}\boldsymbol{\nabla}_r\times\left(\boldsymbol{\sigma}^{(1)}-\boldsymbol{\sigma}^{(2)}\right) + \mathcal{O}\left(M^{-2}r^0, M^{-1}r^1, M^0r^3\right)\,, \qquad (2.115)
\end{aligned}$$

in which only four undetermined coefficients remain.

2.3.3 Invariance of the Lagrangian

Singlet Sector

As was shown in the previous section, the boost generators have to satisfy the commutation relation Eq. (2.28)

$$\begin{aligned}[1-i\boldsymbol{\xi}\cdot\boldsymbol{K},1-i\boldsymbol{\eta}\cdot\boldsymbol{K}]S = \Big((\boldsymbol{\xi}\times\boldsymbol{\eta})\cdot(\boldsymbol{R}\times\boldsymbol{\nabla}_R) - \left[\boldsymbol{\xi}\cdot\hat{\boldsymbol{k}}_S, \boldsymbol{\eta}\cdot\hat{\boldsymbol{k}}_S\right] \\ - i\left(\boldsymbol{\eta}\partial_0\cdot\boldsymbol{\delta}_\nabla + (\boldsymbol{\eta}\times\boldsymbol{B}^a)\cdot\boldsymbol{\delta}_E^a - (\boldsymbol{\eta}\times\boldsymbol{E}^a)\cdot\boldsymbol{\delta}_B^a\right)(\boldsymbol{\xi}\cdot\hat{\boldsymbol{k}}_S) \\ + i\left(\boldsymbol{\xi}\partial_0\cdot\boldsymbol{\delta}_\nabla + (\boldsymbol{\xi}\times\boldsymbol{B}^a)\cdot\boldsymbol{\delta}_E^a - (\boldsymbol{\xi}\times\boldsymbol{E}^a)\cdot\boldsymbol{\delta}_B^a\right)(\boldsymbol{\eta}\cdot\hat{\boldsymbol{k}}_S)\Big)S\,,\end{aligned} \tag{2.116}$$

which at leading order in $1/M$ evaluates to

$$\begin{aligned}&(\boldsymbol{\xi}\times\boldsymbol{\eta})\cdot(\boldsymbol{R}\times\boldsymbol{\nabla}_R) - \left[\boldsymbol{\xi}\cdot\hat{\boldsymbol{k}}_S, 2M\boldsymbol{\eta}\cdot\boldsymbol{R}\right] + \left[\boldsymbol{\eta}\cdot\hat{\boldsymbol{k}}_S, 2M\boldsymbol{\xi}\cdot\boldsymbol{R}\right] + \mathcal{O}(M^{-1}) \\ &= (\boldsymbol{\xi}\times\boldsymbol{\eta})\cdot(\boldsymbol{R}\times\boldsymbol{\nabla}_R) + (\boldsymbol{\xi}\times\boldsymbol{\eta})\cdot(k_{Sa'}^{(1,0)}\boldsymbol{r}\times\boldsymbol{\nabla}_r) + \frac{ik_{Sc}^{(1,0)}}{2}(\boldsymbol{\xi}\times\boldsymbol{\eta})\cdot(\boldsymbol{\sigma}^{(1)}+\boldsymbol{\sigma}^{(2)}) \\ &\quad - \frac{ik_{Sd''}^{(1,0)}}{2r^2}(\boldsymbol{\xi}\times\boldsymbol{\eta})\cdot\left(\boldsymbol{r}\times\left(\boldsymbol{r}\times\left(\boldsymbol{\sigma}^{(1)}+\boldsymbol{\sigma}^{(2)}\right)\right)\right) + \mathcal{O}(M^{-1}) \\ &\overset{!}{=} (\boldsymbol{\xi}\times\boldsymbol{\eta})\cdot\left(\boldsymbol{R}\times\boldsymbol{\nabla}_R + \boldsymbol{r}\times\boldsymbol{\nabla}_r + \frac{i}{2}\left(\boldsymbol{\sigma}^{(1)}+\boldsymbol{\sigma}^{(2)}\right)\right).\end{aligned} \tag{2.117}$$

This fixes three further coefficients: $k_{Sa'}^{(1,0)} = k_{Sc}^{(1,0)} = 1$, and $k_{Sd''}^{(1,0)} = 0$.

The last remaining coefficient $k_{SD}^{(1,0)}$ is fixed when we apply the boost transformation to the singlet sector of the Lagrangian up to $\mathcal{O}(M^{-2})$ (where we follow the notation from Ref. [58])

$$\begin{aligned}\mathcal{L}_{\text{pNRQCD}}^{(S)} = \int d^3r\,\mathrm{Tr}\Big[S^\dagger\Big(&i\partial_0 + \frac{1}{2M}\left\{c_S^{(1,-2)}, \boldsymbol{\nabla}_r^2\right\} + \frac{c_S^{(1,0)}}{4M}\boldsymbol{\nabla}_R^2 - V_S^{(0)} - \frac{V_S^{(1)}}{M} + \frac{V_{rS}}{M^2} \\ &+ \frac{V_{P^2Sa}}{8M^2}\boldsymbol{\nabla}_R^2 + \frac{1}{2M^2}\left\{V_{p^2Sb}, \boldsymbol{\nabla}_r^2\right\} + \frac{V_{L^2Sa}}{4M^2r^2}(\boldsymbol{r}\times\boldsymbol{\nabla}_R)^2 + \frac{V_{L^2Sb}}{4M^2r^2}(\boldsymbol{r}\times\boldsymbol{\nabla}_r)^2 \\ &- \frac{V_{S_{12}S}}{M^2r^2}\left(3(\boldsymbol{r}\cdot\boldsymbol{\sigma}^{(1)})(\boldsymbol{r}\cdot\boldsymbol{\sigma}^{(2)}) - r^2(\boldsymbol{\sigma}^{(1)}\cdot\boldsymbol{\sigma}^{(2)})\right) - \frac{V_{S^2S}}{4M^2}\boldsymbol{\sigma}^{(1)}\cdot\boldsymbol{\sigma}^{(2)} \\ &+ \frac{iV_{LSSa}}{4M^2}(\boldsymbol{r}\times\boldsymbol{\nabla}_R)\cdot(\boldsymbol{\sigma}^{(1)}-\boldsymbol{\sigma}^{(2)}) + \frac{iV_{LSSb}}{4M^2}(\boldsymbol{r}\times\boldsymbol{\nabla}_r)\cdot(\boldsymbol{\sigma}^{(1)}+\boldsymbol{\sigma}^{(2)})\Big)S\Big].\end{aligned} \tag{2.118}$$

The transformed Lagrangian has to be invariant up to total derivatives; omitting the original form, the extra terms are:

$$\begin{aligned}\partial_\mu\widehat{\Delta}^\mu\mathcal{L}^{(S)} = \int d^3r\,\mathrm{Tr}\Big[\boldsymbol{\eta}\cdot S^\dagger\Big(&i\left(1-c_S^{(1,0)}\right)\boldsymbol{\nabla}_R - \frac{1}{2M}\left(k_{SD}^{(1,0)} - c_S^{(1,0)}\right)\boldsymbol{\nabla}_R\partial_0 \\ &- \frac{i}{M}\left(V_{P^2Sa} + V_{L^2Sa} + \frac{1}{2}V_S^{(0)}\right)\boldsymbol{\nabla}_R + \frac{i}{Mr^2}\left(V_{L^2Sa} + \frac{r}{2}V_S^{(0)\prime}\right)\boldsymbol{r}(\boldsymbol{r}\cdot\boldsymbol{\nabla}_R) \\ &+ \frac{1}{2M}\left(V_{LSSa} + \frac{1}{2r}V_S^{(0)\prime}\right)\left(\boldsymbol{\sigma}^{(1)}-\boldsymbol{\sigma}^{(2)}\right)\times\boldsymbol{r}\Big)S\Big],\end{aligned} \tag{2.119}$$

where the prime means derivative with respect to r. None of these terms have the form of a total derivative, so all coefficients have to vanish, which gives the following constraints:

$$k_{SD}^{(1,0)} = c_S^{(1,0)} = 1\,,\quad V_{P^2Sa} = \frac{r}{2}V_S^{(0)\prime} - \frac{1}{2}V_S^{(0)}\,,\quad V_{L^2Sa} = -\frac{r}{2}V_S^{(0)\prime}\,,\quad V_{LSSa} = -\frac{1}{2r}V_S^{(0)\prime}\,. \tag{2.120}$$

These coincide with the results in the literature [58]. Note that with the last coefficient fixed the boost generator for the singlet field up to this order is exactly the same as in the $g \to 0$ limit, i.e. there are no loop corrections to any of the coefficients. Remember, however, that this form of the boost generator has been a particular choice obtained through certain field redefinitions; other choices are equally possible and may change the constraints derived above. Our choice also corresponds to the one taken in [58].

Octet Sector

The calculation of the commutator of two boosts is completely analogous to the singlet case, so also for the octet we have $k^{(1,0)}_{Oa'} = k^{(1,0)}_{Oc} = 1$ and $k^{(1,0)}_{Od''} = 0$. The only remaining boost coefficient is again $k^{(1,0)}_D$.

In [58], the octet sector of the pNRQCD Lagrangian is given as

$$
\begin{aligned}
\mathcal{L}^{(O)}_{\text{pNRQCD}} = \int d^3r\, \mathrm{Tr} \Bigg\{ O^\dagger \Bigg(& iD_0 + \frac{1}{2M}\left\{c_O^{(1,-2)}, \boldsymbol{\nabla}_r^2\right\} + \frac{c_O^{(1,0)}}{4M}\boldsymbol{D}_R^2 - V_O^{(0)} - \frac{V_O^{(1)}}{M} - \frac{V_{rO}}{M^2} \\
& + \frac{V_{P^2Oa}}{4M^2}\boldsymbol{D}_R^2 + \frac{1}{2M^2}\left\{V_{p^2Ob}, \boldsymbol{\nabla}_r^2\right\} + \frac{V_{L^2Oa}}{4M^2r^2}(\boldsymbol{r}\times\boldsymbol{D}_R)^2 + \frac{V_{L^2Ob}}{M^2r^2}(\boldsymbol{r}\times\boldsymbol{\nabla}_r)^2 \\
& - \frac{V_{S_{12}O}}{M^2r^2}\left(3\left(\boldsymbol{r}\cdot\boldsymbol{\sigma}^{(1)}\right)\left(\boldsymbol{r}\cdot\boldsymbol{\sigma}^{(2)}\right) - r^2\left(\boldsymbol{\sigma}^{(1)}\cdot\boldsymbol{\sigma}^{(2)}\right)\right) - \frac{V_{S^2O}}{4M^2}\boldsymbol{\sigma}^{(1)}\cdot\boldsymbol{\sigma}^{(2)} \\
& + \frac{iV_{LSOa}}{4M^2}(\boldsymbol{r}\times\boldsymbol{D}_R)\cdot\left(\boldsymbol{\sigma}^{(1)} - \boldsymbol{\sigma}^{(2)}\right) + \frac{iV_{LSOb}}{2M^2}(\boldsymbol{r}\times\boldsymbol{\nabla}_r)\cdot\left(\boldsymbol{\sigma}^{(1)} + \boldsymbol{\sigma}^{(2)}\right)\Bigg) O \\
& + \Bigg[O^\dagger \Bigg(\frac{V_{OO}^{(0,1)}}{2}\boldsymbol{r}\cdot g\boldsymbol{E} + \frac{iV_{OOa}^{(0,2)}}{8}\left[(\boldsymbol{r}\cdot\boldsymbol{D}_R), (\boldsymbol{r}\cdot g\boldsymbol{E})\right] + \frac{iV_{OOb}^{(0,2)}}{8}r^2\left[\boldsymbol{D}_R\cdot, g\boldsymbol{E}\right] \\
& + \frac{iV_{OOa}^{(1,0)}}{8M}\left\{\boldsymbol{\nabla}_r\cdot, \boldsymbol{r}\times g\boldsymbol{B}\right\} + \frac{c_F V_{OOb}^{(1,0)}}{2M}g\boldsymbol{B}\cdot\boldsymbol{\sigma}^{(1)} - \frac{V_{O\otimes Ob}^{(1,0)}}{2M}g\boldsymbol{B}\cdot\boldsymbol{\sigma}^{(2)} \\
& + \frac{V_{OOc}^{(1,0)}}{2Mr^2}(\boldsymbol{r}\cdot g\boldsymbol{B})\left(\boldsymbol{r}\cdot\boldsymbol{\sigma}^{(1)}\right) - \frac{V_{O\otimes Oc}^{(1,0)}}{2Mr^2}(\boldsymbol{r}\cdot g\boldsymbol{B})\left(\boldsymbol{r}\cdot\boldsymbol{\sigma}^{(2)}\right) + \frac{V_{OOd}^{(1,0)}}{2Mr}\boldsymbol{r}\cdot g\boldsymbol{E} \\
& - \frac{iV_{OO}^{(1,1)}}{8M}\{(\boldsymbol{r}\times\boldsymbol{D}_R)\cdot, g\boldsymbol{B}\} \\
& + \frac{ic_S V_{OOa}^{(2,0)}}{16M^2}\left[\boldsymbol{D}_R\times, g\boldsymbol{E}\right]\cdot\boldsymbol{\sigma}^{(1)} - \frac{iV_{O\otimes Oa}^{(2,0)}}{16M^2}\left[\boldsymbol{D}_R\times, g\boldsymbol{E}\right]\cdot\boldsymbol{\sigma}^{(2)} \\
& + \frac{iV_{OOb'}^{(2,0)}}{16M^2r^2}\left\{(\boldsymbol{r}\times\boldsymbol{D}_R)\cdot, g\boldsymbol{E}\right\}(\boldsymbol{r}\cdot\boldsymbol{\sigma}^{(1)}) - \frac{iV_{OOb''}^{(2,0)}}{16M^2r^2}\left\{\left((\boldsymbol{r}\times\boldsymbol{D}_R)\cdot\boldsymbol{\sigma}^{(1)}\right), (\boldsymbol{r}\cdot g\boldsymbol{E})\right\} \\
& - \frac{iV_{O\otimes Ob'}^{(2,0)}}{16M^2r^2}\left\{(\boldsymbol{r}\times\boldsymbol{D}_R)\cdot, g\boldsymbol{E}\right\}(\boldsymbol{r}\cdot\boldsymbol{\sigma}^{(2)}) + \frac{iV_{O\otimes Ob''}^{(2,0)}}{16M^2r^2}\left\{\left((\boldsymbol{r}\times\boldsymbol{D}_R)\cdot\boldsymbol{\sigma}^{(2)}\right), (\boldsymbol{r}\cdot g\boldsymbol{E})\right\} \\
& + \frac{1}{16M^2}\left\{V_{OOc'}^{(2,0)}(\boldsymbol{r}\cdot g\boldsymbol{E}), (\boldsymbol{\nabla}_r\cdot\boldsymbol{D}_R)\right\} + \frac{1}{16M^2}\left\{V_{OOc''}^{(2,0)}r_i g E_j, (\nabla_r)_j (D_R)_i\right\} \\
& + \frac{1}{16M^2}\left\{V_{OOc'''}^{(2,0)}r_i g E_j, (\nabla_r)_i (D_R)_j\right\} + \frac{1}{16M^2}\left\{\frac{V_{OOd}^{(2,0)}}{r^2}r_i r_j (\boldsymbol{r}\cdot g\boldsymbol{E}), (\nabla_r)_i (D_R)_j\right\} \\
& - \frac{iV_{OOe}^{(2,0)}}{8M^2r}\left\{(\boldsymbol{r}\times\boldsymbol{D}_R)\cdot, g\boldsymbol{B}\right\}\Bigg) O + c.c.\Bigg]\Bigg\}\,,
\end{aligned}
\tag{2.121}
$$

where *c.c.* refers to the charge conjugate of every term inside the angular brackets. In the terms of order $M^{-1}r^1$ and $M^{-2}r^0$ we include only those that contain a covariant derivative acting on the octet field, because otherwise they do not contribute in the boost transformation at the order we are interested in.

Note that in Ref. [58] the identity (2.97) was not used, so there a set of operators is included that is not linearly independent. In particular, there are two other potentials $V^{(2,0)}_{OOb'''}$ and $V^{(2,0)}_{O\otimes Ob'''}$, which we have chosen to neglect in order to work only with linearly independent operators. Ultimately, these potentials are found to be zero in [58] and the other constraints do not depend on them, so the results remain unchanged.

Applying the boost operation to this Lagrangian, one obtains the following extra terms, which have to vanish:

$$
\begin{aligned}
\partial_\mu \widehat{\Delta}^\mu \mathcal{L}^{(O)} = \int d^3r\, \mathrm{Tr}\Bigg\{ & O^\dagger \Bigg(i\left(1 - c_O^{(1,0)}\right)(\boldsymbol{\eta}\cdot\boldsymbol{D}_R) - \frac{1}{4M}\left(k_{OD}^{(1,0)} - c_O^{(1,0)}\right)\boldsymbol{\eta}\cdot\{D_0, \boldsymbol{D}_R\} \\
& - \frac{i}{M}\left(V_{P^2Oa} + V_{L^2Oa} + \frac{1}{2}k_{OD}^{(1,0)}V_O^{(0)}\right)(\boldsymbol{\eta}\cdot\boldsymbol{D}_R) \\
& + \frac{i}{Mr^2}\left(V_{L^2Oa} + \frac{r}{2}V_O^{(0)\prime}\right)(\boldsymbol{\eta}\cdot\boldsymbol{r})(\boldsymbol{r}\cdot\boldsymbol{D}_R) \\
& - \frac{1}{2M}\left(V_{LSOa} + \frac{1}{2r}V_O^{(0)\prime}\right)(\boldsymbol{\eta}\times\boldsymbol{r})\cdot\left(\boldsymbol{\sigma}^{(1)} - \boldsymbol{\sigma}^{(2)}\right)\Bigg) O \\
& + \Bigg[O^\dagger \Bigg(\frac{1}{2}\left(V_{OO}^{(1,1)} - V_{OO}^{(0,1)}\right)(\boldsymbol{\eta}\times\boldsymbol{r})\cdot g\boldsymbol{B} \\
& + \frac{1}{4M}\left(c_S V_{OOa}^{(2,0)} - 2c_F V_{OOb}^{(1,0)} + \frac{1}{2}V_{OO}^{(0,1)} + \frac{1}{2}\right)(\boldsymbol{\eta}\times g\boldsymbol{E})\cdot\boldsymbol{\sigma}^{(1)} \\
& - \frac{1}{4M}\left(V_{O\otimes Oa}^{(2,0)} - 2V_{O\otimes Ob}^{(1,0)} + \frac{1}{2}V_{OO}^{(0,1)} - \frac{1}{2}\right)(\boldsymbol{\eta}\times g\boldsymbol{E})\cdot\boldsymbol{\sigma}^{(2)} \\
& - \frac{1}{4Mr^2}\left(V_{OOb'}^{(2,0)} - 2V_{OOc}^{(1,0)}\right)((\boldsymbol{\eta}\times\boldsymbol{r})\cdot g\boldsymbol{E})\left(\boldsymbol{r}\cdot\boldsymbol{\sigma}^{(1)}\right) \\
& + \frac{1}{4Mr^2}\left(V_{O\otimes Ob'}^{(2,0)} - 2V_{O\otimes Oc}^{(1,0)}\right)((\boldsymbol{\eta}\times\boldsymbol{r})\cdot g\boldsymbol{E})\left(\boldsymbol{r}\cdot\boldsymbol{\sigma}^{(2)}\right) \\
& + \frac{1}{4Mr^2}\left(V_{OOb''}^{(2,0)} + \frac{r}{2}V_{OO}^{(0,1)\prime}\right)\left((\boldsymbol{\eta}\times\boldsymbol{r})\cdot\boldsymbol{\sigma}^{(1)}\right)(\boldsymbol{r}\cdot g\boldsymbol{E}) \\
& - \frac{1}{4Mr^2}\left(V_{O\otimes Ob''}^{(2,0)} + \frac{r}{2}V_{OO}^{(0,1)\prime}\right)\left((\boldsymbol{\eta}\times\boldsymbol{r})\cdot\boldsymbol{\sigma}^{(2)}\right)(\boldsymbol{r}\cdot g\boldsymbol{E}) \\
& - \frac{i}{8M}\left\{\left(V_{OOc'}^{(2,0)} + V_{OOa}^{(1,0)}\right)(\boldsymbol{r}\cdot g\boldsymbol{E}), (\boldsymbol{\eta}\cdot\boldsymbol{\nabla}_r)\right\} \\
& - \frac{i}{8M}\left\{\left(V_{OOc''}^{(2,0)} - V_{OOa}^{(1,0)} + 2\right)(\boldsymbol{\eta}\cdot\boldsymbol{r}), (\boldsymbol{\nabla}_r\cdot g\boldsymbol{E})\right\} \\
& - \frac{i}{8M}\left\{V_{OOc'''}^{(2,0)}(\boldsymbol{\eta}\cdot g\boldsymbol{E})\boldsymbol{r}\cdot, \boldsymbol{\nabla}_r\right\} - \frac{i}{8M}\left\{\frac{V_{OOd}^{(2,0)}}{r^2}(\boldsymbol{\eta}\cdot\boldsymbol{r})(\boldsymbol{r}\cdot g\boldsymbol{E})\boldsymbol{r}\cdot, \boldsymbol{\nabla}_r\right\} \\
& + \frac{1}{2Mr}\left(V_{OOe}^{(2,0)} - V_{OOd}^{(1,0)}\right)(\boldsymbol{\eta}\times\boldsymbol{r})\cdot g\boldsymbol{B}\Bigg) O + c.c.\Bigg]\Bigg\}\,. \qquad (2.122)
\end{aligned}
$$

Thus, one obtains the following constraints:

$$
\begin{aligned}
k_{OD}^{(1,0)} &= c_O^{(1,0)} = 1\,, & V_{P^2Oa} &= \frac{r}{2}V_O^{(0)\prime} - \frac{1}{2}V_O^{(0)}\,,\\
V_{L^2Oa} &= -\frac{r}{2}V_O^{(0)\prime}\,, & V_{LSOa} &= -\frac{1}{2r}V_O^{(0)\prime}\,,\\
c_S V_{OOa}^{(2,0)} &= 2c_F V_{OOb}^{(1,0)} - \frac{1}{2}V_{OO}^{(0,1)} - \frac{1}{2}\,, & V_{O\otimes Oa}^{(2,0)} &= 2V_{O\otimes Ob}^{(1,0)} - \frac{1}{2}V_{OO}^{(0,1)} + \frac{1}{2}\,,\\
V_{OOb'}^{(2,0)} &= 2V_{OOc}^{(1,0)}\,, & V_{O\otimes Ob'}^{(2,0)} &= 2V_{O\otimes Oc}^{(1,0)}\\
V_{OOb''}^{(2,0)} &= -\frac{r}{2}V_{OO}^{(0,1)\prime}\,, & V_{O\otimes Ob''}^{(2,0)} &= -\frac{r}{2}V_{OO}^{(0,1)\prime}\,,\\
V_{OOc'}^{(2,0)} &= -V_{OOa}^{(1,0)}\,, & V_{OOc''}^{(2,0)} &= V_{OOa}^{(1,0)} - 2\,,\\
V_{OOc'''}^{(2,0)} &= 0\,, & V_{OOd}^{(2,0)} &= 0\,,\\
V_{OOe}^{(2,0)} &= V_{OOd}^{(1,0)}\,, & V_{OO}^{(1,1)} &= V_{OO}^{(0,1)}\,,
\end{aligned}
\tag{2.123}
$$

which are in agreement with [58] once the linearly dependent operators are removed. Note that in [58] the same field redefinitions have been performed as in this work. Again, the boost coefficient $k_{OD}^{(1,0)}$ is fixed to unity, so the boost generator for the octet field coincides with the one expected from the $g \to 0$ limit with covariant derivatives for the center-of-mass coordinate.

Singlet-Octet Sector

Finally, moving on to the singlet-octet sector, several terms that appear in the octet-octet sector are absent due to cancellation by charge conjugate counterparts. Following [58], the Lagrangian is given by:

$$
\begin{aligned}
\mathcal{L}_{\text{pNRQCD}}^{(SO,\,h)} = \int d^3r\,\mathrm{Tr}\Bigg[S^\dagger \Bigg(& V_{SO}^{(0,1)} \boldsymbol{r}\cdot g\boldsymbol{E} + \frac{c_F V_{SOb}^{(1,0)}}{2M} g\boldsymbol{B}\cdot\left(\boldsymbol{\sigma}^{(1)} - \boldsymbol{\sigma}^{(2)}\right)\\
& + \frac{V_{SOc}^{(1,0)}}{2Mr^2}(\boldsymbol{r}\cdot g\boldsymbol{B})\left(\boldsymbol{r}\cdot\left(\boldsymbol{\sigma}^{(1)} - \boldsymbol{\sigma}^{(2)}\right)\right) + \frac{V_{SOd}^{(1,0)}}{Mr}\boldsymbol{r}\cdot g\boldsymbol{E}\\
& - \frac{i}{4M}V_{SO}^{(1,1)}\left\{(\boldsymbol{r}\times\boldsymbol{D}_R)\cdot, g\boldsymbol{B}\right\} + \frac{ic_S}{16M^2}V_{SOa}^{(2,0)}\left[\boldsymbol{D}_R\times, g\boldsymbol{E}\right]\cdot\left(\boldsymbol{\sigma}^{(1)} - \boldsymbol{\sigma}^{(2)}\right)\\
& + \frac{iV_{SOb'}^{(2,0)}}{16M^2r^2}\left\{(\boldsymbol{r}\times\boldsymbol{D}_R)\cdot, g\boldsymbol{E}\right\}\left(\boldsymbol{r}\cdot\left(\boldsymbol{\sigma}^{(1)} - \boldsymbol{\sigma}^{(2)}\right)\right)\\
& - \frac{iV_{SOb''}^{(2,0)}}{16M^2r^2}\left\{\left((\boldsymbol{r}\times\boldsymbol{D}_R)\cdot\left(\boldsymbol{\sigma}^{(1)} - \boldsymbol{\sigma}^{(2)}\right)\right), (\boldsymbol{r}\cdot g\boldsymbol{E})\right\}\\
& - \frac{iV_{SOe}^{(2,0)}}{4M^2r}\left\{(\boldsymbol{r}\times\boldsymbol{D}_R)\cdot, g\boldsymbol{B}\right\}\Bigg) O + h.c.\Bigg]\,,
\end{aligned}
\tag{2.124}
$$

where again we only include terms with covariant derivatives acting on the quarkonium fields in the order $M^{-1}r^1$ and $M^{-2}r^0$ terms, and we have neglected the linearly dependent operator with potential $V_{SOb'''}^{(2,0)}$.

Here we have included an index h to the Lagrangian, because all operators between the round brackets are hermitian. In the pure singlet or octet sectors, these are the only operators that are allowed, but in the singlet-octet sector, one may in principle also add antihermitian

operators. Instead of canceling, they give terms of the form $S^\dagger h O - O^\dagger h S$. We are not aware of any argument that would exclude such terms a priori, so we give here also the singlet-octet Lagrangian for the antihermitian operators:

$$\begin{aligned}\mathcal{L}^{(SO,\,a)}_{\rm pNRQCD} = \int d^3r\,{\rm Tr}\Bigg[S^\dagger\Bigg(&\frac{1}{2M}\left\{rV^{(1,0)}_{SOe},\boldsymbol{\nabla}_r\cdot g\boldsymbol{E}\right\}+\frac{iV^{(1,0)}_{SOf}}{2Mr}(\boldsymbol{r}\times g\boldsymbol{E})\cdot\left(\boldsymbol{\sigma}^{(1)}+\boldsymbol{\sigma}^{(2)}\right)\\
&-\frac{i}{4M^2}\left\{rV^{(2,0)}_{SOf}g\boldsymbol{B}\cdot,(\boldsymbol{\nabla}_r\times\boldsymbol{D}_R)\right\}+\frac{V^{(2,0)}_{SOg'}}{16M^2r}\left\{(\boldsymbol{r}\cdot g\boldsymbol{B}),\left(\boldsymbol{D}_R\cdot\left(\boldsymbol{\sigma}^{(1)}+\boldsymbol{\sigma}^{(2)}\right)\right)\right\}\\
&+\frac{V^{(2,0)}_{SOg''}}{16M^2r}\left\{(\boldsymbol{r}\cdot\boldsymbol{D}_R),\left(g\boldsymbol{B}\cdot\left(\boldsymbol{\sigma}^{(1)}+\boldsymbol{\sigma}^{(2)}\right)\right)\right\}\\
&+\frac{V^{(2,0)}_{SOg'''}}{16M^2r}\left(\boldsymbol{r}\cdot\left(\boldsymbol{\sigma}^{(1)}+\boldsymbol{\sigma}^{(2)}\right)\right)\left\{\boldsymbol{D}_R\cdot,g\boldsymbol{B}\right\}\Bigg)O+h.c.\Bigg]\,.\end{aligned}\tag{2.125}$$

Such terms were not considered in [58].

The extra terms after the boost transformation are the following:

$$\begin{aligned}\partial_\mu\widehat{\Delta}^\mu\mathcal{L}^{(SO,\,h)} = \int d^3r\,{\rm Tr}\Big[S^\dagger\Big(&\left(V^{(1,1)}_{SO}-V^{(0,1)}_{SO}\right)(\boldsymbol{\eta}\times\boldsymbol{r})\cdot g\boldsymbol{B}\\
&+\frac{1}{4M}\left(c_SV^{(2,0)}_{SOa}-2c_FV^{(1,0)}_{SOb}+V^{(0,1)}_{SO}\right)(\boldsymbol{\eta}\times g\boldsymbol{E})\left(\boldsymbol{\sigma}^{(1)}-\boldsymbol{\sigma}^{(2)}\right)\\
&-\frac{1}{4Mr^2}\left(V^{(2,0)}_{SOb'}-2V^{(1,0)}_{SOc}\right)((\boldsymbol{\eta}\times\boldsymbol{r})\cdot g\boldsymbol{E})\left(\boldsymbol{r}\cdot\left(\boldsymbol{\sigma}^{(1)}-\boldsymbol{\sigma}^{(2)}\right)\right)\\
&+\frac{1}{4Mr^2}\left(V^{(2,0)}_{SOb''}+rV^{(0,1)\prime}_{SO}\right)\left((\boldsymbol{\eta}\times\boldsymbol{r})\cdot\left(\boldsymbol{\sigma}^{(1)}-\boldsymbol{\sigma}^{(2)}\right)\right)(\boldsymbol{r}\cdot g\boldsymbol{E})\\
&+\frac{1}{Mr}\left(V^{(2,0)}_{SOe}-V^{(1,0)}_{SOd}\right)(\boldsymbol{\eta}\times\boldsymbol{r})\cdot g\boldsymbol{B}\Big)O+h.c.\Big]\,,\end{aligned}\tag{2.126}$$

$$\begin{aligned}\partial_\mu\widehat{\Delta}^\mu\mathcal{L}^{(SO,\,a)} = \int d^3r\,{\rm Tr}\Bigg[S^\dagger\Bigg(&\frac{1}{2M}\left\{r\left(V^{(2,0)}_{SOf}-V^{(1,0)}_{SOe}\right),(\boldsymbol{\eta}\times\boldsymbol{\nabla}_r)\cdot g\boldsymbol{B}\right\}\\
&-\frac{i}{4Mr}\left(V^{(2,0)}_{SOg'}-2V^{(1,0)}_{SOf}\right)\left(\boldsymbol{\eta}\cdot\left(\boldsymbol{\sigma}^{(1)}+\boldsymbol{\sigma}^{(2)}\right)\right)(\boldsymbol{r}\cdot g\boldsymbol{B})\\
&-\frac{i}{4Mr}\left(V^{(2,0)}_{SOg''}+2V^{(1,0)}_{SOf}\right)(\boldsymbol{\eta}\cdot\boldsymbol{r})\left(g\boldsymbol{B}\cdot\left(\boldsymbol{\sigma}^{(1)}+\boldsymbol{\sigma}^{(2)}\right)\right)\\
&-\frac{iV^{(2,0)}_{SOg'''}}{4Mr}(\boldsymbol{\eta}\cdot g\boldsymbol{B})\left(\boldsymbol{r}\cdot\left(\boldsymbol{\sigma}^{(1)}+\boldsymbol{\sigma}^{(2)}\right)\right)\Bigg)O+h.c.\Bigg]\,,\end{aligned}\tag{2.127}$$

which brings us to the constraints

$$\begin{aligned}&V^{(0,1)}_{SO}=V^{(1,1)}_{SO}\,, && c_SV^{(2,0)}_{SOa}=2c_FV^{(1,0)}_{SOb}-V^{(0,1)}_{SO}\,, && V^{(2,0)}_{SOb'}=2V^{(1,0)}_{SOc}\,,\\
&V^{(2,0)}_{SOb''}=-rV^{(0,1)\prime}_{SO}\,, && V^{(2,0)}_{SOe}=V^{(1,0)}_{SOd}\,, && V^{(2,0)}_{SOf}=V^{(1,0)}_{SOe}\,,\\
&V^{(2,0)}_{SOg'}=2V^{(1,0)}_{SOf}\,, && V^{(2,0)}_{SOg''}=-2V^{(1,0)}_{SOf}\,, && V^{(2,0)}_{SOg'''}=0\,.\end{aligned}\tag{2.128}$$

These are in agreement with [58] as well, after performing the field redefinitions, except for the new potentials $V^{(1,0)}_{SOe}$, $V^{(1,0)}_{SOf}$, $V^{(2,0)}_{SOf}$, $V^{(2,0)}_{SOg'}$, $V^{(2,0)}_{SOg''}$, and $V^{(2,0)}_{SOg'''}$.

Chapter 3

Hybrid Quarkonium with Effective Field Theories

3.1 Introduction

After discussing the conceptional issues of hidden symmetries in EFTs in the previous chapter, we now want to turn our attention towards the application of EFTs to the study of exotics, which is of great relevance as we have argued in the beginning of this work. The effective theories discussed in the previous chapter were instrumental in providing a well defined theoretical framework for the study of heavy quarkonia away from threshold [9, 10, 35, 64–66]. Also in the case of exotic quarkonia, the mass scale can be considered larger than any other scale of the system, so one may integrate it out and arrive at NRQCD. However, the second step, i.e. arriving at an effective field theory of the type of pNRQCD, whose matching coefficients are the interaction potentials and the leading order dynamical equation is of the Schrödinger type, is more difficult.

While in the case of quarkonium systems away from the threshold a dynamically generated gap exists [35, 64–66], allowing us to integrate out the other degrees of freedom, when we consider quarkonium systems at or above the strong decay threshold, this is no longer the case. There is no mass gap between the heavy quarkonium and the creation of a heavy-light pair or a heavy quark pair with gluonic excitations. Thus, constructing the effective field theory entails considering, besides the heavy quark operators, all gauge invariant operators containing light quarks, heavy quarks, and excited glue operators, e.g. pions, some heavy-light mesons, quarkonium hybrids, and glueballs. We discussed in the beginning how phenomenological models just pick up some of these possible degrees of freedom and attach to them some phenomenological interaction. In an effective field theory description, one should identify an appropriate expansion parameter and establish a power counting weighting the operators. This is, at the moment, still difficult.

In this chapter we restrict ourselves to considering a heavy quark, a heavy antiquark, and excited glue degrees of freedom, aiming at a description of heavy quarkonium hybrids under some special conditions. Heavy quarkonium hybrids (for a review see e.g. [67]) have traditionally been described in models like the flux tube model [68, 69], the bag model [70], the constituent gluon model [71], or in the so-called Born-Oppenheimer (BO) approximation applied to QCD [67, 72, 73]. The adiabatic BO approximation has been the standard method to describe the interaction between electrons and nuclei in molecules bound by electromagnetism

since the early days of quantum mechanics [74, 75] up to now [76]. The BO approximation assumes that the lighter electrons adjust adiabatically to the motion of the heavier nuclei. It exploits the fact that the masses of the nuclei are much larger than the electron masses and, consequently, the time scales for the dynamics of the two types of particles are very different. It entails no restriction on the strength of the coupling between the slow and the fast degrees of freedom. In concrete terms, the BO approximation provides a method to obtain the molecular energies by solving the Schrödinger equation for the nuclei with a potential given by the electronic static energies at fixed nuclei positions. In particular, in the case of the diatomic molecule the electronic static energies turn out to be labeled by molecular quantum numbers corresponding to the symmetries of the diatomic molecular system.

This procedure is rooted in the existence of two classes of degrees of freedom, the "fast" and "slow" ones, and in the symmetries of the diatomic molecular system. This is the reason why the same framework can be used to describe systems of different nature but with similar characteristics. This turns out to be the case for heavy quarkonium hybrids, systems formed by a heavy quark, a heavy antiquark, and excited glue. The BO approximation has been used in this case, identifying the slow and fast degrees of freedom with the heavy quark-antiquark pair and the gluons, respectively [67, 72, 73]. In the static limit the quark and the antiquark serve as color source and sink at distance $\boldsymbol{r}$, and the gluonic field arranges itself in configurations described by the quantum numbers fixed by the symmetry of the system. The gluonic dynamics are, however, collective and non-perturbative. Nevertheless, the gluonic static energies (that are the analog of the electronic static energies) have been extracted from the large time behavior of lattice evaluations of generalized quark-antiquark Wilson loops at fixed spatial distance with initial and final states of the appropriate symmetry [72, 73, 77–82]. This method provides, in principle, these gluonic static energies, but does not provide the gluonic wave functions.

Then, relying on a kind of BO approximation, the gluonic static energies have been introduced as potentials in a Schrödinger-like equation [75] and some level structure has been obtained [73, 83]. The structure of the hybrid multiplets has also been discussed in Ref. [17, 84, 85] using the BO approximation and complementary information from the lattice. These works relied on the adiabatic and single channel BO approximation, meaning respectively that only the static potential and no mixing between different static energies have been considered. To our knowledge, up to now no analytical description of quarkonium hybrids has been worked out directly from QCD by constructing an effective field theory that realizes the physical scale hierarchy typical of the system.[1] This is what we address in the present chapter.

This chapter is organized as follows. In section 3.2 we introduce the Non-Relativistic QCD Hamiltonian and discuss the description of the heavy quarkonium hybrid systems in NRQCD in the static limit, defining the Fock states, their symmetries, and the corresponding static energies. In section 3.3 we give the same characterization using potential NRQCD, i.e. integrating out the soft scale of the momentum transfer and in case multipole expanding.

In particular, we match the NRQCD states and Hamiltonian to the corresponding objects in pNRQCD. In this way, glueballs and gluelumps naturally emerge in pNRQCD, where the gluelumps are defined as the color singlet combination of an octet color source coupled to a gluonic field. The hybrid static potentials appear as matching coefficients of pNRQCD. The higher degree of symmetry of the lower energy EFT induces a pattern of degeneracy in the gluelump multiplets.

[1] This refers to the hybrid spectroscopy. Applications of NRQCD to hybrid production can be found in [86].

In section 3.4 we introduce existing lattice evaluations of the hybrid static energies and we relate them to the definitions and the discussion given in the previous sections. In section 3.5 we add the first correction to the static limit, introducing operators of order $1/m$ in NRQCD and pNRQCD. This allows us to obtain the appropriate Schrödinger equations as dynamical equations in pNRQCD. At this time we still neglect the spin. We work out the radial Schrödinger equations coupling the Σ_u^- and the Π_u gluonic states (due to the so-called Λ-doubling term) in detail, as these will generate all the lowest mass hybrid multiplets. We characterize the hybrid multiplets by their J^{PC} quantum numbers, and we discuss the relation with the pattern of hybrid multiplets obtained in the BO approximation and other approaches.

In section 3.6 we solve the Schrödinger equation to get the masses of the predicted hybrid multiplets. The static potentials appearing in the Schrödinger equation have been defined in pNRQCD in section 3.3, they depend in the short range on two non-perturbative parameters. We fix the first one from lattice determinations of the gluelump mass, and we extract the second from a fit to the gluonic static energies. Then, we define an appropriate renormalon-free scheme (RS) and we obtain the heavy quarkonium hybrid masses for $c\bar{c}$, $b\bar{c}$, and $b\bar{b}$ systems.

In section 3.7 we compare our results for hybrid mass multiplets to the existing experimental candidates and to results obtained using the BO approximation, direct lattice computations, and QCD sum rules. The appendices contain detailed information about the symmetry of the static system (appendix A.1), the RS scheme (appendix A.2), the derivation of the radial Schrödinger equation (appendix A.3), and the numerical solution of coupled Schrödinger equations (appendix A.4).

3.2 Static NRQCD: Symmetries of the Static System and Definition of the Gluonic Static Energies

We are considering a bound system made by a heavy quark Q, a heavy antiquark $\bar{Q}$ and some gluonic excitations: this we will generically call a heavy hybrid state.[2] Since the quark mass m_Q is much larger than the typical hadronic scale $\Lambda_{\rm QCD}$, we can use NRQCD [30, 32] to describe such a system. The Hamiltonian of NRQCD for the one-quark-one-antiquark sector of the Fock space reads

$$H_{\rm NRQCD} = H^{(0)} + \frac{1}{m_Q} H^{(1,0)} + \frac{1}{m_{\bar{Q}}} H^{(0,1)} + \dots \,, \tag{3.1}$$

$$H^{(0)} = \int d^3x \, \frac{1}{2} \left(\boldsymbol{E}^a \cdot \boldsymbol{E}^a + \boldsymbol{B}^a \cdot \boldsymbol{B}^a \right) - \sum_{l=1}^{n_f} \int d^3x \, \bar{q}_l \, i\boldsymbol{D} \cdot \boldsymbol{\gamma} \, q_l \,, \tag{3.2}$$

$$H^{(1,0)} = -\frac{1}{2} \int d^3x \, \psi^\dagger \left(\boldsymbol{D}^2 + c_F \, \boldsymbol{\sigma} \cdot g\boldsymbol{B} \right) \psi \,, \tag{3.3}$$

$$H^{(0,1)} = \frac{1}{2} \int d^3x \, \chi^\dagger \left(\boldsymbol{D}^2 + c_F \, \boldsymbol{\sigma} \cdot g\boldsymbol{B} \right) \chi \,, \tag{3.4}$$

where we explicitly allowed for the heavy quark and the antiquark to have different masses m_Q and $m_{\bar{Q}}$. The matching coefficient c_F is equal to one up to loop corrections of order $\alpha_{\rm s}$. The

[2] Usually the term hybrid identifies systems where $Q\bar{Q}$ is in a color octet configuration. In the present treatment the distinction between this type of hybrid and $Q\bar{Q}$ in a color singlet state plus a glueball is often irrelevant, therefore we will make it only when necessary.

physical states are constrained to satisfy the Gauss law[3]

$$(\boldsymbol{D}\cdot\boldsymbol{E})^a\,|\text{phys}\rangle = g\Big(\psi^\dagger T^a\psi + \chi^\dagger T^a\chi + \sum_{l=1}^{n_f}\bar{q}_l\gamma^0 T^a q_l\Big)|\text{phys}\rangle\,. \tag{3.5}$$

Even though we include the light quarks here in the Hamiltonian and in the Gauss law, we will not consider them as external dynamical sources in the rest of this chapter, in the sense that we exclude excitations with nonzero isospin,[4] transitions through light mesons, or decays into heavy-light mesons, but we still allow for them to appear in the form of sea quarks, as in light quark loops in perturbation theory or unquenched lattice calculations. The lowest gluonic excitations are stable under these conditions, since the only remaining transitions require the emission of a glueball, and this is only possible if the mass gap between initial and final state is larger than the glueball mass.

In the static limit $m_Q,\, m_{\bar{Q}} \to \infty$ we have

$$H_{\text{NRQCD}} = H^{(0)}\,, \tag{3.6}$$

which still contains the kinetic terms associated to the gluons, while the kinetic terms of the heavy quarks vanish. In the static limit the one-quark–one-antiquark sector of the Fock space is spanned by [35, 64, 65]

$$|\underline{n};\boldsymbol{x}_1,\boldsymbol{x}_2\rangle^{(0)} = \psi^\dagger(\boldsymbol{x}_1)\chi(\boldsymbol{x}_2)|n;\boldsymbol{x}_1,\boldsymbol{x}_2\rangle^{(0)}, \qquad \forall \boldsymbol{x}_1,\boldsymbol{x}_2\,, \tag{3.7}$$

where $|\underline{n};\boldsymbol{x}_1,\boldsymbol{x}_2\rangle^{(0)}$ is a gauge-invariant eigenstate of $H^{(0)}$ (defined up to a phase and satisfying the Gauss law) with energy $E_n^{(0)}(\boldsymbol{x}_1,\boldsymbol{x}_2)$; $|n;\boldsymbol{x}_1,\boldsymbol{x}_2\rangle^{(0)}$ encodes the purely gluonic content of the state, and it is annihilated by $\chi^\dagger(\boldsymbol{x})$ and $\psi(\boldsymbol{x})$ for any $\boldsymbol{x}$. It transforms like $3_{\boldsymbol{x}_1}\otimes 3^*_{\boldsymbol{x}_2}$ under color $SU(3)$. The normalizations are taken as follows

$${}^{(0)}\langle n;\boldsymbol{x}_1,\boldsymbol{x}_2|m;\boldsymbol{x}_1,\boldsymbol{x}_2\rangle^{(0)} = \delta_{nm}\,, \tag{3.8}$$

$${}^{(0)}\langle \underline{n};\boldsymbol{x}_1,\boldsymbol{x}_2|\underline{m};\boldsymbol{y}_1,\boldsymbol{y}_2\rangle^{(0)} = \delta_{nm}\delta^{(3)}(\boldsymbol{x}_1-\boldsymbol{y}_1)\delta^{(3)}(\boldsymbol{x}_2-\boldsymbol{y}_2)\,. \tag{3.9}$$

Notice that since $H^{(0)}$ does not contain any heavy fermion field, $|n;\boldsymbol{x}_1,\boldsymbol{x}_2\rangle^{(0)}$ itself is also an eigenstate of $H^{(0)}$ with energy $E_n^{(0)}(\boldsymbol{x}_1,\boldsymbol{x}_2)$. We have made it explicit that the positions $\boldsymbol{x}_1$ and $\boldsymbol{x}_2$ of the quark and antiquark, respectively, are good quantum numbers for the static solution $|\underline{n};\boldsymbol{x}_1,\boldsymbol{x}_2\rangle^{(0)}$, while n generically denotes the remaining quantum numbers.

In static NRQCD, the gluonic excitations between static quarks have the same symmetries as the diatomic molecule [75]. In the center-of-mass system, these correspond to the symmetry group $D_{\infty h}$ (substituting the parity operation by CP). According to that symmetry, the mass eigenstates are classified in terms of the angular momentum along the quark-antiquark axis ($\Lambda = 0,1,2,\dots$, to which one gives the traditional names $\Sigma,\Pi,\Delta,\dots$), CP (g for even or u for odd), and the reflection properties with respect to a plane that passes through the quark-antiquark axis (+ for even or − for odd). Only the Σ states are not degenerate with respect to the reflection symmetry. See appendix A.1 for more details.

[3] Since $\boldsymbol{\Pi}^a = \boldsymbol{E}^a + O(1/m^2)$ we use the chromoelectric field $\boldsymbol{E}^a$ instead of the canonical momentum $\boldsymbol{\Pi}^a$ here and in the Hamiltonian above.

[4] States induced by the inclusion of these light degrees of freedom have been discussed in the BO approximation in [17, 84, 85].

Translational invariance implies that $E_n^{(0)}(\boldsymbol{x}_1, \boldsymbol{x}_2) = E_n^{(0)}(r)$, where $\boldsymbol{r} = \boldsymbol{x}_1 - \boldsymbol{x}_2$. This means that the gluonic static energies are functions of r and of the only other scale of the system in the static limit, Λ_{QCD}. The ground-state energy $E_{\Sigma_g^+}^{(0)}(r)$ is associated to the static quark-antiquark energy, while the other gluonic static energies $E_n^{(0)}(r)$, $n \neq 0$, are associated to gluonic excitations between static quarks. Following the analogy with the diatomic molecule, the $E_n^{(0)}(r)$ play the same role as the electronic static energies. However, in the present case they are non-perturbative quantities and can be obtained in lattice QCD from generalized static Wilson loops in the limit of large interaction times T [72, 73, 77–82]

Since the static energies are eigenvalues of the static Hamiltonian, one can exploit the following relation:

$$^{(0)}\langle \underline{n}; \boldsymbol{x}_1, \boldsymbol{x}_2, T/2 |\, \underline{n}; \boldsymbol{x}_1, \boldsymbol{x}_2, -T/2\rangle^{(0)} = \mathcal{N} \exp\left[-iE_n^{(0)}(r)\, T\right] , \tag{3.10}$$

where $\mathcal{N} = \left[\delta^{(3)}(\mathbf{0})\right]^2$ is a normalization constant following from (3.9). Since the static states $|\underline{n}; \boldsymbol{x}_1, \boldsymbol{x}_2\rangle^{(0)}$ form a complete basis, any state $|X_n\rangle$ can be written as an expansion in them:

$$|X_n\rangle = c_n\, |\underline{n}; \boldsymbol{x}_1, \boldsymbol{x}_2\rangle^{(0)} + c_{n'}\, |\underline{n}'; \boldsymbol{x}_1, \boldsymbol{x}_2\rangle^{(0)} + \dots . \tag{3.11}$$

From Eq. (3.10), it then follows

$$\langle X_n, T/2 | X_n, -T/2\rangle = \mathcal{N}|c_n|^2 \exp\left[-iE_n^{(0)}(r)\, T\right] + \mathcal{N}|c_{n'}|^2 \exp\left[-iE_{n'}^{(0)}(r)\, T\right] + \dots . \tag{3.12}$$

For large T the exponentials will be highly oscillatory, or in the Euclidean time of lattice QCD highly suppressed, so such a correlator will be dominated by the lowest static energy. This allows us to obtain the lowest static energies without knowing the static states explicitly

$$E_n^{(0)}(r) = \lim_{T\to\infty} \frac{i}{T} \ln\langle X_n, T/2 | X_n, -T/2\rangle . \tag{3.13}$$

The only condition that $|X_n\rangle$ has to satisfy is that it needs to have a nonvanishing overlap with the static state, $c_n \neq 0$. This can be ensured by requiring $|X_n\rangle$ to have the same quantum numbers n as the static state. Doing this also allows us to not only get the ground state energy, but also the lowest static energy for any set of excited quantum numbers n, because, if the quantum numbers of $|X_n\rangle$ are fixed, then it can only have an overlap with static states of the same quantum numbers.

A convenient choice for these $|X_n\rangle$ states gives the static energies in terms of Wilson loops, so we define

$$|X_n\rangle = \chi(\boldsymbol{x}_2)\phi(\boldsymbol{x}_2, \boldsymbol{R}) T^a P_n^a(\boldsymbol{R}) \phi(\boldsymbol{R}, \boldsymbol{x}_1)\psi^\dagger(\boldsymbol{x}_1)|\mathrm{vac}\rangle . \tag{3.14}$$

Here the strings $\phi(\boldsymbol{x}_2, \boldsymbol{x}_1)$ are Wilson lines from $\boldsymbol{x}_1$ to $\boldsymbol{x}_2$, which are defined in general as

$$\phi(x_2, x_1) = \mathcal{P} \exp\left[-ig \int_{x_1}^{x_2} dx^\mu\, A_\mu(x)\right] , \tag{3.15}$$

where $\mathcal{P}$ denotes the path ordering operator. By $|\mathrm{vac}\rangle$ we mean the NRQCD vacuum, and P_n is some gluonic operator that generates the right quantum numbers n. A list of possible operators P_n is given in Table 3.1. The large time correlator of these states is given by a static Wilson loop with insertions of P_n in the strings at the center-of-mass. These generalized static Wilson loops are in principle the same quantities as those that are used to obtain the gluonic

static energies on the lattice, but with suitable lattice definitions for the operators P_n and allowing for further manipulations like smearing. For more details see section 3.4.

For the ground state energy $E^{(0)}_{\Sigma_g^+}(r)$ one has to insert a color-neutral gluonic operator with J^{PC} quantum numbers 0^{++} instead of $T^a P^a_n$. For the simplest choice, i.e. the unit matrix, this then coincides with the usual static Wilson loop without insertions and gives the quark-antiquark static energy. One can also replace $T^a P^a_n$ by a color-neutral gluonic operator with excited J^{PC} quantum numbers. In this case one selects the lowest mass singlet plus glueball states consistent with those J^{PC} quantum numbers. It is possible to get additional information about and a characterization of these gluonic static energies by using the lower energy effective field theory called pNRQCD.

3.3 Static pNRQCD: Characterization of the Gluonic Static Energies at Short Distances and Form of the Potentials

In this section we discuss how it is possible to obtain a model independent characterization of the gluonic static energies at short distance and a definition of the hybrid potential using the low-energy effective field theory called pNRQCD [9, 10].

In the static limit and at leading order in the multipole expansion, the pNRQCD Hamiltonian is:

$$\mathcal{H}^{(0)} = \int d^3R\, d^3r\, \left(V_s(r) S^\dagger(\boldsymbol{r},\boldsymbol{R}) S(\boldsymbol{r},\boldsymbol{R}) + V_o(r) O^{a\,\dagger}(\boldsymbol{r},\boldsymbol{R}) O^a(\boldsymbol{r},\boldsymbol{R})\right) + \mathcal{H}_{YM} + \mathcal{O}(r)\,. \quad (3.16)$$

We will use the symbol $\mathcal{H}$ to distinguish pNRQCD Hamiltonians from the NRQCD symbol H. We assume that the theory has been quantized in an $A^a_0 = 0$ gauge for simplicity. At leading order in the multipole expansion, the singlet and octet degrees of freedom decouple, but the octet is still coupled to gluons because of the Gauss law. $V_s(r)$ and $V_o(r)$ are pNRQCD matching coefficients corresponding to the static quark-antiquark potential in a singlet and in an octet color configuration respectively (referred to as $V^{(0)}_{S/O}$ in chapter 2). These potential terms are generated by soft gluons, which are still dynamical in NRQCD but integrated out in pNRQCD, so their effect has to be included explicitly in the Hamiltonian.

$\mathcal{H}_{YM}$ has the same form as the pure Yang-Mills plus light-quark part of the NRQCD Hamiltonian given in Eq. (3.2), but all fields are now understood as ultrasoft. The same conditions on the light quarks as discussed in the previous chapter also apply here. The inclusion or omissions of light quarks as sea quarks seems not to critically affect the pattern of the lowest hybrid masses. This is indicated by the few existing unquenched lattice calculations of the gluelump masses [87] and static energies [82].

In the $r \to 0$ limit extra symmetries for the gluonic excitations between static quarks appear. The glue dynamics no longer involve the relative coordinate $\boldsymbol{r}$, in particular, there is no longer a special direction dictated by the quark-antiquark axis. Therefore, the glue associated with a gluonic excitation between static quarks acquires a spherical symmetry. So in the center-of-mass system gluonic excitations between static quarks are classified according to representations of $\mathrm{O}(3) \otimes \mathrm{C}$ [9], as opposed to the $D_{\infty h}$ group in NRQCD. We will indicate these quantum numbers by K^{PC}, where $\boldsymbol{K}$ is the angular momentum operator of the gluons.

Accordingly, in the short distance limit the static states have to be given through glueball and gluelump operators, which we will call G and G^a respectively. While a gluelump itself consists of the color singlet combination of a color octet source with gluons, here we will always use the term "gluelump operator" to refer only to the gluonic operator, since the source will always be given by the quarkonium octet field. The glueball and gluelump operators are normalized as

$$\langle 0|G_{m,\,i}(\boldsymbol{R})G_{n,\,j}(\boldsymbol{R})|0\rangle = \delta_{mn}\delta_{ij}\,, \quad \text{and} \quad \langle 0|G^a_{m,\,i}(\boldsymbol{R})G^b_{n,\,j}(\boldsymbol{R})|0\rangle = \frac{1}{8}\delta_{mn}\delta_{ij}\delta^{ab}\,. \tag{3.17}$$

Here the operators are assumed to be real. The first indices m and n label different types of glueballs or gluelumps, the second indices i and j label the different components of the respective K^{PC} representation.

We can then match the eigenstates of the static NRQCD Hamiltonian to pNRQCD through

$$|\underline{n};\boldsymbol{x}_1,\boldsymbol{x}_2\rangle^{(0)} \mathrel{\tilde{=}} \left(S^\dagger(\boldsymbol{r},\boldsymbol{R})\,\hat{n}_i\;G_{n,\,i}(\boldsymbol{R}) + \mathcal{O}(r)\right)|0\rangle \tag{3.18}$$

for the singlet plus glueball states and

$$|\underline{n};\boldsymbol{x}_1,\boldsymbol{x}_2\rangle^{(0)} \mathrel{\tilde{=}} \left(O^{a\,\dagger}(\boldsymbol{r},\boldsymbol{R})\,\hat{n}_i\;G^a_{n,\,i}(\boldsymbol{R}) + \mathcal{O}(r)\right)|0\rangle \tag{3.19}$$

for the gluelump states, where $\hat{n}$ is some unit projection vector that fixes the $D_{\infty h}$ quantum numbers. Higher order terms in the multipole expansion will also be operators of this form, so the states will no longer be purely singlet plus glueball or gluelump, but a combination of all of these states with the right $D_{\infty h}$ quantum numbers. We use the symbol $\mathrel{\tilde{=}}$ to read "matches to", meaning that, although the states or operators on both sides are defined in different Fock spaces, calculating amplitudes in either theory gives the same results. In this case the matching condition is that acting with the static Hamiltonian of either theory on the respective state gives the same static energy.

Since the projection vector $\hat{n}$ does not influence the static energy at leading order in the multipole expansion, several static energies are degenerate in the short distance limit $r \ll 1/\Lambda_{\rm QCD}$. We can see this for the gluelump states by calculating that

$$\begin{aligned} H^{(0)}\,|\underline{n};\boldsymbol{x}_1,\boldsymbol{x}_2\rangle \mathrel{\tilde{=}} & \left[\int d^3R'\,d^3r'\,V_o(r)O^{a'\,\dagger}(\boldsymbol{r}',\boldsymbol{R}')O^{a'}(\boldsymbol{r}',\boldsymbol{R}'),O^{a\,\dagger}(\boldsymbol{r},\boldsymbol{R})\right]\,\hat{n}_i\,G^a_{n,\,i}(\boldsymbol{R})\,|0\rangle \\ & + O^{a\,\dagger}(\boldsymbol{r},\boldsymbol{R})\,\hat{n}_i\,\left[\mathcal{H}_{YM},G^a_{n,\,i}(\boldsymbol{R})\right]|0\rangle + \mathcal{O}(r) \\ = & \left(V_o(r)+\Lambda_H+\mathcal{O}\left(r^2\right)\right)\left(O^{a\,\dagger}(\boldsymbol{r},\boldsymbol{R})\,\hat{n}_i\,G^a_{n,\,i}(\boldsymbol{R})+\mathcal{O}(r)\right)|0\rangle\,. \end{aligned} \tag{3.20}$$

For the singlet plus glueball states the calculation goes analogously. The glueball or gluelump mass Λ_H is the energy eigenvalue of the states generated by G or G^a under the Yang-Mills Hamiltonian. It depends on n but it is the same for any component of G or G^a, so the projections have no influence on the leading order of the static energy. This approximate degeneracy for small r is a direct consequence of the extension of the $D_{\infty h}$ symmetry group to $\mathrm{O}(3)\otimes\mathrm{C}$.

The glueball and gluelump masses Λ_H are well defined as eigenvalues of the Yang-Mills Hamiltonian, however, the operators that create the corresponding eigenstates are unknown. This situation is similar to the previous section, where it is also unknown how to express the exact static NRQCD states $|\underline{n};\boldsymbol{x}_1,\boldsymbol{x}_2\rangle^{(0)}$ in terms of NRQCD fields. So one can use the same approach here to determine the values of Λ_H: one uses operators with the same quantum

Λ_η^σ	K^{PC}	P^a
Σ_u^-	1^{+-}	$\hat{\boldsymbol{r}}\cdot\boldsymbol{B}$, $\hat{\boldsymbol{r}}\cdot(\boldsymbol{D}\times\boldsymbol{E})$
Π_u	1^{+-}	$\hat{\boldsymbol{r}}\times\boldsymbol{B}$, $\hat{\boldsymbol{r}}\times(\boldsymbol{D}\times\boldsymbol{E})$
$\Sigma_g^{+\prime}$	1^{--}	$\hat{\boldsymbol{r}}\cdot\boldsymbol{E}$, $\hat{\boldsymbol{r}}\cdot(\boldsymbol{D}\times\boldsymbol{B})$
Π_g	1^{--}	$\hat{\boldsymbol{r}}\times\boldsymbol{E}$, $\hat{\boldsymbol{r}}\times(\boldsymbol{D}\times\boldsymbol{B})$
Σ_g^-	2^{--}	$(\hat{\boldsymbol{r}}\cdot\boldsymbol{D})(\hat{\boldsymbol{r}}\cdot\boldsymbol{B})$
Π_g'	2^{--}	$\hat{\boldsymbol{r}}\times((\hat{\boldsymbol{r}}\cdot\boldsymbol{D})\boldsymbol{B}+\boldsymbol{D}(\hat{\boldsymbol{r}}\cdot\boldsymbol{B}))$
Δ_g	2^{--}	$(\hat{\boldsymbol{r}}\times\boldsymbol{D})^i(\hat{\boldsymbol{r}}\times\boldsymbol{B})^j+(\hat{\boldsymbol{r}}\times\boldsymbol{D})^j(\hat{\boldsymbol{r}}\times\boldsymbol{B})^i$
Σ_u^+	2^{+-}	$(\hat{\boldsymbol{r}}\cdot\boldsymbol{D})(\hat{\boldsymbol{r}}\cdot\boldsymbol{E})$
Π_u'	2^{+-}	$\hat{\boldsymbol{r}}\times((\hat{\boldsymbol{r}}\cdot\boldsymbol{D})\boldsymbol{E}+\boldsymbol{D}(\hat{\boldsymbol{r}}\cdot\boldsymbol{E}))$
Δ_u	2^{+-}	$(\hat{\boldsymbol{r}}\times\boldsymbol{D})^i(\hat{\boldsymbol{r}}\times\boldsymbol{E})^j+(\hat{\boldsymbol{r}}\times\boldsymbol{D})^j(\hat{\boldsymbol{r}}\times\boldsymbol{E})^i$

Table 3.1: Gluonic excitation operators at leading order in the multipole expansion in pNRQCD up to mass dimension 3; $\hat{\boldsymbol{r}}$ denotes the unit vector in the direction of the quark-antiquark distance $\boldsymbol{r}$. Different projections of the same fields correspond to different $D_{\infty h}$ representations, which are degenerate in the small distance limit. The cross product with $\hat{\boldsymbol{r}}$ has two linearly independent components, which correspond to the two components of $\Lambda \geq 1$ representations of $D_{\infty h}$; the same applies for the symmetric tensor operators of the Δ representations. Note that the K^{PC} quantum numbers refer only to the gluon fields, not the transformation properties of $\hat{\boldsymbol{r}}$, which is P and C odd. The Σ_g^+ is not shown since it corresponds to the ground state. This table is taken from [9].

numbers as G or G^a and projects out the lowest energy eigenvalue through the large time limit.

The NRQCD states $|X_n\rangle$ defined in (3.14) match in pNRQCD at leading order in the multipole expansion to

$$|X_n\rangle \stackrel{\sim}{=} \left(Z_n(r)\, O^{a\,\dagger}(\boldsymbol{r},\boldsymbol{R}) P_n^a(\hat{\boldsymbol{r}},\boldsymbol{R}) + \mathcal{O}(r)\right)|0\rangle\,. \tag{3.21}$$

The matching constant Z_n accounts for effects at the scale $1/r$, which have been integrated out in pNRQCD, and so it depends on r in a non-analytic way. However, it gives a vanishing term in the large time correlator (3.13), so it has no influence on the static energies. Table 3.1 shows a set of convenient gluon operators P_n^a corresponding to the lowest hybrid quantum numbers. The expected pattern of degeneracies in the short distance limit also can be read off from this table:

$$\begin{aligned} \Sigma_u^- &\sim \Pi_u\,, & \Sigma_g^- &\sim \Pi_g' \sim \Delta_g\,, \\ \Sigma_g^{+\prime} &\sim \Pi_g\,, & \Sigma_u^+ &\sim \Pi_u' \sim \Delta_u\,, \end{aligned} \tag{3.22}$$

where a prime indicates an excited state [9] (see also [88]).

The large time correlators are then given by

$$\langle X_n, T/2 | X_n, -T/2\rangle = \mathcal{N} e^{-iV_o(r)T} \langle 0| P_n^a(T/2)\phi_A^{ab}(T/2,-T/2) P_n^b(-T/2)|0\rangle + \mathcal{O}\left(r^2\right)\,. \tag{3.23}$$

The temporal Wilson line in the gluonic correlator ensures the gauge invariance of the expression. In $A_0^a = 0$ gauges, which we assumed in the Hamiltonian, it can be replaced by a

Kronecker delta, but in other gauges it is needed. The gluonic correlator can only be evaluated non-perturbatively, since it contains no physical scale except for $\Lambda_{\rm QCD}$, but on general grounds we can argue that

$$\langle 0|P_n^a(T/2)\phi_A^{ab}(T/2,-T/2)P_n^b(-T/2)|0\rangle = |c_n|^2 e^{-i\Lambda_H T} + |c_{n'}|^2 e^{-i\Lambda_{H'} T} + \dots\,, \tag{3.24}$$

so that we achieve the following matching condition between the static energy $E_n^{(0)}(r)$ in NRQCD and the static potential $V_o(r)$ in pNRQCD [cf. Eq. (3.13)]

$$E_n^{(0)}(r) = \lim_{T\to\infty} \frac{i}{T} \ln\langle X_n, T/2|X_n, -T/2\rangle = V_o(r) + \Lambda_H + \mathcal{O}\left(r^2\right)\,. \tag{3.25}$$

Again, for the singlet plus glueball states the calculation is analogous. The ground state corresponds to a singlet without a glueball operator, so

$$E_{\Sigma_g^+}^{(0)}(r) = V_s(r) + \mathcal{O}\left(r^2\right)\,. \tag{3.26}$$

At small distances, $r \ll 1/\Lambda_{\rm QCD}$, V_s and V_o can be calculated perturbatively. They are known at three loops with some partial results at four loops [89–95]. For a detailed comparison of V_s to the lattice data in the short range, see [96–98].

Equations (3.25) and (3.26) can be systematically improved by calculating higher orders in the multipole expansion. In particular, one can look at how the O(3) $\otimes$ C symmetry is softly broken to $D_{\infty h}$ in the short-distance limit. The leading correction coming from the multipole expansion to (3.25) and (3.26) is at $\mathcal{O}(r^2)$ and can be calculated in pNRQCD in terms of non-perturbative correlators to be eventually evaluated on the lattice or in QCD vacuum models. Such a correction is necessary in order to form a bound state, since $V_o(r)$ itself is repulsive.

In this chapter we consider only states of the lowest lying symmetry multiplet, i.e. the Σ_u^- and Π_u states. They are generated from a gluelump with quantum numbers 1^{+-}. A good gluonic operator P^a overlapping with this gluelump, which can be used in the large time correlator (3.25), is the chromomagnetic field $\boldsymbol{B}^a$, so we will call this gluelump operator $\boldsymbol{G}_B^a$.

For the projection on the Σ_u^- state the unit vector $\hat{\boldsymbol{r}} = (\sin\theta\cos\varphi, \sin\theta\sin\varphi, \cos\theta)^T$ will be used, which gives the direction of the quark-antiquark axis. The other two projection vectors for the Π_u states have to be orthogonal to $\hat{\boldsymbol{r}}$ and each other, but apart from that we are free to take any two convenient vectors. We will use $\hat{\boldsymbol{r}}^\pm = \left(\hat{\boldsymbol{\theta}} \pm i\hat{\boldsymbol{\varphi}}\right)/\sqrt{2}$, where $\hat{\boldsymbol{\theta}} = (\cos\theta\cos\varphi, \cos\theta\sin\varphi, -\sin\theta)^T$ and $\hat{\boldsymbol{\varphi}} = (-\sin\varphi, \cos\varphi, 0)^T$ are the usual local unit vectors in a spherical coordinate system. The advantage of this choice is that with these complex vectors the projections of the gluelump operator transform as $\hat{\boldsymbol{r}}^\pm \cdot \boldsymbol{G}_B^a \to e^{\pm i\alpha}\, \hat{\boldsymbol{r}}^\pm \cdot \boldsymbol{G}_B^a$ under rotations by an angle α around the quark-antiquark axis.

The leading order matching condition is then given by

$$\left|1\Sigma_u^-; \boldsymbol{x}_1, \boldsymbol{x}_2\right\rangle^{(0)} \mathrel{\widehat{=}} O^{a\,\dagger}(\boldsymbol{r}, \boldsymbol{R})\, \hat{\boldsymbol{r}} \cdot \boldsymbol{G}_B^a(\boldsymbol{R})\,|0\rangle + \mathcal{O}(r)\,, \tag{3.27}$$

$$\left|1\Pi_u^\pm; \boldsymbol{x}_1, \boldsymbol{x}_2\right\rangle^{(0)} \mathrel{\widehat{=}} O^{a\,\dagger}(\boldsymbol{r}, \boldsymbol{R})\, \hat{\boldsymbol{r}}^\pm \cdot \boldsymbol{G}_B^a(\boldsymbol{R})\,|0\rangle + \mathcal{O}(r)\,. \tag{3.28}$$

Note that by this definition the index $\pm$ on the Π_u states refers to the sign under rotations, while the index $-$ of the Σ_u^- state refers to the sign under reflections.

3.4 Lattice Determination of the Gluonic Static Energies in NRQCD

The gluonic NRQCD static energies are calculated on the lattice through the logarithm of large time generalized static Wilson loops introduced in Eq. (3.13) divided by the interaction time. The generalized static Wilson loops are constructed using for the initial and final states NRQCD operators with the quantum numbers needed to select the desired static energy [see, for instance, Eq. (3.14)].

The static energies for heavy quark-antiquark pairs have been computed in lattice QCD by several authors [72, 73, 77–82]. In this section we review the latest available data sets obtained by Juge, Kuti, and Morningstar in [73, 81] and by Bali and Pineda in [99], which have been used in this chapter.

Static energies were obtained in quenched lattice QCD by Juge, Kuti, and Morningstar on anisotropic lattices using an improved gauge action introduced in [100]. They extracted the static energies from Monte Carlo estimates of generalized large Wilson loops for a large set of operators projected onto the different representations of the $D_{\infty h}$ group. The distance r between the heavy quark-antiquark pair is fixed in the starting time slice. The use of anisotropic lattices with the temporal spacing much smaller than the spatial spacing is crucial to resolve the gluon excitation spectrum. The static energies for the Σ, Π and Δ gluonic excitations were first computed in [73] and then in larger lattice volumes in [81]. The lattice data from the latter reference consists of four different runs with lattice volumes: $(18^2\times 24)\times 54$, $(16^2 \times 20) \times 80$, $14^3 \times 56$, and the final one is a finite volume check. The corresponding lattice spacings for these runs are ~ 0.12 fm, ~ 0.19 fm, ~ 0.22 fm, and ~ 0.27 fm.

Lattice simulations were carried out by Bali and Pineda in [99] focusing on the short range static energies for the Π_u and Σ_u^- potentials. They performed two sets of computations using a Wilson gauge action in the quenched approximation. The first set was performed on an isotropic lattice with volume $24^3 \times 48$ at $\beta = 6.2$ and lattice spacing ≈ 0.07 fm, the second set on three anisotropic lattices with spatial spacings ≈ 0.16, 0.11, 0.08 fm and temporal spacing of one fourth of the spatial spacing, with $\beta = 5.8$, 6.0, 6.2, respectively. The isotropic data was used as a consistency check and the anisotropic data was extrapolated to the continuum limit.

The static energies computed on the lattice using generalized static Wilson loops contain divergent self-energy contributions in the temporal lines, in principle associated to the heavy quark mass. These self-energy contributions have to be removed in order to obtain the absolute value of the static energies. They could be removed by comparing the ground state static energy, Σ_g^+, with the Coulombic potential computed in perturbation theory at very short distances. In practice, however, lattice data is not available for such short distances in which the perturbative regime is valid. Instead, to remove the divergence, Juge, Kuti, and Morningstar fitted the Σ_g^+ static energy to $\Lambda_0+e_c/r+\kappa r$ and subtracted the value Λ_0, while Bali and Pineda chose to give the values of the static energies relative to the value of the Σ_g^+ static energy at $r = r_0 \approx 0.5$ fm.

The ground state static energy, Σ_g^+, and the first gluonic excitation, Π_u, have been computed in unquenched lattice simulations in [82]. The light quarks have unphysically large masses which are equivalent to a pion mass of 650 MeV. Two lattice volumes were used, $16^3 \times 32$ and $24^3 \times 40$ with $\beta = 5.6$ and a lattice spacing of ≈ 0.076 fm. Two quenched calculations were carried out in the same work and the results were found to agree within errors with the

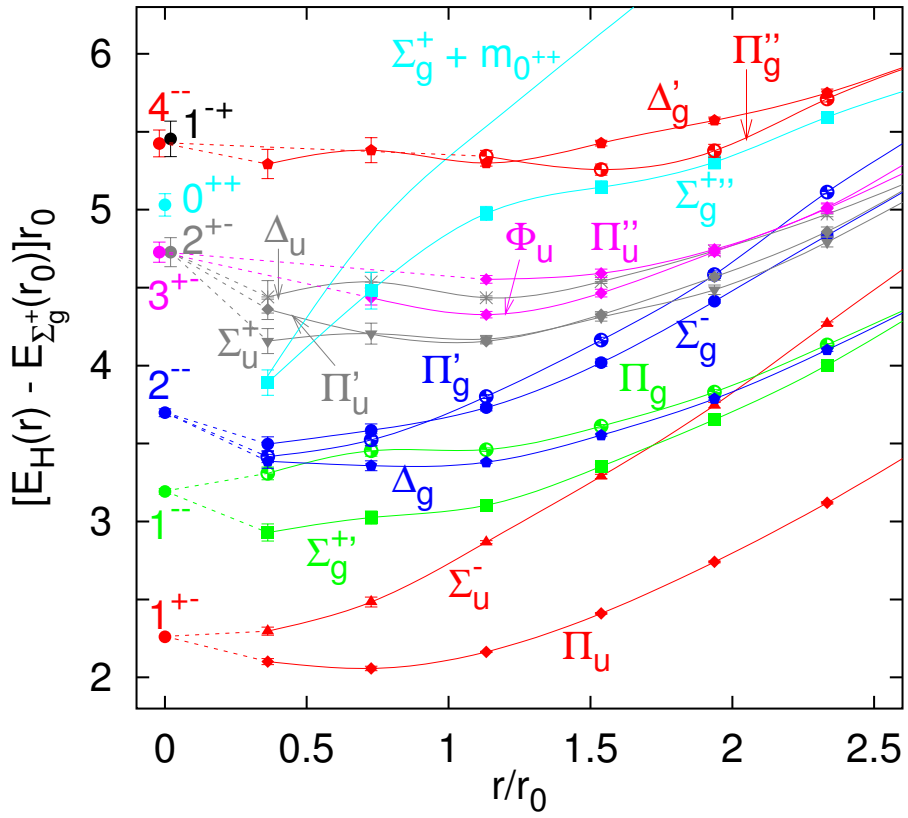

Figure 3.1: The lowest hybrid static energies [81] and gluelump masses [88] in units of $r_0 \approx 0.5$ fm. The absolute values have been fixed such that the ground state Σ_g^+ static energy (not displayed) is zero at r_0. The behavior of the static energies at short distances becomes rather unreliable for some hybrids, especially the higher exited ones. This is largely due to the difficulty in lattice calculations to distinguish between states with the same quantum numbers, which mix. For example, the $\Sigma_g^{+\prime\prime}$ static energy approaches the shape corresponding to a singlet plus 0^{++} glueball state (also displayed) instead of the 0^{++} gluelump. This picture is taken from [99].

unquenched Σ_g^+ and Π_u static energies below the quark-antiquark string breaking distance.

As explained in the previous section, in the short distance limit the heavy quark-antiquark pair gives origin to a local octet source, and the spectrum of gluonic static energies is related to the gluelump spectrum. In Fig. 3.1 the lattice data from Ref. [81] is plotted and compared with the gluelump spectrum, computed also on the lattice, of Ref. [88]. We can see that the two lowest-lying hybrid static energies are the Π_u and Σ_u^- states and they clearly tend to form a degenerate multiplet in the short range. The $\Pi_g - \Sigma_g^{+\prime}$, $\Delta_g - \Sigma_g^- - \Pi_g'$ and $\Delta_u - \Pi_u' - \Sigma_u^+$ multiplets are also expected to be degenerate in the short range [9], cf. Table 3.1.

3.5 The Schrödinger Equation: Matching at $\mathcal{O}(1/m)$

3.5.1 Beyond the Static Limit

In this section we go beyond the static limit to obtain the bound state equation that gives the hybrid masses. Therefore, we consider the $1/m$ corrections to the NRQCD static Hamiltonian,

see Eqs. (3.3) and (3.4). We then match the NRQCD states and Hamiltonian to pNRQCD, obtaining the Schrödinger equation that describes the hybrids and the corresponding eigenstates.

The spectrum of the static Hamiltonian $H^{(0)}$, as of any Hermitian operator, provides a full basis of the corresponding Fock space. Therefore, we can express any state, in particular also the eigenstates $|N\rangle$ of the full Hamiltonian H, as a superposition of static states:

$$|N\rangle = \sum_n \int d^3x_1\, d^3x_2\, |n; \boldsymbol{x}_1, \boldsymbol{x}_2\rangle^{(0)} \psi_n^{(N)}(\boldsymbol{x}_1, \boldsymbol{x}_2)\,. \tag{3.29}$$

In this notation, N is a shorthand for all quantum numbers of the system described by the full Hamiltonian, which are generally different from the static quantum numbers n. The relation in Eq. (3.29) is written in the most general way, but quantum numbers that are incompatible with N do not, in fact, appear in the sum over n. For example, if a certain static quantum number is also a good quantum number in the non-static system, then the sum in Eq. (3.29) can only contain one value for it. By writing the integrations over $\boldsymbol{x}_1$ and $\boldsymbol{x}_2$ explicitly, we already anticipate that the heavy quark and antiquark positions are not good quantum numbers, which is natural in the non-static system of the full Hamiltonian.

We want to use quantum mechanical perturbation theory in order to determine the leading coefficients in (3.29) in the $1/m$ expansion. An important distinction to make here is whether to use degenerate or non-degenerate perturbation theory. In any quantum mechanical system with a Hamiltonian $H^{(0)} + \Delta H$ and a full set of unperturbed eigenstates satisfying $H^{(0)}|n\rangle^{(0)} = E_n^{(0)}|n\rangle^{(0)}$, the first two perturbative corrections to a non-degenerate energy eigenvalue of $H^{(0)}$ are given by

$$E_n = E_n^{(0)} + {}^{(0)}\langle n|\Delta H|n\rangle^{(0)} + \sum_{n'\neq n} \frac{\left|{}^{(0)}\langle n'|\Delta H|n\rangle^{(0)}\right|^2}{E_n^{(0)} - E_{n'}^{(0)}} + \dots\,. \tag{3.30}$$

The first correction to the leading term is usually small for a suitably chosen ΔH, but the second correction term can only be considered small if $\langle \Delta H\rangle / \Delta E^{(0)} \ll 1$, otherwise the second correction would be of the same order as the first, and the perturbative series would break down. If there is no degeneracy between the energies, i.e. $\Delta E^{(0)} \sim E_n^{(0)}$, then this condition is satisfied. The corresponding full eigenstate is given at leading order by exactly one unperturbed state.

However, if some of the energies are close enough or even identical, then because of the vanishing denominator in the second order term this expansion cannot be valid. Instead, one has to calculate the matrix elements of $H^{(0)} + \Delta H$ between all degenerate states and diagonalize the result. The full eigenstates at leading order are then no longer a single unperturbed state but a superposition of the degenerate states, and the coefficients of this superposition form the eigenvectors that diagonalize $H^{(0)} + \Delta H$ in the degenerate sector. The next correction to the energy is given by a term similar to the second order in the non-degenerate case, but the sum over n' now contains none of the degenerate states (so there is no vanishing denominator), and the single state $|n\rangle$ and the energy $E_n^{(0)}$ have to be replaced by the superposition of degenerate states and the corresponding energy eigenvalue, respectively.

In our case the static states are clearly degenerate regarding the quark and antiquark positions $\boldsymbol{x}_1$ and $\boldsymbol{x}_2$. The question whether there are degeneracies related to the other quantum numbers n of the static states is harder to answer. We know that in the short distance limit the states belonging to the same gluelump multiplet are degenerate, and we can assume a

mass gap of order $\Lambda_{\rm QCD}$ between the lowest gluelump and higher excited multiplets as well as the ground state (cf. Fig. 3.1 and Ref. [87]). Neglecting pion contributions is crucial for this assumption. At larger distances $r \sim \Lambda_{\rm QCD}^{-1}$ it is also reasonable to assume a mass gap of order $\Lambda_{\rm QCD}$ between the Π_u and Σ_u^- states, while at even larger distances the Σ_u^- static energy starts to cross with higher excited states, although we do not expect those crossover regions to be of importance to the low lying hybrids. In any case at very large distance open flavor channels that we neglect will also play a role. So depending on the value of r the static energies may or may not be degenerate, but since the lowest lying hybrids are expected to be located around the minimum of the potential, which is close to the short distance part, we will use degenerate perturbation theory with respect to the Π_u and Σ_u^- states.

The leading term for the energy in degenerate perturbation theory is obtained by diagonalizing the matrix elements between the degenerate states. For the static plus $1/m$ Hamiltonian, this can be done in two steps. We can write the matrix elements as

$$ {}^{(0)}\langle \underline{n}'; \boldsymbol{x}_1', \boldsymbol{x}_2' | H^{(0)} + H^{(1)} | \underline{n}; \boldsymbol{x}_1, \boldsymbol{x}_2 \rangle^{(0)} = \left(\delta_{n'n} E_n^{(0)} + E_{n'n}^{(1)} \right) \delta^{(3)}(\boldsymbol{x}_1' - \boldsymbol{x}_1) \delta^{(3)}(\boldsymbol{x}_2' - \boldsymbol{x}_2) \,, \quad (3.31) $$

where we use the abbreviation $H^{(1)} = H^{(1,0)}/m_Q + H^{(0,1)}/m_{\bar{Q}}$. The new energy term $E_{n'n}^{(1)}$ in this expression is a matrix-valued differential operator acting on the delta functions. Diagonalizing the matrix elements corresponds to finding the sets of eigenfunctions $\psi_n^{(N)}$ of $E^{(0)} + E^{(1)}$ satisfying

$$ \sum_n \left(\delta_{n'n} E_n^{(0)} + E_{n'n}^{(1)} \right) \psi_n^{(N)} = \mathcal{E}_N \, \psi_{n'}^{(N)} \,, \quad (3.32) $$

where the eigenvalue $\mathcal{E}_N$ gives the mass of the hybrid state as $m_H = m_Q + m_{\bar{Q}} + \mathcal{E}_N$ up to corrections of order $1/m^2$. So the first step corresponds to determining this differential operator, the second to solving the resulting eigenvalue problem.

We will first determine $E_{n'n}^{(1)}$ in the short distance limit, since it is in this regime where we have a strong degeneracy between the Σ_u^- and Π_u states. Accordingly, we will not calculate the matrix elements for the full $1/m$ Hamiltonian, but only for the leading order in the multipole expansion. The importance of each term can be determined by the standard power counting of weakly-coupled pNRQCD. All powers of $1/r$ including derivatives in r scale as mv with $v \ll 1$, while all other dynamical fields scale as the next lower energy scale, which can either be $\Lambda_{\rm QCD}$ or mv^2, which is the scale of the potential terms. In this case the hierarchy $mv \gg \Lambda_{\rm QCD} \gg mv^2$ seems more appropriate.

In the octet sector the $1/m$ pNRQCD Hamiltonian is given by

$$ \mathcal{H}^{(1)} = \int d^3R \, d^3r \, O^{a\,\dagger}(\boldsymbol{r}, \boldsymbol{R}) \left[-\frac{\boldsymbol{\nabla}_r^2 \delta^{ab}}{m} - \frac{(\boldsymbol{D}_R^2)^{ab}}{4m} + \frac{V^{(1)}(r)\delta^{ab}}{m} + \dots \right] O^b(\boldsymbol{r}, \boldsymbol{R}) \,. \quad (3.33) $$

Here we have assumed for simplicity that the quark and the antiquark have the same mass m, otherwise we would have to distinguish between reduced and total mass, i.e. replace the first denominator by $2m_Q m_{\bar{Q}}/(m_Q + m_{\bar{Q}})$ and the second by $2(m_Q + m_{\bar{Q}})$ etc. These are not all $1/m$ operators, the dots contain other terms that involve the gauge fields $\boldsymbol{E}$ and $\boldsymbol{B}$ at the same or higher orders in the multipole expansion, including spin interactions.

According to the power counting, the first term of $\mathcal{H}^{(1)}$, which is the kinetic term for the relative distance, scales as mv^2, while all other terms scale at most as $\Lambda_{\rm QCD}^2/m$ (in the weak coupling regime $V^{(1)}$ is of order m^2v^4 [64, 65]). We will include only the kinetic term,

which means that our calculation will be valid up to corrections of order $\Lambda_{\rm QCD}^2/m$. The static Hamiltonian $\mathcal{H}^{(0)}$ itself is of order mv^2 in the heavy quark part, which contains the singlet and octet potentials, and of order $\Lambda_{\rm QCD}$ in the Yang-Mills part, which gives rise to the gluelump mass. So we see that at least the potential term of $\mathcal{H}^{(0)}$ and the kinetic term of $\mathcal{H}^{(1)}$ are of the same order, which is in accordance with the virial theorem of standard quantum mechanics.

In the long-distance limit, we cannot rely on the multipole expansion. Both $E_n^{(0)}$ and $E_{n'n}^{(1)}$ may be expressed as the expectation value of some generalized Wilson loop acting on quark-antiquark color singlet states. These generalized Wilson loops, involving the insertion of gauge fields in a static Wilson loop, can in principle be determined from lattice calculations. They have been in the case of $E_n^{(0)}$, see section 3.4, but they have not been in the case of $E_{n'n}^{(1)}$. Hence we will be able to use the full non-perturbative information only for the static energies, while we will have to rely on short distance approximations, and in particular on the leading order term in the multipole expansion, in the case of the $1/m$ terms. This is a reasonable approximation for the lowest hybrid states that are expected to lie near the minimum of the potential, which is sufficiently close to the origin (a quantitative analysis can be found in section 3.6).

In summary, we will use nearly degenerate perturbation theory for the static states Π_u and Σ_u^- belonging to the same 1^{+-} gluelump multiplet at short distances. We will use both perturbative and non-perturbative information for the static energies, $E_n^{(0)}$, while we will evaluate $E_{n'n}^{(1)}$ at short distances at leading order in the multipole expansion.

We turn to the evaluation of the matrix elements of the kinetic term in the short distance limit, which will lead to a coupled Schrödinger equation. The kinetic term acts on the static states corresponding to the lowest gluelump in the following way:

$$\begin{aligned} H_{\rm kin}\,|\underline{n};\boldsymbol{x}_1,\boldsymbol{x}_2\rangle^{(0)} &\stackrel{\simeq}{=} -\left[\int d^3R'\,d^3r'\,O^{a'\,\dagger}(\boldsymbol{r}',\boldsymbol{R}')\frac{\boldsymbol{\nabla}_{r'}^2}{m}O^{a'}(\boldsymbol{r}',\boldsymbol{R}'),O^{a\,\dagger}(\boldsymbol{r},\boldsymbol{R})\right]\hat{\boldsymbol{n}}\cdot\boldsymbol{G}_B^a(\boldsymbol{R})\,|0\rangle \\ &= -\left(\frac{\boldsymbol{\nabla}_r^2}{m}O^{a\,\dagger}(\boldsymbol{r},\boldsymbol{R})\right)\hat{\boldsymbol{n}}\cdot\boldsymbol{G}_B^a(\boldsymbol{R})\,|0\rangle\ , \end{aligned} \tag{3.34}$$

where $\hat{\boldsymbol{n}}$ can be either $\hat{\boldsymbol{r}}$ or $\hat{\boldsymbol{r}}^{\pm}$ for Σ_u^- or Π_u, respectively. The matrix elements are then given by

$$\begin{aligned} &{}^{(0)}\langle\underline{n}';\boldsymbol{x}_1',\boldsymbol{x}_2'|\,H_{\rm kin}\,|\underline{n};\boldsymbol{x}_1,\boldsymbol{x}_2\rangle^{(0)} \\ &= -\langle 0|\,\hat{\boldsymbol{n}}'^*\cdot\boldsymbol{G}_B^{a'}(\boldsymbol{R}')\left[O^{a'}(\boldsymbol{r}',\boldsymbol{R}'),\left(\frac{\boldsymbol{\nabla}_r^2}{m}O^{a\,\dagger}(\boldsymbol{r},\boldsymbol{R})\right)\right]\hat{\boldsymbol{n}}\cdot\boldsymbol{G}_B^a(\boldsymbol{R})\,|0\rangle \\ &= -\langle 0|\,\hat{\boldsymbol{n}}'^*\cdot\boldsymbol{G}_B^a(\boldsymbol{R})\,\hat{\boldsymbol{n}}\cdot\boldsymbol{G}_B^a(\boldsymbol{R})\,|0\rangle\,\frac{\boldsymbol{\nabla}_r^2}{m}\delta^{(3)}(\boldsymbol{r}-\boldsymbol{r}')\delta^{(3)}(\boldsymbol{R}-\boldsymbol{R}') \\ &= -\hat{\boldsymbol{n}}'^*(\theta',\varphi')\cdot\hat{\boldsymbol{n}}(\theta,\varphi)\frac{\boldsymbol{\nabla}_r^2}{m}\delta^{(3)}(\boldsymbol{r}-\boldsymbol{r}')\delta^{(3)}(\boldsymbol{R}-\boldsymbol{R}')\,. \end{aligned} \tag{3.35}$$

To evaluate the expectation value of the gluonic operators we have used the fact that the gluelump operators create orthonormal states. The dependence on the coordinates of the projection vectors has been made explicit in the last line.

If we now let the differential operator corresponding to these matrix elements act on the wave functions, which is equivalent to a convolution of Eq. (3.35) with $\psi_n^{(N)}(\boldsymbol{r})$, then we obtain the following differential equation (replacing $\boldsymbol{r}'$ with $\boldsymbol{r}$)

$$\sum_{n=\Sigma,\,\Pi^{\pm}}\hat{\boldsymbol{n}}'^*(\theta,\varphi)\cdot\left(-\frac{\boldsymbol{\nabla}_r^2}{m}+E_n^{(0)}(r)\right)\hat{\boldsymbol{n}}(\theta,\varphi)\,\Psi_n^{(N)}(\boldsymbol{r})=\mathcal{E}_N\,\Psi_{n'}^{(N)}(\boldsymbol{r})\,. \tag{3.36}$$

Comparing this result with Eq. (3.32), the scalar product of $\hat{\boldsymbol{n}}'$ and $\hat{\boldsymbol{n}}$ gives the $\delta_{n'n}$ in front of the static energy, and the first term gives the differential operator $E^{(1)}_{n'n}$, which will have a more complicated expression, because the derivatives act not only on the wave function, but also on $\hat{\boldsymbol{n}}$. The wave functions only need to depend on $\boldsymbol{r}$, because we have neglected the kinetic term for $\boldsymbol{R}$, so the center-of-mass coordinate is still a good quantum number. This corresponds to a hybrid at rest without any recoil effects between heavy quarks and gluons.

3.5.2 The Radial Schrödinger Equation

The Laplace operator $\boldsymbol{\nabla}_r^2$ can be split into a radial and an angular part, such that

$$-\frac{\boldsymbol{\nabla}_r^2}{m} = -\frac{1}{m\,r^2}\left(\partial_r\, r^2\,\partial_r + \partial_x\left(1-x^2\right)\partial_x + \frac{1}{1-x^2}\,\partial_\varphi^2\right), \tag{3.37}$$

where we have replaced the angle θ by $x = \cos\theta$. The radial part $\partial_r\, r^2\,\partial_r$ acts only on the wave function $\Psi_n(\boldsymbol{r})$, and the scalar product of the projection vectors just gives a Kronecker delta: $\hat{\boldsymbol{n}}' \cdot \hat{\boldsymbol{n}} = \delta_{n'n}$.

The angular part usually has eigenfunctions in the spherical harmonics, however, the presence of the projection vectors modifies the defining differential equations in the diagonal entries $n' = n$ to

$$-\left[\partial_x\left(1-x^2\right)\partial_x + \frac{1}{1-x^2}\left(\partial_\varphi^2 - 2i\lambda x\partial_\varphi - \lambda^2\right)\right] v^\lambda_{l,\,m}(x,\varphi) = l(l+1)v^\lambda_{l,\,m}(x,\varphi)\,, \tag{3.38}$$

where λ labels the different projection vectors, $\lambda = 0$ for $\hat{\boldsymbol{r}}$ and $\lambda = \pm 1$ for $\hat{\boldsymbol{r}}^\pm$. An explicit solution for these orbital wave functions can be given as

$$v^\lambda_{l,\,m}(x,\varphi) = \frac{(-1)^{m+\lambda}}{2^l}\sqrt{\frac{2l+1}{4\pi}\frac{(l-m)!}{(l+m)!(l-\lambda)!(l+\lambda)!}}\,P^\lambda_{l,\,m}(x)e^{im\varphi}\,, \tag{3.39}$$

$$P^\lambda_{l,\,m}(x) = (1-x)^{(m-\lambda)/2}(1+x)^{(m+\lambda)/2}\,\partial_x^{l+m}(x-1)^{l+\lambda}(x+1)^{l-\lambda}\,. \tag{3.40}$$

A derivation of these functions can be found in textbooks such as [75]. They are defined for $|m| \le l$ and $|\lambda| \le l$, and for $\lambda = 0$ they are identical to the spherical harmonics.

The quantum numbers l and m correspond to the eigenvalues of the angular momentum $\boldsymbol{L} = \boldsymbol{L}_{Q\bar{Q}} + \boldsymbol{K}$, where $\boldsymbol{L}_{Q\bar{Q}}$ is the angular momentum operator of the heavy quarks, and $\boldsymbol{K}$ is the gluon angular momentum operator. These eigenvalues appear when the operator acts on the state, not only the wave function:

$$\boldsymbol{L}^2\int d\Omega\,\left(v^\lambda_{l,\,m}\,\hat{\boldsymbol{r}}^\lambda\cdot\boldsymbol{G}^a_B\,O^{a\,\dagger}\right)|0\rangle = l(l+1)\int d\Omega\,\left(v^\lambda_{l,\,m}\,\hat{\boldsymbol{r}}^\lambda\cdot\boldsymbol{G}^a_B\,O^{a\,\dagger}\right)|0\rangle\,, \tag{3.41}$$

$$L_3\int d\Omega\,\left(v^\lambda_{l,\,m}\,\hat{\boldsymbol{r}}^\lambda\cdot\boldsymbol{G}^a_B\,O^{a\,\dagger}\right)|0\rangle = m\int d\Omega\,\left(v^\lambda_{l,\,m}\,\hat{\boldsymbol{r}}^\lambda\cdot\boldsymbol{G}^a_B\,O^{a\,\dagger}\right)|0\rangle\,. \tag{3.42}$$

The states with the orbital wave functions $v^\lambda_{l,\,m}$ are eigenstates of the angular momentum, but not yet of parity and charge conjugation, because acting with P or C turns λ into $-\lambda$. We list here the transformation properties of all elements of the states:

$$v^\lambda_{l,\,m} \xrightarrow{P} (-1)^l v^{-\lambda}_{l,\,m}\,, \qquad v^\lambda_{l,m} \xrightarrow{C} (-1)^l v^{-\lambda}_{l,\,m}\,, \tag{3.43}$$

$$\hat{\boldsymbol{r}}^\lambda \xrightarrow{P} (-1)^{\lambda+1}\hat{\boldsymbol{r}}^{-\lambda}\,, \qquad \hat{\boldsymbol{r}}^\lambda \xrightarrow{C} (-1)^{\lambda+1}\hat{\boldsymbol{r}}^{-\lambda}\,, \tag{3.44}$$

	l	$J^{PC}\{s=0, s=1\}$	$E_n^{(0)}$
H_1	1	$\{1^{--}, (0,1,2)^{-+}\}$	Σ_u^-, Π_u
H_2	1	$\{1^{++}, (0,1,2)^{+-}\}$	Π_u
H_3	0	$\{0^{++}, 1^{+-}\}$	Σ_u^-
H_4	2	$\{2^{++}, (1,2,3)^{+-}\}$	Σ_u^-, Π_u
H_5	2	$\{2^{--}, (1,2,3)^{-+}\}$	Π_u

Table 3.2: J^{PC} multiplets with $l \leq 2$ for the Σ_u^- and Π_u gluonic states. We follow the naming notation H_i used in [17, 83–85], which orders the multiplets from lower to higher mass. The last column shows the gluonic static energies that appear in the Schrödinger equation of the respective multiplet.

$$\boldsymbol{G}_B^a \xrightarrow{P} \boldsymbol{G}_B^a\,, \qquad \boldsymbol{G}_B^a \xrightarrow{C} -(-)^a \boldsymbol{G}_B^a\,, \tag{3.45}$$

$$O_s^a \xrightarrow{P} -O_s^a\,, \qquad O_s^a \xrightarrow{C} (-1)^s (-)^a O_s^a\,. \tag{3.46}$$

The factor $(-)^a$ comes from $T^a = (-)^a (T^a)^T$, but since it appears in front of the octet field and of the gluelump operator, it cancels for the gluelump states. The quantum number s labels the total spin of the quark and the antiquark and can have values 0 or 1.

For $\lambda = 0$ we already have parity and charge conjugation eigenstates:

$$v^0_{l,m}\, \hat{\boldsymbol{r}} \cdot \boldsymbol{G}_B^a\, O^{a\,\dagger}|0\rangle \xrightarrow{P} (-1)^l \quad v^0_{l,m}\, \hat{\boldsymbol{r}} \cdot \boldsymbol{G}_B^a\, O^{a\,\dagger}|0\rangle\,, \tag{3.47}$$

$$v^0_{l,m}\, \hat{\boldsymbol{r}} \cdot \boldsymbol{G}_B^a\, O^{a\,\dagger}|0\rangle \xrightarrow{C} (-1)^{l+s}\, v^0_{l,m}\, \hat{\boldsymbol{r}} \cdot \boldsymbol{G}_B^a\, O^{a\,\dagger}|0\rangle\,. \tag{3.48}$$

For $|\lambda| = 1$ we can define even and odd parity or charge conjugation states:

$$\frac{1}{\sqrt{2}} \left(v^1_{l,m}\, \hat{\boldsymbol{r}}^+ \pm v^{-1}_{l,m}\, \hat{\boldsymbol{r}}^-\right) \cdot \boldsymbol{G}_B^a\, O^{a\,\dagger}|0\rangle \xrightarrow{P} \mp(-1)^l \quad \frac{1}{\sqrt{2}} \left(v^1_{l,m}\, \hat{\boldsymbol{r}}^+ \pm v^{-1}_{l,m}\, \hat{\boldsymbol{r}}^-\right) \cdot \boldsymbol{G}_B^a\, O^{a\,\dagger}|0\rangle\,, \tag{3.49}$$

$$\frac{1}{\sqrt{2}} \left(v^1_{l,m}\, \hat{\boldsymbol{r}}^+ \pm v^{-1}_{l,m}\, \hat{\boldsymbol{r}}^-\right) \cdot \boldsymbol{G}_B^a\, O^{a\,\dagger}|0\rangle \xrightarrow{C} \mp(-1)^{l+s}\, \frac{1}{\sqrt{2}} \left(v^1_{l,m}\, \hat{\boldsymbol{r}}^+ \pm v^{-1}_{l,m}\, \hat{\boldsymbol{r}}^-\right) \cdot \boldsymbol{G}_B^a\, O^{a\,\dagger}|0\rangle\,. \tag{3.50}$$

We see that the combination with a relative minus sign has the same P and C transformation properties as the $\lambda = 0$ state, while the positive combination has opposite behavior.

Now the angular momentum $\boldsymbol{L}$ and the spin $\boldsymbol{S}$ can be combined with the usual Clebsch-Gordan coefficients to form eigenstates of the total angular momentum $\boldsymbol{J} = \boldsymbol{L} + \boldsymbol{S}$. Since at this level of the approximation nothing depends on the spin, all the different spin combinations have the same energy and appear as degenerate multiplets. The J^{PC} quantum numbers are then $\{l^{\pm\pm}; (l-1)^{\pm\mp}, l^{\pm\mp}, (l+1)^{\pm\mp}\}$, where the first entry corresponds to the spin 0 combination and the next three entries to the spin 1 combinations. For $l = 0$ there is only one spin 1 combination as well as only one parity or charge conjugation state (see below), so we have $\{0^{++}, 1^{+-}\}$. In Table 3.2 the first five degenerate multiplets that can be obtained are shown, arranged according to their energy eigenvalues (see section 3.6).

The $\lambda = 0$ state will be convoluted with the radial wave functions $\psi_\Sigma^{(N)}(r)$, while the radial wave functions $\psi_{\pm\Pi}^{(N)}(r)$ will be convoluted with the $|\lambda| = 1$ states that have the relative $\pm$ sign between the two projection vectors and orbital wave functions. The differential term $\hat{\boldsymbol{n}}' \cdot \nabla_r^2\, \hat{\boldsymbol{n}}$ in the coupled Schrödinger equation not only changes the differential equations for the orbital

wave functions, it also adds additional diagonal and offdiagonal terms. The offdiagonal terms change the radial Σ wave function to Π and vice versa, however, they can not change the parity of the states. This means that $\psi_{\Sigma}^{(N)}$ mixes only with $\psi_{-\Pi}^{(N)}$, and $\psi_{+\Pi}^{(N)}$ decouples. We then have the following coupled radial Schrödinger equation for one parity state,

$$\left[-\frac{1}{mr^2}\,\partial_r r^2 \partial_r + \frac{1}{mr^2}\begin{pmatrix} l(l+1)+2 & 2\sqrt{l(l+1)} \\ 2\sqrt{l(l+1)} & l(l+1)\end{pmatrix} + \begin{pmatrix} E_{\Sigma}^{(0)} & 0 \\ 0 & E_{\Pi}^{(0)}\end{pmatrix}\right]\begin{pmatrix}\psi_{\Sigma}^{(N)} \\ \psi_{-\Pi}^{(N)}\end{pmatrix} = \mathcal{E}_N \begin{pmatrix}\psi_{\Sigma}^{(N)} \\ \psi_{-\Pi}^{(N)}\end{pmatrix}, \tag{3.51}$$

and for the other we get the conventional radial Schrödinger equation

$$\left[-\frac{1}{mr^2}\,\partial_r\, r^2\,\partial_r + \frac{l(l+1)}{mr^2} + E_{\Pi}^{(0)}\right]\psi_{+\Pi}^{(N)} = \mathcal{E}_N\,\psi_{+\Pi}^{(N)}\,. \tag{3.52}$$

There is a special case for $l = 0$ in that the offdiagonal terms in the coupled equation vanish, so the radial Schrödinger equations for $\psi_{\Sigma}^{(N)}$ and $\psi_{-\Pi}^{(N)}$ also decouple. In fact, $\psi_{-\Pi}^{(N)}$ is irrelevant, since there are no orbital wave functions with $|\lambda| = 1$ for $l = 0$. The same applies to $\psi_{+\Pi}^{(N)}$. So for $l = 0$ there exists only one parity state, and its radial wave function is given by an almost ordinary Schrödinger equation with the $E_{\Sigma}^{(0)}$ potential, the only unusual element is that the angular part is $2/mr^2$ even though $l = 0$.

In appendix A.3 we describe the derivation of the radial Schrödinger equations in more detail. For the uncoupled radial Schrödinger equations there exist well established numerical methods to find the wave functions and eigenvalues. These can also be extended to the coupled case, more details on the specific approach that we chose to get the numerical results are given in appendix A.4 and [101].

3.5.3 Comparison with Other Descriptions of Hybrids

We now compare the pattern of hybrid spin-symmetry multiplets that we have obtained in our approach with the one obtained in different pictures. The BO approximation for hybrids, as it has been employed in Refs. [17, 70, 72, 73, 84, 85], produces spin-symmetry multiplets with the same J^{PC} constituents as our H_i multiplets in Table 3.2, however, in all the existing BO papers the masses of opposite parity states are degenerate.

In Ref. [17, 84, 85] the underlying assumptions of the BO approximation are given in more detail. Two main points are identified, an adiabatic approximation and a single-channel approximation. The adiabatic approximation states that the time scales for heavy and light degrees of freedom are very different, such that the light degrees of freedom adapt instantaneously to changes in the quark and antiquark positions and therefore always form a static eigenstate. This is equivalent to the $1/m$ expansion we have used here, where the hybrid states are expressed in terms of static states. The single-channel approximation states that at leading order the light degrees of freedom remain always in the same static eigenstate, because transitions to other states are suppressed by a mass gap of order Λ_{QCD}. We make the same assumption regarding transitions to static states corresponding to excited gluelumps, but for the lowest gluelump states we go beyond the single-channel approximation, since at short distances they are nearly degenerate.

Consequently, we obtain terms that mix the static states through a coupled Schrödinger equation, in a way that is firmly based on QCD. Taking into account these mixing terms, we find that the degeneracy between opposite parity states is broken. In the BO approximation

in the context of atomic molecules this effect is also known as Λ-*doubling* [75]. In the context of hybrids, Λ-doubling and the modified orbital wave functions $v^{\lambda}_{l,m}$ have been discussed here for the first time.

In the constituent gluon picture [71], hybrids are assumed to be composed of a gluonic excitation bound to a heavy-quark antiquark pair. The gluons are assumed to appear in J^{PC} representations unlike the case of pNRQCD or BO descriptions, in which the gluonic states appear in Λ^{σ}_{η} representations. The quantum numbers of the resulting hybrid are obtained by adding those of the gluon and those of the heavy-quark antiquark pair using the standard rules for addition of angular momentum. In this way one gets the same J^{PC} quantum numbers as we do, but they are arranged in larger multiplets.

If, in the constituent gluon picture, we couple a chromomagnetic (i.e. 1^{+-}) gluonic excitation with an S-wave heavy-quark antiquark pair in a spin singlet $\{0^{-+}\}$ or spin triplet $\{1^{--}\}$ state, then we get exactly the quantum numbers of H_1. Similarly, for P-wave quarkonium with quantum numbers $\{1^{+-}, (0,1,2)^{++}\}$ (corresponding to different spin states) we get $H_2 \cup H_3 \cup H_4$. H_5 would then be included in the combination with the next quarkonium quantum numbers. Since for pNRQCD in the limit $r \to 0$ we recover spherical symmetry, we can see the constituent gluon picture as the short distance limit of the pNRQCD or BO pictures. Furthermore, one can interpret the finer multiplet structure of pNRQCD with respect to the constituent gluon picture as the effect of the finite distance r between the heavy-quark pair.

The flux tube model [68, 69] (for a more recent comparison of the flux tube model with the constituent gluon picture see e.g. [102]) arises from the idea that for QCD in the strong-coupling regime one can think of the gluonic degrees of freedom as having condensed into a collective stringlike flux tube. In this picture the spectrum of gluonic static energies can be interpreted as the vibrational excitation levels of the string. The lowest excitations of such a string will correspond to non-relativistic, small, transverse displacement oscillations and as such should be well described by the Hamiltonian of a continuous string. The eigenstates of such a Hamiltonian are characterized by the phonon occupation number and their polarizations, while the spectrum corresponds to the different phonon occupation numbers.

The hybrid quantum numbers are constructed by specifying the gluonic states via phonon operators. The value of Λ corresponds to the number of phonons with clockwise polarization minus the number of phonons with anticlockwise polarization. From here one can construct the J^{PC} quantum numbers of the hybrid states in an analogous way to the BO picture. The first excited energy level is a one-phonon state, which necessarily corresponds to a $\Lambda = 1$ state, unlike in the pNRQCD case, where the first excited energy level can be $\Lambda = 0$, 1. Thus, the pattern of the spin-symmetry multiplets emerging from the flux tube model in the case of the first excited static energy is the one in Table 3.2 except for the nonexistence of H_3.

3.6 Solving the Schrödinger Equation: Hybrid Potentials and Masses

In order to obtain the hybrid masses, we have to identify the specific form of the hybrid potentials $E_{\Sigma}(r)$ and $E_{\Pi}(r)$ to be used in the coupled Schrödinger equations in (3.51) and (3.52). In section 3.3 we have reviewed the EFT understanding of these potentials arriving at the expression for the short distance hybrid potential in Eq. (3.20) and the matching condition with the static energies given in Eq. (3.25).

It is well known that the quark mass depends on the renormalon subtraction scheme used. This dependence is canceled in standard quarkonium by the analogous dependence of the singlet potential V_s [103, 104], leaving the total static energy of the singlet, which corresponds to the physical observable, scheme invariant. Similarly, the hybrid static energies are scheme independent, but not V_o and Λ_H, which depend on the renormalon subtraction scheme used. It has been shown that in the On-Shell (OS) scheme the perturbative expansion of the octet potential has a poor convergence. This bad behavior is due to the presence of singularities in the Borel transform of the perturbative series. These singularities are, however, artificial and cancel out in physical observables such as the static energies.

One of the several possible schemes to improve the convergence of the matching coefficients is the so-called Renormalon Subtracted (RS) scheme. In the RS scheme the singularities in the Borel plane (renormalons) are subtracted from the matching coefficients. In Ref. [105] this scheme has been worked out for the heavy quark mass and the static singlet potential, in Ref. [99] the analogous work was done for the octet potential and the lowest gluelump mass. Note that, when working in the RS scheme for the octet potential and gluelump mass, the quark mass in the hybrid static energy also has to be taken in the RS scheme. We have used the RS octet potential $V_o^{RS}(r)$ up to order $\alpha_{\rm s}^3$ in perturbation theory and Λ_H^{RS} at the subtraction scale $\nu_f = 1$ GeV. We have summarized the necessary formulas for the octet potential in the RS scheme in appendix A.2.

The next-to-leading order corrections to the hybrid static energies at short distances are proportional to r^2. The specific proportionality constant depends on non-perturbative dynamics and can be expressed in terms of chromoelectric and chromomagnetic field correlators in the EFT. It could be calculated on the lattice, but no calculations of these objects exist at the moment, or in QCD vacuum models.[5] We choose to fix this coefficient through a fit to the lattice data for the static energies. We are going to consider that this term takes different values for hybrid static energies corresponding to different representations of $D_{\infty h}$, thus breaking the degeneracy of the short range pNRQCD description of the Π_u and Σ_u^- static energies at leading order in the multipole expansion. The final form for the short distance hybrid potential we are going to use is then [cf. Eq. (3.25)]

$$E_n(r) = V_o^{RS}(\nu_f) + \Lambda_H^{RS}(\nu_f) + b_n r^2\,, \quad \nu_f = 1\,\mathrm{GeV}\,, \tag{3.53}$$

and the values of the heavy quark and the 1^{+-} gluelump masses in the RS scheme at $\nu_f = 1$ GeV are: $m_c^{RS} = 1.477(40)$ GeV, $m_b^{RS} = 4.863(55)$ GeV, and $\Lambda_H^{RS} = 0.87(15)$ GeV [99, 105].

We have prepared two different fits for the hybrid potentials to be used in the Schrödinger equations. The first relies only on information from the short distance regime and fits the quadratic term to the lattice data only up to distances where weakly coupled pNRQCD no longer makes sense. Going to larger distances in this potential is inconsistent. The second fit uses the short distance expression for the potential only for distances where weakly coupled pNRQCD is expected to work well, and uses some generic fit function to describe the lattice data of the static energies for larger distances. Comparing the results obtained from both of these fits gives some idea of the importance of the long range regime for hybrids.

In order to obtain the short range quadratic coefficients b_n of Eq. (3.53) in either case, we use lattice data from Refs. [81, 99] described in section 3.4. To do these fits, it must be taken into account that the two sources of lattice data have different energy offsets with respect to the theoretical hybrid potential due to the different methods for the subtractions of the mass

[5] For a computation in the framework of the stochastic vacuum model see [106].

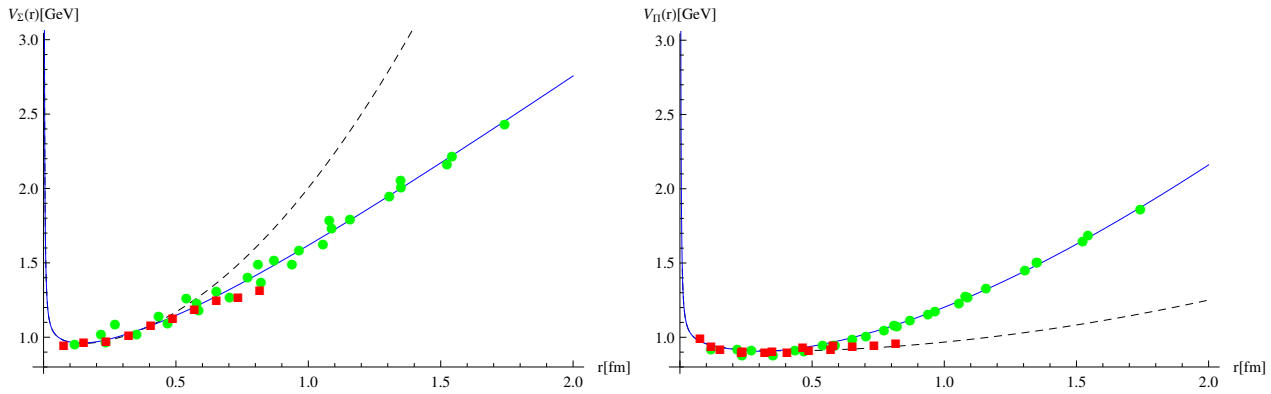

Figure 3.2: Lattice data from Bali and Pineda [99] is represented by red squares, the data from Juge, Kuti, and Morningstar [81] is represented by the green dots. In the left (right) figure we have plotted the data corresponding to Σ_u^- (Π_u). The lattice data has been corrected by the offsets of (3.55). The black dashed line corresponds to $V_\Sigma^{(0.5)}$ ($V_\Pi^{(0.5)}$), the blue continuous line to $V_\Sigma^{(0.25)}$($V_\Pi^{(0.25)}$), see text.

divergence of the lattice calculations. We extract b_n and the energy offsets from both sets of lattice data by fitting the function

$$\mathcal{V}(r) = V_o^{RS} + c + b_n r^2 \,, \tag{3.54}$$

with c and b_n as free parameters.

The RS scheme does not affect the coefficient of the quadratic term b_n. The constant term c is affected both by the RS scheme and by the subtraction scheme used in the lattice calculation, however, at leading order in the multipole expansion the Π_u and Σ_u^- potentials are degenerate. Therefore, we perform a fit of both potentials of the form (3.54) to the lattice data of both groups, restricting the value of c to be the same for both potentials but different for each group and, conversely, restricting the value of b_n to be the same for both groups but different for each potential.

We first give the results for the short range fit. The weakly-coupled pNRQCD description of the hybrid static energy of (3.53) is only valid up to $r \lesssim 1/\Lambda_{\rm QCD}$. Taking perturbation theory up to its limit of validity, we fit (3.54) to lattice data in the range of $r = 0 - 0.5$ fm. We obtain the following offsets for the two lattice data sources

$$c_{\rm BP} = 0.105\,{\rm GeV}, \quad c_{\rm KJM} = -0.471\,{\rm GeV}\,, \tag{3.55}$$

and the values for the coefficient of the quadratic term are

$$b_\Sigma^{(0.5)} = 1.112\,{\rm GeV/fm^2}, \quad b_\Pi^{(0.5)} = 0.110\,{\rm GeV/fm^2}\,. \tag{3.56}$$

The potentials obtained from using the coefficients of the quadratic terms of (3.56) in Eq. (3.53) will be called $V_\Pi^{(0.5)}$ and $V_\Sigma^{(0.5)}$ respectively (corresponding to the Π_u and Σ_u^- configurations). We have plotted $V_\Pi^{(0.5)}$ and $V_\Sigma^{(0.5)}$ in Fig. 3.2 with the lattice data corrected for the different offsets using the values from (3.55).

For the second potential fit, which includes as much information as possible from the long range lattice data, we proceed as follows. For $r \leq 0.25$ fm we use the potential from (3.53) with different b_n factors for each of the low lying hybrid static energies Π_u and Σ_u^-. Accordingly,

we will call the potentials from this fit $V^{(0.25)}$. The b_n factors are obtained through a fit of the function (3.54) for each potential to lattice data up to $r = 0.25$ fm from both sources with the offsets of (3.55). The quadratic term factors resulting from this fit are

$$b_\Sigma^{(0.25)} = 1.246\,\mathrm{GeV/fm}^2, \qquad b_\Pi^{(0.25)} = 0.000\,\mathrm{GeV/fm}^2\,. \tag{3.57}$$

For $r \geq 0.25$ fm we use a fit of the function

$$\mathcal{V}'(r) = \frac{a_1}{r} + \sqrt{a_2\, r^2 + a_3} + a_4\,, \tag{3.58}$$

to all the lattice data with $r \geq 0.25$ fm using the offsets of (3.55). The particular form of (3.58) is not related to a specific model, but approaches the generally expected behavior at short and large distances. Indeed, in the long distance a linear behavior in r is expected as a string picture emerges [81, 107–109]. The parameters have been left unconstrained (e.g. no universal string tension or short-range coupling have been imposed) to better reproduce the lattice data in the distance region where it is available. To ensure a smooth transition between the two pieces of the potential, we impose continuity up to first derivatives. The parameters obtained are

$$\begin{aligned} &a_1^\Sigma = 0.000\,\mathrm{GeVfm}\,, \quad a_2^\Sigma = 1.543\,\mathrm{GeV}^2/\mathrm{fm}^2, \quad a_3^\Sigma = 0.599\,\mathrm{GeV}^2, \quad a_4^\Sigma = 0.154\,\mathrm{GeV}\,, \\ &a_1^\Pi = 0.023\,\mathrm{GeVfm}\,, \quad a_2^\Pi = 2.716\,\mathrm{GeV}^2/\mathrm{fm}^2, \quad a_3^\Pi = 11.091\,\mathrm{GeV}^2, \quad a_4^\Pi = -2.536\,\mathrm{GeV}\,. \end{aligned} \tag{3.59}$$

In Fig. 3.2 we can see both potential fits together with the lattice data. The $V^{(0.25)}$ potentials do a good job reproducing the whole range of lattice data, in fact, fitting with a potential of the form (3.58) also for $r < 0.25$ fm does not change the results significantly. The $V^{(0.5)}$ potentials describe the lattice data well up to $r \lesssim 0.55 - 0.65$ fm, which corresponds to $1/r \gtrsim 0.36 - 0.30$ GeV.

We have solved the coupled Schrödinger equations with both $V^{(0.5)}$ and $V^{(0.25)}$ potentials using the RS heavy quark masses. The results are displayed in Table 3.3. The states obtained with $V^{(0.25)}$ lie above the ones obtained using $V^{(0.5)}$. The masses of the states with smaller sizes have a better agreement, since both potentials agree in the short range. The largest source of uncertainties for the hybrid masses lies in the RS gluelump mass, which is known with an uncertainty of ± 0.15 GeV.

If we look at the results obtained with $V^{(0.5)}$ for the average of the inverse distance $\langle 1/r \rangle$, which are displayed in Table 3.3, we see that for the lowest states the condition that $\langle 1/r \rangle$ falls inside the region where the lattice data is well described by the fit is only marginally fulfilled. The condition that $\langle 1/r \rangle \gtrsim E_{\mathrm{kin}}$, which is at the base of the multipole expansion, is instead fulfilled by almost all the states. Interestingly, adding a long range tail to the potential, as we do for $V^{(0.25)}$, pushes the heavy quarks closer together, in this way better justifying the short distance expansion of the matrix element of H_{kin} that we performed in (3.36). For this reason we will use the $V^{(0.25)}$ potential in the following section as our reference potential for the comparison with data and other approaches.

3.7 Comparison with Experimental Data and Other Determinations of the Hybrid Masses

We compare our results for the hybrid masses with experimental observations in section 3.7.1, predictions obtained using the leading Born-Oppenheimer approximation in section 3.7.2, and direct lattice results and sum rule calculations in sections 3.7.3 and 3.7.4, respectively.

multiplet	J^{PC}	$c\bar{c}$				$b\bar{c}$				$b\bar{b}$			
		m_H	$\langle 1/r \rangle$	$E_{\rm kin}$	P_Π	m_H	$\langle 1/r \rangle$	$E_{\rm kin}$	P_Π	m_H	$\langle 1/r \rangle$	$E_{\rm kin}$	P_Π
H_1	$\{1^{--}, (0,1,2)^{-+}\}$	4.05	0.29	0.11	0.94	7.40	0.31	0.08	0.94	10.73	0.36	0.06	0.95
H_1'		4.23	0.27	0.20	0.91	7.54	0.30	0.16	0.91	10.83	0.36	0.11	0.92
H_2	$\{1^{++}, (0,1,2)^{+-}\}$	4.09	0.21	0.13	1.00	7.43	0.23	0.10	1.00	10.75	0.27	0.07	1.00
H_2'		4.30	0.19	0.24	1.00	7.60	0.21	0.19	1.00	10.87	0.25	0.13	1.00
H_3	$\{0^{++}, 1^{+-}\}$	4.69	0.37	0.42	0.00	7.92	0.42	0.34	0.00	11.09	0.50	0.23	0.00
H_4	$\{2^{++}, (1,2,3)^{+-}\}$	4.17	0.19	0.17	0.97	7.49	0.25	0.14	0.97	10.79	0.29	0.09	0.98
H_5	$\{2^{--}, (1,2,3)^{-+}\}$	4.20	0.17	0.18	1.00	7.51	0.19	0.15	1.00	10.80	0.22	0.10	1.00
H_1	$\{1^{--}, (0,1,2)^{-+}\}$	4.15	0.42	0.16	0.82	7.48	0.46	0.13	0.83	10.79	0.53	0.09	0.86
H_1'		4.51	0.34	0.34	0.87	7.76	0.38	0.27	0.87	10.98	0.47	0.19	0.87
H_2	$\{1^{++}, (0,1,2)^{+-}\}$	4.28	0.28	0.24	1.00	7.58	0.31	0.19	1.00	10.84	0.37	0.13	1.00
H_2'		4.67	0.25	0.42	1.00	7.89	0.28	0.34	1.00	11.06	0.34	0.23	1.00
H_3	$\{0^{++}, 1^{+-}\}$	4.59	0.32	0.32	0.00	7.85	0.37	0.27	0.00	11.06	0.46	0.19	0.00
H_4	$\{2^{++}, (1,2,3)^{+-}\}$	4.37	0.28	0.27	0.83	7.65	0.31	0.22	0.84	10.90	0.37	0.15	0.87
H_5	$\{2^{--}, (1,2,3)^{-+}\}$	4.48	0.23	0.33	1.00	7.73	0.25	0.27	1.00	10.95	0.30	0.18	1.00
H_6	$\{3^{--}, (2,3,4)^{-+}\}$	4.57	0.22	0.37	0.85	7.82	0.25	0.30	0.87	11.01	0.30	0.20	0.89
H_7	$\{3^{++}, (2,3,4)^{+-}\}$	4.67	0.19	0.43	1.00	7.89	0.22	0.35	1.00	11.05	0.26	0.24	1.00

Table 3.3: Hybrid energies obtained from solving the Schrödinger equation with the RS heavy quark masses for the $V^{(0.5)}$ potentials (upper table) and for the $V^{(0.25)}$ potentials (lower table). All values are given in units of GeV. The values of the heavy quark and the 1^{+-} gluelump masses in the RS scheme at $\nu_f = 1$ GeV are: $m_c^{RS} = 1.477(40)$ GeV, $m_b^{RS} = 4.863(55)$ GeV, and $\Lambda_H^{RS} = 0.87(15)$ GeV (see [99, 105]). For the $b\bar{c}$ systems we have used the corresponding reduced mass in the Schrödinger equation. The first row for each multiplet corresponds to the ground state, the second row corresponds to the first excited state. P_Π is the integral over the square of the wave function associated with the Π_u potential. It can be interpreted as the probability to find the hybrid in a Π_u configuration, thus it gives a measure of the mixing effects.

3.7.1 Identification of Hybrids with Experimental States

The list of candidates for heavy quark hybrids consists of the neutral heavy quark mesons above open flavor threshold. An updated list [1] of the states fulfilling these conditions can be found in Table 3.4. Most of the candidates have 1^{--} or $0^{++}/2^{++}$, since the main observation channels are production by e^+e^- or $\gamma\gamma$ annihilation, respectively, which constrains the J^{PC} quantum numbers. It is important to keep in mind that the main source of uncertainty of our results in section 3.6 is the uncertainty of the gluelump mass $\Lambda_H^{RS} = 0.87 \pm 0.15$ GeV. We have plotted the candidate experimental states in Fig. 3.3, except for the single one corresponding to the bottomonium sector, overlaid onto our results using the $V^{(0.25)}$ potential with error bands corresponding to the uncertainty of the gluelump mass.

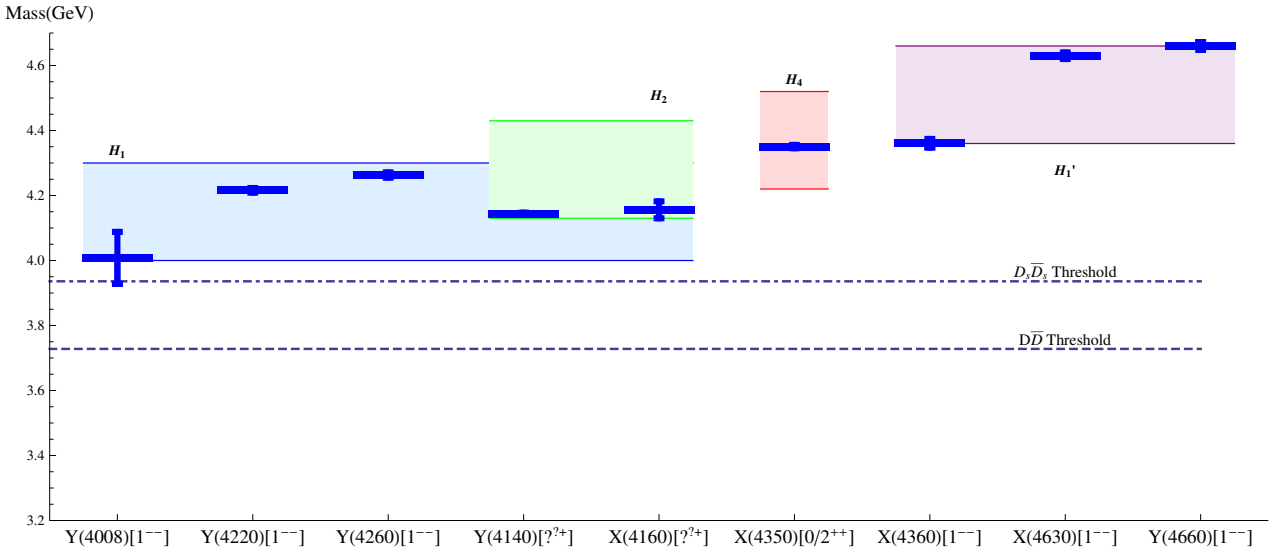

Figure 3.3: Comparison of the experimental candidate masses for the charmonium sector with our results using the $V^{(0.25)}$ potential. The experimental states are plotted in solid blue lines with error bars corresponding to the average of the lower and upper mass uncertainties (see Table 3.4). Our results for the H_1, H_2, H_4 and H_1' multiplets have been plotted in error bands corresponding to the gluelump mass uncertainty of ± 0.15 GeV.

Three 1^{--} states fall close to our mass for the charmonium hybrid from the H_1 multiplet,[6] the $Y(4008)$, $Y(4230)$, and $Y(4260)$. The 1^{--} hybrid from the H_1 multiplet is a spin singlet state, and as such the decays to spin triplet products are suppressed by one power of the heavy quark mass due to heavy quark spin symmetry. All these three candidate states decay to spin triplet charmonium, which in principle disfavors the hybrid interpretation. Nevertheless, there might be enough heavy quark spin symmetry violation to explain those decays [110]. On the other hand, the interpretation of these states as charmonium hybrids would make the decay into two S-wave open charm mesons forbidden [111], which would explain why such decays have not been observed for the $Y(4260)$. Nevertheless, the recent observation of the transition $Y(4260) \to X(3872)\gamma$ [112] makes the identification of $Y(4260)$ as a hybrid highly unlikely.

The $Y(4220)$ is a narrow structure proposed in [113] to fit the line shape of the annihilation processes $e^+e^- \to h_c\pi^+\pi^-$ observed by BESIII and CLEO-c experiments. Its mass is quite close to the one of the H_1 multiplet. Like the previous states, it is a 1^{--} state that would be identified as a spin singlet hybrid. However, unlike the previous states, the $Y(4220)$ has been observed decaying to spin singlet quarkonium, which makes it a very good candidate for a charmonium hybrid. However, the $Y(4220)$ falls very close to the $Y(4230)$ [114] and it is possible that they are the same structure observed in different decay channels.

The J^{PC} quantum numbers of the $Y(4140)$ and $Y(4160)$ have not yet been fully determined, however, their charge conjugation and mass suggest that they can be candidates for the spin triplet 1^{-+} member of the H_1 multiplet. Nevertheless, their mass is also compatible within uncertainties with the spin singlet 1^{++} member of the H_2 multiplet. In the case of the $Y(4160)$, it decays into $D^*\bar{D}^*$ which favors a molecular interpretation of this state.

If the $X(4350)$ turns out to be a 2^{++} state it can be a candidate for the spin singlet

[6] Note that our hybrid multiplets are spin degenerate, i.e. do not include corrections to the mass due to spin effects.

State	M (MeV)	Γ (MeV)	J^{PC}	Decay modes	1st observation
$X(3823)$	3823.1 ± 1.9	< 24	$?^{?-}$	$\chi_{c1}\gamma$	Belle 2013
$X(3872)$	3871.68 ± 0.17	< 1.2	1^{++}	$J/\psi\,\pi^+\pi^-$, $J/\psi\,\pi^+\pi^-\pi^0$, $D^0\bar{D}^0\pi^0$, $D^0\bar{D}^0\gamma$, $J/\psi\,\gamma$, $\psi(2S)\,\gamma$	Belle 2003
$X(3915)$	3917.5 ± 1.9	20 ± 5	0^{++}	$J/\psi\,\omega$	Belle 2004
$\chi_{c2}(2P)$	3927.2 ± 2.6	24 ± 6	2^{++}	$D\bar{D}$	Belle 2005
$X(3940)$	3942^{+9}_{-8}	37^{+27}_{-17}	$?^{?+}$	$D^*\bar{D}$, $D\bar{D}^*$	Belle 2007
$G(3900)$	3943 ± 21	52 ± 11	1^{--}	$D\bar{D}$	Babar 2007
$Y(4008)$	$4008^{+121}_{-\ 49}$	226 ± 97	1^{--}	$J/\psi\,\pi^+\pi^-$	Belle 2007
$Y(4140)$	4144.5 ± 2.6	$15^{+11}_{-\ 7}$	$?^{?+}$	$J/\psi\,\phi$	CDF 2009
$X(4160)$	4156^{+29}_{-25}	139^{+113}_{-65}	$?^{?+}$	$D^*\bar{D}^*$	Belle 2007
$Y(4220)$	4216 ± 7	39 ± 17	1^{--}	$h_c(1P)\,\pi^+\pi^-$	BESIII 2013
$Y(4230)$	4230 ± 14	38 ± 14	1^{--}	$\chi_{c0}\,\omega$	BESIII 2014
$Y(4260)$	4263^{+8}_{-9}	95 ± 14	1^{--}	$J/\psi\,\pi^+\pi^-$, $J/\psi\,\pi^0\pi^0$, $Z_c(3900)\,\pi$	Babar 2005
$Y(4274)$	4293 ± 20	35 ± 16	$?^{?+}$	$J/\psi\,\phi$	CDF 2010
$X(4350)$	$4350.6^{+4.6}_{-5.1}$	$13.3^{+18.4}_{-10.0}$	$0/2^{++}$	$J/\psi\,\phi$	Belle 2009
$Y(4360)$	4354 ± 11	78 ± 16	1^{--}	$\psi(2S)\,\pi^+\pi^-$	Babar 2007
$X(4630)$	$4634^{+\ 9}_{-11}$	92^{+41}_{-32}	1^{--}	$\Lambda_c^+\Lambda_c^-$	Belle 2007
$Y(4660)$	4665 ± 10	53 ± 14	1^{--}	$\psi(2S)\,\pi^+\pi^-$	Belle 2007
$Y_b(10890)$	10888.4 ± 3.0	$30.7^{+8.9}_{-7.7}$	1^{--}	$\Upsilon(nS)\pi^+\pi^-$	Belle 2010

Table 3.4: Neutral mesons above open flavor threshold excluding isospin partners of charged states.

charmonium state of the H_4 multiplet, although its decay violates heavy quark spin symmetry.

The three higher mass 1^{--} charmonia, the $X(4360)$, $X(4630)$, and $Y(4660)$,[7] have a mass that is compatible with the excited spin singlet member of the H_1 multiplet within uncertainties, although none of them falls very close to the central value. The $X(4360)$ and $Y(4660)$ decay into a spin triplet product, which violates heavy quark spin symmetry.

There is so far only one bottomonium candidate for a hybrid state, the $Y_b(10890)$, which can be identified with the spin singlet 1^{--} state of the H_1 bottomonium hybrid multiplet. However, its decay to the Υ violates heavy quark spin symmetry, which is expected to be a good symmetry for bottomonium states.

3.7.2 Comparison with the Leading Born-Oppenheimer Approximation

In a recently published paper Braaten, Langmack, and Smith [17, 84, 85] used the BO approximation to obtain the hybrid masses from the gluonic static energies computed on the lattice.

[7] It has been suggested that $X(4630)$ and $X(4660)$ might actually be the same particle [115].

	$cg\bar{c}$	$bg\bar{b}$
$H_{1/2}$	4.246	10.864
H_3	4.566	11.097
$H_{4/5}$	4.428	10.964
$H'_{1/2}$	4.596	11.071

Table 3.5: Predicted multiplet masses from [17, 84, 85] before adjusting to lattice data. The prime on a multiplet stands for the first excited state of that multiplet. All values are given in units of GeV.

They did not consider the hybrid potential mixing in the Schrödinger equation, which leads to the Λ-doubling effect, cf. section 3.5.3. Considering the mixing terms results in the breaking of the degeneracy between the H_1 and H_2 multiplets as well as the H_4 and H_5 multiplets. In their approach they account for the breaking of this degeneracy by using different energy offsets for positive and negative parity potentials. These offsets were set in the charmonium sector to reproduce the spin averages of the hybrids from the direct lattice calculations of Ref. [116] and in the bottomonium sector to reproduce the mass splittings between the 1^{--}, 1^{++}, and 0^{++} states from the NRQCD lattice computations of Ref. [83].

We have listed the results from [17, 84, 85] suitable for comparison with our results in Table 3.5, and we have plotted them together with our results obtained using the $V^{(0.25)}$ potential in Fig. 3.4 for both charmonium and bottomonium hybrids. The predicted $H_{1/2}$ mass from Braaten *et al.* (before adjusting to lattice data) should be compared with our H_2 mass, since this multiplet is a pure Π_u potential state. Similarly, their $H_{4/5}$ mass should be compared with our H_5 mass. The H_3 multiplet is a pure Σ_u^- potential state in both approaches and can also be compared. We can see that there is a good agreement with our results from Table 3.3. If we shift the masses by the difference in the $H_{1/2}$ state ~ 30 MeV, then the other states agree within 40 MeV. The mass shift of 30 MeV should be accounted for through the uncertainty of the gluelump mass and other systematic errors, so we can take the 40 MeV discrepancy between our results and those of [17, 84, 85] to be the uncertainty coming from the fitting of the potentials and the solution of the Schrödinger equation. Overall, comparing with the results from [17, 84, 85], we can see that the effect of introducing the Λ-doubling terms lowers the masses of the multiplets that have mixed contributions from the two hybrid static energies.

3.7.3 Comparison with Direct Lattice Computations

The spectrum of hybrids in the charmonium sector has recently been calculated by the Hadron Spectrum Collaboration [116] using unquenched lattice QCD. The calculations were done using an anisotropic lattice with a Shekholeslami-Wohlert fermion action with tree-level tadpole improvements and three-dimensional stout-link smearing of the gauge fields. The calculations were performed on two lattice volumes $16^3 \times 128$ and $24^3 \times 128$ with a spatial spacing of ~ 0.12 fm. The light quarks were given unphysically heavy masses equivalent to a pion mass of ≈ 400 MeV.

To interpret their results, the Hadron Spectrum Collaboration organizes the hybrid states into spin-symmetry multiplets. They generate these spin-symmetry multiplets in the constituent gluon picture. The spin-symmetry multiplet resulting from combining a 1^{+-} gluonic

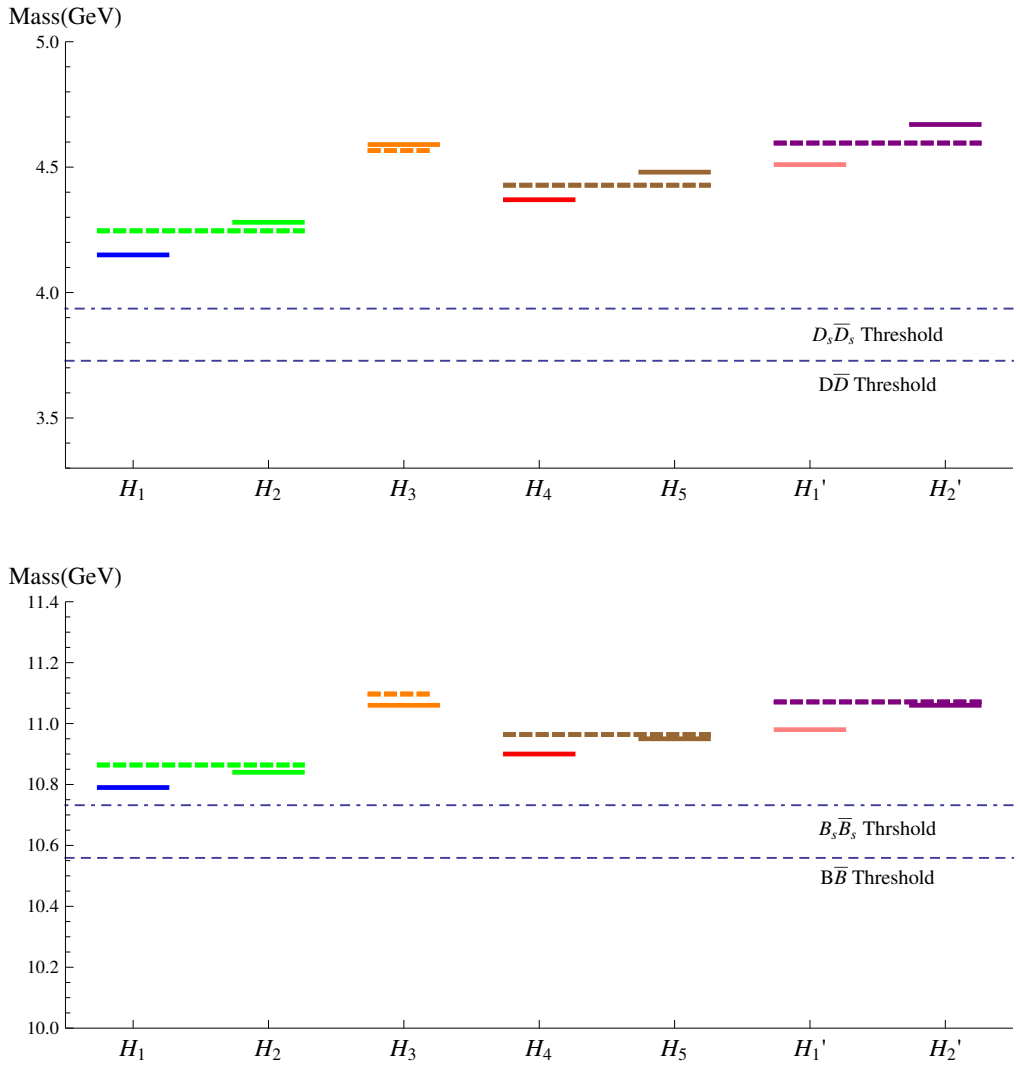

Figure 3.4: Comparison of the hybrid multiplet masses in the charmonium (upper figure) and bottomonium (lower figure) sectors obtained by Braaten *et al.* [17, 84, 85] (before adjusting to lattice data) with the results obtained using the $V^{(0.25)}$ potential. The Braaten *et al.* results correspond to the dashed lines, while the solid lines correspond to the results obtained using $V^{(0.25)}$. The degeneracy of the masses of the $H_{1/2}$ and $H_{4/5}$ multiplets in Braaten *et al.* is broken by the introduction of the mixing terms in our approach.

constituent with an S-wave heavy-quark pair generates the J^{PC} quantum numbers corresponding to our H_1 multiplet. The P-wave heavy-quark pair generates a multiplet with the J^{PC} quantum numbers corresponding to the ones in our H_2, H_3 and H_4 multiplets. Then the lattice results can be assigned to the S-wave or P-wave multiplets according to their J^{PC} quantum numbers. The Hadron Spectrum Collaboration then argues that the closeness in the masses of the states of each multiplet validates the constituent gluon picture.

Similarly, the direct lattice results can be assigned to the pNRQCD (or BO) multiplets of Table 3.2, however, this assignment is ambiguous because some J^{PC} quantum numbers appear more than once in the H_2, H_3, and H_4 multiplets. We choose to work with the same assignment as was used in [17, 84, 85] (see Table 3.6), which assigns states to a specific multiplet based on the closeness in mass. Looking at Fig. 3.5, the direct lattice calculation seems to support

multiplet	J^{PC}	m	spin average
H_1	1^{--}	4.285(14)	4.281(16)
	0^{-+}	4.195(13)	
	1^{-+}	4.217(16)	
	2^{-+}	4.334(17)	
H_2	1^{++}	4.399(14)	4.383(30)
	0^{+-}	4.386(09)	
	1^{+-}	4.344(38)	
	2^{+-}	4.395(40)	
H_3	0^{++}	4.472(30)	4.476(22)
	1^{+-}	4.477(19)	
H_4	2^{++}	4.492(21)	4.517(23)
	1^{+-}	4.497(39)	
	2^{+-}	4.509(18)	
	3^{+-}	4.548(22)	

Table 3.6: Spectrum of charmonium hybrids calculated by the Hadron Spectrum Collaboration [116]. We have added the experimental value $m_{\eta_c} = 2.9837(7)$ GeV. All values are given in units of GeV.

the result of the pNRQCD and BO approaches that the hybrid states appear in three distinct multiplets (H_2, H_3, and H_4) as compared to the constituent gluon picture, where they are assumed to form one supermultiplet together (cf. also the discussion in [17, 84, 85]).

The results from [116] are given with the η_c mass subtracted and are not extrapolated to the continuum limit. In Table 3.6 we list their results with the experimental value of $m_{\eta_c} = 2.9837(7)$ GeV added. In Fig. 3.5 the results from [116] have been plotted together with our results using the $V^{(0.25)}$ potential. We have also computed the spin averaged mass of each multiplet in order to compare with our results from Table 3.3.

Comparing the spin averages of the masses of the hybrid states from [116] to our results, we see that the masses obtained using the $V^{(0.25)}$ potentials are closer to the direct lattice calculations than the ones obtained using the $V^{(0.5)}$ potentials. For the states obtained from $V^{(0.25)}$ our masses are $0.1 - 0.14$ GeV lower except for the H_3 multiplet, which is 0.11 GeV higher. It is interesting to note that the H_3 multiplet is the only one dominated by the Σ_u^- potential. For the states obtained using $V^{(0.5)}$ the differences roughly double.

To further illustrate this comparison, we give the mass splittings between the different multiplets in Table 3.7. Again, we find a better agreement of the lattice data with our calculation with the $V^{(0.25)}$ potentials. In particular, the mass difference between H_1 and H_2, which in our calculation is directly related to the Λ-doubling effect, is very close to our mass difference. The worst agreement is again found for the H_3 multiplet.

In the bottomonium sector direct lattice calculations have been carried out by Juge, Kuti, and Morningstar [83] and by Liao and Manke [117]. Juge, Kuti, and Morningstar did quenched simulations using anisotropic lattices with improved gauge-field actions for the gluons. The heavy quarks were treated in NRQCD for anisotropic lattices containing just a covariant tem-

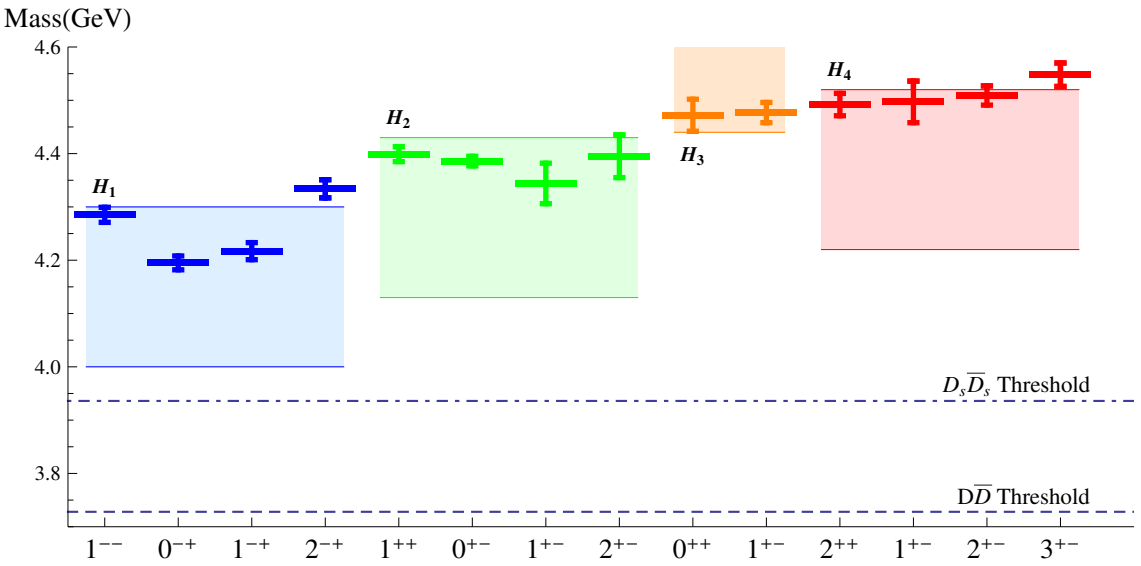

Figure 3.5: Comparison of the results from direct lattice computations of the masses for charmonium hybrids [116] with our results using the $V^{(0.25)}$ potential. The direct lattice mass predictions are plotted in solid lines with error bars corresponding to the mass uncertainties. Our results for the H_1, H_2, H_3, and H_4 multiplets have been plotted in error bands corresponding to the gluelump mass uncertainty of ± 0.15 GeV.

splitting	Ref. [116]	$V^{(0.5)}$	$V^{(0.25)}$
$\delta m_{H_2-H_1}$	0.10	0.04	0.13
$\delta m_{H_4-H_1}$	0.24	0.12	0.22
$\delta m_{H_4-H_2}$	0.13	0.08	0.09
$\delta m_{H_3-H_1}$	0.20	0.64	0.44
$\delta m_{H_3-H_2}$	0.09	0.60	0.31

Table 3.7: Mass splittings between H_1, H_2, H_3, and H_4 charmonium hybrid multiplets for the potentials $V^{(0.5)}$ and $V^{(0.25)}$ compared with the spin averages from the direct lattice calculation of [116]. All values are given in units of GeV.

poral derivative term. Since the hybrid masses were expected to be large, anisotropic lattices with the temporal lattice spacing much smaller than the spatial spacing were used to reduce the statistical fluctuations. Two lattice volumes were used, $15^3 \times 45$ with $\beta = 3.0$ and $10^3 \times 30$ with $\beta = 2.6$.

They studied the correlation functions of five operators on the lattice, three of them corresponding to hybrid operators. They identified three hybrid states corresponding to the ground states of the H_1, H_2, and H_3 multiplets and one excited state of the H_1' multiplet. Since no spin (or any relativistic) effects were included, the results given by Juge, Kuti, and Morningstar are the masses of the degenerate multiplets, which correspond to the ones in Table 3.2.

In Ref. [83] the values of the multiplet mass splitting are given in units of r_0 relative to the mass of the $1S$ bottomonium states. We have used the most up-to-date value for $r_0 = 0.486 \pm 0.004$ fm from [5]. Using this value as well as the spin average of the $1S$ bottomonium mass states we have computed the values for the multiplet masses from their

multiplet	Ref. [83]	J^{PC}(multiplet)	Ref. [117]
H_1	10.830(30)	$1^{-+}(H_1)$	11.39(15)
H_2	10.865(54)	$0^{+-}(H_2)$	10.99(33)
H_3	11.138(28)	$2^{+-}(H_2)$	12.16(14)
H_1'	11.216(37)		

Table 3.8: Masses of the bottomonium hybrids from direct lattice calculations. We present the results of the runs with size $10^3 \times 30$, $\beta = 3.0$, and spatial lattice spacing $a \approx 1.13$ fm of Ref. [83] and with size $16^3 \times 128$, $\beta = 6.3$, and $a \approx 0.0521$ fm from Ref. [117]. All values are given in units of GeV.

splitting	Ref. [83]	$V^{(0.5)}$	$V^{(0.25)}$
$\delta m_{H_2-H_1}$	0.04	0.02	0.05
$\delta m_{H_3-H_1}$	0.31	0.36	0.27
$\delta m_{H_3-H_2}$	0.27	0.34	0.22
$\delta m_{H_1'-H_1}$	0.39	0.10	0.19

Table 3.9: Mass splittings between the H_1, H_2, H_3, and H_1' bottomonium hybrid multiplets for the potentials $V^{(0.5)}$ and $V^{(0.25)}$ compared with the values from Ref. [83]. All values are given in units of GeV.

largest lattice volume in Table 3.8.

Liao and Manke [117] calculated the bottomonium spectrum using quenched lattice QCD on an anisotropic lattice. They were able to go beyond the non-relativistic approximation by using a very fine discretization in the temporal spacing, which also allowed them to extrapolate the results for the hyperfine splitting of the standard bottomonium to the continuum. They used a standard Wilson action for the gluons with various link smearing, while for the heavy quarks in the gluonic background they used an anisotropic clover action. They explored five different lattice spacings from 0.04 fm to 0.17 fm and two anisotropy ratios.

They determined the masses for three $b\bar{b}$ mesons with explicit exotic quantum numbers. The results for the level splittings are presented in an analogous way to the Juge, Kuti, and Morningstar paper, and we have used the same spin independent masses for the $1S$ and $1P$ bottomonium states in order to generate the values displayed in Table 3.8.

We have plotted the results from Juge, Kuti, and Morningstar and the ones from Liao and Manke together with our predictions for the masses of the bottomonium hybrid multiplets in Fig. 3.6. If we compare our results from Table 3.3 with the values from direct lattice calculations from Table 3.8, we observe that our results are systematically lower by $0.05 - 0.15$ GeV except for the excited H_1' state, for which the deviation is larger: 0.4 GeV and 0.26 GeV for the potentials $V^{(0.5)}$ and $V^{(0.25)}$, respectively. To eliminate possible systematic uncertainties we can look at the level splitting displayed in Table 3.9. The values of the level splitting show considerable agreement, improving from using the $V^{(0.5)}$ potentials to using the $V^{(0.25)}$ potentials, with the only exception of the H_1' state. In particular, the Λ-doubling effects seen in the mass splitting between H_2 and H_1 agree quite well with lattice predictions.

In general, the comparison of our results with direct lattice computations of hybrid masses shows a systematic energy offset but a reasonable agreement for the mass splittings between

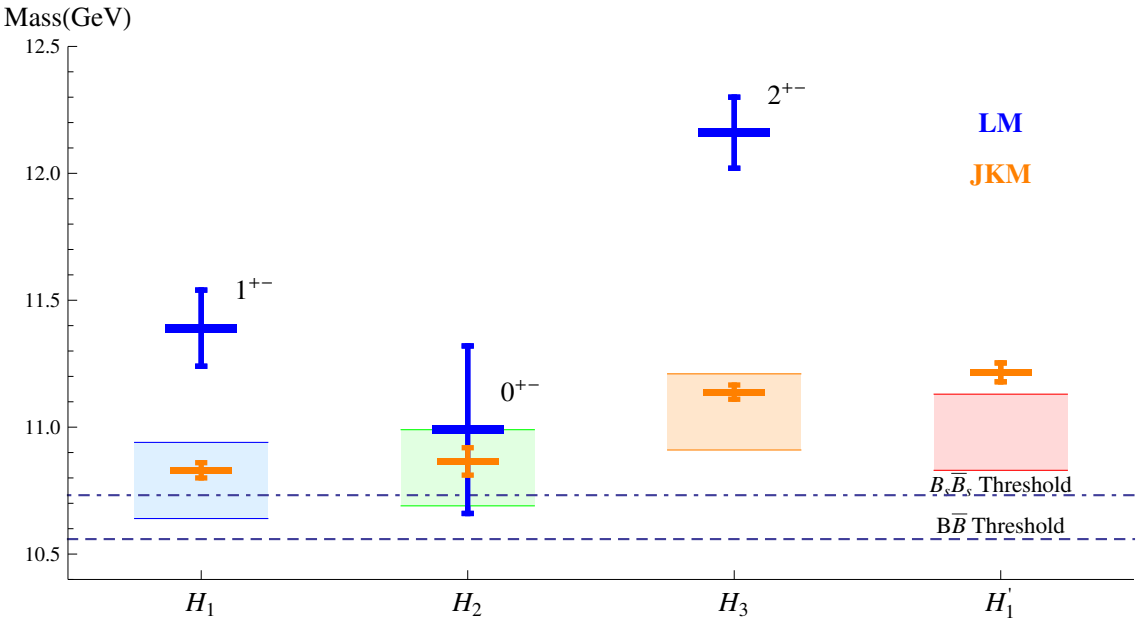

Figure 3.6: Comparison of the results from direct lattice computations of the masses for bottomonium hybrids from Juge, Kuti, and Morningstar (JKM) [83] and Liao and Manke (LM) [117] with our results using the $V^{(0.25)}$ potential. The direct lattice mass predictions are plotted in solid lines with error bars corresponding the mass uncertainties. Orange lines correspond to the results of JKM and blue lines to the ones of LM. The J^{PC} quantum numbers in the figure correspond to the LM states. Our results for the H_1, H_2, H_3, and H_1' multiplets have been plotted in error bands corresponding to the gluelump mass uncertainty of ± 0.15 GeV.

multiplets, particularly for the lower mass ones. The bottomonium sector results show more consistency with direct lattice computations than the charmonium sector, as expected.

3.7.4 Comparison with QCD Sum Rules

The method of QCD sum rules consists of a treatment in which hadrons are represented by their interpolating quark currents, taken at large virtualities, instead of in terms of constituent quarks. The correlation function of these currents is treated in the context of the operator product expansion, where the short and long distance physics are separated. The former is calculated using perturbation theory, whereas the latter is parametrized in terms of universal vacuum condensates or light-cone distribution amplitudes. The result of the calculation can then be related via dispersion relations to a sum over hadronic states.

A recent analysis of QCD sum rules for hybrid operators has been performed by Chen *et al.* for $b\bar{b}$ and $c\bar{c}$ hybrids in [118] and for $b\bar{c}$ hybrids in [119]. Using hybrid operators and computing correlation functions and spectral functions up to dimension six condensates, they stabilized the sum rules and gave mass predictions for the heavy quark hybrids.

The pattern of hybrid states encountered by Chen *et al.* in [118], which we show in Table 3.10 and, plotted against our results using the $V^{(0.25)}$ potential, in Fig. 3.7, is the same for $c\bar{c}$ and $b\bar{b}$ hybrid states. The lightest set of states they found corresponds to our H_1 multiplet. The next set of states consists of 0^{+-}, 1^{+-}, and 1^{++}, which belong to the H_2 multiplet, 2^{++} and 0^{++}, which are part of the multiplets H_3 and H_4, respectively, and 0^{--}, which does not

multiplet	J^{PC}	$c\bar{c}$	$b\bar{b}$	J^P	$b\bar{c}$
H_1	1^{--}	3.36(15)	9.70(12)	1^-	6.83(16)
	0^{-+}	3.61(21)	9.68(29)	0^-	6.90(22)
	1^{-+}	3.70(21)	9.79(22)	1^-	6.95(22)
	2^{-+}	4.04(23)	9.93(21)	2^-	7.15(23)
H_2	0^{+-}	4.09(23)	10.17(22)	0^+	7.37(31)
	1^{+-}	4.53(23)	10.70(53)	1^+	7.77(24)
	1^{++}	5.06(44)	11.09(60)	1^+	8.28(37)
H_4	2^{++}	4.45(27)	10.64(33)	2^+	7.67(18)
H_3	0^{++}	5.34(45)	11.20(48)	0^+	8.55(44)
	0^{--}	5.51(50)	11.48(75)	0^-	8.48(67)

Table 3.10: Left panel: masses of the $c\bar{c}$ and $b\bar{b}$ hybrids obtained using QCD sum rules from [118]. Right panel: masses of $b\bar{c}$ hybrids from [119]. All values are given in units of GeV.

appear in any of the multiplets we have considered.

For charmonium the masses of the H_1 multiplet are between 3.36 GeV and 4.04 GeV with a spin average of 3.75(20) GeV, which is lower than our result for the H_1 multiplet (see Table 3.3). The elements of H_2 show an important dispersion, but overall tend to be larger than our value for the mass of the H_2 multiplet, like in the case of the 2^{++} and 0^{++} masses when compared with our results for H_3 and H_4. A similar pattern emerges for $b\bar{b}$ hybrids. The H_1 multiplet ranges between 9.7 GeV and 9.93 GeV with a spin average of 9.81(19) GeV, which is about 1 GeV below our estimates. Nevertheless, the 1^{+-}, 1^{++}, 2^{++}, and 0^{++} states are within errors of our results.

The $b\bar{c}$ hybrids have also been studied with QCD sum rules by Chen *et al.* in [119]. In this case, since the heavy quark and antiquark are not the same, the interpolating currents that couple to the hybrids have no definite C-parity. The assignment of the $b\bar{c}$ states to each multiplet has been done by analogy of the interpolating currents that generate these states in $Q\bar{Q}$ and $b\bar{c}$. In Fig. 3.8 the results from Chen *et al.* for $b\bar{c}$ hybrids are plotted alongside our results using the $V^{(0.25)}$ potential. The spin average for the $b\bar{c}$ H_1 multiplet is 7.00(16) GeV, which falls about 0.5 GeV below our result.

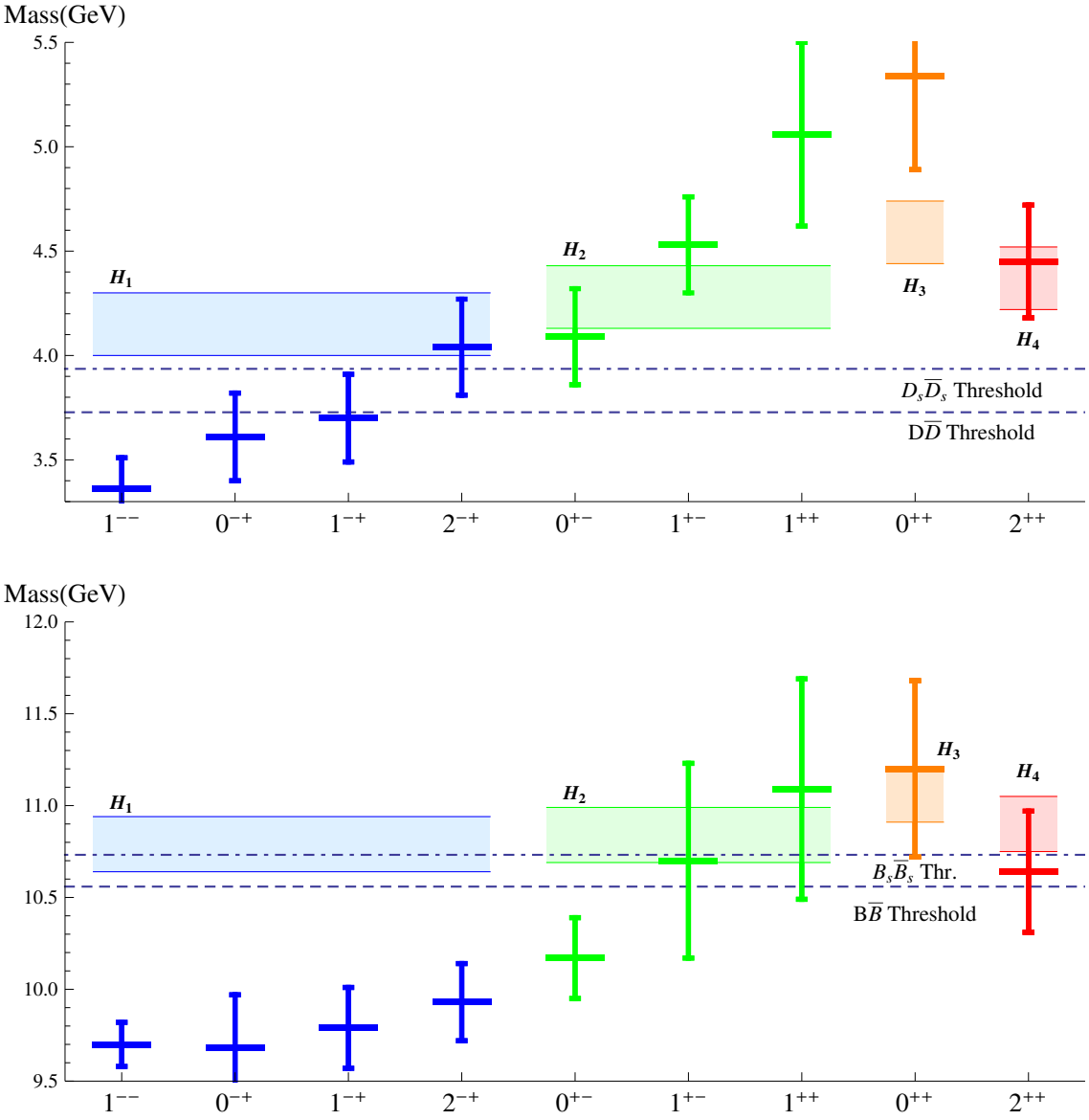

Figure 3.7: Comparison of the mass predictions for charmonium hybrids in the upper figure and for bottomonium hybrids in the lower figure, obtained using QCD sum rules [118], with our results using the $V^{(0.25)}$ potential. The solid lines correspond to the QCD sum rules masses with error bars corresponding to their uncertainties. Our results for the H_1, H_2, H_3, and H_4 multiplets have been plotted in error bands corresponding to the gluelump mass uncertainty of ± 0.15 GeV.

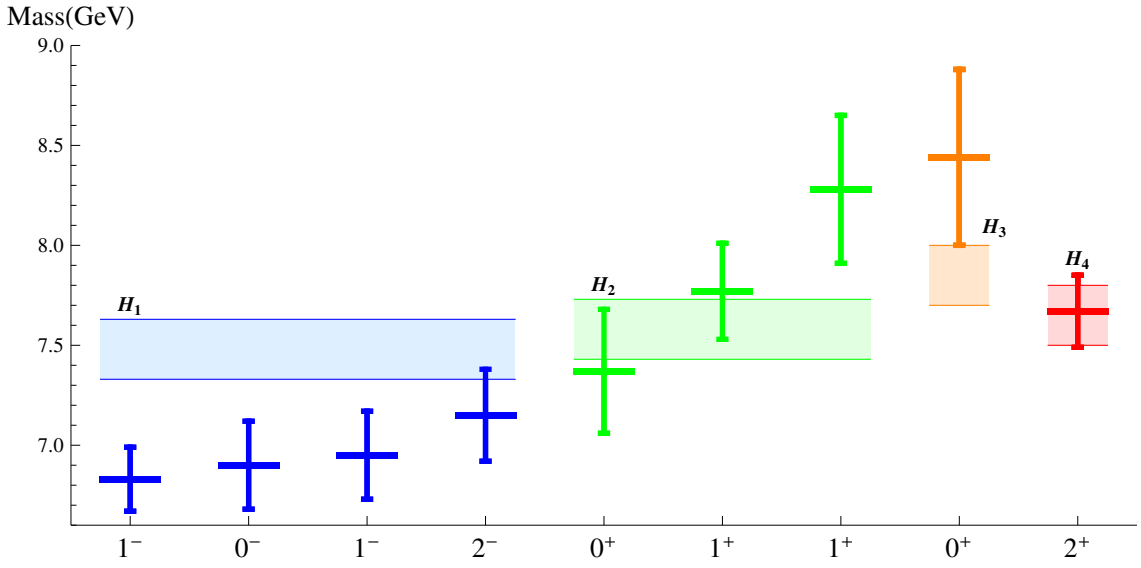

Figure 3.8: Comparison of the mass predictions for $b\bar{c}$ hybrids, obtained using QCD sum rules [119], with our results using the $V^{(0.25)}$ potential. The solid lines correspond to the QCD sum rules masses with error bars corresponding to their uncertainties. Our results for the H_1, H_2, H_3, and H_4 multiplets have been plotted in error bands corresponding to the gluelump mass uncertainty of ± 0.15 GeV.

Chapter 4

The Polyakov Loop and the Polyakov Loop Correlator at NNLO

4.1 Introduction

The Polyakov loop is an order parameter for deconfinement in pure SU(N) gauge theories at non-zero temperature T. It is defined as the thermal average over the trace of the Polyakov loop operator[1]:

$$L = \langle \widetilde{\mathrm{Tr}}[L(\boldsymbol{r})] \rangle \equiv \frac{1}{d_R} \mathrm{Tr} \left\langle \mathcal{P} \exp\left[ig \int_0^{1/T} d\tau A_0(\tau, \boldsymbol{r}) \right] \right\rangle , \tag{4.1}$$

where $\mathcal{P}$ denotes path ordering of the exponential of the temporal component of the gauge field A_0 integrated along the compactified imaginary time direction, and g is the coupling constant[2]. Here we have defined the Polyakov loop in a general representation R of SU(N), so the gauge fields are understood as matrices in this representation R, and the normalized trace $\widetilde{\mathrm{Tr}}$ is divided by the dimension d_R of this representation. The thermal expectation value of a single Polyakov loop is invariant under translations, so we can choose it to be at the origin in the following.

The non-zero expectation value of the Polyakov loop above some temperature indicates the onset of color screening and thus deconfinement [120]. Early lattice studies of the Polyakov loop and its correlators were instrumental in establishing the existence of a deconfinement transition in non-Abelian gauge theories from first principle calculations [121, 122]. The physical interpretation of the logarithm of the Polyakov loop expectation value is the free energy of a static quark $F_Q/T = -\ln L$ (see e.g. discussions in Ref. [122]). The free energy of a static quark in a gluonic plasma is finite due to color screening, but becomes infinite below the phase transition temperature T_c.

While in the presence of $n_f > 0$ flavors of light quarks the Polyakov loop is no longer an order parameter for deconfinement [123], its value at sufficiently high temperatures is still a measure of the screening properties of the deconfined medium. It is easy to see that at leading nontrivial order the Polyakov loop expectation value is $L = 1 + C_R \alpha_s m_D / 2T$, or equivalently

[1] We will use the symbol L both for the (matrix valued) operator and its traced thermal expectation value. It should be clear from context, i.e. whether it appears inside a thermal average or not, which one is meant.

[2] Note that this definition implies $D_0 = \partial_0 - igA_0$, which we choose simply to minimize the number of minus signs.

$F_Q = -C_R \alpha_s m_D/2$, where C_R is the quadratic Casimir of the representation R defined by $T_R^a T_R^a = C_R \mathbb{1}_{d_R}$. For the fundamental and adjoint representations, the quadratic Casimirs are $C_F = (N^2-1)/2N$ and $C_A = N$. The Debye mass m_D is given by

$$m_D^2 = \left(\frac{N}{3} + \frac{n_f}{6}\right) g^2 T^2 \,, \tag{4.2}$$

The next-to-leading-order (NLO) contribution to the Polyakov loop is of $\mathcal{O}(g^4)$. The first calculation of the NLO contribution was performed long ago [124]. However, several years later, it was shown that this calculation was not correct and the correct NLO contribution was calculated independently by two groups [125, 126].

The Polyakov loop has been studied in lattice QCD both in SU(N) gauge theories [127–130] and in the physically relevant case of 2+1 flavor QCD [4, 5, 131–136]. For the understanding of the screening properties of the deconfined medium it is important to connect lattice calculations with perturbative calculations at high temperatures and to see to what extent these calculations agree. In this perspective it is important to compute next-to-next-to-leading order (NNLO) corrections, which will considerably reduce the uncertainties of the NLO result by fixing the scale dependence of the coupling constant at leading order. The computation of the Polyakov loop at NNLO accuracy is one purpose of this chapter.

One feature of the lattice results on the Polyakov loop is Casimir scaling [130], the property that the ratio of static quark free energies in different representations should be given by the ratio of the quadratic Casimirs of those respective representations. One outcome of our analysis is that Casimir scaling holds up to $\mathcal{O}(g^7)$. This is important for understanding the lattice results for the Polyakov loops in higher representations [130, 137, 138].

In analogy to a single Polyakov loop, the correlator of two traced Polyakov loops gives the free energy of a static quark-antiquark pair [122]. This operator does not have an interpretation as an order parameter, since a quark and an antiquark are also allowed to exist in the vacuum in the form of a quarkonium bound state. But the Polyakov loop correlator is related to the interactions of heavy quarks in a thermal medium and may be an important quantity to study the thermal modifications of interquark potentials. It can be decomposed into color singlet and adjoint contributions, which is why the related free energy has also been called the color averaged potential.

The Polyakov loop correlator has been extensively studied on the lattice both in pure SU(N) gauge theories [127, 129, 139] as well as in QCD [136, 140, 141], calling for a more thorough understanding in analytic calculations for weak coupling. It is presently known at NNLO [122, 126], and a matching to pNRQCD in the small distance limit has also been performed, clarifying the relation to singlet and adjoint contributions. The new result for the Polyakov loop will allow us to give the correlator at one higher order. We will also present an exponentiated expression for the Polyakov loop correlator, which greatly reduces the number of relevant Feynman diagrams, and in which a separation into singlet and adjoint contributions naturally emerges. This however is not identical to the one in pNRQCD, which we will clarify in a matching.

The rest of this chapter is organized as follows. In the next section we outline our strategy for the perturbative calculation to $\mathcal{O}(g^5)$ and discuss the power counting. The calculation of the necessary loop integrals is presented in section 4.3, which also contains the main result of the chapter. In section 4.4, we comment on the higher order perturbative terms discussing Casimir scaling and outlining the $\mathcal{O}(g^6)$ calculation. In section 4.5, we compare the perturbative $\mathcal{O}(g^5)$ result with available lattice results.

The Polyakov loop correlator, its exponentiation, and its relation to singlet and adjoint free energies is then explained in more detail in section 4.6. The explicit calculation is given in section 4.7, and finally section 4.8 discusses the matching to pNRQCD. Several technical details of the calculations are presented in appendices B.

4.2 Outline of the Perturbative Calculation

In this section, we will outline the perturbative calculation of the Polyakov loop. We will perform calculations directly in QCD as well as using the effective field theory approach. The direct calculation of the NNLO correction to the Polyakov loop is rather involved and its details will be discussed in the next section. On the other hand, as we will see, the calculation that relies on the effective field theory approach is rather simple, because we can draw on previous results.

4.2.1 The Structure of the Perturbative Series

The following way of defining the path ordered exponential is particularly suited for perturbative expansions:

$$\begin{aligned} L &= \frac{1}{d_R}\mathrm{Tr}\left\langle \mathcal{P}\exp\left[ig\int_0^{1/T} d\tau A_0(\tau,\mathbf{0})\right]\right\rangle \\ &= \sum_{n=0}^{\infty}(ig)^n\int_0^{1/T}d\tau_1\int_0^{\tau_1}d\tau_2\cdots\int_0^{\tau_{n-1}}d\tau_n\,\frac{1}{d_R}\mathrm{Tr}\big\langle A_0(\tau_1,\mathbf{0})A_0(\tau_2,\mathbf{0})\cdots A_0(\tau_n,\mathbf{0})\big\rangle\,. \end{aligned} \tag{4.3}$$

The Feynman diagrams for the Polyakov loop can then be drawn as a straight line from 0 to $1/T$ in the imaginary time direction to which n gluons are attached. The line represents the contour integrations over the gauge fields. In the gauges we are going to use for this calculation, where the gluon propagator is diagonal in color space, it is possible to split each diagram into a color coefficient and a kinematic part. The color coefficient contains the trace over the color matrices from the gauge fields and any structure constants coming from interaction vertices as well as symmetry factors, while the kinematic part contains the integrations over Euclidean time, spatial momenta, etc., as well as the propagators and the Lorentz structures.[3]

It has been shown in [142, 143] that the perturbative series for any closed Wilson line can be rearranged such that it takes the form of an exponential of a series over the same diagrams but with altered color coefficients, several of which are zero. This result has been generalized in [144, 145] for the exponentiation of any Wilson line operator. In the case of the Polyakov loop we have

$$\begin{aligned} L &= 1+\mathcal{K}\Bigg(C_R\;\;+C_R^2\;\;+C_R\left(C_R-\frac{N}{2}\right)\;\;+C_R^2\;\;\Bigg)+\dots \\ &= \exp\left[C_R\,\mathcal{K}\Big(\;\;\Big)-\frac{1}{2}C_R N\,\mathcal{K}\Big(\;\;\Big)+\dots\right] = \exp\left(D_1+D_2+\dots\right), \end{aligned} \tag{4.4}$$

[3] Since three- and four-gluon vertices contain a sum over several terms, it may be necessary for some diagrams to split each term separately into color coefficient and kinematic part. This is not required for any diagram appearing in this chapter; only in the case of tadpoles there appear two terms from the vertex, but they give the same contribution, so we just include a factor 2 in the color coefficient.

where we use $\mathcal{K}$ for the kinematic part of a diagram. Here we have written the color coefficients explicitly, but in the following we will generically use the symbol $\mathcal{C}$ for the color coefficient of a diagram and $\widetilde{\mathcal{C}}$ for the exponentiated coefficient. The gluon propagators are understood as resummed. The dots represent diagrams with three or more gluons, which are at least $\mathcal{O}(g^6)$ and therefore beyond our accuracy. There is also a diagram with three propagators connected by a three-gluon vertex, which would be $\mathcal{O}(g^4)$ at leading order, but since a three-gluon vertex with only temporal indices vanishes, this diagram gives no contribution in all gauges where the propagator is block diagonal in the temporal and spatial components, so it has been neglected in the expression above. We note that the free energy of the static charge corresponding to the above expression is proportional to C_R and thus obeys Casimir scaling at this order. We use the abbreviations D_1 and D_2 for the product of kinematic part and color factor of the remaining one- and two-gluon diagrams in the exponent.

First, we perform the integral over the Euclidean time in the expression for D_1 and D_2 to get

$$D_1 = C_R(ig)^2 \int_0^{1/T} d\tau_1 \int_0^{\tau_1} d\tau_2 \sum\!\!\!\!\!\!\int_K e^{ik_0(\tau_1-\tau_2)} D_{00}(K) = -\frac{C_R g^2}{2T} \int_k D_{00}(0,\boldsymbol{k})\,, \tag{4.5}$$

$$\begin{aligned} D_2 &= -\frac{1}{2} C_R N (ig)^4 \int_0^{1/T} d\tau_1 \int_0^{\tau_1} d\tau_2 \int_0^{\tau_2} d\tau_3 \int_0^{\tau_3} d\tau_4 \sum\!\!\!\!\!\!\int_{K,Q} e^{ik_0(\tau_1-\tau_3)} e^{iq_0(\tau_2-\tau_4)} D_{00}(K) D_{00}(Q) \\ &= -\frac{C_R N g^4}{4T} \int_{k,\,q} \left[\frac{1}{12T} D_{00}(0,\boldsymbol{k}) D_{00}(0,\boldsymbol{q}) - {\sum_{k_0}}' \frac{1}{k_0^2} D_{00}(K) \big(2D_{00}(0,\boldsymbol{q}) - D_{00}(k_0,\boldsymbol{q}) \big) \right]. \end{aligned} \tag{4.6}$$

The sum with a prime denotes a Matsubara sum without the zero mode. Up to this point the discussion is independent of the choice of gauge for the perturbative calculations. In this chapter we will use Feynman gauge, static gauge, and Coulomb gauge. In appendix B.1, we discuss the gluon propagators and self-energies in these gauges.

The integration momenta $\boldsymbol{k}$ and $\boldsymbol{q}$ can either be of the order of the temperature scale πT or of the scale of the Debye mass m_D. In principle, they may also scale with the nonperturbative magnetic mass m_M. The magnetic mass enters the temporal propagators not directly but only through self-energies. Hence, as we will show at the end of this section, momentum regions scaling with m_M contribute only to $\mathcal{O}(g^7)$. We use dimensional regularization to treat both infrared and ultraviolet divergences. In this regularization scheme the different momentum scales can be separated by expanding the integrand according to the hierarchy $\pi T \gg m_D \gg m_M$.

We start considering D_1. Separating out the contributions from the scales πT, m_D, and m_M we write

$$\begin{aligned} D_1 &= -\frac{C_R g^2}{2T} \int_k \frac{1}{k^2 + \Pi(0,k)} \\ &= -\frac{C_R g^2}{2T} \left\{ \int_{k\sim\pi T} \frac{-\Pi_T^{(1)}(0,k)}{k^4} + \int_{k\sim m_D} \left[\frac{1}{k^2+m_D^2} - \frac{\Pi_{m_D}^{(1)}(0,k)}{(k^2+m_D^2)^2} + \frac{\Pi_{m_D}^{(1)}(0,k)^2}{(k^2+m_D^2)^3} \right.\right. \\ &\quad \left.\left. - \frac{1}{(k^2+m_D^2)^2} \left(\frac{d\Pi_T^{(1)}}{dk^2}(0,0)\, k^2 + \Pi_T^{(2)}(0,0) + \Pi_{m_D}^{(2)}(0,k) + \Pi_{m_M}^{(1)}(0,k) \right) \right] \right\} + \mathcal{O}\left(g^6\right). \end{aligned} \tag{4.7}$$

Here $\Pi_T^{(i)}$, $\Pi_{m_D}^{(i)}$, and $\Pi_{m_M}^{(i)}$ denote the contributions to the self-energy of the A_0 field at i-loop order coming from loop momenta of order πT, m_D, and m_M. There can also be self-energies where the loop momenta are not all of the same scale, but these do not contribute until $\mathcal{O}(g^6)$. The self-energies entering the above equation depend on the choice of gauge. The terms proportional to $\Pi_T^{(1)}$ and $\Pi_{m_D}^{(1)}$, together with tree-level D_2, give rise to the known $\mathcal{O}(g^4)$ term in the expression of the Polyakov loop [125, 126]. The 2-loop scale πT contribution to the self-energy $\Pi_T^{(2)}$ as well as the $\dfrac{d\Pi_T^{(1)}}{dk^2}(0,0)\,k^2$ term give rise to terms of $\mathcal{O}(g^5)$, some of which have been identified in Ref. [126] and are related to the running of the coupling constant. The terms proportional to $\Pi_{m_D}^{(2)}$ and $\left(\Pi_{m_D}^{(1)}\right)^2$ are new and also contribute at $\mathcal{O}(g^5)$ to the Polyakov loop. In section 4.3, we will discuss the calculation of these terms in detail. Finally, the term proportional to $\Pi_{m_M}^{(1)}$ does not contribute to the Polyakov loop at $\mathcal{O}(g^5)$ and $\mathcal{O}(g^6)$. This will also be shown in section 4.3.

Concerning D_2, it is easy to see that the leading order contribution of the first term in Eq. (4.6) in any gauge comes only from the scale m_D and is of $\mathcal{O}(g^6)$, which is beyond the accuracy of this calculation. It was already identified in Ref. [126]. The second and third terms in Eq. (4.6) do not contribute in static gauge because $D_{00}(K)$ vanishes for non-zero k_0. In Coulomb gauge the second term starts to contribute at $\mathcal{O}(g^7)$ and the third at $\mathcal{O}(g^8)$, since the leading order propagators with non-zero Matsubara frequencies are scaleless and need at least one loop insertion in order not to vanish. In Feynman gauge the second term in Eq. (4.6) contributes already at $\mathcal{O}(g^5)$ for $k \sim \pi T$ and $q \sim m_D$, while the third starts to contribute at $\mathcal{O}(g^4)$ when both momenta are of the scale πT. There is no $\mathcal{O}(g^5)$ contribution from the third term, since the scale m_D can only enter Feynman gauge propagators with non-zero frequencies through loops, which would at least be of $\mathcal{O}(g^7)$.

In summary we see that the $\mathcal{O}(g^5)$ contribution to the Polyakov loop receives two different contributions. The first comes from terms with mixed scales like the two-loop self-energy at a scale m_D with loop momenta of order πT or two-gluon exchange. The second comes from the two-loop self energy with loop momenta of order m_D. In the effective field theory approach that will be discussed in the next subsection these two contributions correspond to two different steps of the calculation: the determination of the matching coefficients and the calculation of the correlators in the effective theory, respectively.

4.2.2 The Polyakov Loop in an Effective Field Theory Approach

The separation between the scales πT and m_D that was used in the calculation of the previous section can also be achieved with EQCD, which has already been described in the introduction 1.4.2. In this chapter we will also need the effective four-field interactions, for which the Lagrangian is given by:

$$\begin{aligned}\mathcal{L}_{\mathrm{EQCD}} = &\frac{1}{2}\mathrm{Tr}\left[\widetilde{F}_{ij}^2\right]^2 + \mathrm{Tr}\left[\left[\widetilde{D}_i, \widetilde{A}_0\right]^2\right] + m_E^2\,\mathrm{Tr}\left[\widetilde{A}_0^2\right] \\ &+ \lambda_E\left(\mathrm{Tr}\left[\widetilde{A}_0^2\right]\right)^2 + \bar{\lambda}_E\left(\mathrm{Tr}\left[\widetilde{A}_0^4\right] - \frac{1}{2}\left(\mathrm{Tr}\left[\widetilde{A}_0^2\right]\right)^2\right) + \dots\,, \end{aligned} \tag{4.8}$$

where at leading order $\lambda_E = (6+N-n_f)g^4T/24\pi^2$ and $\bar{\lambda}_E = (N-n_f)g^4T/12\pi^2$ (see e.g. [38]). In this case it is more convenient to write the fields as matrices in color space in the usual way $\widetilde{A}_0 = \widetilde{A}_0^a T^a$, where the color matrices are understood in the fundamental representation.

The second quartic interaction is a vanishing operator for $N = 2$ or $N = 3$, so any result can only depend on $\bar{\lambda}_E$ if $N > 3$. The couplings g_E, λ_E, and $\bar{\lambda}_E$ have been calculated to next-to-leading order (NLO) [38]. The three-dimensional gauge coupling g_E is known to next-to-next-to-leading order [146]. The NLO correction to m_E^2 has been calculated in Ref. [37]

$$m_E^2 = m_D^2 \left[1 + \frac{\alpha_\mathrm{s}}{4\pi}\left(\frac{5}{3}N + \frac{2}{3}n_f\,(1 - 4\ln 2) + 2\beta_0\left(\gamma_E + \ln\frac{\mu}{4\pi T}\right)\right)\right] - C_F n_f \alpha_\mathrm{s}^2 T^2\,. \tag{4.9}$$

Here and in the rest of this section we express all matching parameters in terms of the renormalized coupling. Thus the pole that appears with the first coefficient of the beta function $\beta_0 = 11N/3 - 2n_f/3$ has already been canceled.

In EQCD we can write the Polyakov loop in the following way [125]

$$L = \mathcal{Z}_0 - \mathcal{Z}_2 \frac{g^2}{2\,d_R\,T}\mathrm{Tr}\big\langle \widetilde{A}_0^2\big\rangle + \mathcal{Z}_4 \frac{g^4}{24\,d_R\,T^2}\mathrm{Tr}\big\langle \widetilde{A}_0^4\big\rangle + \dots\,. \tag{4.10}$$

The matching coefficients $\mathcal{Z}_n$ are equal to 1 at leading order; at higher orders they can be written as an expansion in α_s, i.e. only in even powers of g. In the power counting of EQCD, every power of $\widetilde{A}_0$ counts as $\sqrt{gT}$, so the term proportional to $\mathcal{Z}_4$ starts to contribute at $\mathcal{O}\,(g^6)$. In EQCD only the scales m_D and m_M are still dynamical, which means that no loop momenta of order πT appear in the evaluation of the Feynman diagrams. The contributions of such loops are contained in higher order corrections to the matching coefficients $\mathcal{Z}_n$ and the EQCD parameters.

For the determination of $\mathcal{Z}_0$ and $\mathcal{Z}_2$ from QCD it is convenient to use the static gauge. In this gauge we can write

$$L = 1 - \frac{g^2}{2\,d_R\,T^2}\,\mathrm{Tr}\,\big\langle A_0^2\big\rangle + \frac{g^4}{24\,d_R\,T^4}\,\mathrm{Tr}\,\big\langle A_0^4\big\rangle + \dots\,. \tag{4.11}$$

Now we can separate each contribution into a static and a nonstatic piece, i.e. we can write

$$\big\langle A_0^2\big\rangle = \big\langle A_0^2\big\rangle_\mathrm{s} + \big\langle A_0^2\big\rangle_\mathrm{ns}\,. \tag{4.12}$$

The notation $\langle\dots\rangle_\mathrm{ns}$ means that there appear only loop momenta of order πT in the evaluation of the corresponding Feynman diagrams, which corresponds to a strict perturbative expansion in g without any resummation of self-energies. The notation $\langle\dots\rangle_\mathrm{s}$ then means that some or all loop momenta are of order m_D or m_M. The corresponding Matsubara frequencies have to be zero, hence the name "static". We can write down a similar decomposition for $\mathrm{Tr}\big\langle A_0^4\big\rangle$.

The sum over all nonstatic pieces exactly gives $\mathcal{Z}_0$. Since in static gauge the scale πT can enter the temporal propagators only through loops, the nonstatic part of the A_0^4 contribution will contribute first at $\mathcal{O}\,(\alpha_\mathrm{s}^4)$. The leading order result for the A_0^2 piece can be found in Ref. [126] and gives

$$\mathcal{Z}_0 = 1 + \frac{C_R\alpha_s^2}{2}\left[N\left(\frac{1}{2\epsilon} + 1 - \gamma_E + \ln\frac{\pi\mu^2}{T^2}\right) - n_f\ln 2\right] + \mathcal{O}\left(\alpha_s^3\right)\,. \tag{4.13}$$

The pole in ϵ is not related to charge renormalization, but corresponds to an infrared divergence in the nonstatic part that cancels against an ultraviolet divergence in the static piece, or equivalently in the EQCD calculation.

The sum over the static pieces then contains all contributions from the scales m_D and m_M and thus corresponds to the EQCD representation of the Polyakov loop without the unit operator. Up to $\mathcal{O}(g^5)$ it is sufficient to consider only the quadratic terms, i.e. $\langle A_0^2\rangle_{\mathrm{s}} = \mathcal{Z}_2\langle \widetilde{A}_0^2\rangle$. The two gauge fields in $\langle A_0^2\rangle_{\mathrm{s}}$ themselves can carry either momenta $k \ll \pi T$ or $k \sim \pi T$, however, in the latter case they only start to contribute to the static piece at three-loop order. The first loop from the two gauge fields in the correlator is scaleless, so another loop is needed to introduce the scale πT and a third one to include the scale m_D in order to be counted towards the static piece. This corresponds to diagrams like L_{10} and L_{12} in Fig. 4.1 when only the tadpole or the subloop momentum is of order m_D and the two other momenta are of order πT. The two scale πT integrations give a contribution of $\mathcal{O}(\alpha_{\mathrm{s}}^2)$ to $\mathcal{Z}_2$ and only one propagator with a momentum of order m_D remains, which corresponds to the leading order of $\langle \widetilde{A}_0^2\rangle$.

In the former case we can relate the QCD field A_0 to $\sqrt{Z_2}\widetilde{A}_0$ in EQCD, where the wave function normalization constant Z_2 can be obtained from the small momentum expansion of the propagator:

$$D_{00}^{\mathrm{QCD}}(k \ll \pi T) = Z_2 D_{00}^{\mathrm{EQCD}}(k) + \dots \,. \tag{4.14}$$

The dots stand for higher powers in the small k^2 expansion, which correspond to higher order two-point interactions in EQCD. From this expression it follows that

$$Z_2 = \left(1 + \frac{d\Pi_T}{dk^2}\left(k^2 = 0\right)\right)^{-1}, \tag{4.15}$$

and with the result from [126] we have up to corrections of $\mathcal{O}(\alpha_{\mathrm{s}}^2)$

$$\mathcal{Z}_2 = Z_2 = 1 + \frac{\alpha_{\mathrm{s}}}{4\pi}\left[\frac{11}{3}N + \frac{2}{3}n_f(1 - 4\ln 2) + 2\beta_0\left(\gamma_E + \ln\frac{\mu}{4\pi T}\right)\right]. \tag{4.16}$$

Now that we have determined the matching coefficients to the desired order, we can write the weak coupling expansion for $\langle \widetilde{A}_0^2\rangle$ as

$$\frac{1}{d_R}\mathrm{Tr}\langle \widetilde{A}_0^2\rangle = -\frac{C_R m_E}{4\pi}\left(1 + a_1\frac{g_E^2}{m_E} + a_2\frac{g_E^4}{m_E^2} + a_3\frac{g_E^6}{m_E^3} + a_4\frac{\lambda_E}{m_E} + \dots\right), \tag{4.17}$$

using simple dimensional analysis. In the above expression we explicitly wrote down all the terms contributing up to $\mathcal{O}(g^6)$ and ignored the magnetic mass scale m_M. We will return to the contribution from the scale m_M later.

In Eq. (4.17) the terms proportional to a_i come from the i-loop self-energy of the $\widetilde{A}_0$ field. The coefficient a_1 is known [125, 126]. We are primarily interested in the NNLO, i.e. $\mathcal{O}(g^5)$ contribution to L. It is evident from Eqs. (4.9), (4.16), and (4.17) that the mixed scale contributions from the previous section come from the $\mathcal{O}(\alpha_{\mathrm{s}})$ corrections to $\mathcal{Z}_2$ and m_E^2, while the pure scale m_D term comes from the two-loop self-energy contribution contained in the coefficient a_2. One can perform a similar analysis for $\langle \widetilde{A}_0^4\rangle$ and see that it contributes at orders $\alpha_{\mathrm{s}}^2 m_E^2$, $\alpha_{\mathrm{s}}^3 m_E$, etc. It is also easy to generalize the analysis for $\langle \widetilde{A}_0^{2n}\rangle$, $n \geq 3$, and see that these terms do not contribute at $\mathcal{O}(g^5)$.

The only remaining task is now to calculate the coefficient a_2. This can be done using the EQCD calculation of the pressure [37]

$$p = -T\left(f_E + f_M - \frac{1}{V}\ln Z_{\mathrm{MQCD}}\right). \tag{4.18}$$

Here we use the same notation as in Ref. [37], i.e. f_E denotes the contribution from the scale πT, f_M denotes the contribution from the scale m_D, and Z_{MQCD} is the partition function of MQCD, which is completely nonperturbative. Ignoring the contribution from MQCD it is easy to see that since

$$f_M = -\frac{1}{V} \ln \int \mathcal{D}\widetilde{A}_0^a \mathcal{D}\widetilde{A}_i^a \, \exp\left[- \int d^3x \, \mathcal{L}_{\mathrm{EQCD}} \right] , \tag{4.19}$$

it follows that

$$\frac{1}{d_R} \mathrm{Tr} \langle \widetilde{A}_0^2 \rangle = \frac{C_R}{N^2-1} \langle \widetilde{A}_0^a \widetilde{A}_0^a \rangle = \frac{2C_R}{N^2-1} \frac{\partial f_M}{\partial m_E^2} . \tag{4.20}$$

Using the expression for f_M from [37] we get

$$\begin{aligned} \frac{1}{d_R} \mathrm{Tr} \langle \widetilde{A}_0^2 \rangle = & - \frac{C_R m_E}{4\pi} + \frac{C_R N g_E^2}{(4\pi)^2} \left[\frac{1}{2\epsilon} + \frac{1}{2} - \gamma_E + \ln \frac{\pi \mu^2}{m_E^2} \right] \\ & + \frac{2C_R N^2}{(4\pi)^3} \frac{g_E^4}{m_E} \left(\frac{89}{48} - \frac{11}{12} \ln 2 + \frac{\pi^2}{12} \right) + \mathcal{O}\left(g^4\right) . \end{aligned} \tag{4.21}$$

The first term corresponds to the well-known leading order result. The second term is identical to the $\mathcal{O}\left(g^4\right)$ static contribution to $\langle A_0^2 \rangle$ (cf. Eq. (44) of Ref. [126]). The $1/\epsilon$ pole in this term is exactly the ultraviolet divergence that cancels against the infrared pole in the nonstatic contribution to $\langle A_0^2 \rangle$ [126]. The scale dependence cancels in the same way. The last term gives the coefficient a_2 we are interested in.

We still need to calculate the $\mathcal{O}\left(g^5\right)$ contribution arising from the $\mathcal{O}\left(\alpha_{\mathrm{s}}\right)$ corrections to m_E and $\mathcal{Z}_2$ times the leading order result for $\mathrm{Tr}\langle \widetilde{A}_0^2 \rangle / d_R = -C_R m_D / 4\pi$. Using Eqs. (4.9) and (4.16) we find that this $\mathcal{O}\left(g^5\right)$ contribution is

$$\frac{3C_R \alpha_{\mathrm{s}}^2 m_D}{16\pi T} \left[3N + \frac{2}{3} n_f (1 - 4\ln 2) + 2\beta_0 \left(\gamma_E + \ln \frac{\mu}{4\pi T} \right) \right] - \frac{C_R C_F n_f \alpha_{\mathrm{s}}^3 T}{4 m_D} . \tag{4.22}$$

With this result and Eq. (4.21) we find the $\mathcal{O}\left(g^5\right)$ contribution to the Polyakov loop

$$\begin{aligned} L \Big|_{g^5} = & \frac{3C_R \alpha_{\mathrm{s}}^2 m_D}{16\pi T} \left[3N + \frac{2}{3} n_f (1 - 4\ln 2) + 2\beta_0 \left(\gamma_E + \ln \frac{\mu}{4\pi T} \right) \right] \\ & - \frac{C_R N^2 \alpha_{\mathrm{s}}^3 T}{m_D} \left(\frac{89}{48} - \frac{11}{12} \ln 2 + \frac{\pi^2}{12} \right) - \frac{C_R C_F n_f \alpha_{\mathrm{s}}^3 T}{4 m_D} . \end{aligned} \tag{4.23}$$

The above equation is one of the main results of this chapter. In the next section we will obtain this result via direct calculations in QCD.

The contribution from the scale m_M to $\langle \widetilde{A}_0^2 \rangle$, which we have neglected so far, can be calculated using MQCD, the effective theory obtained from EQCD by integrating out the electric scale $m_E \sim m_D$. The only scale in MQCD is the dimensionful coupling constant $g_M \sim \sqrt{m_M}$, which is given at leading order as $g_M = g_E$. Since in this theory we have only the three-dimensional gauge fields, we write

$$L = \mathcal{Z}_0^M + \frac{\mathcal{Z}_1^M}{2 m_D^3} \langle \widetilde{F}_{ij}^a \widetilde{F}_{ij}^a \rangle_{\mathrm{MQCD}} + \ldots . \tag{4.24}$$

The matching constant $\mathcal{Z}_0^M$ contains the contributions to L from the scales πT and m_D, so $\mathcal{Z}_0^M = L$ up to $\mathcal{O}\left(g^5\right)$. The matching constant $\mathcal{Z}_1^M$ has been calculated in Ref. [147] for

the fundamental representation. We have repeated that calculation, but allowed for general representations; the result is

$$\mathcal{Z}_1^M = \frac{C_R N \alpha_s^2 \pi}{12\,(N^2-1)} + \mathcal{O}\left(g^5\right) , \tag{4.25}$$

and for $C_R = C_F$ one obtains the expression from [147]. Since $\left\langle \widetilde{F}_{ij}^a \widetilde{F}_{ij}^a \right\rangle \sim m_M^3 \sim g_M^6$, we see that the contribution from the magnetic scale first appears at $\mathcal{O}\left(g^7\right)$. Through the explicit calculations presented in section 4.3 and appendix B.3 we will see that the magnetic contributions at $\mathcal{O}\left(g^5\right)$ and $\mathcal{O}\left(g^6\right)$ indeed vanish.

The $\mathcal{O}\left(g^7\right)$ contribution to the Polyakov loop can be obtained using lattice calculations in MQCD. However, for interesting temperature ranges the separation of the scales m_D and m_M is not obvious. Therefore, it is more practical to calculate $\left\langle \widetilde{A}_0^2 \right\rangle$ using lattice calculations in EQCD. Such lattice calculations have been performed with the aim to estimate the QCD pressure using the EQCD approach in Ref. [148]. We will use this lattice EQCD result when comparing the weak coupling expansion of the Polyakov loop with lattice results in QCD in section 4.5.

4.3 Calculation of the $\mathcal{O}\left(g^5\right)$ Correction to the Polyakov Loop

In this section we will present the calculations of the $\mathcal{O}\left(g^5\right)$ contribution to the Polyakov loop directly in QCD. From the discussion in the previous section it is clear that the diagrams that contribute at $\mathcal{O}\left(g^5\right)$ always have at least one momentum integral of order m_D, while the self-energy contributions may arise from the scales πT, m_D, or m_M. In what follows we will refer to them as contributions from the scale πT, m_D, or m_M, even though all the loop diagrams also involve the scale m_D. We will perform the calculations in Coulomb gauge and in Feynman gauge. The contribution from the diagram D_2 is only relevant in Feynman gauge. It involves one integral over the scale m_D and another sum-integral over the scale πT, so we will refer to it as a part of the contribution from the scale πT.

4.3.1 Contribution from the Scale πT

All self-energies relevant for the contribution from the scale πT in Feynman gauge are known and can be found in Ref. [37] (they use a slightly different convention for the $\overline{\text{MS}}$-scheme, which can be converted into our convention by replacing the renormalization scale Λ^2 in their expressions by $4\pi e^{-\gamma_E}\mu^2$):

$$\begin{aligned}\Pi_T^{(1)}(0,0) \equiv m_D^2(\epsilon) = \frac{g^2T^2}{3}\Bigg[\left(N+\frac{1}{2}n_F\right) + N\left(-\gamma_E + 2\frac{\zeta'(-1)}{\zeta(-1)} + \ln\frac{\mu^2}{4\pi T^2}\right)\epsilon \\ + \frac{1}{2}n_f\left(1-\gamma_E + 2\frac{\zeta'(-1)}{\zeta(-1)} + \ln\frac{\mu^2}{16\pi T^2}\right)\epsilon\Bigg] ,\end{aligned} \tag{4.26}$$

$$\frac{d\Pi_T^{(1)}}{dk^2}(0,0) = -\frac{g^2}{(4\pi)^2}\left[\frac{5}{3}N\left(\frac{1}{\epsilon} - \frac{1}{5} + \gamma_E + \ln\frac{\mu^2}{4\pi T^2}\right) - \frac{2}{3}n_f\left(\frac{1}{\epsilon} - 1 + \gamma_E + \ln\frac{4\mu^2}{\pi T^2}\right)\right], \tag{4.27}$$

$$\Pi_T^{(2)}(0,0) = \frac{g^4T^2}{(4\pi)^2}\left[\frac{2}{3}N^2\left(\frac{1}{\epsilon}+1+2\frac{\zeta'(-1)}{\zeta(-1)}+2\ln\frac{\mu^2}{4\pi T^2}\right)\right.$$
$$\left.+\frac{1}{3}Nn_f\left(\frac{1}{\epsilon}+2+2\frac{\zeta'(-1)}{\zeta(-1)}+2\ln\frac{\mu^2}{8\pi T^2}\right)-C_Fn_F\right]$$
$$=\frac{g^2}{(4\pi)^2}\left[2Nm_D^2(\epsilon)\left(\frac{1}{\epsilon}+1+\gamma_E+\ln\frac{\mu^2}{4\pi T^2}\right)-g^2T^2C_Fn_f\right]. \tag{4.28}$$

In the last line we have reexpressed some terms through $m_D^2(\epsilon)$, i.e. the leading order Debye mass with $\mathcal{O}(\epsilon)$ corrections. This will be crucial for the cancellation of the $1/\epsilon$-poles. The $\mathcal{O}(\epsilon)$ terms of $m_D^2(\epsilon)$ are necessary at this point.

With these we can calculate the first scale πT contribution from diagram D_1 at $\mathcal{O}(g^5)$ in Feynman gauge (FG):

$$D_1\Big|^{FG}_{g^5,\,\pi T} = \frac{C_Rg^2}{2T}\int_{k\sim m_D}\frac{1}{\left(k^2+m_D^2\right)^2}\left(\frac{d\Pi_T^{(1)}}{dk^2}(0,0)\,k^2+\Pi_T^{(2)}(0,0)\right)$$
$$=\frac{3C_R\alpha_s^2m_D(\epsilon)}{16\pi T}\left[\frac{7}{3}N\left(\frac{1}{\epsilon}+\frac{23}{21}+2\ln\frac{\mu^2}{2Tm_D}\right)-\frac{2}{3}n_f\left(\frac{1}{\epsilon}+\frac{1}{3}+2\ln\frac{2\mu^2}{Tm_D}\right)\right]$$
$$-\frac{C_RC_Fn_f\alpha_s^3T}{4m_D}. \tag{4.29}$$

The scale πT contribution from D_2 is given by

$$D_2\Big|^{FG}_{g^5,\,\pi T} = \frac{C_RNg^4}{2T}{\sum_{q_0}}'\int_{q\sim\pi T}\int_{k\sim m_D}\frac{1}{q_0^2\left(q_0^2+q^2\right)\left(k^2+m_D^2\right)}$$
$$=\frac{C_RN\alpha_s^2m_D(\epsilon)}{4\pi T}\left(\frac{1}{\epsilon}+4+2\ln\frac{\mu^2}{2Tm_D}\right), \tag{4.30}$$

and together they give

$$(D_1+D_2)\Big|^{FG}_{g^5,\,\pi T} = -\frac{C_RC_Fn_f\alpha_s^3T}{4m_D}$$
$$+\frac{3C_R\alpha_s^2m_D(\epsilon)}{16\pi T}\left[\frac{11}{3}N\left(\frac{1}{\epsilon}+\frac{71}{33}+2\ln\frac{\mu^2}{2Tm_D}\right)-\frac{2}{3}n_f\left(\frac{1}{\epsilon}+\frac{1}{3}+2\ln\frac{2\mu^2}{Tm_D}\right)\right]. \tag{4.31}$$

We see now that the coefficient of the $1/\epsilon$-terms is proportional to the first coefficient of the beta function $\beta_0 = 11N/3 - 2n_f/3$. This suggests that they are removed through charge renormalization, which is indeed the case. The first counterterm comes from charge renormalization of the $\mathcal{O}(g^3)$ term. We need to be careful with the $\epsilon\to 0$ limit, so we will keep the dimension d general until the last step:

$$D_1\Big|_{g^3} = -\frac{C_Rg^2}{2T}\int_{k\sim m_D}\frac{1}{k^2+m_D^2} = -\frac{C_Rg^2\Gamma\left(1-\frac{d}{2}\right)m_D^{d-2}\mu^{2\epsilon}}{2(4\pi)^{\frac{d}{2}}T}$$
$$\overset{g_B\to g_R}{\longrightarrow} -\frac{C_Rg^2\Gamma\left(1-\frac{d}{2}\right)m_D^{d-2}(\epsilon)\mu^{2\epsilon}}{2(4\pi)^{\frac{d}{2}}T}\left[1-\frac{d}{2}\frac{\alpha_s\beta_0}{4\pi}\left(\frac{1}{\epsilon}-\gamma_E+\ln 4\pi\right)+\mathcal{O}\left(\alpha_s^2\right)\right]. \tag{4.32}$$

The factor $d/2$ comes from the power of α_s: $g^2 m_D^{d-2} \propto \alpha_\mathrm{s}^{d/2}$. Including the counterterm for the charge renormalization we get the full contribution from the scale πT:

$$(D_1 + D_2)\Big|_{g^5,\,\pi T} = \frac{3C_R\alpha_\mathrm{s}^2 m_D}{16\pi T}\left[3N + \frac{2}{3}n_f\left(1 - 4\ln 2\right) + 2\beta_0\left(\gamma_E + \ln\frac{\mu}{4\pi T}\right)\right] - \frac{C_R C_F n_f \alpha_\mathrm{s}^3 T}{4m_D}\,. \tag{4.33}$$

We no longer indicate Feynman gauge in this final result for the scale πT contribution, because it is gauge invariant.

The corresponding calculation goes the same way for both Coulomb (CG) and static gauge (SG). D_2 is scaleless at $\mathcal{O}\left(g^5\right)$, so only D_1 contributes. It has been shown in [37] that the electric mass parameter m_E of EQCD is given up to $\mathcal{O}\left(\alpha_\mathrm{s}^2\right)$ by

$$m_E^2 = \Pi_T^{(1)}(0,0) + \Pi_T^{(2)}(0,0) - \Pi_T^{(1)}(0,0)\frac{d\Pi_T^{(1)}}{dk^2}(0,0)\,. \tag{4.34}$$

Since m_E is a gauge invariant parameter, we can eliminate $\Pi_T^{(2)}(0,0)$ in Coulomb or static gauge from this equation and express it through the Feynman gauge results and $\dfrac{d\Pi_T^{(1)}}{dk^2}(0,0)$, which is the same for Coulomb and static gauge and can be found e.g. in [126]:

$$\frac{d\Pi_T^{(1)}}{dk^2}(0,0) = -\frac{g^2}{(4\pi)^2}\left[\frac{11}{3}N + \frac{2}{3}n_f\left(1 - 4\ln 2\right) + \beta_0\left(\frac{1}{\epsilon} + \gamma_E + \ln\frac{\mu^2}{4\pi T^2}\right)\right]\,. \tag{4.35}$$

With this we have

$$\begin{aligned}\Pi_T^{(2)}\Big|^{CG/SG} &= \left(\Pi_T^{(2)} - m_D^2(\epsilon)\frac{d\Pi_T^{(1)}}{dk^2}\right)\Big|^{FG} + m_D^2(\epsilon)\frac{d\Pi_T^{(1)}}{dk^2}\Big|^{CG/SG} \\ &= -\frac{g^2}{(4\pi)^2}\left(2Nm_D^2 + g^2T^2C_F n_f\right)\,.\end{aligned} \tag{4.36}$$

The contributions from the scale πT are now

$$\begin{aligned}D_1\Big|^{CG/SG}_{g^5,\,\pi T} &= \frac{C_R g^2}{2T}\int_{k\sim m_D}\frac{1}{k^2 + m_D^2}\left(\frac{d\Pi^{(1)}}{dk^2}(0,0) + \Pi^{(2)}(0,0)\right) \\ &= \frac{3C_R\alpha_\mathrm{s}^2 m_D(\epsilon)}{16\pi T}\left[\frac{71}{9}N - \frac{2}{9}n_f\left(1 + 12\ln 2\right) + \beta_0\left(\frac{1}{\epsilon} + 2\ln\frac{\mu^2}{2Tm_D}\right)\right] \\ &\quad - \frac{C_R C_F n_f \alpha_\mathrm{s}^3 T}{4m_D}\,.\end{aligned} \tag{4.37}$$

This is the same result that we got in Feynman gauge from $D_1 + D_2$, so including the counterterm we obtain the same scale πT contribution in Coulomb and static gauge:

$$(D_1 + D_2)\Big|_{g^5,\,\pi T} = \frac{3C_R\alpha_\mathrm{s}^2 m_D}{16\pi T}\left[3N + \frac{2}{3}n_f\left(1 - 4\ln 2\right) + 2\beta_0\left(\gamma_E + \ln\frac{\mu}{4\pi T}\right)\right] - \frac{C_R C_F n_f \alpha_\mathrm{s}^3 T}{4m_D}\,. \tag{4.38}$$

4.3.2 Contribution from the Scale m_D

The contribution from the scale m_D consists of the two-loop self-energy and the square of the one-loop self-energy. It corresponds to the full g_E^4 contribution of $\left\langle \widetilde{A}_0^2 \right\rangle$ in EQCD. The relevant

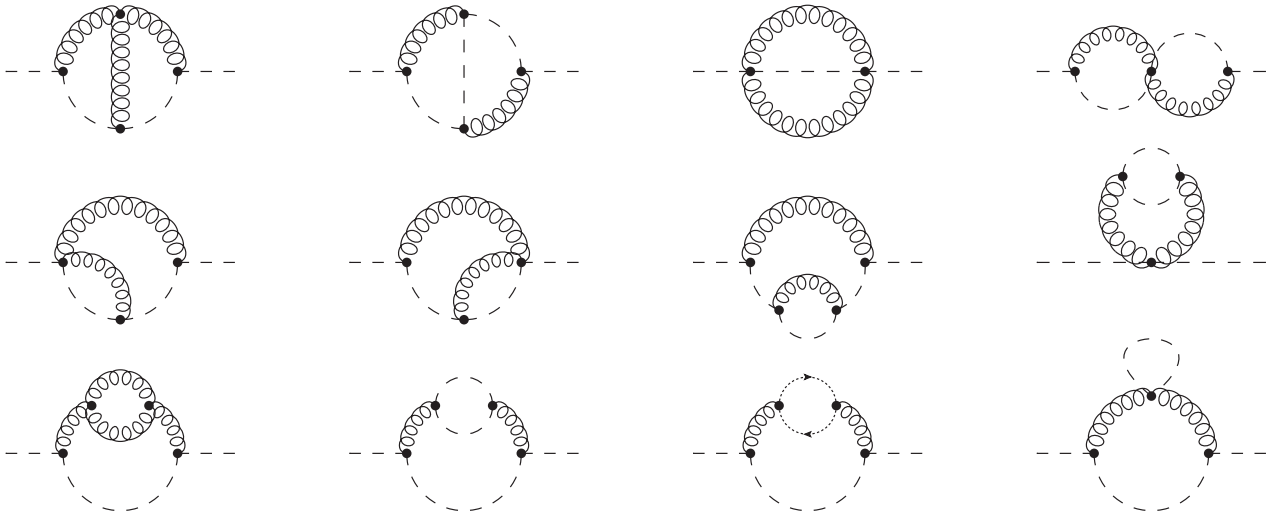

Figure 4.1: All Feynman diagrams contributing to $\Pi^{(2)}_{m_D}(0, k \sim m_D)$. Dashed lines represent temporal gluons, curly lines spatial gluons, and dotted lines with arrows are ghost propagators. The diagrams are labeled $L_1, \ldots, L_{12}$ from top-left to bottom-right. $L_7, \ldots, L_{12}$ are self-energy insertions into one-loop diagrams, while $L_1, \ldots, L_6$ are new two-loop configurations.

diagrams for the two-loop self-energy are given in Fig. 4.1. The contribution from the square of the one-loop self-energy is not displayed, it corresponds to two one-loop insertions into the temporal gluon propagator. Together they also give a gauge invariant result:

$$\begin{aligned} D_1\Big|_{g^5,\, m_D} &= -\frac{C_R g^2}{2T} \int_{k\sim m_D} \left[-\frac{\Pi^{(2)}_{m_D}(0,k)}{\left(k^2+m_D^2\right)^2} + \frac{\Pi^{(1)}_{m_D}(0,k)^2}{\left(k^2+m_D^2\right)^3} \right] \\ &= -\frac{C_R N^2 \alpha_\mathrm{s}^3 T}{m_D} \left[\frac{89}{48} + \frac{\pi^2}{12} - \frac{11}{12} \ln 2 \right] . \end{aligned} \tag{4.39}$$

The calculation itself is quite involved, so we will not go into further details here. We use the method of integration by parts to reduce the three-loop integrals corresponding to each diagram down to a handful of known master integrals. A list of all integrals and their results in different gauges is given in appendix B.2.

4.3.3 Contribution from the Scale m_M

Finally, we have to consider the contribution from the scale m_M. The temporal gluon momentum k cannot be of order m_M, because then the propagator would have to be expanded in $1/m_D^2$ and the k integration would be scaleless. But the loop momenta in the self-energy diagrams may be of order m_M and such diagrams start to contribute at $\mathcal{O}(g^5)$. However, by the arguments from EQCD and MQCD in the previous section we expect the scale m_M to enter the Polyakov loop only at $\mathcal{O}(g^7)$, so the $\mathcal{O}(g^5)$ contributions have to vanish, which is indeed the case.

There are two diagrams at this order (cf. Fig. 4.2); both have one spatial gluon that carries the momentum of order m_M. The first is the diagram, where the spatial gluon connects at two three-gluon vertices, and the second is the tadpole diagram, where the spatial gluon connects at a four-gluon vertex. From the three-gluon vertices there comes a factor $(2k+q)_i(2k+q)_j$,

Figure 4.2: All $\mathcal{O}(g^5)$ diagrams that can give a contribution from the scale m_M. The bubble stands for the resummed propagator.

where k is the momentum of order m_D and q is of order m_M, but only $4k_ik_j$ needs to be kept, because the rest is of higher order. According to the power counting, each power of q in the numerator adds a power of g to the result, while terms with odd powers of the momenta in the numerator vanish. So the first higher order contributions (i.e. the terms quadratic in q) are of $\mathcal{O}(g^7)$. For the same reason, we only have to expand the propagator of the temporal gluon with momentum $\boldsymbol{k}+\boldsymbol{q}$ in the left diagram of Fig. 4.2 to leading order in q. Then we have

$$\begin{aligned} D_1\Big|_{g^5,\,m_M} &= \frac{C_R g^2}{2T}\int_{k\sim m_D}\frac{\Pi^{(1)}_{m_M}(0,k)}{\left(k^2+m_D^2\right)^2} \\ &= \frac{C_R N g^4}{2}\int_{q\sim m_M} D_{ij}(0,\boldsymbol{q})\int_{k\sim m_D}\left[\frac{\delta_{ij}}{\left(k^2+m_D^2\right)^2}-\frac{4k_ik_j}{\left(k^2+m_D^2\right)^3}\right] \\ &= \frac{C_R N g^4}{2}\int_{q\sim m_M} D_{ii}(0,\boldsymbol{q})\,\frac{\Gamma\left(2-\frac{d}{2}\right)}{(4\pi)^{\frac{d}{2}}m_D^{4-d}}\left[1-\frac{4\,\Gamma\left(1+\frac{d}{2}\right)}{d\,\Gamma(3)\Gamma\left(\frac{d}{2}\right)}\right]=0\,. \end{aligned} \tag{4.40}$$

Also the $\mathcal{O}(g^6)$ contributions from the scale m_M need to vanish. These are the two-loop self-energy diagrams with one loop momentum of order m_M. We have also checked their cancellation explicitly; the details of this are given in appendix B.3.

4.3.4 Result

Now we have all contributions to the Polyakov loop at $\mathcal{O}(g^5)$:

$$\begin{aligned} \ln L = {} & \frac{C_R\alpha_{\mathrm{s}}m_D}{2T}+\frac{C_R\alpha_{\mathrm{s}}^2}{2}\left[N\left(\frac{1}{2}+\ln\frac{m_D^2}{T^2}\right)-n_f\ln 2\right] \\ & +\frac{3C_R\alpha_{\mathrm{s}}^2m_D}{16\pi T}\left[3N+\frac{2}{3}n_f\left(1-4\ln 2\right)+2\beta_0\left(\gamma_E+\ln\frac{\mu}{4\pi T}\right)\right]-\frac{C_RC_Fn_f\alpha_{\mathrm{s}}^3T}{4m_D} \\ & -\frac{C_RN^2\alpha_{\mathrm{s}}^3T}{m_D}\left[\frac{89}{48}+\frac{\pi^2}{12}-\frac{11}{12}\ln 2\right]+\mathcal{O}\left(g^6\right)\,. \end{aligned} \tag{4.41}$$

The second line contains the contribution from the scale πT and the third line the contribution from the scale m_D.

Figure 4.3: Connected three-gluon diagrams.

4.4 Higher Order Contributions

4.4.1 Casimir Scaling

It is known from lattice calculations that the logarithm of the Polyakov loop obeys Casimir scaling, at least approximately [130, 137, 138]. Casimir scaling is observed by any quantity, in our case the free energy F_Q of a static charge in representation R, if it is proportional to the quadratic Casimir operator C_R of that representation. In other words, F_Q/C_R should be independent of the representation R.

A necessary condition for the breaking of Casimir scaling is the appearance of a term not proportional to C_R. A term like that was identified for $L-1$ in Ref. [126] at $\mathcal{O}(g^6)$. The term is

$$\delta\langle L\rangle = \frac{1}{2}\left(\frac{C_R\alpha_{\rm s}m_D}{2T}\right)^2 . \tag{4.42}$$

This term, however, does not break the Casimir scaling of the free energy F_Q, since it is nothing else than the second order term in the expansion of $\exp(-F_Q/T)$, when F_Q is taken at leading order. In fact, this term does not appear in F_Q. Note that the exponentiation formula given in (4.4) provides a way of calculating F_Q directly. It is then clear that at the level of two-gluon diagrams there is no breaking of Casimir scaling. Hence, we may ask, to which order of the perturbative series can Casimir scaling be observed?

There are several equivalent prescriptions on how the color coefficients in the logarithm of a closed Wilson line can be determined. It will not be necessary here to go into details on how they are calculated exactly (see appendix B.6 and section 4.6); it is sufficient to know that for so-called connected diagrams, where every gluon is connected to every other gluon through gluon, ghost, or light quark propagators, the standard color factor and the one in the logarithm are the same.

At the three-gluon level we have several unconnected diagrams (cf. Fig. B.6) and a few connected diagrams. By three-gluon diagrams we mean diagrams that correspond to three sum-integrals. We exclude sum-integrals from self-energy or vertex-function insertions from this definition, because if the corresponding tree-level diagram obeys Casimir scaling then also any self-energy or vertex-function insertion does.

The unconnected three-gluon diagrams are all scaleless in Coulomb or static gauge unless each gluon carries a momentum of order m_D, which means that they start to contribute at $\mathcal{O}(g^9)$. We will see below that Casimir scaling is already broken at a lower order, so we can ignore the unconnected three-gluon diagrams in Coulomb gauge on the basis of this argument. In other gauges these diagrams contribute at $\mathcal{O}(g^6)$, but, as we will show in appendix B.6, their color coefficients obey Casimir scaling.

The connected three-gluon diagrams are shown in Fig. 4.3. Their color factors are all given by $-C_RN^2/4$, except for the second from left where it is 0. All of these depend linearly on C_R, so at the three-gluon level Casimir scaling is still observed.

In general, the color factor of any diagram without light quarks is given as the trace over a product of color matrices in the respective representation divided by the dimension of the representation, where every color index is contracted with that of another color matrix or a structure constant from the interaction vertices. By repeated use of the commutation relation, the Jacobi identity or the quadratic Casimir

$$\left[T_R^a, T_R^b\right] = i f^{abc} T_R^c \,, \qquad f^{abe} f^{ecd} + f^{bce} f^{ead} + f^{bde} f^{eca} = 0 \,, \tag{4.43}$$

$$T_R^a T_R^a = C_R \mathbb{1} \,, \qquad f^{acd} f^{bcd} = N \delta^{ab} \,, \tag{4.44}$$

one can express every such color factor as a combination of the following terms

$$C_R^{(n)} = f^{i_1 a_1 i_2} f^{i_2 a_2 i_3} \cdots f^{i_n a_n i_1} \frac{1}{d_R} \mathrm{Tr}\left[T_R^{a_1} T_R^{a_2} \cdots T_R^{a_n}\right] \tag{4.45}$$

and C_R or N.

$C_R^{(1)}$ is trivially zero and $C_R^{(2)}$ and $C_R^{(3)}$ can be calculated independently of the representation:

$$C_R^{(2)} = -C_R N \,, \qquad C_R^{(3)} = -\frac{i}{4} C_R N^2 \,. \tag{4.46}$$

But starting from $C_R^{(4)}$ there is no longer a simple unique formula like Eq. (4.46) valid for all representations. For the fundamental and the adjoint representation one can replace every structure constant by color matrices and then use the Fierz identity to calculate the $C_R^{(n)}$ explicitly:

$$f^{abc} = -2i \,\mathrm{Tr}\left[T_F^a \left[T_F^b, T_F^c\right]\right] \,, \tag{4.47}$$

$$\left(T_F^a\right)_{ij} \left(T_F^a\right)_{kl} = \frac{1}{2}\left(\delta_{il}\delta_{kj} - \frac{1}{N}\delta_{ij}\delta_{kl}\right) \,. \tag{4.48}$$

In this way we obtain

$$C_F^{(4)} = \frac{1}{8} C_F N^2 \left(3N - 4C_F\right) \,, \qquad C_A^{(4)} = \frac{1}{8} N^3 \left(13N - 24 C_F\right) \,, \tag{4.49}$$

or alternatively

$$\frac{C_F^{(4)}}{C_A^{(4)}} = \frac{C_F}{N} \frac{N^2 + 2}{N^2 + 12} \,. \tag{4.50}$$

If we can find a diagram whose color coefficient is given by $C_R^{(4)}$, then we have found a Casimir scaling breaking term. Such a diagram can appear only at $\mathcal{O}\left(g^8\right)$ or higher, because in the Feynman rules of QCD every color matrix and structure constant comes with a factor of g. Figure 4.4 shows some similar diagrams where the dependence on $C_R^{(4)}$ is immediately apparent. The diagram on the left has the color coefficient $C_R^{(4)}$ exactly and the other two have $C_R^{(4)} + C_R N^3/8$, because in both cases two color matrices have to be commuted to get the form of $C_R^{(4)}$ and the commutator gives $iC_R^{(3)} N/2$.

If we add up the contributions proportional to $C_R^{(4)}$ from all three diagrams, then the contour integrations simplify a lot and we get Kronecker deltas for the Matsubara frequencies of each of the four gluon propagators attached to the Polyakov loop contour times a coefficient of $1/8T^4$. One of these four Kronecker deltas is redundant and the Matsubara frequency in the

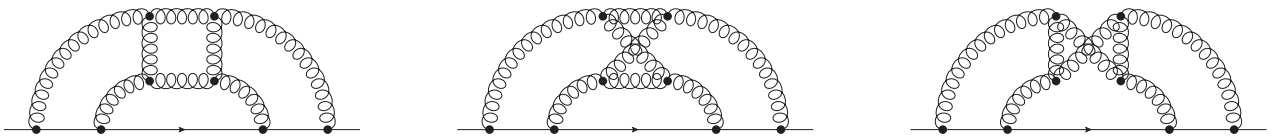

Figure 4.4: Diagrams at $\mathcal{O}(g^8)$ with a color coefficient $C_R^{(4)}$.

internal loop (the square in the left diagram, or the twisted square in the other two diagrams) remains different from zero. So the momentum integrals are not scaleless, because the scale πT remains in the calculation, and we have a possible genuinely nonvanishing contribution at $\mathcal{O}(g^8)$ that breaks Casimir scaling.

There are other diagrams similar to these three, which can be obtained from Fig. 4.4 by contracting one or two propagators in the internal loop to a four-gluon vertex. Their color coefficients also involve $C_R^{(4)}$, so they will give other terms of $\mathcal{O}(g^8)$ that break Casimir scaling. In principle, light quark loops can also give rise to color factors that break Casimir scaling. If such a light quark loop has two or three external gluon legs, then it can be included as a contribution to the self-energy or the vertex function and it will not affect Casimir scaling. With four or more external legs the color factor is no longer proportional to the quadratic Casimir, which can be checked in a similar calculation to the one above replacing the internal gluons in Fig. 4.4 with light quark propagators, but such diagrams also start to contribute at $\mathcal{O}(g^8)$.

One could in principle imagine that all those terms cancel and only Casimir scaled terms remain, but that would imply some underlying mechanism that enforces Casimir scaling to all orders of perturbation theory. Such a mechanism, if it exists, has not been discovered so far. The approximate Casimir scaling observed in lattice calculations may be explained by the strong suppression of the $\mathcal{O}(g^8)$ contributions that possibly violate Casimir scaling.

4.4.2 Outline of the $\mathcal{O}\left(g^6\right)$ Calculation

We will outline here the necessary steps for the calculation of the $\mathcal{O}(g^6)$ contributions, the last order accessible by perturbation theory. The amount of work one has to do is greatly reduced by choosing the appropriate gauge. As explained above, all the unconnected three-gluon diagrams (see Fig. B.6) are scaleless at leading order and start to contribute only at $\mathcal{O}(g^9)$ in Coulomb or static gauge. In Feynman gauge, however, the six diagrams of Fig. B.6 whose modified color coefficients in the logarithm of the Polyakov loop do not vanish all contribute at $\mathcal{O}(g^6)$, so this is not the most efficient gauge to perform this calculation.

There are also unconnected three-gluon diagrams consisting of only two unconnected pieces, a single gluon and a piece of three propagators connected by a three-gluon vertex. These are not displayed in Fig. B.6, because in gauges that are diagonal in temporal and spatial indices they vanish on account of the three-gluon vertex with three temporal indices, just like the corresponding two gluon diagram, but in nondiagonal gauges they also have to be considered.

The connected diagrams of Fig. 4.3 can only contribute at $\mathcal{O}(g^6)$ when all momenta are of the scale πT; the scale m_D contributions are of higher order. However, in Coulomb or static gauge all of them vanish. The first three diagrams are essentially the same gluonic configuration, but with different path ordering prescriptions along the Polyakov loop contour, so we will only discuss the leftmost diagram; the others are analogous (apart from the second having a vanishing color coefficient). In static gauge all Matsubara frequencies have to be zero

because of the temporal propagators, so the integrals are scaleless and vanish. In Coulomb gauge the Matsubara frequencies are not necessarily all zero, but the integrand vanishes by itself: Call $\boldsymbol{k}$ the momentum flowing from the first to the last point on the Polyakov loop contour, $\boldsymbol{p}$ the momentum flowing from the first to the second point, and $\boldsymbol{q}$ the momentum flowing from the third to the fourth point. The results of the $\boldsymbol{p}$ and $\boldsymbol{q}$ integrations can only be proportional to $\boldsymbol{k}$ because of rotational symmetry, where each vector comes from the three-gluon vertices. But these vectors $\boldsymbol{k}$ are then contracted with the transverse projector from the spatial propagator, which gives zero. The rightmost diagram in Fig. 4.3 vanishes because of the four-gluon vertex in all gauges where the gluon propagator is diagonal in temporal and spatial indices.

The two-gluon diagram D_2 has already been discussed above; only the first term in Eq. (4.6) contributes in Coulomb or static gauge at $\mathcal{O}(g^6)$. It gives a contribution of $-C_R N \alpha_s^2 m_D^2/48T^2$ when both momenta are of the scale m_D. When one or both momenta are of the scale πT, then the first nonvanishing contribution is of $\mathcal{O}(g^7)$ or $\mathcal{O}(g^8)$, respectively.

The $\mathcal{O}(g^6)$ contribution from diagram D_1 contains several different elements: the three-loop self-energy with all momenta of order m_D, products of one-loop and two-loop self-energies [essentially the last line of Eq. (4.7) times $\Pi^{(1)}_{m_D}(k)/(k^2+m_D^2)$] or the one-loop self-energy cubed from the expansion of the resummed propagator, the two-loop self-energy at the scale m_D with one loop momentum of order πT and the other of order m_D, and the two-loop or square of one-loop self-energy with all momenta of order πT.

Fortunately, most of these contributions can be inferred in the EFT approach from an already existing EQCD calculation. As explained previously [see Eq. (4.20)], the correlator of two $\widetilde{A}_0$ fields in EQCD can be obtained from the pressure or vacuum energy density, which has been calculated at the four-loop level in [149]. From this we get

$$\begin{aligned}\frac{1}{d_R}\mathrm{Tr}\big\langle \widetilde{A}_0^2\big\rangle_s = &-\frac{C_R m_E}{4\pi} + \frac{C_R N g_E^2}{(4\pi)^2}\left[\frac{1}{2\epsilon}+\frac{1}{2}-\gamma_E+\ln\frac{\pi\mu^2}{m_E^2}\right]\\ &+\frac{2C_R N^2}{(4\pi)^3}\frac{g_E^4}{m_E}\left(\frac{89}{48}-\frac{11}{12}\ln 2+\frac{\pi^2}{12}\right)\\ &+\frac{C_R\,(N^2+1)\,\lambda_E}{2(4\pi)^2}+\frac{C_R\bar{\lambda}_E}{4(4\pi)^2}\left(\frac{4N^2-6}{N}-N^2-1\right)\\ &+\frac{C_R N^3 g_E^6}{(4\pi)^4 m_E^2}\left(\frac{43}{4}-\frac{491\pi^2}{768}\right)+\mathcal{O}\left(g^5\right)\,. \end{aligned} \tag{4.51}$$

If we now insert the explicit expression for λ_E and $\bar{\lambda}_E$ in terms of g and the one-loop corrections to g_E, m_E, and $\mathcal{Z}_2$, then we have almost the full $\mathcal{O}(g^6)$ contribution to the logarithm of the Polyakov loop. The only thing that is missing is the contribution from D_2 given above and the two-loop and square of one-loop self-energy contributions with all momenta of order πT in Coulomb or static gauge.

The one-loop correction to the EQCD coupling constant is given by [38]

$$g_E^2 = g^2 T\left\{1+\frac{\alpha_s}{4\pi}\left[\frac{1}{3}N-\frac{8}{3}n_f\ln 2+\beta_0\left(\frac{1}{\epsilon}+\gamma_E+\ln\frac{\mu^2}{4\pi T^2}\right)\right]\right\}\,. \tag{4.52}$$

Because of the $1/\epsilon$ pole in the g_E^2 term in Eq. (4.51) we also need the $\mathcal{O}(\epsilon)$ terms of both

g_E^2 [146] and $\mathcal{Z}_2$:

$$g_E^2\Big|_{\mathcal{O}(\epsilon)} = \frac{g^4 T\epsilon}{(4\pi)^2}\left[\beta_0\left(\frac{1}{2}\left(\gamma_E + \ln\frac{\mu^2}{4\pi T^2}\right)^2 + \frac{\pi^2}{4} - 2\gamma_E^2 - 4\gamma_1\right)\right.$$
$$\left. + \left(\frac{1}{3}N - \frac{8}{3}n_f \ln 2\right)\left(\gamma_E + \ln\frac{\mu^2}{4\pi T^2}\right) - \frac{8}{3}n_f(\ln 2)^2\right], \tag{4.53}$$

$$\mathcal{Z}_2\Big|_{\mathcal{O}(\epsilon)} = \frac{\alpha_s\epsilon}{4\pi}\left[\beta_0\left(\frac{1}{2}\left(\gamma_E + \ln\frac{\mu^2}{4\pi T^2}\right)^2 + \frac{\pi^2}{4} - 2\gamma_E^2 - 4\gamma_1\right)\right.$$
$$\left. + \left(\frac{11}{3}N + \frac{2}{3}n_f(1 - 4\ln 2)\right)\left(\gamma_E + \ln\frac{\mu^2}{4\pi T^2}\right) + \frac{23}{3}N - \frac{8}{3}n_f(\ln 2)^2\right]. \tag{4.54}$$

Here γ_1 is the coefficient of the linear term in the expansion of $\zeta(1-x)$ for small x. Combining all these terms and inserting the renormalized coupling, we then have

$$\begin{aligned}\ln L\Big|_{\mathcal{O}(g^6)} = &-\frac{C_R\alpha_s^3}{8\pi}\left[\beta_0 N\left(\frac{1}{2}\left(\gamma_E + \ln\frac{\mu^2}{4\pi T^2}\right)^2 + \frac{\pi^2}{4} - 2\gamma_E^2 - 4\gamma_1\right)\right.\\
&+ N\left(2N + \frac{1}{3}n_f(1 - 8\ln 2)\right)\left(\gamma_E + \ln\frac{\mu^2}{4\pi T^2}\right)\\
&+ 8N^2 + \frac{1}{3}Nn_f\left(1 + 4\ln 2 - 8(\ln 2)^2\right) + 4C_F n_f\\
&\left.+ N\left(4N + \frac{2}{3}n_f(1 - 8\ln 2) + 4\beta_0\left(\gamma_E + \ln\frac{\mu}{4\pi T}\right)\right)\left(\frac{1}{2\epsilon} - \gamma_E + \ln\frac{\pi\mu^2}{m_D^2}\right)\right]\\
&- \frac{C_R N\alpha_s^4 T^2}{m_D^2}\left(N^2\left(\frac{43}{8} - \frac{491\pi^2}{1536}\right) + \frac{1}{2}C_F n_f\right) - \frac{C_R N\alpha_s^2 m_D^2}{48T^2}\\
&- \frac{C_R g^2}{2T}\int_{k\sim\pi T}\frac{1}{k^6}\left[\left(\Pi_T^{(1)}(0,k) + \frac{\beta_0\alpha_s}{4\pi}\left(\frac{1}{\epsilon} - \gamma_E + \ln 4\pi\right)k^2\right)^2 - k^2\,\Pi_T^{(2)}(0,k)\right].\end{aligned} \tag{4.55}$$

The first $1/\epsilon$ pole, a UV divergence from the scale m_D, has to cancel against a corresponding IR divergence in the scale πT integrals. The $1/\epsilon$ pole in the last line comes from the charge renormalization in the $\overline{\text{MS}}$ scheme of the $\mathcal{O}(g^4)$ contribution from the scale πT, i.e. the first term in Eq. (4.7), and it cancels the UV divergence in the one-loop vacuum part of the self-energy.

There are also $\mathcal{O}(g^6)$ contributions from two-loop diagrams with two momenta of order m_D and one momentum of order m_M. From the MQCD analysis of the Polyakov loop we know that the scale m_M can only appear first at $\mathcal{O}(g^7)$, so these contributions ultimately have to cancel. We have checked this cancellation explicitly in appendix B.3.

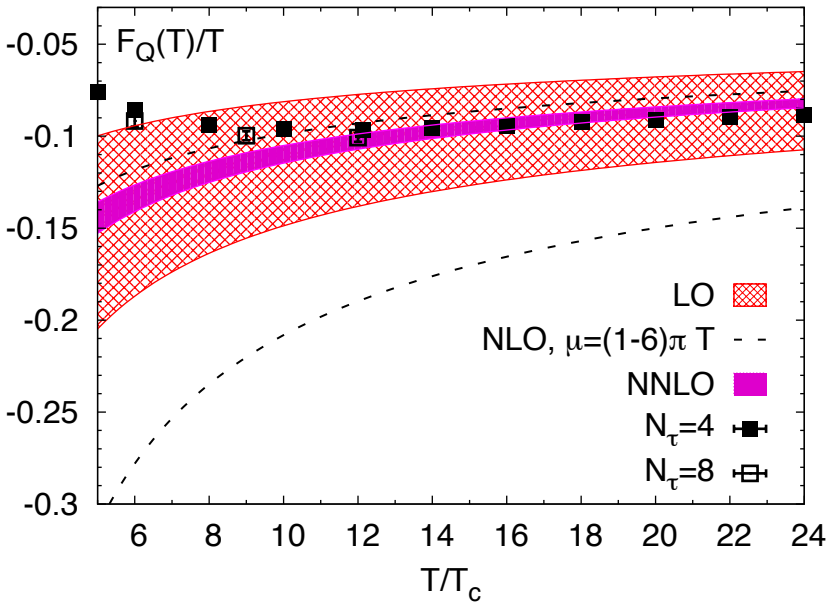

Figure 4.5: The free energy of a static quark F_Q for the SU(3) gauge theory in weak coupling expansion at LO, NLO and NNLO. The bands are obtained by varying the renormalization scale μ between πT and $6\pi T$. Also shown are the lattice data for F_Q obtained on lattices with temporal extent $N_\tau = 4$ and 8 [137].

4.5 Convergence of the Perturbative Series and Comparison with the Lattice Results

In this section, we discuss the convergence of the perturbative series for the Polyakov loop, or equivalently the free energy of a static quark, and compare the weak coupling results with lattice QCD results. For a reliable comparison of the lattice and the weak coupling results we need to consider a temperature range that extends to sufficiently high temperatures. We will start with a comparison to pure SU(3) lattice data (i.e. $n_f = 0$), which have been calculated in [137] up to temperatures of $24T_c$, with T_c being the deconfinement transition temperature. Later we will also comment on the results of a more recent full QCD calculation with $n_f = 3$ published in [150].

In Fig. 4.5 we show the perturbative results for the free energy of a static quark at various orders in perturbation theory for pure SU(3) gauge theory ($n_f = 0$). We use one-loop running for α_s. To determine the renormalization scale for different values of T/T_c we used the relation $r_0 T_c = 0.7498(50)$ [151], where r_0 is the Sommer scale [152]. The value of $\Lambda_{\overline{\rm MS}}$ was determined in Ref. [96]: $r_0\Lambda_{\overline{\rm MS}} = 0.637^{+0.032}_{-0.030}$. With this we get $T_c/\Lambda_{\overline{\rm MS}} = 1.177$. One can see that the scale dependence of the leading order (LO) results is quite large and becomes even larger at NLO. The scale dependence of F_Q is first reduced at NNLO and is, in fact, quite small, making a meaningful comparison with the lattice results possible. In Fig. 4.5 we also show the lattice results for the static quark free energy for $n_f = 0$ from Ref. [137]. The lattice results appear to agree with the LO and NLO results, given their large scale uncertainty, but are slightly larger than the NNLO results at small T.

We should keep in mind, however, that the comparison of the lattice and the perturbative

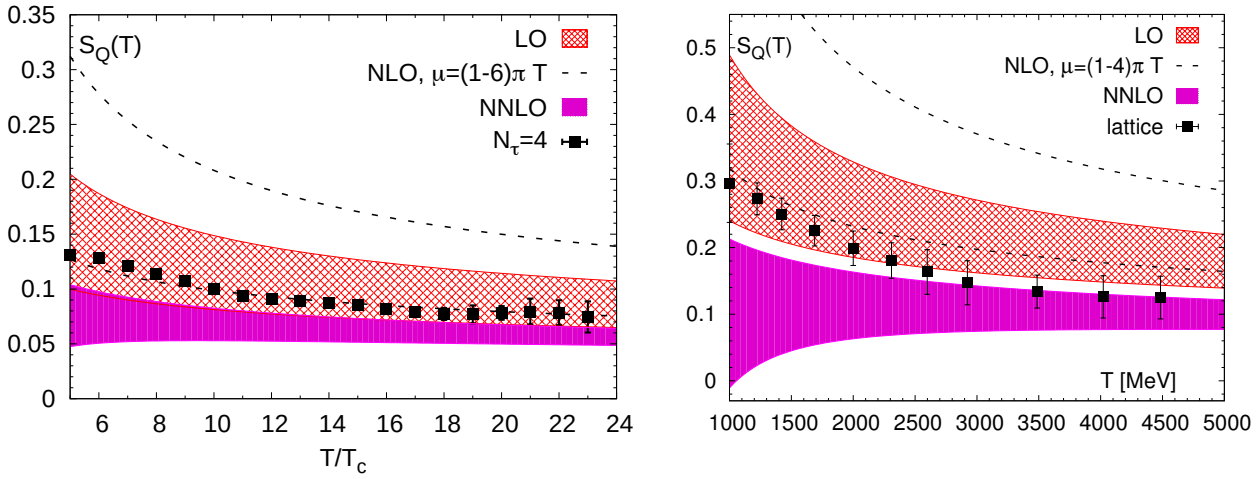

Figure 4.6: The entropy of a static quark S_Q for $n_f = 0$ (left) and $n_f = 3$ (right, picture taken from [150]) in weak coupling expansion at LO, NLO and NNLO. The bands are obtained by varying the renormalization scale μ between πT and $6\pi T$ (left) or $4\pi T$ (right). Also shown are the lattice results for S_Q; cf. the description in the text.

results for F_Q is not as straightforward as Fig. 4.5 may suggest. This fact seems to be generally overlooked in the literature. The perturbative calculations are performed in the $\overline{\text{MS}}$ scheme, while on the lattice the calculation is performed in a scheme in which the static quark-antiquark energy at zero temperature is normalized such that it is equal to the string potential $V(r) = -\pi/(12r) + \sigma r$ at large distances, with σ being the string tension. To match the two schemes one has to normalize the static energy at zero temperature in the perturbative calculation at each order to the lattice potential at short distances. This then corresponds to a constant shift C_{shift} in physical units of the perturbative static energy, which is different at different orders of perturbation theory.

This matching has been carried out for both $n_f = 0$ [96] and $n_f = 3$ [97]. The shift of the static energy implies that one has to add $C_{\text{shift}}/2$ to the perturbative result for F_Q before the comparison with the lattice results can be made. However, C_{shift} is sensitive to the perturbative order, to the resummation of the logarithms associated with the running coupling constant, as well as to the ultrasoft scale (see e.g. discussions in Ref. [98]). Thus, the uncertainty in the determination of C_{shift} will be the dominant systematic uncertainty in the comparison of the weak coupling and lattice calculations for F_Q. For this reason we did not add C_{shift} in the comparison of the lattice and the perturbative result for F_Q in Fig. 4.5.

We can avoid this problem by calculating the entropy of the static quark defined as

$$S_Q = -\frac{\partial F_Q(T)}{\partial T}. \tag{4.56}$$

In this quantity the normalization constant C_{shift} drops out. In perturbation theory it is straightforward to calculate the entropy of a static quark by taking the temperature derivative of Eq. (4.41) times T. In order to calculate the entropy of a static quark on the lattice, we use the lattice data on the renormalized Polyakov loop obtained on $N_\tau = 4$ lattices in Ref. [137]. We interpolate these data using different smoothing splines and calculate the derivatives of the splines using the R package [153]. The statistical errors of the interpolation and the derivative were calculated using the bootstrap method. Furthermore, we considered different spline

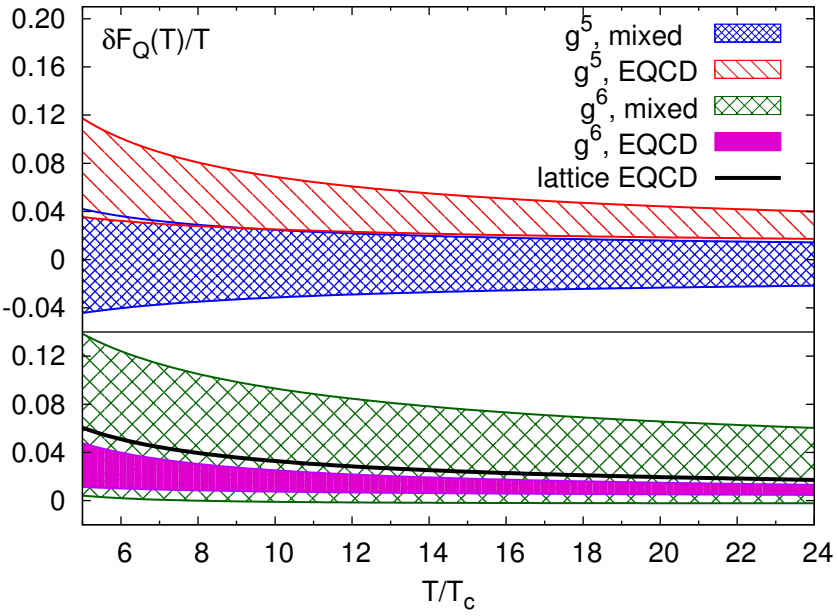

Figure 4.7: EQCD type and mixed contributions to F_Q at $\mathcal{O}(g^5)$ (upper panel) and $\mathcal{O}(g^6)$ (lower panel) for $n_f = 0$. The bands correspond to the variation of the renormalization scale from πT to $6\pi T$. The thick black line corresponds to the higher order EQCD type contributions from lattice EQCD estimated in Ref. [148] for the renormalization scale $\mu = 4\pi T$; cf. the description in the text.

interpolations, varying the number of knots and the value of the smoothing parameter. We enlarged the statistical error to take into account the difference between the different splines, if those were outside the statistical error. In this way we obtained the total error for the entropy in lattice QCD.

In Fig. 4.6 we compare the entropy of a static quark estimated in lattice QCD and in the weak coupling calculations. As in the case of the static quark free energy, the scale dependence of the LO and NLO results is quite large. Within this large scale uncertainty the perturbative calculations and the lattice data agree. The scale dependence of the NNLO result is much smaller. The NNLO result, however, lies below the lattice data. The same also applies for the $n_f = 3$ lattice data from [150] also shown in Fig. 4.6 (taken directly from that reference). The analytic plots in that picture were created using the result of this work, and one-loop running α_s with $\Lambda_{\overline{\rm MS}} = 315$ MeV. The agreement for larger temperatures is somewhat better for $n_f = 3$, though still not perfect. This implies that higher order corrections in the weak coupling expansion may still be important. In view of this, below we discuss some higher order terms in the weak coupling expansion of the static quark free energy and have a closer look on the convergence of the perturbative series.

As discussed above, in the weak coupling expansion we have three types of contributions, purely nonstatic, i.e. arising from the scale πT, purely static contributions corresponding to the scales m_D and m_M, which can be calculated within EQCD, and mixed contributions, where some loop momenta are of order m_D or m_M and others are of order πT. Here we will discuss the latter two types of contributions, referring to them as EQCD type and mixed type contributions, respectively. Together they have been called the static contribution in the previous sections, but here we want to distinguish between them.

The EQCD type contributions arise from the weak coupling expansion of $\mathrm{Tr}\langle \widetilde{A}_0^2 \rangle$ with the expansion parameter $N g_E^2/(4\pi m_E)$ [c.f. Eq. (4.51)], using only the leading order results for the matching parameters $\mathcal{Z}_2$, g_E, and m_E and neglecting quartic or higher order interactions. Beyond four-loop order the condensate $\mathrm{Tr}\langle \widetilde{A}_0^2 \rangle$ contains a nonperturbative contribution of order g_E^8/m_E^3, which was calculated using lattice simulations of EQCD [148]. Furthermore, in Ref. [148] a simple parametrization of those higher order contributions to the condensate beyond four-loop order was given.

In Fig. 4.7 we show the EQCD type contributions at $\mathcal{O}(g^5)$ and $\mathcal{O}(g^6)$ as well as the sum of all higher order contributions calculated in lattice EQCD, which we plot using Eq. (4.1) of Ref. [148]. The bands shown in the figure correspond to the variation of the renormalization scale μ from πT to $6\pi T$. The magnitude of the different contributions is decreasing with increasing order, the $\mathcal{O}(g^6)$ contribution is smaller than the $\mathcal{O}(g^5)$ contribution, and the sum of all the higher order contributions to $g^2/(2Td_R) \times \mathrm{Tr}\langle \widetilde{A}_0^2 \rangle$ [starting from $\mathcal{O}(g^7)$], which includes the nonperturbative contributions, is about the same size as the $\mathcal{O}(g^6)$ contribution. Thus, we conclude that the weak coupling expansion for the purely static contribution is converging reasonably well and there are no large nonperturbative corrections to the Polyakov loop from the static chromomagnetic sector. Furthermore, as shown in Fig. 4.7, the sum of the higher order corrections to the static quark free energy is positive and thus would shift the perturbative result away from the lattice data.

Now let us discuss the mixed contributions, which come from higher order corrections to the matching parameters and higher interaction terms in EQCD. In Fig. 4.7 we show the $\mathcal{O}(g^5)$ and $\mathcal{O}(g^6)$ mixed contributions. The latter is evaluated by using Eq. (4.55) and omitting the last two lines as well as the $1/\epsilon$ pole. In contrast to the EQCD type contributions, the mixed contributions can be positive or negative depending on the choice of the renormalization scale. At $\mathcal{O}(g^5)$ the mixed contribution is smaller than the EQCD type contribution, while at $\mathcal{O}(g^6)$ the mixed contribution is of the same size or larger (depending on the renormalization scale). Furthermore, the two mixed contributions are about the same size, which means that the full $\mathcal{O}(g^6)$ contribution might be large. Clearly, for rigorous statements about the convergence of the weak coupling expansion and comparison with lattice QCD results a complete calculation of the $\mathcal{O}(g^6)$ contribution will be necessary.

4.6 Free Energies for a Static Quark-Antiquark System

In analogy to the relation between the free energy of a static quark and the Polyakov loop, the free energy of a static quark-antiquark pair is correspondingly given by the Polyakov loop correlator [122]:

$$\exp\left[-\frac{F_{Q\bar{Q}}(r)}{T}\right] = \frac{1}{N^2}\left\langle \mathrm{Tr}\big[L(\boldsymbol{r})\big]\,\mathrm{Tr}\left[L^\dagger(\boldsymbol{0})\right]\right\rangle . \tag{4.57}$$

The dagger on the second Polyakov loop, which corresponds to the antiquark contribution, turns the fundamental into the antifundamental representation. This quantity depends only on the relative distance r. Just like for the single Polyakov loop, the free energy is defined with respect to the medium, i.e. $F_{Q\bar{Q}}$ is the difference between the free energy of the medium in the presence of a static quark-antiquark pair and the free energy of the medium without static quarks. This time we will restrict ourselves to quarks in the fundamental representation.

In the weak coupling regime (i.e. for large temperatures) this quantity can be calculated in perturbation theory. For the Polyakov loop we have found an exponentiation formula in

Sec. 4.2, which makes it possible to express the free energy directly through a set of Feynman diagrams. For the correlator we will also obtain a similar expression here (cf. also appendix B.10 for an alternative though less useful exponentiation).

The method we use is the replica trick for Wilson lines [144, 145], which we will outline here. First, consider the Polyakov loop correlator as an amplitude with uncontracted indices:

$$\exp\left[-\frac{F_{Q\bar{Q}}(r)}{T}\right] = \frac{\delta_{ij}\delta_{kl}}{N^2}\,\langle L_{ij}(\boldsymbol{r})L^*_{kl}(\boldsymbol{0})\rangle \equiv \frac{\delta_{ij}\delta_{kl}}{N^2}\langle\mathcal{M}\rangle_{ij,\,kl}\,, \tag{4.58}$$

where i and k are the color indices of the Polyakov loop operator at imaginary time $\tau = 1/T$, while j and l are at $\tau = 0$. Then define a multiplication of amplitudes $\mathcal{A}$ and $\mathcal{B}$ as $\mathcal{A}_{ij',\,kl'}\mathcal{B}_{j'j,\,l'l}$ (note that herein lies the difference to appendix B.10, where the indices k and l are exchanged). Exponentiation is to be understood as a power series with respect to this multiplication. In order to find the exponentiated expression of the thermal average of the amplitude $\langle\mathcal{M}\rangle$, we have to determine an amplitude that can be interpreted as the logarithm of $\langle\mathcal{M}\rangle$.

Now consider the nth power of this amplitude and expand in n:

$$\langle\mathcal{M}\rangle^n_{ij,\,kl} = \exp[n\ln\langle\mathcal{M}\rangle]_{ij,\,kl} = \delta_{ij}\delta_{kl} + n\ln\langle\mathcal{M}\rangle_{ij,\,kl} + \mathcal{O}\left(n^2\right)\,, \tag{4.59}$$

so in order to find the logarithm of $\langle\mathcal{M}\rangle$, we have to calculate the linear term in an expansion of $\langle\mathcal{M}\rangle^n$ in n. There is an alternative way of doing this. We can define a theory that contains n exact copies or replicas of the QCD fields, which interact like in QCD for each replica, but there is no interaction between different replica fields. In this theory, we can write the nth power of the thermal average of the amplitude as the thermal average of n replicas of the amplitude:

$$\langle\mathcal{M}\rangle^n_{ij,\,kl} = \left\langle \mathcal{M}^{(n)}_{ii',\,kk'}\mathcal{M}^{(n-1)}_{i'i'',\,k'k''}\cdots\mathcal{M}^{(1)}_{j'j,\,l'l}\right\rangle\,, \tag{4.60}$$

where the upper indices label the different replicas.

The Feynman diagrams in this replica theory are almost the same as in QCD, except that now there is replica path ordering: all color matrices associated to gluons of a higher replica index ρ are to be placed to the left of those associated to a lower index, regardless of where the gluons are attached to the Polyakov loop contours. Again, this is to be understood in the context of splitting the Feynman diagrams $\mathcal{D}$ into a color and a kinematic part, where the color part $\mathcal{C}$ contains all color matrices, structure constants, or symmetry factors, and the kinematic part $\mathcal{K}$ contains all propagators, contour integrations and other coefficients:

$$\mathcal{D}^{\{\rho\}}_{ij,\,kl} = \mathcal{C}^{\{\rho\}}_{ij,\,kl}(\mathcal{D})\mathcal{K}(\mathcal{D})\,, \tag{4.61}$$

where $\{\rho\}$ denotes the set of all replica indices, while the absence of such an index denotes the corresponding expression in QCD without replicas. Replica path ordering affects only the color coefficients, the kinematic parts are just like in QCD, so the sum over different replica indices and the expansion in n can be performed exclusively in the color part. Consequently, the amplitude $\langle\mathcal{M}\rangle$ and its logarithm can be written as a sum over the same Feynman diagrams, but the color parts for each diagram have to be modified in the following way:

$$\langle\mathcal{M}\rangle_{ij,\,kl} = \sum_{\mathcal{D}}\mathcal{C}_{ij,\,kl}(\mathcal{D})\mathcal{K}(\mathcal{D}) = \exp\big[\ln\langle\mathcal{M}\rangle\big]_{ij,\,kl} = \exp\left[\sum_{\mathcal{D}}\widetilde{\mathcal{C}}(\mathcal{D})\mathcal{K}(\mathcal{D})\right]_{ij,\,kl}\,, \tag{4.62}$$

where

$$\sum_{\{\rho\}} \mathcal{C}^{\{\rho\}}_{ij,\,kl}(\mathcal{D}) = \delta_{ij}\delta_{kl} + n\,\widetilde{\mathcal{C}}_{ij,\,kl}(\mathcal{D}) + \mathcal{O}\left(n^2\right)\,. \tag{4.63}$$

We will present an explicit example of such a determination of the coefficients of the logarithm shortly.

First, we will show how the exponential can be evaluated, after the coefficient has been determined. In principle, it is nothing but the matrix exponential of an $N^2 \times N^2$ matrix, however, in this case it will turn out to be much simpler. We can use the Fierz identity

$$\delta_{ij}\delta_{kl} = \frac{1}{N}\delta_{ik}\delta_{lj} + 2T^a_{ik}T^a_{lj} \equiv (P_S)_{ik}(P_S)^*_{jl} + (P_A)^a_{ik}(P_A)^{a\,*}_{jl}\,, \tag{4.64}$$

where the first part can be understood as a projector on the color singlet space with $(P_S)_{ik} = \delta_{ik}/\sqrt{N}$ and the second part as a projector on the color adjoint space with $(P_A)^a_{ik} = \sqrt{2}T^a_{ik}$. As projectors they satisfy

$$(P_R)^{a\,*}_{ik}(P_{R'})^b_{ik} = \delta_{RR'}\delta^{ab}\,, \tag{4.65}$$

where the representation indices R and R' can stand for either singlet S or adjoint A, and the color indices a and b are absent for the singlet or run from 1 to N^2-1 for the adjoint projector.

With these projectors we can split any amplitude $\mathcal{A}$ like

$$\mathcal{A}_{ij,\,kl} = (P_R)^a_{ik}(P_R)^{a\,*}_{i'k'}\mathcal{A}_{i'j',\,k'l'}(P_{R'})^b_{j'l'}(P_{R'})^{b\,*}_{jl} \equiv (P_R)^a_{ik}\mathcal{A}^{ab}_{RR'}(P_{R'})^{b\,*}_{jl}\,, \tag{4.66}$$

and because of the orthogonality of the projectors the exponential of $\mathcal{A}$ can be expressed as

$$\exp[\mathcal{A}]_{ij,\,kl} = \exp[P^a_R\mathcal{A}^{ab}_{RR'}P^{b\,*}_{R'}]_{ij,\,kl} = (P_R)^a_{ik}\exp[\mathcal{A}]^{ab}_{RR'}(P_{R'})^{b\,*}_{jl}\,. \tag{4.67}$$

In principle, what we did up until now is nothing but a basis transformation for the amplitudes; the matrix exponential with the new indices R, R' and a, b still has $N^2 \times N^2$ elements. But through the specific nature of the Feynman diagrams the exponential in this basis will be greatly simplified.

All color coefficients $\widetilde{\mathcal{C}}$ can be expressed as linear combinations of products of color matrices with all color indices contracted. We can use the Fierz identity (4.64) to show that any two fundamental color matrices with their color indices contracted can be expressed entirely through Kronecker deltas, so we can write any color coefficient as:

$$\widetilde{\mathcal{C}}_{ij,\,kl} = c_1\delta_{ij}\delta_{kl} + c_2\delta_{ik}\delta_{jl}\,. \tag{4.68}$$

With this and the other properties of the fundamental color matrices, i.e. tracelessness and orthogonality, it is straightforward to see that the projected color coefficients satisfy

$$\widetilde{\mathcal{C}}^{ab}_{RR'} = (P_R)^{a\,*}_{ik}\widetilde{\mathcal{C}}_{ij,\,kl}(P_{R'})^b_{jl} = \widetilde{\mathcal{C}}_R\delta_{RR'}\delta^{ab}\,. \tag{4.69}$$

This means that $\ln\langle\mathcal{M}\rangle$ is diagonal in this projection and exponentiation is trivial:

$$\begin{aligned}\exp\left[-\frac{F_{Q\bar{Q}}}{T}\right] &= \frac{\delta_{ij}\delta_{kl}}{N^2}\exp\left[\sum_{\mathcal{D}}\widetilde{\mathcal{C}}(\mathcal{D})\mathcal{K}(\mathcal{D})\right]_{ij,\,kl} \\ &= \frac{\delta_{ij}\delta_{kl}}{N^2}(P_R)^a_{ik}\exp\left[\sum_{\mathcal{D}}\widetilde{\mathcal{C}}(\mathcal{D})\mathcal{K}(\mathcal{D})\right]^{ab}_{RR'}(P_{R'})^{b\,*}_{jl}\end{aligned}$$

$$
\begin{aligned}
&= \frac{\delta_{ij}\delta_{kl}}{N^2}\Bigg((P_S)_{ik} \exp\left[\sum_{\mathcal{D}} \widetilde{\mathcal{C}}_S(\mathcal{D})\mathcal{K}(\mathcal{D})\right](P_S)^*_{jl} \\
&\qquad + (P_A)^a_{ik} \exp\left[\sum_{\mathcal{D}} \widetilde{\mathcal{C}}_A(\mathcal{D})\mathcal{K}(\mathcal{D})\right](P_A)^{a\,*}_{jl}\Bigg) \\
&= \frac{1}{N^2}\exp\left[\sum_{\mathcal{D}} \widetilde{\mathcal{C}}_S(\mathcal{D})\mathcal{K}(\mathcal{D})\right] + \frac{N^2-1}{N^2}\exp\left[\sum_{\mathcal{D}} \widetilde{\mathcal{C}}_A(\mathcal{D})\mathcal{K}(\mathcal{D})\right] \\
&\equiv \frac{1}{N^2}\exp\left[-\frac{F_S}{T}\right] + \frac{N^2-1}{N^2}\exp\left[-\frac{F_A}{T}\right] . \qquad (4.70)
\end{aligned}
$$

In this way we have split the free energy of a static quark-antiquark pair into a singlet and an adjoint free energy, which can be defined directly as

$$
\exp\left[-\frac{F_S}{T}\right] = \frac{1}{N}\left\langle \mathrm{Tr}\left[L(\boldsymbol{r})L^\dagger(\boldsymbol{0})\right]\right\rangle , \qquad (4.71)
$$

$$
\exp\left[-\frac{F_A}{T}\right] = \frac{2}{N^2-1}\left\langle \mathrm{Tr}\left[L(\boldsymbol{r})T^aL^\dagger(\boldsymbol{0})T^a\right]\right\rangle . \qquad (4.72)
$$

This procedure can easily be generalized to similar correlators of Polyakov loops in different representations or with more than two loops. For example, in a diquark Polyakov loop correlator (i.e. a correlator of two Polyakov loops without complex conjugation) one has antitriplet and sextet projectors (or rather $N(N\pm1)/2$-plet projectors for general N) that together form unity instead of Eq. (4.64), and the projected color coefficients are still diagonal as in Eq. (4.69), which gives an analogous definition of antitriplet and sextet free energies (cf. appendix B.10).

Or in the case of a baryonic Polyakov loop correlator (consisting of three Polyakov loops with $N = 3$), one has one singlet, two octet, and one decuplet projector, but the projected color coefficients are no longer fully diagonal: the two octet representations can mix, reflecting the ambiguity in which color indices to (anti)symmetrize, so Eq. (4.69) has to be modified as

$$
\widetilde{\mathcal{C}}^{ab}_{RR'} = \widetilde{\mathcal{C}}_{RR'}\delta_{d(R)d(R')}\delta^{ab} , \qquad (4.73)
$$

where $d(R)$ is the dimension of the respective representation. In fact, this version of Eq. (4.69) also applies to the diquark or quark-antiquark Polyakov loop correlators, so it may be true for any combination of representations and loops, although we will not attempt a general proof here. In any case, this projection of the amplitudes in the baryonic Polyakov loop correlator then defines a singlet and a decuplet free energy through simple exponentials and two octet free energies through the trace of the exponential of a 2×2 matrix:

$$
\exp\left[-\frac{F_{3Q}}{T}\right] = \frac{1}{27}\exp\left[-\frac{F_1}{T}\right] + \frac{8}{27}\mathrm{Tr}\left\{\exp\left[-\frac{1}{T}\begin{pmatrix} F_{88} & F_{88'} \\ F_{8'8} & F_{8'8'}\end{pmatrix}\right]\right\} + \frac{10}{27}\exp\left[-\frac{F_{10}}{T}\right] . \qquad (4.74)
$$

There are, however, two major problems related to the definition of singlet, adjoint, or other free energies such as these. First, the definition is gauge dependent, and second, each of these free energies contains UV divergences, which cancel only in the full expression for the Polyakov loop correlator.

Let us first discuss the divergences (and return to the quark-antiquark case). There are two types of divergences, the first is a linear divergence proportional to the length of a Wilson

line, so in this case $1/T$, and can be understood as a mass correction to the (infinite) mass of the static quark. They factorize, which means that they affect singlet and adjoint free energies in the same way, and can be removed by multiplication with $\exp[-2\Lambda_F/T]$, where Λ_F is a divergent constant and the index F refers to the fundamental representation. In dimensional regularization such divergences are absent.

The second kind of divergence is logarithmic and comes from gluons clustering around the endpoints of a Polyakov loop [154–156]. All gluons contributing to this divergence have to be contained in an infinitesimal area around the endpoints, which means that the divergence does not depend on any characteristics of the Wilson line like length or curvature, except for when two or more endpoints coincide (i.e. at cusps or intersections), in which case the divergence also depends on the angles at this point. There may also be more than one divergent cluster, in which case the ones closer to the singular point constitute a subdivergence with respect to the other ones. Such divergent clusters can be added to any Feynman diagram[4] and will factorize from the sum over all diagrams (cf. figure 16 in [156]), so the divergence of the correlator is proportional to the correlator itself.

Keeping in mind that the divergences at the endpoints of the two Polyakov loops are unrelated, we can write for the divergent part of the amplitude:

$$\mathrm{Div}\langle\mathcal{M}\rangle_{ij,\,kl} = \Delta_{ii',\,jj'}\langle\mathcal{M}\rangle_{i'j',\,kl} + \langle\mathcal{M}\rangle_{ij,\,k'l'}\Delta_{ll',\,kk'} - \Delta_{ii',\,jj'}\langle\mathcal{M}\rangle_{i'j',\,k'l'}\Delta_{ll',\,kk'}\,, \tag{4.75}$$

where we have used the fact that both Polyakov loops have exactly the same configuration at their endpoints[5], so accordingly the divergences Δ have to be identical. The last term is there to remove a double counting of terms with divergences at both Polyakov loops.

Then we define the renormalized correlator through the subtraction of the divergent part:

$$\begin{aligned}\langle\mathcal{M}\rangle^{(R)}_{ij,\,kl} &= \langle\mathcal{M}\rangle_{ij,\,kl} - \mathrm{Div}\langle\mathcal{M}\rangle_{ij,\,kl} = (\delta_{ii'}\delta_{jj'} - \Delta_{ii',\,jj'})\langle\mathcal{M}\rangle_{i'j',\,k'l'}(\delta_{ll'}\delta_{kk'} - \Delta_{ll',\,kk'}) \\ &\equiv Z_{ii',\,jj'}\langle\mathcal{M}\rangle_{i'j',\,k'l'}Z_{ll',\,kk'}\,.\end{aligned} \tag{4.76}$$

We can invert this relation and insert Eq. (4.75) iteratively to further illustrate the divergence structure:

$$\begin{aligned}\langle\mathcal{M}\rangle &= \langle\mathcal{M}\rangle^{(R)} + \mathrm{Div}\langle\mathcal{M}\rangle = \langle\mathcal{M}\rangle^{(R)} + \Delta\langle\mathcal{M}\rangle + \langle\mathcal{M}\rangle\Delta - \Delta\langle\mathcal{M}\rangle\Delta \\ &= \langle\mathcal{M}\rangle^{(R)} + \Delta\langle\mathcal{M}\rangle^{(R)} + \langle\mathcal{M}\rangle^{(R)}\Delta \\ &\quad + \Delta^2\langle\mathcal{M}\rangle + \Delta\langle\mathcal{M}\rangle\Delta + \langle\mathcal{M}\rangle\Delta^2 - \Delta^2\langle\mathcal{M}\rangle\Delta - \Delta\langle\mathcal{M}\rangle\Delta^2 \\ &= \langle\mathcal{M}\rangle^{(R)} + \Delta\langle\mathcal{M}\rangle^{(R)} + \langle\mathcal{M}\rangle^{(R)}\Delta + \Delta^2\langle\mathcal{M}\rangle^{(R)} + \Delta\langle\mathcal{M}\rangle^{(R)}\Delta + \langle\mathcal{M}\rangle^{(R)}\Delta^2 \\ &\quad + \Delta^3\langle\mathcal{M}\rangle + \Delta^2\langle\mathcal{M}\rangle\Delta + \Delta\langle\mathcal{M}\rangle\Delta^2 + \langle\mathcal{M}\rangle\Delta^3 - \Delta^3\langle\mathcal{M}\rangle\Delta - \Delta^2\langle\mathcal{M}\rangle\Delta^2 - \Delta\langle\mathcal{M}\rangle\Delta^3 \\ &= \cdots = \left(\sum_{m=0}^{\infty}\Delta^m\right)\langle\mathcal{M}\rangle^{(R)}\left(\sum_{n=0}^{\infty}\Delta^n\right)\,.\end{aligned} \tag{4.77}$$

So with Eq. (4.75) the divergences and subdivergences for each loop really do form a geometric series (which was implicit in the previous discussion), wherein Δ corresponds to irreducible gluon clusters, and the renormalization tensors Z are the inverse of that series.

[4] If that diagram is already divergent, then adding such a cluster generates a subdivergence.

[5] A Wilson line with final endpoint k and initial endpoint l in the antifundamental representation is equivalent to a Wilson line with final endpoint l and initial endpoint k in the fundamental representation.

Again, we can use Eq. (4.64) to argue that

$$Z_{ii',\,jj'} = z_1\delta_{ii'}\delta_{jj'} + z_2\delta_{ij}\delta_{i'j'}\,. \tag{4.78}$$

Of course, we can multiply the renormalization tensors $Z_{ii',\,jj'}$ by some finite tensor, which corresponds to a different renormalization scheme. The scheme also depends on which finite terms are included in Δ. If we take the traces over the Polyakov loops, then the contour is smooth at this point, which means that there are no logarithmic divergences [154, 155]. So we can partially fix the renormalization scheme by requiring that the renormalized Polyakov loop correlator be identical to the unrenormalized one with respect to the logarithmic divergences, so $\delta_{ij}Z_{ii',\,jj'} = \delta_{i'j'}$, from which it follows that

$$z_1 + Nz_2 = 1\,. \tag{4.79}$$

If we now use the same projectors for the renormalized singlet and adjoint free energies as for the unrenormalized, then we have:

$$\begin{aligned}
\exp\left[-\frac{F_S^{(R)}}{T}\right] &= (P_S)^*_{ik}\langle\mathcal{M}\rangle^{(R)}_{ij,\,kl}(P_S)_{jl} = (P_S)^*_{ik}Z_{ii',\,jj'}\langle\mathcal{M}\rangle_{i'j',\,k'l'}Z_{ll',\,kk'}(P_S)_{jl} \\
&= (P_S)^*_{ik}Z_{ii',\,jj'}\left((P_S)_{i'k'}\exp\left[-\frac{F_S}{T}\right](P_S)^*_{j'l'}\right. \\
&\quad \left. + (P_A)^a_{i'k'}\exp\left[-\frac{F_A}{T}\right](P_A)^{a\,*}_{j'l'}\right)Z_{ll',\,kk'}(P_S)_{jl} \\
&= \frac{1+(N^2-1)z_1^2}{N^2}\exp\left[-\frac{F_S}{T}\right] + \frac{(N^2-1)(1-z_1^2)}{N^2}\exp\left[-\frac{F_A}{T}\right] \\
&\equiv (1-Z_S)\exp\left[-\frac{F_S}{T}\right] + Z_S\exp\left[-\frac{F_A}{T}\right]\,,
\end{aligned} \tag{4.80}$$

$$\begin{aligned}
\exp\left[-\frac{F_A^{(R)}}{T}\right] &= \frac{1}{N^2-1}(P_A)^{a\,*}_{ik}\langle\mathcal{M}\rangle^{(R)}_{ij,\,kl}(P_A)^a_{jl} = \frac{1}{N^2-1}(P_A)^{a\,*}_{ik}Z_{ii',\,jj'}\langle\mathcal{M}\rangle_{i'j',\,k'l'}Z_{ll',\,kk'}(P_A)^a_{jl} \\
&= \frac{1}{N^2-1}(P_A)^{a\,*}_{ik}Z_{ii',\,jj'}\left((P_S)_{i'k'}\exp\left[-\frac{F_S}{T}\right](P_S)^*_{j'l'}\right. \\
&\quad \left. + (P_A)^b_{i'k'}\exp\left[-\frac{F_A}{T}\right](P_A)^{b\,*}_{j'l'}\right)Z_{ll',\,kk'}(P_A)^a_{jl} \\
&= \frac{1-z_1^2}{N^2}\exp\left[-\frac{F_S}{T}\right] + \frac{N^2-1+z_1^2}{N^2}\exp\left[-\frac{F_A}{T}\right] \\
&\equiv Z_A\exp\left[-\frac{F_S}{T}\right] + (1-Z_A)\exp\left[-\frac{F_A}{T}\right]\,.
\end{aligned} \tag{4.81}$$

So we see that the singlet and adjoint free energies mix under renormalization, which makes their definition somewhat ambiguous.

Here we have introduced the renormalization constants

$$Z_S = (N^2-1)Z_A = \frac{N^2-1}{N^2}(1-z_1^2)\,, \tag{4.82}$$

such that Z_S, $Z_A = \mathcal{O}(\alpha_\mathrm{s})$. These relations can also be inverted as

$$\exp\left[-\frac{F_S}{T}\right] = \left(1-\widetilde{Z}_S\right)\exp\left[-\frac{F_S^{(R)}}{T}\right] + \widetilde{Z}_S\exp\left[-\frac{F_A^{(R)}}{T}\right]\,, \tag{4.83}$$

$$\exp\left[-\frac{F_A}{T}\right] = \widetilde{Z}_A \exp\left[-\frac{F_S^{(R)}}{T}\right] + \left(1-\widetilde{Z}_A\right)\exp\left[-\frac{F_A^{(R)}}{T}\right], \tag{4.84}$$

with

$$\widetilde{Z}_S = (N^2-1)\widetilde{Z}_A = \frac{-Z_S}{1-Z_S-Z_A} = \frac{N^2-1}{N^2}\frac{z_1^2-1}{z_1^2}. \tag{4.85}$$

We also see that we can construct a multiplicatively renormalizable quantity through

$$\begin{aligned}\exp\left[-\frac{F_S^{(R)}}{T}\right] - \exp\left[-\frac{F_A^{(R)}}{T}\right] &= (1-Z_S-Z_A)\left(\exp\left[-\frac{F_S}{T}\right] - \exp\left[-\frac{F_A}{T}\right]\right)\\ &= z_1^2\left(\exp\left[-\frac{F_S}{T}\right] - \exp\left[-\frac{F_A}{T}\right]\right).\end{aligned} \tag{4.86}$$

As it turns out, both singlet and adjoint free energy seem to be free of logarithmic divergences in Coulomb gauge, at least up to the currently known perturbative orders. This is why they are usually calculated only in this gauge[6]. The general renormalization properties demonstrated here may give another motivation that considering these gauge dependent quantities in Coulomb gauge may be meaningful: in general gauges the separation into singlet and adjoint is somewhat arbitrary, since both free energies have to be mixed in order to obtain a finite result. But if there are no divergences in Coulomb gauge, then $Z_{S/A} = 0$ and there is no mixing between singlet and adjoint.

It is quite interesting to note that performing a gauge transformation leads to expressions of exactly the same form. Under gauge transformations described by the local SU(N) matrix $U(x)$ the uncontracted Polyakov loop correlator transforms as:

$$\langle\mathcal{M}\rangle_{ij,\,kl} \to U_{ii'}(\boldsymbol{r})U^*_{kk'}(\boldsymbol{0})\langle\mathcal{M}\rangle_{i'j',\,k'l'}U^*_{jj'}(\boldsymbol{r})U_{ll'}(\boldsymbol{0}), \tag{4.87}$$

where we have suppressed the imaginary time argument $\tau = 0$. The singlet and adjoint free energies then transform as:

$$\begin{aligned}\exp\left[-\frac{F_S}{T}\right] &\to (P_S)^*_{ik}U_{ii'}(\boldsymbol{r})U^*_{kk'}(\boldsymbol{0})\langle\mathcal{M}\rangle_{i'j',\,k'l'}U^*_{jj'}(\boldsymbol{r})U_{ll'}(\boldsymbol{0})(P_S)_{jl}\\ &= (P_S)^*_{ik}U_{ii'}(\boldsymbol{r})U^*_{kk'}(\boldsymbol{0})\left((P_S)_{i'k'}\exp\left[-\frac{F_S}{T}\right](P_S)^*_{j'l'}\right.\\ &\quad\left.+\,(P_A)^a_{i'k'}\exp\left[-\frac{F_A}{T}\right](P_A)^{a\,*}_{j'l'}\right)U^*_{jj'}(\boldsymbol{r})U_{ll'}(\boldsymbol{0})(P_S)_{jl}\\ &= \frac{1}{N^2}\mathrm{Tr}\left[U(\boldsymbol{r})U^\dagger(\boldsymbol{0})\right]\mathrm{Tr}\left[U(\boldsymbol{0})U^\dagger(\boldsymbol{r})\right]\exp\left[-\frac{F_S}{T}\right]\\ &\quad+\frac{2}{N}\mathrm{Tr}\left[U(\boldsymbol{r})T^aU^\dagger(\boldsymbol{0})\right]\mathrm{Tr}\left[U(\boldsymbol{0})T^aU^\dagger(\boldsymbol{r})\right]\exp\left[-\frac{F_A}{T}\right]\\ &\equiv (1-u(\boldsymbol{r}))\exp\left[-\frac{F_S}{T}\right] + u(\boldsymbol{r})\exp\left[-\frac{F_A}{T}\right],\end{aligned} \tag{4.88}$$

[6]Another reason is that in the small distance limit they reproduce the vacuum static potentials divided by the temperature.

$$
\begin{aligned}
\exp\left[-\frac{F_A}{T}\right] &\to (P_A)^{a\,*}_{ik} U_{ii'}(\boldsymbol{r}) U^*_{kk'}(\boldsymbol{0}) \langle \mathcal{M} \rangle_{i'j',\,k'l'} U^*_{jj'}(\boldsymbol{r}) U_{ll'}(\boldsymbol{0}) (P_A)^a_{jl} \\
&= (P_A)^{a\,*}_{ik} U_{ii'}(\boldsymbol{r}) U^*_{kk'}(\boldsymbol{0}) \left((P_S)_{i'k'} \exp\left[-\frac{F_S}{T}\right] (P_S)^*_{j'l'} \right. \\
&\quad \left. + (P_A)^b_{i'k'} \exp\left[-\frac{F_A}{T}\right] (P_A)^{b\,*}_{j'l'} \right) U^*_{jj'}(\boldsymbol{r}) U_{ll'}(\boldsymbol{0}) (P_A)^a_{jl} \\
&= \frac{2}{N(N^2-1)} \mathrm{Tr}\left[U^\dagger(\boldsymbol{0}) T^a U(\boldsymbol{r})\right] \mathrm{Tr}\left[U^\dagger(\boldsymbol{r}) T^a U(\boldsymbol{0})\right] \exp\left[-\frac{F_S}{T}\right] \\
&\quad + \frac{4}{N^2-1} \mathrm{Tr}\left[U^\dagger(\boldsymbol{0}) T^a U(\boldsymbol{r}) T^b\right] \mathrm{Tr}\left[U^\dagger(\boldsymbol{r}) T^a U(\boldsymbol{0}) T^b\right] \exp\left[-\frac{F_A}{T}\right] \\
&\equiv \frac{u(\boldsymbol{r})}{N^2-1} \exp\left[-\frac{F_S}{T}\right] + \left(1 - \frac{u(\boldsymbol{r})}{N^2-1}\right) \exp\left[-\frac{F_A}{T}\right] . \qquad (4.89)
\end{aligned}
$$

Again, the transformed free energies, expressed through the old free energies, depend only on one quantity:

$$
u(\boldsymbol{r}) = 1 - \left| \frac{1}{N} \mathrm{Tr}\left[U(\boldsymbol{r}) U^\dagger(\boldsymbol{0})\right] \right|^2 . \qquad (4.90)
$$

Also here we see that the separation of the Polyakov loop correlator into singlet and adjoint free energies is not unique, as performing a gauge transformation mixes the two expressions. Here the transformation constant may also depend on the distance between the two loops, in contrast to the renormalization constant.

In this calculation we have assumed that the gauge transformation does not depend on the gauge fields themselves. However, this does not include all possible transformations. In order to go from Feynman to Coulomb gauge, for instance, there is not one local SU(N) matrix U that turns every gauge field that satisfies the Feynman gauge condition into one that satisfies the Coulomb gauge condition. Different field configurations will need different transformation matrices, so in order to go from one gauge to the other, we need a field dependent transformation. This means that it is not possible to pull such matrices out of the thermal average.

However, we may perform the above calculation just as well for the operators inside the correlators for the singlet and adjoint free energies given in Eqs. (4.71) and (4.72) before taking the thermal average. The corresponding expressions for the transformation behavior of those operators are valid also for field dependent transformations. This will be relevant for the matching to pNRQCD in section 4.8.

4.7 Calculation of the Normalized Polyakov Loop Correlator

The great advantage of exponentiated formulas, such as were derived in the previous section, is that they reduce the number of Feynman diagrams one has to calculate at a given order in perturbation theory, since many of the color coefficients in the exponent are zero. We will show this explicitly for the two-gluon diagrams. First, all diagrams where no gluons are exchanged between the two loops have color coefficients that are proportional to the identity $\delta_{ij}\delta_{kl}$, so they trivially factorize out of the exponentiation. They give a contribution that corresponds to the

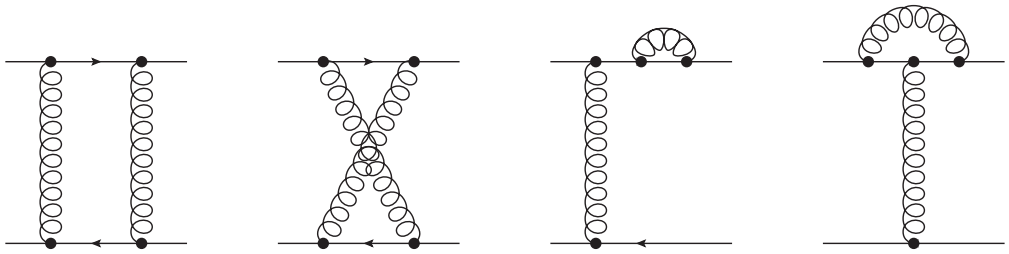

Figure 4.8: All unconnected diagrams. Some diagrams can be flipped to give four other diagrams that are not explicitly displayed. The line with the right arrow is the Polyakov loop for the quark, and the line with the left arrow corresponds to the antiquark.

individual contributions of each Polyakov loop, i.e. $\exp[-2F_Q/T]$. So it makes sense to divide the Polyakov loop correlator by these two Polyakov loops, which corresponds to calculating $F_{Q\bar{Q}} - 2F_Q$ and can be interpreted as the interaction part of the correlator, because it contains only those diagrams where gluons are exchanged between the loops.

For connected diagrams, i.e. diagrams where every gluon is connected to every other gluon through vertices or propagators, the color coefficient in the exponent is the same as the standard coefficient in QCD, so the first diagrams where the modification of the color coefficient obtained from the replica trick becomes relevant are the two-gluon diagrams shown in Fig. 4.8. For each diagram we have to sum over every possible assignment of replica indices and perform the corresponding replica path ordering:

$$\sum_{\{\rho\}} \mathcal{C}^{\{\rho\}} \left(\right) = n(n-1)\, \mathcal{C} \left(\right) + n\, \mathcal{C} \left(\right) ,$$

$$\sum_{\{\rho\}} \mathcal{C}^{\{\rho\}} \left(\right) = n(n-1)\, \mathcal{C} \left(\right) + n\, \mathcal{C} \left(\right) ,$$

$$\sum_{\{\rho\}} \mathcal{C}^{\{\rho\}} \left(\right) = \frac{n(n-1)}{2}\, \mathcal{C} \left(\right) + \frac{n(n-1)}{2}\, \mathcal{C} \left(\right) + n\, \mathcal{C} \left(\right) ,$$

$$\sum_{\{\rho\}} \mathcal{C}^{\{\rho\}} \left(\right) = \frac{n(n-1)}{2}\, \mathcal{C} \left(\right) + \frac{n(n-1)}{2}\, \mathcal{C} \left(\right) + n\, \mathcal{C} \left(\right) , \qquad (4.91)$$

where the first term counts the possibilities of having two gluons with different replica indices and the second term counts the possibilities of them having the same replica index. For the latter two diagrams the first term is split into the possibilities of one gluon having a higher or a lower index than the other gluon, a distinction that is in fact unnecessary, because both orderings have the same standard color coefficient.

We see that for the first diagram the terms linear in n cancel trivially, so this diagram does not contribute to the logarithm of the Polyakov loop correlator. For the third diagram it is straightforward to see that both standard color coefficients are equal, since the gluon attached only to the top Polyakov loop contributes only with a unity matrix to the color coefficient, because $(T^a T^a)_{ij} = \delta_{ij}(N^2-1)/2N$, so also here the linear order of n cancels. These two diagrams are the first examples of a more general statement: whenever one can draw a line crossing both Polyakov loops such that there are gluons on both sides of it but no gluon crosses the line, then this diagram does not contribute to the logarithm of the correlator.

This can be shown in the following way. Whenever it is possible to draw such a line, then the color coefficient $\mathcal{C}$ can be written as a product of two coefficients $\mathcal{A}$ and $\mathcal{B}$, one for the left and one for the right part. The statement that each color coefficient can be written through Kronecker deltas applies to both parts separately, so we can write

$$\begin{aligned}\mathcal{C}_{ij,\,kl} &= \mathcal{A}_{ij',\,kl'}\mathcal{B}_{j'j,\,l'l} = (a_1\delta_{ij'}\delta_{kl'} + a_2\delta_{ik}\delta_{j'l'})(b_1\delta_{j'j}\delta_{l'l} + b_2\delta_{j'l'}\delta_{jl}) \\ &= a_1b_1\delta_{ij}\delta_{kl} + (a_1b_2 + a_2b_1 + a_2b_2N)\delta_{ik}\delta_{jl} = (b_1\delta_{ij'}\delta_{kl'} + b_2\delta_{ik}\delta_{j'l'})(a_1\delta_{j'j}\delta_{l'l} + a_2\delta_{j'l'}\delta_{jl}) \\ &= \mathcal{B}_{ij',\,kl'}\mathcal{A}_{j'j,\,l'l}\,, \end{aligned} \tag{4.92}$$

which means that the two parts (and in fact any two color coefficients) commute. But then the replica path ordering and counting of replica indices can be done for each part separately:

$$\sum_{\{\rho\}} \mathcal{C}^{\{\rho\}}_{ij,\,kl} = \sum_{\{\rho_1\}} \mathcal{A}^{\{\rho_1\}}_{ij',\,kl'} \sum_{\{\rho_2\}} \mathcal{B}^{\{\rho_2\}}_{j'j,\,l'l}\,. \tag{4.93}$$

Since each part is at least of order n, the sum over every replica index combination for the whole color coefficient will be at least of order n^2.

Before calculating the projected color coefficients for the nonvanishing diagrams, we will clarify some conventions related to the complex conjugation on the antiquark Polyakov loop. There is a minus sign from the ig factor in the exponent, which we will use to revert the direction of the contour integration in the kinematic parts of the diagrams (indicated as an arrow to the left in Fig. 4.8), so for the calculation of the color coefficients we will only use charge conjugated color matrices without this minus sign. Then we have

$\widetilde{\mathcal{C}}_S$ 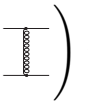 $= \mathcal{C}_S$ 
$$= \frac{\delta_{ik}\delta_{jl}}{N} T^a_{ij} T^{a\,*}_{kl} = \frac{1}{N}\mathrm{Tr}\big[T^aT^a\big] = \frac{1}{2N}(N^2-1)\,, \tag{4.94}$$

$\widetilde{\mathcal{C}}_A$  $= \mathcal{C}_A$ 
$$= \frac{2T^{b\,*}_{ik}T^b_{jl}}{N^2-1} T^a_{ij} T^{a\,*}_{kl} = \frac{2}{N^2-1}\mathrm{Tr}\big[T^aT^bT^aT^b\big] = -\frac{1}{2N}\,, \tag{4.95}$$

$\widetilde{\mathcal{C}}_S$  $= \mathcal{C}_S$  $- \mathcal{C}_S$
$$= \frac{\delta_{ik}\delta_{jl}}{N}\big[(T^aT^b)_{ij}(T^{b\,*}T^{a\,*})_{kl} - (T^aT^b)_{ij}(T^{a\,*}T^{b\,*})_{kl}\big]$$
$$= \frac{1}{N}\mathrm{Tr}\big[T^aT^bT^aT^b - T^aT^bT^bT^a\big] = -\frac{1}{4}(N^2-1)\,, \tag{4.96}$$

$\widetilde{\mathcal{C}}_A$ 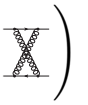 $= \mathcal{C}_A$  $- \mathcal{C}_A$
$$= \frac{2T^{c\,*}_{ik}T^c_{jl}}{N^2-1}\big[(T^aT^b)_{ij}(T^{b\,*}T^{a\,*})_{kl} - (T^aT^b)_{ij}(T^{a\,*}T^{b\,*})_{kl}\big]$$
$$= \frac{2}{N^2-1}\mathrm{Tr}\big[T^aT^bT^cT^aT^bT^c - T^aT^bT^cT^bT^aT^c\big] = \frac{1}{4}\,, \tag{4.97}$$

$\widetilde{\mathcal{C}}_S$ $= \mathcal{C}_S$  $- \mathcal{C}_S$
$$= \frac{\delta_{ik}\delta_{jl}}{N}\big[(T^aT^bT^a)_{ij}T^{b\,*}_{kl} - (T^aT^bT^b)_{ij}T^{a\,*}_{kl}\big]$$
$$= \frac{1}{N}\mathrm{Tr}\big[T^aT^bT^aT^b - T^aT^bT^bT^a\big] = -\frac{1}{4}(N^2-1)\,, \tag{4.98}$$

$\widetilde{\mathcal{C}}_A$  $= \mathcal{C}_A$  $- \mathcal{C}_A$
$$= \frac{2T^{c\,*}_{ik}T^c_{jl}}{N^2-1}\big[(T^aT^bT^a)_{ij}T^{b\,*}_{kl} - (T^aT^bT^b)_{ij}T^{a\,*}_{kl}\big]$$
$$= \frac{2}{N^2-1}\mathrm{Tr}\big[T^aT^bT^aT^cT^bT^c - T^aT^bT^bT^cT^aT^c\big] = \frac{1}{4}\,. \tag{4.99}$$

Continuing in the same way for the three-gluon diagrams, we get

$$\frac{2F_Q - F_S}{T} = \mathcal{K}\Bigg\{ \frac{N^2-1}{2N} \; - \frac{N^2-1}{4}\Bigg(\; + \; + \; \Bigg) + \frac{N(N^2-1)}{8}\Bigg(2 \; + 2 \;$$
$$+ \; + \; + \; + \; + \; + \; + \; + \; + \; + \;$$
$$+ 2 \; + 2 \; + \; + \; + \; + \; + 2 \; - \; - \;$$
$$- \; - \; - \; - \; \Bigg) + \dots \Bigg\}, \tag{4.100}$$

$$\frac{2F_Q - F_A}{T} = \mathcal{K}\Bigg\{ -\frac{1}{2N} \; + \frac{1}{4}\Bigg(\; + \; + \; \Bigg) - \frac{N}{8}\Bigg(2 \; + 2 \; + \; + \;$$
$$+ \; + \; + \; + \; + \; + \; + \; + \; - \; - \;$$
$$- \; - \; + \; + 2 \; - \; - \; - \; - \; - \; \Bigg) + \dots \Bigg\}, \tag{4.101}$$

where the dots include four-gluon diagrams and higher. Here we have neglected several other diagrams that vanish trivially in gauges where the gluon propagator is diagonal with respect to temporal and spatial components, such as Coulomb gauge, static gauge, or Feynman gauge. At the present order, there are 22 diagrams that vanish because a three-gluon vertex with three temporal indices gives zero, and 3 diagrams that vanish because a four-gluon vertex with four temporal indices gives zero.

We can expand the resulting expression for the normalized Polyakov loop correlator:

$$\begin{aligned}
\exp\left[\frac{2F_Q - F_{Q\bar{Q}}}{T}\right] &= \frac{1}{N^2}\exp\left[\frac{2F_Q - F_S}{T}\right] + \frac{N^2-1}{N^2}\exp\left[\frac{2F_Q - F_A}{T}\right] \\
&= 1 + \frac{N^2-1}{8N^2}\mathcal{K}^2\left(\; \right) + \frac{(N^2-1)(N^2-2)}{48N^3}\mathcal{K}^3\left(\; \right) \\
&\quad + \frac{N^2-1}{4N}\mathcal{K}\left(\; + \; + \; + \; + \; + \; + \; - \; - \; \right) \\
&\quad - \frac{N^2-1}{8N}\mathcal{K}\left(\; \right)\mathcal{K}\left(\; + \; + \; \right) + \mathcal{O}\left(\alpha_{\mathrm{s}}^4\right).
\end{aligned} \tag{4.102}$$

Note that this expansion is only valid for $\alpha_{\mathrm{s}}(1/r) \ll rT$, since the leading term in each free energy is the singlet or adjoint static potential, which are proportional to $\alpha_{\mathrm{s}}(1/r)/rT$. So if rT is too small, then the denominator overtakes the α_{s}-suppression from the numerator and the whole expression becomes large. In this case the Polyakov loop correlator is essentially given by the singlet free energy alone, since the contribution from the adjoint free energy is exponentially suppressed and the singlet term is exponentially enhanced.

The kinetic parts of the remaining diagrams will be determined through the method of integration by regions. This means that the integration over each gluon momentum is split into regions where the momentum scales the same as one of the relevant physical scales of the system, as was also explained in section 4.2. In this case we have the inverse distance $1/r$ between the two Polyakov loops, the temperature scale πT, and the Debye mass scale m_D, and we assume the hierarchy $1/r \gg \pi T \gg m_D$. The magnetic mass scale m_M is also present, but does not enter the calculation at this order. In each region the integrand is expanded according to this hierarchy. Depending on the scale of the gluon momentum, the propagator can either be free or resummed.

The evaluation of the kinetic parts becomes particularly simple in Coulomb gauge, because then all unconnected diagrams except for the one-gluon exchange vanish at this order. This can be seen by calculating the free propagator for the temporal gluons in position space:

$$D_{00}(\tau, \boldsymbol{r}) = \sum\!\!\!\!\!\!\int_K \frac{e^{ik_0\tau + i\boldsymbol{k}\cdot\boldsymbol{r}}}{\boldsymbol{k}^2} = \frac{\Gamma\left(\frac{d}{2}-1\right)}{4\pi^{\frac{d}{2}} r^{d-2}} \sum_{n\in\mathbb{Z}} \delta\left(\tau - \frac{n}{T}\right) . \tag{4.103}$$

For all practical purposes, only the $\delta(\tau)$ term is relevant, since the argument of the propagator will always lie inside $(-1/T, 1/T)$, and the endpoints do not contribute to any integral. This delta function requires the propagators to have the same imaginary time arguments at both ends, so any two- or three-gluon diagram in Eq. (4.102) with crossed propagators vanishes when the free propagator is used, which happens for $k \sim 1/r$ and $k \sim \pi T$. For $k \sim m_D$ one has to use a resummed propagator, which depends on k_0 and this relation cannot be used. We will discuss this case in more detail below.

We want to calculate the normalized Polyakov loop correlator in the short distance limit up to order g^7, which means that we have to calculate the one- and two-gluon exchange diagrams up to order g^5 and the three-gluon exchange diagrams up to order g^7. We will label the kinetic parts of the one- and two-gluon diagrams by D_I, D_X and D_T, such that the last line of Eq. (4.102) reads $-(N^2-1)/8N \times D_I(D_X + 2D_T)$ (the last two diagrams are identical for symmetry reasons, so each of them gives D_T). We will start with the calculation of D_I:

$$D_I = (ig)^2 \int_0^{1/T} d\tau_1 \int_{1/T}^{0} d\tau_2 \sum\!\!\!\!\!\!\int_K e^{ik_0(\tau_1-\tau_2)+i\boldsymbol{k}\cdot\boldsymbol{r}} D_{00}(k_0, \boldsymbol{k}) = \frac{g^2}{T} \int_k e^{i\boldsymbol{k}\cdot\boldsymbol{r}} D_{00}(0, \boldsymbol{k}) . \tag{4.104}$$

Splitting the integration into the different momentum regions, we have for $k \sim 1/r$:

$$\begin{aligned}
D_{I,1/r} &= \frac{g^2}{T} \int_{k\sim 1/r} \frac{e^{i\boldsymbol{k}\cdot\boldsymbol{r}}}{k^2} \left(1 - \frac{\Pi(0, k \gg \pi T)}{k^2} + \mathcal{O}\left(g^4\right)\right) \\
&= \frac{g^2}{T} \int_{k\sim 1/r} \frac{e^{i\boldsymbol{k}\cdot\boldsymbol{r}}}{k^2} \left(1 + \frac{g^2}{(4\pi)^2}\left[\frac{31}{9}N - \frac{10}{9}n_f + 2\beta_0 \ln\frac{\mu}{k}\right]\right. \\
&\qquad \left. + \frac{Ng^2}{18}\frac{T^2}{k^2} - \left(\frac{44}{225}N + \frac{7}{45}n_f\right) g^2\pi^2 \frac{T^4}{k^4} + \mathcal{O}\left((T/k)^6, g^4\right)\right) \\
&= \frac{\alpha_\mathrm{s}}{rT}\left(1 + \frac{\alpha_\mathrm{s}}{4\pi}\left[\frac{31}{9}N - \frac{10}{9}n_f + 2\beta_0(\gamma_E + \ln \mu r)\right]\right) \\
&\quad + \alpha_\mathrm{s}^2 \left[-\frac{N}{9} r\pi T - \left(\frac{22}{675}N + \frac{7}{270}n_f\right)(r\pi T)^3 + \mathcal{O}\left((r\pi T)^5, \alpha_\mathrm{s}^3\right)\right] .
\end{aligned} \tag{4.105}$$

Here we have used the (charge-renormalized) temporal gluon self-energy in Coulomb gauge, expanded for momenta much larger than the temperature. The second line gives the result for loop momenta of the same order as k, which corresponds to the vacuum part, while the third line gives the contributions coming from loop momenta of order πT, which corresponds to the matter part. Accordingly, the first part of the result gives the static potential in the vacuum (without the color factor) and the second part gives thermal corrections as a series in $r\pi T$.

The next contribution comes from the region $k \sim \pi T$, where we have to expand the numerator $\exp[i\boldsymbol{k}\cdot\boldsymbol{r}]$ for small r:

$$\begin{aligned} D_{I,\pi T} &= \frac{g^2}{T}\int_{k\sim\pi T}\frac{1-\frac{1}{2}(\boldsymbol{k}\cdot\boldsymbol{r})^2}{k^2}\left(1-\frac{\Pi(0,k\sim\pi T)}{k^2}+\mathcal{O}\left((kr)^4,g^4\right)\right) \\ &= \alpha_{\mathrm{s}}^2\left[N\left(-\frac{1}{2\varepsilon}-1+\gamma_E+\ln\frac{T^2}{\pi\mu^2}\right)+n_f\ln 2+\left(\frac{4}{3}N+n_f\right)\zeta(3)(rT)^2\right]+\mathcal{O}\left(\alpha_{\mathrm{s}}^3\right)\,. \end{aligned} \tag{4.106}$$

The first term in the expansion of the numerator does not depend on r and is exactly the same as -2 times the scale πT contribution to a single Polyakov loop (without the color factor), which can be found in [126]. The second order term in this expansion can be calculated by the same methods. The integrals without the self-energy are all scaleless, and it can be shown that the higher powers in r all vanish in the integral with the one-loop self-energy, so there are no $(r\pi T)^4$ or higher thermal corrections at order α_{s}^2. There also exists a result for all orders of $r\pi T$ in [125], which corresponds to $D_{I,1/r}+D_{I,\pi T}$, see appendix B.7.

The last contribution comes from the region $k\sim m_D$, where again the numerator is expanded, but now also the expansion of the denominator in terms of the self-energy is different:

$$\begin{aligned} D_{I,m_D} &= \frac{g^2}{T}\int_{k\sim m_D}\frac{1-\frac{1}{2}(\boldsymbol{k}\cdot\boldsymbol{r})^2}{k^2+m_D^2}\left(1-\frac{\Pi(0,k\sim m_D)-m_D^2}{k^2+m_D^2}+\frac{\left(\Pi(0,k\sim m_D)-m_D^2\right)^2}{\left(k^2+m_D^2\right)^2}-\dots\right) \\ &= -\frac{\alpha_{\mathrm{s}}m_D}{T}+N\alpha_{\mathrm{s}}^2\left[\frac{1}{2\varepsilon}+\frac{1}{2}-\gamma_E+\ln\frac{\pi\mu^2}{m_D^2}\right]+\frac{(N^2-1)n_f}{4N}\frac{\alpha_{\mathrm{s}}^3T}{m_D} \\ &\quad -\frac{3\alpha_{\mathrm{s}}^2m_D}{8\pi T}\left[3N+\frac{2}{3}n_f(1-4\ln 2)+2\beta_0\left(\gamma_E+\ln\frac{\mu}{4\pi T}\right)\right] \\ &\quad +\frac{N^2\alpha_{\mathrm{s}}^3T}{m_D}\left[\frac{89}{24}+\frac{\pi^2}{6}-\frac{11}{6}\ln 2\right]-\frac{\alpha_{\mathrm{s}}m_D^3}{6T^3}(rT)^2+\mathcal{O}\left(\alpha_{\mathrm{s}}^3\right)\,. \end{aligned} \tag{4.107}$$

Again, the terms coming from the zeroth order expansion of the numerator are equal to -2 times the scale m_D contribution to a single Polyakov loop. The second order term in this expansion is a standard integral in dimensional regularization. Higher terms in r also come with higher powers of m_D by dimensional analysis, so they are suppressed by additional powers of g.

Combining the contributions from the different scales, we have:

$$\begin{aligned} D_I &= \frac{\alpha_{\mathrm{s}}}{rT}\left(1+\frac{\alpha_{\mathrm{s}}}{4\pi}\left[\frac{31}{9}N-\frac{10}{9}n_f+2\beta_0(\gamma_E+\ln\mu r)\right]\right) \\ &\quad -\frac{\alpha_{\mathrm{s}}m_D}{T}+\alpha_{\mathrm{s}}^2\left[N\left(-\frac{1}{2}+\ln\frac{T^2}{m_D^2}\right)+n_f\ln 2\right] \\ &\quad -\frac{3\alpha_{\mathrm{s}}^2m_D}{8\pi T}\left[3N+\frac{2}{3}n_f(1-4\ln 2)+2\beta_0\left(\gamma_E+\ln\frac{\mu}{4\pi T}\right)\right] \end{aligned}$$

$$
\begin{aligned}
&+\frac{N^2\alpha_{\rm s}^3 T}{m_D}\left[\frac{89}{24}+\frac{\pi^2}{6}-\frac{11}{6}\ln 2\right]+\frac{(N^2-1)n_f}{4N}\frac{\alpha_{\rm s}^3 T}{m_D}\\
&-\frac{N\alpha_{\rm s}^2}{9}r\pi T+\alpha_{\rm s}^2\left(\frac{4}{3}N+n_f\right)\zeta(3)(rT)^2-\frac{\alpha_{\rm s}m_D^3}{6T^3}(rT)^2\\
&-\alpha_{\rm s}^2\left(\frac{22}{675}N+\frac{7}{270}n_f\right)(r\pi T)^3+\mathcal{O}\left((r\pi T)^5,\alpha_{\rm s}^3\right)\,, \qquad (4.108)
\end{aligned}
$$

where the terms are ordered with increasing power of r and g. The scale of $\alpha_{\rm s}$ is μ everywhere (so as yet undetermined); however, the logs of μ can be absorbed in an $\alpha_{\rm s}$ evaluated at a different scale, which is identical to this expression up to terms of higher order:

$$
\begin{aligned}
D_I=&\frac{\alpha_{\rm s}(1/r)}{rT}+\frac{\alpha_{\rm s}^2}{4\pi rT}\left[\frac{31}{9}N-\frac{10}{9}n_f+2\beta_0\gamma_E\right]\\
&-\frac{\alpha_{\rm s}(4\pi T)m_D(4\pi T)}{T}+\alpha_{\rm s}^2\left[N\left(-\frac{1}{2}+\ln\frac{T^2}{m_D^2}\right)+n_f\ln 2\right]\\
&-\frac{3\alpha_{\rm s}^2 m_D}{8\pi T}\left[3N+\frac{2}{3}n_f(1-4\ln 2)+2\beta_0\gamma_E\right]\\
&+\frac{N^2\alpha_{\rm s}^3 T}{m_D}\left[\frac{89}{24}+\frac{\pi^2}{6}-\frac{11}{6}\ln 2\right]+\frac{(N^2-1)n_f}{4N}\frac{\alpha_{\rm s}^3 T}{m_D}\\
&-\frac{N\alpha_{\rm s}^2}{9}r\pi T+\alpha_{\rm s}^2\left(\frac{4}{3}N+n_f\right)\zeta(3)(rT)^2-\frac{\alpha_{\rm s}m_D^3}{6T^3}(rT)^2\\
&-\alpha_{\rm s}^2\left(\frac{22}{675}N+\frac{7}{270}n_f\right)(r\pi T)^3+\mathcal{O}\left((r\pi T)^5,\alpha_{\rm s}^3\right)\,. \qquad (4.109)
\end{aligned}
$$

This transformation is to a certain extent arbitrary, since e.g. also the $\beta_0\gamma_E$ terms may be included by an extra factor $\exp[-\gamma_E]$ in the scale of $\alpha_{\rm s}$. We choose not to do this simply because it is rather unconventional.

For the Polyakov loop correlator we need the square and cubic powers of this expression up to $\mathcal{O}\left(g^7\right)$:

$$
\begin{aligned}
D_I^2=&\frac{\alpha_{\rm s}^2(1/r)}{r^2T^2}+\frac{\alpha_{\rm s}(1/r)\alpha_{\rm s}^2}{2\pi r^2T^2}\left[\frac{31}{9}N-\frac{10}{9}n_f+2\beta_0\gamma_E\right]\\
&-\frac{2\alpha_{\rm s}(1/r)\alpha_{\rm s}(4\pi T)m_D(4\pi T)}{rT^2}+\frac{\alpha_{\rm s}^2\alpha_{\rm s}(4\pi T)m_D(4\pi T)}{2\pi rT^2}\left[\frac{31}{9}N-\frac{10}{9}n_f+2\beta_0\gamma_E\right]\\
&+\frac{2\alpha_{\rm s}(1/r)\alpha_{\rm s}^2}{rT}\left[N\left(-\frac{1}{2}+\ln\frac{T^2}{m_D^2}\right)+n_f\ln 2\right]+\frac{(N^2-1)n_f}{2N}\frac{\alpha_{\rm s}(1/r)\alpha_{\rm s}^3}{rm_D}\\
&-\frac{3\alpha_{\rm s}(1/r)\alpha_{\rm s}^2 m_D}{4\pi rT^2}\left[3N+\frac{2}{3}n_f(1-4\ln 2)+2\beta_0\gamma_E\right]\\
&+\frac{2N^2\alpha_{\rm s}(1/r)\alpha_{\rm s}^3}{rm_D}\left[\frac{89}{24}+\frac{\pi^2}{6}-\frac{11}{6}\ln 2\right]-\frac{2\pi N\alpha_{\rm s}(1/r)\alpha_{\rm s}^2}{9}+\frac{\alpha_{\rm s}^2(4\pi T)m_D^2(4\pi T)}{T^2}\\
&-\frac{2\alpha_{\rm s}^2\alpha_{\rm s}(4\pi T)m_D(4\pi T)}{T}\left[N\left(-\frac{1}{2}+\ln\frac{T^2}{m_D^2}\right)+n_f\ln 2\right]\\
&+2\alpha_{\rm s}(1/r)\alpha_{\rm s}^2\left(\frac{4}{3}N+n_f\right)\zeta(3)rT-\frac{\alpha_{\rm s}(1/r)\alpha_{\rm s}m_D^3}{3T^3}rT+\frac{2\pi N\alpha_{\rm s}^2\alpha_{\rm s}(4\pi T)m_D(4\pi T)}{9T}rT
\end{aligned}
$$

$$
\begin{aligned}
&- 2\pi\alpha_{\rm s}(1/r)\alpha_{\rm s}^2\left(\frac{22}{675}N+\frac{7}{270}n_f\right)(r\pi T)^2 \\
&- \frac{2\alpha_{\rm s}^2\alpha_{\rm s}(4\pi T)m_D(4\pi T)}{T}\left(\frac{4}{3}N+n_f\right)\zeta(3)(rT)^2 \\
&+ \frac{2\alpha_{\rm s}^2\alpha_{\rm s}(4\pi T)m_D(4\pi T)}{T}\left(\frac{22}{675}N+\frac{7}{270}n_f\right)(r\pi T)^3+\mathcal{O}\left((r\pi T)^4,\alpha_{\rm s}^4\right)\,, \qquad (4.110)
\end{aligned}
$$

$$
D_I^3=\frac{\alpha_{\rm s}^3(1/r)}{r^3T^3}-\frac{3\alpha_{\rm s}^2(1/r)\alpha_{\rm s}(4\pi T)m_D(4\pi T)}{r^2T^3}+\mathcal{O}\left(\alpha_{\rm s}^4\right)\,. \qquad (4.111)
$$

We have explicitly kept the same scale dependence of $\alpha_{\rm s}$ as in D_I.

We will next discuss the third line of Eq. (4.102). This is a product of two diagrams. Since the first is at least of $\mathcal{O}(\alpha_{\rm s})$, the others need to be calculated at $\mathcal{O}\left(g^5\right)$, so we do not have to consider loop insertions. All these diagrams have crossed gluons, so in Coulomb gauge they all vanish at tree level (see above). Tree level propagators are used when the gluon momentum is of order r or πT, for m_D one uses the resummed propagator and diagrams with crossed gluons no longer vanish. But since gluons with a momentum of order m_D increase the order of the diagram by g, only one gluon is allowed to have such a momentum, otherwise the diagram would be $\mathcal{O}\left(\alpha_{\rm s}^3\right)$.

In the two D_T diagrams, if the scale m_D momentum is carried by the gluon connecting the two Polyakov loops, then the other gluon gives a scaleless integral. If this gluon carries a momentum of order πT instead, then this integral is scaleless without loop insertions. So the only contribution to D_T comes when the gluon connecting the Polyakov loops carries a momentum of order $1/r$ and the other of order m_D. Also in D_X one gluon momentum needs to be of order $1/r$ and the other of order m_D, but here there are two possible distributions of these momenta.

We will now show that at leading order the sum of D_X and $2D_T$ vanishes. This can be seen in the following way: for the gluon with the scale m_D momentum the separation r between the two Polyakov loops vanishes at leading order, and the time arguments of the other gluon are identical because of the delta function in the Coulomb gauge propagator. So the scale m_D gluon in D_X has the same contour integration as in D_T (one endpoint to the left and one to the right of the other gluon), but there is a relative minus because of the opposite orientation of the two loops. In D_X there is also a factor 2 because of the different possibilities to distribute the momenta. In the multipole expansion of D_X there are higher terms $m_D^2r^2$ etc, which are not canceled by $2D_T$, but those are suppressed by higher powers in g and can be neglected.

We will now show this in the explicit calculation. We can use the Coulomb gauge propagator (4.103) with $d=3$ (there are no divergences at this point), and the d-dimensional integral of $\left(k^2+m_D^2\right)^{-1}$ gives $-m_D/4\pi$ for $d\to 3$. Then we have

$$
\begin{aligned}
D_X\Big|_{\mathcal{O}(g^5)} &= (ig)^4\int_{1/T}^0 d\tau_1\int_{1/T}^{\tau_1}d\tau_2\int_0^{1/T}d\tau_3\int_0^{\tau_3}d\tau_4\left(\frac{T\delta(\tau_1-\tau_3)}{4\pi r}+\frac{T\delta(\tau_2-\tau_4)}{4\pi r}\right)\int_k\frac{1}{k^2+m_D^2} \\
&= g^4\left(\int_{1/T}^0 d\tau_1\int_{1/T}^{\tau_1}d\tau_2\int_0^{\tau_1}d\tau_4+\int_{1/T}^0 d\tau_1\int_{1/T}^{\tau_1}d\tau_2\int_{\tau_2}^{1/T}d\tau_3\right)\left(-\frac{Tm_D}{(4\pi)^2r}\right) \\
&= g^4\int_{1/T}^0 d\tau_1\left(-\tau_1\left(\frac{1}{T}-\tau_1\right)-\frac{1}{2}\left(\frac{1}{T}-\tau_1\right)^2\right)\left(-\frac{Tm_D}{(4\pi)^2r}\right) \\
&= -\frac{\alpha_{\rm s}^2m_D}{3rT^2}\,, \qquad (4.112)
\end{aligned}
$$

$$
\begin{aligned}
D_T\Big|_{\mathcal{O}(g^5)} &= (ig)^4 \int_{1/T}^{0} d\tau_1 \int_0^{1/T} d\tau_2 \int_0^{\tau_2} d\tau_3 \int_0^{\tau_3} d\tau_4 \, \frac{T\delta(\tau_1-\tau_3)}{4\pi r} \int_k \frac{1}{k^2+m_D^2} \\
&= -g^4 \int_0^{1/T} d\tau_2 \int_0^{\tau_2} d\tau_3 \int_0^{\tau_3} d\tau_4 \left(-\frac{T m_D}{(4\pi)^2 r}\right) \\
&= \frac{\alpha_s^2 m_D}{6 r T^2} \,, \qquad (4.113)
\end{aligned}
$$

where we labeled the imaginary time coordinates in clockwise order starting from the antiquark loop. So the combination $D_X + 2D_T$ is $\mathcal{O}(g^7)$ and therefore the third line of Eq. (4.102) does not contribute to the Polyakov loop correlator until $\mathcal{O}(g^9)$.

A similar thing happens to the unconnected diagrams of the second line of Eq. (4.102) (i.e. all except for the last two). We need to calculate these diagrams at $\mathcal{O}(g^7)$. If all gluon momenta are larger than m_D then each of these diagrams vanishes in Coulomb gauge because of the crossed propagators, but on the other hand only one gluon may carry a momentum of order m_D, because otherwise it would be $\mathcal{O}(\alpha_s^4)$ or smaller. For the first two unconnected diagrams and the last one it does not matter which gluon carries the scale m_D momentum; any choice leaves two other gluons of higher scale momenta that are crossed and therefore vanish in Coulomb gauge. For each of the remaining four diagrams there is only one possibility to choose the scale m_D gluon such that the other gluons are not crossed. The scale πT does not appear, since the corresponding integrals are scaleless at tree level, and loop insertions are not allowed at this order in g, so the remaining gluons each carry a momentum of order $1/r$.

Again, the sum over all these unconnected diagrams, which we will collectively call D_{3g}, vanishes at leading order. The argument is analogous to the previous case: the scale m_D gluon does not distinguish between the two Polyakov loops, it starts in front of and ends behind the two parallel gluons connecting the two loops in each case, but for two of them the direction of the integration is the opposite of the other two. We also give the explicit calculation (where we use the fact, that a diagram turned upside down is identical to the original diagram for symmetry reasons):

$$
\begin{aligned}
D_{3g}\Big|_{\mathcal{O}(g^7)} &= 2(ig)^6 \int_{1/T}^{0} d\tau_1 \int_{1/T}^{\tau_1} d\tau_2 \int_0^{1/T} d\tau_3 \int_0^{\tau_3} d\tau_4 \int_0^{\tau_4} d\tau_5 \int_0^{\tau_5} d\tau_6 \\
&\quad \times \frac{T\delta(\tau_1-\tau_5)\delta(\tau_2-\tau_4)}{(4\pi r)^2} \int_k \frac{1}{k^2+m_D^2} \\
&\quad + 2(ig)^6 \int_{1/T}^{0} d\tau_1 \int_{1/T}^{\tau_1} d\tau_2 \int_{1/T}^{\tau_2} d\tau_3 \int_0^{1/T} d\tau_4 \int_0^{\tau_4} d\tau_5 \int_0^{\tau_5} d\tau_6 \\
&\quad \times \frac{T\delta(\tau_2-\tau_6)\delta(\tau_3-\tau_5)}{(4\pi r)^2} \int_k \frac{1}{k^2+m_D^2} \\
&= -2g^6 \int_0^{1/T} d\tau_3 \int_0^{\tau_3} d\tau_4 \int_0^{\tau_4} d\tau_5 \int_0^{\tau_5} d\tau_6 \left(-\frac{T m_D}{(4\pi)^3 r^2}\right) \\
&\quad - 2g^6 \int_{1/T}^{0} d\tau_1 \int_{1/T}^{\tau_1} d\tau_2 \int_{1/T}^{\tau_2} d\tau_3 \int_{\tau_3}^{1/T} d\tau_4 \left(-\frac{T m_D}{(4\pi)^3 r^2}\right) \\
&= \frac{\alpha_s^3 m_D}{12 r^2 T^3} - \frac{\alpha_s^3 m_D}{12 r^2 T^3} = 0 \,. \qquad (4.114)
\end{aligned}
$$

In this calculation, the first two lines give the sum of the third and fourth diagram in the second line of Eq. (4.102), while the next two lines correspond to the fifth and sixth diagram.

The remaining contributions to the Polyakov loop come from the last two diagrams in the second line of Eq. (4.102). The sum of those, which we will call D_H, is much simpler to calculate than the individual diagrams, because in this case the contour integrations can be combined in such a way, that they yield the condition that all Matsubara frequencies in the gluon propagators have to be zero. So D_H is given by $g^4/2T$ times the spatial momentum integrals for the gluon propagators and vertices, which we will call D'_H.

This can be shown in the following way. We will label the gluon momenta in the two diagrams in the same way, so that they are easier to combine. In the H-shaped diagram, the momentum k flows from the antiquark loop to the quark loop along the temporal gluons on the left side, the momentum p flows from the antiquark loop to the quark loop along the temporal gluons on the right side, and the momentum q flows through the spatial gluon connecting the two temporal gluon legs from left to right, starting and ending on the quark loop. So if we again use the same labels for the imaginary time coordinates as before, then τ_1 connects to a propagator with momentum k, τ_2 to p, τ_3 to $p+q$, and τ_4 to $k-q$. In the case of the second diagram, the lower two temporal gluon legs are crossed, so τ_1 and τ_2 change their roles.

In Coulomb gauge and with these momentum labels, we may drop the q-terms from the three-gluon vertices, since those cancel in the product with the spatial propagator. The other momenta appear with a factor 2 in the vertices:

$$D'_H(k_0,p_0,q_0) = 4g^2 \int_k \int_p \int_q e^{i\boldsymbol{k}\cdot\boldsymbol{r}} D_{00}(K) D_{00}(K-Q) \big(k_i D_{ij}(Q) p_j\big) D_{00}(P) D_{00}(P+Q) e^{i\boldsymbol{p}\cdot\boldsymbol{r}} \,. \tag{4.115}$$

The result of the contour integrations is:

$$\begin{aligned}
D_H &= (ig)^4 \int_{1/T}^{0} d\tau_1 \int_{1/T}^{\tau_1} d\tau_2 \int_0^{1/T} d\tau_3 \int_0^{\tau_3} d\tau_4 \\
&\quad \times \sum_{k_0,p_0,q_0} \left(e^{-ik_0\tau_1} e^{-ip_0\tau_2} + e^{-ip_0\tau_1} e^{-ik_0\tau_2}\right) e^{i(p_0+q_0)\tau_3} e^{i(k_0-q_0)\tau_4} D'_H(k_0,p_0,q_0) \\
&= g^4 \left(\int_{1/T}^{0} d\tau_1 \int_{1/T}^{\tau_1} d\tau_2 + \int_{1/T}^{0} d\tau_1 \int_{\tau_1}^{0} d\tau_2 \right) \int_0^{1/T} d\tau_3 \int_0^{\tau_3} d\tau_4 \\
&\quad \times \sum_{k_0,p_0,q_0} e^{-ik_0\tau_1} e^{-ip_0\tau_2} e^{i(p_0+q_0)\tau_3} e^{i(k_0-q_0)\tau_4} D'_H(k_0,p_0,q_0) \\
&= g^4 \int_0^{1/T} d\tau_3 \int_0^{\tau_3} d\tau_4 \sum_{k_0,p_0,q_0} \frac{\delta_{k_0}}{T} \frac{\delta_{p_0}}{T} e^{i(p_0+q_0)\tau_3} e^{i(k_0-q_0)\tau_4} D'_H(k_0,p_0,q_0) \\
&= g^4 \int_0^{1/T} d\tau_3 \int_0^{\tau_3} d\tau_4 \sum_{q_0} e^{iq_0(\tau_3-\tau_4)} D'_H(0,0,q_0) \\
&= g^4 \sum_{q_0} \left(\frac{\delta_{q_0}}{2T^2} + \frac{1-\delta_{q_0}}{iq_0 T} \right) D'_H(0,0,q_0) \\
&= \frac{g^4}{2T} D'_H(0,0,0) \,,
\end{aligned} \tag{4.116}$$

where in the second step we exchanged the integration variables τ_1 with τ_2 and rewrote the boundaries of the integrations, δ_{k_0} means a Kronecker delta that selects the zero mode (so $\delta_{k_0} = \delta_{0n_k}$ for $k_0 = 2\pi T n_k$), and the second term in the next-to-last line vanishes because it is odd in q_0 while D'_H is even.

In the calculation of D'_H, again only the scale $1/r$ contributes at leading order, since the scale πT in any of the propagators leads to scaleless integrals. The result reads:

$$D'_H(0,0,0) = -\frac{g^2}{(4\pi)^3 r}\left(3 - \frac{\pi^2}{4}\right) + \mathcal{O}\left(g^3\right) . \tag{4.117}$$

We have calculated this result explicitly (see appendix B.8), however, it can also be obtained by comparison to the $\mathcal{O}\left(\alpha_s^3\right)$ result for the Polyakov loop correlator from [126] (where static gauge was used instead of Coulomb gauge); we will see when we collect the different contributions to the final result for the Polyakov loop that with this value for D'_H the two calculations agree.

In order to study if there can be a contribution of $\mathcal{O}\left(g^3\right)$ from D'_H, we will discuss the cases when one, two, or three momenta are of scale m_D. If only k or p are of scale m_D while all other momenta are still of order $1/r$ (in order to avoid scaleless integrals or higher powers of g), then we get an $\mathcal{O}\left(g^5\right)$ contribution, because there is always a power of k or p in the numerator and another power is required from the expansions of the propagators or exponentials in order to obtain an integrand that is even in the momenta, so the result is proportional to m_D^3. If only q is of the scale m_D then there is no contribution, because all propagators except for the spatial have to be expanded in q, and m_D does not appear in the spatial propagator, so that integral is scaleless.

Also when $k \sim q \sim m_D$ and $p \sim 1/r$ (or equivalently $p \sim q \sim m_D$ and $k \sim 1/r$) the scale m_D integrations of the leading order expansions of the propagators and exponentials are odd under a simultaneous sign change of both momenta, so only the next order in the expansion contributes, which leads to a result proportional to m_D^2 and therefore of $\mathcal{O}\left(g^4\right)$.

This leaves only the case when all gluon momenta are of the scale m_D and both exponentials need to be expanded:

$$D'_H(0,0,0)\Big|_{g^3} = 4g^2 \int_k \int_p \int_q \frac{(\boldsymbol{k}\cdot\boldsymbol{p})\boldsymbol{q}^2 - (\boldsymbol{k}\cdot\boldsymbol{q})(\boldsymbol{p}\cdot\boldsymbol{q}) + \dots}{\left(\boldsymbol{k}^2 + m_D^2\right)\left((\boldsymbol{k}-\boldsymbol{q})^2 + m_D^2\right)\left(\boldsymbol{q}^2\right)^2\left((\boldsymbol{p}+\boldsymbol{q})^2 + m_D^2\right)\left(\boldsymbol{p}^2 + m_D^2\right)} . \tag{4.118}$$

The k and p integrations both have a vector $\boldsymbol{k}$ or $\boldsymbol{p}$ in the numerator, and the only other momentum in the denominator is $\boldsymbol{q}$, so the results of both these integrals have to be proportional to $\boldsymbol{q}$ for symmetry reasons. When these are then contracted with the transverse projector from the spatial gluon propagator, then they also vanish. This means that only the first order contributions from the expansions of both exponentials contribute, which is of $\mathcal{O}\left(g^5\right)$. So there are no contributions to D'_H at all at $\mathcal{O}\left(g^3\right)$, and we have:

$$D_H = -\frac{\alpha_s^3}{rT}\left(\frac{3}{2} - \frac{\pi^2}{8}\right) + \mathcal{O}\left(\alpha_s^4\right) . \tag{4.119}$$

We now can put all the different contributions together to get the final perturbative result for the Polyakov loop. We will first collect all terms up to $\mathcal{O}\left(\alpha_s^3\right)$ and compare with the result from [126]:

$$
\begin{aligned}
\exp\left[\frac{2F_Q - F_{Q\bar{Q}}}{T}\right] &= 1 + \frac{N^2-1}{8N^2} D_I^2 + \frac{(N^2-1)(N^2-2)}{48N^3} D_I^3 - \frac{N^2-1}{4N} D_H + \dots \\
&= 1 + \frac{N^2-1}{8N^2}\left\{ \frac{\alpha_{\rm s}^2(1/r)}{r^2T^2} + \frac{\alpha_{\rm s}(1/r)\alpha_{\rm s}^2}{2\pi r^2T^2}\left(\frac{31}{9}N - \frac{10}{9}n_f + 2\beta_0\gamma_E\right)\right. \\
&\quad - \frac{2\alpha_{\rm s}(1/r)\alpha_{\rm s}(4\pi T) m_D(4\pi T)}{rT^2} + \frac{2\alpha_{\rm s}(1/r)\alpha_{\rm s}^2}{rT}\left[N\left(-\frac{1}{2} + \ln\frac{T^2}{m_D^2}\right) + n_f \ln 2\right] \\
&\quad - \frac{2\pi N \alpha_{\rm s}(1/r)\alpha_{\rm s}^2}{9} + \frac{\alpha_{\rm s}^2(4\pi T) m_D^2(4\pi T)}{T^2} + 2\alpha_{\rm s}(1/r)\alpha_{\rm s}^2\left(\frac{4}{3}N + n_f\right)\zeta(3) rT \\
&\quad - 2\pi\alpha_{\rm s}(1/r)\alpha_{\rm s}^2\left(\frac{22}{675}N + \frac{7}{270}n_f\right)(r\pi T)^2 + \frac{N^2-2}{6N}\frac{\alpha_{\rm s}^3(1/r)}{r^3T^3} \\
&\quad \left. + \frac{N\alpha_{\rm s}^3}{rT}\left(3 - \frac{\pi^2}{4}\right)\right\} + \mathcal{O}\left((r\pi T)^4, g^7\right) \\
&= 1 + \frac{N^2-1}{8N^2}\left\{ \frac{N^2-2}{6N}\frac{\alpha_{\rm s}^3(1/r)}{r^3T^3} + \frac{\alpha_{\rm s}^2(1/r)}{r^2T^2} + \frac{\alpha_{\rm s}(1/r)\alpha_{\rm s}^2}{2\pi r^2T^2}\left(\frac{31}{9}N - \frac{10}{9}n_f + 2\beta_0\gamma_E\right)\right. \\
&\quad - \frac{2\alpha_{\rm s}(1/r)\alpha_{\rm s}(4\pi T) m_D(4\pi T)}{rT^2} + \frac{2\alpha_{\rm s}(1/r)\alpha_{\rm s}^2}{rT}\left[N\left(1 - \frac{\pi^2}{8} + \ln\frac{T^2}{m_D^2}\right) + n_f \ln 2\right] \\
&\quad - \frac{2\pi N \alpha_{\rm s}(1/r)\alpha_{\rm s}^2}{9} + \frac{\alpha_{\rm s}^2(4\pi T) m_D^2(4\pi T)}{T^2} + 2\alpha_{\rm s}(1/r)\alpha_{\rm s}^2\left(\frac{4}{3}N + n_f\right)\zeta(3) rT \\
&\quad \left. - 2\pi\alpha_{\rm s}(1/r)\alpha_{\rm s}^2\left(\frac{22}{675}N + \frac{7}{270}n_f\right)(r\pi T)^2\right\} + \mathcal{O}\left((r\pi T)^4, g^7\right) \,. \qquad (4.120)
\end{aligned}
$$

This result agrees exactly with the one in [126], except that we have added a few more powers of $r\pi T$, and that we could also fix the scale of $\alpha_{\rm s}$ in some more terms through the relation to the one-gluon exchange diagram.

The next order is then:

$$
\begin{aligned}
\exp\left[\frac{2F_Q - F_{Q\bar{Q}}}{T}\right]_{g^7} &= \frac{N^2-1}{8N^2}\left\{ -\frac{N^2-2}{2N}\frac{\alpha_{\rm s}^2(1/r)\alpha_{\rm s}(4\pi T) m_D(4\pi T)}{r^2T^3}\right. \\
&\quad - \frac{2\alpha_{\rm s}^2\alpha_{\rm s}(4\pi T) m_D(4\pi T)}{4\pi rT^2}\left(\frac{31}{9}N - \frac{10}{9}n_f + 2\beta_0\gamma_E\right) \\
&\quad - \frac{3\alpha_{\rm s}(1/r)\alpha_{\rm s}^2 m_D}{4\pi rT^2}\left[3N + \frac{2}{3}n_f(1 - 4\ln 2) + 2\beta_0\gamma_E\right] \\
&\quad + \frac{(N^2-1)n_f}{2N}\frac{\alpha_{\rm s}(1/r)\alpha_{\rm s}^3}{rm_D} + \frac{2N^2\alpha_{\rm s}(1/r)\alpha_{\rm s}^3}{rm_D}\left[\frac{89}{24} + \frac{\pi^2}{6} - \frac{11}{6}\ln 2\right] \\
&\quad - \frac{2\alpha_{\rm s}^2\alpha_{\rm s}(4\pi T) m_D(4\pi T)}{T}\left[N\left(-\frac{1}{2} + \ln\frac{T^2}{m_D^2}\right) + n_f \ln 2\right] \\
&\quad - \frac{\alpha_{\rm s}(1/r)\alpha_{\rm s} m_D^3}{3T^3} rT + \frac{2\pi N\alpha_{\rm s}^2\alpha_{\rm s}(4\pi T) m_D(4\pi T)}{9T} rT \\
&\quad - \frac{2\alpha_{\rm s}^2\alpha_{\rm s}(4\pi T) m_D(4\pi T)}{T}\left(\frac{4}{3}N + n_f\right)\zeta(3)(rT)^2 \\
&\quad \left. + \frac{2\alpha_{\rm s}^2\alpha_{\rm s}(4\pi T) m_D(4\pi T)}{T}\left(\frac{22}{675}N + \frac{7}{270}n_f\right)(r\pi T)^3\right\} \,. \qquad (4.121)
\end{aligned}
$$

4.8 Free Energies in pNRQCD

The Polyakov loop correlator can be written as the correlator of static color sources ψ and χ at a distance r from imaginary time 0 to $1/T$:

$$\exp\left[-\frac{F_{Q\bar{Q}}}{T}\right] = \frac{1}{N^2\delta^6(0)}\mathrm{Tr}\left\langle\left(\psi(1/T,\boldsymbol{r})\chi^\dagger(1/T,\boldsymbol{0})\right)\left(\chi(0,\boldsymbol{0})\psi^\dagger(0,\boldsymbol{r})\right)\right\rangle \tag{4.122}$$

Accordingly, the singlet and adjoint free energies are given by:

$$\exp\left[-\frac{F_S}{T}\right] = \frac{1}{N\delta^6(0)}\left\langle\mathrm{Tr}\left[\psi(1/T,\boldsymbol{r})\chi^\dagger(1/T,\boldsymbol{0})\right]\mathrm{Tr}\left[\chi(0,\boldsymbol{0})\psi^\dagger(0,\boldsymbol{r})\right]\right\rangle\,, \tag{4.123}$$

$$\exp\left[-\frac{F_A}{T}\right] = \frac{2}{(N^2-1)\delta^6(0)}\left\langle\mathrm{Tr}\left[T^a\psi(1/T,\boldsymbol{r})\chi^\dagger(1/T,\boldsymbol{0})\right]\mathrm{Tr}\left[T^a\chi(0,\boldsymbol{0})\psi^\dagger(0,\boldsymbol{r})\right]\right\rangle\,. \tag{4.124}$$

Since the sources are static, their dynamics involve only the (imaginary) time direction. So one only has to add the following terms to the QCD Lagrangian:

$$\mathcal{L}_{\psi\chi} = \int d^3x\left[\psi^\dagger D_0\psi + \chi^\dagger D_0\chi\right]\,. \tag{4.125}$$

This corresponds to the NRQCD Lagrangian at leading order in the $1/M$ expansion, which is also called the static limit. In this theory, ψ is the operator that annihilates the heavy (static) quark, and χ is the operator that creates the heavy (static) antiquark. The spin indices that are present in NRQCD are to be neglected in this case.

Since we have assumed the hierarchy $1/r \gg \pi T \gg m_D$, we may use another EFT where the expansion for small r is systematically incorporated: pNRQCD. In this theory, the effective degrees of freedom are quark-antiquark fields in color singlet or octet configurations: S and O^a. Up until this point we have always kept the number of colors N general, however, pNRQCD is usually defined only for $N = 3$, hence the name octet for the adjoint field. But since the generalization to arbitrary N is straightforward, we will keep N general while still calling the adjoint field "octet" out of convention.

The Lagrangian density for static fields up to linear order in r is given by:

$$\begin{aligned}\mathcal{L}_{\mathrm{pNRQCD}} = &\int d^3r\left[S^\dagger(\partial_0 + V_s)S + O^{\dagger\,a}\left(D_0^{ab} + V_o\delta^{ab}\right)O^b\right] + \frac{1}{4}F^a_{\mu\nu}F^a_{\mu\nu} + \sum_{l=1}^{n_f}\bar{q}_l D_\mu\gamma_\mu q_l \\ &- \int d^3r\left[\frac{V_A}{\sqrt{2N}}\left(S^\dagger(\boldsymbol{r}\cdot ig\boldsymbol{E}^a)O^a + O^{\dagger\,a}(\boldsymbol{r}\cdot ig\boldsymbol{E}^a)S\right) + \frac{V_B}{2}d^{abc}O^{\dagger\,a}(\boldsymbol{r}\cdot ig\boldsymbol{E}^b)O^c\right]\,,\end{aligned} \tag{4.126}$$

where the singlet and octet fields S and O^a depend on both the relative coordinate $\boldsymbol{r}$ and the center-of-mass coordinate $\boldsymbol{R}$, while gluons and light quarks depend only on $\boldsymbol{R}$. The Wilson coefficients at next-to leading order are given by

$$\begin{aligned}V_s(r) = -(N^2-1)V_o(r) = -\frac{N^2-1}{2N}\frac{\alpha_{\mathrm{s}}(1/r)}{r}\left[1 + \frac{\alpha_{\mathrm{s}}}{4\pi}\left(\frac{31N}{9} - \frac{10n_f}{9} + 2\beta_0\gamma_E\right)\right]\,,\\ V_A(r) = V_B(r) = 1\,.\end{aligned} \tag{4.127}$$

In this theory, one can also define singlet and octet (adjoint) free energies:

$$\begin{aligned}
\frac{f_s}{T} \equiv & -\ln\frac{1}{\delta^6(0)}\left\langle S(1/T,\boldsymbol{R},\boldsymbol{r})S^\dagger(0,\boldsymbol{R},\boldsymbol{r})\right\rangle \\
= & -\frac{N^2-1}{2N}\frac{\alpha_{\rm s}(1/r)}{rT}\left[1+\frac{\alpha_{\rm s}}{4\pi}\left(\frac{31N}{9}-\frac{10n_f}{9}+2\beta_0\gamma_E\right)\right]+\frac{\pi}{9}\left(N^2-1\right)\alpha_{\rm s}^2 rT \\
& +\frac{N^2-1}{2N}\left(\frac{4N}{3}+n_f\right)\zeta(3)\alpha_{\rm s}^2 r^2T^2+\frac{(N^2-1)\alpha_{\rm s}}{12N}\frac{m_D^3}{T^3}r^2T^2+\mathcal{O}\left(r^3T^3,\alpha_{\rm s}^3\right), \qquad (4.128) \\
\frac{f_o}{T} \equiv & -\ln\frac{1}{(N^2-1)\delta^6(0)}\left\langle O^a(1/T,\boldsymbol{R},\boldsymbol{r})O^{a\,\dagger}(0,\boldsymbol{R},\boldsymbol{r})\right\rangle \\
= & -\frac{1}{N^2-1}\frac{f_s}{T}-\frac{N\alpha_{\rm s}(4\pi T)m_D(4\pi T)}{2T}+\frac{N\alpha_{\rm s}^2}{2}\left[N\left(-\frac{1}{2}+\ln\frac{T^2}{m_D^2}\right)+n_f\ln 2\right] \\
& -\frac{3N\alpha_{\rm s}^2 m_D}{16\pi T}\left[3N+\frac{2}{3}n_f(1-4\ln 2)+2\beta_0\gamma_E\right]+\frac{N^3\alpha_{\rm s}^3 T}{m_D}\left[\frac{89}{48}+\frac{\pi^2}{12}-\frac{11}{12}\ln 2\right] \\
& +\frac{(N^2-1)n_f}{8}\frac{\alpha_{\rm s}^3 T}{m_D}+\mathcal{O}\left(r^3T^3,\alpha_{\rm s}^3\right). \qquad (4.129)
\end{aligned}$$

We have taken these results from [126] and added the information from Sec. 4.3 about the $\mathcal{O}\left(g^5\right)$ Polyakov loop. The value of the center of mass coordinate is irrelevant because of translational invariance, however, by comparison to the expressions for the NRQCD correlators we set it to $\boldsymbol{R}=\boldsymbol{r}/2$. We can also express the Polyakov loop correlator with these free energies:

$$\exp\left[-\frac{F_{Q\bar{Q}}}{T}\right]=\frac{1}{N^2}\exp\left[-\frac{f_s}{T}\right]+\frac{N^2-1}{N^2}\exp\left[-\frac{f_o}{T}\right]+\mathcal{O}\left(r^4\right). \qquad (4.130)$$

If we compare them to the free energies defined with the exponentiation formula (in Coulomb gauge):

$$\begin{aligned}
\frac{F_S}{T} = & -\frac{N^2-1}{2N}D_I+\frac{2F_Q}{T}+\mathcal{O}\left(\alpha_{\rm s}^3\right), \qquad (4.131) \\
\frac{F_A}{T} = & \frac{1}{2N}D_I+\frac{2F_Q}{T}+\mathcal{O}\left(\alpha_{\rm s}^3\right), \qquad (4.132) \\
\frac{F_Q}{T} = & -\frac{(N^2-1)\alpha_{\rm s}(4\pi T)m_D(4\pi T)}{4NT}+\frac{(N^2-1)\alpha_{\rm s}^2}{4N}\left[N\left(-\frac{1}{2}+\ln\frac{T^2}{m_D^2}\right)+n_f\ln 2\right] \\
& -\frac{3(N^2-1)\alpha_{\rm s}^2 m_D}{32N\pi T}\left[3N+\frac{2}{3}n_f(1-4\ln 2)+2\beta_0\gamma_E\right] \\
& +\frac{N(N^2-1)\alpha_{\rm s}^3 T}{m_D}\left[\frac{89}{96}+\frac{\pi^2}{24}-\frac{11}{24}\ln 2\right]+\frac{(N^2-1)^2 n_f}{16N^2}\frac{\alpha_{\rm s}^3 T}{m_D}+\mathcal{O}\left(\alpha_{\rm s}^3\right), \qquad (4.133)
\end{aligned}$$

we see that they almost agree, but there is a difference of a factor 2 in the linear term in rT.

In order to understand this difference, we must match the two correlators in both theories. It is rather straightforward to see that they are not the same in principle; after all, F_S and F_A depend on the choice of gauge while f_s and f_o do not. In addition, f_s and f_o give the Polyakov loop correlator only at leading order in the small r expansion. But still we can quantify the difference by a proper matching calculation.

More specifically, we will match the operator $\psi(\boldsymbol{r})\chi^\dagger(\boldsymbol{0})$. This transforms as $N_{\boldsymbol{r}}\times\overline{N_{\boldsymbol{0}}}$ under gauge transformations, which in principle also the matching pNRQCD operators have

to satisfy. However, all pNRQCD operators transform locally at the center of mass in either representation. We therefore have to introduce spatial Wilson lines ϕ in order to transport the gauge dependence to the quark or antiquark positions from NRQCD:

$$\phi(\boldsymbol{x}_1, \boldsymbol{x}_2) \equiv \mathcal{P} \exp\left[ig \int_0^1 ds (\boldsymbol{x}_1 - \boldsymbol{x}_2) \cdot \boldsymbol{A}(s\boldsymbol{x}_1 + (1-s)\boldsymbol{x}_2)\right], \tag{4.134}$$

where we suppressed the imaginary time argument.

But in pNRQCD all gauge fields need to be multipole expanded. So the Wilson lines going from $\boldsymbol{R}$ to $\boldsymbol{R} \pm \boldsymbol{r}/2$ have to be rewritten in an expanded form:

$$\begin{aligned}\phi(\boldsymbol{R} \pm \boldsymbol{r}/2, \boldsymbol{R}) &= 1 \pm \frac{1}{2}\int_0^1 ds\, \boldsymbol{r} \cdot ig\boldsymbol{A}(\boldsymbol{R} \pm s\boldsymbol{r}/2) \\ &\quad + \frac{1}{4}\int_0^1 ds_1 \int_0^{s_1} ds_2\, (\boldsymbol{r} \cdot ig\boldsymbol{A}(\boldsymbol{R} \pm s_1\boldsymbol{r}/2))(\boldsymbol{r} \cdot ig\boldsymbol{A}(\boldsymbol{R} \pm s_2\boldsymbol{r}/2)) + \ldots \\ &= 1 \pm \frac{1}{2}\boldsymbol{r} \cdot ig\boldsymbol{A}(\boldsymbol{R}) + \frac{1}{8}(\boldsymbol{r} \cdot \boldsymbol{\nabla}_R)(\boldsymbol{r} \cdot ig\boldsymbol{A}(\boldsymbol{R})) + \frac{1}{8}(\boldsymbol{r} \cdot ig\boldsymbol{A}(\boldsymbol{R}))^2 + \mathcal{O}\left(r^3\right).\end{aligned} \tag{4.135}$$

This expansion of the Wilson line does not include matching coefficients, because the gauge transport only works if all coefficients are exactly like in the expression above.

So the matching of $\psi(\boldsymbol{r})\chi^\dagger(\boldsymbol{0})$ consists of a series of pNRQCD operators with these expanded Wilson lines to the left and right. The other operators also need to have the same behavior under P, C, and T transformations, which $S\mathbb{1}$ and O^aT^a as well as the Wilson lines automatically satisfy. Since all operators need to involve exactly one singlet or octet field because of heavy quark number conservation, the additional operators need to be neutral under P, C, and T[7].

So at $\mathcal{O}(r^2)$ in the multipole expansion, we have:

$$\begin{aligned}\psi(\boldsymbol{r})\chi^\dagger(\boldsymbol{0}) = \phi(\boldsymbol{r}, \boldsymbol{r}/2) \Bigg[&\frac{Z_s}{\sqrt{N}} S\mathbb{1} + \sqrt{2}Z_o O^a T^a + \sqrt{2}Z_{Es}\, r\, (\boldsymbol{r} \cdot ig\boldsymbol{E}^a)\, ST^a \\ &+ \frac{Z_{Eo}\, r}{\sqrt{N}} (\boldsymbol{r} \cdot ig\boldsymbol{E}^a)\, O^a\mathbb{1} + \sqrt{2}Z'_{Eo}\, d^{abc}\, r\, (\boldsymbol{r} \cdot ig\boldsymbol{E}^a)\, O^bT^c + \mathcal{O}\left(r^3\right)\Bigg] \phi^\dagger(\boldsymbol{0}, \boldsymbol{r}/2).\end{aligned} \tag{4.136}$$

All the fields inside the square brackets have $\boldsymbol{R} = \boldsymbol{r}/2$. The matching coefficients have been chosen such that Z_s and Z_o are $1 + \mathcal{O}(\alpha_s)$. The different projections of this operator which generate F_S and F_A are then given by:

$$\begin{aligned}\frac{1}{\sqrt{N}}\mathrm{Tr}\left[\psi\chi^\dagger\right] &= Z_s S + \frac{Z_o}{\sqrt{2N}} (\boldsymbol{r} \cdot ig\boldsymbol{A}^a)\, O^a + \frac{Z_s}{4N} (\boldsymbol{r} \cdot ig\boldsymbol{A}^a)(\boldsymbol{r} \cdot ig\boldsymbol{A}^a)\, S \\ &\quad + \frac{Z_o}{4\sqrt{2N}} d^{abc} (\boldsymbol{r} \cdot ig\boldsymbol{A}^a)\left(\boldsymbol{r} \cdot ig\boldsymbol{A}^b\right) O^c + Z_{Eo}\, r\, (\boldsymbol{r} \cdot ig\boldsymbol{E}^a)\, O^a + \mathcal{O}\left(r^3\right),\end{aligned} \tag{4.137}$$

[7]Note that in imaginary time $\tau = it \xrightarrow{T} (-i)(-t) = \tau$, and thus $A_0 \xrightarrow{T} -A_0$, $\boldsymbol{A} \xrightarrow{T} -\boldsymbol{A}$, and $\boldsymbol{E} \xrightarrow{T} -\boldsymbol{E}$, while all coefficients are still complex conjugated.

$$\begin{aligned}\sqrt{2}\mathrm{Tr}\left[T^a\psi\chi^\dagger\right] &= Z_o O^a + \frac{Z_s}{\sqrt{2N}}\left(\boldsymbol{r}\cdot ig\boldsymbol{A}^a\right)S + \frac{Z_o}{2}d^{abc}\left(\boldsymbol{r}\cdot ig\boldsymbol{A}^b\right)O^c \\ &+ \frac{Z_s}{4\sqrt{2N}}d^{abc}\left(\boldsymbol{r}\cdot ig\boldsymbol{A}^b\right)\left(\boldsymbol{r}\cdot ig\boldsymbol{A}^c\right)S + \frac{Z_o}{4N}\left(\boldsymbol{r}\cdot ig\boldsymbol{A}^a\right)\left(\boldsymbol{r}\cdot ig\boldsymbol{A}^b\right)O^b \\ &+ \frac{Z_o}{8}d^{abe}d^{ecd}\left(\boldsymbol{r}\cdot ig\boldsymbol{A}^b\right)\left(\boldsymbol{r}\cdot ig\boldsymbol{A}^c\right)O^d + \frac{Z_o}{8}if^{abc}\left[(\boldsymbol{r}\cdot\boldsymbol{\nabla}),\left(\boldsymbol{r}\cdot ig\boldsymbol{A}^b\right)\right]O^c \\ &+ Z_{Es}\,r\left(\boldsymbol{r}\cdot ig\boldsymbol{E}^a\right)S + Z'_{Eo}\,d^{abc}\,r\left(\boldsymbol{r}\cdot ig\boldsymbol{E}^b\right)O^c + \mathcal{O}\left(r^3\right)\,. \end{aligned} \tag{4.138}$$

Now we can calculate the corrections to the pNRQCD free energies, by inserting these matching relations into the respective correlators[8]:

$$\begin{aligned}\exp\left[-\frac{F_S}{T}\right] &= \frac{1}{N\delta^6(0)}\left\langle\mathrm{Tr}\left[\psi(1/T)\chi^\dagger(1/T)\right]\mathrm{Tr}\left[\chi(0)\psi^\dagger(0)\right]\right\rangle \\ &= \frac{|Z_s|^2}{\delta^6(0)}\left\langle S(1/T)S^\dagger(0)\right\rangle + \frac{Z_s^*Z_o}{\sqrt{2N}\delta^6(0)}\left\langle\left(\boldsymbol{r}\cdot ig\boldsymbol{A}^a\right)O^a(1/T)S^\dagger(0)\right\rangle \\ &\quad - \frac{Z_o^*Z_s}{\sqrt{2N}\delta^6(0)}\left\langle S(1/T)\left(\boldsymbol{r}\cdot ig\boldsymbol{A}^a\right)O^{a\,\dagger}(0)\right\rangle \\ &\quad + \frac{|Z_s|^2}{2N\delta^6(0)}\left\langle\left(\boldsymbol{r}\cdot ig\boldsymbol{A}^a\right)\left(\boldsymbol{r}\cdot ig\boldsymbol{A}^a\right)S(1/T)S^\dagger(0)\right\rangle \\ &\quad - \frac{|Z_o|^2}{2N\delta^6(0)}\left\langle\left(\boldsymbol{r}\cdot ig\boldsymbol{A}^a\right)\left(\boldsymbol{r}\cdot ig\boldsymbol{A}^b\right)O^a(1/T)O^{b\,\dagger}(0)\right\rangle + \mathcal{O}\left(r^3\right)\,, \end{aligned} \tag{4.139}$$

$$\begin{aligned}(N^2-1)\exp\left[-\frac{F_A}{T}\right] &= \frac{2}{\delta^6(0)}\left\langle\mathrm{Tr}\left[T^a\psi(1/T)\chi^\dagger(1/T)\right]\mathrm{Tr}\left[T^a\chi(0)\psi^\dagger(0)\right]\right\rangle \\ &= \frac{|Z_o|^2}{\delta^6(0)}\left\langle O^a(1/T)O^a(0)\right\rangle - \frac{Z_s^*Z_o}{\sqrt{2N}\delta^6(0)}\left\langle\left(\boldsymbol{r}\cdot ig\boldsymbol{A}^a\right)O^a(1/T)S^\dagger(0)\right\rangle \\ &\quad + \frac{Z_o^*Z_s}{\sqrt{2N}\delta^6(0)}\left\langle S(1/T)\left(\boldsymbol{r}\cdot ig\boldsymbol{A}^a\right)O^{a\,\dagger}(0)\right\rangle \\ &\quad - \frac{|Z_s|^2}{2N\delta^6(0)}\left\langle\left(\boldsymbol{r}\cdot ig\boldsymbol{A}^a\right)\left(\boldsymbol{r}\cdot ig\boldsymbol{A}^a\right)S(1/T)S^\dagger(0)\right\rangle \\ &\quad + \frac{|Z_o|^2}{2N\delta^6(0)}\left\langle\left(\boldsymbol{r}\cdot ig\boldsymbol{A}^a\right)\left(\boldsymbol{r}\cdot ig\boldsymbol{A}^b\right)O^a(1/T)O^{b\,\dagger}(0)\right\rangle + \mathcal{O}\left(r^3\right)\,. \end{aligned} \tag{4.140}$$

We have suppressed the time arguments of the gauge fields; since they obey periodic boundary conditions, it does not matter if they are evaluated at imaginary time 0 or $1/T$. Some terms have been neglected, because they do not contribute at this order in r, and several terms cancel. We see again that the corrections to the pNRQCD free energies are gauge dependent, because they involve the gauge fields $\boldsymbol{A}$ instead of the gauge invariant combinations $\boldsymbol{E}$ or $\boldsymbol{B}$.

The calculation of the correlators for the leading order corrections can be done in the

[8] We have seen in section 4.6 that singlet and adjoint free energies are in general mixed under renormalization. Since f_s and f_o are finite, such a divergence structure can only be reproduced in pNRQCD, if also in the matching the two correlators are mixed. However, as we have seen before, these divergences are absent in Coulomb gauge. So we may ignore any mixing effects and thus get a consistent result in the way presented here.

following way. The quark-antiquark fields can be replaced by the leading order propagators:

$$\begin{aligned}\left\langle (\boldsymbol{r}\cdot ig\boldsymbol{A}^a)\,(\boldsymbol{r}\cdot ig\boldsymbol{A}^a)\,S(1/T)S^\dagger(0)\right\rangle &= \delta^6(0)e^{-V_s/T}\left\langle (\boldsymbol{r}\cdot ig\boldsymbol{A}^a)\,(\boldsymbol{r}\cdot ig\boldsymbol{A}^a)\right\rangle + \mathcal{O}\left(r^4\right)\,,\\ \left\langle (\boldsymbol{r}\cdot ig\boldsymbol{A}^a)\left(\boldsymbol{r}\cdot ig\boldsymbol{A}^b\right)O^a(1/T)O^{b\,\dagger}(0)\right\rangle &= \delta^6(0)e^{-V_o/T}\left\langle (\boldsymbol{r}\cdot ig\boldsymbol{A}^a)\,(\boldsymbol{r}\cdot ig\boldsymbol{A}^a)\right\rangle + \mathcal{O}\left(g^5,r^4\right)\,.\end{aligned} \tag{4.141}$$

When both singlet and octet fields appear, then the insertion of a vertex is necessary:

$$\begin{aligned}\left\langle (\boldsymbol{r}\cdot ig\boldsymbol{A}^a)\,O^a(1/T)S^\dagger(0)\right\rangle &= \frac{V_A\delta^6(0)}{\sqrt{2N}}\int_0^{1/T} d\tau\, e^{-V_o(1/T-\tau)-V_s\tau}\left\langle (\boldsymbol{r}\cdot ig\boldsymbol{E}^a(\tau))\,(\boldsymbol{r}\cdot ig\boldsymbol{A}^a)\right\rangle\\ &\quad + \mathcal{O}\left(g^5,r^4\right)\,, \end{aligned}\tag{4.142}$$

$$\begin{aligned}\left\langle (\boldsymbol{r}\cdot ig\boldsymbol{A}^a)\,S(1/T)O^{a\,\dagger}(0)\right\rangle &= \frac{V_A\delta^6(0)}{\sqrt{2N}}\int_0^{1/T} d\tau\, e^{-V_s(1/T-\tau)-V_o\tau}\left\langle (\boldsymbol{r}\cdot ig\boldsymbol{E}^a(\tau))\,(\boldsymbol{r}\cdot ig\boldsymbol{A}^a)\right\rangle\\ &\quad + \mathcal{O}\left(g^5,r^4\right)\,. \end{aligned}\tag{4.143}$$

The leading contribution from the electric fields comes from the $-\partial_\tau \boldsymbol{A}^a$ term, and we can use the imaginary time derivative to integrate by parts:

$$\begin{aligned}\int_0^{1/T} d\tau\, e^{-V_o(1/T-\tau)-V_s\tau}\left\langle (\boldsymbol{r}\cdot ig\boldsymbol{E}^a(\tau))\,(\boldsymbol{r}\cdot ig\boldsymbol{A}^a)\right\rangle &= \left(e^{-V_o/T}-e^{-V_s/T}\right)\left\langle (\boldsymbol{r}\cdot ig\boldsymbol{A}^a)\,(\boldsymbol{r}\cdot ig\boldsymbol{A}^a)\right\rangle\\ &\quad + \mathcal{O}\left(\alpha_{\rm s}^3\right)\,, \end{aligned}\tag{4.144}$$

$$\begin{aligned}\int_0^{1/T} d\tau\, e^{-V_s(1/T-\tau)-V_o\tau}\left\langle (\boldsymbol{r}\cdot ig\boldsymbol{E}^a(\tau))\,(\boldsymbol{r}\cdot ig\boldsymbol{A}^a)\right\rangle &= \left(e^{-V_s/T}-e^{-V_o/T}\right)\left\langle (\boldsymbol{r}\cdot ig\boldsymbol{A}^a)\,(\boldsymbol{r}\cdot ig\boldsymbol{A}^a)\right\rangle\\ &\quad + \mathcal{O}\left(\alpha_{\rm s}^3\right)\,. \end{aligned}\tag{4.145}$$

We can also replace the coefficients Z_s, Z_o, and V_A by 1, because higher order corrections to these coefficients are beyond the accuracy of this calculation. The corrections to the free energies then simplify to:

$$\exp\left[-\frac{F_S}{T}\right] = \exp\left[-\frac{f_s}{T}\right] + \frac{e^{-V_o/T}-e^{-V_s/T}}{2N}\left\langle (\boldsymbol{r}\cdot ig\boldsymbol{A}^a)\,(\boldsymbol{r}\cdot ig\boldsymbol{A}^a)\right\rangle + \mathcal{O}\left(g^5,r^3\right)\,, \tag{4.146}$$

$$\exp\left[-\frac{F_A}{T}\right] = \exp\left[-\frac{f_o}{T}\right] - \frac{e^{-V_o/T}-e^{-V_s/T}}{2N(N^2-1)}\left\langle (\boldsymbol{r}\cdot ig\boldsymbol{A}^a)\,(\boldsymbol{r}\cdot ig\boldsymbol{A}^a)\right\rangle + \mathcal{O}\left(g^5,r^3\right)\,. \tag{4.147}$$

For the calculation of the gauge field correlator, we need to use the same gauge as for F_S and F_A, i.e. Coulomb gauge:

$$\begin{aligned}\left\langle (\boldsymbol{r}\cdot ig\boldsymbol{A}^a)\,(\boldsymbol{r}\cdot ig\boldsymbol{A}^a)\right\rangle &= -g^2\sum\!\!\!\!\!\!\int_K \frac{(\boldsymbol{r}^2\boldsymbol{k}^2-(\boldsymbol{r}\cdot\boldsymbol{k})^2)\,\delta^{aa}}{\boldsymbol{k}^2\,(k_0^2+\boldsymbol{k}^2)} = -g^2(N^2-1)\frac{d-1}{d}\sum\!\!\!\!\!\!\int_K \frac{r^2}{k_0^2+\boldsymbol{k}^2}\\ &= -\frac{g^2(N^2-1)r^2T^{d-1}\mu^{3-d}}{2\pi^{2-\frac{d}{2}}}\frac{d-1}{d}\Gamma\left(1-\tfrac{d}{2}\right)\zeta(2-d)\\ &\overset{d=3}{=} -\frac{2\pi}{9}(N^2-1)\alpha_{\rm s}r^2T^2\,. \end{aligned}\tag{4.148}$$

When we insert this into the expression above, then we also expand the exponentials of the potentials, since they also are of $\mathcal{O}(\alpha_{\rm s})$. Then the leading order corrections are:

$$\exp\left[-\frac{F_S}{T}\right] = \exp\left[-\frac{f_s}{T}\right] + \frac{\pi}{18}(N^2-1)\alpha_{\rm s}^2r^2T^2 + \mathcal{O}\left(g^5,r^3\right)\,, \tag{4.149}$$

$$\exp\left[-\frac{F_A}{T}\right] = \exp\left[-\frac{f_o}{T}\right] - \frac{\pi}{18}\alpha_{\rm s}^2r^2T^2 + \mathcal{O}\left(g^5,r^3\right)\,. \tag{4.150}$$

In this way we can exactly reproduce the difference between the free energies in NRQCD and pNRQCD at the given order.

We have seen that there are no corrections at $\mathcal{O}(g^5)$. However, there are several contributions at this order that we have neglected in this calculation. We do not attempt here to show that they all cancel, but this should be a straightforward extension of the arguments presented here.

Chapter 5

Conclusions and Outlook

In this thesis, the behavior of heavy quarks has been studied both in the vacuum and in a hot medium. For the vacuum part, this work constitutes the first treatment of hybrid quarkonia in an EFT framework. At finite temperature, we present a new perturbative order in the calculation of both the Polyakov loop and the Polyakov loop correlator for weak coupling. In all these studies, effective field theories have proved to be an extremely useful tool, for whose construction the study of the symmetries of the respective system is pivotal as a guiding principle. Therefore, in the first part of this work, we have first studied how the hidden boost symmetry in non-relativistic EFTs can be used to derive exact relations between the matching parameters in chapter 2.

The following application of NRQCD and pNRQCD to the description of hybrids in chapter 3 is only the first step towards a fully consistent framework for hybrids. Still, this first EFT discussion of hybrids has already yielded some advancements over previous work, introducing the concept of Λ-doubling, which has been known in the context of atomic molecules and is responsible for the mass splitting between nearly degenerate states with opposite parity. This is reflected in the appearance of coupled radial Schrödinger equations for the heavy quark content of the hybrid states, which mix contributions from different static states. Our results are in agreement with lattice calculations and also fall into the mass range of experimental candidates for exotic quarkonia, although a clear identification is not yet possible.

In chapter 4, we have calculated the Polyakov loop in perturbation theory at the third non-trivial order, in an EFT framework as well as in a direct calculation. In a comparison to existing lattice data in a temperature range well beyond the critical temperature, where perturbation theory is supposed to work, we found that the perturbative result is reasonably close, but still does not quite agree with the lattice result within statistical errors (at least in the pure gauge case $n_f = 0$). We conclude that there is still room for the disagreement to be settled with the next perturbative correction. This is an issue that should be addressed in the future by calculating the next order of the Polyakov loop in perturbation theory. Beyond this order the perturbative expansion breaks down due to effects at the magnetic scale, so this result would give the best attainable (purely) perturbative expression for the Polyakov loop. A better knowledge of the Polyakov loop would in turn lead to new results for the correlator, in the same way as has been demonstrated in the latter half of chapter 4, where we have calculated the correlator to NNNLO in the short distance limit.

This research provides ample opportunity for extension in some of the following directions. The principle of using non-linear field transformations for not explicitly realized symmetries can be applied to any other EFT as well, whenever a symmetry is not explicitly realized in

the EFT but has to be hidden in some form.

In order to improve our theoretical knowledge about the hybrids, studies that go beyond leading order in the expansion parameters are required for more reliable results. In particular, the inclusion of spin dependent terms would be very interesting, since the effects of these terms, while not being NLO because of their higher suppression in $1/M$, would still give very clear signals as they are the only contributions that can differentiate between the otherwise degenerate spin-symmetry multiplets. Another important direction is the description of decays and production mechanisms of hybrids. Then, this framework may also be applied to the study of tetraquarks, as proposed in [17]. This would require the determination of the static energies with a non-trivial light-quark content, but the derivation of coupled Schrödinger equations would be analogous and the discussion on the quantum numbers would apply as well.

At finite temperature, there are several other quantities which can be expressed through Wilson line operators apart from the Polyakov loop. Among these are the jet quenching parameter or the heavy quark diffusion coefficient, which describe energy loss in the medium. As such they are relevant for comparisons with experimental results, so an improved theoretical knowledge is desirable. The methods for the Polyakov loop calculation, and maybe also to some extent the results, can be used to study these parameters.

The Wilson line operator that relates to the interquark potential is the rectangular Wilson loop, both in the vacuum and at finite temperature. This operator depends on a rectangular path in space-time. If like in this case such a path has corners, so-called cusps, then there are divergences associated to these cusps and the corresponding renormalization group equation depends on the cusp anomalous dimension. This cusp anomalous dimension is a universal function that depends only on the angles at the cusp, and has applications to many other quantities related to Wilson line operators. For example, it has been shown that the cusp anomalous dimension and the static potential agree in a certain limit at low orders in perturbation theory. At higher orders [157] deviations from this relation are expected, but it should be possible to calculate them with the same techniques as for the potential. Since the cusp anomalous dimension has many applications to other fields in QCD, like heavy quark production or parton distribution functions, such a study would definitely be worthwhile.

Another very promising approach to obtain results at finite temperature is through a spectral function representation. If a Euclidean expression is written as the Laplace transform of a spectral function, then the Minkowski analog is given by the Fourier transform of that function. This makes the spectral function a very powerful tool, because it contains information on both the real and the imaginary time behavior. Unfortunately, the extraction of the spectral function out of a finite set of lattice data is a mathematically ill-posed problem, so some prior knowledge on the function is required. Therefore, an analytic study of the spectral function would be of great importance.

In all these proposed directions, effective field theories may lead to very elegant descriptions of the respective problem, enhancing our knowledge of the physical processes of the system and guiding theoretical approaches through the systematic use of fundamental or emergent symmetries.

Appendices

Appendix A

Vacuum

A.1 Symmetries of the Static System

A system of two static opposite color sources (in our case the system formed by a heavy quark in position $\boldsymbol{x}_1$ and a heavy antiquark in position $\boldsymbol{x}_2$) remains invariant under the following symmetry transformations: rotations $R(\alpha)$ by an angle $\alpha \in]-\pi, \pi]$ around the axis defined by the two sources, space inversion P in combination with charge conjugation C, reflections M across a plane containing the two sources, and combinations thereof. These transformations form the group $D_{\infty h}$, which is the symmetry group of a cylinder.

Since the static Hamiltonian is invariant under these transformations, we can use the quantum numbers of the representations of $D_{\infty h}$ to label its eigenstates. The conventional notation for the representations of $D_{\infty h}$ is Λ_η^σ. Λ is the rotational quantum number, it can take non-negative integer values $0, 1, 2, 3, \ldots$, which are traditionally represented by capital Greek letters $\Sigma, \Pi, \Delta, \Phi, \ldots$ corresponding to the atomic orbitals $s, p, d, f, \ldots$, respectively. The eigenvalue of CP is given as the index η. It can take the values $+1$ or -1, for which the labels g (*gerade*, i.e. even) and u (*ungerade*, i.e. odd) are used. The other index σ gives the sign under reflections as $+$ or $-$, however, it is only written explicitly for the Σ-states, because for $\Lambda \geq 1$ the states with opposite σ are degenerate with respect to the static energy.

Physically, this can be understood in the following way. The static system itself has no preferred orientation for the plane across which the reflections are defined. In fact, through a combination of rotation and reflection operations one can define a new reflection operation $M' = R(-\alpha)MR(\alpha)$, where the reflection plane is rotated by an angle α. The Σ-states are rotationally invariant, so M and M' give the same eigenvalue, but for $\Lambda \geq 1$ they do not. If in the simplest case α is chosen to be $\pi/2$, then M and M' have opposite eigenvalues. However, the static Hamiltonian $H^{(0)}$ does not depend on the choice of M or M', so consequently its eigenvalues, the static energies, cannot depend on σ unless $\Lambda = 0$.

Mathematically, this can be explained by looking at the irreducible representations of $D_{\infty h}$. We can write $D_{\infty h} = O(2) \otimes Z_2$, where Z_2 corresponds to the sign η under CP transformations. There are two different one-dimensional irreducible representations of $O(2)$ and countably infinite two-dimensional ones. The two one-dimensional representations both map the rotations to unity and differ by the sign under reflections. These correspond to $\Lambda = 0$ and positive or negative σ.

The two-dimensional representations are given by

$$R(\alpha) = \begin{pmatrix} \cos\Lambda\alpha & \sin\Lambda\alpha \\ -\sin\Lambda\alpha & \cos\Lambda\alpha \end{pmatrix}, \qquad M = \begin{pmatrix} 1 & 0 \\ 0 & -1 \end{pmatrix}. \tag{A.1}$$

The basis for these representations was chosen such that M is diagonal. It is possible to make a basis transformation that takes $M \to -M$ while $R(\alpha)$ remains the same. This means that the sign under reflections is irrelevant for the two-dimensional representations and σ cannot label different representations. Since the static energies depend only on the representation, they must be independent of σ for $\Lambda \geq 1$.

It is also possible to make a basis transformation that takes $R(\alpha) \to R(-\alpha)$ while M remains the same. This means that negative values for Λ do not correspond to a different representation but just to a different choice of basis, so by convention Λ is defined to be non-negative. Λ can only take integer values, because $R(2\pi)$ is required to be unity. Note that for $\Lambda = 0$ the two-dimensional representation is diagonal and reduces to the two one-dimensional representations.

In the context of the spectrum of the static Hamiltonian, the two-dimensionality of the irreducible representations of $D_{\infty h}$ means that any eigenstate of $H^{(0)}$ with $\Lambda \geq 1$ consists of two components, which correspond to $\sigma = \pm 1$ in the basis given above. For the calculations in this chapter it is advantageous to choose a different basis such that $R(\alpha)$ is diagonal:

$$R(\alpha) = \begin{pmatrix} e^{i\Lambda\alpha} & 0 \\ 0 & e^{-i\Lambda\alpha} \end{pmatrix}, \qquad M = \begin{pmatrix} 0 & \sigma_M^* \\ \sigma_M & 0 \end{pmatrix}. \tag{A.2}$$

There are many ways in which one can make such a basis transformation, and this manifests itself in the phase σ_M appearing in M, which is completely arbitrary. In this basis we can label the two components by $\lambda = \pm\Lambda$ such that they transform with $e^{i\lambda\alpha}$ under rotations. Because M now is offdiagonal, irrespective of the choice of σ_M, the two components are exchanged under reflections, i.e. $\lambda \xrightarrow{M} -\lambda$.

The advantage of this choice of basis is that, if we introduce the angular momentum operator $\boldsymbol{K}$ of the light degrees of freedom, then λ is the eigenvalue of $\hat{\boldsymbol{r}} \cdot \boldsymbol{K}$, where $\hat{\boldsymbol{r}}$ is the orientation of the quark-antiquark axis. Λ is then given by the absolute value of $\hat{\boldsymbol{r}} \cdot \boldsymbol{K}$, which is also true for $\Lambda = 0$. The operator $\boldsymbol{K}^2$ represents the fully three-dimensional rotations, i.e. the group $SO(3)$, so the static states are not eigenstates of $\boldsymbol{K}^2$ except for the limit of vanishing quark-antiquark distance, where this symmetry is restored.

A.2 RS Scheme

The RS octet potential is defined as follows [99, 105]

$$V_o^{RS}(\nu_f) = V_o - \delta V_o^{RS}(\nu_f), \tag{A.3}$$

with

$$V_o(r,\nu) = \left(\frac{C_A}{2} - C_F\right) \frac{\alpha_{V_o}(\nu)}{r}, \tag{A.4}$$

$$\delta V_o^{RS}(\nu_f) = \sum_{n=1}^{\infty} N_{V_o} \nu_f \left(\frac{\beta_0}{2\pi}\right)^n \alpha_{\mathrm{s}}^{n+1}(\nu_f) \sum_{k=0}^{\infty} c_k \frac{\Gamma(n+1+b-k)}{\Gamma(1+b-k)}. \tag{A.5}$$

The value of $N_{V_o} = 0.114001$ was computed in Ref. [99]. The value of α_{V_o} up to order α_s^3 is given by [158]

$$\alpha_{V_o}(\nu) = \alpha_{V_s}(\nu) - \left(\frac{3}{4} - \frac{\pi^2}{16}\right) C_A^2 \alpha_s^3(\nu) + \mathcal{O}\left(\alpha_s^4\right) , \tag{A.6}$$

where α_{V_s} is

$$\begin{aligned}\alpha_{V_s}(\nu) = \alpha_s(\nu) \Bigg(1 + (a_1 + 2\gamma_E\beta_0)\frac{\alpha_s(\nu)}{4\pi} \\ + \left[\gamma_E(4a_1 + \beta_0 + 2\beta_1) + \left(\frac{\pi^2}{3} + 4\gamma_E^2\right)\beta_0^2 + a_2\right]\frac{\alpha_s^2(\nu)}{16\pi^2}\Bigg) .\end{aligned} \tag{A.7}$$

The parameters b and the first three c_k appearing in δV_o^{RS} are given by

$$\begin{aligned} b &= \frac{\beta_1}{2\beta_0^2} , \qquad c_0 = 1 , \qquad c_1 = \frac{1}{4b\beta_0^3}\left(\frac{\beta_1^2}{\beta_0} - \beta_2\right) , \\ c_2 &= \frac{1}{32b(b-1)\beta_0^8}\left(\beta_1^4 + 4\beta_0^3\beta_1\beta_2 - 2\beta_0\beta_1^2\beta_2 + \beta_0^2(\beta_2^2 - 2\beta_1^3) - 2\beta_0^4\beta_3\right) . \end{aligned} \tag{A.8}$$

A.3 Derivation of the Radial Schrödinger Equation in Detail

The Laplace operator $\boldsymbol{\nabla}_r^2$ can be split into a radial and an angular part, such that

$$-\frac{\boldsymbol{\nabla}_r^2}{m} = -\frac{1}{m\,r^2}\left(\partial_r\, r^2\,\partial_r + \partial_x\left(1-x^2\right)\partial_x + \frac{1}{1-x^2}\partial_\varphi^2\right) , \tag{A.9}$$

with the variable $x = \cos\theta$. The angular part of this acts on both the wave function and the projection vector in (3.36), and since we know $\hat{\boldsymbol{n}}$ explicitly for the 1^{+-} gluelump, we can work out the action of the angular part of $\hat{\boldsymbol{n}}' \cdot (-\boldsymbol{\nabla}_r^2/m)\,\hat{\boldsymbol{n}}$ in the form of a matrix acting on the three-component wave function $\Psi^{(N)}$. Then we get

$$\left[-\frac{1}{mr^2}\partial_r\, r^2\,\partial_r + \frac{1}{mr^2}\left(\Delta_x + \Delta_\varphi\right) + V(r)\right]\Psi^{(N)}(\boldsymbol{r}) = \mathcal{E}_N\Psi^{(N)}(\boldsymbol{r}) , \tag{A.10}$$

where we have defined $V(r) = \mathrm{diag}\left(E_\Sigma^{(0)}(r), E_\Pi^{(0)}(r), E_\Pi^{(0)}(r)\right)$ and

$$\Delta_x = \begin{pmatrix} -\partial_x\left(1-x^2\right)\partial_x + 2 & -\sqrt{2}\partial_x\sqrt{1-x^2} & -\sqrt{2}\partial_x\sqrt{1-x^2} \\ \sqrt{2}\sqrt{1-x^2}\partial_x & -\partial_x\left(1-x^2\right)\partial_x + \dfrac{1}{1-x^2} & 0 \\ \sqrt{2}\sqrt{1-x^2}\partial_x & 0 & -\partial_x\left(1-x^2\right)\partial_x + \dfrac{1}{1-x^2} \end{pmatrix} , \tag{A.11}$$

$$\Delta_\varphi = \begin{pmatrix} -\dfrac{1}{1-x^2}\partial_\varphi^2 & \dfrac{\sqrt{2}}{\sqrt{1-x^2}}i\partial_\varphi & -\dfrac{\sqrt{2}}{\sqrt{1-x^2}}i\partial_\varphi \\ \dfrac{\sqrt{2}}{\sqrt{1-x^2}}i\partial_\varphi & -\dfrac{1}{1-x^2}\left(\partial_\varphi^2 - 2xi\partial_\varphi\right) & 0 \\ -\dfrac{\sqrt{2}}{\sqrt{1-x^2}}i\partial_\varphi & 0 & -\dfrac{1}{1-x^2}\left(\partial_\varphi^2 + 2xi\partial_\varphi\right) \end{pmatrix} . \tag{A.12}$$

The three columns correspond to $\hat{\boldsymbol{n}} = \hat{\boldsymbol{r}}, \hat{\boldsymbol{r}}^+, \hat{\boldsymbol{r}}^-$ and the three rows to $\hat{\boldsymbol{n}}' = \hat{\boldsymbol{r}}, \hat{\boldsymbol{r}}^+, \hat{\boldsymbol{r}}^-$ in that order.

This is a coupled Schrödinger equation, which differs from the standard example of the hydrogen atom by the appearance of different potentials for the different wave function components and the more complicated angular part. But like the hydrogen atom, it can be solved by a separation ansatz $\Psi^{(N)}(\boldsymbol{r}) = \psi_m(\varphi)\,\psi_l(x)\,\psi^{(N)}(r)$. The angular wave functions $\psi_m(\varphi)$ and $\psi_l(x)$ are matrices acting on the vector $\psi^{(N)}(r)$. They are eigenfunctions of their respective differential operators Δ_φ and Δ_x in the following sense:

$$\Delta_\varphi \psi_m(\varphi) = \psi_m(\varphi) M\,, \quad \text{and} \quad (\Delta_x + M)\psi_l(x) = \psi_l(x) L\,, \tag{A.13}$$

where M and L are matrices. If we also require $\psi_m(\varphi)$ and $\psi_l(x)$ to commute with the potential matrix $V(r)$, and in addition $\psi_m(\varphi)$ to commute with Δ_x, then the full Schrödinger equation reduces to a coupled radial Schrödinger equation for $\psi^{(N)}(r)$ with an effective potential $V_{eff}(r) = V(r) + L/mr^2$:

$$\begin{aligned}
0 &= \left[-\frac{1}{mr^2}\partial_r\, r^2\,\partial_r + \frac{1}{mr^2}\left(\Delta_x + \Delta_\varphi\right) + V(r) - \mathcal{E}_N\right]\psi_m(\varphi)\,\psi_l(x)\,\psi^{(N)}(r) \\
&= \psi_m(\varphi)\left[-\frac{1}{mr^2}\partial_r\, r^2\,\partial_r + \frac{1}{mr^2}\left(\Delta_x + M\right) + V(r) - \mathcal{E}_N\right]\psi_l(x)\,\psi^{(N)}(r) \qquad \text{(A.14)} \\
&= \psi_m(\varphi)\,\psi_l(x)\left[-\frac{1}{mr^2}\partial_r\, r^2\,\partial_r + \frac{1}{mr^2}L + V(r) - \mathcal{E}_N\right]\psi^{(N)}(r) \qquad \text{(A.15)} \\
&= \psi_m(\varphi)\,\psi_l(x)\left[-\frac{1}{mr^2}\partial_r\, r^2\,\partial_r + V_{eff}(r) - \mathcal{E}_N\right]\psi^{(N)}(r)\,. \qquad \text{(A.16)}
\end{aligned}$$

We will now show that such matrices do indeed exist. A solution for $\psi_m(\varphi)$ can immediately be found by making the ansatz $\psi_m(\varphi) = e^{im\varphi}\,\mathbb{1}$, where $\mathbb{1}$ is the unit matrix. With this we have

$$\Delta_\varphi \psi_m(\varphi) = \psi_m(\varphi)\begin{pmatrix} \frac{m^2}{1-x^2} & -\frac{\sqrt{2}m}{\sqrt{1-x^2}} & \frac{\sqrt{2}m}{\sqrt{1-x^2}} \\ -\frac{\sqrt{2}m}{\sqrt{1-x^2}} & \frac{m^2-2mx}{1-x^2} & 0 \\ \frac{\sqrt{2}m}{\sqrt{1-x^2}} & 0 & \frac{m^2+2mx}{1-x^2} \end{pmatrix}. \tag{A.17}$$

Also for the next wave function $\psi_l(x)$, a solution in the form of a diagonal matrix can be found, although now the diagonal entries differ from each other. The diagonal elements of $\Delta_x + M$ (without constant terms) all have the same form

$$-\,\partial_x\left(1-x^2\right)\partial_x + \frac{m^2 - 2\lambda m x + \lambda^2}{1-x^2}\,, \tag{A.18}$$

with $\lambda = 0, 1, -1$ for the first, second, and third entries, respectively. The eigenfunctions of this differential operator are generalizations of the associated Legendre polynomials, for $\lambda = 0$ they even coincide, and their derivation can be found in textbooks such as [75].

Including the factor $e^{im\varphi}$ and proper normalization, they are given by

$$v^\lambda_{l,\,m}(x,\varphi) = \frac{(-1)^{m+\lambda}}{2^l}\sqrt{\frac{2l+1}{4\pi}\frac{(l-m)!}{(l+m)!(l-\lambda)!(l+\lambda)!}}\,P^\lambda_{l,\,m}(x)e^{im\varphi}\,, \tag{A.19}$$

$$P^\lambda_{l,\,m}(x) = (1-x)^{\frac{m-\lambda}{2}}(1+x)^{\frac{m+\lambda}{2}}\partial_x^{l+m}(x-1)^{l+\lambda}(x+1)^{l-\lambda}\,. \tag{A.20}$$

The eigenvalue is $l(l+1)$, and just like for the spherical harmonics, solutions exist only for l a non-negative integer, $|m| \leq l$, and $|\lambda| \leq l$. They are normalized such that

$$\int d\Omega \, v^{\lambda\,*}_{l',m'}(x,\varphi) v^{\lambda}_{l,m}(x,\varphi) = \delta_{l'l}\delta_{m'm}\,, \tag{A.21}$$

and they also satisfy the orthogonality relations

$$\sum_{m=-l}^{l} v^{\lambda'\,*}_{l,m}(x,\varphi) v^{\lambda}_{l,m}(x,\varphi) = \frac{2l+1}{4\pi}\delta^{\lambda'\lambda}\,, \tag{A.22}$$

$$\sum_{\lambda=-l}^{l} v^{\lambda\,*}_{l,m'}(x,\varphi) v^{\lambda}_{l,m}(x,\varphi) = \frac{2l+1}{4\pi}\delta_{m'm}\,. \tag{A.23}$$

The easiest way to construct these functions is to use ladder operators for m and λ. These operators and their action on the $v^{\lambda}_{l,m}$ functions are given by

$$\left(\mp\sqrt{1-x^2}\,\partial_x - \frac{mx-\lambda}{\sqrt{1-x^2}}\right) e^{\pm i\varphi}\, v^{\lambda}_{l,m}(x,\varphi) = \sqrt{l(l+1)-m(m\pm 1)}\, v^{\lambda}_{l,m\pm 1}(x,\varphi)\,, \tag{A.24}$$

$$\left(\pm\sqrt{1-x^2}\,\partial_x - \frac{m-\lambda x}{\sqrt{1-x^2}}\right) v^{\lambda}_{l,m}(x,\varphi) = \sqrt{l(l+1)-\lambda(\lambda\pm 1)}\, v^{\lambda\pm 1}_{l,m}(x,\varphi)\,. \tag{A.25}$$

If we now look at the offdiagonal elements of $\Delta_x + M$, we see that they are given exactly by the ladder operators for λ. So for $\psi_m(\varphi)\,\psi_l(x) = \mathrm{diag}\left(v^0_{l,m}(x,\varphi), v^1_{l,m}(x,\varphi), v^{-1}_{l,m}(x,\varphi)\right)$ Eq. (A.13) becomes

$$(\Delta_x + \Delta_\varphi)\,\psi_m(\varphi)\,\psi_l(x) = \psi_m(\varphi)\,\psi_l(x) \begin{pmatrix} l(l+1)+2 & \sqrt{2l(l+1)} & -\sqrt{2l(l+1)} \\ \sqrt{2l(l+1)} & l(l+1) & 0 \\ -\sqrt{2l(l+1)} & 0 & l(l+1) \end{pmatrix}. \tag{A.26}$$

Before we write down the resulting radial Schrödinger equation, we will exploit the fact that we are free to multiply this expression by any constant matrix, which gives another solution to the angular differential equation with a modified but equivalent eigenvalue matrix L. If this constant matrix is $(1,2)$-block diagonal, then also $V(r)$ remains unchanged. In this way we will define a new orbital wave function matrix $\psi_{l,m}(x,\varphi)$ as

$$\psi_{l,m}(x,\varphi) = \frac{1}{\sqrt{2}} \begin{pmatrix} \sqrt{2}\, v^0_{l,m}(x,\varphi) & 0 & 0 \\ 0 & v^1_{l,m}(x,\varphi) & v^1_{l,m}(x,\varphi) \\ 0 & -v^{-1}_{l,m}(x,\varphi) & v^{-1}_{l,m}(x,\varphi) \end{pmatrix}. \tag{A.27}$$

The advantage of this redefinition is that now in the radial Schrödinger equation the effective potential is $(2,1)$-block diagonal.

$$\begin{aligned} &\left[-\frac{1}{mr^2}\partial_r\, r^2\,\partial_r + \frac{1}{mr^2}\,(\Delta_x+\Delta_\varphi) + V(r)\right]\psi_{l,m}(x,\varphi)\,\psi^{(N)}(r) \\ &= \psi_{l,m}(x,\varphi)\left[-\frac{1}{mr^2}\partial_r\, r^2\,\partial_r + \frac{1}{mr^2}\begin{pmatrix} l(l+1)+2 & 2\sqrt{l(l+1)} & 0 \\ 2\sqrt{l(l+1)} & l(l+1) & 0 \\ 0 & 0 & l(l+1) \end{pmatrix} + V(r)\right]\psi^{(N)}(r) \\ &= \mathcal{E}_N\,\psi_{l,m}(x,\varphi)\,\psi^{(N)}(r)\,. \end{aligned} \tag{A.28}$$

We see here explicitly the decoupling of the opposite parity states described in the main part of this chapter. One solution is of the form $\left(\psi_{\Sigma}^{(N)}(r), \psi_{-\Pi}^{(N)}(r), 0\right)^T$, the other $\left(0, 0, \psi_{+\Pi}^{(N)}(r)\right)^T$.

If those are multiplied by the orbital wave function matrix $\psi_{l,m}(x,\varphi)$, and spin and angular momentum indices are combined through Clebsch-Gordan coefficients, then we get the following expressions for the hybrid states:

$$\sum_{m_l,\, m_s} \int d^3r\, C^{m_l,\, m_s}_{j,\, m;\, l,\, s} \left[v^0_{l,\, m_l} \hat{\boldsymbol{r}}\, \psi_{\Sigma}^{(N)} + \frac{1}{\sqrt{2}} \left(v^1_{l,\, m_l} \hat{\boldsymbol{r}}^+ - v^{-1}_{l,\, m_l} \hat{\boldsymbol{r}}^- \right) \psi_{-\Pi}^{(N)} \right] \cdot \boldsymbol{G}^a_B\, O^{a\,\dagger}_{s,\, m_s} |0\rangle\,, \tag{A.29}$$

$$\sum_{m_l,\, m_s} \int d^3r\, C^{m_l,\, m_s}_{j,\, m;\, l,\, s} \frac{1}{\sqrt{2}} \left(v^1_{l,\, m_l} \hat{\boldsymbol{r}}^+ + v^{-1}_{l,\, m_l} \hat{\boldsymbol{r}}^- \right) \psi_{+\Pi}^{(N)} \cdot \boldsymbol{G}^a_B\, O^{a\,\dagger}_{s,\, m_s} |0\rangle\,. \tag{A.30}$$

The first gives the hybrid multiplets H_1, H_1', H_3, H_4, and H_6, the second gives H_2, H_2', H_5, and H_7, for different values of l, s, and N. Note that the different P and C eigenstate combinations come out correct.

We will now show that the hybrid states we have constructed are in fact eigenstates of the total angular momentum operator $\boldsymbol{L} = \boldsymbol{L}_{Q\bar{Q}} + \boldsymbol{K}$, where $\boldsymbol{K}$ is the angular momentum operator of the gluons and $\boldsymbol{L}_{Q\bar{Q}}$ the one of the relative coordinate of the quark-antiquark system. The center-of-mass coordinate $\boldsymbol{R}$ is fixed in the current approximation, which corresponds to a hybrid at rest, so there is no contribution to the total angular momentum from this coordinate.

The 1^{+-} gluelump operator is a (pseudo) vector, so $\boldsymbol{K}$ acts on it as

$$\left[K_i, G^a_{B\,j}\right] = i\, \epsilon_{ijk} G^a_{B\,k}\,. \tag{A.31}$$

The relative angular momentum operator in the octet sector is given by

$$\boldsymbol{L}_{Q\bar{Q}} = \int d^3r\, d^3R\, O^{a\,\dagger}(\boldsymbol{r}, \boldsymbol{R}) \begin{pmatrix} -i\sqrt{1-x^2}\sin\varphi\, \partial_x + \dfrac{ix\cos\varphi}{\sqrt{1-x^2}}\, \partial_\varphi \\ i\sqrt{1-x^2}\cos\varphi\, \partial_x + \dfrac{ix\sin\varphi}{\sqrt{1-x^2}}\, \partial_\varphi \\ -i\partial_\varphi \end{pmatrix} O^a(\boldsymbol{r}, \boldsymbol{R})\,. \tag{A.32}$$

Acting with $\boldsymbol{L}_{Q\bar{Q}}$ on the hybrid states is equivalent to acting with the differential operator between the two octet fields on the wave functions and projection vectors. In a slight abuse of notation, we will also use the symbol $\boldsymbol{L}_{Q\bar{Q}}$ for this differential operator. It should be clear which one is meant by whether it acts on a state or on a wave function.

It is straightforward to show that

$$-i\partial_\varphi\, \hat{\boldsymbol{n}}^T(x,\varphi) = \hat{\boldsymbol{n}}^T(x,\varphi) \begin{pmatrix} -i\partial_\varphi & -i & 0 \\ i & -i\partial_\varphi & 0 \\ 0 & 0 & -i\partial_\varphi \end{pmatrix} \quad \text{for all} \quad \hat{\boldsymbol{n}} = \hat{\boldsymbol{r}},\, \hat{\boldsymbol{r}}^{\pm}\,, \tag{A.33}$$

and by construction the orbital wave functions satisfy $-i\partial_\varphi\, v^\lambda_{l,\,m}(x,\varphi) = m\, v^\lambda_{l,\,m}(x,\varphi)$. So acting with L_3 on the hybrid states (before combining spin and angular momentum indices) gives

$$L_3 \int d^3r\, O^{a\,\dagger}(\boldsymbol{r}, \boldsymbol{R}) \sum_{n,\, i} \hat{n}_i(x,\varphi) G^a_{B\,i}(\boldsymbol{R}) \Psi_n^{(N)}(\boldsymbol{r}) |0\rangle$$

$$= \int d^3r\, O^{a\,\dagger}(\boldsymbol{r}, \boldsymbol{R}) \sum_{n,\, i,\, j} \hat{n}_i(x,\varphi) \left[\begin{pmatrix} -i\partial_\varphi & -i & 0 \\ i & -i\partial_\varphi & 0 \\ 0 & 0 & -i\partial_\varphi \end{pmatrix} + \begin{pmatrix} 0 & i & 0 \\ -i & 0 & 0 \\ 0 & 0 & 0 \end{pmatrix} \right]_{ij} G^a_{B\,j}(\boldsymbol{R}) \Psi_n^{(N)}(\boldsymbol{r}) |0\rangle$$

$$= \int d^3r\, O^{a\,\dagger}(\boldsymbol{r},\boldsymbol{R}) \sum_{n,\,i} \hat{n}_i(x,\varphi) G^a_{B\,i}(\boldsymbol{R}) \left(-i\partial_\varphi\, \Psi^{(N)}_n(\boldsymbol{r})\right) |0\rangle$$

$$= m \int d^3r\, O^{a\,\dagger}(\boldsymbol{r},\boldsymbol{R}) \sum_{n,\,i} \hat{n}_i(x,\varphi) G^a_{B\,i}(\boldsymbol{R}) \Psi^{(N)}_n(\boldsymbol{r}) |0\rangle\,. \tag{A.34}$$

For L^2 we can write

$$L^2 = L^2_{Q\bar{Q}} + 2\boldsymbol{L}_{Q\bar{Q}} \cdot \boldsymbol{K} + K^2\,. \tag{A.35}$$

We already know the effect of $L^2_{Q\bar{Q}}$ on $\hat{\boldsymbol{n}}$ from the previous section:

$$L^2_{Q\bar{Q}}\, \hat{\boldsymbol{n}} = \left(-\partial_x \left(1-x^2\right) \partial_x - \frac{1}{1-x^2}\partial^2_\varphi\right) \hat{\boldsymbol{n}} = \sum_{n'} \hat{\boldsymbol{n}}' \left(\Delta_x + \Delta_\varphi\right)_{n'n}\,. \tag{A.36}$$

Note that here and in the following we use the indices n and n' to denote matrices that are defined in the basis of the different static states, Σ^-_u and $\Pi^\pm_u$, which correspond to the projection vectors $\hat{\boldsymbol{r}}$ and $\hat{\boldsymbol{r}}^\pm$, respectively. In contrast, the indices i and j will always be used for the components of vectors and matrices defined in three-dimensional position space.

The last term in Eq. (A.35) K^2 just gives a constant factor $k(k+1)$, which is equal to 2 in our case. So there only remains to determine the effect of $\boldsymbol{L}_{Q\bar{Q}} \cdot \boldsymbol{K}$ on $\hat{\boldsymbol{n}}$. We can write it as a matrix of differential operators, where the matrix nature comes from the action of the $\boldsymbol{K}$ part on the gluelump. An explicit calculation gives

$$\begin{aligned}
\boldsymbol{L}_{Q\bar{Q}} \cdot \boldsymbol{K}\, \hat{n}_i =& \sum_j \begin{pmatrix} 0 & 0 & -\sqrt{1-x^2}\cos\varphi\partial_x \\ 0 & 0 & -\sqrt{1-x^2}\sin\varphi\partial_x \\ \sqrt{1-x^2}\cos\varphi\partial_x & \sqrt{1-x^2}\sin\varphi\partial_x & 0 \end{pmatrix}_{ij} \hat{n}_j \\
&+ \sum_j \begin{pmatrix} 0 & -\partial_\varphi & -\dfrac{x\sin\varphi}{\sqrt{1-x^2}}\partial_\varphi \\ \partial_\varphi & 0 & \dfrac{x\cos\varphi}{\sqrt{1-x^2}}\partial_\varphi \\ \dfrac{x\sin\varphi}{\sqrt{1-x^2}}\partial_\varphi & -\dfrac{x\cos\varphi}{\sqrt{1-x^2}}\partial_\varphi & 0 \end{pmatrix}_{ij} \hat{n}_j \\
=& \sum_{n'} \hat{n}'_i \begin{pmatrix} -2 & \dfrac{1}{\sqrt{2}}\partial_x\sqrt{1-x^2} & \dfrac{1}{\sqrt{2}}\partial_x\sqrt{1-x^2} \\ -\dfrac{1}{\sqrt{2}}\sqrt{1-x^2}\partial_x & -1 & 0 \\ -\dfrac{1}{\sqrt{2}}\sqrt{1-x^2}\partial_x & 0 & -1 \end{pmatrix}_{n'n} \\
&+ \sum_{n'} \hat{n}'_i \begin{pmatrix} 0 & -\dfrac{i}{\sqrt{2}}\dfrac{1}{\sqrt{1-x^2}}\partial_\varphi & \dfrac{i}{\sqrt{2}}\dfrac{1}{\sqrt{1-x^2}}\partial_\varphi \\ -\dfrac{i}{\sqrt{2}}\dfrac{1}{\sqrt{1-x^2}}\partial_\varphi & 0 & 0 \\ \dfrac{i}{\sqrt{2}}\dfrac{1}{\sqrt{1-x^2}}\partial_\varphi & 0 & 0 \end{pmatrix}_{n'n}\,.
\end{aligned} \tag{A.37}$$

We now see that in $L^2_{Q\bar{Q}} + 2\boldsymbol{L}_{Q\bar{Q}} \cdot \boldsymbol{K} + K^2$ all offdiagonal elements of Δ_x and Δ_φ cancel,

as well as all constant terms in the diagonal elements. What remains is

$$\begin{aligned}
&\left(L^2_{Q\bar{Q}} + 2\boldsymbol{L}_{Q\bar{Q}} \cdot \boldsymbol{K} + K^2\right) \sum_n \hat{\boldsymbol{n}}(x,\varphi)\Psi^{(N)}_n(\boldsymbol{r}) \\
&= \sum_{n,\,n'} \hat{\boldsymbol{n}}'(x,\varphi) \begin{pmatrix} L^2_{Q\bar{Q}} & 0 & 0 \\ 0 & L^2_{Q\bar{Q}} + \dfrac{2ix\partial_\varphi + 1}{1-x^2} & 0 \\ 0 & 0 & L^2_{Q\bar{Q}} + \dfrac{-2ix\partial_\varphi + 1}{1-x^2} \end{pmatrix}_{n'n} \Psi^{(N)}_n(\boldsymbol{r}) \\
&= l(l+1) \sum_n \hat{\boldsymbol{n}}(x,\varphi)\Psi^{(N)}_n(\boldsymbol{r})\,. \qquad \text{(A.38)}
\end{aligned}$$

The last equality follows, because the diagonal entries are exactly the defining differential equations for the orbital wave functions.

A.4 Numerical Solution of the Schrödinger Equations

The Schrödinger equations in (3.51) and (3.52) can be solved numerically (see e.g. [159, 160]). In the uncoupled case the nodal theorem can be used to determine the energy eigenvalues. Any value $\mathcal{E}$ one inserts in these equations in the place of $\mathcal{E}_N$ defines a linear differential equation of second order. These have in general two linearly independent solutions. Such a solution can only be interpreted as a wave function, if it is normalizable.

Two independent solutions can be distinguished by their behavior at the origin,

$$\psi^{(N)}_{+\Pi}(r) \propto r^l + \mathcal{O}(r^{l+1}) \qquad \text{or} \qquad \psi^{(N)}_{+\Pi}(r) \propto r^{-l-1} + \mathcal{O}\left(r^{-l}\right)\,. \qquad \text{(A.39)}$$

The second expression is singular at the origin and therefore not normalizable. The first expression defines initial conditions for the wave function and its derivative, such that for any value of $\mathcal{E}$ the differential equation (3.52) has a unique solution. This solution generally diverges for large r, only for particular values of $\mathcal{E} = \mathcal{E}_N$ does it approach zero and is normalizable. These are the desired wave function solutions of the Schrödinger equation. The order N of the eigenvalue is equal to the number of zeros in the wave function. For the special case of $l = 0$ the initial conditions for $\psi^{(N)}_{\Sigma}$ are the same as for $\psi^{(N)}_{+\Pi}$ with $l = 1$.

A similar approach can be used to determine the energy eigenvalues of the coupled Schrödinger equation (3.51) for $l \geq 1$. A system of two linearly coupled differential equations of second order has in general four linearly independent solutions, of which now two are singular at the origin. The remaining two can also be distinguished by their behavior at the origin, which is given by

$$\begin{pmatrix} \psi^{(N1)}_{\Sigma}(r) \\ \psi^{(N1)}_{-\Pi}(r) \end{pmatrix} \propto \begin{pmatrix} \sqrt{l}\, r^{l-1} \\ -\sqrt{l+1}\, r^{l-1} \end{pmatrix} + \mathcal{O}\left(r^l\right)\,, \qquad \text{(A.40)}$$

or

$$\begin{pmatrix} \psi^{(N2)}_{\Sigma}(r) \\ \psi^{(N2)}_{-\Pi}(r) \end{pmatrix} \propto \begin{pmatrix} \sqrt{l+1}\, r^{l+1} \\ \sqrt{l}\, r^{l+1} \end{pmatrix} + \mathcal{O}\left(r^{l+2}\right)\,. \qquad \text{(A.41)}$$

Again, the solutions to the two coupled differential equations with these initial conditions diverge for general $\mathcal{E}$ at large r. For particular values of $\mathcal{E} = \mathcal{E}_N$ there exists one linear

combination

$$\begin{pmatrix} \psi_{\Sigma}^{(N)}(r) \\ \psi_{-\Pi}^{(N)}(r) \end{pmatrix} = \begin{pmatrix} \psi_{\Sigma}^{(N1)}(r) \\ \psi_{-\Pi}^{(N1)}(r) \end{pmatrix} + \nu \begin{pmatrix} \psi_{\Sigma}^{(N2)}(r) \\ \psi_{-\Pi}^{(N2)}(r) \end{pmatrix} , \tag{A.42}$$

which approaches zero for large r, while any other combination with a different ν will still diverge. This gives the desired wave functions.

So now one has to tune two independent parameters in order to find the solutions, $\mathcal{E}$ and ν. Fortunately, the two can be determined separately. Instead of counting zeros of the wave function in order to find the eigenvalues $\mathcal{E}_N$ like in the uncoupled case, one now has to look at the determinant of the two independent solutions [161]

$$U(r) = \det \begin{pmatrix} \psi_{\Sigma}^{(N1)}(r) & \psi_{\Sigma}^{(N2)}(r) \\ \psi_{-\Pi}^{(N1)}(r) & \psi_{-\Pi}^{(N2)}(r) \end{pmatrix} . \tag{A.43}$$

This function diverges in the large r limit for general $\mathcal{E}$ but converges for $\mathcal{E} = \mathcal{E}_N$ and then has exactly N zeros. In this way $\mathcal{E}_N$ can be determined without knowledge of ν.

Then in order to obtain the wave functions $\psi_{\Sigma}^{(N)}(r)$ and $\psi_{-\Pi}^{(N)}(r)$ one can determine ν through

$$\nu = -\lim_{r\to\infty} \frac{\psi_{\Sigma}^{(N1)}(r)}{\psi_{\Sigma}^{(N2)}(r)} = -\lim_{r\to\infty} \frac{\psi_{-\Pi}^{(N1)}(r)}{\psi_{-\Pi}^{(N2)}(r)} , \tag{A.44}$$

after $\mathcal{E}$ has been fixed to the eigenvalue $\mathcal{E}_N$ from the previous step. Alternatively, $(1, \nu)^T$ is the eigenvector of the wave function matrix (i.e. the matrix of which $U(r)$ is the determinant) at $r \to \infty$ with eigenvalue zero.

These properties of the solutions of the radial Schrödinger equations can be exploited in an algorithm to numerically find the eigenvalues and wave functions. The details of this will be described elsewhere [101].

Appendix B

Finite Temperature

B.1 Gluon Propagators

B.1.1 Feynman Gauge

Feynman gauge is obtained by adding the gauge fixing term $\left(\partial_\mu A^a_\mu\right)^2/2$ to the Lagrangian, as well as the ghost Lagrangian $\left(\partial_\mu \bar{c}^a\right) D^{ab}_\mu c^b$. Then the free propagators for gluons D_0 and ghosts G_0 are given by

$$D_0 = \frac{\delta_{\mu\nu}}{k_0^2 + k^2} \quad \text{and} \quad G_0 = \frac{1}{k_0^2 + k^2}\,. \tag{B.1}$$

We will not explicitly display color indices, because they only appear in Kronecker deltas.

For the resummed gluon propagators we need to sum over all one-particle reducible diagrams, i.e., over all bubble insertions in a propagator, where the bubbles define the self-energy tensor $-\Pi_{\mu\nu}$. We can parametrize the self-energy tensor in the following way

$$\Pi = \begin{pmatrix} \Pi_{00} & \Pi_A k_0 k_j \\ \Pi_A k_i k_0 & \Pi_B \delta_{ij} + \Pi_C k_i k_j \end{pmatrix}, \tag{B.2}$$

which comprises all tensor structures allowed by rotational symmetry. Even though Feynman gauge is designed to be fully covariant under Lorentz transformations, the existence of the medium explicitly breaks the full Lorentz symmetry down to the rotational symmetry in the rest frame of the medium, so that the temporal and mixed components of the self-energy tensor Π_{00} and $\Pi_{i0} = \Pi_{0i}$ may have different coefficients than the corresponding tensor structures in the spatial components Π_{ij}. In other words, $\Pi_{00} \neq \Pi_B + \Pi_C k_0^2$ and $\Pi_A \neq \Pi_C$.

The sum over one-particle reducible diagrams constitutes a geometric series. So the resummed propagators are given by

$$D = D_0 \sum_{n=0}^{\infty} (-\Pi D_0)^n = D_0 (1 + \Pi D_0)^{-1} = \left(D_0^{-1} + \Pi\right)^{-1}, \tag{B.3}$$

and similarly for the ghosts. By inverting this matrix we get

$$D_{00} = \frac{k_0^2 + k^2 + \Pi_B + \Pi_C k^2}{\left(k_0^2 + k^2 + \Pi_{00}\right)\left(k_0^2 + k^2 + \Pi_B + \Pi_C k^2\right) - \Pi_A^2 k_0^2 k^2}, \tag{B.4}$$

$$D_{i0} = \frac{-\Pi_A k_i k_0}{\left(k_0^2 + k^2 + \Pi_{00}\right)\left(k_0^2 + k^2 + \Pi_B + \Pi_C k^2\right) - \Pi_A^2 k_0^2 k^2}, \tag{B.5}$$

$$D_{ij} = \frac{1}{k_0^2 + k^2 + \Pi_B} \left(\delta_{ij} - \frac{k_i k_j}{k^2} \right) + \frac{k_0^2 + k^2 + \Pi_{00}}{(k_0^2 + k^2 + \Pi_{00})(k_0^2 + k^2 + \Pi_B + \Pi_C k^2) - \Pi_A^2 k_0^2 k^2} \frac{k_i k_j}{k^2} \,. \tag{B.6}$$

We can rewrite these expressions in terms of the self-energy tensor as

$$D_{00} = \frac{1}{k_0^2 + k^2 + \Pi} \quad \text{and} \quad D_{ij} = \frac{1}{k_0^2 + k^2 + \Sigma_1} \left(\delta_{ij} - \frac{k_i k_j}{k^2} \right) + \frac{1}{k_0^2 + k^2 + \Sigma_2} \frac{k_i k_j}{k^2} \,, \tag{B.7}$$

where

$$\Pi = \Pi_{00} - \frac{\Pi_A^2 k_0^2 k^2}{k_0^2 + k^2 + \Pi_B + \Pi_C k^2} = \Pi_{00} - \frac{\Pi_{0i}\Pi_{i0}}{k_0^2 + k^2 + \Pi_{ij} k_i k_j / k^2} \,, \tag{B.8}$$

$$\Sigma_1 = \Pi_B = \frac{1}{d-1} \left(\Pi_{ii} - \frac{\Pi_{ij} k_i k_j}{k^2} \right) \,, \tag{B.9}$$

$$\Sigma_2 = \Pi_B + \Pi_C k^2 - \frac{\Pi_A^2 k_0^2 k^2}{k_0^2 + k^2 + \Pi_{00}} = \frac{\Pi_{ij} k_i k_j}{k^2} - \frac{\Pi_{0i}\Pi_{i0}}{k_0^2 + k^2 + \Pi_{00}} \,, \tag{B.10}$$

and

$$D_{0l} = \frac{-\Pi_{0l}}{(k_0^2 + k^2 + \Pi_{00})(k_0^2 + k^2 + \Pi_{ij} k_i k_j / k^2) - \Pi_{0i}\Pi_{i0}} \,. \tag{B.11}$$

We see that, although the free Feynman propagator is diagonal, the resummed propagator is not.

The free ghost propagator G_0 as well as the ghost self-energy Γ are scalar functions, so the resummation of the geometric series for the full ghost propagator G is trivial:

$$G = \left(G_0^{-1} + \Gamma \right)^{-1} = \frac{1}{k_0^2 + k^2 + \Gamma} \,. \tag{B.12}$$

B.1.2 Static Gauge

Static gauge [41] satisfies the gauge condition $\partial_0 A_0 = 0$, but this condition alone does not give an invertible propagator, so we need to modify it in order to fix the gauge also for the spatial gluons. This can be done by adding the gauge fixing term $\left(\partial_0 A_0 + \sqrt{\alpha/\xi}\, \boldsymbol{\nabla} \cdot \boldsymbol{A}^a \right)^2 / 2\alpha$ and taking the limit $\alpha \to 0$, which gives back the original gauge condition. This limit would diverge in the Lagrangian, but leads to a finite propagator. The freedom in how to fix the gauge for the spatial gluons is reflected in the residual gauge fixing parameter ξ. The gauge condition on the spatial gluons is lifted for $\xi \to \infty$ and accordingly the propagator diverges in this limit.

The inverse of the free propagator can be read from the Lagrangian:

$$D_0^{-1} = \begin{pmatrix} \dfrac{k_0^2}{\alpha} + k^2 & -\left(1 - \dfrac{1}{\sqrt{\alpha\xi}} \right) k_0 k_j \\ -\left(1 - \dfrac{1}{\sqrt{\alpha\xi}} \right) k_i k_0 & \left(k_0^2 + k^2 \right) \delta_{ij} - \left(1 - \dfrac{1}{\xi} \right) k_i k_j \end{pmatrix} \,, \tag{B.13}$$

which can be inverted to

$$D_0 = \begin{pmatrix} \dfrac{\alpha\left(\xi k_0^2 + k^2\right)}{\left(\sqrt{\xi} k_0^2 + \sqrt{\alpha} k^2\right)^2} & \dfrac{\left(\alpha\xi - \sqrt{\alpha\xi}\right) k_0 k_j}{\left(\sqrt{\xi} k_0^2 + \sqrt{\alpha} k^2\right)^2} \\ \dfrac{\left(\alpha\xi - \sqrt{\alpha\xi}\right) k_i k_0}{\left(\sqrt{\xi} k_0^2 + \sqrt{\alpha} k^2\right)^2} & \dfrac{1}{k_0^2 + k^2} \left(\delta_{ij} - \dfrac{k_i k_j}{k^2} \right) + \dfrac{\xi\left(k_0^2 + \alpha k^2\right)}{\left(\sqrt{\xi} k_0^2 + \sqrt{\alpha} k^2\right)^2} \dfrac{k_i k_j}{k^2} \end{pmatrix}$$

$$\overset{\alpha\to 0}{=} \begin{pmatrix} \dfrac{\delta_{k_0}}{k^2} & 0 \\ 0 & \dfrac{1-\delta_{k_0}}{k_0^2+k^2}\left(\delta_{ij}-\dfrac{k_i k_j}{k_0^2}\right)+\dfrac{\delta_{k_0}}{k^2}\left(\delta_{ij}-(1-\xi)\dfrac{k_i k_j}{k^2}\right) \end{pmatrix}, \tag{B.14}$$

where by δ_{k_0} we mean for $k_0 = 2\pi T n$ with $n \in \mathbb{Z}$ that $\delta_{k_0} = \delta_{0n}$, i.e., selecting only the zero mode in the Matsubara sum. We see that the free propagator explicitly distinguishes between zero and non-zero modes. In particular, the 00 component of the propagator contains only the zero mode, which means that in position space it does not depend on the imaginary time coordinate, as required by the gauge condition.

The ghost Lagrangian is given by

$$\mathcal{L}_{gh} = \frac{1}{\sqrt{\alpha}} \left(\partial_0 \bar{c}^a\right) D_0^{ab} c^b + \frac{1}{\sqrt{\xi}} \left(\boldsymbol{\nabla} \bar{c}^a\right) \cdot \boldsymbol{D}^{ab} c^b \,, \tag{B.15}$$

from which it follows that the free ghost propagator is

$$G_0 = \frac{\sqrt{\alpha\xi}}{\sqrt{\xi} k_0^2 + \sqrt{\alpha} k^2} \overset{\alpha\to 0}{=} \frac{\sqrt{\xi}\delta_{k_0}}{k^2} \,. \tag{B.16}$$

There is a ghost vertex with a temporal gluon that is proportional to $1/\sqrt{\alpha}$, so the $\alpha \to 0$ limit may potentially be problematic in this interaction. However, this vertex is also proportional to the Matsubara frequency k_0 of the outgoing ghost propagator, which means that only non-zero modes can participate in this interaction. The number of ghost propagators and ghost-gluon vertices is always the same in any loop diagram, so in the most singular diagrams, where all vertices are with a temporal gluon, the powers of $\sqrt{\alpha}$ cancel exactly between the vertices and the numerators of the propagators. Then the $\alpha \to 0$ limit can be taken without problems and all propagators are given by $1/k_0^2$, which is not singular because the zero-modes do not contribute. This makes all loop integrations scaleless and therefore vanish. If there are some vertices with spatial gluons, then there are more powers of $\sqrt{\alpha}$ in the numerator than in the denominator and the diagram vanishes trivially in the $\alpha \to 0$ limit.

So we see that the ghosts completely decouple from the temporal gluons. For the interactions with the spatial gluons the $\alpha \to 0$ limit is unproblematic. There is a factor of $1/\sqrt{\xi}$ at each vertex, which exactly cancels the $\sqrt{\xi}$ factor in the ghost propagators. So we can in fact simplify the ghost sector considerably, because as we have just shown the non-zero Matsubara frequencies, the parameter ξ, or interactions with temporal gluons are irrelevant. Therefore the modified ghost Lagrangian and free propagator

$$\mathcal{L}_{gh} = \left(\boldsymbol{\nabla} \bar{c}^a\right) \cdot \boldsymbol{D}^{ab} c^b \qquad \text{and} \qquad G_0 = \frac{\delta_{k_0}}{k^2} \tag{B.17}$$

with static (i.e., independent of the imaginary time coordinate) ghost fields give exactly the same contributions as the more complicated Lagrangian given above.

For the resummed propagator we can use the same parametrization of the self-energy tensor as in Feynman gauge. Then we get

$$D_{00} = \frac{k_0^2 + k^2/\xi + \Pi_B + \Pi_C k^2}{\left(k_0^2/\alpha + k^2 + \Pi_{00}\right)\left(k_0^2 + k^2/\xi + \Pi_B + \Pi_C k^2\right) - \left(1 - 1/\sqrt{\alpha\xi} - \Pi_A\right)^2 k_0^2 k^2} \overset{\alpha\to 0}{=} \frac{\delta_{k_0}}{k^2 + \Pi_{00}} \,, \tag{B.18}$$

$$D_{i0} = \frac{\left(1 - 1/\sqrt{\alpha\xi} - \Pi_A\right) k_i k_0}{\left(k_0^2/\alpha + k^2 + \Pi_{00}\right)\left(k_0^2 + k^2/\xi + \Pi_B + \Pi_C k^2\right) - \left(1 - 1/\sqrt{\alpha\xi} - \Pi_A\right)^2 k_0^2 k^2} \overset{\alpha\to 0}{=} 0\,, \tag{B.19}$$

$$\begin{aligned} D_{ij} &= \frac{1}{k_0^2 + k^2 + \Pi_B}\left(\delta_{ij} - \frac{k_i k_j}{k^2}\right) \\ &\quad + \frac{k_0^2/\alpha + k^2 + \Pi_{00}}{\left(k_0^2/\alpha + k^2 + \Pi_{00}\right)\left(k_0^2 + k^2/\xi + \Pi_B + \Pi_C k^2\right) - \left(1 - 1/\sqrt{\alpha\xi} - \Pi_A\right)^2 k_0^2 k^2}\frac{k_i k_j}{k^2} \\ &\overset{\alpha\to 0}{=} \frac{1 - \delta_{k_0}}{k_0^2 + k^2 + \Pi_B}\left(\delta_{ij} + \frac{\left(1 - \Pi_C\right) k_i k_j}{k_0^2 + \Pi_B + \Pi_C k^2}\right) + \frac{\delta_{k_0}}{k^2 + \Pi_B}\left(\delta_{ij} - \frac{\left(1 - \xi + \xi\Pi_C\right) k_i k_j}{k^2 + \xi\left(\Pi_B + \Pi_C k^2\right)}\right). \end{aligned} \tag{B.20}$$

Or in analogy to the functions Π, Σ_1, and Σ_2 that we defined in Feynman gauge we can also write

$$D_{00} = \frac{\delta_{k_0}}{k^2 + \Pi}\,, \tag{B.21}$$

$$D_{i0} = D_{0j} = 0\,, \tag{B.22}$$

$$D_{ij} = \frac{1 - \delta_{k_0}}{k_0^2 + k^2 + \Sigma_1}\left(\delta_{ij} - \frac{k_i k_j}{k^2}\right) + \frac{1 - \delta_{k_0}}{k_0^2 + \Sigma_2}\frac{k_i k_j}{k^2} + \frac{\delta_{k_0}}{k^2 + \Sigma_1}\left(\delta_{ij} - \frac{k_i k_j}{k^2}\right) + \frac{\xi\delta_{k_0}}{k^2 + \xi\Sigma_2}\frac{k_i k_j}{k^2}\,, \tag{B.23}$$

where now

$$\Pi = \Pi_{00}\,, \quad \Sigma_1 = \Pi_B = \frac{1}{(d-1)k^2}\left(k^2\Pi_{ii} - \Pi_{ij}k_i k_j\right)\,, \quad \text{and} \quad \Sigma_2 = \Pi_B + \Pi_C k^2 = \frac{\Pi_{ij}k_i k_j}{k^2}\,. \tag{B.24}$$

The resummed ghost propagator follows trivially from the modified ghost Lagrangian.

$$G = \frac{\delta_{k_0}}{k^2 + \Gamma}\,. \tag{B.25}$$

For $\xi = 1$ the static part of the gluon propagator (i.e., $k_0 = 0$) has the same form as in Feynman gauge, which is why this choice is also called Feynman static gauge. The self-energy functions still differ between the two gauges. For $\xi = 0$ the static part of the propagator has the same form as in Coulomb gauge, so this choice could be called Coulomb static gauge.

B.1.3 Coulomb Gauge

Coulomb gauge is defined by the gauge condition $\boldsymbol{\nabla}\cdot\boldsymbol{A}^a = 0$. It can be implemented by adding the gauge fixing term $\left(\boldsymbol{\nabla}\cdot\boldsymbol{A}^a\right)^2/2\xi$ to the Lagrangian as well as the ghost Lagrangian $(\boldsymbol{\nabla}\bar{c}^a)\cdot\boldsymbol{D}^{ab}c^b$ with the limit $\xi \to 0$. If we compare this to the gauge fixing term in static gauge, we see that Coulomb gauge can also be obtained from there by first taking the limit $\alpha \to \infty$ and then $\xi \to 0$, so we can reuse all results from the previous section.

The free propagator is then given by

$$D_0 \overset{\xi\to 0}{=} \begin{pmatrix} \dfrac{1}{k^2} & 0 \\ 0 & \dfrac{1}{k_0^2 + k^2}\left(\delta_{ij} - \dfrac{k_i k_j}{k^2}\right) \end{pmatrix}, \tag{B.26}$$

and the resummed propagator by

$$D \overset{\xi\to 0}{=} \begin{pmatrix} \dfrac{1}{k^2+\Pi} & 0 \\ 0 & \dfrac{1}{k_0^2+k^2+\Sigma_1}\left(\delta_{ij}-\dfrac{k_i k_j}{k^2}\right) \end{pmatrix}, \tag{B.27}$$

where the self-energy functions Π and Σ_1 are defined as in static gauge.

The temporal component of the propagator is the same as in static gauge, except that in Coulomb gauge also the non-zero Matsubara frequencies are allowed (although they do not appear explicitly in the free propagator). The spatial part of the propagator is transversely polarized with respect to $\boldsymbol{k}$ and the mixed temporal and spatial components vanish, such that the gauge condition is explicitly satisfied as $k_i D_{i\nu} = 0$. This relation holds for both the free and the resummed propagator, and only the coefficient Σ_1 of the transversely polarized part of the self-energy tensor remains in the propagator after the resummation.

After a redefinition of the ghost fields $(\bar{c}, c) \to \xi^{1/4}(\bar{c}, c)$, the limit $\xi \to 0$ eliminates the first term in (B.15) and the free and resummed propagators are given by

$$G_0 = \frac{1}{k^2} \quad \text{and} \quad G = \frac{1}{k^2+\Gamma}\,. \tag{B.28}$$

The ghosts only couple to spatial gluons like in static gauge.

Quantization in Coulomb gauge generates the so-called Schwinger-Christ-Lee term [162, 163]. This term is an α_{s}^2 suppressed term that involves a nonlocal interaction with transverse gluons. It is beyond the accuracy of the present work.

B.1.4 Phase-Space Coulomb Gauge

There exists an alternative formulation of Coulomb gauge QCD that is defined in the so-called phase-space formalism [164], which we will adapt here to the Euclidean space of the imaginary time formalism. An auxiliary field $\boldsymbol{E}$ is introduced in the action S:

$$\begin{aligned} e^{-S} &= \exp\left[-\int_0^{1/T} d\tau \int d^3x \left(\frac{1}{4}F_{ij}^a F_{ij}^a + \frac{1}{2}F_{0i}^a F_{0i}^a\right)\right] \\ &= \mathcal{N}^{-1}\int \mathcal{D}E_i \exp\left[-\int_0^{1/T} d\tau \int d^3x \left(\frac{1}{4}F_{ij}^a F_{ij}^a + iE_i^a F_{0i}^a + \frac{1}{2}E_i^a E_i^a\right)\right]. \end{aligned} \tag{B.29}$$

This step can be interpreted such that now the chromoelectric field is treated as a dynamical variable. This interpretation originates from the equations of motion for the $\boldsymbol{E}$-field, which are $E_i^a = -iF_{0i}^a$ (the factor i is an effect of the imaginary time formalism, in Minkowski space it is absent). So we will call $\boldsymbol{E}$ the electric field for the rest of this section. One can easily return to the original action, up to some irrelevant constant $\mathcal{N}$, by explicitly carrying out the path integral over the electric field, which is possible because it only appears in quadratic terms in the exponential.

With this new action we can calculate as if there was a seven-component gluon field A_α, where $\alpha = 0$ corresponds to A_0, $\alpha = 1, 2, 3$ to $\boldsymbol{A}$, and $\alpha = 4, 5, 6$ to $\boldsymbol{E}$. The free propagator $(D_0)_{\alpha\beta}$ will be the 7×7 matrix given through the quadratic terms of this gluon field as

$A_\alpha \left(D_0^{-1}\right)_{\alpha\beta} A_\beta$. In order to distinguish between the spatial gluon and electric field components in this unified description, we will use the propagator indices i, j and m, n exclusively for $\alpha, \beta = 1, 2, 3$ and $\alpha, \beta = 4, 5, 6$ respectively.

In order to fix the gauge we again introduce the terms $\left(\boldsymbol{\nabla} \cdot \boldsymbol{A}^a\right)^2 / 2\xi$ and $\left(\boldsymbol{\nabla} \bar{c}^a\right) \cdot \boldsymbol{D}^{ab} c^b$ into the Lagrangian. The ghost sector remains unchanged compared to standard Coulomb gauge, so we will only discuss the gluonic sector. Going from position to momentum space in the free action,

$$\begin{aligned} S_0 &= \int_0^{1/T} d\tau \int d^3x \left[\frac{1}{2} \left(\partial_i A_j^a\right) \left(\partial_i A_j^a\right) - \frac{1}{2} \left(\partial_i A_j^a\right) \left(\partial_j A_i^a\right) + \frac{1}{2\xi} \left(\partial_i A_i^a\right) \left(\partial_j A_j^a\right) \right. \\ &\qquad \left. + i E_i^a \partial_0 A_i^a - i E_i^a \partial_i A_0^a + \frac{1}{2} E_i^a E_i^a \right] \\ &= \sum\!\!\!\!\!\!\int_K \frac{1}{2} \left[A_i^a(-K) \left(k^2 \delta_{ij} - \frac{\xi - 1}{\xi} k_i k_j \right) A_j^a(K) - E_i^a(-K) k_0 A_i^a(K) + A_i^a(-K) k_0 E_i^a(K) \right. \\ &\qquad \left. + E_i^a(-K) k_i A_0^a(K) - A_0^a(-K) k_i E_i^a(K) + \frac{1}{2} E_i(-K)^a E_i^a(K) \right] \\ &= \sum\!\!\!\!\!\!\int_K \left[\frac{1}{2} A_\alpha^a(-K) \left(D_0^{-1}\right)_{\alpha\beta} A_\beta^a(K) \right] , \end{aligned} \tag{B.30}$$

we get the inverse of the propagator as

$$D_0^{-1} = \begin{pmatrix} 0 & 0 & -k_n \\ 0 & k^2\, \delta_{ij} - (1 - 1/\xi)\, k_i k_j & k_0\, \delta_{in} \\ k_m & -k_0\, \delta_{mj} & \delta_{mn} \end{pmatrix} , \tag{B.31}$$

where we have written the 7×7 matrix in terms of $(1, 3, 3) \times (1, 3, 3)$ blocks. Inverting this and taking the $\xi \to 0$ limit, we get the free propagator:

$$D_0 = \begin{pmatrix} \dfrac{1}{k^2} & 0 & \dfrac{k_n}{k^2} \\ 0 & \dfrac{1}{k_0^2 + k^2} \left(\delta_{ij} - \dfrac{k_i k_j}{k^2} \right) & -\dfrac{k_0}{k_0^2 + k^2} \left(\delta_{in} - \dfrac{k_i k_n}{k^2} \right) \\ -\dfrac{k_m}{k^2} & \dfrac{k_0}{k_0^2 + k^2} \left(\delta_{mj} - \dfrac{k_m k_j}{k^2} \right) & \dfrac{k^2}{k_0^2 + k^2} \left(\delta_{mn} - \dfrac{k_m k_n}{k^2} \right) \end{pmatrix} . \tag{B.32}$$

We see that the temporal and spatial components still have the same propagators as in the standard formalism, in particular they do not mix with each other for $\xi = 0$, but both do mix with the electric field. Also note that $D_0^T(K) = D_0(-K)$. This is of relevance for the off-diagonal terms, which have odd powers of the momentum in the numerator (the reason is that A_0 and $\boldsymbol{A}$ are of mass dimension 1, while $\boldsymbol{E}$ is of dimension 2).

The interaction part of the action is given by

$$S_{int} = \int_0^{1/T} d\tau \int d^3x \left[g f^{abc} \left(\partial_i A_j^a\right) A_i^b A_j^c + \frac{g^2}{4} f^{abe} f^{cde} A_i^a A_j^b A_i^c A_j^d - i g f^{abc} A_0^a E_i^b A_i^c \right] . \tag{B.33}$$

This gives the same three- and four-gluon vertices as in standard Coulomb gauge if only spatial gluons are involved, but the temporal gluons now interact with the spatial gluons only through

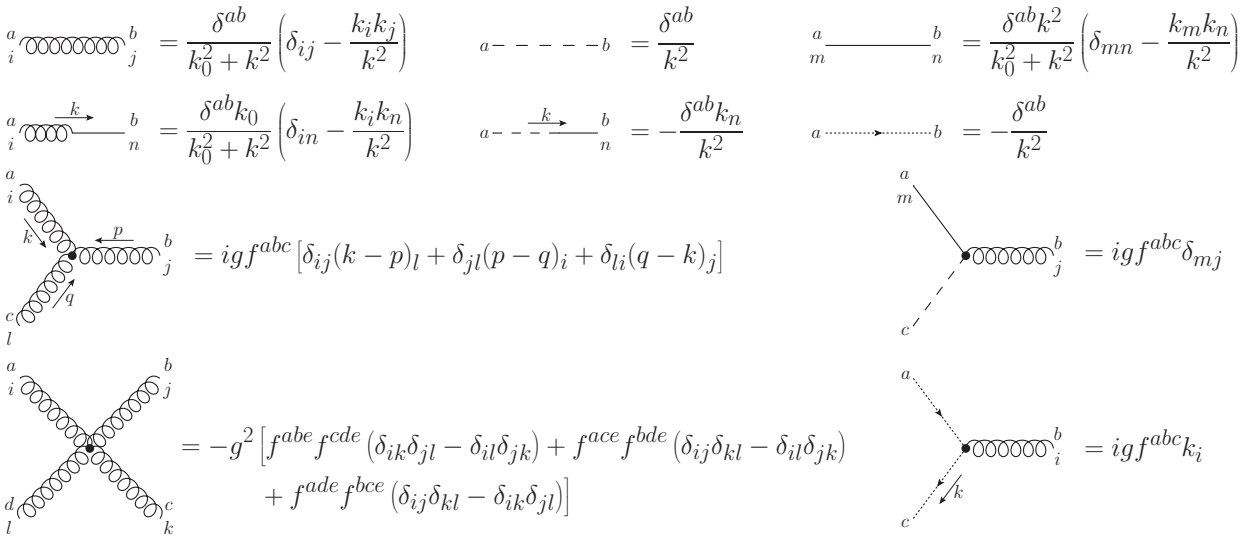

Figure B.1: All free propagators and interaction vertices in phase-space Coulomb gauge. Whenever there is an arrow specifying the direction of a momentum over a mixed propagator, opposite momenta will give the negative propagator.

a three-field vertex with an additional electric field and the simple coefficient $igf^{abc}\delta_{im}$. All Feynman rules of phase-space Coulomb gauge are shown in Fig. B.1.

For the resummed propagator we need to introduce a new parametrization of the self-energy tensor in the form a 7×7-matrix:

$$\Pi = \begin{pmatrix} \Pi_{tt} & k_0k_j\,\Pi_{ts} & -k_n\,\Pi_{te} \\ k_ik_0\,\Pi_{ts} & \Pi_{ss1}\,\delta_{ij}+\Pi_{ss2}\,\dfrac{k_ik_j}{k^2} & k_0\left(\Pi_{se1}\,\delta_{in}+\Pi_{se2}\,\dfrac{k_ik_n}{k^2}\right) \\ k_m\,\Pi_{te} & -k_0\left(\Pi_{se1}\,\delta_{mj}+\Pi_{se2}\,\dfrac{k_mk_j}{k^2}\right) & \Pi_{ee1}\,\delta_{mn}+\Pi_{ee2}\,\dfrac{k_mk_n}{k^2} \end{pmatrix}, \tag{B.34}$$

where the labels t, s, and e stand for temporal, spatial, and electric respectively. Then the resummed propagators are

$$D_{00} = \frac{1+\Pi_{ee1}+\Pi_{ee2}}{k^2\left(1+\Pi_{te}\right)^2+\left(1+\Pi_{ee1}+\Pi_{ee2}\right)\Pi_{tt}}\,, \tag{B.35}$$

$$D_{0j} = D_{i0} = 0\,, \tag{B.36}$$

$$D_{0n} = \frac{\left(1+\Pi_{te}\right)k_n}{k^2\left(1+\Pi_{te}\right)^2+\left(1+\Pi_{ee1}+\Pi_{ee2}\right)\Pi_{tt}}\,, \tag{B.37}$$

$$D_{m0} = \frac{-\left(1+\Pi_{te}\right)k_m}{k^2\left(1+\Pi_{te}\right)^2+\left(1+\Pi_{ee1}+\Pi_{ee2}\right)\Pi_{tt}}\,, \tag{B.38}$$

$$D_{ij} = \frac{1+\Pi_{ee1}}{k_0^2\left(1+\Pi_{se1}\right)^2+k^2\left(1+\Pi_{ee1}\right)+\left(1+\Pi_{ee1}\right)\Pi_{ss1}}\left(\delta_{ij}-\frac{k_ik_j}{k^2}\right)\,, \tag{B.39}$$

$$D_{in} = \frac{-\left(1+\Pi_{se1}\right)k_0}{k_0^2\left(1+\Pi_{se1}\right)^2+k^2\left(1+\Pi_{ee1}\right)+\left(1+\Pi_{ee1}\right)\Pi_{ss1}}\left(\delta_{in}-\frac{k_ik_n}{k^2}\right)\,, \tag{B.40}$$

$$D_{mj} = \frac{(1+\Pi_{se1})\,k_0}{k_0^2\,(1+\Pi_{se1})^2 + k^2\,(1+\Pi_{ee1}) + (1+\Pi_{ee1})\,\Pi_{ss1}} \left(\delta_{mj} - \frac{k_m k_j}{k^2}\right), \tag{B.41}$$

$$D_{mn} = \frac{k^2+\Pi_{ss1}}{k_0^2\,(1+\Pi_{se1})^2 + k^2\,(1+\Pi_{ee1}) + (1+\Pi_{ee1})\,\Pi_{ss1}} \left(\delta_{mn} - \frac{k_m k_n}{k^2}\right) + \frac{\Pi_{tt}}{k^2\,(1+\Pi_{te})^2 + (1+\Pi_{ee1}+\Pi_{ee2})\,\Pi_{tt}} \frac{k_m k_n}{k^2}. \tag{B.42}$$

We see that the self-energy components that are proportional to k_i or k_j (i.e., Π_{ts}, Π_{ss2}, and Π_{se2}) do not appear at all, while the ones that are proportional only to k_m or k_n (i.e., Π_{te} and Π_{ee2}), appear only in D_{00}, D_{m0}, D_{0n}, and D_{mn}. The reason for this is that every free propagator with a spatial gluon index i or j is proportional to the transverse projector $\delta_{ij} - k_i k_j/k^2$, so the self-energy components Π_{ts}, Π_{ss2}, and Π_{se2} drop out of the geometric series. Since only the δ_{ij} self-energy terms remain in the geometric series for D_{ij}, D_{in}, and D_{mj}, also the resummed propagators are proportional to the transverse projector. A mixing of temporal and spatial gluons is still not possible, because $(D_0)_{i0}$ and $(D_0)_{0j}$ are zero from the outset and intermediate electric field contributions like, e.g., $(D_0)_{in}\,\Pi_{nm}\,(D_0)_{m0}$ or $(D_0)_{in}\,\Pi_{n0}\,(D_0)_{00}$ always involve a contraction of the transverse projector with the momentum k_m, either from the self-energy or the $(D_0)_{m0}$ propagator. In the case of the propagators D_{00}, D_{m0}, D_{0n}, and D_{mn}, there appear terms in the geometric series without any transverse projectors, so those propagators also depend on the self-energy terms Π_{te} and Π_{ee2}. Also note that, in contrast to the free propagator, the resummed D_{mn} contains a part that is not proportional to the transverse projector, which comes, e.g., from terms like $(D_0)_{m0}\,\Pi_{00}\,(D_0)_{0n}$.

B.1.5 Expansions of the Propagators

In the small coupling case the two energy scales πT and $m_D \sim gT$ are well separated, so we expand the propagators accordingly. The Matsubara frequencies are always of order πT and the momentum k can be either of order πT or m_D. The self-energy functions are at least of order g^2T^2, so if k is of order πT then the propagators have to be expanded in the self-energy, which is equivalent to using free propagators instead of resummed propagators.

If k is of order m_D but k_0 is not zero, then the propagators also have to be expanded in k^2/k_0^2, which leads to scaleless integrals in most cases (and in all integrals appearing in this chapter). An exception to this are the temporal propagators in static and Coulomb gauge, which do not have a k_0^2 term in the denominator.

If k is of order m_D and k_0 is zero, then the leading term of the self-energy may be of the same order as k^2 and the propagator has to be expanded in the next-to-leading terms. It is known that only the self-energy in the temporal propagator has a term of order g^2T^2, which is gauge invariant and given by the square of the Debye mass m_D^2, see Eq. (4.2). In Coulomb gauge, the free propagator is independent of the Matsubara frequencies. The self-energy, however, is such that it is of order g^2T^2 for the zero mode, while it is of higher order for the other frequencies. The self-energies in the spatial propagator start at order g^4T^2, therefore the spatial propagator has to be expanded and we can use the free one.

It is a straightforward calculation to show that also in the phase-space Coulomb gauge (PSCG) only Π_{tt} has a term of order g^2T^2 and this is again given by m_D^2. All other self-energies need to be expanded; see Eqs. (B.35)-(B.42). Therefore, the spatial and mixed spatial-electric propagators remain massless, but the electric and mixed temporal-electric propagators also get massive denominators.

We summarize here the propagators in different gauges in the leading order expansion for $k_0 = 0$ and $k \sim m_D$.

$$D^{FG} = \begin{pmatrix} \dfrac{1}{k^2+m_D^2} & 0 \\ 0 & \dfrac{\delta_{ij}}{k^2} \end{pmatrix}, \quad D^{SG} = \begin{pmatrix} \dfrac{1}{k^2+m_D^2} & 0 \\ 0 & \dfrac{1}{k^2}\left(\delta_{ij} - (1-\xi)\dfrac{k_i k_j}{k^2}\right) \end{pmatrix}, \tag{B.43}$$

$$D^{CG} = D^{SG}\big|_{\xi=0}, \quad D^{PSCG} = \begin{pmatrix} \dfrac{1}{k^2+m_D^2} & 0 & \dfrac{k_n}{k^2+m_D^2} \\ 0 & \dfrac{1}{k^2}\left(\delta_{ij} - \dfrac{k_i k_j}{k^2}\right) & 0 \\ -\dfrac{k_m}{k^2+m_D^2} & 0 & \delta_{mn} - \dfrac{k_m k_n}{k^2+m_D^2} \end{pmatrix}. \tag{B.44}$$

B.2 Electric Scale Two-Loop Integrals

In this appendix, we will explicitly write down the integrals and their results for all the two-loop self-energy diagrams at the scale m_D. In order to calculate the integrals we make use of an algorithm that systematically reduces the integrals to a handful of master integrals by the method of integration by parts and then replaces these master integrals by their known values. More details on this algorithm can be found in appendix B.4.

All relevant diagrams for $\Pi^{(2)}_{m_D}(0, k \sim m_D)$ are shown in Fig. 4.1, where also the diagrams labels are explained. As explained in appendix B.1.5, only temporal gluons carry the Debye mass in the propagator, so it makes sense to visually distinguish between temporal and spatial gluons in the diagrams. All Matsubara frequencies are assumed to be zero, which means that a vertex with one temporal gluon and two spatial gluons or ghosts (if they are required by the chosen gauge) cannot appear, because it would be proportional to the Matsubara frequencies. This is why there are no three-gluon vertices with just one temporal gluon in all the diagrams of Fig. 4.1. Tadpole diagrams with only spatial gluons or ghosts are scaleless and therefore have been omitted in Fig. 4.1. Fermion propagators do not have zero-modes, so also light quark loops cannot contribute to $\Pi^{(2)}_{m_D}(0, k \sim m_D)$.

We will do the calculation explicitly in Feynman, Coulomb, and phase-space Coulomb gauge. In the case of the static gauge we will not perform the calculation for a generic gauge fixing parameter ξ. For $\xi = 1$ and $\xi = 0$ the calculation is identical to the one in Feynman and Coulomb gauge, respectively.

The color factors of the two-loop self-energy can be calculated using the quadratic Casimir of the adjoint representation and the Jacobi identity:

$$\mathrm{Tr}\big[T_A^a T_A^b\big] = (-if^{acd})(-if^{bdc}) = f^{acd} f^{bcd} = N\,\delta^{ab}\,, \tag{B.45}$$

$$f^{abe} f^{ecd} + f^{bce} f^{ead} + f^{cae} f^{ebd} = 0\,. \tag{B.46}$$

With these we get

$$f^{acd} f^{dce} f^{egh} f^{hgb} = (-N\,\delta^{ae})(-N\,\delta^{eb}) = N^2\,\delta^{ab}\,, \tag{B.47}$$

$$f^{acd} f^{dgh} f^{hge} f^{ecb} = -N f^{acd} f^{dcb} = N^2\,\delta^{ab}\,, \tag{B.48}$$

$$f^{acd}f^{cge}f^{deh}f^{hgb} = -\frac{1}{2}f^{acd}\big(f^{cge}f^{edh} + f^{che}f^{egd}\big)f^{hgb} = \frac{1}{2}f^{acd}f^{dce}f^{egh}f^{hgb} = \frac{1}{2}N^2\,\delta^{ab}\,. \quad \text{(B.49)}$$

All color factors are given by these expressions or combinations thereof. Symmetry factors appear only when gluons of the same type (temporal or spatial) can be exchanged, which is the case for L_3, L_8, L_9, L_{10}, and L_{12}, although in the case of L_3, L_8, and L_{12} one symmetry factor $1/2$ is compensated by a factor 2 from the four-gluon vertices. From the vertices we either get $(ig)^4$, $(ig)^2(-g^2)$ or $(-g^2)^2$, which is equal to g^4 in each case. So no additional signs arise from the vertices, but the ghost loop gets a minus due to its Grassmann nature. Then we have

$$\mathcal{C}(L_1) = \mathcal{C}(L_2) = -\mathcal{C}(L_8) = \mathcal{C}(L_9) = \mathcal{C}(L_{10}) = \frac{1}{2}N^2\,, \quad \text{(B.50)}$$

$$\mathcal{C}(L_7) = -\mathcal{C}(L_{11}) = -\mathcal{C}(L_{12}) = N^2\,, \quad \text{(B.51)}$$

$$\mathcal{C}(L_3) = -\mathcal{C}(L_4) = -\mathcal{C}(L_5) = -\mathcal{C}(L_6) = \frac{3}{2}N^2\,. \quad \text{(B.52)}$$

B.2.1 Feynman Gauge

We will call the momenta in the diagrams of Fig. 4.1 in such a way that k appears in each temporal gluon propagator (even in the temporal gluon loops in L_8, L_{10} and L_{12} through a shift of the loop momentum by k), while the additional loop momenta will be called p and q. In the denominator only the combinations $\boldsymbol{k}+\boldsymbol{p}$, $\boldsymbol{k}+\boldsymbol{q}$, and either $\boldsymbol{k}+\boldsymbol{p}+\boldsymbol{q}$ or $\boldsymbol{p}-\boldsymbol{q}$ can appear. The reason for this choice is that with this momentum configuration the integrals are already in the form required by the algorithm described in appendix B.4. We will use the abbreviation $P(\boldsymbol{k}) = \boldsymbol{k}^2 + m_D^2$. L_5 and L_6 are the same up to a relabeling of the momenta, so we will calculate them together. Then we have

$$\begin{aligned}
L_1 &= -\frac{C_R N^2 g^6}{4}\int\!\!\!\int\!\!\!\int_{k,\,p,\,q\sim m_D} \frac{2T(2k_i+p_i)(p^2\delta_{ij}-p_ip_j+q^2\delta_{ij}-q_iq_j-(\boldsymbol{p}\cdot\boldsymbol{q})\delta_{ij}+p_iq_j)(2k_j+q_j)}{\boldsymbol{p}^2\,(\boldsymbol{p}-\boldsymbol{q})^2\,\boldsymbol{q}^2\,P(\boldsymbol{k}+\boldsymbol{p})P(\boldsymbol{k}+\boldsymbol{q})P(\boldsymbol{k})^2} \\
&= \frac{C_R N^2\alpha_s^3 T}{m_D}\left[-\frac{1}{32\epsilon} - \frac{7}{32} + \frac{3}{32}\gamma_E - \frac{\pi^2}{24} - \frac{3}{32}\ln\frac{\pi\mu^2}{m_D^2} + \mathcal{O}(\epsilon)\right], \quad \text{(B.53)} \\
L_2 &= -\frac{C_R N^2 g^6}{4}\int\!\!\!\int\!\!\!\int_{k,\,p,\,q\sim m_D} \frac{T\left[(2\boldsymbol{k}+\boldsymbol{p})\cdot(2\boldsymbol{k}+\boldsymbol{p}+2\boldsymbol{q})\right]\left[(2\boldsymbol{k}+\boldsymbol{q})\cdot(2\boldsymbol{k}+2\boldsymbol{p}+\boldsymbol{q})\right]}{\boldsymbol{p}^2\,\boldsymbol{q}^2\,P(\boldsymbol{k}+\boldsymbol{p})\,P(\boldsymbol{k}+\boldsymbol{q})\,P(\boldsymbol{k}+\boldsymbol{p}+\boldsymbol{q})\,P(\boldsymbol{k})^2} \\
&= \frac{C_R N^2\alpha_s^3 T}{m_D}\left[-\frac{1}{32\epsilon} - \frac{1}{4} + \frac{3}{32}\gamma_E - \frac{\pi^2}{12} - \frac{3}{32}\ln\frac{\pi\mu^2}{256m_D^2} + \mathcal{O}(\epsilon)\right], \quad \text{(B.54)} \\
L_3 &= -\frac{3C_R N^2 g^6}{4}\int\!\!\!\int\!\!\!\int_{k,\,p,\,q\sim m_D} \frac{T\,d}{\boldsymbol{p}^2\,(\boldsymbol{p}-\boldsymbol{q})^2\,P(\boldsymbol{k}+\boldsymbol{q})\,P(\boldsymbol{k})^2} \\
&= \frac{C_R N^2\alpha_s^3 T}{m_D}\left[-\frac{9}{32\epsilon} - \frac{3}{8} + \frac{27}{32}\gamma_E - \frac{27}{32}\ln\frac{\pi\mu^2}{m_D^2} + \mathcal{O}(\epsilon)\right], \quad \text{(B.55)} \\
L_4 &= \frac{3C_R N^2 g^6}{4}\int\!\!\!\int\!\!\!\int_{k,\,p,\,q\sim m_D} \frac{T\,(2\boldsymbol{k}+\boldsymbol{p})\cdot(2\boldsymbol{k}+\boldsymbol{q})}{\boldsymbol{p}^2\,\boldsymbol{q}^2\,P(\boldsymbol{k}+\boldsymbol{p})\,P(\boldsymbol{k}+\boldsymbol{q})\,P(\boldsymbol{k})^2} \\
&= \frac{C_R N^2\alpha_s^3 T}{m_D}\left[\frac{39}{32} + \mathcal{O}(\epsilon)\right], \quad \text{(B.56)}
\end{aligned}$$

$$L_5 + L_6 = \frac{3C_R N^2 g^6}{4} \int\!\!\int\!\!\int_{k,\,p,\,q\sim m_D} \frac{2T\,(2\boldsymbol{k}+\boldsymbol{p})\cdot(2\boldsymbol{k}+\boldsymbol{p}+\boldsymbol{q})}{\boldsymbol{p}^2\,(\boldsymbol{p}-\boldsymbol{q})^2\,P(\boldsymbol{k}+\boldsymbol{p})\,P(\boldsymbol{k}+\boldsymbol{q})\,P(\boldsymbol{k})^2}$$

$$= \frac{C_R N^2 \alpha_{\mathrm{s}}^3 T}{m_D}\left[\frac{9}{32\epsilon} - \frac{3}{16} - \frac{27}{32}\gamma_E + \frac{\pi^2}{8} + \frac{27}{32}\ln\frac{\pi\mu^2}{m_D^2} + \mathcal{O}(\epsilon)\right], \tag{B.57}$$

$$L_7 = -\frac{C_R N^2 g^6}{2} \int\!\!\int\!\!\int_{k,\,p,\,q\sim m_D} \frac{T\,(2\boldsymbol{k}+\boldsymbol{p})^2\,(2\boldsymbol{k}+\boldsymbol{p}+\boldsymbol{q})^2}{\boldsymbol{p}^2\,(\boldsymbol{p}-\boldsymbol{q})^2\,P(\boldsymbol{k}+\boldsymbol{p})^2\,P(\boldsymbol{k}+\boldsymbol{q})\,P(\boldsymbol{k})^2}$$

$$= \frac{C_R N^2 \alpha_{\mathrm{s}}^3 T}{m_D}\left[-\frac{1}{8\epsilon} - \frac{9}{8} + \frac{3}{8}\gamma_E - \frac{3}{8}\ln\frac{\pi\mu^2}{m_D^2} + \mathcal{O}(\epsilon)\right], \tag{B.58}$$

$$L_8 = \frac{C_R N^2 g^6}{4} \int\!\!\int\!\!\int_{k,\,p,\,q\sim m_D} \frac{T\,(2\boldsymbol{k}+\boldsymbol{p}+\boldsymbol{q})^2}{((\boldsymbol{p}-\boldsymbol{q})^2)^2\,P(\boldsymbol{k}+\boldsymbol{p})\,P(\boldsymbol{k}+\boldsymbol{q})\,P(\boldsymbol{k})^2}$$

$$= \frac{C_R N^2 \alpha_{\mathrm{s}}^3 T}{m_D}\left[-\frac{1}{32\epsilon} + \frac{3}{32}\gamma_E - \frac{3}{32}\ln\frac{\pi\mu^2}{m_D^2} + \mathcal{O}(\epsilon)\right], \tag{B.59}$$

$$L_9 = -\frac{C_R N^2 g^6}{4} \int\!\!\int\!\!\int_{k,\,p,\,q\sim m_D} \frac{T\,(2k_i+p_i)\,(2k_j+p_j)}{P(\boldsymbol{k}+\boldsymbol{p})\,P(\boldsymbol{k})^2}$$
$$\times \frac{(5p^2\delta_{ij} - (6-d)p_i p_j + 2q^2\delta_{ij} - (6-4d)q_i q_j - 2(\boldsymbol{p}\cdot\boldsymbol{q})\delta_{ij} + (6-4d)p_i q_j)}{(\boldsymbol{p}^2)^2\,(\boldsymbol{p}-\boldsymbol{q})^2\,\boldsymbol{q}^2}$$

$$= \frac{C_R N^2 \alpha_{\mathrm{s}}^3 T}{m_D}\left[\frac{13}{64\epsilon} - \frac{19}{32} - \frac{39}{64}\gamma_E + \frac{39}{64}\ln\frac{\pi\mu^2}{m_D^2} + \mathcal{O}(\epsilon)\right], \tag{B.60}$$

$$L_{10} = -\frac{C_R N^2 g^6}{4} \int\!\!\int\!\!\int_{k,\,p,\,q\sim m_D} \frac{T\,[(2\boldsymbol{k}+\boldsymbol{p})\cdot(2\boldsymbol{k}+\boldsymbol{p}+2\boldsymbol{q})]^2}{(\boldsymbol{p}^2)^2\,P(\boldsymbol{k}+\boldsymbol{p})\,P(\boldsymbol{k}+\boldsymbol{q})\,P(\boldsymbol{k}+\boldsymbol{p}+\boldsymbol{q})\,P(\boldsymbol{k})^2}$$

$$= \frac{C_R N^2 \alpha_{\mathrm{s}}^3 T}{m_D}\left[-\frac{5}{48} + \frac{1}{6}\ln 2 + \mathcal{O}(\epsilon)\right], \tag{B.61}$$

$$L_{11} = \frac{C_R N^2 g^6}{2} \int\!\!\int\!\!\int_{k,\,p,\,q\sim m_D} \frac{T\,[(2\boldsymbol{k}+\boldsymbol{p})\cdot(-\boldsymbol{q})]\,[(2\boldsymbol{k}+\boldsymbol{p})\cdot(\boldsymbol{p}-\boldsymbol{q})]}{(\boldsymbol{p}^2)^2\,(\boldsymbol{p}-\boldsymbol{q})^2\,\boldsymbol{q}^2\,P(\boldsymbol{k}+\boldsymbol{p})\,P(\boldsymbol{k})^2}$$

$$= \frac{C_R N^2 \alpha_{\mathrm{s}}^3 T}{m_D}\left[\frac{1}{64\epsilon} - \frac{1}{32} - \frac{3}{64}\gamma_E + \frac{3}{64}\ln\frac{\pi\mu^2}{m_D^2} + \mathcal{O}(\epsilon)\right], \tag{B.62}$$

$$L_{12} = \frac{C_R N^2 g^6}{2} \int\!\!\int\!\!\int_{k,\,p,\,q\sim m_D} \frac{T\,(2\boldsymbol{k}+\boldsymbol{p})^2}{(\boldsymbol{p}^2)^2\,P(\boldsymbol{k}+\boldsymbol{p})\,P(\boldsymbol{k}+\boldsymbol{q})\,P(\boldsymbol{k})^2}$$

$$= \frac{C_R N^2 \alpha_{\mathrm{s}}^3 T}{m_D}\left[\frac{1}{8} + \mathcal{O}(\epsilon)\right]. \tag{B.63}$$

We also have to include the contribution from the square of the one-loop self-energy in order to get a gauge invariant result. This contribution can also be put into the form required by the algorithm:

$$-\frac{C_R g^2}{2T}\int_{k\sim m_D} \frac{\left(\Pi_{m_D}^{(1)}(0,k)\right)^2}{(k^2+m_D^2)^3} = -\frac{C_R N^2 g^6}{2} \int\!\!\int\!\!\int_{k,\,p,\,q\sim m_D} \frac{T\,(2\boldsymbol{k}+\boldsymbol{p})^2\,(2\boldsymbol{k}+\boldsymbol{q})^2}{\boldsymbol{p}^2\,\boldsymbol{q}^2\,P(\boldsymbol{k}+\boldsymbol{p})\,P(\boldsymbol{k}+\boldsymbol{q})\,P(\boldsymbol{k})^3}$$
$$= \frac{C_R N^2 \alpha_{\mathrm{s}}^3 T}{m_D}\left[-\frac{5}{16} - \frac{\pi^2}{12} + \mathcal{O}(\epsilon)\right]. \tag{B.64}$$

The sum of all these terms then gives the $\mathcal{O}(g^5)$ contribution from the scale m_D:

$$D_1\Big|_{g^5,\,m_D} = -\frac{C_R N^2 \alpha_{\rm s}^3 T}{m_D}\left[\frac{89}{48}+\frac{\pi^2}{12}-\frac{11}{12}\ln 2\right]. \tag{B.65}$$

B.2.2 Coulomb Gauge

In Coulomb gauge we have

$$\begin{aligned}
L_1 &= -\frac{C_R N^2 g^6}{4}\int\!\!\!\int\!\!\!\int_{k,\,p,\,q\sim m_D}\frac{-16T}{\boldsymbol{p}^2\,(\boldsymbol{p}-\boldsymbol{q})^2\,\boldsymbol{q}^2\,P(\boldsymbol{k}+\boldsymbol{p})\,P(\boldsymbol{k}+\boldsymbol{q})\,P(\boldsymbol{k})^2}\\
&\quad\times\left[\left(\boldsymbol{k}\cdot\boldsymbol{q}-\frac{(\boldsymbol{k}\cdot\boldsymbol{p})(\boldsymbol{p}\cdot\boldsymbol{q})}{\boldsymbol{p}^2}\right)\left(\boldsymbol{k}\cdot\boldsymbol{p}-\frac{(\boldsymbol{k}\cdot\boldsymbol{q})(\boldsymbol{p}\cdot\boldsymbol{q})}{\boldsymbol{q}^2}\right)\left(1+\frac{\boldsymbol{k}\cdot(\boldsymbol{p}+\boldsymbol{q})}{(\boldsymbol{p}-\boldsymbol{q})^2}\right)\right.\\
&\quad+\left(\boldsymbol{k}^2-\frac{(\boldsymbol{k}\cdot\boldsymbol{p})^2}{\boldsymbol{p}^2}\right)\left(\boldsymbol{k}\cdot\boldsymbol{p}-\frac{(\boldsymbol{k}\cdot\boldsymbol{q})(\boldsymbol{p}\cdot\boldsymbol{q})}{\boldsymbol{q}^2}\right)\left(1-\frac{\boldsymbol{q}^2}{(\boldsymbol{p}-\boldsymbol{q})^2}\right)\\
&\quad+\left(\boldsymbol{k}\cdot\boldsymbol{q}-\frac{(\boldsymbol{k}\cdot\boldsymbol{p})(\boldsymbol{p}\cdot\boldsymbol{q})}{\boldsymbol{p}^2}\right)\left(\boldsymbol{k}^2-\frac{(\boldsymbol{k}\cdot\boldsymbol{q})^2}{\boldsymbol{q}^2}\right)\left(1-\frac{\boldsymbol{p}^2}{(\boldsymbol{p}-\boldsymbol{q})^2}\right)\\
&\quad\left.-\frac{\boldsymbol{p}^2\boldsymbol{q}^2-(\boldsymbol{p}\cdot\boldsymbol{q})^2}{(\boldsymbol{p}-\boldsymbol{q})^2}\left(\boldsymbol{k}^2-\frac{(\boldsymbol{k}\cdot\boldsymbol{p})^2}{\boldsymbol{p}^2}-\frac{(\boldsymbol{k}\cdot\boldsymbol{q})^2}{\boldsymbol{q}^2}+\frac{(\boldsymbol{k}\cdot\boldsymbol{p})(\boldsymbol{k}\cdot\boldsymbol{q})(\boldsymbol{p}\cdot\boldsymbol{q})}{\boldsymbol{p}^2\,\boldsymbol{q}^2}\right)\right]\\
&= \frac{C_R N^2\alpha_{\rm s}^3 T}{m_D}\left[\frac{1}{8}-\frac{\pi^2}{24}+\mathcal{O}(\epsilon)\right],
\end{aligned}\tag{B.66}$$

$$\begin{aligned}
L_2 &= -\frac{C_R N^2 g^6}{4}\int\!\!\!\int\!\!\!\int_{k,\,p,\,q\sim m_D}\frac{16T}{\boldsymbol{p}^2\,\boldsymbol{q}^2\,P(\boldsymbol{k}+\boldsymbol{p})\,P(\boldsymbol{k}+\boldsymbol{q})\,P(\boldsymbol{k}+\boldsymbol{p}+\boldsymbol{q})\,P(\boldsymbol{k})^2}\\
&\quad\times\left[\boldsymbol{k}\cdot(\boldsymbol{k}+\boldsymbol{q})-\frac{(\boldsymbol{k}\cdot\boldsymbol{p})(\boldsymbol{k}\cdot\boldsymbol{p}+\boldsymbol{p}\cdot\boldsymbol{q})}{\boldsymbol{p}^2}\right]\left[\boldsymbol{k}\cdot(\boldsymbol{k}+\boldsymbol{p})-\frac{(\boldsymbol{k}\cdot\boldsymbol{q})(\boldsymbol{k}\cdot\boldsymbol{q}+\boldsymbol{p}\cdot\boldsymbol{q})}{\boldsymbol{q}^2}\right]\\
&= \frac{C_R N^2\alpha_{\rm s}^3 T}{m_D}\left[\frac{1}{8}+\frac{3}{4}\ln 2-\frac{\pi^2}{12}+\mathcal{O}(\epsilon)\right],
\end{aligned}\tag{B.67}$$

$$\begin{aligned}
L_3 &= -\frac{3C_R N^2 g^6}{4}\int\!\!\!\int\!\!\!\int_{k,\,p,\,q\sim m_D}\frac{T}{\boldsymbol{p}^2\,\boldsymbol{q}^2\,P(\boldsymbol{k}+\boldsymbol{p}+\boldsymbol{q})\,P(\boldsymbol{k})^2}\left[d-2+\frac{(\boldsymbol{p}\cdot\boldsymbol{q})^2}{\boldsymbol{p}^2\,\boldsymbol{q}^2}\right]\\
&= \frac{C_R N^2\alpha_{\rm s}^3 T}{m_D}\left[-\frac{9}{64\epsilon}-\frac{3}{64}+\frac{27}{64}\gamma_E-\frac{27}{64}\ln\frac{\pi\mu^2}{m_D^2}+\mathcal{O}(\epsilon)\right],
\end{aligned}\tag{B.68}$$

$$\begin{aligned}
L_4 &= \frac{3C_R N^2 g^6}{4}\int\!\!\!\int\!\!\!\int_{k,\,p,\,q\sim m_D}\frac{4T\left[\boldsymbol{k}^2\boldsymbol{p}^2\boldsymbol{q}^2-(\boldsymbol{k}\cdot\boldsymbol{p})^2\boldsymbol{q}^2-(\boldsymbol{k}\cdot\boldsymbol{q})^2\boldsymbol{p}^2+(\boldsymbol{k}\cdot\boldsymbol{p})(\boldsymbol{k}\cdot\boldsymbol{q})(\boldsymbol{p}\cdot\boldsymbol{q})\right]}{(\boldsymbol{p}^2)^2\,(\boldsymbol{q}^2)^2\,P(\boldsymbol{k}+\boldsymbol{p})\,P(\boldsymbol{k}+\boldsymbol{q})\,P(\boldsymbol{k})^2}\\
&= \frac{C_R N^2\alpha_{\rm s}^3 T}{m_D}\left[\frac{15}{8}-\frac{\pi^2}{8}+\mathcal{O}(\epsilon)\right],
\end{aligned}\tag{B.69}$$

$$\begin{aligned}
L_5+L_6 &= \frac{3C_R N^2 g^6}{2}\int\!\!\!\int\!\!\!\int_{k,\,p,\,q\sim m_D}\frac{4T}{\boldsymbol{p}^2\,\boldsymbol{q}^2\,P(\boldsymbol{k}+\boldsymbol{p})\,P(\boldsymbol{k}+\boldsymbol{p}+\boldsymbol{q})\,P(\boldsymbol{k})^2}\\
&\quad\times\left[\boldsymbol{k}^2-\frac{(\boldsymbol{k}\cdot\boldsymbol{p})^2}{\boldsymbol{p}^2}-\frac{(\boldsymbol{k}\cdot\boldsymbol{q})(\boldsymbol{k}\cdot\boldsymbol{q}+\boldsymbol{p}\cdot\boldsymbol{q})}{\boldsymbol{q}^2}+\frac{(\boldsymbol{k}\cdot\boldsymbol{p})(\boldsymbol{k}\cdot\boldsymbol{q}+\boldsymbol{p}\cdot\boldsymbol{q})(\boldsymbol{p}\cdot\boldsymbol{q})}{\boldsymbol{p}^2\boldsymbol{q}^2}\right]\\
&= \frac{C_R N^2\alpha_{\rm s}^3 T}{m_D}\left[-\frac{3}{2}+\frac{\pi^2}{4}+\mathcal{O}(\epsilon)\right],
\end{aligned}\tag{B.70}$$

$$L_7 = -\frac{C_R N^2 g^6}{2} \int\!\!\!\int\!\!\!\int_{k,\,p,\,q\sim m_D} \frac{16T\left[\boldsymbol{k}^2\boldsymbol{p}^2 - (\boldsymbol{k}\cdot\boldsymbol{p})^2\right]\left[(\boldsymbol{k}+\boldsymbol{p})^2\boldsymbol{q}^2 - (\boldsymbol{k}\cdot\boldsymbol{q}+\boldsymbol{p}\cdot\boldsymbol{q})^2\right]}{\left(\boldsymbol{p}^2\right)^2\left(\boldsymbol{q}^2\right)^2 P(\boldsymbol{k}+\boldsymbol{p})^2\, P(\boldsymbol{k}+\boldsymbol{p}+\boldsymbol{q})\, P(\boldsymbol{k})^2}$$
$$= \frac{C_R N^2 \alpha_{\rm s}^3 T}{m_D}\left[-\frac{9}{8} + \mathcal{O}(\epsilon)\right], \tag{B.71}$$
$$L_8 = \frac{C_R N^2 g^6}{4} \int\!\!\!\int\!\!\!\int_{k,\,p,\,q\sim m_D} \frac{4T\left[(\boldsymbol{k}+\boldsymbol{q})^2\boldsymbol{p}^2 - (\boldsymbol{k}\cdot\boldsymbol{p}+\boldsymbol{p}\cdot\boldsymbol{q})^2\right]}{\left(\boldsymbol{p}^2\right)^3 P(\boldsymbol{k}+\boldsymbol{q})\, P(\boldsymbol{k}+\boldsymbol{p}+\boldsymbol{q})\, P(\boldsymbol{k})^2}$$
$$= \frac{C_R N^2 \alpha_{\rm s}^3 T}{m_D}\left[-\frac{1}{32\epsilon} + \frac{3}{32}\gamma_E - \frac{3}{32}\ln\frac{\pi\mu^2}{m_D^2} + \mathcal{O}(\epsilon)\right], \tag{B.72}$$
$$L_9 = -\frac{C_R N^2 g^6}{4} \int\!\!\!\int\!\!\!\int_{k,\,p,\,q\sim m_D} \frac{16T}{\left(\boldsymbol{p}^2\right)^2 (\boldsymbol{p}-\boldsymbol{q})^2\,\boldsymbol{q}^2\, P(\boldsymbol{k}+\boldsymbol{p})\, P(\boldsymbol{k})^2}$$
$$\times\left[\left(\boldsymbol{k}^2 - \frac{(\boldsymbol{k}\cdot\boldsymbol{p})^2}{\boldsymbol{p}^2}\right)\left(\boldsymbol{p}^2\boldsymbol{q}^2 - (\boldsymbol{p}\cdot\boldsymbol{q})^2\right)\left(\frac{1}{(\boldsymbol{p}-\boldsymbol{q})^2} + \frac{1}{\boldsymbol{q}^2}\right)\right.$$
$$\left. + \left(\boldsymbol{k}\cdot\boldsymbol{q} - \frac{(\boldsymbol{k}\cdot\boldsymbol{p})(\boldsymbol{p}\cdot\boldsymbol{q})}{\boldsymbol{p}^2}\right)^2\left(d - 1 - \frac{\boldsymbol{p}^2\boldsymbol{q}^2 - (\boldsymbol{p}\cdot\boldsymbol{q})^2}{(\boldsymbol{p}-\boldsymbol{q})^2\,\boldsymbol{q}^2}\right)\right]$$
$$= \frac{C_R N^2 \alpha_{\rm s}^3 T}{m_D}\left[\frac{5}{32\epsilon} - \frac{43}{64} - \frac{15}{32}\gamma_E + \frac{15}{32}\ln\frac{\pi\mu^2}{m_D^2} + \mathcal{O}(\epsilon)\right], \tag{B.73}$$
$$L_{10} = -\frac{C_R N^2 g^6}{4} \int\!\!\!\int\!\!\!\int_{k,\,p,\,q\sim m_D} \frac{16T\left[(\boldsymbol{k}^2 + \boldsymbol{k}\cdot\boldsymbol{q})\,\boldsymbol{p}^2 - (\boldsymbol{k}\cdot\boldsymbol{p})(\boldsymbol{k}\cdot\boldsymbol{p}+\boldsymbol{p}\cdot\boldsymbol{q})\right]^2}{\left(\boldsymbol{p}^2\right)^4 P(\boldsymbol{k}+\boldsymbol{p})\, P(\boldsymbol{k}+\boldsymbol{q})\, P(\boldsymbol{k}+\boldsymbol{p}+\boldsymbol{q})\, P(\boldsymbol{k})^2}$$
$$= \frac{C_R N^2 \alpha_{\rm s}^3 T}{m_D}\left[-\frac{5}{48} + \frac{1}{6}\ln 2 + \mathcal{O}(\epsilon)\right], \tag{B.74}$$
$$L_{11} = \frac{C_R N^2 g^6}{2} \int\!\!\!\int\!\!\!\int_{k,\,p,\,q\sim m_D} \frac{4T\left[(\boldsymbol{k}\cdot\boldsymbol{q})\boldsymbol{p}^2 - (\boldsymbol{k}\cdot\boldsymbol{p})(\boldsymbol{p}\cdot\boldsymbol{q})\right]^2}{\left(\boldsymbol{p}^2\right)^4 (\boldsymbol{p}-\boldsymbol{q})^2\,\boldsymbol{q}^2\, P(\boldsymbol{k}+\boldsymbol{p})\, P(\boldsymbol{k})^2}$$
$$= \frac{C_R N^2 \alpha_{\rm s}^3 T}{m_D}\left[\frac{1}{64\epsilon} - \frac{1}{32} - \frac{3}{64}\gamma_E + \frac{3}{64}\ln\frac{\pi\mu^2}{m_D^2} + \mathcal{O}(\epsilon)\right], \tag{B.75}$$
$$L_{12} = \frac{C_R N^2 g^6}{2} \int\!\!\!\int\!\!\!\int_{k,\,p,\,q\sim m_D} \frac{4T\left[\boldsymbol{k}^2\boldsymbol{p}^2 - (\boldsymbol{k}\cdot\boldsymbol{p})^2\right]}{\left(\boldsymbol{p}^2\right)^3 P(\boldsymbol{k}+\boldsymbol{p})\, P(\boldsymbol{k}+\boldsymbol{q})\, P(\boldsymbol{k})^2}$$
$$= \frac{C_R N^2 \alpha_{\rm s}^3 T}{m_D}\left[\frac{1}{8} + \mathcal{O}(\epsilon)\right]. \tag{B.76}$$

The square of the one-loop self-energy from the scale m_D gives the contribution

$$-\frac{C_R g^2}{2T}\int_{k\sim m_D}\frac{\left(\Pi^{(1)}_{m_D}(0,k)\right)^2}{\left(k^2+m_D^2\right)^3} = -\frac{C_R N^2 g^6}{2}\int\!\!\!\int\!\!\!\int_{k,\,p,\,q\sim m_D}\frac{16T\left[\boldsymbol{k}^2\boldsymbol{p}^2 - (\boldsymbol{k}\cdot\boldsymbol{p})^2\right]\left[\boldsymbol{k}^2\boldsymbol{q}^2 - (\boldsymbol{k}\cdot\boldsymbol{q})^2\right]}{\left(\boldsymbol{p}^2\right)^2\left(\boldsymbol{q}^2\right)^2 P(\boldsymbol{k}+\boldsymbol{p})\, P(\boldsymbol{k}+\boldsymbol{q})\, P(\boldsymbol{k})^3}$$
$$= \frac{N^2\alpha_{\rm s}^3 T}{m_D}\left[-\frac{5}{8} - \frac{\pi^2}{12} + \mathcal{O}(\epsilon)\right], \tag{B.77}$$

and after summing up all these terms, we again obtain the same result as in Feynman gauge:

$$D_1\Big|_{g^5,\,m_D} = -\frac{C_R N^2 \alpha_{\rm s}^3 T}{m_D}\left[\frac{89}{48} + \frac{\pi^2}{12} - \frac{11}{12}\ln 2\right]. \tag{B.78}$$

Figure B.2: All diagrams relevant for the cancellation of the non-zero modes in the one-loop spatial gluon self-energy in Coulomb gauge.

There is a subtlety in Coulomb gauge regarding the non-zero modes. In Feynman gauge all Matsubara frequencies have to be zero, because otherwise the necessary expansions of the propagators only lead to scaleless or higher order contributions. But in Coulomb gauge the frequencies do not appear explicitly in the temporal gluon or ghost propagators, the only dependence on the frequencies is that the Debye mass appears in the temporal gluon propagator only for the zero mode. So, in principle, the propagators do not have to be expanded and there is nothing preventing also non-zero frequencies to appear in the Matsubara sums, as long as they do not appear in spatial gluon propagators.

In most diagrams there is only the zero mode because of the contour integration, but in diagrams L_8, L_{10}, L_{11}, and L_{12} the momentum of the temporal gluon or ghost loop can have a non-zero frequency without it entering a spatial gluon propagator. This poses a problem, because those loops do not depend on the frequency, so the Matsubara sums contain an infinite sum over a constant, which is divergent and not regulated by dimensional regularization.

However, these sums are canceled by a diagram that we could ignore so far, because it vanishes for the zero mode. This is the last diagram in Fig. B.2 and the Matsubara frequencies in the numerator from the vertices exactly cancel the denominator of the spatial gluon after it has been expanded. Then the sum over all diagrams of Fig. B.2 gives from left to right

$$g^2 N \sum\!\!\!\!\!\!\int_Q{}' \left[\frac{1}{2}\frac{4q_iq_j}{(\boldsymbol{p}-\boldsymbol{q})^2\boldsymbol{q}^2} - \frac{q_iq_j}{(\boldsymbol{p}-\boldsymbol{q})^2\boldsymbol{q}^2} - \frac{\delta_{ij}}{(\boldsymbol{p}-\boldsymbol{q})^2} + \frac{q_0^2}{(\boldsymbol{p}-\boldsymbol{q})^2}\frac{1}{q_0^2}\left(\delta_{ij}-\frac{q_iq_j}{\boldsymbol{q}^2}\right)\right] = 0\,. \quad \text{(B.79)}$$

We have used the momentum $\boldsymbol{p}-\boldsymbol{q}$ instead of just $\boldsymbol{q}$ in the tadpole loop so that its cancellation becomes more apparent, and we do not have to consider the higher order expansion terms of the spatial gluon propagator in the last diagram, because they only contain scaleless integrals.

So even though each diagram contains a divergent series, the sum of all four of them is finite, because for each particular value of the frequency the sum cancels. In static gauge with $\xi = 0$ this problem does not arise, because the temporal gluon and ghost propagators vanish for non-zero frequencies. Since the last diagram of Fig. B.2 gives no other contribution apart from canceling the non-zero-frequency contributions of the other diagrams in Coulomb gauge, the corresponding diagram has not been displayed in Fig. 4.1.

B.2.3 Phase-Space Coulomb Gauge

In phase-space Coulomb gauge there are less diagram types, because temporal gluons only couple in a three-gluon vertex. These types are shown in Fig. B.3. But because the massive propagators now can be temporal, electric, or mixed, there are more diagrams in total. However, it is possible for each diagram type to factorize the massive propagators from the spatial gluon propagators, so that we can sum over all possibilities for the massive propagators before multiplying them with the spatial gluons. This sum over all massive propagators is represented by the double-line propagators in Fig. B.3.

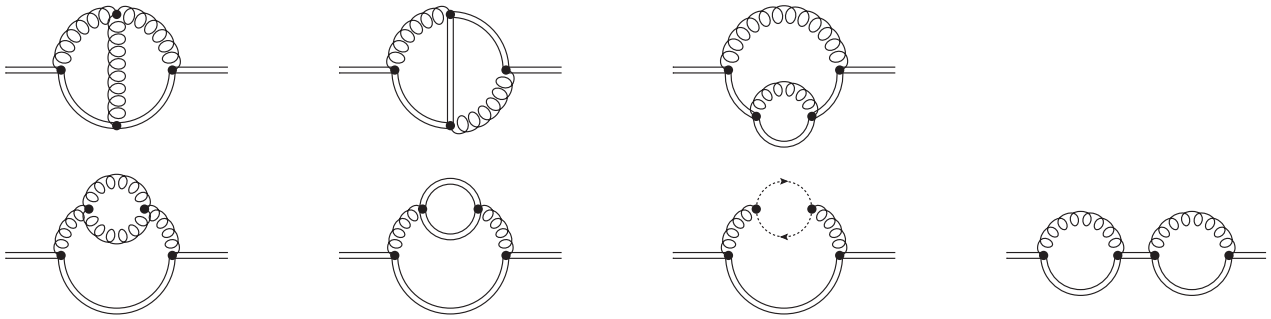

Figure B.3: All two-loop diagram configurations in phase-space Coulomb gauge. The double-line propagators can represent either a temporal, an electric, or a mixed propagator. Also the diagram with two one-loop bubbles is displayed in the bottom-right corner. We will label the diagrams $\widetilde{L}_1, \dots, \widetilde{L}_7$ from top left to bottom right.

We have included the one-particle reducible diagram $\widetilde{L}_7$ in Fig. B.3, which corresponds to the second order expansion of the resummed propagator. In this case the reexpanded temporal propagator depends on several different self-energy functions, so it is easier to just calculate this diagram explicitly.

We will denote the sum over massive propagators by $D_{\alpha\beta}^{m_1 m_2 \cdots}(\boldsymbol{k}_0, \boldsymbol{k}_1, \boldsymbol{k}_2, \dots)$. The indices m_i correspond to the vector indices at each vertex i, which can then be contracted with the spatial gluon propagator. The initial momentum of the series of propagators is $\boldsymbol{k}_0$ and the $\boldsymbol{k}_i$ are the incoming momenta at each vertex i. The final and initial indices of the propagator series are α and β, respectively. We will need temporal indices for most diagrams, but also mixed indices for the double line loop in diagram $\widetilde{L}_5$.

We will show the summation over massive propagators explicitly in one case for illustration and just give the result for the other relevant cases. Figure B.4 shows the double line propagator with two vertices in terms of temporal, electric, and mixed propagators. By the phase-space Coulomb gauge Feynman rules this gives

$$\begin{aligned}
D_{00}^{m_1 m_2}(\boldsymbol{k}_0, \boldsymbol{k}_1, \boldsymbol{k}_2) = &- D_{00}(\boldsymbol{k}_0 + \boldsymbol{k}_1 + \boldsymbol{k}_2) D_{m_2 m_1}(\boldsymbol{k}_0 + \boldsymbol{k}_1) D_{00}(\boldsymbol{k}_0) \\
&+ D_{00}(\boldsymbol{k}_0 + \boldsymbol{k}_1 + \boldsymbol{k}_2) D_{m_2 0}(\boldsymbol{k}_0 + \boldsymbol{k}_1) D_{m_1 0}(\boldsymbol{k}_0) \\
&+ D_{0 m_2}(\boldsymbol{k}_0 + \boldsymbol{k}_1 + \boldsymbol{k}_2) D_{0 m_1}(\boldsymbol{k}_0 + \boldsymbol{k}_1) D_{00}(\boldsymbol{k}_0) \\
&- D_{0 m_2}(\boldsymbol{k}_0 + \boldsymbol{k}_1 + \boldsymbol{k}_2) D_{00}(\boldsymbol{k}_0 + \boldsymbol{k}_1) D_{m_1 0}(\boldsymbol{k}_0) \\
= &- \frac{1}{P(\boldsymbol{k}_0 + \boldsymbol{k}_1 + \boldsymbol{k}_2)} \left(\delta_{m_2 m_1} - \frac{(k_0 + k_1)_{m_2} (k_0 + k_1)_{m_1}}{P(\boldsymbol{k}_0 + \boldsymbol{k}_1)} \right) \frac{1}{P(\boldsymbol{k}_0)} \\
&+ \frac{1}{P(\boldsymbol{k}_0 + \boldsymbol{k}_1 + \boldsymbol{k}_2)} \frac{-(k_0 + k_1)_{m_2}}{P(\boldsymbol{k}_0 + \boldsymbol{k}_1)} \frac{-(k_0)_{m_1}}{P(\boldsymbol{k}_0)} \\
&+ \frac{(k_0 + k_1 + k_2)_{m_2}}{P(\boldsymbol{k}_0 + \boldsymbol{k}_1 + \boldsymbol{k}_2)} \frac{(k_0 + k_1)_{m_1}}{P(\boldsymbol{k}_0 + \boldsymbol{k}_1)} \frac{1}{P(\boldsymbol{k}_0)} \\
&- \frac{(k_0 + k_1 + k_2)_{m_2}}{P(\boldsymbol{k}_0 + \boldsymbol{k}_1 + \boldsymbol{k}_2)} \frac{1}{P(\boldsymbol{k}_0 + \boldsymbol{k}_1)} \frac{-(k_0)_{m_1}}{P(\boldsymbol{k}_0)} \\
= &- \frac{1}{P(\boldsymbol{k}_0 + \boldsymbol{k}_1 + \boldsymbol{k}_2)} \left(\delta_{m_1 m_2} - \frac{4(k_0 + k_1)_{m_2} (k_0)_{m_1}}{P(\boldsymbol{k}_0 + \boldsymbol{k}_1)} \right) \frac{1}{P(\boldsymbol{k}_0)} \,. \qquad \text{(B.80)}
\end{aligned}$$

Here we have used the fact that all vector indices are contracted with gluon propagators that are proportional to the transverse propagator, which means that all terms $(k_i)_{m_i}$ cancel in the

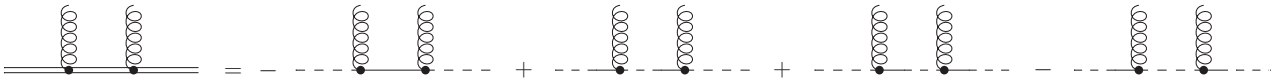

Figure B.4: Explicit expression for a double line propagator with two vertices in terms of temporal, electric, and mixed propagators.

numerator and can be neglected. The different signs in front of the propagators come from the two color structure functions in the vertices, which are even or odd depending on whether the temporal, electric, and spatial fields are attached with the same ordering or the opposite one compared to the three-field vertex shown in Fig. B.1.

In the same way one can calculate double line propagators with more vertices or different initial and final indices:

$$
\begin{aligned}
&D_{00}^{m_1m_2m_3}(\boldsymbol{k}_0,\boldsymbol{k}_1,\boldsymbol{k}_2,\boldsymbol{k}_3)\\
&= \frac{2(k_0+k_1+k_2)_{m_3}\delta_{m_2m_1}}{P(\boldsymbol{k}_0+\boldsymbol{k}_1+\boldsymbol{k}_2+\boldsymbol{k}_3)P(\boldsymbol{k}_0+\boldsymbol{k}_1+\boldsymbol{k}_2)P(\boldsymbol{k}_0)} + \frac{2\delta_{m_3m_2}(k_0)_{m_1}}{P(\boldsymbol{k}_0+\boldsymbol{k}_1+\boldsymbol{k}_2+\boldsymbol{k}_3)P(\boldsymbol{k}_0+\boldsymbol{k}_1)P(\boldsymbol{k}_0)}\\
&- \frac{8(k_0+k_1+k_2)_{m_3}(k_0+k_1)_{m_2}(k_0)_{m_1}}{P(\boldsymbol{k}_0+\boldsymbol{k}_1+\boldsymbol{k}_2+\boldsymbol{k}_3)P(\boldsymbol{k}_0+\boldsymbol{k}_1+\boldsymbol{k}_2)P(\boldsymbol{k}_0+\boldsymbol{k}_1)P(\boldsymbol{k}_0)}\,,
\end{aligned}
\tag{B.81}
$$

$$
\begin{aligned}
&D_{00}^{m_1m_2m_3m_4}(\boldsymbol{k}_0,\boldsymbol{k}_1,\boldsymbol{k}_2,\boldsymbol{k}_3,\boldsymbol{k}_4)\\
&= \frac{1}{P(\boldsymbol{k}_0+\boldsymbol{k}_1+\boldsymbol{k}_2+\boldsymbol{k}_3+\boldsymbol{k}_4)}\left(\delta_{m_4m_3} - \frac{4(k_0+k_1+k_2+k_3)_{m_4}(k_0+k_1+k_2)_{m_3}}{P(\boldsymbol{k}_0+\boldsymbol{k}_1+\boldsymbol{k}_2+\boldsymbol{k}_3)}\right)\\
&\quad\times\frac{1}{P(\boldsymbol{k}_0+\boldsymbol{k}_1+\boldsymbol{k}_2)}\left(\delta_{m_2m_1} - \frac{4(k_0+k_1)_{m_2}(k_0)_{m_1}}{P(\boldsymbol{k}_0+\boldsymbol{k}_1)}\right)\frac{1}{P(\boldsymbol{k}_0)}\\
&\quad- \frac{4(k_0+k_1+k_2+k_3)_{m_4}\delta_{m_3m_2}(k_0)_{m_1}}{P(\boldsymbol{k}_0+\boldsymbol{k}_1+\boldsymbol{k}_2+\boldsymbol{k}_3+\boldsymbol{k}_4)P(\boldsymbol{k}_0+\boldsymbol{k}_1+\boldsymbol{k}_2+\boldsymbol{k}_3)P(\boldsymbol{k}_0+\boldsymbol{k}_1)P(\boldsymbol{k}_0)}\,,
\end{aligned}
\tag{B.82}
$$

$$
D_{0n}^{m_1}(\boldsymbol{k}_0,\boldsymbol{k}_1) = -\frac{1}{P(\boldsymbol{k}_0+\boldsymbol{k}_1)}\left(\delta_{m_1n} - \frac{2(k_0)_{m_1}(k_0)_n}{P(\boldsymbol{k}_0)}\right)\,. \tag{B.83}
$$

With these we can write the phase-space Coulomb gauge diagrams in a rather compact form:

$$
\begin{aligned}
\widetilde{L}_1 &= -\frac{C_RN^2g^6T}{4}\int\!\!\!\int\!\!\!\int_{k,\,p,\,q\sim m_D} D_{00}^{ijl}(\boldsymbol{k},\boldsymbol{p},\boldsymbol{q}-\boldsymbol{p},-\boldsymbol{q})D_{ii'}(\boldsymbol{p})D_{jj'}(\boldsymbol{q}-\boldsymbol{p})D_{ll'}(-\boldsymbol{q})\\
&\qquad\qquad\times\left[\delta_{i'j'}(2p-q)_{l'}+\delta_{j'l'}(2q-p)_{i'}-\delta_{l'i'}(p+q)_{j'}\right]\\
&= \frac{C_RN^2\alpha_{\mathrm{s}}^3T}{m_D}\left[\frac{1}{8}-\frac{\pi^2}{24}+\mathcal{O}(\epsilon)\right]\,,
\end{aligned}
\tag{B.84}
$$

$$
\begin{aligned}
\widetilde{L}_2 &= -\frac{C_RN^2g^6T}{4}\int\!\!\!\int\!\!\!\int_{k,\,p,\,q\sim m_D} D_{00}^{iji'j'}(\boldsymbol{k},\boldsymbol{p},\boldsymbol{q},-\boldsymbol{p},-\boldsymbol{q})D_{ii'}(\boldsymbol{p})D_{jj'}(\boldsymbol{q})\\
&= \frac{C_RN^2\alpha_{\mathrm{s}}^3T}{m_D}\left[-\frac{3}{64\epsilon}+\frac{15}{64}+\frac{9}{64}\gamma_E-\frac{\pi^2}{24}+\frac{3}{4}\ln 2-\frac{9}{64}\ln\frac{\pi\mu^2}{m_D^2}+\mathcal{O}(\epsilon)\right]\,,
\end{aligned}
\tag{B.85}
$$

$$\widetilde{L}_3 = -\frac{C_R N^2 g^6 T}{2} \iiint\limits_{k,\,p,\,q\sim m_D} D_{00}^{ijj'i'}(\boldsymbol{k},\boldsymbol{p},\boldsymbol{q},-\boldsymbol{q},-\boldsymbol{p}) D_{ii'}(\boldsymbol{p}) D_{jj'}(\boldsymbol{q})$$

$$= \frac{C_R N^2 \alpha_{\mathrm{s}}^3 T}{m_D} \left[-\frac{3}{32\epsilon} - \frac{69}{32} + \frac{9}{32}\gamma_E + \frac{\pi^2}{6} - \frac{9}{32}\ln\frac{\pi\mu^2}{m_D^2} + \mathcal{O}(\epsilon) \right], \tag{B.86}$$

$$\widetilde{L}_4 = -\frac{C_R N^2 g^6 T}{2} \iiint\limits_{k,\,p,\,q\sim m_D} D_{00}^{ij}(\boldsymbol{k},\boldsymbol{p},-\boldsymbol{p}) D_{ii'}(\boldsymbol{p}) D_{jj'}(-\boldsymbol{p}) \frac{2}{(\boldsymbol{p}-\boldsymbol{q})^2\boldsymbol{q}^2}$$

$$\times \left[\left(\boldsymbol{p}^2\boldsymbol{q}^2 - (\boldsymbol{p}\cdot\boldsymbol{q})^2\right) \left(\frac{1}{\boldsymbol{q}^2} + \frac{1}{(\boldsymbol{p}-\boldsymbol{q})^2} \right) \delta_{i'j'} + \left(d - 1 - \frac{\boldsymbol{p}^2\boldsymbol{q}^2 - (\boldsymbol{p}\cdot\boldsymbol{q})^2}{(\boldsymbol{p}-\boldsymbol{q})^2\boldsymbol{q}^2} \right) q_{i'} q_{j'} \right]$$

$$= \frac{C_R N^2 \alpha_{\mathrm{s}}^3 T}{m_D} \left[\frac{5}{32\epsilon} - \frac{43}{64} - \frac{15}{32}\gamma_E + \frac{15}{32}\ln\frac{\pi\mu^2}{m_D^2} + \mathcal{O}(\epsilon) \right], \tag{B.87}$$

$$\widetilde{L}_5 = -\frac{C_R N^2 g^6 T}{2} \iiint\limits_{k,\,p,\,q\sim m_D} D_{00}^{ij}(\boldsymbol{k},\boldsymbol{p},-\boldsymbol{p}) D_{ii'}(\boldsymbol{p}) D_{jj'}(-\boldsymbol{p}) D_{0n}^{j'}(\boldsymbol{k}+\boldsymbol{q},\boldsymbol{p}) \delta_{i'n}$$

$$= \frac{C_R N^2 \alpha_{\mathrm{s}}^3 T}{m_D} \left[-\frac{1}{32\epsilon} + \frac{1}{48} + \frac{3}{32}\gamma_E + \frac{1}{6}\ln 2 - \frac{3}{32}\ln\frac{\pi\mu^2}{m_D^2} + \mathcal{O}(\epsilon) \right], \tag{B.88}$$

$$\widetilde{L}_6 = -\frac{C_R N^2 g^6 T}{2} \iiint\limits_{k,\,p,\,q\sim m_D} D_{00}^{ij}(\boldsymbol{k},\boldsymbol{p},-\boldsymbol{p}) D_{ii'}(\boldsymbol{p}) D_{jj'}(-\boldsymbol{p}) \frac{q_{i'} q_{j'}}{(\boldsymbol{p}-\boldsymbol{q})^2\boldsymbol{q}^2}$$

$$= \frac{C_R N^2 \alpha_{\mathrm{s}}^3 T}{m_D} \left[\frac{1}{64\epsilon} - \frac{1}{32} - \frac{3}{64}\gamma_E + \frac{3}{64}\ln\frac{\pi\mu^2}{m_D^2} + \mathcal{O}(\epsilon) \right], \tag{B.89}$$

$$\widetilde{L}_7 = -\frac{C_R N^2 g^6 T}{2} \iiint\limits_{k,\,p,\,q\sim m_D} D_{00}^{ii'jj'}(\boldsymbol{k},\boldsymbol{p},-\boldsymbol{p},\boldsymbol{q},-\boldsymbol{q}) D_{ii'}(\boldsymbol{p}) D_{jj'}(\boldsymbol{q})$$

$$= \frac{C_R N^2 \alpha_{\mathrm{s}}^3 T}{m_D} \left[\frac{5}{8} - \frac{\pi^2}{6} + \mathcal{O}(\epsilon) \right]. \tag{B.90}$$

We have changed the momenta in the double line loop of diagram $\widetilde{L}_5$ from $\boldsymbol{p}+\boldsymbol{q}$ and $\boldsymbol{q}$ to $\boldsymbol{k}+\boldsymbol{p}+\boldsymbol{q}$ and $\boldsymbol{k}+\boldsymbol{q}$ by a shift of the integration momentum $\boldsymbol{q}$, such that the integrals are all of the form required by the algorithm of appendix B.4.

We see that the sum of these integrals gives the same result as in standard Coulomb gauge and in Feynman gauge. But we can make the correspondence between phase-space and standard Coulomb gauge even clearer. The propagator of the electric field [cf. Eq. (B.44)] contains a part that is just a Kronecker delta, which gives exactly the same contribution as if the electric propagator were contracted to a point and replaced by a four-gluon vertex in standard Coulomb gauge. The second part of the electric propagator contains components of the momentum in the numerator and a massive denominator. This term has the same form as a corresponding three-gluon vertex in Coulomb gauge, where the momentum components in the numerator come from the vertex and not the propagator. The same applies for mixed temporal-electric propagators.

The correspondence is not one-to-one, for example diagrams $\widetilde{L}_2$ and $\widetilde{L}_3$ both give diagram L_3 in standard Coulomb gauge when we replace the second and fourth double-line propagator by a Kronecker delta. But if we look at the color coefficients $C_R N^2/2$ of $\widetilde{L}_2$ and $C_R N^2$ of $\widetilde{L}_3$, we see that they add up exactly to the color coefficient $3C_R N^2/2$ of L_3. So ultimately it is only a matter of combinatorics to see that phase-space and standard Coulomb gauge generate

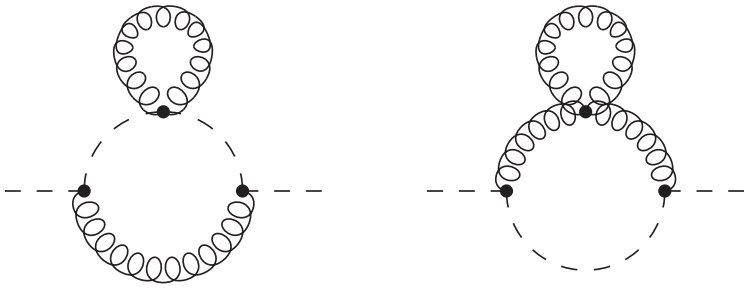

Figure B.5: Additional diagrams carrying the scale m_M at $\mathcal{O}(g^6)$.

exactly the same integrals.

A simpler check of this statement is to compare certain classes of diagrams between phase-space and standard Coulomb gauge, which have unique configurations in both gauge formulations. In our case, L_1 and $\widetilde{L}_1$ are the only diagrams with a vertex of three spatial gluons, and diagrams $L_8, \ldots, L_{12}$, and $\widetilde{L}_4, \ldots, \widetilde{L}_6$ are the only ones with a one-loop self-energy in a spatial propagator. So accordingly, we find the equalities

$$\widetilde{L}_1 = L_1\,, \tag{B.91}$$

$$\widetilde{L}_2 + \widetilde{L}_3 + \widetilde{L}_7 = L_2 + L_3 + L_4 + L_5 + L_6 + L_7 + L_{13}\,, \tag{B.92}$$

$$\widetilde{L}_4 + \widetilde{L}_5 + \widetilde{L}_6 = L_8 + L_9 + L_{10} + L_{11} + L_{12}\,, \tag{B.93}$$

where we used L_{13} to denote the contribution from the square of the one-loop self-energy at the scale m_D.

The cancellation of the non-zero frequency contributions is a bit simpler in this formulation than in standard Coulomb gauge. The double-line loop in diagram $\widetilde{L}_5$ of Fig. B.3 gives rise to two contributions, one where the loop contains a temporal and an electric propagator and one where both propagators are mixed temporal-electric. The first contribution is unproblematic, since the electric propagator for non-zero frequencies contains the denominator $q_0^2 + q^2$, for which the Matsubara sum is finite. The second contribution exactly cancels the ghost loop diagram.

B.3 Magnetic Scale Cancellation at $\mathcal{O}(g^6)$

We will list here all contributions at $\mathcal{O}(g^6)$ that involve the scale m_M. At $\mathcal{O}(g^5)$ those were one-loop diagrams where the spatial gluon carries a momentum of order m_M and the temporal gluon carries a momentum of order m_D (see Sec. 4.3.3). At $\mathcal{O}(g^6)$ it is the same principle: two-loop diagrams with all propagators carrying momenta of order m_D except for one spatial gluon with a momentum of order m_M. In three-gluon vertices only the momenta of order m_D are to be kept in the numerator.

We refer again to Fig. 4.1, which essentially gives all relevant diagrams for this calculation. In diagrams $L_1, \ldots, L_7$ any of the spatial gluons can be the one that carries the scale m_M, in diagram L_9 it is only the gluons in the subloop. So L_1 contains three and $L_2, \ldots, L_7, L_9$ each contain two different contributions. In addition, there are two new diagrams not displayed in Fig. 4.1, which we give in Fig. B.5. They correspond to the diagrams L_7 and L_9 from Fig. 4.1 with the subloop replaced by a tadpole, so we will include the contributions of the left and

right diagram in Fig. B.5 in the following expressions for L_7 and L_9, respectively. Diagrams L_8, L_{10}, and L_{12} do not contribute, because if the spatial gluons were of the scale m_M, then these would correspond to the one-loop diagram with a resummed spatial propagator, which we have already considered in the $\mathcal{O}(g^5)$ calculation. Diagram L_{11} with one ghost propagator of the scale m_M does not contribute, because from the gluon-ghost vertices there is a factor of the loop momentum squared in the numerator, so this diagram is of $\mathcal{O}(g^8)$.

We will do this calculation in Feynman gauge, because the expressions are somewhat shorter. We will label the momenta such that $k, p \sim m_D$ and $q \sim m_M$. Since we have to expand everything in q/m_D, we can just ignore q in all other propagators at leading order. This simplifies the q integration, which now contains only one propagator:

$$\int_{q\sim m_M} D_{ij}(0,q) = \frac{\delta_{ij}}{d} \int_{q\sim m_M} D_{kk}(0,q)\,. \tag{B.94}$$

The Kronecker delta can then be used to contract all indices in the k and p integrations, which can be carried out by the same methods as in the $\mathcal{O}(g^5)$ calculation.

The calculation of the different diagrams gives

$$\begin{aligned}
L_1 &= -C_R N^2 g^6 T \int_{k,\,p\sim m_D,\,q\sim q_M} \left(\frac{4\,(\boldsymbol{k}^2\boldsymbol{p}^2 - (\boldsymbol{k}\cdot\boldsymbol{p})^2)}{(\boldsymbol{p}^2)^2\,P(\boldsymbol{k}+\boldsymbol{p})\,P(\boldsymbol{k})^3} + \frac{2\,(\boldsymbol{k}^2\boldsymbol{p}^2 - (\boldsymbol{k}\cdot\boldsymbol{p})^2)}{(\boldsymbol{p}^2)^2\,P(\boldsymbol{k}+\boldsymbol{p})^2\,P(\boldsymbol{k})^2} \right) \frac{D_{ii}(0,q)}{d} \\
&= -\frac{2\pi}{3} \frac{C_R N^2 \alpha_s^3 T}{m_D^2} \int_{q\sim m_M} D_{ii}(0,q)\,, \qquad \text{(B.95)} \\
L_2 &= -C_R N^2 g^6 T \int_{k,\,p\sim m_D,\,q\sim q_M} \frac{2(2\boldsymbol{k}+\boldsymbol{p})^2\,(\boldsymbol{k}^2+\boldsymbol{k}\cdot\boldsymbol{p})}{\boldsymbol{p}^2\,P(\boldsymbol{k}+\boldsymbol{p})^2\,P(\boldsymbol{k})^3} \frac{D_{ii}(0,q)}{d} \\
&= -\frac{2\pi}{3} \frac{C_R N^2 \alpha_s^3 T}{m_D^2} \int_{q\sim m_M} D_{ii}(0,q)\,, \qquad \text{(B.96)} \\
L_3 &= -\frac{3}{2} C_R N^2 g^6 T \int_{k,\,p\sim m_D,\,q\sim q_M} \frac{d}{\boldsymbol{p}^2\,P(\boldsymbol{k}+\boldsymbol{p})\,P(\boldsymbol{k})^2} \frac{D_{ii}(0,q)}{d} \\
&= -\frac{3\pi}{2} \frac{C_R N^2 \alpha_s^3 T}{m_D^2} \int_{q\sim m_M} D_{ii}(0,q)\,, \qquad \text{(B.97)} \\
L_4 &= C_R N^2 g^6 T \int_{k,\,p\sim m_D,\,q\sim q_M} \frac{3\,(2\boldsymbol{k}^2+\boldsymbol{k}\cdot\boldsymbol{p})}{\boldsymbol{p}^2\,P(\boldsymbol{k}+\boldsymbol{p})\,P(\boldsymbol{k})^3} \frac{D_{ii}(0,q)}{d} \\
&= \pi \frac{C_R N^2 \alpha_s^3 T}{m_D^2} \int_{q\sim m_M} D_{ii}(0,q)\,, \qquad \text{(B.98)} \\
L_5 + L_6 &= C_R N^2 g^6 T \int_{k,\,p\sim m_D,\,q\sim q_M} \left(\frac{3(2\boldsymbol{k}+\boldsymbol{p})\cdot(\boldsymbol{k}+\boldsymbol{p})}{\boldsymbol{p}^2\,P(\boldsymbol{k}+\boldsymbol{p})^2\,P(\boldsymbol{k})^2} + \frac{3\,(2\boldsymbol{k}^2+\boldsymbol{k}\cdot\boldsymbol{p})}{\boldsymbol{p}^2\,P(\boldsymbol{k}+\boldsymbol{p})\,P(\boldsymbol{k})^3} \right) \frac{D_{ii}(0,q)}{d} \\
&= 2\pi \frac{C_R N^2 \alpha_s^3 T}{m_D^2} \int_{q\sim m_M} D_{ii}(0,q)\,, \qquad \text{(B.99)}
\end{aligned}$$

$$L_7 = -\frac{1}{2} C_R N^2 g^6 T \int\limits_{k,\, p\sim m_D,\, q\sim q_M} \left(\frac{4(2\boldsymbol{k}+\boldsymbol{p})^2(\boldsymbol{k}+\boldsymbol{p})^2}{\boldsymbol{p}^2\, P(\boldsymbol{k}+\boldsymbol{p})^3\, P(\boldsymbol{k})^2} + \frac{4\boldsymbol{k}^2(2\boldsymbol{k}+\boldsymbol{p})^2}{\boldsymbol{p}^2\, P(\boldsymbol{k}+\boldsymbol{p})\, P(\boldsymbol{k})^4} - \frac{d(2\boldsymbol{k}+\boldsymbol{p})^2}{\boldsymbol{p}^2\, P(\boldsymbol{k}+\boldsymbol{p})^2\, P(\boldsymbol{k})^2} \right) \frac{D_{ii}(0,q)}{d}$$

$$= -\frac{5\pi}{9} \frac{C_R N^2 \alpha_{\rm s}^3 T}{m_D^2} \int\limits_{q\sim m_M} D_{ii}(0,q)\,, \tag{B.100}$$

$$L_9 = -\frac{1}{2} C_R N^2 g^6 T \int\limits_{k,\, p\sim m_D,\, q\sim q_M} \left(\frac{20\boldsymbol{k}^2\boldsymbol{p}^2 - 4(6-d)(\boldsymbol{k}\cdot\boldsymbol{p})^2 - 4(1-d)(\boldsymbol{k}\cdot\boldsymbol{p})^2\boldsymbol{p}^2 - (1-d)\left(\boldsymbol{p}^2\right)^2}{\left(\boldsymbol{p}^2\right)^3 P(\boldsymbol{k}+\boldsymbol{p})\, P(\boldsymbol{k})^2} - \frac{(d-1)(2\boldsymbol{k}+\boldsymbol{p})^2}{\left(\boldsymbol{p}^2\right)^2 P(\boldsymbol{k}+\boldsymbol{p})\, P(\boldsymbol{k})^2} \right) \frac{D_{ii}(0,q)}{d}$$

$$= \frac{\pi}{2} \frac{C_R N^2 \alpha_{\rm s}^3 T}{m_D^2} \int\limits_{q\sim m_M} D_{ii}(0,q)\,. \tag{B.101}$$

From the square of the one-loop self-energy we have

$$-\frac{C_R g^2}{2T} \int\limits_{k\sim m_D} \frac{\Pi^{(1)}_{m_D}(0,k)\Pi^{(1)}_{m_M}(0,k)}{\left(k^2+m_D^2\right)^3}$$

$$= -C_R N^2 g^6 T \int\limits_{k,\, p\sim m_D,\, q\sim q_M} \left(\frac{4\boldsymbol{k}^2(2\boldsymbol{k}+\boldsymbol{p})^2}{\boldsymbol{p}^2\, P(\boldsymbol{k}+\boldsymbol{p})\, P(\boldsymbol{k})^4} - \frac{d\,(2\boldsymbol{k}+\boldsymbol{p})^2}{\boldsymbol{p}^2\, P(\boldsymbol{k}+\boldsymbol{p})\, P(\boldsymbol{k})^3} \right) \frac{D_{ii}(0,q)}{d}$$

$$= -\frac{\pi}{9} \frac{C_R N^2 \alpha_{\rm s}^3 T}{m_D^2} \int\limits_{q\sim m_M} D_{ii}(0,q)\,. \tag{B.102}$$

The sum of all these terms gives zero.

B.4 Automatic Reduction to Master Integrals

The method of how to solve the three-loop integrals appearing in this calculation has been described in [165]. Minimal modifications are required in order to account for the Euclidean metric. All integrals can be put in the two following forms:

$$B_M(i_1,i_2,i_3,i_4,i_5,i_6) = \int_k \int_p \int_q \frac{1}{(\boldsymbol{p}^2)^{i_1}((\boldsymbol{p}-\boldsymbol{q})^2)^{i_2}(\boldsymbol{q}^2)^{i_3} P(\boldsymbol{k}+\boldsymbol{p})^{i_4} P(\boldsymbol{k}+\boldsymbol{q})^{i_5} P(\boldsymbol{k})^{i_6}}\,, \tag{B.103}$$

$$B_N(i_1,i_2,i_3,i_4,i_5,i_6) = \int_k \int_p \int_q \frac{1}{(\boldsymbol{p}^2)^{i_1}(\boldsymbol{q}^2)^{i_2} P(\boldsymbol{k}+\boldsymbol{p})^{i_3} P(\boldsymbol{k}+\boldsymbol{q})^{i_4} P(\boldsymbol{k}+\boldsymbol{p}+\boldsymbol{q})^{i_5} P(\boldsymbol{k})^{i_6}}\,, \tag{B.104}$$

with $P(\boldsymbol{k}) = k^2 + m_D^2$. In this framework, the exponents $i_1, \ldots, i_6$ are integers.

By relabeling or shifting the integration variables $\boldsymbol{k}$, $\boldsymbol{p}$, and $\boldsymbol{q}$ several identities between the different B_M and B_N can be established:

$$\begin{aligned}
&B_M(i_1,i_2,i_3,i_4,i_5,i_6) = B_M(i_2,i_1,i_3,i_4,i_6,i_5)\\
&= B_M(i_3,i_1,i_2,i_6,i_4,i_5) = B_M(i_3,i_2,i_1,i_5,i_4,i_6)\\
&= B_M(i_2,i_3,i_1,i_5,i_6,i_4) = B_M(i_1,i_3,i_2,i_6,i_5,i_4)\,, \qquad \text{(B.105)}\\
&B_N(i_1,i_2,i_3,i_4,i_5,i_6) = B_N(i_1,i_2,i_5,i_6,i_3,i_4)\\
&= B_N(i_1,i_2,i_4,i_3,i_6,i_5) = B_N(i_1,i_2,i_6,i_5,i_4,i_3)\\
&= B_N(i_2,i_1,i_4,i_3,i_5,i_6) = B_N(i_2,i_1,i_5,i_6,i_4,i_3)\\
&= B_N(i_2,i_1,i_3,i_4,i_6,i_5) = B_N(i_2,i_1,i_6,i_5,i_3,i_4)\,. \qquad \text{(B.106)}
\end{aligned}$$

In addition, any B_N with an index $i_3,\ldots,i_6$ zero or negative can be turned into a B_M. The obvious relation is

$$B_N(i_1,i_2,i_3,i_4,0,i_6) = B_M(i_1,0,i_2,i_3,i_4,i_6)\,. \qquad \text{(B.107)}$$

If i_5 is negative, one can expand the numerator after substituting

$$(\boldsymbol{k}+\boldsymbol{p}+\boldsymbol{q})^2+m_D^2 = \boldsymbol{p}^2-(\boldsymbol{p}-\boldsymbol{q})^2+\boldsymbol{q}^2+\left((\boldsymbol{k}+\boldsymbol{p})^2+m_D^2\right)+\left((\boldsymbol{k}+\boldsymbol{q})^2+m_D^2\right)-\left(\boldsymbol{k}^2+m_D^2\right)\,. \qquad \text{(B.108)}$$

All these terms appear to some power in the denominator, so they can be canceled to give proper B_M integrals. If any of the other indices $i_3,\ldots,i_6$ is zero or negative, then one can use the identities above to shift that to the fifth position and then use the relation for $i_5 \leq 0$.

Other identities can be found by acting with $\boldsymbol{\nabla}_i \cdot \boldsymbol{k}_j$ on the integrand, where $\boldsymbol{k}_i$ and $\boldsymbol{k}_j$ can be any of the three loop momenta. The total expression has to be zero, since it is an integral over a total derivative, but calculating the derivative explicitly gives a number of other B_M and B_N integrals. These new identities include integrals with changed indices $i_1,\ldots,i_6$, while the identities above just shift them:

$$\begin{aligned}
&(d-2i_1-i_2-i_4)\,B_M\left(i_1,i_2,i_3,i_4,i_5,i_6\right)\\
&= i_2 B_M\left(i_1-1,i_2+1,i_3,i_4,i_5,i_6\right) - i_2 B_M\left(i_1,i_2+1,i_3-1,i_4,i_5,i_6\right)\\
&\quad + i_4 B_M\left(i_1-1,i_2,i_3,i_4+1,i_5,i_6\right) - i_4 B_M\left(i_1,i_2,i_3,i_4+1,i_5,i_6-1\right)\,, \qquad \text{(B.109)}\\
&(d-i_1-i_3-2i_6)\,B_M\left(i_1,i_2,i_3,i_4,i_5,i_6\right) = -2i_6 m_D^2 B_M\left(i_1,i_2,i_3,i_4,i_5,i_6+1\right)\\
&\quad + i_1 B_M\left(i_1+1,i_2,i_3,i_4,i_5,i_6-1\right) - i_1 B_M\left(i_1+1,i_2,i_3,i_4-1,i_5,i_6\right)\\
&\quad + i_3 B_M\left(i_1,i_2,i_3+1,i_4,i_5,i_6-1\right) - i_3 B_M\left(i_1,i_2,i_3+1,i_4,i_5-1,i_6\right)\,, \qquad \text{(B.110)}\\
&(d-i_1-2i_4-i_6)\,B_N\left(i_1,i_2,i_3,i_4,i_5,i_6\right)\\
&= i_1 B_N\left(i_1+1,i_2,i_3,i_4-1,i_5,i_6\right) - i_1 B_N\left(i_1+1,i_2,i_3,i_4,i_5-1,i_6\right)\\
&\quad + i_6 B_N\left(i_1,i_2,i_3,i_4-1,i_5,i_6+1\right) - i_6 B_N\left(i_1,i_2-1,i_3,i_4,i_5,i_6+1\right)\\
&\quad - 2i_4 m_D^2 B_N\left(i_1,i_2,i_3,i_4+1,i_5,i_6\right) - 2i_6 m_D^2 B_N\left(i_1,i_2,i_3,i_4,i_5,i_6+1\right)\,, \qquad \text{(B.111)}\\
&\left(i_1+i_2+i_3+i_4+i_5+i_6-\frac{3d}{2}\right) B_N\left(i_1,i_2,i_3,i_4,i_5,i_6\right)\\
&= i_3 m_D^2 B_N\left(i_1,i_2,i_3+1,i_4,i_5,i_6\right) + i_4 m_D^2 B_N\left(i_1,i_2,i_3,i_4+1,i_5,i_6\right)\\
&\quad + i_5 m_D^2 B_N\left(i_1,i_2,i_3,i_4,i_5+1,i_6\right) + i_6 m_D^2 B_N\left(i_1,i_2,i_3,i_4,i_5,i_6+1\right)\,. \qquad \text{(B.112)}
\end{aligned}$$

There are 16 further identities, which can be obtained from these four by combining them with the index shifts given above.

By repeated use of these identities every B_N integral can be reduced to $B_N(0,0,1,1,1,1)$ plus a bunch of B_M integrals. In the same way, every B_M integral can be reduced down to $B_M(0,0,0,1,1,1)$ plus B_M integrals where at least one of the indices $i_4,\ldots,i_6$ is zero or negative, for which there exists a general solution. So all integrals appearing in our calculation can be put into the form of a few master integrals. The needed results for those can be found in [37, 165, 166].[1]

B.5 Calculation of the Master Integrals

For the sake of completeness, we attach here how the master integrals, whose results are given in [37, 165, 166], can be calculated. The simplest one is $B_M(0,0,0,1,1,1)$, because in this case all three loop integrations decouple by shifting $\boldsymbol{p}\to\boldsymbol{p}-\boldsymbol{k}$ and $\boldsymbol{q}\to\boldsymbol{q}-\boldsymbol{k}$:

$$B_M(0,0,0,1,1,1)=\left(\int_k\frac{1}{k^2+m_D^2}\right)^3=\frac{\Gamma\left(1-\frac{d}{2}\right)^3}{(4\pi)^{\frac{3d}{2}}}\,m_D^{3d-6}\,. \tag{B.113}$$

For the other B_M integrals instead of a closed expression we will rather give another algorithm for their solution. We will assume that the zero or negative index is i_4, because if it is i_5 or i_6 instead then one can exchange those with i_4 by one of the identities. After also performing the shift $\boldsymbol{p}\to\boldsymbol{p}-\boldsymbol{k}$ and $\boldsymbol{q}\to\boldsymbol{q}-\boldsymbol{k}$ we can integrate over $\boldsymbol{p}$ without problems, because it no longer appears in a massive denominator:

$$\begin{aligned}
&\int_p\frac{\left(p^2+m_D^2\right)^{-i_4}}{\left((\boldsymbol{p}-\boldsymbol{k})^2\right)^{i_1}\left((\boldsymbol{p}-\boldsymbol{q})^2\right)^{i_2}}\\
&=\frac{\Gamma(i_1+i_2)}{\Gamma(i_1)\Gamma(i_2)}\int_0^1dx\int_p\frac{\left(p^2+m_D^2\right)^{-i_4}x^{i_1-1}(1-x)^{i_2-1}}{\left(p^2-2x\boldsymbol{p}\cdot\boldsymbol{k}-2(1-x)\boldsymbol{p}\cdot\boldsymbol{q}+xk^2+(1-x)q^2\right)^{i_1+i_2}}\\
&=\frac{\Gamma(i_1+i_2)}{\Gamma(i_1)\Gamma(i_2)}\int_0^1dx\int_p\frac{\left((\boldsymbol{p}+x\boldsymbol{k}+(1-x)\boldsymbol{q})^2+m_D^2\right)^{-i_4}x^{i_1-1}(1-x)^{i_2-1}}{\left(p^2+x(1-x)(\boldsymbol{k}-\boldsymbol{q})^2\right)^{i_1+i_2}}\,.
\end{aligned} \tag{B.114}$$

Now we have to expand the numerator, which we can do because $-i_4$ is a non-negative integer, and then use the identity

$$\begin{aligned}
\int_p(\boldsymbol{p}\cdot\boldsymbol{q})^n f\left(p^2\right)&=\frac{2}{(4\pi)^{\frac{d-1}{2}}\Gamma\left(\frac{d-1}{2}\right)}\int_{-\infty}^{\infty}\frac{dp_\parallel}{2\pi}\int_0^\infty dp_\perp\,p_\perp^{d-2}(p_\parallel q)^n f\left(p_\parallel^2+p_\perp^2\right)\\
&=\frac{4}{(4\pi)^{\frac{d+1}{2}}\Gamma\left(\frac{d-1}{2}\right)}\int_0^\infty dp\int_{-1}^1dx\frac{p}{\sqrt{1-x^2}}\left(\sqrt{1-x^2}\,p\right)^{d-2}(xpq)^n f\left(p^2\right)\\
&=\frac{4}{(4\pi)^{\frac{d+1}{2}}\Gamma\left(\frac{d-1}{2}\right)}\int_0^\infty dp\int_0^1dx\,(1-x)^{\frac{d-3}{2}}x^{\frac{n-1}{2}}p^{d-1+n}q^n f\left(p^2\right)\\
&=\frac{\Gamma\left(\frac{n+1}{2}\right)\Gamma\left(\frac{d}{2}\right)}{\sqrt{\pi}\,\Gamma\left(\frac{d+n}{2}\right)}\int_p p^nq^n f\left(p^2\right)=\frac{\Gamma(n)\Gamma\left(\frac{d}{2}\right)}{2^{n-1}\Gamma\left(\frac{n}{2}\right)\Gamma\left(\frac{d+n}{2}\right)}\int_p p^nq^n f\left(p^2\right)\,,
\end{aligned} \tag{B.115}$$

if n is even, or 0 if it is odd. Then the expanded numerator consists only of a sum of powers of p^2, m_D^2, and $(x\boldsymbol{k}+(1-x)\boldsymbol{q})^2$, the last of which can be reexpressed as

$$(x\boldsymbol{k}+(1-x)\boldsymbol{q})^2=x(k^2+m_D^2)-x(1-x)(\boldsymbol{k}-\boldsymbol{q})^2+(1-x)(q^2+m_D^2)-m_D^2\,. \tag{B.116}$$

[1] As a check that our programs are running correctly we have calculated all the integrals given in the appendix of [37] and reproduced their results.

The p and x integrations now all have the form

$$\begin{aligned}
&\int_0^1 dx \int_p \frac{x^{\alpha-1}(1-x)^{\beta-1}p^{2\gamma}}{\left(p^2+x(1-x)(\boldsymbol{k}-\boldsymbol{q})^2\right)^\delta} \\
&= \frac{\Gamma\left(\delta-\gamma-\frac{d}{2}\right)\Gamma\left(\frac{d}{2}+\gamma\right)}{(4\pi)^{\frac{d}{2}}\Gamma(\delta)\Gamma\left(\frac{d}{2}\right)} \int_0^1 dx\, \frac{x^{\alpha+\gamma+\frac{d}{2}-\delta-1}(1-x)^{\beta+\gamma+\frac{d}{2}-\delta-1}}{\left((\boldsymbol{k}-\boldsymbol{q})^2\right)^{\delta-\gamma-\frac{d}{2}}} \\
&= \frac{\Gamma\left(\delta-\gamma-\frac{d}{2}\right)\Gamma\left(\frac{d}{2}+\gamma\right)\Gamma\left(\alpha+\gamma+\frac{d}{2}-\delta\right)\Gamma\left(\beta+\gamma+\frac{d}{2}-\delta\right)\mu^{3-d}}{(4\pi)^{\frac{d}{2}}\Gamma(\delta)\Gamma\left(\frac{d}{2}\right)\Gamma(\alpha+\beta+2\gamma+d-2\delta)\left((\boldsymbol{k}-\boldsymbol{q})^2\right)^{\delta-\gamma-\frac{d}{2}}}\,. \qquad \text{(B.117)}
\end{aligned}$$

We see that the remaining loop momenta $\boldsymbol{k}$ and $\boldsymbol{q}$ appear only in the combination $(\boldsymbol{k}-\boldsymbol{q})^2$ in the denominator, which can be combined with the term $\left((\boldsymbol{k}-\boldsymbol{q})^2\right)^{i_3}$ from the original B_M integral. The numerator has already been expressed through terms appearing in the denominator, which can also be combined so that we have a sum of integrals of the form

$$\begin{aligned}
&\int_k \int_q \frac{1}{\left((\boldsymbol{k}-\boldsymbol{q})^2\right)^\alpha (k^2+m_D)^\beta (q^2+m_D^2)^\gamma} \\
&= \frac{\Gamma(\alpha+\beta)}{\Gamma(\alpha)\Gamma(\beta)} \int_0^1 dx \int_k \int_q \frac{(1-x)^{\alpha-1}x^{\beta-1}}{(k^2+x(1-x)q^2+xm_D^2)^{\alpha+\beta}(q^2+m_D^2)^\gamma} \\
&= \frac{\Gamma\left(\alpha+\beta-\frac{d}{2}\right)}{(4\pi)^{\frac{d}{2}}\Gamma(\alpha)\Gamma(\beta)} \int_q \frac{(1-x)^{\alpha-1}x^{\frac{d}{2}-\alpha-1}\mu^{3-d}}{((1-x)q^2+m_D^2)^{\alpha+\beta-\frac{d}{2}}(q^2+m_D^2)^\gamma} \\
&= \frac{\Gamma\left(\alpha+\beta+\gamma-\frac{d}{2}\right)}{(4\pi)^{\frac{d}{2}}\Gamma(\alpha)\Gamma(\beta)\Gamma(\gamma)} \int_0^1 dx \int_0^1 dy \int_q \frac{(1-x)^{\alpha-1}x^{\frac{d}{2}-\alpha-1}(1-y)^{\gamma-1}y^{\alpha+\beta-\frac{d}{2}-1}\mu^{3-d}}{\left((1-xy)q^2+m_D^2\right)^{\alpha+\beta+\gamma-\frac{d}{2}}} \\
&= \frac{\Gamma(\alpha+\beta+\gamma-d)}{(4\pi)^d\Gamma(\alpha)\Gamma(\beta)\Gamma(\gamma)} \int_0^1 dx \int_0^1 dy\, \frac{(1-x)^{\alpha-1}x^{\frac{d}{2}-\alpha-1}(1-y)^{\gamma-1}y^{\alpha+\beta-\frac{d}{2}-1}\mu^{6-2d}}{(1-xy)^{\frac{d}{2}}m_D^{2\alpha+2\beta+2\gamma-2d}}\,. \qquad \text{(B.118)}
\end{aligned}$$

If we now perform the substitution

$$z = \frac{(1-y)x}{1-xy}\,, \qquad 1-z = \frac{1-x}{1-xy}\,, \qquad dz = \frac{1-y}{(1-xy)^2}dx\,, \qquad \text{(B.119)}$$

where for x from 0 to 1 also z ranges from 0 to 1 independently of y, then the two Feynman parameter integrations decouple:

$$\begin{aligned}
&\int_k \int_q \frac{1}{\left((\boldsymbol{k}-\boldsymbol{q})^2\right)^\alpha (k^2+m_D)^\beta (q^2+m_D^2)^\gamma} \\
&= \frac{\Gamma(\alpha+\beta+\gamma-d)}{(4\pi)^d\Gamma(\alpha)\Gamma(\beta)\Gamma(\gamma)} \int_0^1 dy \int_0^1 dz\, \frac{(1-z)^{\alpha-1}z^{\frac{d}{2}-\alpha-1}(1-y)^{\alpha+\gamma-\frac{d}{2}-1}y^{\alpha+\beta-\frac{d}{2}-1}\mu^{6-2d}}{m_D^{2\alpha+2\beta+2\gamma-2d}} \\
&= \frac{\Gamma(\alpha+\beta+\gamma-d)\Gamma\left(\frac{d}{2}-\alpha\right)\Gamma\left(\alpha+\beta-\frac{d}{2}\right)\Gamma\left(\alpha+\gamma-\frac{d}{2}\right)\mu^{6-2d}}{(4\pi)^d\Gamma(\beta)\Gamma(\gamma)\Gamma\left(\frac{d}{2}\right)\Gamma(2\alpha+\beta+\gamma-d)m_D^{2\alpha+2\beta+2\gamma-2d}}\,. \qquad \text{(B.120)}
\end{aligned}$$

In this way all B_M integrals with a zero or negative index $i_4, \ldots, i_6$ can be expressed through gamma functions.

The final missing integral $B_N(0,0,1,1,1,1)$ is more complicated and we are not aware of a solution for general d, so we will show how to calculate it to $\mathcal{O}(\epsilon^0)$. In fact, it is easier to

calculate $B_N(0,0,2,1,1,2)$, because unlike $B_N(0,0,1,1,1,1)$ this integral is finite. Through the algorithm described above we get the relation

$$B_N(0,0,2,1,1,2) = \frac{(3d-8)(3d-10)(d-3)}{64(d-4)m^4} B_N(0,0,1,1,1,1) + \frac{(d-2)^3\Gamma\left(1-\frac{d}{2}\right)^3 \mu^{3d-9}}{32(d-4)(4\pi)^{\frac{3d}{2}} m_D^{3d-6}} \,. \tag{B.121}$$

We see that, because of the coefficient $(d-3)$, in order to get $B_N(0,0,1,1,1,1)$ to $\mathcal{O}(\epsilon^0)$ we need to calculate $B_N(0,0,2,1,1,2)$ to $\mathcal{O}(\epsilon^1)$. After performing the shift $\boldsymbol{p} \to \boldsymbol{p} - \boldsymbol{k}$ the $\boldsymbol{p}$ and $\boldsymbol{k}$ integrations are identical:

$$\begin{aligned}
B_N(0,0,2,1,1,2) &= \int_k \int_p \int_q \frac{1}{\left(p^2+m_D^2\right)^2 \left((\boldsymbol{k}+\boldsymbol{q})^2+m_D^2\right) \left((\boldsymbol{p}+\boldsymbol{q})^2+m_D^2\right) \left(k^2+m_D^2\right)^2} \\
&= \int_q \left(\int_k \frac{1}{\left((\boldsymbol{k}+\boldsymbol{q})^2+m_D^2\right)\left(k^2+m_D^2\right)^2} \right)^2 \\
&= \int_q \left(\int_0^1 dx \int_k \frac{2x}{\left(k^2+x(1-x)q^2+m_D^2\right)^3} \right)^2 \\
&= \int_q \left(\frac{\Gamma\left(3-\frac{d}{2}\right)}{(4\pi)^{\frac{d}{2}}} \int_0^1 dx \frac{x\,\mu^{3-d}}{\left(x(1-x)q^2+m_D^2\right)^{3-\frac{d}{2}}} \right)^2 \\
&= \int_0^\infty dq\, \frac{2q^{d-1}\mu^{3-d}}{(4\pi)^{\frac{d}{2}}\Gamma\left(\frac{d}{2}\right)} \left(\frac{1}{8\pi m_D \left(q^2+4m_D^2\right)} \left(1 - \gamma_E\,\epsilon + \ln\frac{\mu^2\pi}{m_D^2}\,\epsilon\right) + \frac{\tan^{-1}\frac{q}{2m_D}}{2\pi q\left(q^2+4m_D^2\right)}\,\epsilon \right)^2 \\
&= \int_0^\infty dq\, \frac{q^2}{128\pi^4 m_D^2 \left(q^2+m_D^2\right)^2} \left(1 + 2\epsilon - 3\gamma_E\,\epsilon + \ln\frac{\mu^6\pi^3}{m_D^4 q^2}\,\epsilon + \frac{8m_D}{q}\tan^{-1}\frac{q}{2m_D}\,\epsilon\right) \\
&= \frac{1}{16(4\pi)^3 m_D^3} \left(1 + 2\epsilon - 3\gamma_E\,\epsilon - 2\ln 2\,\epsilon + 3\ln\frac{\mu^2\pi}{m_D^2}\,\epsilon\right) + \mathcal{O}\left(\epsilon^2\right) \,.
\end{aligned} \tag{B.122}$$

From these two results we obtain

$$B_N(0,0,1,1,1,1) = \frac{m_D}{(4\pi)^3}\left(-\frac{1}{\epsilon} - 8 + 3\gamma_E + 4\ln 2 - 3\ln\frac{\mu^2\pi}{m_D^2}\right) + \mathcal{O}(\epsilon)\,. \tag{B.123}$$

B.6 Color Coefficients of the Unconnected Three-Gluon Diagrams

All unconnected three-gluon diagrams are given in Fig. B.6. The standard color coefficients are labeled $\mathcal{C}_{ij}$ according to the caption, while the coefficients that appear in the logarithm are called $\widetilde{\mathcal{C}}_{ij}$. These indices bear no relation to and should not be confused with the color indices used for the coefficients of the uncontracted diagrams appearing in the calculation for the Polyakov loop correlator.

The most straightforward prescription to calculate the coefficients in the logarithm comes from the replica trick [144, 145]. First one attaches an index from 1 to n to each gluon, where n is some integer, then rearranges each diagram such that gluons with a higher index are moved along the Polyakov loop contour to the right of gluons with a lower index, while gluons

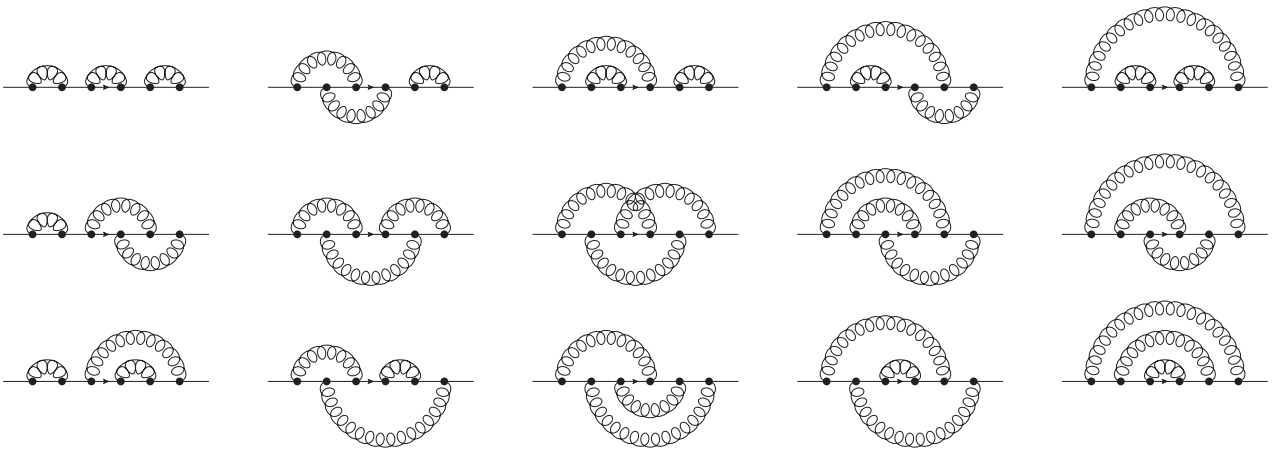

Figure B.6: All unconnected three-gluon diagrams. The corresponding color coefficients are labeled $\mathcal{C}_{ij}$, where i denotes the row and j the column in which the diagram is listed.

with the same index keep their current configuration. After summing over all combinations of indices one expands in n and takes the coefficient of the linear term.

Here we have three different possibilities: either all three gluons have a different index, two have the same but the third index is different, or all three indices are the same. It is then only a matter of combinatorics to count the number of possible index combinations. For three different indices there are $n(n-1)(n-2)$ possibilities, while when all three are the same there are n. When only two are the same there are $n(n-1)$ index combinations and 3 ways to choose the one gluon that has a different index. Rearranging the gluons according to their index number always gives $\mathcal{C}_{11} = C_R^3$ for three different indices and the standard (i.e., QCD) color coefficient when all indices are the same. When only two are the same, then in half of the index combinations the single index will be smaller then the double index and larger for the other half, but in both cases the color coefficient is the same, so we do not have to differentiate between them. The 3 different ways to choose the single index gluon may or may not give different color coefficients after rearranging the gluons according to their indices.

The standard color factors are

$$
\begin{aligned}
&\mathcal{C}_{11} = C_R^3\,, && \mathcal{C}_{21} = C_R^2\left(C_R - \frac{1}{2}N\right)\,, && \mathcal{C}_{31} = C_R^3\,,\\
&\mathcal{C}_{12} = C_R^2\left(C_R - \frac{1}{2}N\right)\,, && \mathcal{C}_{22} = C_R\left(C_R - \frac{1}{2}N\right)^2\,, && \mathcal{C}_{32} = C_R^2\left(C_R - \frac{1}{2}N\right)\,,\\
&\mathcal{C}_{13} = C_R^3\,, && \mathcal{C}_{23} = C_R\left(C_R - \frac{1}{2}N\right)(C_R - N)\,, && \mathcal{C}_{33} = C_R\left(C_R - \frac{1}{2}N\right)^2\,,\\
&\mathcal{C}_{14} = C_R^2\left(C_R - \frac{1}{2}N\right)\,, && \mathcal{C}_{24} = C_R\left(C_R - \frac{1}{2}N\right)^2\,, && \mathcal{C}_{34} = C_R^2\left(C_R - \frac{1}{2}N\right)\,,\\
&\mathcal{C}_{15} = C_R^3\,, && \mathcal{C}_{25} = C_R^2\left(C_R - \frac{1}{2}N\right)\,, && \mathcal{C}_{35} = C_R^3\,.
\end{aligned}
\tag{B.124}
$$

Then we can calculate the coefficients in the logarithm:

$$\widetilde{\mathcal{C}}_{11} = n\mathcal{C}_{11} + 3n(n-1)\mathcal{C}_{11} + n(n-1)(n-2)\mathcal{C}_{11}\Big|_{\mathcal{O}(n)} = 0\,, \tag{B.125}$$

$$\widetilde{\mathcal{C}}_{12} = n\mathcal{C}_{12} + 2n(n-1)\mathcal{C}_{11} + n(n-1)\mathcal{C}_{12} + n(n-1)(n-2)\mathcal{C}_{11}\Big|_{\mathcal{O}(n)} = 0\,, \tag{B.126}$$

$$\widetilde{\mathcal{C}}_{13} = n\mathcal{C}_{13} + 2n(n-1)\mathcal{C}_{11} + n(n-1)\mathcal{C}_{13} + n(n-1)(n-2)\mathcal{C}_{11}\Big|_{\mathcal{O}(n)} = 0\,, \tag{B.127}$$

$$\begin{aligned}\widetilde{\mathcal{C}}_{14} &= n\mathcal{C}_{14} + n(n-1)\mathcal{C}_{11} + n(n-1)\mathcal{C}_{12} + n(n-1)\mathcal{C}_{13} + n(n-1)(n-2)\mathcal{C}_{11}\Big|_{\mathcal{O}(n)} \\ &= \mathcal{C}_{11} - \mathcal{C}_{12} - \mathcal{C}_{13} + \mathcal{C}_{14} = 0\,,\end{aligned} \tag{B.128}$$

$$\begin{aligned}\widetilde{\mathcal{C}}_{15} &= n\mathcal{C}_{15} + n(n-1)\mathcal{C}_{11} + 2n(n-1)\mathcal{C}_{13} + n(n-1)(n-2)\mathcal{C}_{11}\Big|_{\mathcal{O}(n)} \\ &= \mathcal{C}_{11} - 2\mathcal{C}_{13} + \mathcal{C}_{15} = 0\,,\end{aligned} \tag{B.129}$$

$$\widetilde{\mathcal{C}}_{21} = n\mathcal{C}_{21} + 2n(n-1)\mathcal{C}_{11} + n(n-1)\mathcal{C}_{21} + n(n-1)(n-2)\mathcal{C}_{11}\Big|_{\mathcal{O}(n)} = 0\,, \tag{B.130}$$

$$\begin{aligned}\widetilde{\mathcal{C}}_{22} &= n\mathcal{C}_{22} + 2n(n-1)\mathcal{C}_{21} + n(n-1)\mathcal{C}_{11} + n(n-1)(n-2)\mathcal{C}_{11}\Big|_{\mathcal{O}(n)} \\ &= \mathcal{C}_{22} - 2\mathcal{C}_{21} + \mathcal{C}_{11} = \frac{1}{4}C_R N^2\,,\end{aligned} \tag{B.131}$$

$$\begin{aligned}\widetilde{\mathcal{C}}_{23} &= n\mathcal{C}_{23} + 3n(n-1)\mathcal{C}_{21} + n(n-1)(n-2)\mathcal{C}_{11}\Big|_{\mathcal{O}(n)} \\ &= \mathcal{C}_{23} - 3\mathcal{C}_{21} + 2\mathcal{C}_{11} = \frac{1}{2}C_R N^2\,,\end{aligned} \tag{B.132}$$

$$\begin{aligned}\widetilde{\mathcal{C}}_{24} &= n\mathcal{C}_{24} + 2n(n-1)\mathcal{C}_{21} + n(n-1)\mathcal{C}_{31} + n(n-1)(n-2)\mathcal{C}_{11}\Big|_{\mathcal{O}(n)} \\ &= \mathcal{C}_{24} - 2\mathcal{C}_{21} - \mathcal{C}_{31} + 2\mathcal{C}_{11} = \frac{1}{4}C_R N^2\,,\end{aligned} \tag{B.133}$$

$$\begin{aligned}\widetilde{\mathcal{C}}_{25} &= n\mathcal{C}_{25} + n(n-1)\mathcal{C}_{21} + 2n(n-1)\mathcal{C}_{31} + n(n-1)(n-2)\mathcal{C}_{11}\Big|_{\mathcal{O}(n)} \\ &= \mathcal{C}_{25} - \mathcal{C}_{21} - 2\mathcal{C}_{31} + 2\mathcal{C}_{11} = 0\,,\end{aligned} \tag{B.134}$$

$$\widetilde{\mathcal{C}}_{31} = n\mathcal{C}_{31} + 2n(n-1)\mathcal{C}_{11} + n(n-1)\mathcal{C}_{31} + n(n-1)(n-2)\mathcal{C}_{11}\Big|_{\mathcal{O}(n)} = 0\,, \tag{B.135}$$

$$\begin{aligned}\widetilde{\mathcal{C}}_{32} &= n\mathcal{C}_{32} + n(n-1)\mathcal{C}_{11} + n(n-1)\mathcal{C}_{21} + n(n-1)\mathcal{C}_{31} + n(n-1)(n-2)\mathcal{C}_{11}\Big|_{\mathcal{O}(n)} \\ &= \mathcal{C}_{32} - \mathcal{C}_{21} - \mathcal{C}_{31} + \mathcal{C}_{11} = 0\,,\end{aligned} \tag{B.136}$$

$$\begin{aligned}\widetilde{\mathcal{C}}_{33} &= n\mathcal{C}_{33} + 2n(n-1)\mathcal{C}_{21} + n(n-1)\mathcal{C}_{31} + n(n-1)(n-2)\mathcal{C}_{11}\Big|_{\mathcal{O}(n)} \\ &= \mathcal{C}_{33} - 2\mathcal{C}_{21} - \mathcal{C}_{31} + 2\mathcal{C}_{11} = \frac{1}{4}C_R N^2\,,\end{aligned} \tag{B.137}$$

$$\begin{aligned}\widetilde{\mathcal{C}}_{34} &= n\mathcal{C}_{34} + n(n-1)\mathcal{C}_{21} + 2n(n-1)\mathcal{C}_{31} + n(n-1)(n-2)\mathcal{C}_{11}\Big|_{\mathcal{O}(n)} \\ &= \mathcal{C}_{34} - \mathcal{C}_{21} - 2\mathcal{C}_{31} + 2\mathcal{C}_{11} = 0\,,\end{aligned} \tag{B.138}$$

$$\begin{aligned}\widetilde{\mathcal{C}}_{35} &= n\mathcal{C}_{35} + 3n(n-1)\mathcal{C}_{31} + n(n-1)(n-2)\mathcal{C}_{11}\Big|_{\mathcal{O}(n)} \\ &= \mathcal{C}_{35} - 3\mathcal{C}_{31} + 2\mathcal{C}_{11} = 0\,.\end{aligned} \tag{B.139}$$

Here we see the general property confirmed that only two-particle irreducible diagrams

appear in the logarithm. This means that the color coefficient in the logarithm vanishes for any diagram where one can cut the (closed) Polyakov loop contour in two points such that there are no gluons connecting from one segment of the contour to the other. These are the so-called two-particle reducible diagrams, the diagrams where this is not possible are called two-particle irreducible. Here the considerable reduction in the number of diagrams is even more apparent than in the two-gluon diagrams: out of 15 unconnected three-gluon diagrams only 4 survive in the logarithm.

We also see that all higher power terms of C_R are canceled; only the linear term remains and only the two-particle irreducible diagrams have a linear term. This is in accordance with the theorem shown in [145] that the color coefficients in the logarithm all correspond to those of fully connected diagrams. The coefficients of fully connected diagrams depend only linearly on C_R or the $C_R^{(n)}$. So the only terms that can break Casimir scaling come from the $C_R^{(n)}$, see Eq. (4.45).

B.7 Unexpanded Result for D_I

In Ref. [125], an unexpanded result for the contributions to diagram D_I from the scales $1/r$ and πT has been presented. This result is also valid when $1/r \sim \pi T$, and when it is expanded for small r, then one obtains the expression given in the main section. We add the contribution from the scale m_D, for which we still assume $\pi T \gg m_D$.

$$\begin{aligned}
D_I = {} & \frac{\alpha_s}{rT}\left\{1+\frac{\alpha_s}{4\pi}\left[\frac{11N}{3}+\frac{2n_f}{3}(1-4\ln 2)+2\beta_0\left(\gamma_E+\log\frac{\mu}{4\pi T}\right)\right]\right\} \\
& + N\alpha_s^2\left(-\frac{1}{24r^2T^2}+\frac{1}{r\pi T}\int_1^\infty dx\,\left(-1+\frac{1}{x^2}-\frac{1}{2x^4}\right)\log\left(1-\exp\left[-4r\pi Tx\right]\right)\right) \\
& + \alpha_s^2 n_f\frac{1}{2r\pi T}\int_1^\infty dx\,\left(\frac{1}{x^2}-\frac{1}{x^4}\right)\log\frac{1+\exp\left[-2r\pi Tx\right]}{1-\exp\left[-2r\pi Tx\right]}+\left(\frac{2N}{3}+\frac{n_f}{3}\right)\alpha_s^2 r\pi T \\
& - \frac{\alpha_s m_D}{T}+2N\alpha_s^2\left[1-\gamma_E-\ln 2-\ln rm_D\right]+\frac{(N^2-1)n_f}{4N}\frac{\alpha_s^3 T}{m_D} \\
& - \frac{3\alpha_s^2 m_D}{8\pi T}\left[3N+\frac{2}{3}n_f(1-4\ln 2)+2\beta_0\left(\gamma_E+\ln\frac{\mu}{4\pi T}\right)\right] \\
& + \frac{N^2\alpha_s^3 T}{m_D}\left[\frac{89}{24}+\frac{\pi^2}{6}-\frac{11}{6}\ln 2\right]-\frac{\alpha_s r^2 m_D^3}{6T}+\mathcal{O}\left(\alpha_s^3\right)\,. \qquad \text{(B.140)}
\end{aligned}$$

We see that here the natural scale for α_s seems to be $4\pi T$ also for the leading $1/rT$ term, which makes sense considering that this result is appropriate for $1/r \sim \pi T$. For $1/r \gg \pi T$ the expansion of the integrals yields some nonanalytic terms that cancel the temperature dependence in the logarithms of the first line and change the natural scale for α_s back to $1/r$.

In that paper, also a result valid for $r \sim m_D$ was given. However, this is only available at $\mathcal{O}(g^4)$, and it is not possible to infer the next order from the Polyakov loop at $\mathcal{O}(g^5)$ like for $r \gg m_D$ (because then it is not allowed to expand $\exp[i\boldsymbol{k}\cdot\boldsymbol{r}]$ in the scale m_D contribution to D_I), so we do not include this result here in order to consistently work at $\mathcal{O}(g^5)$.

B.8 The H-Shaped Diagrams

Using the same labels for the gluon momenta as in the main section, the $\mathcal{O}(\alpha_s^3)$ contribution from the H-shaped diagrams in Eq. (4.102) is given by:

$$D_H = \frac{(ig)^6}{2T}\int_k\int_p\int_q \frac{-4\left((\boldsymbol{k}\cdot\boldsymbol{p})\boldsymbol{q}^2-(\boldsymbol{k}\cdot\boldsymbol{q})(\boldsymbol{p}\cdot\boldsymbol{q})\right)e^{i\boldsymbol{k}\cdot\boldsymbol{r}}e^{i\boldsymbol{p}\cdot\boldsymbol{r}}}{\boldsymbol{k}^2(\boldsymbol{k}-\boldsymbol{q})^2\left(\boldsymbol{q}^2\right)^2(\boldsymbol{p}+\boldsymbol{q})^2\boldsymbol{p}^2}\,. \tag{B.141}$$

We shift the momenta $\boldsymbol{k}\to\boldsymbol{k}-\boldsymbol{p}$ and $\boldsymbol{q}\to\boldsymbol{q}-\boldsymbol{p}$. Then the integral contains only one momentum in the exponential:

$$D_H = \frac{2g^6}{T}\int_k\int_p\int_q \frac{(k-p)_i\left(\delta_{ij}(\boldsymbol{q}-\boldsymbol{p})^2-(q-p)_i(q-p)_j\right)p_j e^{i\boldsymbol{k}\cdot\boldsymbol{r}}}{(\boldsymbol{k}-\boldsymbol{p})^2(\boldsymbol{k}-\boldsymbol{q})^2\left((\boldsymbol{q}-\boldsymbol{p})^2\right)^2\boldsymbol{q}^2\boldsymbol{p}^2}\,. \tag{B.142}$$

The p and q integrations can be put into the form of general k-dependent integrals:

$$I_k(n_1,n_2,n_3,n_4,n_5)\equiv\int_p\int_q\frac{1}{\left((\boldsymbol{k}-\boldsymbol{p})^2\right)^{n_1}\left((\boldsymbol{k}-\boldsymbol{q})^2\right)^{n_2}\left((\boldsymbol{p}-\boldsymbol{q})^2\right)^{n_3}\left(\boldsymbol{p}^2\right)^{n_4}\left(\boldsymbol{q}^2\right)^{n_5}}\,. \tag{B.143}$$

Through redefinitions of the integration momenta one can show the following identities:

$$I_k(n_1,n_2,n_3,n_4,n_5)=I_k(n_2,n_1,n_3,n_5,n_4)=I_k(n_4,n_5,n_3,n_1,n_2)=I_k(n_5,n_4,n_3,n_2,n_1)\,. \tag{B.144}$$

Reexpressing the numerator through terms that can be canceled against terms in the denominator and using these identities, we get:

$$\begin{aligned}D_H = \frac{g^6}{T}\int_k e^{i\boldsymbol{k}\cdot\boldsymbol{r}}\Big[&I_k(1,0,2,1,0)-I_k(1,0,2,0,1)+\frac{1}{2}I_k(1,1,0,1,1)\\&-2I_k(1,0,1,1,1)+k^2I_k(1,1,1,1,1)\Big]\,.\end{aligned} \tag{B.145}$$

In the first integral of this expression, the q integration is scaleless, so $I_k(1,0,2,1,0)=0$. The other integrals except for the last can all be calculated with standard methods. In order to simplify the last integral, we can use integration-by-parts relations. In order to obtain these, we insert $\boldsymbol{\nabla}_p\cdot\boldsymbol{p}$ or $\boldsymbol{\nabla}_p\cdot\boldsymbol{q}$ into the general expression for $I_k(n_1,n_2,n_3,n_4,n_5)$. Because it is an integral over a total derivative, each of these expressions vanishes, but if one calculates the derivatives explicitly, then one can also express it through other integrals of this type. Other relations can also be obtained, but in this case those two are sufficient.

$$\begin{aligned}0=&\int_p\int_q(\boldsymbol{\nabla}_p\cdot\boldsymbol{p})\frac{1}{\left((\boldsymbol{k}-\boldsymbol{p})^2\right)^{n_1}\left((\boldsymbol{k}-\boldsymbol{q})^2\right)^{n_2}\left((\boldsymbol{p}-\boldsymbol{q})^2\right)^{n_3}\left(\boldsymbol{p}^2\right)^{n_4}\left(\boldsymbol{q}^2\right)^{n_5}}\\
=&-n_1I_k(n_1+1,n_2,n_3,n_4-1,n_5)+n_1k^2I_k(n_1+1,n_2,n_3,n_4,n_5)\\
&-n_3I_k(n_1,n_2,n_3+1,n_4-1,n_5)+n_3I_k(n_1,n_2,n_3+1,n_4,n_5-1)\\
&+(d-n_1-n_3-2n_4)I_k(n_1,n_2,n_3,n_4,n_5)\,,\end{aligned} \tag{B.146}$$

$$\begin{aligned}0=&\int_p\int_q(\boldsymbol{\nabla}_p\cdot\boldsymbol{q})\frac{1}{\left((\boldsymbol{k}-\boldsymbol{p})^2\right)^{n_1}\left((\boldsymbol{k}-\boldsymbol{q})^2\right)^{n_2}\left((\boldsymbol{p}-\boldsymbol{q})^2\right)^{n_3}\left(\boldsymbol{p}^2\right)^{n_4}\left(\boldsymbol{q}^2\right)^{n_5}}\\
=&-n_1I_k(n_1+1,n_2-1,n_3,n_4,n_5)+n_1I_k(n_1+1,n_2,n_3-1,n_4,n_5)\\
&-n_1I_k(n_1+1,n_2,n_3,n_4-1,n_5)+n_1k^2I_k(n_1+1,n_2,n_3,n_4,n_5)\\
&-n_3I_k(n_1,n_2,n_3+1,n_4-1,n_5)+n_3I_k(n_1,n_2,n_3+1,n_4,n_5-1)\\
&+n_4I_k(n_1,n_2,n_3-1,n_4+1,n_5)-n_4I_k(n_1,n_2,n_3,n_4+1,n_5-1)\\
&+(n_3-n_4)I_k(n_1,n_2,n_3,n_4,n_5)\,.\end{aligned} \tag{B.147}$$

In both expressions one can write $I_k(n_1, n_2, n_3, n_4, n_5)$ in terms of integrals where one index is raised and one is lowered. The only exception to this are the two integrals with a k^2 coefficient. But if we subtract the second relation from the first, then this term vanishes:

$$\begin{aligned} 0 = &(d - n_1 - 2n_3 - n_4) I_k(n_1, n_2, n_3, n_4, n_5) \\ &+ n_1 I_k(n_1 + 1, n_2 - 1, n_3, n_4, n_5) - n_1 I_k(n_1 + 1, n_2, n_3 - 1, n_4, n_5) \\ &- n_4 I_k(n_1, n_2, n_3 - 1, n_4 + 1, n_5) + n_4 I_k(n_1, n_2, n_3, n_4 + 1, n_5 - 1)\,. \end{aligned} \tag{B.148}$$

This relation can be used repeatedly to lower either the index n_2, n_3, or n_5 to 0, at which point the integral is straightforward to calculate. In the case of $I_k(1, 1, 1, 1, 1)$ one iteration is enough:

$$I_k(1, 1, 1, 1, 1) = \frac{2}{4 - d} I_k(2, 0, 1, 1, 1) - \frac{2}{4 - d} I_k(1, 2, 0, 1, 1)\,, \tag{B.149}$$

where we have used the symmetry relations again.

We now give the results of the integrals when one index is 0. Because of the symmetry relations we only need to consider two cases:

$$\begin{aligned} I_k(n_1, 0, n_3, n_4, n_5) &= \int_p \frac{1}{((\boldsymbol{k} - \boldsymbol{p})^2)^{n_1} (\boldsymbol{p}^2)^{n_4}} \int_q \frac{1}{((\boldsymbol{p} - \boldsymbol{q})^2)^{n_3} (\boldsymbol{q}^2)^{n_5}} \\ &= \int_p \frac{1}{((\boldsymbol{k} - \boldsymbol{p})^2)^{n_1} (\boldsymbol{p}^2)^{n_4}} \frac{\mu^{d-3} \Gamma\left(n_3 + n_5 - \frac{d}{2}\right) \Gamma\left(\frac{d}{2} - n_3\right) \Gamma\left(\frac{d}{2} - n_5\right)}{(4\pi)^{d/2} (\boldsymbol{p}^2)^{n_3 + n_5 - d/2} \Gamma(n_3) \Gamma(n_5) \Gamma(d - n_3 - n_5)} \\ &= \frac{(\boldsymbol{k}^2)^{d - n_1 - n_3 - n_4 - n_5} \mu^{6-2d}}{(4\pi)^d} \frac{\Gamma\left(\frac{d}{2} - n_1\right) \Gamma\left(\frac{d}{2} - n_3\right) \Gamma\left(\frac{d}{2} - n_5\right)}{\Gamma(n_1) \Gamma(n_3) \Gamma(n_5)} \\ &\quad \times \frac{\Gamma\left(n_3 + n_5 - \frac{d}{2}\right) \Gamma(d - n_3 - n_4 - n_5) \Gamma(n_1 + n_3 + n_4 + n_5 - d)}{\Gamma(d - n_3 - n_5) \Gamma\left(n_3 + n_4 + n_5 - \frac{d}{2}\right) \Gamma\left(\frac{3d}{2} - n_1 - n_3 - n_4 - n_5\right)}\,, \end{aligned} \tag{B.150}$$

$$\begin{aligned} I_k(n_1, n_2, 0, n_4, n_5) &= \int_p \frac{1}{((\boldsymbol{k} - \boldsymbol{p})^2)^{n_1} (\boldsymbol{p}^2)^{n_4}} \int_q \frac{1}{((\boldsymbol{k} - \boldsymbol{q})^2)^{n_2} (\boldsymbol{q}^2)^{n_5}} \\ &= \frac{\mu^{3-d} \Gamma\left(n_1 + n_4 - \frac{d}{2}\right) \Gamma\left(\frac{d}{2} - n_1\right) \Gamma\left(\frac{d}{2} - n_4\right)}{(4\pi)^{d/2} (\boldsymbol{k}^2)^{n_1 + n_4 - d/2} \Gamma(n_1) \Gamma(n_4) \Gamma(d - n_1 - n_4)} \\ &\quad \times \frac{\mu^{3-d} \Gamma\left(n_2 + n_5 - \frac{d}{2}\right) \Gamma\left(\frac{d}{2} - n_2\right) \Gamma\left(\frac{d}{2} - n_5\right)}{(4\pi)^{d/2} (\boldsymbol{k}^2)^{n_2 + n_5 - d/2} \Gamma(n_2) \Gamma(n_5) \Gamma(d - n_2 - n_5)} \\ &= \frac{(\boldsymbol{k}^2)^{d - n_1 - n_2 - n_4 - n_5} \mu^{6-d}}{(4\pi)^d} \frac{\Gamma\left(\frac{d}{2} - n_1\right) \Gamma\left(\frac{d}{2} - n_2\right) \Gamma\left(\frac{d}{2} - n_4\right) \Gamma\left(\frac{d}{2} - n_5\right)}{\Gamma(n_1) \Gamma(n_2) \Gamma(n_4) \Gamma(n_5)} \\ &\quad \times \frac{\Gamma\left(n_1 + n_4 - \frac{d}{2}\right) \Gamma\left(n_2 + n_5 - \frac{d}{2}\right)}{\Gamma(d - n_1 - n_4) \Gamma(d - n_2 - n_5)}\,. \end{aligned} \tag{B.151}$$

Then we have:

$$\begin{aligned} D_H = \frac{g^6}{T} \int_k e^{i\boldsymbol{k}\cdot\boldsymbol{r}} \Big[&- I_k(1, 0, 2, 0, 1) + \frac{1}{2} I_k(1, 1, 0, 1, 1) - 2 I_k(1, 0, 1, 1, 1) \\ &+ \frac{2k^2}{4 - d} I_k(2, 0, 1, 1, 1) - \frac{2k^2}{4 - d} I_k(2, 1, 0, 1, 1) \Big] \end{aligned}$$

$$
\begin{aligned}
&= \frac{g^6}{T}\int_k \frac{e^{i\boldsymbol{k}\cdot\boldsymbol{r}}\mu^{6-2d}}{(4\pi)^d\left(\boldsymbol{k}^2\right)^{4-d}}\left[-\frac{\Gamma^2\left(\frac{d}{2}-1\right)\Gamma\left(\frac{d}{2}-2\right)\Gamma(4-d)}{\Gamma\left(\frac{3d}{2}-4\right)}+\frac{\Gamma^4\left(\frac{d}{2}-1\right)\Gamma^2\left(2-\frac{d}{2}\right)}{2\Gamma^2(d-2)}\right.\\
&\qquad -\frac{2\Gamma^3\left(\frac{d}{2}-1\right)\Gamma\left(2-\frac{d}{2}\right)\Gamma(d-3)\Gamma(4-d)}{\Gamma(d-2)\Gamma\left(3-\frac{d}{2}\right)\Gamma\left(\frac{3d}{2}-4\right)}\\
&\qquad +\frac{2\Gamma^2\left(\frac{d}{2}-1\right)\Gamma\left(\frac{d}{2}-2\right)\Gamma\left(2-\frac{d}{2}\right)\Gamma(d-3)\Gamma(5-d)}{(4-d)\Gamma(d-2)\Gamma\left(3-\frac{d}{2}\right)\Gamma\left(\frac{3d}{2}-5\right)}\\
&\qquad \left.-\frac{2\Gamma^3\left(\frac{d}{2}-1\right)\Gamma\left(\frac{d}{2}-2\right)\Gamma\left(2-\frac{d}{2}\right)\Gamma\left(3-\frac{d}{2}\right)}{(4-d)\Gamma(d-2)\Gamma(d-3)}\right]\\
&= \frac{g^6(\mu r)^{9-3d}}{4^4\pi^{3d/2}rT}\frac{\Gamma\left(\frac{3d}{2}-4\right)}{\Gamma(4-d)}\left[-\frac{2d\Gamma^3\left(\frac{d}{2}-1\right)\Gamma(4-d)}{(4-d)^2\Gamma\left(\frac{3d}{2}-4\right)}+\frac{(3d-8)\Gamma^4\left(\frac{d}{2}-1\right)\Gamma^2\left(2-\frac{d}{2}\right)}{2(4-d)\Gamma^2(d-2)}\right]\\
&= \frac{\alpha_{\mathrm{s}}^3(\mu r)^{9-3d}}{4\pi^{3d/2-3}rT}\left[-\frac{2d}{(4-d)^2}\Gamma^3\left(\tfrac{d}{2}-1\right)+\frac{\Gamma\left(\frac{3d}{2}-3\right)\Gamma^4\left(\frac{d}{2}-1\right)\Gamma^2\left(2-\frac{d}{2}\right)}{\Gamma(5-d)\Gamma^2(d-2)}\right]. \qquad \text{(B.152)}
\end{aligned}
$$

For $d = 3$ this gives:

$$
D_H = \frac{\alpha_{\mathrm{s}}^3}{rT}\left(-\frac{3}{2}+\frac{\pi^2}{8}\right). \qquad \text{(B.153)}
$$

B.9 Relation to Other Forms of Resummation

The results of section 4.7 relate to a calculation published in [167], which we will discuss here. The authors performed a partial resummation of the perturbative series for the Polyakov loop correlator and the singlet free energy correlator (which they call Wilson loop, but since they neglect any contributions involving the spatial Wilson lines, both functions are identical), and they find an unexpected behavior at short distances. While the calculation itself seems to be correct, some of their conclusions may not be.

The resummation includes all diagrams where tree-level gluons of momentum $\sim 1/r$ are exchanged between the two Polyakov lines, while any loop contributions are neglected. As such it is well-defined, but gauge dependent starting from the two-gluon exchange. They choose static gauge $\partial_0 A_0 = 0$ and we believe this to be the source of their unexpected results. Performing the same kind of resummation in Coulomb gauge leads to a different result.

We may use the exponentiated expression of (4.102). In the corresponding discussion, we have already argued that all diagrams where gluons can be separated into a left and a right part by a line connecting the two Polyakov loops such that no gluon crosses this line do not contribute to the exponent. In other words, it is a necessary condition for tree level diagrams of any order to appear in the exponent that the gluons cross. However, for such diagrams the delta function in the tree level propagators renders all diagrams with more than one gluon equal to zero. So the result of this resummation in Coulomb gauge is simply the exponential of D_I.

Comparing this result to the one in static gauge from [167] for SU(2), we have

$$
\mathcal{W}_{SG} \approx (1+z)\cosh(z) + (2+z)\sinh(z) = 1 + 3z + \frac{3}{2}z^2 + \dots \qquad \text{(B.154)}
$$

$$
\mathcal{W}_{CG} \approx \exp(3z) = 1 + 3z + \frac{9}{2}z^2 + \dots \qquad \text{(B.155)}
$$

where $z = g^2/16\pi rT$ and we have expanded for small z. We see that the first order term is the same, but the second order is not. This confirms our previous statement that starting from two-gluon exchange diagrams this resummation is gauge dependent.

But since the Wilson loop is gauge invariant (if the spatial Wilson lines are included), the difference between both gauges must be contained in terms that were neglected in this resummation. The intention of [167] seems to be to resum all terms where $1/rT$ appears to the same power as g^2, in other words terms of order z^n. But in static gauge this is not equivalent to resumming all tree level diagrams. We will show this at $\mathcal{O}(z^2)$.

There are two sources for the discrepancy between both gauges, the first comes from the singular part in the static gauge gluon self-energy. At one-loop order this is given by (see e.g. [126])

$$\Pi_{00}(0, k \gg \pi T)_{sing} = -\frac{Ng^2|\boldsymbol{k}|^3}{192T}\,. \tag{B.156}$$

If we include this contribution in the one-gluon exchange, we get

$$\frac{3g^2}{4T}\int_k \frac{e^{i\boldsymbol{k}\cdot\boldsymbol{r}}}{\boldsymbol{k}^2 + \Pi_{sing}} = \frac{3}{16\pi rT} + \frac{g^4}{(16\pi)^2 r^2 T^2} + \cdots = 3\left(z + \frac{z^2}{3} + \ldots\right)\,. \tag{B.157}$$

So instead of z one should insert $\widetilde{z} = z + z^2/3 + \ldots$ into the resummed expression for $\mathcal{W}_{SG}$ in SU(2) in order not to neglect any contributions of order z^n.

The second source of the discrepancy comes from the neglected contributions of the spatial Wilson lines. There are three diagrams with one gluon between the two Polyakov lines and one gluon connected to the spatial Wilson lines. In one of them the two gluons cross and in the two others they do not. The former has a color factor $-(N^2-1)/4N^2$ and the latter $(N^2-1)^2/4N^2$, and it is straightforward to show that the sum of the three diagrams is equivalent to the crossed diagram survives with a coefficient $-(N^2-1)/4$.

The spatial gluon propagator for large momenta has a term of order $1/T^2$:

$$D_{ij}(k_0 \neq 0, \boldsymbol{k}) = \frac{k_i k_j}{k_0^2\,\boldsymbol{k}^2} + \mathcal{O}\left(\frac{1}{\boldsymbol{k}^2}\right)\,. \tag{B.158}$$

With this the crossed diagram gives a contribution of order z^2 (again with $N = 2$):

$$\begin{aligned}\delta\mathcal{W} &= -\frac{3}{4}\left(\frac{g^2}{T}\int_k \frac{e^{i\boldsymbol{k}\cdot\boldsymbol{r}}}{\boldsymbol{k}^2}\right)\left((ig)^2\int_0^1 ds_1 r_i \int_1^0 ds_2 r_j \sum_K{}' e^{i\boldsymbol{k}\cdot\boldsymbol{r}(s_1-s_2)}\frac{k_i k_j}{k_0^2\,\boldsymbol{k}^2}\right) \\ &= -\frac{3}{4}\left(\frac{g^2}{4\pi rT}\right)\left(-\frac{g^2}{24\pi rT}\right) = 2z^2\,.\end{aligned} \tag{B.159}$$

Coulomb gauge has neither a singular part in the one-loop self-energy nor a term of order $1/T^2$ in the spatial gluon propagator, so the tree-level one-gluon exchange diagram already contains all terms of order z^n. If we put all contributions in static gauge together, we indeed get now the same result as in Coulomb gauge for the SU(2) Wilson loop:

$$\mathcal{W}_{SG} = 1 + 3\left(z + \frac{1}{3}z^2\right) + \frac{3}{2}z^2 + 2z^2 + \mathcal{O}\left(z\alpha, z^3\right) = 1 + 3z + \frac{9}{2}z^2 + \mathcal{O}\left(z\alpha, z^3\right)\,. \tag{B.160}$$

The other part of [167] deals with the large N limit. The result they obtain in this case for the Wilson loop is given by a Bessel function:

$$\mathcal{W}_{SG} = I_0\left(2\sqrt{z}\right) = 1 + z + \frac{1}{4}z^2 + \ldots\,, \tag{B.161}$$

where now $z = g^2 N/8\pi r T$. For Coulomb gauge nothing changes, so taking the planar limit we have

$$\mathcal{W}_{CG} = \exp z = 1 + z + \frac{1}{2} z^2 + \dots \,. \tag{B.162}$$

Taking the planar limit for the other two results we get $z^2/12$ from the singular part of the self-energy and $z^2/6$. We see also here that if we add these two contributions to the tree-level one-gluon exchange result in static gauge, then both gauges agree up to $\mathcal{O}(z^2)$.

So far we only considered the small z expansions. There is also a discussion of the large z limit in [167], which corresponds to $rT \ll \alpha_\mathrm{s}$ or $rT \ll \alpha_\mathrm{s} N$, and this is where we disagree with their conclusions. In order to take the limit $z \to \infty$ one really has to include all terms of order z^n in the resummation, and as we just saw, this has not been done in [167]. There will also be higher powers of z from multiple gluon exchanges between the spatial Wilson lines and higher powers in the expansion of the propagators in the singular self-energy. Since those terms were not included in the resummations, the results for large z cannot be trusted. The authors have commented on a strange behavior of the Wilson loop for large z and interpreted it as a side effect of the planar limit, while in our view it is rather due to an incomplete resummation and gauge dependence.

In Coulomb gauge there are no contributions of order z^n from gluon exchanges between the spatial Wilson lines and there are also no singular terms in the self-energy up to one-loop order. We do not know if at a higher loop order a singular term can appear in the self energy, but assuming that it does not, then the resummed result of the Wilson loop is also valid in the large z limit and shows exactly the Coulombic behavior that is expected.

Apart from the Wilson loop, Ref. [167] also discusses the Polyakov loop correlator. There the picture is similar, the leading term in the small z expansion of their resummed result reproduces the known expression, but the next order term is missing the contribution from the singular part of the self-energy (compare the cubic part in Eq. (4.120) or Ref. [126]). Then the large z limit does not reproduce the right behavior, because the resummation is incomplete.

Assuming that Coulomb gauge does not have singular contributions from the self energy at higher orders, we may take the $z \to \infty$ limit in Eq. (4.102) without problems. The contribution from the adjoint self energy becomes exponentially suppressed, and the Polyakov loop correlator is given by the exponential of the singlet free energy alone.

B.10 Alternative Exponentiation of the Polyakov Loop Correlator

Instead of the expression given in Eq. (4.58), we now write the Polyakov loop as:

$$\exp\left[-\frac{F_{Q\bar{Q}}(r)}{T}\right] = \frac{\delta_{ij}\delta_{kl}}{N^2} \left\langle L_{ij}(\boldsymbol{r}) \left(L^\dagger\right)_{kl}(\boldsymbol{0}) \right\rangle \equiv \frac{\delta_{ij}\delta_{kl}}{N^2} \langle \mathcal{M} \rangle_{ik,jl} \,, \tag{B.163}$$

where i, k are final and j, l are initial indices with respect to the direction of the Polyakov loops (i.e. from 0 to $1/T$ for the quark loop and from $1/T$ to 0 for the antiquark loop). Exponentiation is now understood with respect to the multiplication:

$$\mathcal{M}^n_{ik,jl} = \mathcal{M}_{ik,i'k'} \mathcal{M}_{i'k',i''k''} \cdots \mathcal{M}_{j'l',jl} \,. \tag{B.164}$$

Note that now also the replica path ordering is different. In section 4.7 gluons with a higher replica index are ordered such that they are closer to $1/T$ than gluons with a lower index, but

here they are ordered such that they are closer to the endpoint of their respective Polyakov loop, which can be $1/T$ or 0 for the quark or antiquark loop.

Because of the Fierz identity (1.7), there remain only two possibilities in which the initial and final indices can be combined in fundamental tensors:

$$(t_1)_{ik,jl} = \delta_{ij}\delta_{kl}\,, \qquad (t_2)_{ik,jl} = \delta_{il}\delta_{kj}\,. \tag{B.165}$$

Then the color coefficients of the one- and two-gluon exchange diagrams are given by

$\widetilde{\mathcal{C}}_{ik,jl}$  $= \mathcal{C}_{ik,jl}$  $= T^a_{ij}T^a_{kl} = \frac{1}{2}\left(\delta_{il}\delta_{kj} - \frac{1}{N}\delta_{ij}\delta_{kl}\right) = -\frac{1}{2N}(t_1)_{ik,jl} + \frac{1}{2}(t_2)_{ik,jl}\,,$ (B.166)

$$\begin{aligned}
\widetilde{\mathcal{C}}_{ik,jl}\,&\text{  } = n(n-1)\,\mathcal{C}_{ik,jl}\,\text{} + n\,\mathcal{C}_{ik,jl}\,\text{}\Big|_{\mathcal{O}(n)} = \mathcal{C}_{ik,jl}\,\text{} - \mathcal{C}_{ik,jl}\,\text{} \\
&= (T^aT^b)_{ij}(T^bT^a)_{kl} - (T^aT^b)_{ij}(T^aT^b)_{kl} = T^a_{im}T^b_{mj}T^b_{kn}T^a_{nl} - T^a_{im}T^b_{mj}T^a_{kn}T^b_{nl} \\
&= \frac{1}{4}\left(\delta_{il}\delta_{nm} - \frac{1}{N}\delta_{im}\delta_{nl}\right)\left(\delta_{mn}\delta_{kj} - \frac{1}{N}\delta_{mj}\delta_{kn}\right) \\
&\quad - \frac{1}{4}\left(\delta_{in}\delta_{km} - \frac{1}{N}\delta_{im}\delta_{kn}\right)\left(\delta_{ml}\delta_{nj} - \frac{1}{N}\delta_{mj}\delta_{nl}\right) \\
&= -\frac{1}{4}(t_1)_{ik,jl} + \frac{N}{4}(t_2)_{ik,jl}\,,
\end{aligned} \tag{B.167}$$

$$\widetilde{\mathcal{C}}_{ik,jl}\,\text{  } = n(n-1)\,\mathcal{C}_{ik,jl}\,\text{} + n\,\mathcal{C}_{ik,jl}\,\text{}\Big|_{\mathcal{O}(n)} = 0\,, \tag{B.168}$$

$$\widetilde{\mathcal{C}}_{ik,jl}\,\text{  } = n(n-1)\,\mathcal{C}_{ik,jl}\,\text{} + n\,\mathcal{C}_{ik,jl}\,\text{}\Big|_{\mathcal{O}(n)} = 0\,, \tag{B.169}$$

$$\begin{aligned}
\widetilde{\mathcal{C}}_{ik,jl}\,&\text{  } = n(n-1)\,\mathcal{C}_{ik,jl}\,\text{} + n\,\mathcal{C}_{ik,jl}\,\text{}\Big|_{\mathcal{O}(n)} = \mathcal{C}_{ik,jl}\,\text{} - \mathcal{C}_{ik,jl}\,\text{} \\
&= (T^aT^bT^a)_{ij}T^b_{kl} - (T^aT^aT^b)_{ij}T^b_{kl} = T^a_{im}T^b_{mn}T^a_{nj}T^b_{kl} - T^a_{im}T^a_{mn}T^b_{nj}T^b_{kl} \\
&= \frac{1}{4}\left(\delta_{ij}\delta_{nm} - \frac{1}{N}\delta_{im}\delta_{nj}\right)\left(\delta_{kn}\delta_{ml} - \frac{1}{N}\delta_{mn}\delta_{kl}\right) \\
&\quad - \frac{1}{4}\left(\delta_{in}\delta_{mm} - \frac{1}{N}\delta_{im}\delta_{mn}\right)\left(\delta_{kj}\delta_{nl} - \frac{1}{N}\delta_{nj}\delta_{kl}\right) \\
&= \frac{1}{4}(t_1)_{ik,jl} - \frac{N}{4}(t_2)_{ik,jl}\,.
\end{aligned} \tag{B.170}$$

In the tensor space of t_1 and t_2, t_1 is the unit element, and t_2 has the property $t_2^2 = t_1$. The exponential of a linear combination of t_1 and t_2 is therefore given by

$$\exp\bigl[At_1 + Bt_2\bigr] = \exp[A]\,\bigl(\cosh[B]\,t_1 + \sinh[B]\,t_2\bigr)\,. \tag{B.171}$$

We can again factorize the unconnected diagrams, because they are always proportional to

only t_1. With $\delta_{ji}\delta_{lk}(t_1)_{ik,jl} = N^2$ and $\delta_{ji}\delta_{lk}(t_2)_{ik,jl} = N$ we get for the connected part:

$$\exp\left[\frac{2F_Q - F_{Q\bar{Q}}}{T}\right] = \exp\left[-\frac{1}{2N}\,\mathcal{K}\left(\right) - \frac{1}{4}\,\mathcal{K}\left(\right) + \dots\right]$$
$$\times\left(\cosh\left[\frac{1}{2}\,\mathcal{K}\left(\right) + \frac{N}{4}\,\mathcal{K}\left(\right) + \dots\right]\right.$$
$$\left. + \frac{1}{N}\sinh\left[\frac{1}{2}\,\mathcal{K}\left(\right) + \frac{N}{4}\,\mathcal{K}\left(\right) + \dots\right]\right)$$
$$= \frac{N-1}{2N}\exp\left[-\frac{N+1}{2N}\,\mathcal{K}\left(\right) - \frac{N+1}{4}\,\mathcal{K}\left(\right) + \dots\right]$$
$$+ \frac{N+1}{2N}\exp\left[\frac{N-1}{2N}\,\mathcal{K}\left(\right) + \frac{N-1}{4}\,\mathcal{K}\left(\right) + \dots\right]$$
$$= 1 + \frac{N^2-1}{8N^2}\mathcal{K}^2\left(\right) - \frac{N^2-1}{24N^3}\mathcal{K}^3\left(\right)$$
$$+ \frac{N^2-1}{8N}\mathcal{K}\left(\right)\mathcal{K}\left(\right) + \dots\,. \tag{B.172}$$

This looks very different than the result we obtained in the calculation of the main section, in particular the appearance of the uncrossed two-gluon diagram and the absence of the crossed diagram. However, we can see the equivalence between both expressions in the expansion of the exponentials, also noting the identity:

$$\mathcal{K}\left(\right) = \frac{1}{2}\,\mathcal{K}^2\left(\right) - \mathcal{K}\left(\right)\,. \tag{B.173}$$

With this the square of the one-gluon diagram as well as the product of one- and two-gluon diagrams are the same in both results. The cubic power of the one-gluon diagram does not come out right yet, because there is a similar identity for the three-gluon diagrams, and since we did not include those here, we are missing a contribution.

The second expression for this way of exponentiation is also very interesting. The coefficients $(N\pm1)/2N$ are exactly the dimensions of the irreducible representations of a quark-quark combination divided by N^2 (in the case of $N = 3$ those are an antitriplet and a sextet). The coefficients of the one-gluon diagram in the exponents are also exactly those of the corresponding potentials, only the sign of the diagram itself is wrong.

This is no surprise. We can turn the $Q\bar{Q}$ Polyakov loop correlator into a QQ correlator simply by flipping the lower line in all diagrams. The exponentiation performed in this appendix is not affected by this, but the multiplication we have defined here then corresponds exactly to the one used in the main section. The different orientation of the lower contour gives a minus sign for all diagrams with an odd number of gluons connecting the two loops and turns the uncrossed two-gluon diagram into the crossed one. Then we get exactly the expected result, the QQ Polyakov loop correlator decomposes into $N(N\pm1)/2$-plet free energies, each of which is given by the corresponding static potential at leading order (now with the right sign).

Acknowledgments

I am deeply grateful to my supervisors Nora Brambilla and Antonio Vairo for their invaluable guidance and continued support. I look back on numerous enlightening discussions and six years of most interesting research. And I am very grateful for having been given the opportunity to attend many conferences, workshops and schools all around the world. I also thank the people who have kindly invited me to their home institutions: Hideo Suganuma to Kyoto University, Péter Petreczky to BNL, and Yukinari Sumino to Tohoku University. Some have turned into fruitful collaborations, and I expect others will in the future.

Then I would like to thank my past or present collaborators Péter Petreczky, Jacopo Ghiglieri, Jaume Tarrús Castellà, and Sungmin Hwang, who were always open to discuss my ideas and helped me tremendously with their insight. I would be very happy if we could continue on those collaborations. Another deep thanks goes out to all my colleagues and friends, who have made my time at TUM such a pleasant experience, both scientifically and personally. Apart from the aforementioned, these are Héctor Martínez, Simone Biondini, Vladyslav Shtabovenko, Michael Benzke, Miguel Escobedo, Piotr Pietrulewicz, Thomas Rosenhammer, Kiesang Jeong, Sebastian Steinbeißer, Johannes Weber, Jorge Segovia, Javad Komijani, and of course our secretary Susanne Tillich, who was always ready to help.

Lastly, I want to thank my family for their constant love and support. I would not be where I am now without you.

Bibliography

[1] N. Brambilla *et al.*, "QCD and Strongly Coupled Gauge Theories: Challenges and Perspectives," Eur. Phys. J. **C74**, 2981 (2014), arXiv:1404.3723 [hep-ph].

[2] N. Brambilla *et al.*, "Heavy quarkonium: progress, puzzles, and opportunities," Eur. Phys. J. **C71**, 1534 (2011), arXiv:1010.5827 [hep-ph].

[3] G. T. Bodwin, E. Braaten, E. Eichten, S. L. Olsen, T. K. Pedlar, and J. Russ, "Quarkonium at the Frontiers of High Energy Physics: A Snowmass White Paper," in *Community Summer Study 2013: Snowmass on the Mississippi (CSS2013)* (2013) arXiv:1307.7425.

[4] S. Borsányi, Z. Fodor, C. Hoelbling, S. D. Katz, S. Krieg, C. Ratti, and K. K. Szabó (Wuppertal-Budapest), "Is there still any T_c mystery in lattice QCD? Results with physical masses in the continuum limit III," JHEP **09**, 073 (2010), arXiv:1005.3508 [hep-lat].

[5] A. Bazavov *et al.*, "The chiral and deconfinement aspects of the QCD transition," Phys. Rev. **D85**, 054503 (2012), arXiv:1111.1710 [hep-lat].

[6] B. Müller, "Investigation of Hot QCD Matter: Theoretical Aspects," *Proceedings, Nobel Symposium 154: The Higgs Boson Discovery and Other Recent LHC Results: Krusenberg, Sweden, May 13-17, 2013*, Phys. Scripta **T158**, 014004 (2013), arXiv:1309.7616 [nucl-th].

[7] T. Matsui and H. Satz, "J/ψ Suppression by Quark-Gluon Plasma Formation," Phys. Lett. **B178**, 416 (1986).

[8] N. Brambilla, J. Ghiglieri, A. Vairo, and P. Petreczky, "Static quark-antiquark pairs at finite temperature," Phys. Rev. **D78**, 014017 (2008), arXiv:0804.0993 [hep-ph].

[9] N. Brambilla, A. Pineda, J. Soto, and A. Vairo, "Potential NRQCD: An Effective theory for heavy quarkonium," Nucl. Phys. **B566**, 275 (2000), arXiv:hep-ph/9907240 [hep-ph].

[10] A. Pineda and J. Soto, "Effective field theory for ultrasoft momenta in NRQCD and NRQED," *Quantum chromodynamics. Proceedings, Conference, QCD'97, Montpellier, France, July 3-9, 1997*, Nucl. Phys. Proc. Suppl. **64**, 428 (1998), arXiv:hep-ph/9707481 [hep-ph].

[11] R. Aaij *et al.* (LHCb), "Observation of $J/\psi p$ Resonances Consistent with Pentaquark States in $\Lambda_b^0 \to J/\psi K^- p$ Decays," Phys. Rev. Lett. **115**, 072001 (2015), arXiv:1507.03414 [hep-ex].

[12] C. B. Lang, L. Leskovec, D. Mohler, S. Prelovsek, and R. M. Woloshyn, "DK and D^*K scattering near threshold," *Proceedings, 32nd International Symposium on Lattice Field Theory (Lattice 2014)*, PoS **LATTICE2014**, 086 (2015), arXiv:1410.6668 [hep-lat].

[13] S. Prelovsek, C. B. Lang, L. Leskovec, and D. Mohler, "Study of the Z_c^+ channel using lattice QCD," Phys. Rev. **D91**, 014504 (2015), arXiv:1405.7623 [hep-lat].

[14] G. Moir, M. Peardon, S. M. Ryan, C. E. Thomas, and L. Liu (Hadron Spectrum), "Excited spectroscopy of mesons containing charm quarks from lattice QCD," *Proceedings, 31st International Symposium on Lattice Field Theory (Lattice 2013)*, PoS **LATTICE2013**, 242 (2014), arXiv:1312.1361 [hep-lat].

[15] C. Morningstar, J. Bulava, B. Fahy, J. Foley, Y. C. Jhang, K. J. Juge, D. Lenkner, and C. H. Wong, "Extended hadron and two-hadron operators of definite momentum for spectrum calculations in lattice QCD," Phys. Rev. **D88**, 014511 (2013), arXiv:1303.6816 [hep-lat].

[16] J. Bulava, B. Fahy, J. Foley, Y.-C. Jhang, K. J. Juge, D. Lenkner, C. Morningstar, and C. H. Wong, "Spectrum of excited states using the stochastic LapH method," *Proceedings, 31st International Symposium on Lattice Field Theory (Lattice 2013)*, PoS **LATTICE2013**, 266 (2014), arXiv:1310.7887 [hep-lat].

[17] E. Braaten, "How the $Z_c(3900)$ Reveals the Spectra of Quarkonium Hybrid and Tetraquark Mesons," Phys. Rev. Lett. **111**, 162003 (2013), arXiv:1305.6905 [hep-ph].

[18] E. Braaten, H. W. Hammer, and T. Mehen, "Scattering of an Ultrasoft Pion and the $X(3872)$," Phys. Rev. **D82**, 034018 (2010), arXiv:1005.1688 [hep-ph].

[19] E. Braaten, "Galilean-invariant effective field theory for the X(3872)," Phys. Rev. **D91**, 114007 (2015), arXiv:1503.04791 [hep-ph].

[20] M. Berwein, N. Brambilla, and A. Vairo, "Renormalization of Loop Functions in QCD," Phys. Part. Nucl. **45**, 656 (2014), arXiv:1312.6651 [hep-th].

[21] M. Berwein, N. Brambilla, J. Tarrus Castella, and A. Vairo, "Quarkonium hybrids with nonrelativistic effective field theories," Phys. Rev. **D92**, 114019 (2015), arXiv:1510.04299 [hep-ph].

[22] M. Berwein, N. Brambilla, P. Petreczky, and A. Vairo, "Polyakov loop at next-to-next-to-leading order," Phys. Rev. **D93**, 034010 (2016), arXiv:1512.08443 [hep-ph].

[23] M. Berwein, N. Brambilla, S. Hwang, and A. Vairo, "Poincaré invariance in NRQCD and pNRQCD," (2016), preprint-no. TUM-EFT 74/15.

[24] M. Berwein, N. Brambilla, P. Petreczky, and A. Vairo, "The Polyakov loop correlator in perturbation theory," (2016), preprint-no. TUM-EFT 80/16.

[25] C. A. Baker *et al.*, "An Improved experimental limit on the electric dipole moment of the neutron," Phys. Rev. Lett. **97**, 131801 (2006), arXiv:hep-ex/0602020 [hep-ex].

[26] E. Braaten and R. D. Pisarski, "Soft Amplitudes in Hot Gauge Theories: A General Analysis," Nucl. Phys. **B337**, 569 (1990).

[27] E. Braaten and R. D. Pisarski, "Simple effective Lagrangian for hard thermal loops," Phys. Rev. **D45**, R1827 (1992).

[28] S. Weinberg, "Phenomenological Lagrangians," Physica **A96**, 327 (1979).

[29] J. Gomis and S. Weinberg, "Are nonrenormalizable gauge theories renormalizable?" Nucl. Phys. **B469**, 473 (1996), arXiv:hep-th/9510087 [hep-th].

[30] W. E. Caswell and G. P. Lepage, "Effective Lagrangians for Bound State Problems in QED, QCD, and Other Field Theories," Phys. Lett. **B167**, 437 (1986).

[31] G. P. Lepage and B. A. Thacker, "Effective Lagrangians for Simulating Heavy Quark Systems," *Field Theory on the Lattice. Proceedings, International Symposium, Seillac, France, September 28 - October 2, 1987*, Nucl. Phys. Proc. Suppl. **4**, 199 (1988).

[32] G. T. Bodwin, E. Braaten, and G. P. Lepage, "Rigorous QCD analysis of inclusive annihilation and production of heavy quarkonium," Phys. Rev. **D51**, 1125 (1995), [Erratum: Phys. Rev. **D55**, 5853 (1997)], arXiv:hep-ph/9407339 [hep-ph].

[33] N. Isgur and M. B. Wise, "Weak Decays of Heavy Mesons in the Static Quark Approximation," Phys. Lett. **B232**, 113 (1989).

[34] N. Isgur and M. B. Wise, "Weak Transition Form-Factors Between Heavy Mesons," *DPF Conf.1990:0459-464*, Phys. Lett. **B237**, 527 (1990).

[35] N. Brambilla, A. Pineda, J. Soto, and A. Vairo, "Effective field theories for heavy quarkonium," Rev. Mod. Phys. **77**, 1423 (2005), arXiv:hep-ph/0410047 [hep-ph].

[36] A. Pineda, "Review of Heavy Quarkonium at weak coupling," Prog. Part. Nucl. Phys. **67**, 735 (2012), arXiv:1111.0165 [hep-ph].

[37] E. Braaten and A. Nieto, "Free energy of QCD at high temperature," Phys. Rev. **D53**, 3421 (1996), arXiv:hep-ph/9510408 [hep-ph].

[38] K. Kajantie, M. Laine, K. Rummukainen, and M. E. Shaposhnikov, "3-D SU(N) + adjoint Higgs theory and finite temperature QCD," Nucl. Phys. **B503**, 357 (1997), arXiv:hep-ph/9704416 [hep-ph].

[39] P. H. Ginsparg, "First Order and Second Order Phase Transitions in Gauge Theories at Finite Temperature," Nucl. Phys. **B170**, 388 (1980).

[40] T. Appelquist and R. D. Pisarski, "High-Temperature Yang-Mills Theories and Three-Dimensional Quantum Chromodynamics," Phys. Rev. **D23**, 2305 (1981).

[41] E. D'Hoker, "Perturbative results on QCD in three-dimensions at finite temperature," Nucl. Phys. **B201**, 401 (1982).

[42] S. Nadkarni, "Dimensional Reduction in Hot QCD," Phys. Rev. **D27**, 917 (1983).

[43] N. P. Landsman, "Limitations to Dimensional Reduction at High Temperature," Nucl. Phys. **B322**, 498 (1989).

[44] T. Reisz, "Realization of dimensional reduction at high temperature," Z. Phys. **C53**, 169 (1992).

[45] P. LaCock, D. E. Miller, and T. Reisz, "Dimensional reduction of SU(2) gauge theory beyond the perturbative horizon," Nucl. Phys. **B369**, 501 (1992).

[46] L. Kärkkäinen, P. Lacock, B. Petersson, and T. Reisz, "Dimensional reduction and color screening in QCD," Nucl. Phys. **B395**, 733 (1993).

[47] L. Kärkkäinen, P. Lacock, D. E. Miller, B. Petersson, and T. Reisz, "The Physical phase of dimensionally reduced gauge theories," Nucl. Phys. **B418**, 3 (1994), arXiv:hep-lat/9310014 [hep-lat].

[48] A. Patkós, P. Petreczky, and Z. Szép, "Coupled gap equations for the screening masses in hot SU(N) gauge theory," Eur. Phys. J. **C5**, 337 (1998), arXiv:hep-ph/9711263 [hep-ph].

[49] F. Karsch, M. Oevers, and P. Petreczky, "Screening masses of hot SU(2) gauge theory from the 3-d adjoint Higgs model," Phys. Lett. **B442**, 291 (1998), arXiv:hep-lat/9807035 [hep-lat].

[50] K. Kajantie, M. Laine, J. Peisa, A. Rajantie, K. Rummukainen, and M. E. Shaposhnikov, "Nonperturbative Debye mass in finite temperature QCD," Phys. Rev. Lett. **79**, 3130 (1997), arXiv:hep-ph/9708207 [hep-ph].

[51] M. Laine and O. Philipsen, "The Nonperturbative QCD Debye mass from a Wilson line operator," Phys. Lett. **B459**, 259 (1999), arXiv:hep-lat/9905004 [hep-lat].

[52] A. Hart and O. Philipsen, "The Spectrum of the three-dimensional adjoint Higgs model and hot SU(2) gauge theory," Nucl. Phys. **B572**, 243 (2000), arXiv:hep-lat/9908041 [hep-lat].

[53] A. Hart, M. Laine, and O. Philipsen, "Static correlation lengths in QCD at high temperatures and finite densities," Nucl. Phys. **B586**, 443 (2000), arXiv:hep-ph/0004060 [hep-ph].

[54] A. Cucchieri, F. Karsch, and P. Petreczky, "Magnetic screening in hot nonAbelian gauge theory," Phys. Lett. **B497**, 80 (2001), arXiv:hep-lat/0004027 [hep-lat].

[55] A. Cucchieri, F. Karsch, and P. Petreczky, "Propagators and dimensional reduction of hot SU(2) gauge theory," Phys. Rev. **D64**, 036001 (2001), arXiv:hep-lat/0103009 [hep-lat].

[56] A. D. Linde, "Infrared Problem in Thermodynamics of the Yang-Mills Gas," Phys. Lett. **B96**, 289 (1980).

[57] M. E. Luke and A. V. Manohar, "Reparametrization invariance constraints on heavy particle effective field theories," Phys. Lett. **B286**, 348 (1992), arXiv:hep-ph/9205228 [hep-ph].

[58] N. Brambilla, D. Gromes, and A. Vairo, "Poincare invariance constraints on NRQCD and potential NRQCD," Phys. Lett. **B576**, 314 (2003), arXiv:hep-ph/0306107 [hep-ph].

[59] E. P. Wigner, "On Unitary Representations of the Inhomogeneous Lorentz Group," Annals Math. **40**, 149 (1939), [Reprint: Nucl. Phys. Proc. Suppl. **6**, 9 (1989)].

[60] J. Heinonen, R. J. Hill, and M. P. Solon, "Lorentz invariance in heavy particle effective theories," Phys. Rev. **D86**, 094020 (2012), arXiv:1208.0601 [hep-ph].

[61] C. Arzt, "Reduced effective Lagrangians," Phys. Lett. **B342**, 189 (1995), arXiv:hep-ph/9304230 [hep-ph].

[62] N. Brambilla, E. Mereghetti, and A. Vairo, "Hadronic quarkonium decays at order v**7," Phys. Rev. **D79**, 074002 (2009), [Erratum: Phys. Rev., **D83**, 079904 (2011)], arXiv:0810.2259 [hep-ph].

[63] R. J. Hill, G. Lee, G. Paz, and M. P. Solon, "NRQED Lagrangian at order $1/M^4$," Phys. Rev. **D87**, 053017 (2013), arXiv:1212.4508 [hep-ph].

[64] N. Brambilla, A. Pineda, J. Soto, and A. Vairo, "The QCD potential at O(1/m)," Phys. Rev. **D63**, 014023 (2001), arXiv:hep-ph/0002250 [hep-ph].

[65] A. Pineda and A. Vairo, "The QCD potential at O (1 / $m^{2)}$: Complete spin dependent and spin independent result," Phys. Rev. **D63**, 054007 (2001), [Erratum: Phys. Rev. **D64**, 039902 (2001)], arXiv:hep-ph/0009145 [hep-ph].

[66] N. Brambilla, D. Eiras, A. Pineda, J. Soto, and A. Vairo, "Inclusive decays of heavy quarkonium to light particles," Phys. Rev. **D67**, 034018 (2003), arXiv:hep-ph/0208019 [hep-ph].

[67] C. A. Meyer and E. S. Swanson, "Hybrid Mesons," Prog. Part. Nucl. Phys. **82**, 21 (2015), arXiv:1502.07276 [hep-ph].

[68] N. Isgur and J. E. Paton, "A Flux Tube Model for Hadrons," Phys. Lett. **B124**, 247 (1983).

[69] N. Isgur and J. E. Paton, "A Flux Tube Model for Hadrons in QCD," Phys. Rev. **D31**, 2910 (1985).

[70] P. Hasenfratz, R. R. Horgan, J. Kuti, and J. M. Richard, "The Effects of Colored Glue in the QCD Motivated Bag of Heavy Quark - anti-Quark Systems," Phys. Lett. **B95**, 299 (1980).

[71] D. Horn and J. Mandula, "A Model of Mesons with Constituent Gluons," Phys. Rev. **D17**, 898 (1978).

[72] L. A. Griffiths, C. Michael, and P. E. L. Rakow, "Mesons With Excited Glue," Phys. Lett. **B129**, 351 (1983).

[73] K. J. Juge, J. Kuti, and C. J. Morningstar, "Gluon excitations of the static quark potential and the hybrid quarkonium spectrum," *Contents of LAT97 proceedings*, Nucl. Phys. Proc. Suppl. **63**, 326 (1998), arXiv:hep-lat/9709131 [hep-lat].

[74] R. Born and R. Oppenheimer, "Zur Quantentheorie der Molekeln," Ann. Phys. **389**, 457 (1927).

[75] L. D. Landau and E. M. Lifshitz, *Quantum Mechanics: Non-Relativistic Theory*, 3rd ed., Course of Theoretical Physics, Vol. 3 (Pergamon Press, 1977).

[76] D. Marx and J. Hutter, *Ab Initio Molecular Dynamics: Basic Theory and Advanced Methods* (Cambridge University Press, 2009).

[77] N. A. Campbell, L. A. Griffiths, C. Michael, and P. E. L. Rakow, "Mesons with excited glue from SU(3) lattice gauge theory," Phys. Lett. **B142**, 291 (1984).

[78] I. J. Ford, R. H. Dalitz, and J. Hoek, "Potentials in Pure QCD on 32^4 Lattices," Phys. Lett. **B208**, 286 (1988).

[79] S. Perantonis and C. Michael, "Static potentials and hybrid mesons from pure SU(3) lattice gauge theory," Nucl. Phys. **B347**, 854 (1990).

[80] P. Lacock, C. Michael, P. Boyle, and P. Rowland (UKQCD), "Hybrid mesons from quenched QCD," Phys. Lett. **B401**, 308 (1997), arXiv:hep-lat/9611011 [hep-lat].

[81] K. J. Juge, J. Kuti, and C. Morningstar, "Fine structure of the QCD string spectrum," Phys. Rev. Lett. **90**, 161601 (2003), arXiv:hep-lat/0207004 [hep-lat].

[82] G. S. Bali, B. Bolder, N. Eicker, T. Lippert, B. Orth, P. Ueberholz, K. Schilling, and T. Struckmann (TXL, T(X)L), "Static potentials and glueball masses from QCD simulations with Wilson sea quarks," Phys. Rev. **D62**, 054503 (2000), arXiv:hep-lat/0003012 [hep-lat].

[83] K. J. Juge, J. Kuti, and C. J. Morningstar, "Ab initio study of hybrid anti-b g b mesons," Phys. Rev. Lett. **82**, 4400 (1999), arXiv:hep-ph/9902336 [hep-ph].

[84] E. Braaten, C. Langmack, and D. H. Smith, "Born-Oppenheimer Approximation for the XYZ Mesons," Phys. Rev. **D90**, 014044 (2014), arXiv:1402.0438 [hep-ph].

[85] E. Braaten, C. Langmack, and D. H. Smith, "Selection Rules for Hadronic Transitions of XYZ Mesons," Phys. Rev. Lett. **112**, 222001 (2014), arXiv:1401.7351 [hep-ph].

[86] G. Chiladze, A. F. Falk, and A. A. Petrov, "Hybrid charmonium production in B decays," Phys. Rev. **D58**, 034013 (1998), arXiv:hep-ph/9804248 [hep-ph].

[87] K. Marsh and R. Lewis, "A lattice QCD study of generalized gluelumps," Phys. Rev. **D89**, 014502 (2014), arXiv:1309.1627 [hep-lat].

[88] M. Foster and C. Michael (UKQCD), "Hadrons with a heavy color adjoint particle," Phys. Rev. **D59**, 094509 (1999), arXiv:hep-lat/9811010 [hep-lat].

[89] N. Brambilla, X. Garcia i Tormo, J. Soto, and A. Vairo, "The Logarithmic contribution to the QCD static energy at N^4LO," Phys. Lett. **B647**, 185 (2007), arXiv:hep-ph/0610143 [hep-ph].

[90] N. Brambilla, A. Vairo, X. Garcia i Tormo, and J. Soto, "The QCD static energy at NNNLL," Phys. Rev. **D80**, 034016 (2009), arXiv:0906.1390 [hep-ph].

[91] A. V. Smirnov, V. A. Smirnov, and M. Steinhauser, "Three-loop static potential," Phys. Rev. Lett. **104**, 112002 (2010), arXiv:0911.4742 [hep-ph].

[92] C. Anzai, Y. Kiyo, and Y. Sumino, "Static QCD potential at three-loop order," Phys. Rev. Lett. **104**, 112003 (2010), arXiv:0911.4335 [hep-ph].

[93] A. Pineda and J. Soto, "The Renormalization group improvement of the QCD static potentials," Phys. Lett. **B495**, 323 (2000), arXiv:hep-ph/0007197 [hep-ph].

[94] A. Pineda and M. Stahlhofen, "The static hybrid potential in D dimensions at short distances," Phys. Rev. **D84**, 034016 (2011), arXiv:1105.4356 [hep-ph].

[95] C. Anzai, M. Prausa, A. V. Smirnov, V. A. Smirnov, and M. Steinhauser, "Color octet potential to three loops," Phys. Rev. **D88**, 054030 (2013), arXiv:1308.1202 [hep-ph].

[96] N. Brambilla, X. Garcia i Tormo, J. Soto, and A. Vairo, "Precision determination of $r_0\Lambda^-_{MS}$ from the QCD static energy," Phys. Rev. Lett. **105**, 212001 (2010), [Erratum: Phys. Rev. Lett. **108**, 269903 (2012)], arXiv:1006.2066 [hep-ph].

[97] A. Bazavov, N. Brambilla, X. Garcia i Tormo, P. Petreczky, J. Soto, and A. Vairo, "Determination of $\alpha_{\rm s}$ from the QCD static energy," Phys. Rev. **D86**, 114031 (2012), arXiv:1205.6155 [hep-ph].

[98] A. Bazavov, N. Brambilla, X. Garcia i Tormo, P. Petreczky, J. Soto, and A. Vairo, "Determination of $\alpha_{\rm s}$ from the QCD static energy: An update," Phys. Rev. **D90**, 074038 (2014), arXiv:1407.8437 [hep-ph].

[99] G. S. Bali and A. Pineda, "QCD phenomenology of static sources and gluonic excitations at short distances," Phys. Rev. **D69**, 094001 (2004), arXiv:hep-ph/0310130 [hep-ph].

[100] C. J. Morningstar and M. J. Peardon, "Efficient glueball simulations on anisotropic lattices," Phys. Rev. **D56**, 4043 (1997), arXiv:hep-lat/9704011 [hep-lat].

[101] M. Berwein and H. E. Martinez, In preparation, preprint-no. TUM-EFT 48/14.

[102] F. Buisseret and C. Semay, "On two- and three-body descriptions of hybrid mesons," Phys. Rev. **D74**, 114018 (2006), arXiv:hep-ph/0610132 [hep-ph].

[103] A. Pineda, *Heavy quarkonium and nonrelativistic effective field theories*, Ph.D. thesis, Barcelona U. (1998).

[104] A. H. Hoang, M. C. Smith, T. Stelzer, and S. Willenbrock, "Quarkonia and the pole mass," Phys. Rev. **D59**, 114014 (1999), arXiv:hep-ph/9804227 [hep-ph].

[105] A. Pineda, "Determination of the bottom quark mass from the Υ(1S) system," JHEP **06**, 022 (2001), arXiv:hep-ph/0105008 [hep-ph].

[106] Müller, K. R., *Investigation of gluonic excitations in the presence of a static quark anti-quark pair by means of the potential non-relativistic QCD (pNRQCD)*, Master's thesis, Ruprecht-Karls-Universität Heidelberg (2003).

[107] M. Luscher, "Symmetry Breaking Aspects of the Roughening Transition in Gauge Theories," Nucl. Phys. **B180**, 317 (1981).

[108] J. F. Arvis, "The Exact $q\bar{q}$ Potential in Nambu String Theory," Phys. Lett. **B127**, 106 (1983).

[109] O. Andreev, "Exotic Hybrid Quark Potentials," Phys. Rev. **D86**, 065013 (2012), arXiv:1207.1892 [hep-ph].

[110] Wang, Qian and Cleven, Martin and Guo, Feng-Kun and Hanhart, Christoph and Meißner, Ulf-G. and Wu, Xiao-Gang and Zhao, Qiang, "$Y(4260)$: hadronic molecule versus hadro-charmonium interpretation," Phys. Rev. **D89**, 034001 (2014), arXiv:1309.4303 [hep-ph].

[111] E. Kou and O. Pene, "Suppressed decay into open charm for the $Y(4260)$ being an hybrid," Phys. Lett. **B631**, 164 (2005), arXiv:hep-ph/0507119 [hep-ph].

[112] M. Ablikim *et al.* (BESIII), "Observation of $e^+e^- \to \gamma X(3872)$ at BESIII," Phys. Rev. Lett. **112**, 092001 (2014), arXiv:1310.4101 [hep-ex].

[113] C.-Z. Yuan, "Evidence for resonant structures in $e^+e^- \to \pi^+\pi^- h_c$," Chin. Phys. **C38**, 043001 (2014), arXiv:1312.6399 [hep-ex].

[114] M. Ablikim *et al.* (BESIII), "Study of $e^+e^- \to \omega\chi_{cJ}$ at center-of-mass energies from 4.21 to 4.42 GeV," Phys. Rev. Lett. **114**, 092003 (2015), arXiv:1410.6538 [hep-ex].

[115] G. Cotugno, R. Faccini, A. D. Polosa, and C. Sabelli, "Charmed Baryonium," Phys. Rev. Lett. **104**, 132005 (2010), arXiv:0911.2178 [hep-ph].

[116] L. Liu, G. Moir, M. Peardon, S. M. Ryan, C. E. Thomas, P. Vilaseca, J. J. Dudek, R. G. Edwards, B. Joo, and D. G. Richards (Hadron Spectrum), "Excited and exotic charmonium spectroscopy from lattice QCD," JHEP **07**, 126 (2012), arXiv:1204.5425 [hep-ph].

[117] X. Liao and T. Manke, "Relativistic bottomonium spectrum from anisotropic lattices," Phys. Rev. **D65**, 074508 (2002), arXiv:hep-lat/0111049 [hep-lat].

[118] W. Chen, R. T. Kleiv, T. G. Steele, B. Bulthuis, D. Harnett, J. Ho, T. Richards, and S.-L. Zhu, "Mass Spectrum of Heavy Quarkonium Hybrids," JHEP **09**, 019 (2013), arXiv:1304.4522 [hep-ph].

[119] W. Chen, T. G. Steele, and S.-L. Zhu, "Masses of the bottom-charm hybrid $\bar{b}Gc$ states," J. Phys. **G41**, 025003 (2014), arXiv:1306.3486 [hep-ph].

[120] A. M. Polyakov, "Thermal Properties of Gauge Fields and Quark Liberation," Phys. Lett. **B72**, 477 (1978).

[121] J. Kuti, J. Polónyi, and K. Szlachányi, "Monte Carlo Study of SU(2) Gauge Theory at Finite Temperature," Phys. Lett. **B98**, 199 (1981).

[122] L. D. McLerran and B. Svetitsky, "Quark Liberation at High Temperature: A Monte Carlo Study of SU(2) Gauge Theory," Phys. Rev. **D24**, 450 (1981).

[123] K. Fukushima, "Thermodynamic limit of the canonical partition function with respect to the quark number in QCD," Annals Phys. **304**, 72 (2003), arXiv:hep-ph/0204302 [hep-ph].

[124] E. Gava and R. Jengo, "Perturbative Evaluation of the Thermal Wilson Loop," Phys. Lett. **B105**, 285 (1981).

[125] Y. Burnier, M. Laine, and M. Vepsäläinen, "Dimensionally regularized Polyakov loop correlators in hot QCD," JHEP **01**, 054 (2010), [Erratum: JHEP **01**, 180 (2013)], arXiv:0911.3480 [hep-ph].

[126] N. Brambilla, J. Ghiglieri, P. Petreczky, and A. Vairo, "The Polyakov loop and correlator of Polyakov loops at next-to-next-to-leading order," Phys. Rev. **D82**, 074019 (2010), arXiv:1007.5172 [hep-ph].

[127] O. Kaczmarek, F. Karsch, P. Petreczky, and F. Zantow, "Heavy quark anti-quark free energy and the renormalized Polyakov loop," Phys. Lett. **B543**, 41 (2002), arXiv:hep-lat/0207002 [hep-lat].

[128] O. Kaczmarek, F. Karsch, F. Zantow, and P. Petreczky, "Static quark anti-quark free energy and the running coupling at finite temperature," Phys. Rev. **D70**, 074505 (2004), [Erratum: Phys. Rev. **D72**, 059903 (2005)], arXiv:hep-lat/0406036 [hep-lat].

[129] S. Digal, S. Fortunato, and P. Petreczky, "Heavy quark free energies and screening in SU(2) gauge theory," Phys. Rev. **D68**, 034008 (2003), arXiv:hep-lat/0304017 [hep-lat].

[130] A. Mykkänen, M. Panero, and K. Rummukainen, "Casimir scaling and renormalization of Polyakov loops in large-N gauge theories," JHEP **05**, 069 (2012), arXiv:1202.2762 [hep-lat].

[131] Y. Aoki, Z. Fodor, S. D. Katz, and K. K. Szabó, "The QCD transition temperature: Results with physical masses in the continuum limit," Phys. Lett. **B643**, 46 (2006), arXiv:hep-lat/0609068 [hep-lat].

[132] M. Cheng *et al.*, "The QCD equation of state with almost physical quark masses," Phys. Rev. **D77**, 014511 (2008), arXiv:0710.0354 [hep-lat].

[133] Y. Aoki, S. Borsányi, S. Dürr, Z. Fodor, S. D. Katz, S. Krieg, and K. K. Szabó, "The QCD transition temperature: results with physical masses in the continuum limit II." JHEP **06**, 088 (2009), arXiv:0903.4155 [hep-lat].

[134] A. Bazavov *et al.*, "Equation of state and QCD transition at finite temperature," Phys. Rev. **D80**, 014504 (2009), arXiv:0903.4379 [hep-lat].

[135] A. Bazavov and P. Petreczky, "Polyakov loop in 2+1 flavor QCD," Phys.Rev. **D87**, 094505 (2013), arXiv:1301.3943 [hep-lat].

[136] S. Borsányi, Z. Fodor, S. D. Katz, A. Pásztor, K. K. Szabó, and C. Török, "Static $\overline{\mathrm{Q}}\mathrm{Q}$ pair free energy and screening masses from correlators of Polyakov loops: continuum extrapolated lattice results at the QCD physical point," JHEP **04**, 138 (2015), arXiv:1501.02173 [hep-lat].

[137] S. Gupta, K. Hübner, and O. Kaczmarek, "Renormalized Polyakov loops in many representations," Phys. Rev. **D77**, 034503 (2008), arXiv:0711.2251 [hep-lat].

[138] P. Petreczky and H. P. Schadler, "Renormalization of the Polyakov loop with gradient flow," Phys. Rev. **D92**, 094517 (2015), arXiv:1509.07874 [hep-lat].

[139] O. Kaczmarek, F. Karsch, E. Laermann, and M. Lutgemeier, "Heavy quark potentials in quenched QCD at high temperature," Phys. Rev. **D62**, 034021 (2000), arXiv:hep-lat/9908010 [hep-lat].

[140] F. Karsch, E. Laermann, and A. Peikert, "Quark mass and flavor dependence of the QCD phase transition," Nucl. Phys. **B605**, 579 (2001), arXiv:hep-lat/0012023 [hep-lat].

[141] P. Petreczky and K. Petrov, "Free energy of a static quark anti-quark pair and the renormalized Polyakov loop in three flavor QCD," Phys. Rev. **D70**, 054503 (2004), arXiv:hep-lat/0405009 [hep-lat].

[142] J. G. M. Gatheral, "Exponentiation of Eikonal Cross-sections in Nonabelian Gauge Theories," Phys. Lett. **B133**, 90 (1983).

[143] J. Frenkel and J. C. Taylor, "Nonabelian Eikonal Exponentiation," Nucl. Phys. **B246**, 231 (1984).

[144] E. Gardi, E. Laenen, G. Stavenga, and C. D. White, "Webs in multiparton scattering using the replica trick," JHEP **11**, 155 (2010), arXiv:1008.0098 [hep-ph].

[145] E. Gardi, J. M. Smillie, and C. D. White, "The Non-Abelian Exponentiation theorem for multiple Wilson lines," JHEP **1306**, 088 (2013), arXiv:1304.7040 [hep-ph].

[146] M. Laine and Y. Schröder, "Two-loop QCD gauge coupling at high temperatures," JHEP **03**, 067 (2005), arXiv:hep-ph/0503061 [hep-ph].

[147] E. Braaten and A. Nieto, "Asymptotic behavior of the correlator for Polyakov loops," Phys. Rev. Lett. **74**, 3530 (1995), arXiv:hep-ph/9410218 [hep-ph].

[148] A. Hietanen, K. Kajantie, M. Laine, K. Rummukainen, and Y. Schröder, "Three-dimensional physics and the pressure of hot QCD," Phys. Rev. **D79**, 045018 (2009), arXiv:0811.4664 [hep-lat].

[149] K. Kajantie, M. Laine, K. Rummukainen, and Y. Schröder, "Four loop vacuum energy density of the SU(N(c)) + adjoint Higgs theory," JHEP **04**, 036 (2003), arXiv:hep-ph/0304048 [hep-ph].

[150] A. Bazavov, N. Brambilla, H. T. Ding, P. Petreczky, H. P. Schadler, A. Vairo, and J. H. Weber, "Polyakov loop in 2+1 flavor QCD from low to high temperatures," Phys. Rev. **D93**, 114502 (2016), arXiv:1603.06637 [hep-lat].

[151] S. Necco, "Universality and scaling behavior of RG gauge actions," Nucl. Phys. **B683**, 137 (2004), arXiv:hep-lat/0309017 [hep-lat].

[152] R. Sommer, "A New way to set the energy scale in lattice gauge theories and its applications to the static force and alpha-s in SU(2) Yang-Mills theory," Nucl. Phys. **B411**, 839 (1994), arXiv:hep-lat/9310022 [hep-lat].

[153] `http://www.r-project.org/`.

[154] A. M. Polyakov, "Gauge Fields as Rings of Glue," Nucl. Phys. **B164**, 171 (1980).

[155] V. S. Dotsenko and S. N. Vergeles, "Renormalizability of Phase Factors in the Nonabelian Gauge Theory," Nucl. Phys. **B169**, 527 (1980).

[156] R. A. Brandt, F. Neri, and M.-a. Sato, "Renormalization of Loop Functions for All Loops," Phys. Rev. **D24**, 879 (1981).

[157] A. Grozin, J. M. Henn, G. P. Korchemsky, and P. Marquard, "The three-loop cusp anomalous dimension in QCD and its supersymmetric extensions," JHEP **01**, 140 (2016), arXiv:1510.07803 [hep-ph].

[158] B. A. Kniehl, A. A. Penin, Y. Schroder, V. A. Smirnov, and M. Steinhauser, "Two-loop static QCD potential for general colour state," Phys. Lett. **B607**, 96 (2005), arXiv:hep-ph/0412083 [hep-ph].

[159] P. Falkensteiner, H. Grosse, F. Schöberl, and P. Hertel, "Solving the Schrödinger equation for bound states," Comput. Phys. Commun. **34**, 287 (1985).

[160] W. Lucha and F. F. Schöberl, "Solving the Schrödinger equation for bound states with Mathematica 3.0," Int. J. Mod. Phys. **C10**, 607 (1999), arXiv:hep-ph/9811453 [hep-ph].

[161] H. Amann and P. Quittner, "A nodal theorem for coupled systems of Schrödinger equations and the number of bound states," J. Math. Phys. **36**, 4553 (1995).

[162] J. Schwinger, "NonAbelian gauge fields. Relativistic invariance," Phys. Rev. **127**, 324 (1962).

[163] N. H. Christ and T. D. Lee, "Operator Ordering and Feynman Rules in Gauge Theories," Phys. Rev. **D22**, 939 (1980).

[164] A. Andraši, "The Gluon propagator in the Coulomb gauge," Eur. Phys. J. **C37**, 307 (2004), arXiv:hep-th/0311118 [hep-th].

[165] D. J. Broadhurst, "Three loop on-shell charge renormalization without integration: Lambda-MS (QED) to four loops," Z. Phys. **C54**, 599 (1992).

[166] N. Gray, D. J. Broadhurst, W. Grafe, and K. Schilcher, "Three Loop Relation of Quark (Modified) Ms and Pole Masses," Z. Phys. **C48**, 673 (1990).

[167] R. D. Pisarski and V. V. Skokov, "Correlation functions of Polyakov loops at tree level," (2015), arXiv:1501.06904 [hep-ph].